Deciphering the Mechanisms of Cross-Presentation for Exogenous ROPs Through Their Interaction With Cathepsin S



Alexander John Stephens

Wolfson College

University of Oxford

A thesis submitted to the degree of

Doctor of Philosophy in Oncology

Michaelmas 2023

To my wife – without whom none of this would have been possible.

“All we have to decide is what to do with the time that is given us.”

J.R.R. Tolkien

Statement on the Impact of the COVID-19 Pandemic on This Thesis

During the COVID-19 pandemic lockdowns, I could not access the Oncology laboratories from March until September 2020. During my absence from the laboratory, I used the time to write and publish the review article “Beyond Just Peptide Antigens: The Complex World of Peptide-Based Cancer Vaccines.” This article was partly adapted for the literature review of my thesis introduction.

Between mid-June and the end of July, access was granted for COVID-19 research within the CMD laboratories, but I was not allowed to work on DPhil-related projects. It was not until September 2020 that limited access to the Department of Oncology laboratories was reinstated, necessitating scaling back of the project scope until full-time laboratory access was granted in April 2021.

Because of these challenges, an extension for an additional term was applied for and granted, which gave me the necessary time to complete the remaining experiments. Had the original time been available, the plan was to continue beyond studies on model ROP and implement the ideas presented in this thesis into cancer-antigen ROPs and *in vivo* mouse models.

Declaration of Authentication

The work presented in this thesis is wholly my own, with any contributions made by others acknowledged accordingly. The content submitted here is not part of another thesis in this or any other university. This work was conducted under the supervision of Professor Shisong Jiang and Professor Alex Bullock.

Alexander J Stephens

November 2023

Publication Note

Material from *Introduction 1.5 Peptide Cancer Vaccines* was adapted from the following published review:

Stephens AJ, Burgess-Brown NA and Jiang S (2021) Beyond Just Peptide Antigens: The Complex World of Peptide-Based Cancer Vaccines. *Front. Immunol.* 12:696791. doi: 10.3389/fimmu.2021.696791

Acknowledgements

This journey has been long and arduous, but I have finally reached the other side. I owe everything to those who supported me throughout my DPhil journey. I could not have done this without you.

Firstly, I would like to thank Professor Shisong Jiang, Professor Alex Bullock and my former supervisor, Dr Nicola Burgess-Brown. Your guidance, encouragement, and expertise have been instrumental in shaping my research and academic growth. Your unwavering support and constructive feedback have been invaluable throughout my DPhil. I also wish to thank Oxford Vacmedix for the scholarship that enabled me to conduct my research.

To Yuqian Ou, Sichen Liu, Constantinos Demetriou, Hanjun Zhao and all other Jiang lab members, past and present, thank you for your unwavering support, guidance and friendship throughout the last four years. Our collaborations and discussions have shaped this thesis into what it is here.

To the Seymour lab, including Professor Len Seymour and present lab members, Peter Wan, Emma Page, Mahnoor Nadeem, Kate Friesen, Fernando Jimenez Gallardo, Henry Brigden, Dr Flurin Caviezel, Dr Hena Khalique, Dr Kerry Fisher, Dr Ahmet Hazini, Dr Gulsah Albayrak, along with past-members Dr Richard Baugh, Dr Arthur Dyer and countless others. Thank you all for supporting me and treating me as your own. I could not have completed this thesis without your help and support. You have always been a guide to me when things got tough, and for that, I appreciate you all immeasurably.

To both labs and my dear friends, thank you for your understanding, encouragement, and countless moments of shared laughter. Your support provided a much-needed

balance to the demands of academia, making the journey memorable and fulfilling. To my family, thank you for encouraging me and fostering a supportive environment for me to succeed.

Last but certainly not least, I owe an immeasurable debt of gratitude to my wife. Your unwavering support, patience, and love sustained me through the highs and lows of this DPhil journey. Your belief in me kept me going, and I am profoundly grateful for your sacrifices to see me succeed.

Abstract

Recombinant overlapping peptides (ROPs) are composed of short overlapping peptide sequences formed into one chain encompassing the sequence of a cancer antigen. Each overlapping segment is separated by a cathepsin S cleavage site for processing within dendritic cells to promote antigen cross-presentation and an anti-tumour response. ROPs have been designed with the LRMK linker to target cathepsin S, a key mediator in the vacuolar pathway of cross-presentation. However, the contribution of this pathway to ROP processing is unknown.

Here, we aim to understand the LRMK linker's contribution to cross-presentation by expressing a model ROP designed around the antigen ovalbumin and exploring its processing pathways. OVA-ROP was expressed and cross-presented but relied on detergents to maintain solubility. Therefore, alternative ROP and targeted peptide epitope strategies using Fc-tags and scFvs specific to DCs were employed to discover the feasibility of a DC-targeted approach as a future ROP platform.

We used synthetic peptides containing the LRMK linker from ROP to delve deeper into its contribution to cross-presentation. We demonstrated that cathepsin S is a critical protease in processing LRMK-containing peptides, with chemical inhibition and siRNA knockdown causing a marked reduction in cross-presentation for peptides containing the linker. We also demonstrated the difference in peptide uptake compared to particulate antigens through endocytosis and proteasome inhibitors, uncovering unexpected effects from inhibition.

Overall, the study presented here justifies the LRMK-site within ROP and how its inclusion contributes to ROP processing through the vacuolar cross-presentation pathway, manifesting in ROPs effectiveness as an anti-cancer therapeutic.

Table of Contents

Statement on the Impact of the COVID-19 Pandemic on This Thesis I
Declaration of Authentication II
Publication Note III
Acknowledgements IV
Abstract VI
Table of Contents VII
List of Figures XII
List of Tables XIII
List of Abbreviations XIV
1 Introduction 1
1.1 Cancer 1
1.1.1 What is Cancer? 1
1.1.2 Traditional Cancer Treatments 2
1.1.3 Cancer Immunosurveillance and Immunoediting 4
1.2 Immunotherapy 7
1.2.1 Introduction to Immunotherapy 7
1.2.2 Antibodies and Immune Checkpoint Inhibitors 8
1.2.3 Adoptive Cell Therapy and CAR-T cells 10
1.2.4 Cytokine Therapy 13
1.2.5 Oncolytic Viruses 14
1.2.6 Cancer Vaccines 14
1.3 Antigen Presentation and Cross-Presentation 17
1.3.1 T Cell Activation by Dendritic Cells 17
1.3.2 Antigen Presentation 18
1.3.3 Introduction to Antigen Cross-Presentation 20
1.3.4 Antigen Cross-Presentation – The Cytosolic Pathway 20
1.3.5 Antigen Cross-Presentation – The Vacuolar Pathway 24
1.3.6 Mechanisms of Dendritic Cell Internalisation 26
1.4 Antigen Presentation in Cancer 29
1.4.1 Dendritic Cells in Cancer 29
1.4.2 Cancer Suppression of Dendritic Cells and T cells 31
1.4.3 MHC-I Downregulation in Cancer 34
1.5 Peptide Cancer Vaccines 37
1.5.1 Introduction 37

1.5.2 Synthetic Long Peptides 38
1.5.3 Personalised Peptide Cancer Vaccines 40
1.5.4 Particulate Peptide Cancer Vaccines 41
1.5.5 Targeting Dendritic Cells 44
1.5.6 Peptide Cancer Vaccines in Clinical Trials 46
1.5.7 Recombinant Overlapping Peptides 49
1.6 Thesis Overview and Hypotheses 51
1.6.1 Thesis Overview 51
1.6.2 Hypotheses 53
2 Materials and Methods 54
2.1 Molecular Biology and Cloning 54
2.1.1 Agarose Gel Electrophoresis 54
2.1.2 Bacterial Transformation 54
2.1.3 PCR Colony Screen 55
2.1.4 -80°C Glycerol Stocks of Bacterial Cultures 55
2.1.5 DNA Plasmid Preparation and Quantification 56
2.1.6 DNA Sequencing 56
2.1.7 PCR Amplification and Mutagenesis of Gene Inserts 56
2.1.8 Ligation Independent Cloning of OVA-ROP and DEC-205 scFv Constructs 58
2.1.9 Cloning of OVA-ROP-Fc and pFUSE Constructs 60
2.2 Tissue Culture 63
2.2.1 Cell Lines and Tissue Culturing 63
2.2.2 Cryopreservation of Cell Lines 64
2.3 OVA-ROP Protein Expression and Purification 65
2.3.1 SDS-PAGE and Gel Transfer 65
2.3.2 Protein Concentration Calculation by BCA Assay 66
2.3.3 OVA-ROP Test Expression and Purification From *E. coli* 67
2.3.4 OVA-ROP Inclusion Body Denaturation and Purification 68
2.3.5 Solubility Testing of Denatured OVA-ROP 69
2.3.6 Sarkosyl Solubilisation of OVA-ROP 70
2.3.7 Sarkosyl Turbidimetric Assay 71
2.3.8 TEV Cleavage of OVA-ROP 72
2.3.9 Cathepsin S Protease Assay With Tryptic Digest Tandem Mass Spectrometry 72
2.4 Fc and scFv Fusion Expression and Purification 73
2.4.1 Transfection and Expression Analysis of OVA-ROP-Fc in Mammalian Cells 73

2.4.2 Purification of OVA-ROP-Fc and pFUSE Constructs 75
2.4.3 Expression and Purification of scFv Fusion Proteins 77
2.4.4 Refolding and Tag Removal of SUMO-tagged scFv Fusion Proteins 78
2.5 Synthetic Peptides & Beads 79
2.5.1 Peptide Synthesis 79
2.5.2 Conjugation of OVA to Carboxylate-Modified Latex Beads 80
2.5.3 Cathepsin S siRNA Knockdown of DC2.4 Cells 81
2.5.4 Western Blot Analysis of Cathepsin S Knockdown 83
2.6 Cellular Assays 84
2.6.1 MTS Cytotoxicity Assay 84
2.6.2 Fluorescent Dye Conjugation and Confocal Microscopy 85
2.6.3 Antigen Cross-Presentation Assay by T Cell Receptor-Like Antibody 86
2.6.4 B3Z *LacZ* Antigen Cross-Presentation Assay With Peptides and Proteins 88
2.6.5 B3Z *LacZ* Antigen Cross-Presentation Assay With OVA Beads 90
2.7 Statistical Tests 91
3 Expression and Functional Assessment of OVA-ROP as a Model ROP 92
3.1 Introduction 92
3.1.1 Chapter Aims 96
3.1.2 Hypothesis 96
3.2 Results 97
3.2.1 OVA-ROP is Overexpressed in *E. coli* and Forms Inclusion Bodies 97
3.2.2 Guanidine Solubilises OVA-ROP From Inclusion Bodies 98
3.2.3 Buffer and Additive Refolding Screen of OVA-ROP 100
3.2.4 Sarkosyl Directly Solubilises OVA-ROP From Inclusion Bodies 103
3.2.5 Proteolytic Cleavage of OVA-ROP With TEV and Cathepsin S 106
3.2.6 Sarkosyl-Formulated OVA-ROP is Tolerated by DC2.4 cells in Low Concentrations 107
3.2.7 Visualising the Internalisation and Localisation of OVA-ROP in DC2.4 Cells 109
3.2.8 OVA-ROP is Cross-Presented by DC2.4 Cells 111
3.3 Discussion 113
3.4 Conclusion 121
4 Alternative ROP and Peptide Formulation Strategies 122
4.1 Introduction 122
4.1.1 Chapter Aims 129
4.1.2 Hypotheses 129
4.2 Results 130

4.2.1 tOVA-ROP-Fc Fusions are Expressed in Mammalian Cells 130
4.2.2 tOVA-ROP-Fc is Purifiable From Mammalian Cell Pellets and Displays a Propensity to Cross-Present 133
4.2.3 The Inclusion of IgM Tailpiece Sequence and Q94C Mutation Can Induce Multimerisation of Fc-Tags 137
4.2.4 OVA Epitope DEC-205 scFv Fusion is Expressed, Purified and Refolded From *E. coli* 141
4.2.5 SUMO Tag Removal From OVA-DEC-205 scFv Leads to Precipitation of the Fusion Protein 144
4.2.6 NY-ESO-1 Epitope DEC-205 scFv Fusion is Expressed, Purified and Refolded From *E. coli* 147
4.2.7 SUMO Tag Removal From NY-ESO-1 DEC-205 scFv Leads to Precipitation of the Fusion Protein 148
4.3 Discussion 151
4.4 Conclusion 157
5 Uncovering the Role of the Cathepsin S Sensitive Linker in Antigen Cross-Presentation 158
5.1 Introduction 158
5.1.1 Chapter Aims 165
5.1.2 Hypotheses 165
5.2 Results 166
5.2.1 Brefeldin A Partially Inhibits MHC-I Export of the Synthetic Peptides 166
5.2.2 Endocytosis Inhibition of DC2.4 Cells Reveals Unexpected Enhancement of SIINFEKL Potency 169
5.2.3 Endocytosis Inhibition Shows Similar Internalisation Profiles Between the Synthetic Peptides 171
5.2.4 Proteasome and Cathepsin S Inhibition Reveals Differences in Processing of the Synthetic Peptides 177
5.2.5 High Concentration LHVS Demonstrates Further Inhibition of Cross-Presentation 182
5.2.6 OVA Beads With Inhibitors Uncovers Differences Between Particulate and Soluble Antigen Processing 185
5.2.7 Cathepsin S Knockdown Differentiates the LRMK-Containing Peptide in Antigen Cross-Presentation 187
5.2.8 Cathepsin S Knockdown Validates a Crucial Role of the Vacuolar Pathway in the Cross-Presentation of OVA Beads 191
5.3 Discussion 193
5.4 Conclusion 202
6 Final Discussion 203

6.1 Thesis Overview 203
6.2 Thesis Discussion 209
6.3 Thesis Conclusion 218
References 219
7 Appendices 257
7.1 Appendix I – Supplementary Results 257
7.2 Appendix II – Buffer & Media List 264
7.3 Appendix III – DNA and Protein Sequences 268

List of Figures

Figure 1.1 The Three Signals of T cell Activation 18
Figure 1.2 The Cytosolic and Vacuolar Pathways of Cross-Presentation 24
Figure 1.3 Suppression of Dendritic Cells and T Cells in the Tumour Microenvironment 34
Figure 1.4 Peptide Cancer Vaccine Strategies 38
Figure 1.5 Overview of Recombinant Overlapping Peptides 50
Figure 2.1 Representative Gating Strategy for a Typical Flow Cytometry Experiment on DC2.4 Cells Using an Anti-SIINFEKL/H-2Kb PE Antibody 88
Figure 3.1 Expression of OVA-ROP in *E. coli* 98
Figure 3.2 Solubilisation and Purification of OVA-ROP From Inclusion Bodies 99
Figure 3.3 Screening OVA-ROP for Optimal Solubility Conditions 103
Figure 3.4 Sarkosyl as a Direct Solubilisation Reagent for OVA-ROP Inclusion Bodies 105
Figure 3.5 Proteolytic Activity of TEV Protease and Cathepsin S on OVA-ROP 107
Figure 3.6 Testing Sarkosyl and OVA-ROP Cytotoxicity on DC2.4 cells by MTS assay 108
Figure 3.7 Confocal Microscopy of OVA and OVA-ROP in DC2.4 Cells 110
Figure 3.8 OVA-ROP Cross-Presentation Analysis by T Cell Receptor-Like Antibody 112
Figure 4.1 tOVA-ROP Fc-fusion Protein Expression in HEK293 Cells 132
Figure 4.2 Purification and Antigenicity Assessment of tOVA-ROP-Fc 136
Figure 4.3 Multimerisation of mFc-IgM and mFc_{QC}-IgM Constructs 140
Figure 4.4 Expression and Purification of OVA-DEC-205 scFv Fusion in *E. coli* 143
Figure 4.5 SUMO-Tag Removal From OVA-DEC-205 scFv by SUMO Protease 146
Figure 4.6 Expression and Purification of NYE-DEC-205 scFv Fusion in *E. coli* 148
Figure 4.7 SUMO-Tag Removal From NYE-DEC-205 scFv by SUMO Protease 150
Figure 5.1 Inhibition of Peptide Cross-Presentation by MHC-I Export Blockade 169
Figure 5.2 SIINFEKL Peptide MHC-I Presentation With Endocytosis Inhibitors 171
Figure 5.3 Cross-Presentation of Synthetic Peptides With Endocytosis Inhibition 177
Figure 5.4 Cross-Presentation Profile of Synthetic Peptides With Cathepsin S, Proteasome, and Endosome Acidification Inhibitors 181
Figure 5.5 Effect of Higher LHVS Concentration on Synthetic Peptide Cross-Presentation 184
Figure 5.6 Cross-Presentation of OVA Beads With Inhibitors 187
Figure 5.7 Cross-Presentation of Synthetic Peptides With Cathepsin S siRNA Knockdown 191
Figure 5.8 Cross-Presentation of OVA beads With Cathepsin S siRNA Knockdown 192
Figure 7.1 DDM Concentration in OVA-ROP Detergent Screen 257
Figure 7.2 OVA-ROP Concentration Determination by BCA Assay 257
Figure 7.3 tOVA-ROP-Fc Concentration Determination by BCA Assay 258

Figure 7.4 DC2.4 MTS Cytotoxicity Assessment of Endocytosis Inhibitors 258
Figure 7.5 B3Z Assay Dose-Response Curves of Dynasore and Cytochalasin D With Dynasore 259
Figure 7.6 DC2.4 MTS Cytotoxicity Assessment of Proteasome and Endosome Inhibitors 260
Figure 7.7 B3Z Assay Dose-Response Curves of Epoxomicin and Chloroquine 261
Figure 7.8 Measuring the Yield of OVA Conjugated to Latex Beads Using a BCA Assay ... 262
Figure 7.9 Fluorescein-Conjugated siRNA Transfection Control 263
Figure 7.10 siRNA Knockdown Band Intensity Analysis of Second Band 263

List of Tables

Table 1.1 Key Approved Cancer Immunotherapy Treatments 7
Table 1.2 New Peptide Vaccine Clinical Trials (June 2021 – November 2023) 47
Table 2.1 PCR Conditions for Colony Screen 55
Table 2.2 Amino Acid Sequences for Gene Inserts 57
Table 2.3 PCR Amplification Reaction Conditions 58
Table 2.4 dNTPs for Vector and Insert Polymerisation 59
Table 2.5 Synthetic Peptide Amino Acid Sequences and Length 80
Table 2.6 Inhibitor Concentrations for MTS Assay 84
Table 2.7 Inhibitor Concentrations for B3Z Assay 89
Table 5.1 Endocytosis Inhibitors 169
Table 5.2 Proteasome, Endosome and Protease Inhibitors 177

List of Abbreviations

2xYT	2x yeast extract tryptone
4PL	Four-parameter logistic
ACT	Adoptive cell therapy
ADCC	Antibody-dependent cell-mediated cytotoxicity
ADP	Antibody-dependent phagocytosis
ALL	Acute lymphoblastic leukaemia
ANOVA	Analysis of variance
APC	Antigen-presenting cell
Arg-Glu	Arginine-glutamine
ATP	Adenosine triphosphate
BCA	Bicinchoninic acid
BCMA	B-cell maturation antigen
Bis-Tris	Bis-(2-hydroxy-ethyl)-amino-tris(hydroxymethyl)-methane
BiTE	Bispecific T-cell engager
bp	Base pairs
BSA	Bovine serum albumin
$CaCl_2$	Calcium chloride
CARD	Caspase activation and recruitment domains
CAR-DC	Chimeric antigen receptor dendritic cell
CAR-T	Chimeric antigen receptor T-cell
CCL	Chemokine C-C ligand
CCR	Chemokine C-C receptor
CDC	Complement-mediated cytotoxicity
cDC	Conventional DC
CH	Constant heavy
CHAPS	3-((3-cholamidopropyl) dimethylammonio)-1-propanesulfonate
CLEC-9	C-type lectin domain family 9
CLIP	Class II-associated invariant chain peptide
CMC	Critical micelle concentration
CMD	Centre for Medicines Discovery
CMV	Cytomegalovirus
CO_2	Carbon dioxide
CPA	Cyclophosphamide
CPP	Cell-penetrating peptide
CPRG	Chlorophenol red-β-d-galactopyranoside
CTL	Cytotoxic T lymphocytes
CTLA-4	Cytotoxic T lymphocyte-associated protein 4
ctss	Cathepsin S
CV	Column volume
CXCL	Chemokine C-X-C ligand
CXCR	Chemokine C-X-C receptor
CyDisCo	Cytoplasmic disulphide bond in *E. coli*
Cyto D	Cytochalasin D

DAMP	Damage-associated molecular pattern
DAPI	4′,6-diamidino-2-phenylindole
DC	Dendritic cell
ddH_2O	Double-distilled water
DDM	N-dodecyl-beta-maltoside
DLBCL	Diffuse large B-cell lymphoma
DMEM	Dulbecco's modified eagle medium
DMSO	Dimethylsulphoxide
DNA	Deoxyribonucleic acid
DNAJB1-PRKACA	Dnaj homolog subfamily b member 1- protein kinase camp-activated catalytic subunit alpha
dNTP	Deoxynucleotide triphosphate
DOPE	Dioleoyl phosphatidyl-ethanolamine
DPBS	Dulbecco's phosphate-buffered saline
Dsb	Disulphide bond
DTT	Dithiothreitol
E. coli	*Escherichia coli*
ECL	Enhanced chemiluminescence
EDAC	1-ethyl-3-(3-dimethylaminopropyl) carbodiimide hydrochloride
EDTA	Ethylenediaminetetraacetic acid
EGFR	Epidermal growth factor receptor
EphA2	Ephrin type-a receptor 2
ER	Endoplasmic reticulum
ERAD	ER-associated degradation
ERAP	Endoplasmic reticulum aminopeptidase protein
Erv1p	Essential for respiration and vegetative growth protein 1
EU/mL	Endotoxin units per mL
F/T	Flow-through
Fab	Fragment-antigen binding
FasL	Fas ligand
FBS	Foetal bovine serum
Fc	Fragment crystallisable
FcRn	Neonatal Fc-receptor
FcγR	Fragment crystallisable gamma receptor
FDA	Food and Drug Administration
FLT3L	Fms-like tyrosine kinase 3 ligand
FOLFIRI	Folinic acid, fluorouracil, and irinotecan
FPLC	Fast protein liquid chromatography
GFP	Green fluorescent protein
GM-CSF	Granulocyte-macrophage colony-stimulating factor
gp100	Glycoprotein 100
GPC3	Glypican-3
GSH	Reduced glutathione
GSSG	Oxidised glutathione
GTPase	Guanosine triphosphate hydrolase
GuHCl	Guanidine hydrochloride

GzmB	Granzyme b
HCC	Hepatocellular carcinoma
HCl	Hydrochloride
HCL	Hairy cell leukaemia
HEK293	Human embryonic kidney 293 cells
HEPES	(4-(2-hydroxyethyl)-1-piperazineethanesulfonic acid)
HER2	Human epidermal growth factor receptor 2
HLA	Human leukocyte antigens
HPV	Human papilloma virus
HRP	Horse radish peroxidase
HSV-1	Type 1 herpes simplex virus
IAP	Inhibitor of apoptosis
IB	Inclusion body
IC	Immune complex
ICI	Immune checkpoint inhibitor
ICP	Infected cell protein
IFN	Interferon
Ig	Immunoglobulin
IGEPAL CA-630	Octylphenoxypolyethoxyethanol
IL	Interleukin
iNKT	Invariant natural killer T cells
IPTG	Isopropyl ß-d-1-thiogalactopyranoside
IRAP	Insulin-regulated aminopeptidase
ITAM	Immunoreceptor tyrosine-based activation motif
ITIM	Immunoreceptor tyrosine-based inhibition motif
IVIG	Intravenous immunoglobulin
KCl	Potassium chloride
kDa	Kilodalton
KIR	Killer cell immunoglobulin-like receptor
KLD	Kinase ligase DpnI
KRAS	Kirsten rat sarcoma virus
LAG-3	Lymphocyte-activation gene 3
LB	Lysogeny broth
LDS	Lithium dodecyl sulphate
LFA	Lipofectamine
LHVS	Leucine homophenylalanine vinyl sulfone
LIC	Ligation-independent cloning
Log(ED_{50})	Logarithmic median effective dose
LPS	Lipopolysaccharides
LRPAP1	Low-density lipoprotein receptor-related protein-associated protein 1
mAb	Monoclonal antibody
MAC	Membrane attack complex
MAGE-A3	Melanoma-associated antigen 3
MART-1	Melanoma antigen recognized by T cells 1
MBP	Maltose binding protein

MCA	Methylcholanthrene
MCL	Mantle cell lymphoma
MDA5	Melanoma differentiation-associated protein 5
MDSC	Myeloid-derived suppressor cell
MELOE1	Melanoma-overexpressed antigen 1
MES	2-(n-morpholino)ethanesulphonic acid
mFc-IgM	pFUSE-mIgG2a-Fc2$_{IgM}$
mFc$_{QC}$-IgM	pFUSE-mIgG2a-Fc2$_{Q94C+IgM}$
MgCl2	Magnesium chloride
MHC	Major histocompatibility complex
MI-51	Montanide ISA-51
mIgG2a	mouse IgG2a
MOWSE	Molecular weight search
MPL	Monophosphate lipid A
mRNA	Messenger RNA
MTS	(3-(4,5-dimethylthiazol-2-yl)-5-(3-carboxymethoxyphenyl)-2-(4-sulfophenyl)-2H-tetrazolium)
MUC1	Mucin short variant S1
MWCO	Molecular weight cut-off
MyD88	Myeloid differentiation primary response 88
NaCl	Sodium chloride
NEAA	Non-essential amino acids
NEB	New England Biolabs
NFAT	Nuclear factor of activated T cells
NFW	Nuclease-free water
NF-κB	The nuclear factor kappa-light-chain-enhancer of activated B cells
NHS	N-hydroxysuccinimide ester
Ni^{2+}	Nickel Ion
Ni^{2+} Resin	Ni Sepharose 6 fast flow histidine-tagged protein purification resin
NK	Natural killer
NKG2	Natural killer group 2
NLRC5	Nod-like receptor family card domain containing 5
NOD	Nucleotide-binding oligomerization domain
NOX2	Nicotinamide adenine dinucleotide phosphate oxidase 2
ns	Not significant
NSCLC	Non-small cell lung cancer
NY-ESO-1	New York oesophageal squamous cell carcinoma 1
Opti-MEM	Opti-minimal essential media
OVA	Ovalbumin
OVA-ROP	Ovalbumin-recombinant overlapping peptide
PADRE	Pan HLA-DR epitope
PAMP	Pathogen-associated molecular pattern
PAP	Prostatic acid phosphatase
PBS	Phosphate buffered saline
PBS-T	PBS-Tween
PCR	Polymerase chain reaction

PD-1	Programmed cell death protein 1
PDAC	Pancreatic ductal adenocarcinoma
pDC	Plasmacytoid DC
PD-L1	Programmed death ligand 1
PE	Phycoerythrin
PEI	Polyethylenimine
PeI	Pectate lyase
PES	Polyethersulphone
PFN	Perforin
pFUSE-Fc	pFUSE-mIgG2a-Fc2
PLC	Peptide loading complex
PLGA	Poly(lactic-co-glycolic acid)
poly-ICLC	Polyinosinic-polycytidylic acid with polylysine and carboxy-methylcellulose
PRR	Pathogen-recognition receptor
PSMB8	Proteasome subunit beta type-8
PVDF	Polyvinylidene fluoride
RIPA	Radioimmunoprecipitation assay buffer
RNA	Ribonucleic acid
ROP	Recombinant overlapping peptide
ROS	Reactive oxygen species
RPM	Revolutions per minute
RPMI-1640	Roswell park memorial institute-1640
S/N	Supernatant
Sarkosyl	N-lauroylsarcosine
scFv	Single-chain variable fragment
SD	Standard deviation
SDS	Sodium dodecyl sulphate
SDS-PAGE	Sodium dodecyl sulphate–polyacrylamide gel electrophoresis
siRNA	Small interfering RNA
SIRPα	Signal regulatory protein α
SLP	Synthetic long peptides
SNAP	Soluble N-ethylmaleimide-sensitive factor attachment proteins
SNARE	Snap receptor
SOC	Super optimal broth with catabolite repression
STING	Stimulator of interferon genes
SUMO	Small ubiquitin-like modifier
TAA	Tumour-associated antigen
TAE	Tris(hydroxymethyl) aminomethane-acetate-ethylenediaminetetraacetic acid
TAP	Transporter associated with antigen processing
TAPBPR	Tap-binding protein-related
TB	Terrific broth
TBVA	Tumour blood vessel antigen
TCEP	Tris(2-carboxyethyl)phosphine
TCR	T-cell receptor
TE	Tris-EDTA

TEV	Tobacco etch virus
TGF	Transforming growth factor
Th	T helper
TICAM1	Toll/interleukin-1 receptor domain-containing adaptor molecule
TIL	Tumour-infiltrating lymphocyte
TIM-3	T-cell immunoglobulin and mucin-domain containing 3
TLR	Toll-like receptor
TME	Tumour microenvironment
TMZ	Temozolomide
TNF	Tumour necrosis factor
TRAIL	Tumour necrosis factor-related apoptosis-inducing ligand
Treg	Regulatory T cell
TRIS	Tris(hydroxymethyl)aminomethane
TRP-2	Tyrosinase related protein-2
TSA	Tumour-specific antigen
TSE	Tris/sucrose/EDTA
Uty	Ubiquitously transcribed tetratricopeptide repeat gene on the Y chromosome
v/v	Volume-to-volume
V-ATPase	Vacuolar-type ATP hydrolase
VEGF	Vascular endothelial growth factor
w/v	Weight-to-volume
w/w	Weight-to-weight
Wt-Fc	Wildtype Fc
XCL	Chemokine (C motif) ligand
XCR1	Chemokine C receptor 1
β2M	Beta-2 microglobulin
βME	Beta-mercaptoethanol

1 Introduction

1.1 Cancer

1.1.1 What is Cancer?

Cancer is a heterogeneous disease characterised by aberrant cell proliferation, resulting from a disruption of the regulatory mechanisms which control cell growth and division. Uncontrolled cellular growth culminates in the formation of neoplasms, known as tumours. The breakdown of these regulatory mechanisms can be attributed to genetic mutations, which can be either inherited or acquired through environmental or lifestyle factors.

Cancer can be fundamentally characterised by a set of hallmarks, laid out in the formative review “Hallmarks of Cancer” by Hanahan and Weinberg in 2000 (Hanahan & Weinberg, 2000). Further hallmarks were added in 2011 to provide a more comprehensive understanding of cancer (Hanahan & Weinberg, 2011). The hallmarks characterised include sustained proliferative signalling, evasion of growth suppression, replicative immortality, tumour-promoting inflammation, invasion and metastasis, induction of angiogenesis, genomic instability and mutation, resistance to cell death, reprogramming of cellular metabolism, and immune avoidance (Hanahan & Weinberg, 2011). Finally, in 2022, four more “emerging” hallmarks were described, which include phenotypic plasticity, epigenetic reprogramming, polymorphic microbiomes, and cellular senescence (Hanahan, 2022), underlining our ever-evolving understanding of this complicated set of diseases.

In the UK, between 2016 and 2018, 375,400 people were diagnosed with cancer, with 167,142 deaths from 2017-2019 (Cancer Research UK, 2023). An estimated one in two people in the UK get cancer in their lifetime (Ahmad et al., 2015), making it a

substantial burden on healthcare systems, the public, and society. However, since 2010, 50% of people with cancer have survived for ten years or more in England and Wales, compared to 24% fifty years prior (Cancer Research UK, 2023), showing the strides in cancer treatment made within the last few decades.

1.1.2 Traditional Cancer Treatments

Traditional cancer treatments can be divided into three categories: surgical resection, radiotherapy, and chemotherapy. Surgery is the oldest and most widely used cancer treatment method (Wyld et al., 2015). It entails physically removing cancerous tissue from the body, offering advantages for patients, including relief from symptoms caused by the mass effect of the tumour, and can be curative in some cases (Dallabona et al., 2017; Montagne et al., 2021). However, surgery is often unsuitable in metastatic disease due to its systemic nature (Powell et al., 2022). Surgery can also leave microscopic lesions, potentially reestablishing new primary tumours or metastases (Tohme et al., 2017).

Radiotherapy uses ionising radiation to target and damage or destroy cancer cells. It addresses some of the issues with surgical resection by being non-invasive and preserving organ function. Radiotherapy can eradicate smaller and more inaccessible lesions whilst stimulating an anti-tumour immune response, eliminating cancer cells (Frey et al., 2014; Maccomb & Fletcher, 1957; Schaue et al., 2012; Timke et al., 2011).

While radiotherapy can effectively treat cancer, it comes with certain drawbacks. One of the most prominent is the side effects of radiation, which include nausea and fatigue. Additionally, there is a risk of secondary cancer formation from damage to nearby healthy tissue during radiotherapy treatment (Paris et al., 2001; H. Zhang et al., 2011). Radiotherapy is three times less effective in killing cells within a hypoxic (low oxygen)

environment (Hall & Giaccia, 2006; Rockwell et al., 2009), as radiotherapy relies on the generation of reactive oxygen species (ROS) to damage cell deoxyribonucleic acid (DNA) and kill cancer cells, which is limited in hypoxic environments (Brown & Wilson, 2004; Pouget et al., 2002).

Chemotherapy is a systemic treatment that targets rapidly growing cells within the body, such as cancer cells. As a systemic therapy, chemotherapy targets microscopic lesions and metastatic disease and is customisable depending on the cancer type and molecular target (Chua et al., 2010; O'Shaughnessy, 2005; Swenerton et al., 1979). Most molecular targets are for DNA or ribonucleic acid (RNA) and damage them through cross-linking, alkylation, or inhibiting ribonucleoside reductases and polymerases (Anand et al., 2023). However, the disadvantage of chemotherapy includes toxicity to healthy cells, as it targets any fast-growing cells, which can damage tissue with high cell turnover, such as bone marrow (Lyman et al., 2004; Newman et al., 2016). Cancers can also build resistance to chemotherapy over time through drug inactivation, reduced absorption, increased expulsion, or resistance to apoptosis (Croop et al., 1989; Druker et al., 2001; Higgins, 1992; Townsend & Tew, 2003).

Patient cancer treatment employs a combination of therapies tailored to the cancer type and severity. For example, combining radiotherapy with chemotherapy allows the treatment of the local disease with radiotherapy and systemic disease with chemotherapy to improve curative rate and patient outcomes (Herskovic et al., 1992; Rubens et al., 1980). Similarly, chemotherapy and surgery can be used to kill the remaining cells following surgery (adjuvant) or preceding surgery (neoadjuvant) to shrink the tumour (Eilber et al., 1987; Mieog et al., 2007; Taieb & Gallois, 2020).

1.1.3 Cancer Immunosurveillance and Immunoediting

Immunosurveillance is the immune system's recognition and targeted destruction of abnormal or transformed cells. The concept of the immune system defending against cancer has been recognised since the 19th and early 20th centuries, with Paul Ehrlich being the first to propose the idea (Ehrlich, 1908). Even earlier, in 1893, the surgeon William Bradley Coley, who was inspired by the observation of *streptococcus*-infected patients who experienced tumour regression, discovered that patients injected with heat-inactivated bacteria experienced tumour regression by stimulating the body's immune system (Coley, 1991). It was not until 1964, with the discovery of tumour-specific antigens and the notion that lymphocytes may protect the body from nascent transformed cells, that the immunosurveillance hypothesis was formed (Burnet, 1970; Burnet, 1957; Klein, 1966).

The immunosurveillance hypothesis initially proved challenging to confirm, with studies using immunocompromised and nude mice at the time providing contradictory conclusions (Burstein & Law, 1971; Grant & Miller, 1965; Outzen et al., 1975; Stutman, 1974). However, these studies were flawed as nude mice are now known to not be wholly immunocompromised and have some functional T cell subtypes (Ikehara et al., 1984; Maleckar & Sherman, 1987). Solid evidence of immunosurveillance did not come until the 1990s, with the discovery of interferon (IFN) γ and its role in protection against transplanted and spontaneous or chemically induced cancers (Dighe et al., 1994; Kaplan et al., 1998). Further evidence came from perforin-negative mice, which showed an increased propensity for chemically induced sarcoma formation by methylcholanthrene (MCA) than wild-type mice (van den Broek et al., 1996). Perforin is a protein expressed in cytotoxic T lymphocytes (CTL) and natural killer (NK) cells, which creates a pore in target cell membranes to allow apoptotic proteins such as

granzyme B to enter the cell and induce apoptosis and cell death in target cells (Trapani et al., 1998).

It became apparent in the early 2000s that the immunosurveillance hypothesis did not fully explain the immune system's role in cancer. A pioneering study in 2001 revealed that lymphocytes and IFN-γ could function to protect against the development of induced and spontaneous cancers (Shankaran et al., 2001). However, it can also lead to the selection of tumour cells with reduced immunogenicity (Shankaran et al., 2001), explaining how the immune system prevents cancer formation and affects the evolving immunogenic environment of established malignancies. This discovery led to the coining of the term “cancer immunoediting” (Dunn et al., 2002).

Cancer immunoediting can be split into three phases: elimination, equilibrium, and escape (Dunn et al., 2002). The elimination phase is characterised by the immune system eliminating abnormal cells through direct killing or growth suppression before they are established (Dunn et al., 2002). The elimination phase is a combination of innate and adaptive immune elements. Within the innate immune system, cells such as NK cells are recruited and recognise germline-encoded ligands such as natural killer group 2 (NKG2) D on the cell surface of the tumour cells, stimulating the release of IFN-γ (Arase et al., 1996; Shankaran et al., 2001). IFN-γ directly influences tumour cells by increasing major histocompatibility complex (MHC) -I expression and inducing cell death (Shankaran et al., 2001). The MHC-I expression allows for recognition by the cluster of differentiation (CD) 8^+ CTLs, as well as inducing the release of chemokines and chemoattractants from the tumour and host cells (Cole et al., 1998; Gorbachev et al., 2007; Luster & Ravetch, 1987). In turn, this blocks angiogenesis (Beatty & Paterson, 2001; Lu et al., 2009), increases dendritic cell (DC) uptake of tumour debris, leading to antigen presentation and cross-presentation, and

culminating in the activation of $CD4^+$ T-helper cells and $CD8^+$ CTLs, which produce more IFN-γ (Jorgovanovic et al., 2020). Following this, the CTLs primed against the tumour antigen can perform their effector function by targeting cancer cells displaying antigens on MHC-I and expressing perforin, granzyme B, Fas ligand (FasL) and tumour necrosis factor-related apoptosis-inducing ligand (TRAIL) to induce apoptosis in target tumour cells (Barry & Bleackley, 2002).

The next phase is characterised by a state of equilibrium or tumour dominancy, in which cancer cells survive and are prevented from growing or spreading further in a delicate balance by the immune system (Dunn et al., 2002). Experimental evidence suggests that in MCA-induced mouse sarcoma models, the equilibrium phase is dominated by the adaptive immune system, with antibody blockade of $CD4^+$ and $CD8^+$ T cells, IFN-γ and interleukin (IL) -12 leading to significant growth of late-forming tumours (Koebel et al., 2007). The exact mechanism of tumour regression to the elimination phase or progression to the escape phase is not fully understood. However, the progression to escape is likely from immune pressure driving genetic and epigenetic changes and immune evolution, leading to subclones of resistant cancer cells (Dunn et al., 2002; Shankaran et al., 2001).

The final stage is the escape phase, where the tumour evolves to evade suppression by the immune system and proliferates unhindered (Dunn et al., 2002). Tumour escape is caused by reduced immune recognition, resistance to cell death, or the formation of an immunosuppressive tumour microenvironment (Mittal et al., 2014). One of the critical mechanisms by which cancers in this phase avoid the adaptive immune response is a loss of neoantigens or antigen presentation machinery, such as the transporter associated with antigen processing (TAP) protein or MHC-I, enabling

their evasion from the adaptive immune response (Cromme et al., 1994; Romero et al., 2018; Schrors et al., 2017).

1.2 Immunotherapy

1.2.1 Introduction to Immunotherapy

Immunotherapy is a class of cancer treatment that programmes the body's immune system to identify and target cancer cells for elimination. Immunotherapy aims to provide the immune system with the resources to overcome the immunosuppressive or evasive mechanisms that tumours have developed through immune evasion. It encompasses monoclonal antibodies (mAb), immune checkpoint inhibitors (ICI), adoptive cell therapy (ACT), cytokine therapy, oncolytic virus therapy, and cancer antigen vaccines (Liu et al., 2022). Table 1.1 summarises key approved cancer immunotherapy treatments.

Table 1.1 Key Approved Cancer Immunotherapy Treatments

Type	Name (Approval Year)	Description	Mechanism of action	References
Antibodies	**Rituximab (1997)**	Anti-CD20 mAb for the treatment of non-Hodgkin's lymphoma	Immune modulation through ADCC, CDC and ADP	(James & Dubs, 1997; Maloney et al., 1997; Maloney et al., 2002)
	Trastuzumab (1998)	Anti-HER2 mAb for the treatment of breast cancer	Inhibition of HER2, promoting cell cycle arrest	(Baselga et al., 1996; Le et al., 2003; Yakes et al., 2002)
	Blinatumomab (2014)	Anti-CD3xCD19 BiTE for the treatment of ALL	MHC-independent T cell immunological synapse and activation	(Löffler et al., 2000; Przepiorka et al., 2015)
Immune Checkpoint Inhibitors	**Ipilimumab (2011)**	Anti-CTLA-4 mAb for the treatment of melanoma	Blocks CTLA-4 interaction with B7 on APCs – allowing CD28/B7 Co-stimulation and CTL response	(Keler et al., 2003; Leach et al., 1996; Shrikant et al., 1999; Traynor, 2011)

	Pembrolizumab (2014)	Anti-PD-1 mAb for the treatment of melanoma and NSCLC	Blocks PD-1 binding to PD-L1 – prevents immune suppression of T cells	(Hamid et al., 2013; Sul et al., 2016)
Adoptive Cell Therapy	**Sipuleucel-T (2010)**	Autologous DCs stimulated with GM-CSF and pulsed with PAP peptides for the treatment of prostate cancer.	Enhances tumour antigen-specific adaptive immune response	(Cheever & Higano, 2011; Kantoff et al., 2010)
CAR-T	**Tisagenlecleucel (2017)**	CD19-targeting CAR-T for the treatment of ALL & DLBCL	MHC-Independent T cell-mediated cytotoxicity	(Schuster et al., 2017; Schuster et al., 2019)
	Idecabtagene vicleucel (2021)	BCMA-targeting CAR-T for the treatment of MCL	MHC-Independent T cell-mediated cytotoxicity	(Munshi et al., 2021)
Cytokine Therapy	**IFN-α (1986)**	Recombinant IFN-α for the treatment of HCL	Immune cell expansion and inhibition of HCL growth	(Berneman et al., 1986; Grever et al., 2017; Quesada et al., 1986; Quesada et al., 1984)
	Aldesleukin (1992)	Recombinant IL-2 for the treatment of metastatic renal carcinoma and melanoma	Stimulation and expansion of T cells and NK cells	(Muul et al., 1987; Rosenberg et al., 1985; Rosenberg et al., 1989)
Oncolytic Virus	**Talimogene laherparepvec (T-VEC) (2015)**	HSV-1 with ICP34.5 & 47 deletions encoding GM-CSF for the treatment of metastatic melanoma	Direct oncolysis and promotion of DC differentiation and antigen-presentation	(Andtbacka et al., 2015; Liu et al., 2003)

Abbreviations: antibody-dependent cell-mediated cytotoxicity (ADCC), complement-mediated cytotoxicity (CDC), antibody-dependent phagocytosis (ADP), cytotoxic T-lymphocyte associated protein 4 (CTLA-4), cluster of differentiation (CD), antigen-presenting cell (APC), non-small cell lung cancer (NSCLC), programmed cell death protein 1 (PD-1), programmed death ligand 1 (PD-L1), granulocyte-macrophage colony-stimulating factor (GM-CSF), prostatic acid Phosphatase (PAP), chimeric antigen receptor T cell (CAR-T), acute lymphoblastic leukaemia (ALL), diffuse large B-cell lymphoma (DLBCL), B-cell maturation antigen (BCMA), mantle cell lymphoma (MCL), hairy cell leukaemia (HCL), type 1 herpes simplex virus (HSV-1), infected cell protein (ICP).

1.2.2 Antibodies and Immune Checkpoint Inhibitors

Antibodies with no additional conjugates are called naked antibodies and perform their action either by binding directly to cancer cells to prevent their growth and survival or by targeting them for destruction by the immune system (Le et al., 2003; Maloney et al., 1997) (Table 1.1). Naked antibodies perform this function through three direct mechanisms. First is through antibody-dependent cell-mediated cytotoxicity (ADCC), whereby effector cells, mostly NK cells, bind to the fragment crystallisable (Fc) region

of the cell-bound antibody through the CD16 Fc-receptor, causing their degranulation and release of cytotoxic molecules to kill the tumour cell (Reff et al., 1994; Romee et al., 2013). Secondly is through complement-mediated cytotoxicity (CDC), where C1q of the classical complement system binds to the antibody, leading to a cascade of further complement binding and the formation of the membrane attack complex (MAC) (Beum et al., 2008; Harjunpaa et al., 2000; Idusogie et al., 2000). MAC induces cell lysis in the target cell by forming a pore in the membrane, allowing ions and molecules to enter and induce cell death (Xie et al., 2020). The final mechanism is through antibody-dependent phagocytosis (ADP), where phagocytes, such as macrophages and neutrophils, bind through Fc-gamma receptors (FcγR) to the Fc region of the antibody bound to the tumour and engulf it (Church et al., 2016; Gul et al., 2014). Upon phagocytosis, the phagosome fuses with lysosomes, containing enzymes and proteases which break down the engulfed cell.

The direct effect of monoclonal antibodies through ADCC, CDC and ADP also mediates antigen cross-presentation, as debris from the lysed cells is taken up by DCs and the antigens processed for presentation, culminating in an enhanced tumour-specific CTL response (Selenko et al., 2002).

Antibodies with dual binding sites, known as a bispecific T cell engager (BiTE), attach to T cells via CD3 and a cancer antigen (Löffler et al., 2000). BiTEs facilitate an immunological synapse between the T cells and cancer cells, activating the CTLs in an MHC-independent manner, causing the release of cytotoxic compounds like perforin and granzyme B (Wolf et al., 2005) (Table 1.1).

The immune checkpoint is a process of control for the immune system that balances an appropriate and proportionate response to pathogens and cancer without causing

harm to healthy tissue. T cells express multiple immune checkpoint receptors which suppress T cell functionality to prevent an inappropriate immune response, including T cell immunoglobulin and mucin-domain containing-3 (TIM-3), Lymphocyte-activation gene 3 (LAG-3), CTLA-4 and PD-1, to name a few (Freeman et al., 2000; Huang et al., 2015; Macon-Lemaitre & Triebel, 2005; Walunas et al., 1994). Cancers can evolve to take advantage of these so-called immunological “brakes” by overexpressing ligands such as PD-L1, which interacts with PD-1 on T cells and inhibits their activity, thus contributing to cancer’s immune escape and poor patient prognosis (Jung et al., 2017; Okita et al., 2017) (Table 1.1). Immune checkpoint inhibitors were developed to combat this suppression. For example, anti-CTLA-4 mAb blocks CTLA-4 on T cells interacting with B7 on antigen-presenting cells, allowing the CD28 costimulatory molecule to bind to B7, provoking T cell activation, augmentation and a more robust anti-tumour response (Leach et al., 1996; Shrikant et al., 1999) (Table 1.1). One side-effect of checkpoint inhibitors is that “releasing the brakes” can induce unintended immune activation, known as immune-related adverse events (Ramos-Casals et al., 2020).

1.2.3 Adoptive Cell Therapy and CAR-T cells

Adoptive cell therapy (ACT) takes a patient’s immune cells, expands and modifies them *ex vivo,* and infuses them into the patient to treat their cancer. The only DC therapy approved is Sipuleucel-T (Table 1.1). The phase III trial preceding its approval showed an increase in overall survival for metastatic castration-resistant prostate cancer patients and a three-year survival probability of 31.7% compared to 23.0% for the placebo group (Kantoff et al., 2010).

Most ACTs are T cell therapies and fall into two broad categories. Tumour-infiltrating lymphocyte (TIL) therapy and chimeric antigen receptor T cell (CAR-T) therapy. TIL

treatment involves extracting autologous T cells from the periphery of a patient's tumour, expanding them *ex vivo* and infusing the tumour-derived T cells programmed against the cancer cells back into the patient (Lee et al., 2017). The benefit of this system is that the expanded TILs are polyclonal and can target multiple neoantigens, countering heterogeneous antigen expression (Kvistborg et al., 2012). TIL therapy has also been shown to successfully form a memory response through their differentiation into memory T cells, providing long-term protection from reoccurrence (van den Berg et al., 2020).

Although showing promise within the clinic, TIL therapy does have some drawbacks. For example, not all solid tumours have an abundance of TILs within them; immunosuppressive “cold” tumours lack immune cell infiltration and limit the potential for successful immunogenic TIL extraction and activity following reinfusion (Creelan et al., 2021; Hegde et al., 2016). Despite the challenges, trials in solid tumours are ongoing, with one pioneering study in metastatic melanoma demonstrating that 22% of lymphodepletion patients achieve tumour regression following autologous TIL therapy, with a further 20% having ongoing regression three years later, with a five-year survival rate for the complete responders of 93% (Rosenberg et al., 2011). A highlight of the trial was that 95% of the patients had already received prior treatment of IL-2, chemotherapy, IFN-γ, anti-CTLA-4 or a combination thereof, which did not affect patient outcome (Rosenberg et al., 2011).

A more recent phase one study with TIL treatment for anti-PD-1-resistant metastatic lung cancer showed that out of 13 patients, eleven had a reduced tumour burden, three had a confirmed response, and two patients had a complete ongoing response 18 months after the trial (Creelan et al., 2021). Importantly, they saw persistence and diversity in the cancer antigen-specific TILs (Creelan et al., 2021).

CAR-T cell therapy entails extracting T cells from patients and genetically engineering a chimeric antigen receptor on their cell surface. The artificial receptor contains an antigen-recognition domain on its cell surface composed of a single-chain variable fragment (scFv) specific to a tumour-expressed antigen fused by a linker domain to an intracellular CD3ζ, which forms part of the T cell receptor (TCR) CD3 signalling domain (Bridgeman et al., 2014). First-generation CAR-T cells only had a CD3 signalling domain and were found to not sufficiently prime T cells (Brocker & Karjalainen, 1995). Second-generation CAR-T cells incorporated costimulatory 4-1BB (Krause et al., 1998), while subsequent iterations included multiple costimulatory domains such as 4-1BB with CD28 to increase the downstream activation and potency of the CAR-T cells (Ramos et al., 2018; Subklewe et al., 2019). The patient-derived CAR-T cells are expanded and infused into the patient, where they act on cancer cells in an MHC-independent manner.

Most of the success with CAR-T cell-based therapies has been in haematologic cancers with limited efficacy in solid tumours (Davila et al., 2014; Savoldo et al., 2011) (Table 1.1). These limitations are mainly attributed to tumour antigen escape, immunosuppression by the tumour microenvironment, and lack of tumour tissue penetration (Brudno et al., 2018; Sterner & Sterner, 2021). Researchers have investigated the efficacy of combination therapies to overcome these challenges, particularly with immune checkpoint inhibitors (Li et al., 2018; Yin et al., 2018). One study combined pembrolizumab (anti-PD-1) with a ganglioside-2-targeting third-generation CAR-T cell, an antigen upregulated in melanoma and neuroblastoma cancers (Gargett et al., 2016). They found in metastatic melanoma patients that their CAR-T cells alone would quickly become exhausted in a PD-1/PD-L1-dependent

manner and trigger activation-induced cell death in the CAR-T cells, which was prevented by pembrolizumab (Gargett et al., 2016).

To overcome the issues with tissue penetration, one lab targeted the glypican-3 (GPC3) antigen with a CAR-T cell expressing the chemokine C-X-C receptor (CXCR) 2, both upregulated in hepatocellular carcinoma (HCC) (Liu et al., 2020). The study in mouse models found increased HCC tumour penetration and anti-tumour activity of their CXCR2-expressing GPC3-CAR-T cell compared to their mock CAR-T cell, which only targeted GPC3 (Liu et al., 2020).

1.2.4 Cytokine Therapy

Cytokines are the immune system's regulatory molecules and can enhance or dampen the immune response. In the context of cancer, cytokine therapy aims to improve the recognition and response of the immune system. Two cytokines are approved for cancer treatment, IL-2 and IFN-α (Table 1.1).

IFN-γ was considered for therapeutic use in cancer. However, IFN-γ was found to have both pro-tumour and anti-tumour properties (Abiko et al., 2015; Hao & Tang, 2018; Lo et al., 2019; Song et al., 2019). For instance, IFN-γ increases MHC-II expression on DCs and promotes a T helper (Th) 1 activation (Akbar et al., 1996; Corthay et al., 2005; Zhang et al., 2001). The Th1 response supports and activates immune function by releasing pro-inflammatory cytokines such as IFN-γ and IL-2 (Mosmann & Coffman, 1989), which activate macrophages and promote $CD8^+$ T cell cytolytic function (Abbas et al., 1996; Mosser & Edwards, 2008).

However, IFN-γ also increases regulatory T cell (Treg) and Myeloid-derived suppressor cell (MDSC) development, which dampens the immune response (Medina-Echeverz et al., 2014; Z. Wang et al., 2006). This paradoxical function within

cancer has limited IFN-γ use in the cancer therapeutic setting. Other cytokines trialled include GM-CSF to stimulate antigen-presenting cell expansion and antigen presentation and IL-12 to aid in differentiating T cells (Kurbacher et al., 2005; Li et al., 2020).

1.2.5 Oncolytic Viruses

Oncolytic viruses are engineered for selective replication exclusively in cancer cells, often through deleterious mutations or directed evolution (Koshizuka et al., 2005; Kuhn et al., 2008; Liu et al., 2003). Upon infection of cancer cells, oncolytic viruses destroy them and leave healthy cells intact.

T-VEC was the first oncolytic virus to gain widespread approval in the US and Europe to treat metastatic melanoma (Table 1.1) (Andtbacka et al., 2015; Liu et al., 2003). Combination therapies of oncolytic viruses with immune checkpoint inhibitors improve patient response, with one clinical study showing a 39% objective response with T-VEC in combination with ipilimumab compared to an 18% response rate with ipilimumab alone (Chesney et al., 2018). The study suggests that combining oncolytic virus and immune checkpoint inhibitors induces an anti-tumour response by enhancing antigen presentation, T cell priming and expansion (Chesney et al., 2018; Kohlhapp & Kaufman, 2016).

1.2.6 Cancer Vaccines

Cancer vaccines are formulated to activate the adaptive immune system, encouraging it to identify and eradicate cancer cells. These vaccines prime the immune system and can be structured as whole-cell or antigen-based vaccine strategies. Initial cell-based cancer vaccines used whole tumour cells to stimulate the immune system. This strategy offers the advantage of encompassing the entire cancer cell antigen

repertoire of $CD4^+$ and $CD8^+$ epitopes for antigen presentation and cross-presentation by DCs. However, live tumour cells are poorly immunogenic because of their ability to evade the immune system and the secretion of immunosuppressive molecules such as vascular endothelial growth factor (VEGF), IL-10 and transforming growth factor (TGF) β (Dikov et al., 2001; Groh et al., 2002; Hu et al., 2022; Li et al., 2006; Loercher et al., 1999). Therefore, whole-cancer cell vaccines are often engineered, inactivated, or lysed.

GVAX is an engineered GM-CSF-secreting intact cancer cell developed as a potential whole-cell vaccine strategy (Dranoff et al., 1993). GM-CSF stimulates DC differentiation and survival, and by combining it with irradiated whole-cancer cells, has shown promise in mouse models and human trials, including for melanoma, leukaemia and pancreatic cancer (Laheru et al., 2008; Mach et al., 2000; Zilberberg et al., 2011).

Cancer antigen vaccines start by identifying antigens which are either specific to a cancer cell, known as a tumour-specific antigen (TSA) or neoantigen, or an antigen which is found in normal tissue but is overexpressed in cancer cells, known as a tumour-associated antigen (TAA). Once identified, TSA/TAAs can be made as DNA or messenger RNA (mRNA) vaccines, recombinant whole protein, recombinant peptide or protein fusions, and synthetic peptide derivatives.

DNA and mRNA cancer vaccines encode for the sequence of a tumour antigen. Upon transfection into DCs, the DNA is transcribed and the mRNA is translated into the protein of interest, which is presented and activates a T cell-mediated response (Cafri et al., 2020; Jahanafrooz et al., 2020; Williams et al., 2008). The delivery method of DNA and mRNA cancer vaccines is paramount, as they are rapidly degraded by intracellular nucleases (Lechardeur et al., 2005; Osborn et al., 2011). One approach

is transducing or transfecting DCs *ex vivo* and transfusing them back into patients (Chan et al., 2006). Another is incorporating the nucleic acids into liposome nanoparticles to protect them and promote membrane fusion (Fotoran et al., 2017; U'Ren et al., 2006).

Although no cancer-targeting nucleic acid vaccine has been approved, trials are still ongoing. A recent phase I study used a personalised mRNA-lipoplex nanoparticle against pancreatic ductal adenocarcinoma (PDAC) in combination with the anti-PD-L1 antibody atezolizumab and chemotherapy treatment following surgical resection (Rojas et al., 2023). The personalised mRNA consisted of up to 20 neoantigens derived from individual patients, and in half of the cohort induced neoantigen-specific T cell production, of which half of the patients had T cells specific to more than one neoantigen (Rojas et al., 2023). Finally, after 18 months, none of the patients with these specific T cells showed cancer recurrence, compared to a year for those without a T cell response (Rojas et al., 2023). The personalised approach for nucleic acid-based vaccines has potential in cancer therapy because of their rapid, low-cost manufacturing process (Lorentzen et al., 2022), a limiting factor in many personalised cancer vaccine strategies.

Peptide cancer vaccines contain $CD4^+$ and $CD8^+$ epitopes derived from a cancer antigen. They prime the adaptive immune system to recognise the cancer antigen as foreign to elicit a CTL response. The functionality, design and formulation of peptide-cancer vaccines will be discussed in more detail later in this chapter.

1.3 Antigen Presentation and Cross-Presentation

1.3.1 T Cell Activation by Dendritic Cells

DCs are the primary professional antigen-presenting cells responsible for activating helper and cytotoxic T cells and are the immune system's sentinels, constantly sampling the intercellular space for foreign antigens. DCs function as the bridge between the innate and adaptive immune systems by releasing pro-inflammatory cytokines and presenting exogenously derived antigens for the presentation and activation of T cells.

DCs engage with TCRs on the surface of T cells through MHC-I for CTLs and MHC-II for helper T cells, with the aid of CD8 and CD4 co-receptors, respectively, comprising the first of three signals required for TCR signal activation (Daniels & Jameson, 2000; Janeway, 1992). The second signal comes from the CD80/86 (B7-1/2) co-receptor on DCs interacting with CD28 on the engaged T cells (McAdam et al., 1998). The third signal arises from the cytokines the DC releases, which drives the differentiation of effector T cells and their subsequent function (Curtsinger & Mescher, 2010; Heufler et al., 1996). All three signals are required to initiate T cell-mediated immune response and to overcome immune tolerance, with a lack of CD28 "second signal" resulting in T cell anergy and apoptosis (Schwartz, 2003) (Figure 1.1).

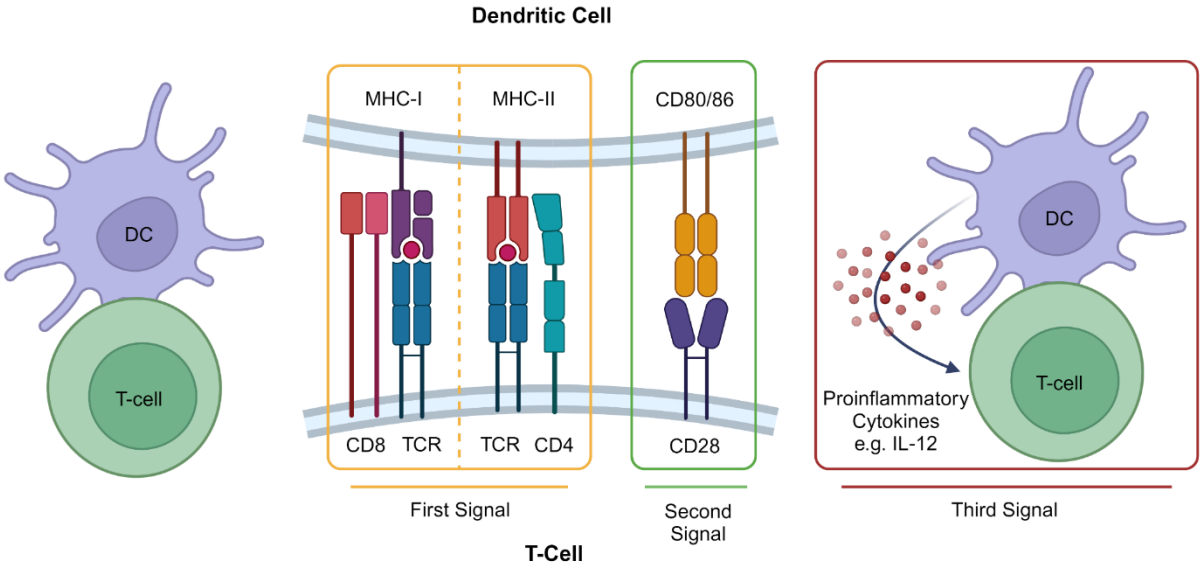


Figure 1.1 The Three Signals of T cell Activation
Three signals are required for complete T cell activation, with any missing signal leading to incomplete activation and T cell anergy. Signal one is provided by the interaction of the TCR on the T cell with the MHC presenting the peptide on the surface of the DC; the CD4 or CD8 co-receptors offer further stimulation. Signal two is through the interaction of CD28 on the T cell with CD80/86 (B7) on the DC. A lack of a second signal is associated with immune tolerance. Pro-inflammatory cytokines released by the DC provide the third signal. In particular, IL-12 stimulates T cell activation and enhances effector function. Created with BioRender.com

1.3.2 Antigen Presentation

All nucleated cells possess the ability to process antigens through the MHC-I pathway. This pathway presents peptides derived from autologous self-proteins, which the immune system tolerates. In damaged, aberrant, or infected cells, endogenous pathogenic antigens are processed by the cell and presented through MHC-I to $CD8^+$ T cells to stimulate an adaptive immune response.

In canonical antigen presentation, the proteasome digests the endogenous antigenic proteins in the cytosol into smaller peptides, where they are translocated into the endoplasmic reticulum (ER) in a TAP-dependent process (van Endert et al., 1994). TAP is an adenosine triphosphate (ATP) -binding cassette transporter whose function is to transport peptides from the cytosol into the ER for loading onto MHC-I (Higgins, 1992; Suh et al., 1994).

MHC-I forms within the ER by association of the heavy chain with β-2 microglobulin (β2M) through the chaperone calnexin (Vassilakos et al., 1996). The peptide loading complex (PLC) then forms, causing calnexin to dissociate and be replaced with calreticulin, which binds to ERp57 (Diedrich et al., 2001; Hughes & Cresswell, 1998). ERp57 also binds to tapasin, associated with the TAP protein (Diedrich et al., 2001). The peptide is then trimmed to 8-11 amino acids in length by ER aminopeptidase (ERAP) and loaded onto MHC-I (Saveanu et al., 2005). If the protein is low affinity, TAP-binding protein-related (TAPBPR) protein can exchange peptides in a PLC-independent manner until a high-affinity peptide is loaded onto the MHC-I (Hermann et al., 2015). After binding to a high-affinity peptide, the MHC-I/peptide complex is exported from the cell via the Golgi apparatus (Spiliotis et al., 2000). Upon export to the cell surface, the MHC-I/peptide complex interacts with TCRs on $CD8^+$ CTLs. The recognition and binding of TCRs on CTLs activate an antigen-specific response and the release of cytolytic compounds (Itoh et al., 1991; Kagi et al., 1994; Peters et al., 1991).

MHC-II antigen presentation is how professional antigen-presenting cells, such as DCs and macrophages, internalise exogenous antigens obtained through phagocytosis and endocytosis. This mechanism plays a critical role in the immune response by facilitating the presentation of antigens to $CD4^+$ helper T cells and their subsequent activation.

Upon entry, antigens are trafficked into lysosomal compartments and digested by proteases, such as cysteine proteases and asparagine endopeptidase, into smaller peptides (Driessen et al., 2001; Honey et al., 2002; Manoury et al., 1998). In particular, the cysteine protease cathepsin L is crucial in generating peptides for MHC-II presentation (Honey et al., 2002). Meanwhile, MHC-II is transported from the ER to

the endosomal compartment, where the class II-associated invariant chain peptide (CLIP) is cleaved off the invariant chain by cathepsin S from the MHC-II peptide binding groove (Driessen et al., 1999; Riese et al., 1996). The typically 12 to 25 amino acid-long degraded peptides are loaded onto MHC-II within the endosome and transported to the cell surface (Falk et al., 1994). The MHC-II molecules present their antigens to $CD4^+$ helper T cells, with co-stimulation by CD40 on DCs with CD40L on $CD4^+$ T cells, resulting in a Th1 response (Cella et al., 1996; Constant & Bottomly, 1997).

1.3.3 Introduction to Antigen Cross-Presentation

During the internalisation of antigens through the MHC-II antigen pathway, a small proportion of exogenous antigens can escape the pathway and be presented on MHC-I molecules in a process known as antigen cross-presentation. This process allows DCs to present and activate $CD8^+$ T cells from external antigen sources.

There are two main cross-presentation pathways. The cytosolic pathway occurs through an escape of antigens from the endosomal compartment into the cytosol, where it is digested by the proteasome and loaded onto MHC-I in a TAP-dependent manner (Burgdorf et al., 2008; Kovacsovics-Bankowski & Rock, 1995). In comparison, the vacuolar pathway is a TAP-independent mechanism occurring through the cysteine-protease cathepsin S, which cleaves and directly loads peptides onto MHC-I within the endosomal compartment (Shen et al., 2004).

1.3.4 Antigen Cross-Presentation – The Cytosolic Pathway

It is unclear how endosomal escape happens, but it starts with preventing rapid protein degradation by alkalising the endosomal compartments. In mice, $CD8^+$ DCs are highly efficient at cross-presentation and have neutral pH endosomes, which prevents rapid

degradation of internalised antigens (den Haan et al., 2000; Pooley et al., 2001; Savina et al., 2009). $CD8^-$ DC cells with a low pH endosome are poor at cross-presentation, as antigens are rapidly degraded (den Haan et al., 2000; Pooley et al., 2001; Savina et al., 2009).

The vacuolar-type ATP hydrolase (V-ATPase) proton-pump regulates the acidification of the endosome, while the recruitment of nicotinamide adenine dinucleotide phosphate oxidase 2 (NOX2) by Ras-related protein Rab27a increases alkalisation (Jancic et al., 2007; Mantegazza et al., 2008). NOX2 releases ROS, which reacts with protons to form hydrogen peroxide, increasing the pH of the endosome and enhancing cross-presentation (Mantegazza et al., 2008; Savina et al., 2006). One study suggests that toll-like receptor (TLR) engagement instigates an up-regulation of NOX2, increasing endosomal pH and promoting cross-presentation (Vulcano et al., 2004). Therefore, a balance exists between V-ATPase and NOX2 expression and activity in cross-presentation regulation. Further evidence is provided by chloroquine, which inhibits endosome acidification and increases cross-presentation and CTL activity (Accapezzato et al., 2005; Garulli et al., 2008; Ratikan et al., 2013).

There is no consensus on the mechanisms of transporting antigens from the endosome into the cytosol. However, one of the prevailing theories is that antigens are transported from the endosome to the cytosol by the ER-associated degradation (ERAD) process (Ackerman et al., 2006). The two main proteins in ERAD theorised in this export are Sec61, which translocates proteins into the cytosol, and the p97 ATPase, which provides energy for the translocation (Koopmann et al., 2000; Zehner et al., 2011). Evidence came from the ability of Sec61 to retro-translocate proteins from the ER into the cytosol and its strong association with endosomal compartments (Houde et al., 2003; Wiertz et al., 1996). Furthermore, the genetic knockdown of Sec61

showed inhibition of cross-presentation. However, as sec61 is involved in transporting proteins and MHC-I into the ER, the independent role of endosomal Sec61 could not be elucidated (Zehner et al., 2015).

Further evidence of ERAD involvement came from the *Pseudomonas aeruginosa* exotoxin A, which blocks Sec61, prompting a significant decrease in antigen cross-presentation (Ackerman et al., 2006). Sec61 blockade also reduced the endosome to cytosol export of the HSV-1 ICP47, which inhibits TAP, evidenced by the decline in inhibition (Ackerman et al., 2006). More recently, the inhibition of Sec61α by mycolactone toxin was shown not to affect the ability of proteins to be transported from the endosome to the cytosol but did strongly inhibit MHC-I presentation and T cell activation (Grotzke et al., 2017). Finally, in a p97 and Sec61 knockout model, the cross-presentation was found to be p97-dependent but not Sec61-dependent with synthetic long peptides (SLP) (Menager et al., 2014), therefore showing a role for ERAD in cross-presentation but not necessarily through Sec61. Together, these studies demonstrate the conflicting views and challenges associated with researching the mechanisms of endosomal export and the ambiguous role of Sec61, p97, and ERAD.

Another proposed approach to antigen export involves membrane disruption, where the generation of ROS by NOX2, along with the resulting hydrogen peroxide, induces lipid peroxidation in the membrane, ultimately leading to membrane permeability and the release of antigens into the cytosol (Dingjan et al., 2016). The most compelling evidence for membrane leaking is the use of mAzami fluorescently tagged galectin-3, which binds to β-galactoside sugars present only on the luminal side of the endosome (Dingjan et al., 2016; Paz et al., 2010). The researchers observed that when galectin-3 expressing DCs were stimulated with lipopolysaccharides (LPS) and ovalbumin

(OVA), galectin-3 clustered around OVA-positive endosomes (Dingjan et al., 2016). This clustering was hindered by α-tocopherol, a compound that inhibits lipid peroxidation (Dingjan et al., 2016). The result demonstrates that lipid peroxidation disrupted the membrane and allowed access to these β-galactoside sugars and galectin-3 to bind, indicating a leak in the membrane (Dingjan et al., 2016). Interestingly, this would imply that NOX2 has a dual purpose in reducing degradation and increasing export.

Evidence suggests that TAP-dependent cytosolic cross-presentation may also occur within endosomal compartments. A study showed that TAP was recruited to early endosomes by engagement of TLR4 by LPS through the signalling molecules myeloid differentiation primary response 88 (MyD88) and toll/interleukin-1 receptor domain-containing adaptor molecule (TICAM1) (Burgdorf et al., 2008). Furthermore, the soluble N-ethylmaleimide-sensitive factor attachment protein (SNAP) receptor (SNARE) Sec22b, involved in membrane fusion, is thought to mediate the transportation of TAP from the ER to endosomal compartments, with Sec22b knockdown compromising cross-presentation but not endogenous MHC-I or MHC-II presentation (Cebrian et al., 2011). Finally, DCs deficient in the endosomal insulin-regulated aminopeptidase (IRAP) were compromised in their antigen cross-presentation ability (Saveanu et al., 2009). Suggesting an alternative mechanism following cytosolic export through the reimport of peptides into endosomes by TAP, where editing occurs by IRAP before MHC-I loading (Burgdorf et al., 2008; Saveanu et al., 2009).

The export machinery transporting antigens from the endosome to the cytosol remains a mystery, with conflicting views and pathways thought to be involved. The potential is

that no single path involves endosomal export and that a combination of redundant pathways may play equal roles in the export of antigens. (Figure 1.2).

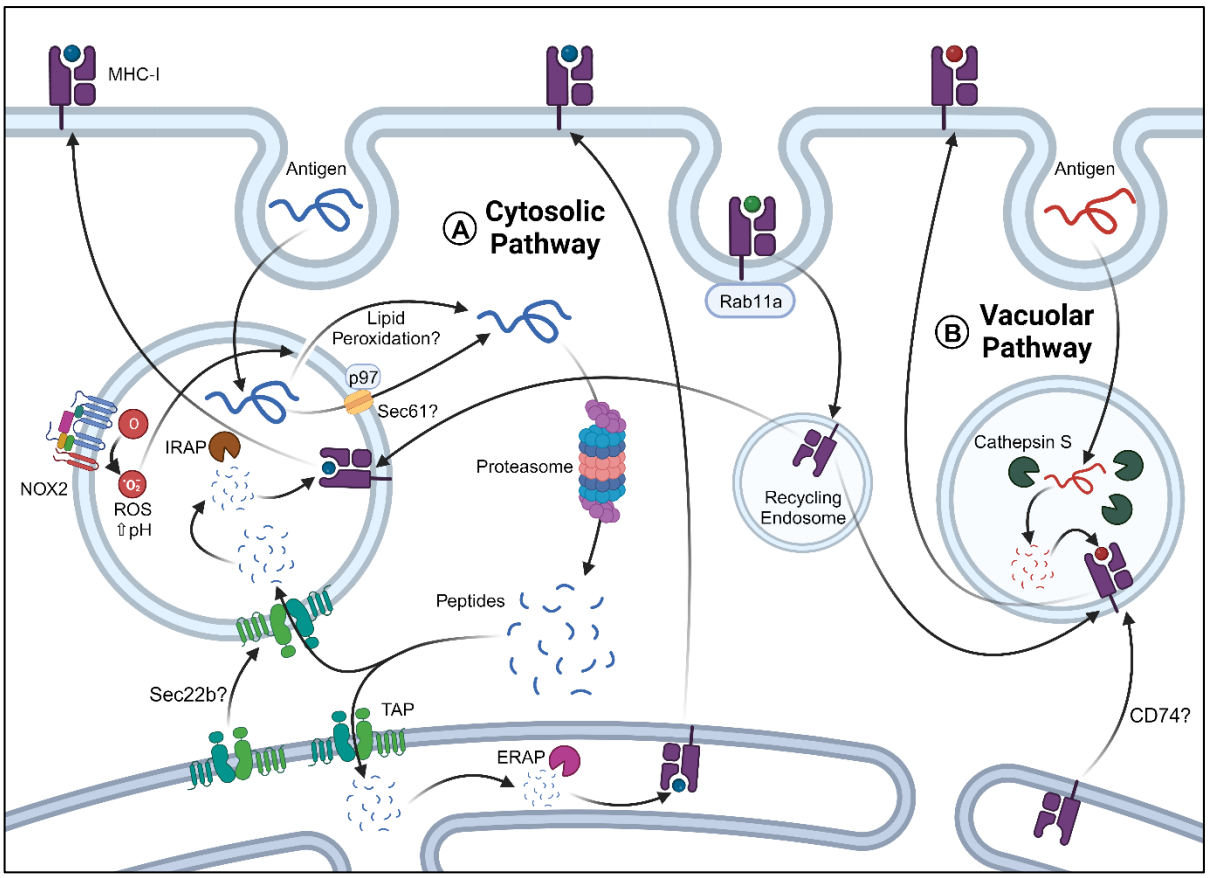


Figure 1.2 The Cytosolic and Vacuolar Pathways of Cross-Presentation
(A) The cytosolic pathway of cross-presentation is characterised by the escape of antigen from the endosomal compartment into the cytosol. This process is thought to occur either through a translocation process or a leaky membrane caused by ROS peroxidation of the lipid bilayer. The ROS are produced by NOX2, which also increases the pH of the endosome, preventing rapid digestion of the antigens. Antigens in the cytosol are then digested by the proteasome and translocated into the ER by TAP. ERAP aminopeptidase trims the peptides into the correct size before they are loaded onto MHC-I and exported to the cell surface via the Golgi. Evidence suggests that TAP is also found in the endosomal compartment, which is believed to be transported by Sec22b. Endosomal TAP imports peptides back into the endosome, trimmed by IRAP and loaded onto MHC-I recycled from the cell surface via Rab11a. **(B)** The vacuolar pathway of cross-presented is characterised by the digestion of the proteins in a TAP and proteasome-independent manner by cysteine protease cathepsin S. Peptides are loaded onto MHC-I either from the recycling endosome or newly synthesised by the ER. Evidence suggests that CD74 (invariant chain) may play a role in this process. Adapted from Embgenbroich & Burgdorf, 2018. Created with Biorender.com

1.3.5 Antigen Cross-Presentation – The Vacuolar Pathway

The vacuolar pathway is an alternative mechanism of cross-presentation where the peptides required for MHC-I loading are generated within the endosomal compartment

without export to the cytosol in a TAP and proteasome-independent manner (Shen et al., 2004; Song & Harding, 1996). The first evidence of an alternative pathway came from experiments with macrophages treated with OVA-latex beads and OVA-expressing bacteria, which showed cross-presentation under proteasome blockade and in TAP knockout cells (Song & Harding, 1996). It was later discovered that cathepsin S was the critical protease involved in this alternative pathway through TAP knockout models with chemical inhibitors of endosomal proteases and genetic knockdown of cathepsin S, which led to complete inhibition of cross-presentation in DC lines and *in vivo* (Shen et al., 2004) (Figure 1.2).

The origin of the MHC-I molecules required for the vacuolar pathway is not fully understood but is thought to originate from either newly synthesised and transported MHC-I from the ER or through recycling endosomes from the cell surface (Basha et al., 2012; Di Pucchio et al., 2008; Nair-Gupta et al., 2014). The trafficking of MHC-I from the ER to the endosomal compartment was demonstrated to be CD74-dependent through MHC-I binding to CD74's endosomal targeting signal (Basha et al., 2012). This association was revealed by CD74 knockout mice, who lost cross-priming ability that was restored following the introduction of CD74, but not with CD74 missing its endosomal targeting signal (Basha et al., 2012). Interestingly, CD74, also known as the invariant chain, is cleaved off MHC-II by cathepsin S in antigen presentation, which could point to a further role of cathepsin S in its dissociation from MHC-I through the vacuolar pathway.

A study in plasmacytoid DCs (pDCs) following viral infection provided evidence for MHC-I originating from recycling endosomes (Di Pucchio et al., 2008). The study showed that the processing of the exogenous viral antigens was proteasome-independent and occurred in distinct recycling endosomes containing MHC-I derived

from the cell surface (Di Pucchio et al., 2008). These recycling endosomes and the subsequent cross-presentation were ablated with primaquine, which inhibits endosome recycling (Di Pucchio et al., 2008). Further research revealed TLR signalling from microbial infection concentrated MHC-I in Ras-related protein Rab11a marked recycling vesicles (Nair-Gupta et al., 2014). The vesicles are recruited and fused with phagosomal compartments for cross-presentation by TLR-signalling-induced phosphorylation of SNAP23, stabilising the SNARE complex required for fusion (Nair-Gupta et al., 2014).

The general contribution of the cytosolic and vacuolar pathways within DCs is unknown. One study using immunoproteasome-depleted proteasome subunit beta type-8 (PSMB8) knockout mice found an inability to process and cross-present the immunodominant H-Y ubiquitously transcribed tetratricopeptide repeat gene on the Y chromosome $(Uty)_{246–254}$ epitope, which was PSMB8 immunoproteasome dependent (Palmowski et al., 2006). However, the study showed that injection of MHC-mismatched cells into the PSMB8 knockout mice produced a strong response against the Uty epitope, suggesting a small proportion was presented through a proteasome-independent pathway, likely the vacuolar pathway (Palmowski et al., 2006). The study demonstrated that the cytosolic pathway was the dominant but not the sole cross-presentation pathway in this context.

1.3.6 Mechanisms of Dendritic Cell Internalisation

Phagocytosis is the process by which antigen-presenting cells, such as macrophages and DCs, engulf dead cells and large (>0.5 μm) antigen particles (Aderem & Underhill, 1999). Dying or infected cells release damage-associated molecular patterns (DAMPs) and pathogen-associated molecular patterns (PAMPs), which are recognised by pattern recognition receptors (PRRs) on the surface of DCs (Fang et

al., 2014; Tang et al., 2012). The PRRs induce downstream signalling, which activates DCs and induces uptake by phagocytosis and endocytosis (Fang et al., 2014; Tang et al., 2012). Apoptotic cells have been shown to release lysophosphatidylcholine in a caspase-3-dependent manner, which acts as a chemoattractant to attract phagocytes to the site of the dying cells (Lauber et al., 2003).

The C-type lectin receptors, which recognise conserved carbohydrates found on bacterial and fungal cell walls, include DEC-205 (CD205), C-type lectin domain family 9 (CLEC9), CD209 and dectin (Brown, 2006; Schreibelt et al., 2012; Shrimpton et al., 2009). CD209 is an endocytic receptor found on DCs and macrophages and is a PRR for mannose oligosaccharides commonly found on viruses, bacteria, and fungi (Geurtsen et al., 2010). DEC-205 is of interest as it has been strongly associated with favourable antigen presentation and cross-presentation, with one study showing a 400-fold increase in antigen cross-presentation with the use of an OVA DEC-205 antibody fusion compared to OVA alone (Bonifaz et al., 2002). However, immunity against rechallenge was only observed with the co-administration of agonist CD40 antibody to promote DC maturation; otherwise, immune tolerance was observed (Bonifaz et al., 2002). The study demonstrated a delicate balance between immune response and tolerance.

In the context of cancer, the macrophage galactose type C-type lectin, which is expressed on macrophages and DCs, has demonstrated recognition of mucin short variant S1 (MUC1), a highly glycosylated, overexpressed antigen in adenocarcinoma (Saeland et al., 2007), revealing the role of DC PRRs in the recognition of aberrant cells.

Fragment crystallisable gamma receptors (FcγR) recognise immunoglobulin (Ig) G through their Fc receptor and bind to opsonised cells or antigen immune complexes (ICs) to initiate internalisation (Ravetch & Bolland, 2001). FcγR subtypes have different affinities for subtypes of IgG and can be excitatory or inhibitory. For example, FcγRI (CD64) is excitatory and has a high affinity for monomeric IgG1 and IgG4 subtypes but not for monomeric IgG2 (Bruhns et al., 2009). Whereas FcγRIIB is inhibitory and binds with lower affinity to IgG1, 2 and 3, and acts to regulate the immune response via an anti-inflammatory function (Bruhns et al., 2009; Karsten et al., 2012).

For efficient internalisation, multiple IgG form ICs with antigens or by opsonising cells, cross-linking multiple Fc receptors, which phosphorylates their associated immunoreceptor tyrosine-based activation motifs (ITAM) for excitatory FcγRs or immunoreceptor tyrosine-based inhibition motifs (ITIM) for inhibitory FcγRs (Billadeau & Leibson, 2002). Upon phosphorylation, the downstream signalling cascade results in the internalisation of the opsonised cell or IC through activation of the phosphatidylinositol-3 and Src kinase pathways for the phagocytosis of large particles (Araki et al., 1996; Z. Y. Huang et al., 2006), or through ubiquitination pathways for endocytosis of smaller soluble ICs (Booth et al., 2002). Upon internalisation, the complexes are trafficked to the lysosome for processing and antigen presentation (Ukkonen et al., 1986). The ITAM-signalling pathway is essential for cross-presenting particulate antigens but is not required for soluble antigens, as they can be internalised through other pathways, such as macropinocytosis (Graham et al., 2007).

Inside the cell, the internal neonatal Fc receptor (FcRn) orchestrates the movement of ICs, guiding them towards lysosomal compartments for degradation and antigen presentation (Qiao et al., 2008). Simultaneously, FcRn directs monomeric IgGs out of the cell to prevent their catabolism and to continue circulating (Qiao et al., 2008). FcRn

has also been shown to enhance cross-presentation by protecting the antigens from the acidic lysosomes in $CD8^-$ DCs, facilitating its retention and subsequent escape (Baker et al., 2011). In experiments with FcRn knockout mouse models, the absence of FcRn resulted in a complete loss of cross-presentation ability in $CD8^-$ DCs (Baker et al., 2011).

One study illustrated the significance of FcγR uptake in antigen cross-presentation by coating myeloma cells with an antibody that targets syndecan, a cancer-testis antigen overexpressed in myeloma (Dhodapkar et al., 2002). The antibody promoted stronger antigen cross-presentation in DCs, which led to a potent $CD8^+$ T cell response against syndecan-bearing tumours compared to DCs that had only been pulsed with peptide or dying myeloma cells (Dhodapkar et al., 2002).

Unlike phagocytosis and endocytosis, macropinocytosis is a non-specific uptake mechanism with sizes ranging from 0.2 to 5 µm (Hewlett et al., 1994). DCs form these macropinosomes from cell ruffling and constantly sample antigens and nutrients from their surroundings (Lim & Gleeson, 2011). Although non-specific, they offer a general entry route for small antigens and peptides for antigen presentation, as their inhibition has been shown to reduce $CD4^+$ T cell activation (Sarkar et al., 2005; von Delwig et al., 2006).

1.4 Antigen Presentation in Cancer

1.4.1 Dendritic Cells in Cancer

In humans, DCs can be broadly categorised into conventional DC (cDC), cDC1 and cDC2, and non-conventional DCs like pDCs, each having different responsibilities and effects in the tumour microenvironment. Other subtypes of DC and antigen-presenting cells, such as monocyte-derived DCs and Langerhans cells, are not discussed here

but have been expertly reviewed elsewhere (Collin & Bigley, 2018; Kushwah & Hu, 2011).

Conventional DCs are characterised by their potent aptitude for cross-presentation, with mouse $CD8^+$ cDC1 being the primary MHC-I presenting cells, while mouse $CD8^-$ cDC2 being primarily focused on MHC-II presentation (Bennett et al., 1997; Binnewies et al., 2019; den Haan et al., 2000). Human cDC1 can be differentiated from cDC2 by their expression of CD141 and the surface markers XCR1 and CLEC9A (Dzionek et al., 2000; Heger et al., 2023; Villani et al., 2017). Both human cDC1 and cDC2 are equally competent at MHC-I presentation (Cohn et al., 2013; Segura et al., 2013; Sittig et al., 2016). However, conflicting data suggests that cDC1 is the primary source of cross-presented antigens (Bachem et al., 2010; Crozat et al., 2010).

DCs form a small but essential proportion of the immune cell repertoire within the tumour. DCs are recruited into the tumour periphery by the secretion of pro-inflammatory cytokines and chemokines. NK cells act as a primary source of initial cDC recruitment in the tumour by secretion of chemokine C-C ligand (CCL) 5 and chemokine (C motif) ligand (XCL) 1 (Bottcher et al., 2018). Interestingly, NK cells have also been implicated in precursor DC differentiation and cDC1 survival by releasing the growth factor fms-like tyrosine kinase 3 ligand (FLT3L) (Barry et al., 2018; Pulendran et al., 1999). Therefore, NK cell penetration and abundance in the tumour microenvironment is an essential precursor to potent T cell-mediated response through DCs.

Upon endocytosis and presentation of tumour antigens, cDCs migrate to lymph nodes via the detection of CCL19 and CCL20 released by stromal cells through the chemokine C-C receptor (CCR) 7 receptor (Forster et al., 1999; Luther et al., 2000).

Upon arrival in the draining lymph nodes, cDCs present their antigen on MHC molecules to naïve T cells, priming their antigen-specific effector function (Mempel et al., 2004). Tumour-resident cDCs then recruit tumour-antigen primed T cells back to the tumour site by releasing chemokine C-X-C ligand (CXCL) 9 and CXCL10 (Spranger et al., 2017), where they can perform their effector functions.

pDCs function in anti-viral immunity by secreting large quantities of type I interferons (IFN-α/β) (Ito et al., 2006). In the context of cancer, pDCs have been implicated with poor prognosis and immune tolerance (Han et al., 2017; Kiessler et al., 2021; Labidi-Galy et al., 2012). Cancer cells recruit pDCs into the periphery through the secretion of CXCL12 to increase tumour immune tolerance and induce pDC secretion of tumour necrosis factor (TNF)-α and IL-8 to increase angiogenesis (Curiel et al., 2004; Zou et al., 2001). In ovarian and breast cancers, pDCs have been shown to enhance immunosuppression through Treg recruitment, suppression of effector T cell response and immune tolerance (Conrad et al., 2012; Sisirak et al., 2012). Tumours exploit pDCs by secreting numerous cytokines, such as TNF-α and IL-10, to prevent pDC maturation and the secretion of IFN-α (Hack et al., 2012).

1.4.2 Cancer Suppression of Dendritic Cells and T cells

Cancer cells have evolved strategies to suppress the function of DCs and T cells by recruiting immunosuppressive cells. Tregs are immunosuppressive T cells defined by their expression of FoxP3 and regulate immune tolerance and prevention of autoimmunity (Fontenot et al., 2003; Takahashi et al., 2000). Treg cells are recruited into the tumour microenvironment by the release of the cytokines CCL1 (Kuehnemuth et al., 2018), CCL5 (Tan et al., 2009), CCL17/22 (Mizukami et al., 2008), and CCL28 (Ren et al., 2016), and act upon DCs through their expression of the immune checkpoint molecule CTLA-4 (Chen et al., 2017; Tekguc et al., 2021). CTLA-4

competes with CD28 for binding to CD80/86 on DCs, preventing T cell activation as CTLA-4 has a higher affinity for CD80/86 (Collins et al., 2002; Stamper et al., 2001). Treg cells also release anti-inflammatory cytokines such as IL-10, TGF-β and IL-35 (Collison et al., 2007; Strauss et al., 2007). Unsurprisingly, a high Treg to $CD8^+$ T cell ratio has been correlated with poor prognosis in some cancers (L. Hu et al., 2021; Sato et al., 2005; Shen et al., 2010).

Myeloid-derived suppressor cells (MDSCs) are a heterogeneous group of immunosuppressive cells that arise from bone marrow precursor cells exposed to prolonged cytokine and growth-factor release by chronic inflammation and cancerous tissue (Almand et al., 2001; Diaz-Montero et al., 2009; Ostrand-Rosenberg & Sinha, 2009). MDSCs have been shown to induce immunosuppressive Treg and M2 macrophage production through the release of IL-10 and IFN-γ, and T cell anergy and apoptosis through expression of PD-L1 (Beury et al., 2014; B. Huang et al., 2006; Lu et al., 2016; Yamauchi et al., 2018). MDSCs also present antigens to T cells and, through this interaction, release ROS to suppress $CD8^+$ T cells (Kusmartsev et al., 2004). T cell suppression is also achieved by arginine depletion by MDSC arginase expression and nitric oxide release, reducing available metabolites for T cell function (Raber et al., 2012; Raber et al., 2014). The suppression of DCs by MDSCs is not as well studied. However, in mouse HCC studies, MDSCs were shown to suppress DC function through IL-10 release and cross-talking, leading to the downregulation of IL-12 production and reduction in T cell stimulation (Hu et al., 2011).

Tumour-associated macrophages (TAMs) are often abundant within the tumour microenvironment and categorised into M1 or M2 types. M1 macrophages are activated by IFN-γ and are characterised by their anti-tumour properties, including the release of proinflammatory cytokines, production of nitric oxide, and the upregulation

of MHC-II molecules for antigen presentation (Boutilier & Elsawa, 2021; Martinez & Gordon, 2014; Pan et al., 2020). M2 macrophages, on the other hand, are pro-tumour and arise from stimulation by anti-inflammatory cytokines, such as IL-10. Their immunosuppressive functions in tissue repair and angiogenesis are characterised by releasing IL-10, VEGF and TGFβ (Boutilier & Elsawa, 2021; Martinez & Gordon, 2014; Pan et al., 2020).

Macrophages display significant plasticity and exist on a spectrum between the M1 and M2 phenotypes, with the phenotype somewhat redirectable (Guiducci et al., 2005; Saccani et al., 2006). Consequently, the M1 to M2 macrophages ratio in the tumour microenvironment (TME) is indicative of cancer prognosis, with a lower M1/M2 ratio associated with a poorer outcome (Cui et al., 2013; Pantano et al., 2013; Petrillo et al., 2015). For DCs, the release of IL-10 by M2-phenotypic TAMs has been demonstrated to suppress the DC expression of IL-12, which is necessary for CTL activation (Rojas et al., 2023).

Figure 1.3 highlights the fundamental suppression mechanisms of immune cells within the tumour microenvironment and the downregulation of MHC-I discussed in the next section.

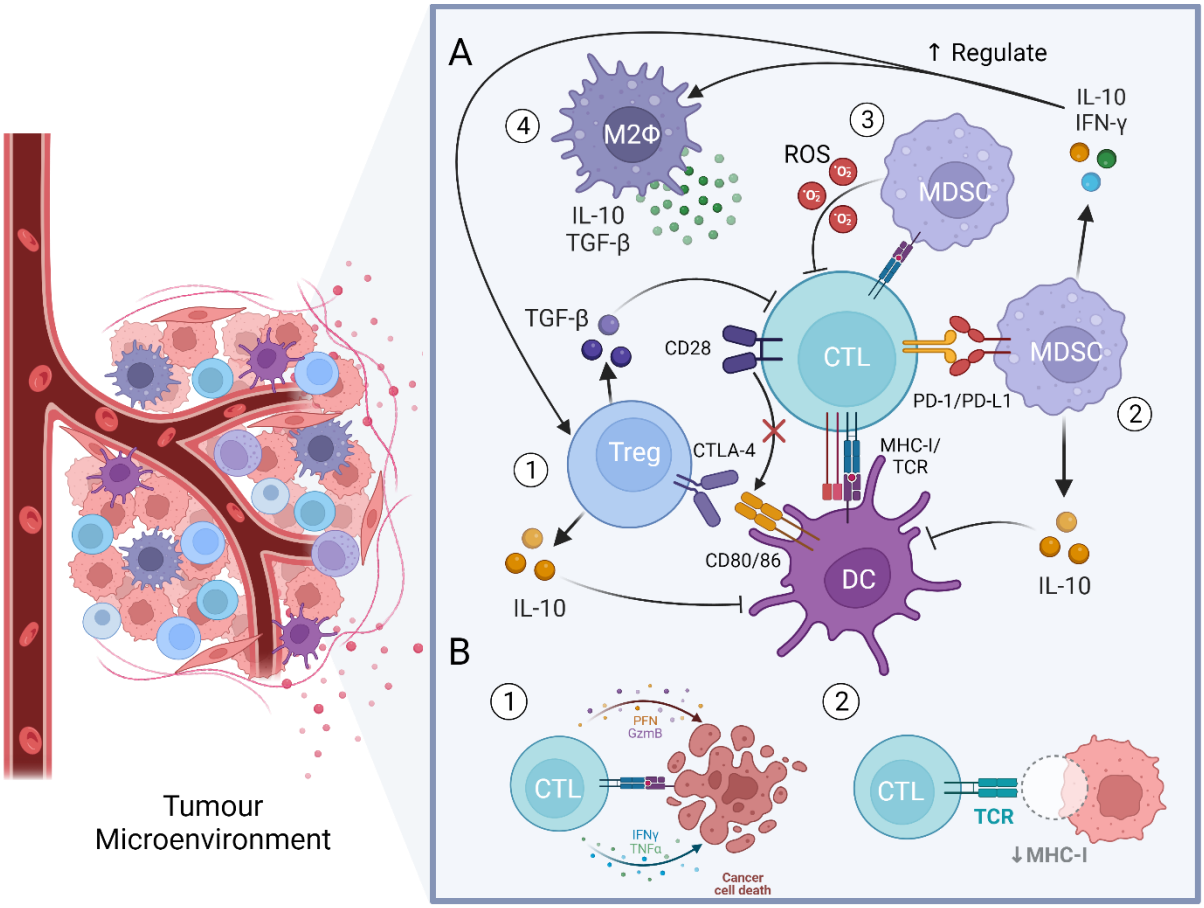


Figure 1.3 Suppression of Dendritic Cells and T Cells in the Tumour Microenvironment
The TME provides a hostile environment for DC and T cells, preventing effective immune response. **(A)** Resident immunosuppressive cells within the TME include (1) Treg cells, which express anti-inflammatory cytokines such as IL-10 and TGF-β to suppress DC and CTL functions. They also express CTLA-4 on their cell surface, which binds to CD80/86 (B7) on DCs, preventing CD28 interaction on CTLs and the "second signal" of T cell activation, leading to T cell anergy. (2) MDSC express cytokines that inhibit DC function and upregulate M2 macrophages (M2Φ) and Treg cells. MDSCs also express PD-L1, which binds to PD-1 on CTLs and suppresses their effector function. (3) MDSCs can present antigens on MHC, which binds to TCRs on the T cells; MDSCs release ROS across the immune synapse, further suppressing CTL functionality. (4) Immunoregulatory M2 macrophages contribute to the overall immunosuppression by releasing anti-inflammatory cytokines such as IL-10 and TGF-β. **(B)** (1) Cancer cells expressing antigens on MHC are targeted by their cognate TCR on CTLs, which induces the release of cytokines and cytotoxic compounds such as perforin (PFN) and granzyme B (GzmB). (2) A common immune evasion strategy is the downregulation of MHC-I on cancer cells, preventing recognition by antigen-specific CTLs and continued cancer proliferation. Created with Biorender.com

1.4.3 MHC-I Downregulation in Cancer

On top of the immune suppression of the tumour microenvironment, cancer cells often downregulate the expression of MHC-I on their cell surface to prevent recognition and apoptosis by effector T cells (Chang et al., 2015; Maeurer et al., 1996). MHC-I downregulation can occur through various methods, including epigenetic silencing

(Luo et al., 2018; Nie et al., 2001), loss of heterozygosity (Maleno et al., 2011; Maleno et al., 2002), genetic mutations and deletions (Shukla et al., 2015; Wang et al., 1999), autophagy (Yamamoto et al., 2020), or downregulation of MHC-I transcription factors and activation pathways (Forloni et al., 2010; Staehli et al., 2012). Loss of MHC-I has been described in numerous cancers and is often associated with poor prognosis (Ito et al., 2016; Pedersen et al., 2017; Simpson et al., 2010).

Loss of MHC-I through epigenetic silencing or downregulation of signalling pathways is reversible. In several cancers, DNA methyltransferase inhibitors have been demonstrated to reverse the hypermethylation of MHC-I and related genes to remove epigenetic silencing (Luo et al., 2018; Siebenkas et al., 2017; Srivastava et al., 2015). IFN-γ has been widely reported to increase MHC-I and TAP expression in certain cancers (Propper et al., 2003; Stifter et al., 2020; Yang et al., 2004), with the NOD-like receptor family CARD domain containing 5 (NLRC5) recognised as an IFN-γ-inducible regulator which was found to increase MHC-I expression in MHC-deficient breast cancer cells (Zhao et al., 2019). Induction of the nuclear factor kappa-light-chain-enhancer of activated B cells (NF-κB) pathway with retinoic acid was also found to increase MHC-I expression in human embryonal carcinoma and neuroblastoma (Farina et al., 2002; Segars et al., 1993).

The stimulator of interferon genes (STING) pathway has a dual ability to upregulate MHC-I expression on cancer cells and activate NK-mediated anti-tumour responses (Grabosch et al., 2019; Nicolai et al., 2020). The STING pathway regulates inflammation in cellular stress and infection, with STING agonists improving antigen-specific T cell responses (Corrales et al., 2015; Rossi et al., 2021). However, the challenge has been that constant STING activation has been associated with upregulation in PD-L1 expression on cancer cells (Lemos et al., 2020), hence why

trials with STING agonists are combined with immune checkpoint blockade to bolster anti-tumour efficacy (Foote et al., 2017; Ghaffari et al., 2018; Le Naour et al., 2020).

Irreversible MHC-I loss through genetic mutations or loss of heterozygosity renders antigen-specific T cell response impossible. As we have already discussed, BiTEs and CAR-T cells can act upon cancer cells in an MHC-independent manner (see sections 1.2.2 and 1.23). However, NK cells have evolved to recognise cells without MHC-I on the cell surface as abnormal and target them for apoptosis, as described by the "missing self" hypothesis (Ljunggren & Karre, 1990).

NK cells recognise "self" through MHC-I molecules, which in humans bind to NKG2A and the killer cell immunoglobulin-like receptor (KIR) family of inhibitory receptors (Borrego et al., 1998; Yokoyama & Kim, 2006). Therefore, the loss of MHC-I from cancer cells reduces KIR and NKG2A inhibition through these receptors. However, NK cell activation also requires the recognition of stress-induced molecules on the target cell through activation receptors such as NKG2D (Radosavljevic et al., 2002; Takada et al., 2008). Through reduced inhibition and enhanced activation, NK cells can exert cytotoxic functions to kill the target cell (Pardo et al., 2002; Screpanti et al., 2001).

1.5 Peptide Cancer Vaccines[1]

1.5.1 Introduction

Peptide cancer vaccines, in their simplest form, are peptides manufactured from a known cancer antigen sequence containing $CD4^+$ and $CD8^+$ epitopes to activate T cell-mediated immune responses against their targets. One of the challenges with peptide cancer vaccines is breaking self-tolerance to produce the desired anti-tumour response.

Creating a cancer vaccine that is effective for a substantial portion of the population requires careful consideration of the peptide sequence and length to ensure that the vaccine encapsulates the widest specificity and affinity to diverse MHC haplotypes. One study demonstrated the subtle differences by studying the binding specificities of human leukocyte antigens (HLA) DRB1*0401, DRB1*0101, and DRB1*0701 haplotypes (Southwood et al., 1998). They found that the different subtypes have overlapping but non-identical recognition of $CD4^+$ epitopes (Southwood et al., 1998). The importance of peptide length for MHC-I binding is also critical, with an earlier study demonstrating differences in HLA-B and HLA-C haplotype binding specificities (Sidney et al., 1995).

The length of peptides affects immunogenicity, with synthetic peptides of minimal $CD8^+$ length producing inferior CTL response compared to an extended-length peptide (Bijker et al., 2008). This inferior response was thought to be caused by the engagement of the peptide with non-professional antigen-presenting cells, which do not have the necessary costimulatory signals for robust T cell activation (Bijker et al., 2008). Figure 1.4 gives an overview of peptide strategies currently being investigated.

[1] The content in this section is partly derived from a published review – see publication note (Page V)

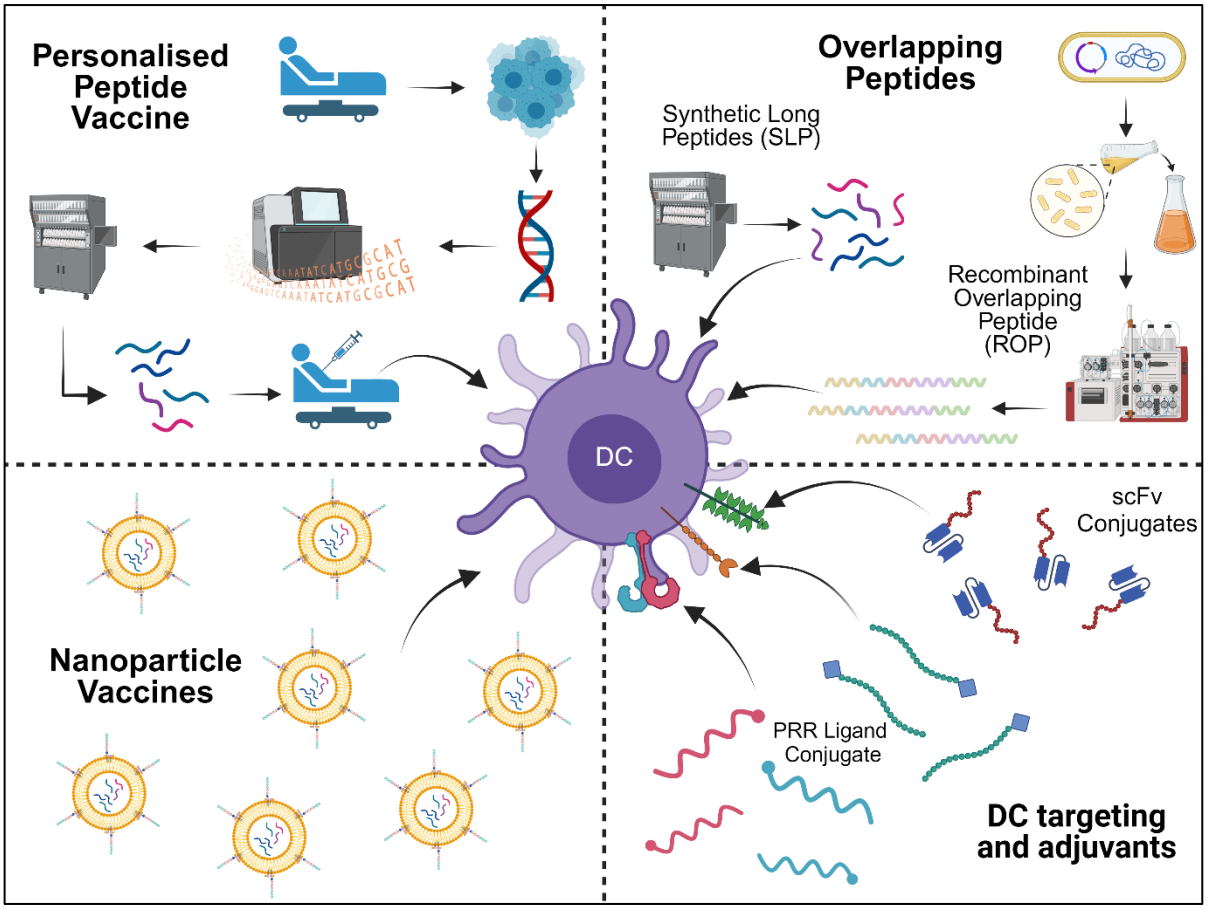


Figure 1.4 Peptide Cancer Vaccine Strategies
An overview of some of the vaccine strategies currently being trialled. Overlapping peptides containing $CD4^+$ and $CD8^+$ epitopes derived from a known cancer antigen can be synthesised as a pool of peptides (SLP) or recombinantly overlapping peptides (ROP). Peptide vaccines can incorporate DC-targeting ligands, antibodies, scFvs, or adjuvants to improve uptake and efficacy. Peptides have a short half-life, which can be enhanced by incorporating peptides into nanoparticles, such as liposomes, to protect the peptides and create a depot of peptides upon uptake. Liposomes can also contain ligands and receptors within their lipid bilayer to increase targeting and uptake. Increasingly, personalised peptide vaccine strategies are being implemented by sequencing patients' cancer antigen repertoire and their mutational burden to provide a fully customisable peptide vaccine treatment. Adapted from Stephens et al., 2021. Created with Biorender.com

1.5.2 Synthetic Long Peptides

Peptide cancer vaccines are diverse in their form and functionality to maximise DC uptake and cross-presentation efficacy. One strategy is to create a synthetic peptide pool of overlapping cancer antigen sequences to encapsulate a cancer antigen sequence (Speetjens et al., 2009; Zwaveling et al., 2002). Synthetic long peptides (SLPs) are synthetic peptide pools consisting of approximately 32 to 35 amino acids long peptides covering a sequence of a cancer antigen (Speetjens et al., 2009;

Zwaveling et al., 2002). The peptides were designed to be long enough to prevent direct MHC-I binding and consideration of known $CD4^+$ and $CD8^+$ epitopes (Zwaveling et al., 2002). In a study with human papilloma virus (HPV) E7 SLPs, this strategy induced strong anti-tumour immunity and reduced tumour burden compared to minimal $CD8^+$ epitope peptides (Zwaveling et al., 2002).

Modified SLPs have also been used to investigate methods of targeting specific pathways in antigen cross-presentation. A study focusing on an SLP derived from melanoma-overexpressed antigen 1 (MELOE1) incorporated a variety of cathepsin-sensitive linkers for cathepsin D, L and S between the MHC-I and II epitopes (Rabu et al., 2019). No change in $CD4^+$ antigen-presentation was observed, but the inclusion of the LLSVGG linker showed a greater efficiency at cross-presentation and $CD8^+$ T cell activation compared to the GGGG linker or native epitope peptide (Rabu et al., 2019), exhibiting the ability of peptide cancer vaccines to be designed to target pathways and proteases to enhance cross-presentation.

TCRs that are reactive to self-antigens are eliminated from the T cell repertoire by central and peripheral immune tolerance mechanisms to prevent autoimmunity and are similarly found in the context of tumour antigen tolerance (Schietinger et al., 2016; Schwartz, 2003; Sebzda et al., 1994). In a study with a survivin vaccine composed of three synthetic long peptides containing $CD4^+$ and $CD8^+$ epitopes of survivin, the vaccine broke self-tolerance and, in four mouse models, generated antigen-specific $CD4^+$ and $CD8^+$ T cells. Additionally, the vaccine elicited the generation of memory T cells without a concurrent increase in Treg cells (Onodi et al., 2018). Survivin is a member of the inhibitor of apoptosis (IAP) family, and its role is to inhibit cell death by blocking caspase-3 and -7 (Ambrosini et al., 1997; Onodi et al., 2018; Tamm et al., 1998). It is expressed at varying levels in many cancers, with expression found in all

sixty cancer cell lines tested as part of the National Cancer Institute's human tumour cell-line screening programme (Ambrosini et al., 1997; Tamm et al., 1998).

1.5.3 Personalised Peptide Cancer Vaccines

Increasingly, researchers are focusing on personalised peptide vaccine strategies to overcome HLA haplotype differences and tumour heterogeneity. One recently concluded trial used a personalised long-peptide approach with twenty peptides derived from eight patients with surgically resected stage III and IV melanoma, combined with polyinosinic-polycytidylic acid with polylysine and carboxy-methylcellulose (poly-ICLC), and a TLR3 and melanoma differentiation-associated protein 5 (MDA5) agonist (Z. Hu et al., 2021). The personalised peptides were identified by a combination of whole-exome sequencing comparing normal cells to tumour cells, expression of mutant alleles by RNA sequencing and using predictive models to assess peptide-HLA binding for these isolated antigens (Z. Hu et al., 2021; Ott et al., 2017). The study found that the patients developed memory T cell response and diversification of antigen-recognition through T cell epitope spreading, particularly after anti-PD-1 therapy (Z. Hu et al., 2021). However, the authors note the recurrence of the tumour in numerous patients, indicating that this strategy alone may not be sufficient (Z. Hu et al., 2021).

Similar studies with personalised cancer vaccines were conducted in glioblastoma patients (Hilf et al., 2019; Keskin et al., 2019). The study combined two personalised approaches, firstly by vaccinating with a pre-manufactured vaccine containing the seven highest ranking immunogenic tumour antigens for each patient, followed by identification of the individual patient's mutated peptides, ranking them, and creating a personalised neoepitope vaccine (Hilf et al., 2019). The study showed that 80% of

the patients had neo-epitope-specific responses, predominantly $CD4^+$ Th1, with only a modest degree of $CD8^+$ specificity (Hilf et al., 2019).

These studies highlight that even with a personalised strategy, peptide cancer vaccines alone have limited immunogenicity, necessitating additional combination therapies to tackle the evolving tumour heterogeneity and suppressive microenvironment.

1.5.4 Particulate Peptide Cancer Vaccines

Nanoparticles provide an elegant packaging system to combine peptides and adjuvants into one delivery vehicle to bolster the immune response and protect their contents from rapid degradation (Stark et al., 2008). Soluble antigens and particles are internalised and processed by DCs using different pathways, with particulate antigens demonstrating enhanced cross-presentation compared to soluble proteins (Harding & Song, 1994; Mant et al., 2012). The size of the particles is essential, with 20-200 nm particles draining rapidly to the lymph nodes and internalised by resident DCs (Manolova et al., 2008). In contrast, larger particles tend to be taken up by DCs at the injection site (Manolova et al., 2008). Because of these unique properties, investigations on particulate-based peptide cancer have been ongoing.

Poly(lactic-co-glycolic acid) (PLGA) is a Food and Drug Administration (FDA) approved biodegradable particle used in drug delivery for its biocompatibility and sustained drug release (Sadat Tabatabaei Mirakabad et al., 2014). Dolen et al. used PLGA nanoparticles containing New York oesophageal squamous cell carcinoma 1 (NY-ESO-1) peptides, a cancer testis antigen, and the α-galactosylceramide analogue, IMM60 (Dolen et al., 2021). IMM60 and α-galactosylceramide are potent activators of invariant natural killer T cells (iNKT), a unique and rare subset of T cells, comprising

less than 1% of the T cell population, that express an invariant TCRα chain (Beckman et al., 1994; Lee et al., 2002; Natori et al., 1994). iNKT does not recognise peptide-MHC complexes but glycolipids presented on CD1d, a non-polymorphic MHC-I-like molecule (Beckman et al., 1994). Alpha-galactosylceramide and its analogues stimulate iNKTs through the CD1d receptor and have been shown to have anti-tumour effects in B16 mouse models (Morita et al., 1995). In mouse models, the PLGA particle containing NY-ESO-1 peptides showed enhanced $CD4^+$ and $CD8^+$ T cell response *in vivo* compared to soluble peptides, which was further enhanced with the addition of IMM60 (Dolen et al., 2021). The authors speculated that the iNKT activation may have enhanced $CD4^+$ activity, demonstrated by the higher IFN-γ release with IMM60 (Dolen et al., 2021).

An earlier experiment used PLGA-encapsulated mouse melanoma antigenic peptides from glycoprotein 100 (gp100) and tyrosinase-related protein-2 (TRP-2) (Z. Zhang et al., 2011). The investigation found an increase in antigen-specific $CD8^+$ immune response compared to soluble peptides but no control of the B16 melanoma tumour mouse model in the therapeutic setting, which was caused by a downregulation of MHC-I (Z. Zhang et al., 2011). IFN-γ was able to recapitulate the MHC-I expression and increase tumour control (Z. Zhang et al., 2011). Nanoparticles that included a TLR4 agonist also demonstrated increased DC maturation, cytokine production and particle uptake than nanoparticles without (Z. Zhang et al., 2011).

Liposomes offer several advantages over a PLGA-based system. The first is their plasticity, which allows for changes in size, charge and composition (Bulbake et al., 2017). Cell membranes are negatively charged, so incorporating cationic lipids into the composition attracts the positively charged liposome to the lipid bilayer, promoting membrane fusion (Bailey & Cullis, 1997). Some lipids also contain unique properties

to enhance cross-presentation; for example, dioleoyl phosphatidyl-ethanolamine (DOPE) liposomes change structure within the acidic environment of the endosomes, allowing them to fuse with the endocytic membrane and release its contents into the cytosol (Connor et al., 1984; Kono et al., 1997).

The second advantage is the liposome's ability to encapsulate hydrophilic compounds in its interior and bind hydrophobic compounds on its lipid layer, including cell-surface receptor ligands and adjuvants (Copland et al., 2003; Guan et al., 1998; Meraz et al., 2014). A comparison study between a PLGA and cationic liposome-based peptide cancer vaccine with SLPs demonstrated a more potent antigen-specific T cell induction with a liposome system than a PLGA system (Varypataki et al., 2016).

Zamani et al. demonstrated the diversity of liposomal delivery systems by using a combination of short peptides and long multi-epitope peptides for human epidermal growth factor receptor 2 (HER2) breast cancer antigen in combination with a pan HLA-DR epitope (PADRE) peptide in a cationic DOPE-liposome (Zamani et al., 2020). PADRE is a synthetic universal $CD4^+$ epitope, as it binds with high affinity to 15 of the 16 most common HLA-DR haplotypes and potently activates a helper T cell response (Agadjanyan et al., 2005; Alexander et al., 2004). Overall, the vaccine strategy was more effective prophylactically than therapeutically but saw increases in antigen-specific $CD8^+$ T cell response and IFN-γ levels than with peptides alone (Zamani et al., 2020). The PADRE contributed to this increase through induction and activation of $CD4^+$ response, along with the HER2 peptides, and together reduced tumour burden and survival in mouse models (Zamani et al., 2020).

Particulate-based peptide cancer vaccines can potentially solve many of the issues with peptide-cancer vaccines, including tumour heterogeneity, by combining multiple

epitopes, protecting peptides from rapid extracellular elimination, and enhancing cross-presentation through adjuvants and controlled peptide release.

1.5.5 Targeting Dendritic Cells

As discussed previously, DCs contain PRRs on their surface to detect PAMPs and DAMPs (see section 1.3.6). These receptors are often endocytic and prompt rapid internalisation, antigen presentation, and cross-presentation. Consequently, methods have been developed to conjugate peptides to ligands and targets of these receptors.

CLEC9a is a C-type lectin receptor expressed in high levels on cDC1 cells in humans and the cross-presentation efficient $CD8^+$ cDC in mice (Caminschi et al., 2008; den Haan et al., 2000). In a study of a CLEC9a-targeting peptide conjugated to antigenic OVA or gp100 melanoma peptide, the targeting enhanced uptake in the $CLEC9a^+$ mouse DCs and inhibited tumour growth in both the more immunogenic OVA-B16 tumour and an immune checkpoint inhibitor-resistant B16 model with gp100 when compared to antigen alone (Gou et al., 2021). The engagement of CLEC9a caused downstream spleen tyrosine kinase activation and the release of IL-21, which enhances $CD4^+$ T cell proliferation, differentiation and cytokine production, as well as $CD8^+$ T cell proliferation, survival and cytotoxicity (Gou et al., 2021; Spolski & Leonard, 2014).

Chemokine C receptor 1 (XCR1) is found exclusively on the surface of cross-presentation efficient human $CD141^+$ cDC1 and $CD8^+$ cDCs in mice (Bachem et al., 2010; Dorner et al., 2009). The XCR1 ligand (XCL1) is released by NK cells during early innate response and $CD8^+$ T cells during the adaptive immune response to attract these specialised DCs (Crozat et al., 2010; Dorner et al., 2002). Targeting XCR1 enhances uptake by DCs, with an XCL1-OVA-SLP fusion protein displaying superior

tumour control in immunogenic E.G7 and the more resistant B16-OVA model compared to OVA-SLP alone (Botelho et al., 2019). Interestingly, uncoupled free XCL1 and SLP performed equally (Botelho et al., 2019), indicating that it may be the more general attraction of DCs rather than any specific benefit of the fusion.

The mixed benefit of XCL1 in fusions continues with a study on a peptide-cancer vaccine strategy combining XCL1 fused to antigenic HSV-1 glycoprotein B and D peptides, a furin/cathepsin B cleavage motif and a cell-penetrating peptide (CPP) (Wylie et al., 2021). CPPs are small peptides that can pass through cell membranes by endocytosis or energy-independent translocation (Henriques et al., 2007; Liu et al., 2011). This study used the CPP to penetrate the endosomal membrane and deliver its cargo to the cytosol (Wylie et al., 2021). Although the vaccine displayed substantial $CD8^+$ T cell expansion, the authors demonstrated that the non-specific $XCL1^-$ CPP vaccine was equally as effective at expanding $CD8^+$ T cells (Wylie et al., 2021), thus demonstrating that targeting specific DC subtypes does not always produce an enhanced immunogenic response and careful consideration of the target is necessary.

Targeting DEC-205 for its endocytic properties and potency in the cross-presentation of conjugated proteins has been demonstrated (see section 1.3.6). Efforts have also been undertaken to apply it within the context of peptide cancer vaccines. One example is a DEC-205 scFv conjugated to an MHC-II restricted melanoma-associated antigen 3 (MAGE-A3) peptide (Birkholz et al., 2010). The scFv fusion bound readily to monocyte-derived DCs and displayed a higher IL-2 secretion by $CD4^+$ T cells from donor and melanoma-patient-derived DCs compared to peptide-pulsed cells (Birkholz et al., 2010). The study was confined to a proof-of-concept with only a $CD4^+$ epitope and observation of the T-helper response, which was insufficient to elicit a complete and robust anti-tumour response.

Liu et al. demonstrated the CTL activation potential of DEC-205 targeting by fusing an scFv to an HPV E7 SLP containing known dominant T cell epitopes (Liu et al., 2016). The scFv fusion bound to DC cells in naïve C57BL/6 mice and demonstrated significant inhibition of HPV-E7^{+} TC-1 tumour growth in the prophylactic and therapeutic setting compared to free E7 peptide and increased CTL response by IFN-γ expression (Liu et al., 2016). A synergistic effect was observed with a combination of the vaccine and anti-PD-L1 therapy, which enhanced anti-tumour efficacy compared to the individual vaccine or anti-PD-L1 (Liu et al., 2016).

Targeting DCs for antigen cross-presentation produced mixed results, with CLEC9a and DEC-205 more promising. Therefore, consideration of the receptor target and its abundance within DC subsets to produce a strong response with the specificity to prevent off-target effects is imperative.

1.5.6 Peptide Cancer Vaccines in Clinical Trials

Peptide cancer vaccines have proven strategies to overcome immune tolerance to self-antigens and an ability to create antigen-specific T cells against a cancer antigen. However, despite achievements in mouse models and preclinical experiments, currently, there are no FDA-approved *in vivo* cancer peptide vaccines, with the only approved *ex vivo* peptide-based cancer vaccine being sipuleucel-T cell therapy (see section 1.2.3) (Cheever & Higano, 2011; Kantoff et al., 2010). Some of the most recent phase I/II trials for peptide cancer vaccines are listed in Table 1.2.

Table 1.2 New Peptide Vaccine Clinical Trials (June 2021 – November 2023)				
Cancer	**Intervention**	**Phase**	**Status**	**NCT Number**
Blood	Calreticulin peptide + P-ICLC	I	R	NCT05025488
	KRAS peptide pool	I/II	R	NCT05841550
	DNAJB1-PRKACA peptide + TLR 1/2 agonist + MI-51	I	R	NCT05937295
Breast	Personalised peptides + P-ICLC + anti-PD-1	I	R	NCT05098210
	Personalised peptides + GM-CSF+ anti-PD-1	I	R	NCT05269381
Colorectal	Novel microbial peptide + anti-PD-1	I/II	R	NCT05589597
	Peptide pool/MI-51 + anti-PD-1	II	ANR	NCT05243862
	Peptide pool/MI-51 + trifluridine/tipiracil	I	C	NCT05130060
	Novel microbial peptide + anti-PD-1	II	R	NCT05350501
Glioblastoma	DCs pulsed with personalised peptides + TMZ	I	R	NCT04968366
	Survivin peptide vaccine + MI-51	II	R	NCT05163080
Glioma	Tetanus-toxoid peptide linked to EphA2, pp65 or Survivin peptides + P-ICLC	I	R	NCT05283109
	Personalised peptides	I	R	NCT04943718
Head & Neck	Liposomal HPV E6/E7 peptide + anti-PD-1	I/II	R	NCT05232851
	Personalised peptides + GM-CSF	I	R	NCT05307835
Kidney	Personalised peptides + GM-CSF	I	R	NCT05641545
	TBVA-derived peptide-pulsed DC	II	R	NCT05127824
Multiple	HER2/3 peptide-pulsed DC	I	R	NCT05809752
	Lipid-conjugate peptides & oligonucleotides	I/II	R	NCT05726864
NSCLC	DCs pulsed with personalised peptides + CPA	I	R	NCT05195619
	LRPAP1 SLP vaccine + MI-51	I/II	R	NCT05898763
	Mutant KRAS SLP pool vaccine + ICI	I	R	NCT05254184
Ovarian	NY-ESO-1 peptides + anti-PD-1	II	R	NCT05479045
Pancreatic	KRAS SLP vaccine	I	R	NCT05013216
	Neoantigen SLP vaccine + P-ICLC adjuvant	I	R	NCT05111353
Prostate	Personalised peptides + P-ICLC/CDX-301	I	R	NCT05010200
Sarcoma	Personalised peptides + TLR1/2 agonist + MI-51	I/II	R	NCT06094101
Solid	EphA2-targeting CAR-DC pulsed with TP53 Peptide + ICI	I	R	NCT05631886
	EphA2-targeting CAR-DC pulsed with KRAS peptides + ICI	I	R	NCT05631899

Abbreviations: recruiting (R), active, not recruiting (ANR), complete (C), non-small cell lung cancer (NSCLC), polyinosinic-polycytidylic acid with polylysine and carboxy-methylcellulose (P-ICLC), toll-like receptor (TLR), temozolomide (TMZ), Montanide ISA-51 (MI-51), ephrin type-A receptor 2 (EphA2), granulocyte-macrophage colony-stimulating factor (GM-CSF), tumour blood vessel antigen (TBVA), human papillomavirus (HPV), cyclophosphamide (CPA), low-density lipoprotein receptor-related protein-associated protein 1 (LRPAP1), human epidermal growth factor receptor 2/3 (HER2/3), immune checkpoint inhibitor (ICI), Kirsten rat sarcoma virus (KRAS), synthetic long peptide (SLP), chimeric-antigen receptor DC (CAR-DC), New York oesophageal squamous cell carcinoma 1 (NY-ESO-1). DnaJ homolog subfamily B member 1- protein kinase cAMP-activated catalytic subunit alpha (DNAJB1-PRKACA).

Similar to the last time the clinical trial environment was reviewed (Stephens et al., 2021), All of the newly submitted trials since June 2021 have been for Phase I/II

(ClinicalTrials.gov, 2023). Peptide vaccines have been trialled against a diverse array of cancer targets. Notably, NSCLC, colorectal cancer, and various blood cancers are among the most explored, underscoring the potential of peptide vaccines in addressing both haematological and solid tumours.

Of the 29 trials, seven (24%) are personalised peptide vaccines, continuing the trend of increased personalised peptide cancer vaccine strategies (ClinicalTrials.gov, 2023). Around one-third of the interventions include one or more immune checkpoint inhibitors, and another third utilise peptide cancer vaccines with adjuvants (e.g., P-ICLC and Montanide ISA-51) (ClinicalTrials.gov, 2023). Interestingly, one vaccine has lipid-conjugated peptides, while another uses a liposomal delivery system, demonstrating peptide cancer vaccine diversity. Finally, six strategies involve *ex vivo* DC peptide pulsing on autologous DC or engineered CAR-DCs, with two autologous DC vaccines pulsed with personalised peptides (ClinicalTrials.gov, 2023). The diversity in cancers treated and intervention types demonstrates the dynamism of a peptide-based cancer vaccine. However, the lack of phase III indicates that the strategy has a way to go before widespread adoption in the clinic.

There are many potential reasons for the lack of peptide vaccines in the clinic. Firstly is tumour heterogeneity, with some vaccines only targeting one antigen out of many, which are expressed at different levels with varying mutations (de Bruin et al., 2014; Gerlinger et al., 2012). Secondly, the immunosuppressive microenvironment hampers peptide activation of the adaptive immune response (Labani-Motlagh et al., 2020; Murciano-Goroff et al., 2020). Combining peptide cancer vaccines with immune checkpoint inhibitors circumvents this hurdle and has shown superior anti-tumour efficacy compared to vaccines administered alone (Karyampudi et al., 2014; Massarelli et al., 2019; Zom et al., 2018). Finally, peptides have a short half-life due to

degradation from extracellular proteases and rapid elimination from the body (Diao & Meibohm, 2013).

1.5.7 Recombinant Overlapping Peptides

Recombinant overlapping peptide (ROP) is a class of peptide cancer vaccines with overlapping sequences engineered to enhance cross-presentation. An ROP is formed from an overlapping library of peptides derived from a cancer antigen sequence. This library is combined sequentially into one long polypeptide chain with a cathepsin S-sensitive linker between the overlapping regions (Cai et al., 2017). The ROPs are then expressed in *Escherichia coli* (*E. coli)*, providing benefits in manufacturing and cost compared with a pool of synthetic peptides (Cai et al., 2017; Jiang et al., 2006). Once internalised by DCs, ROPs are re-cleaved into their constituent peptides by cathepsin S, a major protease in the vacuolar pathway of cross-presentation (see section 1.3.5) (Shen et al., 2004)

The minimal LRMK cathepsin S sensitive sequence within ROP is derived from the cleavage site on the invariant chain of MHC-II, with the amino acid sequence LRMKLPKP (Cai et al., 2017; Ruckrich et al., 2006). Cross-presentation is a redundant process with peptides likely using both the vacuolar and cytosolic pathways, but by including the cathepsin S sequence, both pathways can be targeted to cross-present ROPs (Cai et al., 2017) (Figure 1.5).

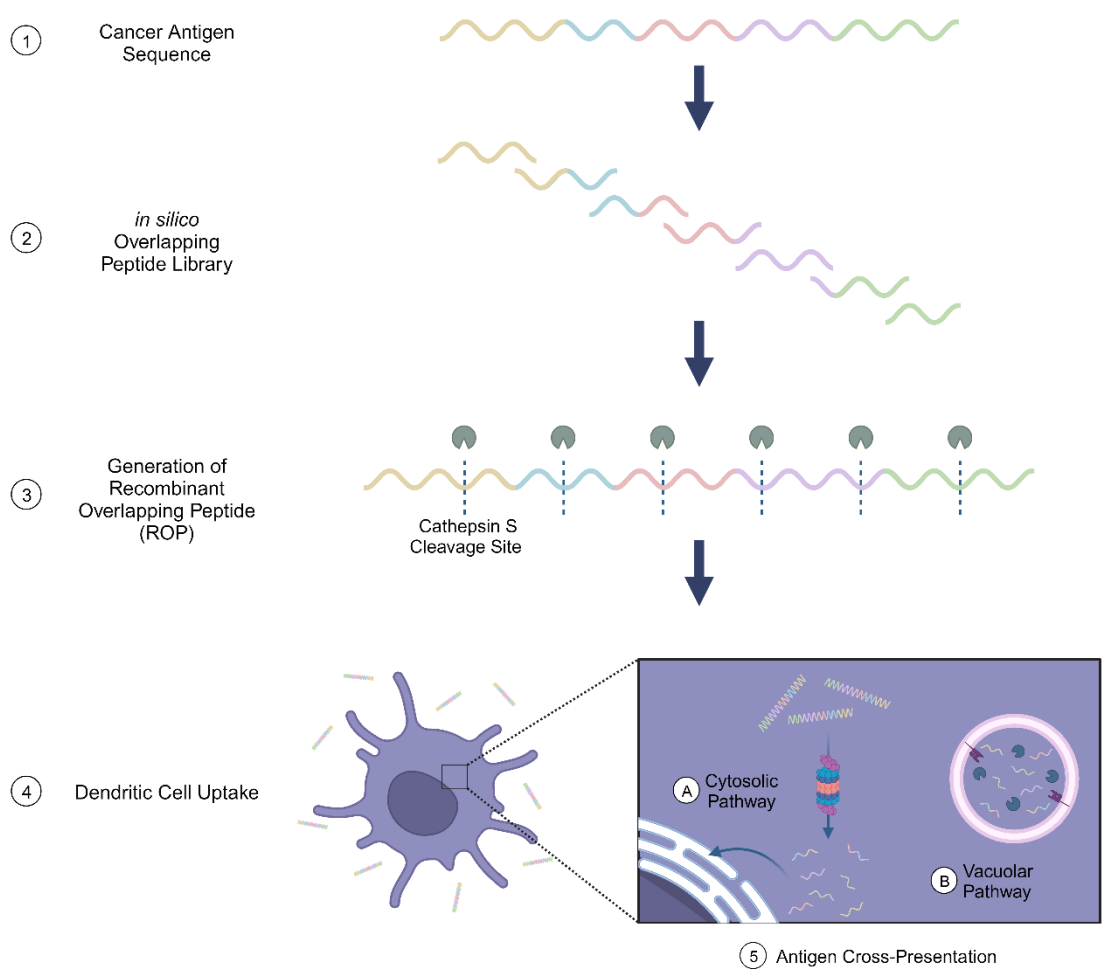


Figure 1.5 Overview of Recombinant Overlapping Peptides
The generation of ROP starts with a cancer antigen and the creation of an overlapping peptide library encompassing the antigen sequence (1,2). The sequence library is joined sequentially with a cathepsin S-sensitive linker between each overlapping region and is recombinantly expressed (3). Upon ROP uptake by DCs, the ROP is processed for antigen presentation and cross-presentation (4,5). ROP is processed by the cytosolic pathway (5A) or by utilising the cathepsin S cleavage site to enhance cross-presentation through the vacuolar pathway (5B). Created with Biorender.com

The inclusion of the overlapping sequence offers several potential advantages. Firstly, the overlapping sequence allows for diversity in HLA haplotype binding, as different MHC-II haplotypes have overlapping recognition of epitopes (Cai et al., 2017; Southwood et al., 1998). Secondly, long overlapping peptides provide multiple epitopes for MHC-I and MHC-II presentation, providing robust helper and CTL response against the antigen target (Cai et al., 2017; Jiang et al., 2006).

Several ROPs have been investigated for their prophylactic and therapeutic potential, including HPV and survivin (Cai et al., 2017; Zhang et al., 2023). A recent study comparing survivin-ROP to wildtype survivin with the adjuvant monophosphate lipid A (MPL) demonstrated that both were similar in the amount of antigen-specific IFN-γ producing T cells (Zhang et al., 2023). However, the T cells were significantly more cytotoxic when co-cultured with survivin-expressing B16 cells (Zhang et al., 2023). In the therapeutic MPL adjuvant setting with survivin-expressing B16 C57/BL6 mice, the ROP significantly reduced tumour burden and overall survival of the mice when compared to wildtype survivin, which correlated with expression, and an increase in survivin-specific lymphocytes (Zhang et al., 2023). Finally, combined with anti-41BB monoclonal antibody, a synergistic effect was observed with a further decrease in tumour burden compared to ROP with MPL (Zhang et al., 2023).

1.6 Thesis Overview and Hypotheses

1.6.1 Thesis Overview

ROPs have demonstrated robust and multifaceted T cell activation and anti-tumour immunity against antigen-bearing tumours with promising preclinical results with HPV and survivin (Cai et al., 2017; Zhang et al., 2023). However, little is understood about ROP's entry, processing mechanisms and the degree to which cathepsin S contributes to their cross-presentation.

Antigen cross-presentation is not a fully understood process, with gaps in the knowledge associated with the contribution of the cytosolic and vacuolar pathways to the overall antigen cross-presentation response. There is considerable redundancy within the cross-presentation pathways, with evidence of multiple sources of MHC-I, TAP and peptide binding locations, including through newly synthesised molecules in

the ER, recycling endosomes, and ER-to-endosomal transportation (Nair-Gupta et al., 2014; Ruckrich et al., 2006; Serwold et al., 2002).

ROPs alone have demonstrated the ability to break self-tolerance through their overlapping sequence and reduced homology, which produces a robust immunogenic response against tumour-associated antigens (Cai et al., 2017; Zhang et al., 2023). However, peptide cancer vaccines have struggled to show progress beyond phase I/II trials (Bezu et al., 2018; Stephens et al., 2021). By understanding more about cross-presentation, its machinery, the role of cathepsin S and the vacuolar pathway in processing ROP, we can understand how to improve its efficacy. A model ROP system was needed to realise cross-presentation mechanisms *in vitro*.

OVA is frequently employed as a model antigen because of its well-characterised and researched $CD4^+$ and $CD8^+$ epitopes, predictable immune response, and its status as a foreign antigen that is not subject to immune tolerance (Schwartz, 2003; Vita et al., 2019). These properties make it a valuable proof-of-concept for new vaccines. Therefore, OVA-ROP will function as a model system for studying cross-presentation and a platform for developing and testing next-generation ROPs with DC targeting tags or multivalency.

Studying cross-presentation pathways with ROP is complex as there are associated challenges with producing an artificial polypeptide, including solubility. Synthetic peptides are replicas of the original protein sequence, offering valuable insights into cellular mechanisms without the complications of recombinant expression and protein folding issues (Gross et al., 2015). By incorporating cathepsin S protease-specific sites upstream from a known $CD8^+$ epitope, we can assess the impact of cathepsin S on their cross-presentation compared to peptides lacking such sites.

Antigen cross-presentation is a complex process that is influenced by numerous factors, both known and unknown. However, by gaining a deeper understanding of this process and the preferences of ROPs, we can create next-generation ROPs that are more stable and have an increased ability to stimulate the immune system.

1.6.2 Hypotheses

1. OVA-ROP can be expressed, endocytosed and cross-presented measurably by DCs.
2. Incorporating fusion tags into ROPs can improve their solubility, targeting and immunogenicity.
3. The expression of multimerised ROPs is a viable strategy for increasing uptake and cross-presentation.
4. Cathepsin S recognises and cleaves at the LRMK site in the vacuolar pathway of cross-presentation.

2 Materials and Methods

2.1 Molecular Biology and Cloning

2.1.1 Agarose Gel Electrophoresis

DNA bands were resolved by agarose gel electrophoresis. 0.8-1.5% (w/v) agarose (#A9539-500G, Sigma-Aldrich) was dissolved in 1 x tris(hydroxymethyl) aminomethane-acetate-ethylenediaminetetraacetic acid (TAE) buffer (Appendix II) and 1 x GelGreen nucleic acid stain (#41005, Biotum). Samples were prepared by dilution in 10 x BlueJuice gel loading dye (#10816015, Invitrogen) and run with 1kb plus DNA ladder (#N3200L, New England Biolabs (NEB)). Gels were run in 1 x TAE buffer at 100 V for 30 minutes and visualised by Biorad ChemiDoc imaging system.

For gel extraction, bands were excised from the gel by scalpel under blue light on the ChemiDoc Imaging System and purified using a QIAquick Gel Extraction kit (#28706, Qiagen) according to the manufacturer's protocol.

2.1.2 Bacterial Transformation

Mach1 (#C862003, Thermo Fisher) and Rosetta (DE3) *E. coli* (#70954, Sigma-Aldrich) were transformed with plasmid DNA using the heat-shock protocol. 50 µl of Cells were thawed on ice, and 1-2 µl of plasmid DNA was added gently to cells and incubated on ice for 30 minutes. Cells were heat-shocked at 42°C in a water bath for 45 seconds and returned to ice for 2 minutes. To each transformant, 100 µl of super optimal broth with catabolite repression (SOC) medium (#11528896, Thermo Fisher) was added and incubated at 37°C for 1 hour. Unless stated, grow-out cultures were plated on pre-warmed lysogeny broth (LB) agar (#L2897, Sigma-Aldrich) plates with 50 µg/mL kanamycin (#K1377-5G, Sigma-Aldrich) and 5% sucrose (#S0389, Sigma-Aldrich) for Mach1 selection and 50 µg/mL kanamycin with 20 µg/mL chloramphenicol (#C0378,

Sigma-Aldrich) for Rosetta selection. The next day, colonies were picked and inoculated into 1-5 mL 2x yeast extract tryptone medium (2xYT, #YDB0102, Formedium) with appropriate antibiotic selection.

2.1.3 PCR Colony Screen

Colonies from agar plates were picked and resuspended in 10 µl of nuclease-free water (NFW, #10793837, Invitrogen), 2 µl was added to 18 µl of polymerase chain reaction (PCR) colony screen master mix from a mixture of 80 µl of 5x MyTaq buffer (#BIO-37112, Bioline), 0.5 µl each of 10 µM primers, 1 µl MyTaq DNA polymerase (#BIO-21106, Bioline), and 259 µl of NFW. Primers used were pLIC-fwd and -rev for pNIC28-Bsa4, pNIC-MBP2-LIC, pNIC-CTH0 and pSUMO-LIC vectors. Other primers used stated as appropriate (Appendix III). Reaction conditions were performed as in Table 2.1 with a SimpliAmp thermal cycler (#A24811, Applied Biosystems)

Table 2.1 PCR Conditions for Colony Screen

Step	Temperature	Time	Cycles
Initial denaturation	95°C	10 min	
Denaturation	95°C	20 sec	x25
Annealing	50°C	20 sec	
Extension	72°C	1 min	
Final extension	72°C	5 min	
Finished	15°C	Hold	

PCR reactions were run on a 1.5% agarose gel (Materials and Methods 2.1.1), and positive colonies, unless otherwise stated, were inoculated into 1 mL of LB Broth with 5% sucrose, 50 µg/mL kanamycin for overnight growth at 37°C, 700 revolutions per minute (RPM).

2.1.4 -80°C Glycerol Stocks of Bacterial Cultures

Glycerol stocks were prepared by combining 30 µl of 60% glycerol (#G7757, Sigma-Aldrich) with 120 µl of overnight culture in a 96-well microtiter plate (#655161, Greiner) and stored at -80°C.

2.1.5 DNA Plasmid Preparation and Quantification

Mach1 colony or glycerol stock inoculated into 3 mL of LB-Broth with 50 µg/mL kanamycin and incubated overnight at 37°C, 200 RPM. Pellets were harvested and processed for plasmid DNA purification using a GenElute miniprep kit (PLN70-1KT, Sigma-Aldrich) according to the manufacturer's protocol. A Thermo Fisher Nanodrop One spectrophotometer was used to quantify DNA concentrations. For large-scale DNA purification, midiprep DNA purification was performed using a GenElute high-performance midiprep kit (#NA0200-1KT, Sigma-Aldrich) using 50 mL of bacterial culture following the manufacturer's protocol.

2.1.6 DNA Sequencing

DNA was sequenced with appropriate primers for each construct (Appendix III) by Sanger sequencing provided by Source Bioscience. Sequences were aligned using SnapGene software to confirm correct insertion and mutagenesis.

2.1.7 PCR Amplification and Mutagenesis of Gene Inserts

Invitrogen GeneArt service was used to synthesise the Ovalbumin-ROP (OVA-ROP) DNA sequence (Appendix III). Forward and reverse primers were designed for insertion into pNIC28-Bsa4, pNIC-MBP2-LIC, pNIC-CTH0 and pSUMO-LIC vectors (SGC, UK) by ligation-independent cloning (LIC) (Bsa4/MBP2-OR-fwd & -rev, CTH0-OR-fwd & -rev, SUMO-OR-fwd & -rev; Appendix III). Full construct maps can be found in Appendix III. Amino acid sequences and features are in Table 2.2

For OVA-DEC-205 scFv and NY-ESO-1-DEC-205 scFv fusion, genes were synthesised as gene fragments by Integrated DNA Technologies Inc. with either a pectate lyase (pel) B periplasmic signal sequence for insertion into pNIC-CTH0 or without pelB for insertion into a pSUMO-LIC vector. Forward and reverse primers were

designed for insertion into pNIC-CTH0 and pSUMO-LIC vectors. For OVA this was pNIC-CTH0-DEC-fwd & -rev and pSUMO-OVA-DEC-fwd & pSUMO-DEC-rev, and for NY-ESO-1 this was pNIC-CTH0-DEC-fwd & -rev and pSUMO-NYE-DEC-fwd & pSUMO-DEC-rev (Appendix III). Amino acid sequences and features are in Table 2.2.

Table 2.2 Amino Acid Sequences for Gene Inserts (Additional Sequences in Appendix III)

Protein Name Molecular weight Extinction coefficient	**Amino acid Sequence** **$CD8^+$ epitope**, **$CD4^+$ epitope**, **Cathepsin S linker**, **IgM Tail**, **$(G_4S)_3$ linker**, **AviTag**, **IL-2 signal**, **Fc-tag**
OVA-ROP 16.1 kDa ε – 15,470 $M^{-1}cm^{-1}$	MSMLVLLPDEVSGLEQLE**SIINFEKL**TEWTSSNVME**LRMK**TEWTSSNV MEERKIKVYLPRMKMEEKYNLTSVLMA**LRMK**KYNLTSVLMAMGITDVFS SSANLSGISSAESLKIS**LRMK**ISSAESLK**ISQAVHAAHAEINEAGR**
tOVA-ROP-Fc 35.6 kDa; ε – 45,420 $M^{-1}cm^{-1}$ (IL-2 signal) 33.4 kDa; ε – 43,805 $M^{-1}cm^{-1}$ (no IL-2 signal)	**MYRMQLLSCIALSLALVTNS**MPDEVSGLEQLE**SIINFEKL**TEWTSS**LRM KLPKP**ESIINFEKL**TEWTSSNVMEERKIKVRS**PRGPTIKPCPPCKCPAP NLLGGPSVFIFPPKIKDVLMISLSPIVTCVVVDVSEDDPDVQISWFVNNV EVHTAQTQTHREDYNSTLRVVSALPIQHQDWMSGKEFKCKVNNKDLP APIERTISKPKGSVRAPQVYVLPPPEEEMTKKQVTLTCMVTDFMPEDIY VEWTNNGKTELNYKNTEPVLDSDGSYFMYSKLRVEKKNWVERNSYS CSVVHEGLHNHHTTKSFSRTPGK**
Fc-tag 26.3 kDa ε – 32,805 $M^{-1}cm^{-1}$	PRGPTIKPCPPCKCPAPNLLGGPSVFIFPPKIKDVLMISLSPIVTCVVVDV SEDDPDVQISWFVNNVEVHTAQTQTHREDYNSTLRVVSALPIQHQDWM SGKEFKCKVNNKDLPAPIERTISKPKGSVRAPQVYVLPPPEEEMTKKQV TLTCMVTDFMPEDIYVEWTNNGKTELNYKNTEPVLDSDGSYFMYSKLR VEKKNWVERNSYSCSVVHEGLHNHHTTKSFSRTPGK
Fc-IgM tag 28.2 kDa ε – 35,410 $M^{-1}cm^{-1}$	PRGPTIKPCPPCKCPAPNLLGGPSVFIFPPKIKDVLMISLSPIVTCVVVDV SEDDPDVQISWFVNNVEVHTAQTQTHREDYNSTLRVVSALPIQHHPICH QDWMSGKEFKCKVNNKDLPAPIERTISKPKGSVRAPQVYVLPPPEEEM TKKQVTLTCMVTDFMPEDIYVEWTNNGKTELNYKNTEPVLDSDGSYFM YSKLRVEKKNWVERNSYSCSVVHEGLHNHHTTKSFSRTPGK**PTLYNVS LIMSDTGGTCY**
Fc-IgM + Q94C mutation 28.2 kDa ε – 35,410 $M^{-1}cm^{-1}$	PRGPTIKPCPPCKCPAPNLLGGPSVFIFPPKIKDVLMISLSPIVTCVVVDV SEDDPDVQISWFVNNVEVHTAQTQTHREDYNSTLRVVSALPI**C**HHPICH QDWMSGKEFKCKVNNKDLPAPIERTISKPKGSVRAPQVYVLPPPEEEM TKKQVTLTCMVTDFMPEDIYVEWTNNGKTELNYKNTEPVLDSDGSYFM YSKLRVEKKNWVERNSYSCSVVHEGLHNHHTTKSFSRTPGK**PTLYNVS LIMSDTGGTCY**
OVA-DEC-205 scFv fusion (NLDC-145) (Demangel et al., 2005; Swiggard et al., 1995) 31.9 kDa ε – 65,110 $M^{-1}cm^{-1}$	EVKLQQSGTEVVKPGASVKLSCKASGYIFTSYDIDWVRQTPEQGLEWIG WIFPGEGSTEYNEKFKGRATLSVDKSSSTAYMELTRLTSEDSAVYFCAR GDYYRRYFDLWGQGTTVTVSS**GGGGSGGGGSGGGGS**DIQMTQSPSF LSTSLGNSITITCHASQNIKGWLAWYQQKSGNAPQLLIYKASSLQSGVP SRFSGSGSGTDYIFTISNLQPEDIATYYCQHYQSFPWTFGGGTKLEIKRA A**GGGGSGGGGSGGGGSSIINFEKLISQAVHAAHAEINEAGRGLNDIFE AQKIEWHE**
NY-ESO-1-DEC-205 scFv fusion (MG38-3) (Birkholz et al., 2010; Guo et al., 2000) 34.1 kDa ε – 58,120 $M^{-1}cm^{-1}$	EVQLQQSGPVLVKPGASVKMSCKASGNTFTDSFMHWMKQSHGKSLE WIGIINPYNGGTSYNQKFKGKATLTVDKSSSTAYMELNSLTSEDSAVYYC ARNGVRYYFDYWGQGTTLTVSSASGA**GGGGSGGGGSGGGGS**AAQPA MADYKQAVVTQESALTTSPGETVTLTCRSSTGAVTISNYANWVQEKPDH LFTGLIGGTNNRAPGVPARFSGSLIGDKAALTITGAQTEDEAIYFCALWY NNQFIFGSGTKVTVL**GGGGSGGGGSGGGGS**ARGPESRLLEFYLAMPF ATPMEAELARRSL**SLLMWITQC**GLNDIFEAQKIEWHE

25 µl PCR amplification was performed with 5 µL Q5 5x reaction buffer (#B9027S, NEB), 0.5 µL 10 mM dNTPs (#N0447, NEB), 1.25 µL of each primer from 10 µM stock, 0.5 µl (5 ng) of template DNA, 0.25 µL of Q5 Hi-Fi DNA polymerase (#M0491S, NEB), and 16.25 µL of NFW. PCR was performed in a SimpliAmp thermal cycler (Table 2.3).

Table 2.3 PCR Amplification Reaction Conditions

Step	Temperature	Time	Cycles
Initial denaturation	98°C	30 sec	
Denaturation	98°C	10 sec	X30
Annealing	**X***	20 sec	
Extension	72°C	**Y*** sec	
Final extension	72°C	2 min	
Finished	4°C	Hold	

***Annealing Temperatures for amplification (Y = 30 sec) (X):**
Bsa4/MBP2 OVA-ROP primers: **65°C**
CTH0 OVA-ROP primers: **61°C**
pSUMO OVA-ROP primers: **62°C**
CTH0 OVA/NY-ESO-1 pelB scFv fusion primers: **66°C**
pSUMO OVA scFv fusion primers: **62°C**
pSUMO NY-ESO-1 scFv fusion primers: **66°C**
pFUSE tOVA-ROP primers: **66°C**

***Annealing Temperatures for mutagenesis (Y = 120 sec) (X):**
pFUSE-mIgG2a-Fc2$_{IgM}$ tailpiece insertion: **67°C**
pFUSE-mIgG2a-Fc2$_{Q94C+IgM}$ mutation: **72°C**

Inserts for pNIC28-Bsa4, pNIC-MBP2-LIC, pNIC-CTH0 and pSUMO-LIC vectors, 3 µl of each PCR product were run on a 1.5% agarose gel to check for correct insert amplification (Materials and Methods 2.1.1) and proceeded to ligation-independent cloning (Materials and Methods 2.1.8).

2.1.8 Ligation Independent Cloning of OVA-ROP and DEC-205 scFv Constructs

Expression vectors underwent restriction digest consisting of 5 µl of CutSmart buffer (#B7204 NEB) for BsaI or 3.1 buffer (#B7203 NEB) for BfuAI, 5 µg of DNA, 1.5 µl of restriction enzymes, made up to 50 µl with NFW. pNIC28-Bsa4, pNIC-MBP2-LIC and pSUMO-LIC vectors (Appendix III) (Centre for Medicines Discovery (CMD), UK) were digested with BsaI (#R0535, NEB) at 37°C for 2 hours. pNIC-CTH0 was treated with BfuAI (#R0701, NEB) at 50°C for 2 hours. Vectors and amplified inserts were purified

by a Qiaquick PCR purification kit (#28106, Qiagen) according to the manufacturer's protocol. Vector and insert were treated with T4 DNA polymerase (#M0203, NEB). For the vectors, 50 µL of digested plasmid was added to 21.5 µL of NFW, 10 µL of CutSmart buffer, 1 µL of bovine serum albumin (BSA, #B9000, NEB), 5 µL of 100 mM dithiothreitol (DTT, #M02712, Fluorochem), 2.5 µL of T4 polymerase, and 10 µL of 25 mM dNTP (#N0446, NEB) depending on the vector (Table 2.4). For the inserts, 5 µL of insert DNA was added to 2.15 µL of water, 1 µL of CutSmart buffer, 0.1 µL of BSA, 0.5 µL of 100 mM DTT, 0.25 µL of T4 DNA polymerase, and 1 µL of 25 mM dNTP depending on vector backbone (Table 2.4). T4 DNA polymerase reaction was performed at 22 °C for 30 minutes, followed by 20-minute heat-inactivation at 75°C.

Table 2.4 dNTPs for Vector and Insert Polymerisation

Vector	dNTP for Vector Polymerisation	dNTP for Insert Polymerisation
pNIC28-Bsa4	dGTP	dCTP
pNIC-MBP2-LIC	dGTP	dCTP
pSUMO-LIC	dTTP	dATP
pNIC-CTH0	dCTP	dGTP

T4-treated vector and insert were annealed by a 1:4 ratio of vector to insert at room temperature for 30 minutes. 3 µl of the annealed sample were transformed into Mach1 competent *E. coli* cells (Materials and Methods 2.1.2).

Colonies were picked and screened by PCR colony screen and overnight cultured (Materials and Methods 2.1.3). Overnight cultures were prepared for glycerol stocks and DNA purified (Materials and Methods 2.1.4 and 2.1.5). Plasmid-prepared constructs were sent off for sequencing using pLIC-fwd and -rev (Appendix III) (Materials and Methods 2.1.6). Sequence-confirmed constructs were transformed into Rosetta (DE3) *E. coli* (Materials and Methods 2.1.2). Glycerol stocks were created (Materials and Methods 2.1.4) and stored at -80°C until needed.

2.1.9 Cloning of OVA-ROP-Fc and pFUSE Constructs

For the zeocin selection of pFUSE mouse IgG2a-FC2 (pFUSE-mFc) vector (Appendix III) (#PFUSE-MG2AFC2, Invivogen), 1 L of autoclaved Luria low salt LB (Appendix II) and 1 L of Luria low salt LB with agar (Appendix II) was prepared and autoclaved. Zeocin antibiotic (#ANT-ZN-1P, Invivogen) at 100 mg/mL (4000x) stock in double distilled water (ddH_2O) was added to a final 25 µg/mL concentration to all cultures. pFUSE-mFc vector was transformed into Mach1 competent *E. coli* (Materials and Methods 2.1.2), plated, grown overnight and inoculated into 1 mL of liquid culture for overnight incubation. Glycerol stocks were created (Materials and Methods 2.1.4), and DNA plasmid preparation was performed (Materials and Methods 2.1.5).

tOVA-ROP was synthesised as a gene fragment by Integrated DNA Technologies Inc. and PCR amplified with primers to insert EcoR1 and BglII restriction sites for insertion into the pFUSE-mFc vector (pFUSE-tOR-fwd & -rev) —sequence and primers in Appendix III. PCR was performed with pFUSE-tOR-fwd & -rev primers (Materials and Methods 2.1.7), and products were run on a 1.5% agarose gel, with the 200 bp insert gel extracted (Materials and Methods 2.1.1). DNA concentration was measured by Nanodrop One spectrophotometer.

pFUSE-mFc vector and tOVA-ROP insert were prepared for ligation by a double restriction digest. For pFUSE-mFc, 5 µg (8 µL) of DNA was added with 5 µl 3.1 buffer, 1.5 µL EcoRI (#R0101, NEB) and 1.5 µL of BglII (#R0144, NEB) enzymes in NFW to a final volume of 50 µL. For the newly synthesised OVA insert, 0.56 ng (34 µL) of DNA was added with the same volumes of buffer and enzyme and made up to 50 µl. Digests were incubated overnight at 37°C.

Double digest of the vector was run on 1.5% agarose gel to confirm the vector's linearisation (Materials and Methods 2.1.1). OVA inserts were purified by a Qiaquick PCR purification kit following the standard manufacturer's protocol. Ligation was performed using a T4 ligase reaction. 50 ng of vector (1 µL) was added to 2 µl of T4 ligase buffer (#B0202S, NEB), 1 µl of T4 ligase (#M0202S, NEB), 1 µL of OVA insert (7.2ng, 1:3 vector to insert ratio) and made up to 20 µl with NFW. A vector-only control was set up to observe the degree of self-ligation.

Ligations were incubated for 30 minutes at room temperature, followed by heat-inactivation at 65°C for 10 minutes. 5 µl of each ligation was transformed into 50 µl of Mach1 *E. coli* (Materials and Methods 2.1.2) and plated onto zeocin$^+$ Low-salt LB agar plates for overnight incubation at 37°C. Colonies were picked and screened by PCR with primers used for gene insert and inoculated into zeocin$^+$ Low-salt LB broth (Materials and Methods 2.1.3). PCR products were run on 1.5% agarose gel (Materials and Methods 2.1.1). Overnight cultures were prepared for glycerol stocks and DNA purified (Materials and Methods 2.1.4 and 2.1.5). Plasmid-prepared constructs were sent off for sequencing using pFUSE-tOR-fwd and -rev primers (Appendix III).

For the development of the pFUSE-mIgG2a-Fc2$_{IgM}$ (mFc-IgM) and pFUSE-mIgG2a-Fc2$_{Q94C+IgM}$ (mFc$_{QC}$-IgM) construct, the process began with inserting the mouse IgM tailpiece into the pFUSE-Fc vector to create mFc-IgM. Primers were designed to insert 54 base pairs using back-to-back flanking primers (Mu IgM Q5 mutagenesis-fwd & -rev; Appendix III) for PCR mutagenesis (Materials and Methods 2.1.7; amino acid sequences and features are in Table 2.2).

10 µl of PCR products were run on 1% agarose gel to confirm the successful reaction (Materials and Methods 2.11). Positive PCR product was processed with kinase ligase

DpnI (KLD) reaction to ligate the blunt ends and remove template DNA. 1 µl of PCR product was mixed with 5 µl of KLD buffer (#B0554A, NEB), 3 µl NFW and 10x KLD enzyme mix (#M0554S, NEB). The reaction was incubated for ten minutes at room temperature. 5 µl of reaction and no KLD treatment control were transformed into Mach1 cells (Materials and Methods 2.1.2) on zeocin$^+$ low salt LB-agar plates for overnight culturing at 37°C. Positive colonies were picked and grown overnight in 1-2 mL of zeocin$^+$ low salt LB at 37°C. Glycerol stocks were made with overnight culture (Materials and Methods 2.1.4), and the remaining DNA was purified by plasmid preparation (Materials and Methods 2.1.5) and quantified by Nanodrop One spectrophotometer. DNA was sent off for sequencing with pFUSE-tOR-fwd and Fc-seq-rev primer (Appendix III) to confirm mutagenesis.

For Q94C single-point mutagenesis (mFc$_{QC}$-IgM), Fc-IgM was used as a template and single-point mutagenesis was performed by Q5 mutagenesis protocol with Q94C mutagenesis-fwd and -rev primers (Appendix III) (Materials and Methods 2.1.7). Reactions confirmed by 0.8% agarose gel (Materials and Methods 2.1.1) and 20 µl of PCR reactions were set up for DpnI digest to remove the parental template. Reactions were performed in 20 µl with 5 µl of CutSmart buffer, 14 µl of NFW and 1 µl DpnI (#R0176, NEB). The reaction was incubated for 30 minutes at 37°C. A Qiaquick PCR purification kit purified samples according to the standard manufacturer's protocol. The sample was measured on a Nanodrop One spectrophotometer. The purified linear construct was prepared for In-Fusion ligation by 2.5 µl (100 ng) of construct added to 5.5 µl of NFW and 2 µl of In-Fusion master mix (#638948, Takara Bio). The reaction proceeded at 50°C for 15 minutes. 5 µl of reaction and vector-only control was transformed into Mach1 cells (Materials and Methods 2.1.2). Transformants plated onto zeocin$^+$ low salt LB agar plates and incubated overnight at 37°C.

Positive colonies were picked and inoculated into zeocin$^+$ low salt LB broth and incubated overnight at 37°C, 700 RPM. Overnight cultures were made into glycerol stocks and plasmid-prepared (Materials and Methods 2.1.4 and 2.1.5). DNA was measured and sent off for sequencing using pFUSE-tOR-fwd and FC-Seq-rev primers (Appendix III).

2.2 Tissue Culture

2.2.1 Cell Lines and Tissue Culturing

DC2.4 cells were a kind gift from Prof. Kenneth L. Rock (University of Massachusetts, USA). B3Z Hybridoma cells were a kind gift from Prof. Edd James (University of Southampton, UK). DC2.4 and B3Z cells were cultured in Roswell Park Memorial Institute-1640 (RPMI-1640) with L-glutamine (R8758-500ML, Sigma-Aldrich), supplemented with 10% heat-inactivated foetal bovine serum (FBS) (#10500064, Gibco), 10 mM (4-(2-hydroxyethyl)-1-piperazineethanesulphonic acid) (HEPES, #H0887, Thermo Fisher), 1 x minimal essential media non-essential amino acids (NEAA) (#11140050, Gibco), 50 µM β-mercaptoethanol (βME) (#31350010, Gibco). βME was added fresh at each passage. Human embryonic kidney 293 cells (HEK293) cells were cultured in high glucose Dulbecco's modified eagle medium (DMEM) with L-glutamine (#11965092, Gibco) supplemented with 10% FBS. All cells were cultured from 96-well to 6-well (Corning) and cell culture flasks from T25 to T175 (Greiner) at 37°C, 5% carbon dioxide (CO_2) in a humidified incubator.

DC2.4 and HEK293 cells were routinely cultured in T75 flasks (#658170, Greiner) and passaged every 3-4 days at a 1:10 ratio. Passaging was performed by removing cell culture media and gently washing the surface twice with Dulbecco's phosphate-buffered saline (DPBS) (#14190144, Gibco), followed by incubation with 0.25% trypsin

and 0.02% ethylenediaminetetraacetic acid (EDTA) (Trypsin-EDTA, #T3924, Sigma-Aldrich) for 5-10 minutes or until cells dissociated. Trypsin was neutralised with media, and cells were pelleted by centrifugation at room temperature, 300 x g, for 5 minutes. The cell pellet was resuspended in media with a split taken depending on the ratio needed.

B3Z is a semi-adherent cell line split by removing adherent cells lightly with a cell scraper (#F238237W, Greiner) and combining them with suspension cells. Cells were counted using a Neubauer haemocytometer (#AC1000, Hawksley) with a 1:2-1:4 ratio of culture to 0.4% trypan blue solution (#T8154-100ML, Sigma-Aldrich) and passaged daily to a density of between 0.20-0.30x10^6 cells/mL in 20-30 mL of media in a T75 flask.

Expi293F suspension cells (#A14528, Life Technologies) were cultured in FreeStyle 293 expression medium (#12338-018 Thermo Fisher) for routine passage in 60 mL cultures in a 250 mL vented, non-baffled cell culture flask (#431144 Corning) at 150 RPM in a 37°C, 8% CO_2, 75% humidity. Cells were seeded at 0.4x10^6 cells/mL and passaged every 3-4 days.

2.2.2 Cryopreservation of Cell Lines

Cells were counted as outlined (Materials and Methods 2.2.1), centrifuged at 300 x g for 5 minutes, and the supernatant discarded. Cells were resuspended in freezing media consisting of 90% FBS with 10% dimethyl sulphoxide (DMSO) (#D8418, Sigma-Aldrich) to a density of 2-4x10^6 cells/mL, with 1 mL aliquoted into 1.5 mL cryogenic vials (#72379992, Sarstedt). Vials were placed in a CoolCell LX freezing container (#432002, Corning) and frozen overnight at 1°C/min in -80°C freezer. Cells were transferred to a vapour-phase liquid nitrogen tank for long-term storage.

Cells were recovered by warming vials in a 37°C water bath until just thawed and slowly topped up to 10 mL with culture media. Cells were centrifuged at 300 x g for 5 minutes, resuspended in fresh culture media, and incubated at 37°C, 5% CO_2 in a humidified cell incubator for 24 hours. After 24 hours, the media was changed with fresh, complete media appropriate for each cell line and returned to the incubator.

2.3 OVA-ROP Protein Expression and Purification

2.3.1 SDS-PAGE and Gel Transfer

For reduced loading, 5 µl of 4x NuPAGE lithium dodecyl sulphate (LDS) sample buffer (#NP0007, Invitrogen) containing 200 mM DTT was added to 2-5 µg of protein and topped up to 20 µl with ddH_2O. For non-reduced loading, 2-5 µg of protein in 15 µl was added to 5 µl 4x NuPAGE LDS sample buffer without DTT. Other volumes were used as described.

Samples were boiled at 95°C for 10 minutes and pulse centrifuged. Samples for sodium dodecyl sulphate–polyacrylamide gel electrophoresis (SDS-PAGE) were run on 1.0 mm 4-12% bis-(2-hydroxy-ethyl)-amino-tris(hydroxymethyl)-methane (Bis-Tris) NuPAGE 26-well gel (#WG1403A, Invitrogen) in NuPAGE midi gel tank (#16611116, Invitrogen) containing 1 L of 1 x 2-(N-morpholino)ethanesulphonic acid (MES) running buffer (Appendix II). For larger volumes (20-30 µl), 4-20% Mini-PROTEAN TGX precast protein gels, 10-well, 50 µl (#4561094, Bio-Rad) were used with Mini-PROTEAN tetra cell tank (#1658004EDU, Bio-Rad).

Samples were run against 10 µl of Precision Plus unstained protein standard (#1610363, Bio-Rad) for SDS-PAGE and PageRuler pre-stained protein ladder (#11832124, Thermo Fisher) for western blot analysis. Gels were run at 180 V for 40-45 minutes.

Ethanol precipitation was performed for guanidine hydrochloride (GuHCl) samples loaded on SDS-PAGE, adapted from the published protocol (Pepinsky, 1991). 5 µl of GuHCl solubilised protein was added to 200 µl of absolute ethanol (#32221-M, Sigma-Aldrich), vortexed briefly and incubated at -20°C for 1 hour. The samples were centrifuged at 16,000 x g at room temperature for 10 minutes, and the supernatant was removed. The pellet was resuspended in 50 µl of 1x NuPAGE LDS sample buffer diluted in DPBS. A 5-10 µl sample was loaded on SDS-PAGE.

For SDS-PAGE analysis, gels were stained with InstantBlue Coomassie protein stain (#ab119211, Abcam) for 1-2 hours, then destained in ddH_2O for 1-2 hours. Gels were imaged on the ChemiDoc imaging system.

For western blot analysis, gels were placed in a Trans-Blot turbo midi 0.2 µm polyvinylidene fluoride (PVDF) transfer pack (#1704157, Bio-Rad) and transferred by Trans-Blot turbo transfer system (Bio-Rad) using the 7-minute turbo transfer protocol. The membrane was washed briefly with 1 x PBS-Tween (PBS-T; 1 x DPBS, 0.1% TWEEN-20 (#P7949, Sigma-Aldrich) and blocked with blocking buffer (Appendix II) for 1 hour. Membranes then progressed to the primary antibody staining, described appropriately.

2.3.2 Protein Concentration Calculation by BCA Assay

The Pierce bicinchoninic acid (BCA) protein assay kit (#23225, Thermo Fisher) was used per the manufacturer's protocol. A 25 µg/mL to 2 mg/mL BSA standard curve was made by serial dilution from 2 mg/mL stock in 100 µl with 25 µl used in triplicate in 96-well plates and included zero blank; other ranges used were indicated. Lysates from cathepsin S small interfering RNA (siRNA) transfection were thawed, diluted 1:2-1:10 in DPBS, and aliquoted at 25 µl per well in a 96-well plate. Purified protein was diluted

based on the estimated concentration from the Nanodrop One spectrophotometer. 200 µl of BCA reaction mixture was made according to the manufacturer's protocol and added to each standard and unknown. Plates were incubated at 37°C for 30 minutes, and absorbance of 562 nm was measured on a Thermo Fisher Varioskan LUX multimode microplate reader. Assay concentrations were calculated using standard curve linear regression and interpolation on GraphPad Prism software.

2.3.3 OVA-ROP Test Expression and Purification From *E. coli*

Rosetta (DE3) glycerol stocks were inoculated into 1 mL of terrific broth (TB) media (TRB0102, Formedium) containing 50 µg/mL of kanamycin and incubated at 37°C, 700 RPM to an absorbance at 600 nm of 2-3. Cultures were cooled to room temperature, induced with 0.1 mM isopropyl ß-D-1-thiogalactopyranoside (IPTG) (#R0392, Thermo Scientific), and incubated at 18°C, 700 RPM overnight. Cultures were harvested by centrifugation at 3,000 x g for 20 minutes. Pellets were resuspended in 200 µl of *E. coli* lysis buffer (Appendix II) and freeze-thawed to break them open. A 3 µl sample of each lysate was diluted in 27 µl of water and 10 µl of sample buffer for SDS-PAGE analysis (Materials and Methods 2.3.1). Lysed cultures were clarified by centrifuging at 3,000 x g for 20 minutes.

50 µl of 50% Ni Sepharose 6 fast flow histidine-tagged protein purification resin (Ni^{2+} Resin, #17531801, Cytiva) resin per sample was aliquoted into a Multiscreen 96-well 1.2 µm filter plate (#MSBVS1210, Merck Millipore) and washed twice with 125 µl of ddH_2O by vacuum filtration, followed by three washes with *E. coli* lysis buffer (Appendix II). Clarified lysate was aliquoted onto the plate, sealed and incubated for 1 hour at 18°C, 400 RPM in a Glas-Col shaking incubator. Clarified lysate was filtered through the resin, followed by three 200 µl washes in wash buffer (Appendix II). The residual wash buffer was removed by centrifuging the plate at 300 x g for 1 minute,

and 40 µl of elution buffer (Appendix II) was added. The plate was sealed and incubated for 20 minutes at 18°C, 400 RPM. Protein was eluted from the resin by centrifuging it into a 96-well plate at 300 x g for 3 minutes. 40 µl eluate (soluble fraction) was mixed with 15 µl of sample buffer for SDS-PAGE analysis (Materials and Methods 2.3.1).

2.3.4 OVA-ROP Inclusion Body Denaturation and Purification

Inoculated 1 L of TB-kanamycin with 10 mL of overnight Rosetta (DE3) *E. coli* cultures, the culture was grown at 37°C, 200 RPM to an absorbance at 600 nm of between 2-3, induced with 0.1 mM IPTG and incubated overnight at 18°C, 200 RPM. Cultures were harvested by centrifugation at 3,000 x g for 20 minutes, and pellets were resuspended in 30 mL *E. coli* lysis buffer (Appendix II), followed by sonication at 35% amplitude, 5 seconds on, 10 seconds off for 40 cycles. Samples were centrifuged at 30,000 x g for 20 minutes to pellet inclusion bodies. The inclusion body (IB) pellet was washed with 40 mL IB wash buffer (Appendix II). IB suspensions were re-centrifuged at 30,000 x g for 20 minutes and weighed. Pellets were suspended into either urea pH 7.5 buffer, urea pH 5.0 buffer, GuHCl pH 7.5 buffer, or GuHCl pH 5.0 buffer (Appendix II) at a w/v ratio of 1:25 or 1:50 (1:10 Urea buffer as control). Resuspended inclusion bodies were incubated for 2 hours at 4°C on a 15 RPM rotating wheel and centrifuged at 30,000 x g for 20 minutes. Samples were filtered by a Minisart 0.2 µm Polyethersulphone (PES) syringe filter (#16532K, Sartorius).

1 mL of Ni^{2+} resin per sample was prepared by washing in 5 mL of water twice, followed by 6 mL of GuHCl pH 7.5 buffer (Appendix II). The prepared resin was added to the 1:25 w/v GuHCl solubilised samples and incubated overnight on a rotating wheel at 4°C, 15 RPM. The resin was pelleted by centrifugation at 600 x g for 5 minutes, and samples of supernatant and resin were taken for SDS-PAGE analysis (Materials and

Methods 2.3.1). The resin was washed with 5 mL of GuHCl wash buffer (Appendix II) and re-centrifuged. 1 mL GuHCl elution buffer (Appendix II) was added to each resin and incubated for two hours, rotating at 4°C, 15 RPM. Eluate was collected by centrifuging at 600 x g for 5 minutes.

2.3.5 Solubility Testing of Denatured OVA-ROP

QuickFold protein refolding kit (#0600, AthenaES) was used to screen refolding conditions according to the manufacturer's protocol. Complete list of buffers in Appendix II. 50 µl of OVA-ROP at 1 mg/mL in GuHCl elution buffer (Appendix II) was added dropwise to 950 µl of each buffer while vortexing. Samples were incubated at room temperature for 1 hour. 12 µl of sample was added to 4 µl of SDS loading buffer for SDS-PAGE analysis (Materials and Methods 2.3.1). Samples from the buffer screen were concentrated by 10 kDa molecular weight cut-off (MWCO) Vivaspin 2mL centrifugal concentrators (#VS02H01, Sartorius) to between 70 and 80 µl. Samples were normalised by volume, and 12 µl was mixed with 4 µl of SDS-PAGE loading buffer and run on SDS-PAGE gel (Materials and Methods 2.3.1).

ROP 'refolding' was assessed with four methods: fast dilution, slow dilution, dialysis, and on-column refolding. Fast dilution was performed by diluting 1 mL of GuHCl purified OVA-ROP samples at 1 mg/mL dropwise into 10 mL of ROP refolding buffer (Appendix II) with and without 50 mM L-arginine (#W381918, Sigma-Aldrich) while vortexing. Samples were incubated on ice for 1 hour. Slow dilution was performed by adding 10 mL of buffer dropwise to the 1 mL of ROP at 1 mg/mL. On-column refolding was assessed by binding to 1 mL of Ni^{2+} resin in GuHCl pH 7.5 buffer (Appendix II) and reducing GuHCl concentration stepwise with five-column volume (CV) washes in 4 M, 2 M, 1 M, and 0 M GuHCl pH 7.5 buffer (Appendix II) before eluting off the column with elution buffer (Appendix II). Dialysis was performed by dialysing 3 mL of OVA-

ROP at 1 mg/mL sequentially in 1 L of 4 M, 2 M, 1 M, and 0 M GuHCl pH 7.5 buffer (Appendix II) with two hours between buffer changes. Samples were concentrated using 10 kDa MWCO 20 mL Vivaspin.

A detergent screen experiment was set up on OVA-ROP using N-dodecyl-beta-maltoside (DDM, #850520P, Avanti), 3-((3-cholamidopropyl)dimethylammonio)-1-propanesulphonate (CHAPS, #850500P, Avanti) and N-lauroylsarcosine (sarkosyl, #61745, Sigma-Aldrich) at 0.1%, 0.5%, and 1.0%. In 20 mL of detergent screen buffer (Appendix II). While vortexing, 500 µg of OVA-ROP from a 1 mg/mL stock was added slowly to each detergent test. Detergent test samples were concentrated using 10 kDa MWCO 20 mL Vivaspin centrifugal concentrators between 1 and 1.5 mL. Samples were taken for SDS-PAGE analysis (Materials and Methods 2.3.1).

2.3.6 Sarkosyl Solubilisation of OVA-ROP

0.5 g of the inclusion body pellet was resuspended in 2 mL of 1% sarkosyl or 10% sarkosyl buffer (Appendix II) and incubated for 1 hour at 4°C. Tubes were centrifuged at 20,000 x g for 10 minutes at 4°C to pellet insoluble material, and samples were taken for SDS-PAGE analysis (Materials and Methods 2.3.1). The 1% and 10% sarkosyl samples were diluted 1 in 4 and 1 in 40 to reduce sarkosyl concentration to <0.25% for compatibility with nickel resin. 0.5 mL of Ni^{2+} resin was prepared per sample by washing twice in 5 mL water and three 5 mL washes in sarkosyl binding buffer (Appendix II) and incubated with samples overnight at 4°C with gentle rotation.

The following day, the resin was pelleted by centrifugation at 500 x g for 5 minutes and washed three times with 5 mL of sarkosyl wash buffer (Appendix II), followed by elution with 1 mL of sarkosyl elution buffer (Appendix II). Samples were concentrated by 10k MWCO 2 mL Vivaspin, then dialysis into ROP dialysis buffer (Appendix II).

Concentration was calculated by BCA assay (Materials and Methods 2.3.2) and sampled for SDS-PAGE analysis (Materials and Methods 2.3.1). Endotoxin was removed by Pierce endotoxin removal kit (#88275, Thermo Scientific) according to the manufacturer's protocol and quantified by Pierce endotoxin quantification kit according to manufacturer's protocol, to be less than 1.0 endotoxin units per mL (EU/mL) (#A39552, Thermo Scientific). Later optimisations allowed protocol with 0.1% sarkosyl binding, washing and elution buffers following the same procedure outlined.

2.3.7 Sarkosyl Turbidimetric Assay

The sarkosyl turbidimetric assay was adapted from the Novagen protein refolding kit protocol and based on published literature (Kurucz et al., 1995). A standard curve from 0% to 0.03% sarkosyl was created in the ROP dialysis buffer (Appendix II). Sarkosyl purified samples from Materials and Methods 2.3.6 protocol at 1 mg/mL were diluted 1:50, 1:75, 1:100, 1:200, and 1:500 in the buffer. The dilutions were repeated for GuHCl solubilised OVA-ROP (Materials and Methods 2.3.4) using the same dilution series in GuHCl pH 7.5 buffer (Appendix II). 200 µl of each sample, and the standard curve was added to a flat-bottomed 96-well plate (#3595, Corning), and 200 µl of buffer only as a negative control. To each sample, standard and control 20 µl of 1 M hydrochloric acid (#1003172510, Merck) was added and incubated at room temperature for 5 minutes. Plates were measured for turbidity by absorbance at 405 nM on the Varioskan LUX multimode microplate reader. A sigmoidal, four-parameter logistic regression curve was generated from the standard curve on GraphPad Prism. The sarkosyl concentration was interpolated from the curve before multiplying by the dilution factor for the final sarkosyl concentration.

2.3.8 TEV Cleavage of OVA-ROP

Tobacco etch virus (TEV) protease cleavage was performed by adding 2 µl of TEV protease (provided by CMD, Oxford, UK) and 1 mM DTT to 48 µl of OVA-ROP at 1.18 mg/mL in 0.1% sarkosyl buffer (Appendix II). A control was set up with ROP only and enzyme only. The reaction was incubated overnight at 4°C. 5 µl of digested samples were run on SDS-PAGE with the controls to analyse (Materials and Methods 2.3.1).

2.3.9 Cathepsin S Protease Assay With Tryptic Digest Tandem Mass Spectrometry

For cathepsin S protease assay, 20 µL of 10 µM (0.18 mg/mL) of OVA-ROP in 0.1% sarkosyl buffer (Appendix II) was diluted with 80 µL of 100 mM sodium acetate (#S2889, Sigma-Aldrich), 4 mM DTT to a final concentration of 20 mM sodium acetate, 1 mM DTT pH 6.5. Recombinant human cathepsin S (#10487-H08H, Sino Biological) and recombinant mouse cathepsin S (#50769-M08H, Sino Biological) were resuspended with 70 µl of DPBS to 0.15 mg/mL and 0.26 mg/mL, respectively. 0.1 µg of either recombinant human or mouse cathepsin S was added to the test samples. A no-enzyme and enzyme-only control test was also performed. Plates were incubated overnight at 37°C. 12 µl of each test and control were loaded onto reducing SDS-PAGE for analysis (Materials and Methods 2.3.1).

Gel band protein identification was performed by excising bands from SDS-PAGE gel and submitting it to the CMD mass spectrometry unit operated by Dr Rod Chalk. Tryptic digestion tandem mass spectrometry was performed on a Bruker high-capacity ion trap liquid chromatography with tandem mass spectrophotometer. Data presented as a Mascot MOWSE (molecular weight search) score compared against the internal CMD Database, containing the OVA-ROP sequence (QQ01OVAGGA-c001) and Swiss-Prot protein database. A score >50 ($p \leq 0.05$) is considered a significant match.

2.4 Fc and scFv Fusion Expression and Purification

2.4.1 Transfection and Expression Analysis of OVA-ROP-Fc in Mammalian Cells

From glycerol stocks, 50 mL of zeocin$^+$ low salt LB broth was inoculated with OVA-ROP-Fc, pFUSE-Fc, mFc-IgM, and mFc$_{QC}$-IgM for overnight incubation at 37°C. Midi-prep DNA plasmid preparation purified the four constructs (Materials and Methods 2.1.5), and DNA concentration was measured by Nanodrop One spectrophotometer. 5 mL of DNA solution was ethanol precipitated by adding 1/10 (0.5 mL) volume of 3 M of ice-cold sodium acetate pH 5.2 followed by 2.5x (12.5 mL) of ice-cold 100% ethanol. The mixture was incubated at -20°C for 1 hour before centrifugation at 14,000 x g for 15 minutes at 4°C. The liquid was discarded, and 200 µL of ice-cold, 70% ethanol was added and mixed to dislodge the pellet into suspension. The tube was centrifuged at 14,000 x g for 10 minutes, ethanol was removed, and the pellet was airdried in a tissue culture hood. The pellet was resuspended with 200 µl of sterile-filtered tris(hydroxymethyl) aminomethane (Tris) -EDTA (TE, #93283, Sigma-Aldrich) buffer to yield 1.31 µg/mL of DNA.

HEK29a cells were seeded at 0.1x10^6 cells/well into 24-well plates (#3524, Corning) in culture media and incubated overnight at 37°C, 5% CO_2. The next day, 4-10 µl of lipofectamine (LFA) 2000 (#11668019, Invitrogen) was added to 100 µl of Opti-minimal essential media (Opti-MEM; #31985062, Gibco), and 5 µg of OVA-ROP-Fc plasmid DNA was added to another 250 µl of Opti-MEM. A no DNA Opti-MEM control and 5 µg CMV-promotor green fluorescent protein (GFP) positive control vector (Kind gift from Prof. Len Seymour, University of Oxford, UK) were also included. 100 µl of the LFA mixes were added to each plasmid (2 µg) or control mixture and incubated at room temperature for 5 minutes. Media was removed from HEK293 overnight wells and

gently washed with DPBS. 0.5 mL of DMEM without FBS was added to each well. 50 µl of transfection or control mixture were added to each well in quadruplicate and incubated for 6 hours. After 6 hours, transfection media was removed and replaced with DMEM with 10% FBS for 48-72 hours at 37°C, 5% CO_2.

Cells were harvested by removing media, washing with 2 mL of ice-cold DPBS, and adding 100 µl of ice-cold radioimmunoprecipitation assay buffer (RIPA) buffer (#89901, Thermo Scientific) containing 1x HALT protease inhibitor cocktail (#78429, Thermo Scientific), and 1:10,000 Benzonase nuclease, >90% purity (#70746, Merck Millipore), incubating on ice for 15 minutes. Debris was pelleted by centrifugation at 15,000 x g, 4°C for 15 minutes and proceeded to BCA assay (Materials and Methods 2.3.2). Normalised samples were run on SDS-PAGE and transferred to a membrane for western blot (Materials and Methods 2.3.1).

Western blot membranes were stained with goat anti-mouse IgG2a and Fc gamma specific antibody (#33416S, Cell Signaling Technology) overnight at 1:5000 in blocking buffer (Appendix II) at 4°C. Membranes were subsequently washed thrice with 10 mL of PBS-T (Appendix II) and developed with 1 mL of SuperSignal West Dura extended duration enhanced chemiluminescence (ECL) substrate (#34075, Thermo Scientific) for 3-5 minutes and imaged on a BioRad ChemiDoc Imager.

Expi293F cells were seeded $2x10^6$ cells/mL in 250 mL of FreeStyle 293 media in a 2 L roller bottle (#430849 Corning) and allowed to settle for 20 minutes. In a sterile 50 mL tube, 250 µg of DNA was added to 5 mL of Opti-MEM (#210231, Greiner). In another tube, 750 µg of linear-polyethylenimine (#765090, Merck) was added to 5 mL of pre-warmed Opti-MEM. Tubes were incubated at room temperature for 5 minutes, and the DNA mixture was added to the PEI mixture (1:3 ratio). The tube was inverted

briefly and incubated at room temperature for 30 minutes. Meanwhile, 10 mM sodium butyrate (#A11079.22, Alfa Aesar) was added to the cells from 1 M stock. After 30 minutes, the DNA-PEI mixture was added slowly to the cells in the roller bottle. The roller bottle was incubated at 37°C, 5% CO_2, and 170 RPM at 75% humidity for 5 days. Cells were harvested by centrifugation at 1,500 x g for 30 minutes, and the supernatant was passed through a Minisart 0.45 µm PES syringe filter (#16533K, Sartorius). Supernatant and pellets were immediately used to purify OVA-ROP-Fc and pFUSE constructs.

2.4.2 Purification of OVA-ROP-Fc and pFUSE Constructs

OVA-ROP-Fc, pFUSE-Fc, mFc-IgM, and mFc$_{QC}$-IgM were purified by 1 mL HiTrap protein A HP column (#29048576, Cytiva). For purification of secreted OVA-ROP-Fc, pFUSE-Fc, mFc-IgM, and mFc$_{QC}$-IgM constructs, 1 mL HiTrap protein A column was prepared by washing with 10 CVs of ddH_2O by a peristaltic pump at 1 mL/min, followed by 10 CVs of 1x phosphate binding buffer (Appendix II). The supernatant volume was measured, and 10x phosphate binding buffer was added to 1/9th of the total volume to reach a 1x concentration. The supernatant was run at 1 mL/min by a peristaltic pump over 1 mL HiTrap protein A column. The column was washed with 10 CVs of binding buffer and eluted with 5 CVs of 100 mM citric acid (#124912500, Thermo Fisher) at pH 3.5. Eluate was fractionated into 400 µl in 1.5 mL centrifuge tubes (#313201, Greiner) containing 100 µl of 1 M Tris hydrochloride (Tris-HCl, #T3253, Sigma-Aldrich) pH 9.0. Concentrations were measured by Nanodrop One spectrophotometer by absorbance at 280 nm for OVA-ROP-Fc, pFUSE-Fc, mFc-IgM, and mFc$_{QC}$-IgM. Using the extinction coefficient for each to calculate concentration (Table 2.2; Materials and Methods 2.1.7).

For non-secreted OVA-ROP-Fc, harvest cell pellets were resuspended in 20 mL of DPBS with 1:1000 dilution of EDTA-free protease inhibitor cocktail (#ab270055, Abcam) and incubated on ice. The suspension was pulse sonicated on ice, 5 seconds on, 10 seconds off, at 35% amplitude for 1 minute. The suspension was centrifuged at 30,000 x g for 60 minutes at 4°C, and the supernatant passed through a Minisart 0.45 µM PES syringe filter. 1 mL of MabSelect protein A resin (#17519902, Cytiva) was resuspended in 5 mL water and aliquoted into a 20 mL gravity-flow chromatography column (#7321010, Bio-Rad). The column was washed with 10 CVs of water and 10 CVs of DPBS. The sample was passed through the column and was followed up with 10 CVs of DPBS. Protein was eluted off the column by 10 CVs of sodium citrate (#C8532, Sigma-Aldrich) pH 3.0 buffer by fractionation in 800 µl aliquots in 1.5 mL centrifuge tubes containing 200 µl of 1 M Tris-HCl pH 9.0 to neutralise. Fractionated samples were measured on a Nanodrop One spectrophotometer at an absorbance of 280 nm using the predicted extinction coefficient (Table 2.2; Materials and Methods 2.1.7). A BCA assay was used to accurately measure OVA-ROP-Fc concentration (Materials and Methods 2.3.2).

Samples were taken throughout the purification process to analyse and confirm the successful purification of OVA-ROP-Fc, pFUSE-Fc, mFc-IgM, and mFc$_{QC}$-IgM for SDS-PAGE and western blot. 30 µl of supernatants and 5 µl of collected pellets were added to 25 µl of DPBS, followed by 10 µl of 4x reduced SDS-PAGE sample buffer. Samples were run on SDS-PAGE for Coomassie staining and gel transfer for western blot analysis (Materials and Methods 2.3.1). Western blot analysis was performed identically to that in (Materials and Methods 2.4.1).

2.4.3 Expression and Purification of scFv Fusion Proteins

20 mL of overnight cultures picked from glycerol stocks were added to complete autoclaved 2 L TB media containing 50 µg/mL kanamycin with 20 µg/mL chloramphenicol and grown at 37°C, 200 RPM to an optical density of 1 to 2 at 600 nm as measured on Nanodrop One spectrophotometer. The flask was cooled to room temperature, and IPTG was added to 0.1 mM concentration to induce expression. Cultures were incubated overnight at 18°C, 200 RPM.

Cultures were harvested by centrifugation at 6,000 x g for 20 minutes at 4°C. The supernatant was discarded, and pellets were washed with 200 mL ice-cold DPBS and re-centrifuged at 6,000 x g for 20 minutes. PelB pellets were resuspended in 50 mL ice-cold Tris/sucrose/EDTA (TSE) buffer (Appendix II) for periplasmic extraction and incubated on ice for 1 hour. The periplasmic lysate was centrifuged at 20,000 x g for 30 minutes, and the supernatant was dialysed three times at 4°C with 2 L for 2 hours each in 7K MWCO SnakeSkin dialysis tubing (# 68700, Thermo Scientific), followed by a fourth round of dialysis overnight at 4°C. Cytoplasmic small ubiquitin-like modifier (SUMO)-tagged pellets were lysed with a SUMO lysis buffer (Appendix II) with pulse sonication at 30% amplitude, 5 seconds on, 10 seconds off for 10 minutes total. SUMO lysate was centrifuged at 20,000 x g for 30 minutes to clarify. The remaining pellet was resuspended in 40 mL of GuHCl pH 7.5 buffer (Appendix II) and incubated overnight, rotating slowly at 4°C.

1 mL of Ni^{2+} resin was prepared each for pelB and SUMO lysate and the denatured SUMO pellet. Nickel resin for pelB was equilibrated with 5 CVs of DPBS containing 10 mM imidazole (#56750, Sigma Aldrich), and SUMO nickel resin was equilibrated with SUMO lysis buffer (Appendix II). Nickel resin for denatured SUMO pellet was equilibrated with 5 CVs of GuHCl pH 7.5 buffer (Appendix II).

Equilibrated resins were incubated with respective lysates and supernatants for two hours. PelB lysate nickel resin was washed with 10 CVs of DPBS, SUMO lysate resin with 10 CVs of SUMO wash buffer (Appendix II), and GuHCl samples with 10 CVs of GuHCl pH 7.5 wash buffer (Appendix II). PelB was eluted from resin with 3 CVs of DPBS with 500 mM imidazole in 1 mL fractions. Denatured SUMO pellet nickel resin was eluted with GuHCl pH 7.5 elution buffer (Appendix II), and the protein concentration of samples was measured by absorbance at 280 nm on a Nanodrop One spectrophotometer using predicted extinction coefficients (Table 2.2; Materials and Methods 2.1.7 and Appendix III). Samples were taken for SDS-PAGE analysis (Materials and Methods 2.3.1).

2.4.4 Refolding and Tag Removal of SUMO-tagged scFv Fusion Proteins

6 mL of denatured and purified SUMO-scFv fusions at 1 mg/mL was dialysed from GuHCl pH 7.5 elution buffer into scFv refolding buffer (Appendix II) using 7K MWCO SnakeSkin dialysis tubing with 2 L of buffer for 72 hours at 4°C with gentle mixing. After 72 hours, the buffer was changed to 2 L of 50 mM TRIS-HCl pH 8.0, 150 mM sodium chloride (NaCl, #S9888, Sigma-Aldrich) and dialysed for 2 hours at 4°C, followed by another buffer change and overnight dialysis at 4°C with gentle mixing. The dialysed sample was centrifuged at 6,000 x g for 20 minutes to pellet aggregates, and the concentration of soluble fraction was measured using absorbance 280 nm on Nanodrop One spectrophotometer with predicted extinction coefficients (Table 2.2; Materials and Methods 2.1.7). Samples were concentrated to >1 mg/mL by 4 mL Amicon 10K MWCO centrifugal concentrator (#UFC801008, Merck Millipore).

SUMO tag removal was facilitated by SUMO protease. SUMO protease (CMD, UK) from 8.6 mg/mL stock was diluted to 1 mg/mL in scFv dilution buffer (Appendix II) and added from 1-5 µl (1:1000-1:20) to SUMO protease reduced or redox master mix

(Appendix II). 100 µg of the fusion protein was mixed with 80 µl of solution containing 50 mM TRIS-HCl pH 8.0, 150 mM NaCl. Then, 20 µl of the master mix was added to achieve a final ratio of SUMO protease to fusion protein (1:1000-1:20). Samples were incubated overnight at 4°C. A control tube without reducing and redox reagents was set up as a control. Tubes were centrifuged at 10,000 x g for 5 minutes to pellet any precipitate. 5 µl of supernatant was run on reduced and non-reduced SDS-PAGE (Materials and Methods 2.3.1).

Following SUMO tag removal, nickel affinity capture was used to remove SUMO protease, cleaved SUMO, and uncleaved scFv fusions. 1 mL Ni^{2+} resin was equilibrated in tag binding buffer (Appendix II). 1 mL of SUMO-treated sample was bound to the column through gravity filtration and washed with 5 mL tag wash buffer (Appendix II) followed by 1 mL of tag elution buffer (Appendix II). 5 µl eluate and resin and 10 µl of flowthrough were run on reduced SDS-PAGE (Materials and Methods 2.3.1).

2.5 Synthetic Peptides & Beads

2.5.1 Peptide Synthesis

SIINFEKL peptide was purchased commercially (#6-7015-901, IBA Life Sciences). All other synthetic peptides were custom synthesised in 4 mg quantities by Hangzhou (China) Allpeptide Biotechnology Ltd. with N-terminal acetylation and C-terminal amidation to a purity of >95% with an additional trifluoroacetic acid removal step. 1mg vials of peptide were reconstituted in DMSO to 20 mg/mL before dilution in DPBS to 100 µM stocks and aliquoted for storage at -80°C. The amino acid sequences for each peptide used in this study are in Table 2.5.

Table 2.5 Synthetic Peptide Amino Acid Sequences and Length		
Peptide Name	**Sequence Length**	**Amino Acid Sequence**
Ctss peptide	21	RENLRMKLPKPSIINFEKLTR
Mutant peptide	21	RENLRMDPPKPSIINFEKLTR
Scrambled peptide	21	RKPPLNLERKMSIINFEKLTR

2.5.2 Conjugation of OVA to Carboxylate-Modified Latex Beads

Chicken egg albumin (OVA) (#A5503, Sigma-Aldrich) was dissolved in DPBS to 1.2 mg/mL in a volume of 10 mL. The conjugation protocol was adapted from the Bangs Laboratories protocol for carboxyl-modified bead conjugation (Bangs Laboratories Inc., 2013). 2.5 mL (100 mg) of 3 µm carboxylate-modified latex beads (#C37484, Invitrogen) were centrifuged at 3,0000 x g for 15 minutes and washed twice in 10 mL of 50 mM MES pH 6.5 buffer with brief vortexing to homogenise. After the second wash, beads were resuspended in 9 mL of 50 mM MES pH 6.5 buffer. 100 mg of 1-ethyl-3-(3-dimethylaminopropyl) carbodiimide hydrochloride (EDAC) (#E2247, Invitrogen) was dissolved in 1 mL of MES pH 6.5 buffer and added immediately to a 9 mL bead solution. The mixture was incubated for 15 minutes at room temperature with constant mixing.

Afterwards, beads were centrifuged at 3,000 x g for 15 minutes and washed twice with 10 mL of DPBS pH 7.4 before resuspending in 5 mL of DPBS. To 5 mL bead suspension, 5 mL of 1.2 mg/mL (6 mg total) of OVA stock was aliquoted onto beads. The OVA bead mixture reacted at room temperature for 3 hours with constant mixing. After 3 hours, beads were centrifuged at 3,000 x g for 15 minutes, and the OVA solution was removed and retained for post-conjugation BCA assay to determine binding efficiency (Materials and Methods 2.3.2). Beads were washed twice with centrifugation in 10 mL of 0.1% glycine (#G7126, Sigma-Aldrich) in DPBS to quench the reaction.

Beads were finally resuspended in 10 mL of 0.1% glycine-DPBS and stored at 4°C until needed.

OVA binding was quantified by samples of OVA solution before and after the conjugation protocol. Protein concentrations were calculated by BCA assay (Materials and Methods 2.3.2). The mass of OVA per million beads was calculated by dividing the bound mass from the BCA assay by the estimated 6.75 x 10^9 beads used. Bead data was derived from the certificate of analysis (Lot #2301726).

2.5.3 Cathepsin S siRNA Knockdown of DC2.4 Cells

DC2.4 cells were seeded at 0.5x10^6 cells per well in 6-well plates containing 2 mL complete RPMI cell culture media. The cells were incubated at 37°C with 5% CO_2 for 24 hours. The next day, cells were observed under a microscope to ensure a confluency of between 70 and 90% for siRNA transfection. Mouse cathepsin S siRNA (#sc-29941, SantaCruz), control siRNA-A (#sc-36869, SantaCruz) and fluorescein-conjugated control siRNA (#sc-36869, SantaCruz) were reconstituted to 10 µM with NFW. Two 1.5 mL centrifuge tubes were prepared for each transfection with 150 µl of Opti-MEM. In one tube, 9 µl of RNAiMAX (#13778150, Thermo Fisher) was aliquoted, and 3 µl (25 pmol; 1x) or 6 µl (50 pmol; 2x) of cathepsin S or control siRNAs in the second tube. 150 µl of siRNA-containing media was added to a tube containing RNAiMAX-media mixture. RNAiMAX-SiRNA complex media was incubated at room temperature for 15 minutes. Media from overnight incubation was removed and replaced with 2 mL of fresh complete media. 250 µl of siRNA-RNAiMAX complexes were added slowly across the well in the 6-well plates (#657160, Greiner). For un-transfected control, 250 µl of Opti-MEM only was added. In total, three wells were set up for cathepsin S, one well for negative control siRNA-A, one well for fluorescein transfection control siRNA, and one well as an un-transfected control.

After 6 hours, media from transfection control siRNA was removed and replaced with 2 mL of DPBS. The plate was observed using a Zeiss Axiovert 25 fluorescent microscope using blue light with a green filter to observe fluorescence for transfection control. The plate was returned to the incubator for 24 hours before the replacement of the transfection mixture with complete DC2.4 media (Materials and Methods 2.2.1). Plates were returned to the incubator for a further 24 hours. Transfections were harvested after 48 hours with RIPA buffer (Materials and Methods 2.4.1). Protein concentration was measured by BCA assay (Materials and Methods 2.3.2) or stored at -20 °C until needed.

For large-scale transfection, cells were seeded at $8x10^6$ cells in 15 mL of media in T75 flasks and incubated at 37°C, 5% CO_2 for 24 hours. Cell confluency was checked under the microscope to be between 60% and 80%. For each flask, 20 µl of 100 µM mouse cathepsin S siRNA, control siRNA-A and fluorescein-conjugated control siRNA were added to 1 mL of Opti-MEM per tube, and 59 µl of RNAiMAX was added to 1 mL of Opti-MEM in another. 1 mL siRNA mixture was added to RNAiMAX mixture and incubated for 15 minutes at room temperature. 2 mL mixture was added to 15 mL of complete DC2.4 media (Materials and Methods 2.2.1) in each of the flasks for transfection. Flasks were incubated for 24 hours at 37°C, with media exchanged and flasks returned to the incubator for a further 24 hours.

Flasks were washed thrice with 15 mL of DPBS, followed by 5 mL of cell-dissociation buffer (#C5914, Sigma-Aldrich) and incubated for 10 minutes to dissociate cells from flasks. Flasks were gently tapped to dislodge cells and aliquoted into 5 mL of DC2.4 media (Materials and Methods 2.2.1). 10 µl sample of each transfection harvest was used for viable cell counting (Materials and Methods 2.2.1). Cells were seeded at 40,000 cells per well in two 96-well round-bottomed plates (#3799, Corning). The cells

were subsequently used for further peptide experimentation by B3Z assay (Materials and Methods 2.6.4).

2.5.4 Western Blot Analysis of Cathepsin S Knockdown

Lysate protein concentration from cathepsin S siRNA transfections was measured by BCA assay (Materials and Methods 2.3.2). 20 µg of lysate was loaded on SDS-PAGE gel, which was transferred to the membrane for western blot analysis (Materials and Methods 2.3.1). After blocking, 5 mL of 1:500 mouse anti-cathepsin S primary polyclonal antibody (#ab232740, Abcam) was added to the blocking buffer (Appendix II). The tube was incubated at 4°C with constant rotation overnight. Membranes were washed thrice for 5 minutes each with 10 mL of PBS-T and incubated for 1 hour at room temperature with 5 mL of 1:3000 dilution of anti-rabbit IgG horse radish peroxidase (HRP) secondary monoclonal antibody (#7074, Cell Signalling). The membrane was washed thrice with 10 mL PBS-T for 5 minutes each. The membrane was developed with 1 mL of 1:1 mixture of SuperSignal West Dura extended duration ECL substrate for 5 minutes. Western blots were placed in plastic film and visualised using a BioRad ChemiDoc imager.

For actin re-probing, membranes were washed twice and stripped using western blot stripping buffer (#21059, Thermo Scientific), re-blocked with blocking buffer and incubated for 1 hour with 1:5000 dilution of DirectBlot HRP anti-β-actin antibody (#643807, Biolegend), before washing as before and developing as before. For semi-quantification of knockdown, images were analysed in ImageJ using band intensity analysis comparing band intensity of cathepsin S normalised against actin.

2.6 Cellular Assays

2.6.1 MTS Cytotoxicity Assay

DC2.4 cells were seeded into two flat-bottomed 96-well plates at a density of $2x10^4$ cells per well in 100 µl of DC2.4 culture media (Materials and Methods 2.2.1); one lane was without cells or samples to function as a background control. OVA-ROP was added to each sample column in a dilution series between 0 to 100 µg/mL from a 0.7 mg/mL stock in 0.1% sarkosyl for the sarkosyl test. Sarkosyl was added to the second plate in each column in a dilution series between 0 and 0.1% in triplicate. The sample and cells were incubated on the plate for 16 hours at 37°C, 5% CO_2 in a humidified incubator. For synthetic peptide inhibitor (3-(4,5-dimethylthiazol-2-yl)-5-(3-carboxymethoxyphenyl)-2-(4-sulphophenyl)-2H-tetrazolium) (MTS) tests, the inhibitors were added at a concentration range as in Table 2.6

Table 2.6 Inhibitor Concentrations for MTS Assay

Inhibitor	Product Code, Company	Concentration or Range Tested
Amiloride	#0215353750, MP Biomedicals	1 mM
Chloroquine	#0219391910, MP Biomedicals	10-60 nM
Cytochalasin D	#1233/1, Bio-Techne	5 µM
Dynasore	#A1605-APE-10mg, Stratech Scientific	30 µM
Epoxomicin	# A2606-APE-1mg, Stratech Scientific	10-80 nM
LHVS	#SML2857-5MG, Merck Life Science	10-1000 nM
MG-132	# A2585-APE-10mg, Stratech Scientific	100-400 nM

Inhibitors were incubated with DC2.4 cells for 4 hours before being removed and incubated with cell culture media for 16 hours at 37°C, 5% CO_2 in a humidified incubator.

Samples were processed using CellTiter 96 AQueous one solution cell proliferation assay kit (#G3580, Promega) according to the manufacturer's protocol and incubated for 2-4 hours at 37°C, 5% CO_2 in a humidified incubator. Absorbance was measured at 490 nm on a Varioskan LUX multimode microplate reader. Cell viability was

calculated by normalising absorbance values against untreated live cells (100%) and no-cell well negative control (0%)—graphs created in GraphPad Prism.

2.6.2 Fluorescent Dye Conjugation and Confocal Microscopy

OVA was dissolved to 10 mg/mL in conjugation sarkosyl buffer (OVA-sarkosyl) (Appendix II). 1mg of Alexa Fluor 488 N-hydroxysuccinimide (NHS) Ester (#A20000, Invitrogen) was reconstituted in 100 µl of DMSO to yield a 10 mg/mL solution. 30 µl of Alexa-488 solution was added to 300 µl of OVA-sarkosyl and OVA-ROP solutions while vortexing gently protected from light. Samples were incubated with continuous, gentle mixing for 1 hour at room temperature. Unconjugated dye was removed by dialysis against 500 mL of the sample's respective buffers in 0.5 mL 7K MWCO Slide-A-Lyzer G2 dialysis cassettes (#66373, Thermo Scientific). A Nanodrop One spectrophotometer calculated concentration using the OVA and OVA-ROP extinction coefficients (Table 2.2; Materials and Methods 2.1.7 and Appendix III). DC2.4 cells were plated into a 96-well black/clear plate (#3904, Corning) at 10,000 cells/well in 100 µl of DC2.4 growth media and incubated overnight at 37°C/5% CO_2.

For confocal microscopy, the following controls were prepared: untreated cells (negative control), OVA-Alexa488 conjugate (#O34781, Invitrogen) with or without LysoTracker Red DND-99 (#L7528, Invitrogen), and LysoTracker only control. Sample wells consisted of OVA-ROP and OVA-sarkosyl with or without LysoTracker. 1mM stock of LysoTracker was diluted to 75 nM in serum-free DC2.4 media, with 100 µl added to required wells and incubated for 1 hour at 37°C, 5% CO_2.

After 1 hour, cells with LysoTracker were washed with DPBS. 50 µg/mL (2.67 µM) of OVA-ROP was prepared from the stock of conjugated samples along with an equimolar concentration of conjugated OVA-sarkosyl from stocks (115 µg/mL; 2.67

μM) in serum-free media. To the negative and LysoTracker wells, media was replaced with 100 μl of fresh serum-free media. To the positive control wells, 100 μl of diluted OVA-Alexa-488 conjugate. To the ROP-containing wells, 100 μl of ROP diluted in serum-free media was added to the well. Finally, 100 μl of respective dilutions in serum-free media were added for the OVA-sarkosyl wells. Plates were incubated for 1 hour at 37°C, 5% CO_2.

Cells were harvested by centrifugation at 300 x g for 5 minutes, with three 100 μL DPBS wash and centrifuge cycles to remove media. Cells were fixed with 100 μL of 10% neutral buffered formalin (#HT501128-4L, Sigma-Aldrich) and incubated at room temperature for 10 minutes. Cells were centrifuged at 300 x g for 5 minutes and washed twice with 100 μL of DPBS. Cell nuclei were stained by 4′,6-diamidino-2-phenylindole (DAPI; #D1306, Thermo Fisher) with 1:1000 dilution in DPBS from 1 mg/mL stock. 100 μl was added to cells and incubated for 10 minutes at room temperature. Cells were washed twice with 100 μL of DPBS and immediately imaged by confocal microscopy. Confocal imaging was performed on Zeiss 710 by 40x/1.3 (magnification/numerical aperture) oil or 63X/1.4 oil objective with excitation laser 488 nm for Alexa-488 (emission: 496 nm), 561 nm excitation for LysoTracker Red (emission: 590 nm), and 405 nm excitation for DAPI (emission: 461 nm). Images are processed in ImageJ by the maximum z-stack projection.

2.6.3 Antigen Cross-Presentation Assay by T Cell Receptor-Like Antibody

DC2.4 cells were seeded into 6-well plates at a density of $1x10^6$ cells per well in 2 mL of DC2.4 culture media. 100 μg of OVA-ROP was added to the wells to 2.7 μM and incubated for 4, 8 or 16 hours at 37°C, 5% CO_2 in a humidified incubator. SIINFEKL peptide was added at 0.3 μM to a well as a positive control and incubated for 2 hours, with one containing no samples as a blank control. Cells were detached from the plate

with gentle pipetting with DPBS and centrifuged at 400 x g for 5 minutes. The pellet was resuspended in 200 µl of MACS buffer (DPBS with 2 mM EDTA and 0.5% BSA (#A9418, Sigma-Aldrich) with 0.5 µg of CD16/32 mouse monoclonal antibody (#14-0161-82, Invitrogen) as an Fc blocker. Samples were incubated at 4°C for 10 minutes. Samples were centrifuged and washed in 200 µl of MACS buffer and counted. $1x10^5$ Cells were aliquoted into three centrifuge tubes for unstained, isotype control, and TCR antibody testing, centrifuged and resuspended in 50 µl of MACS buffer.

50 µl of MACS buffer was added to the unstained sample. 50 µl of mouse IgG1 kappa phycoerythrin (PE) isotype control (#12-4714-82, Invitrogen) in MACS buffer was added to the isotype control. To the TCR sample, 50 µl of SIINFEKL/H-2Kb PE monoclonal antibody (#12-5743-82, Invitrogen) in MACS buffer was added and incubated at 4°C for 1 hour. The sample was washed and centrifuged twice with 100 µl MACS buffer. 1:5000 dilution of near-infrared fixable live/dead stain (#L34975, Invitrogen) was added and incubated for 30 minutes. Cells were washed thrice with 100 µl MACS buffer and fixed in 100 µl of 10% formalin before being washed twice more and resuspended in 200 µl of MACS buffer. Samples were run on the Cytoflex (BD Biosciences) flow cytometer gating for single-cells and PE fluorescence. The gating strategy is represented in Figure 2.1.

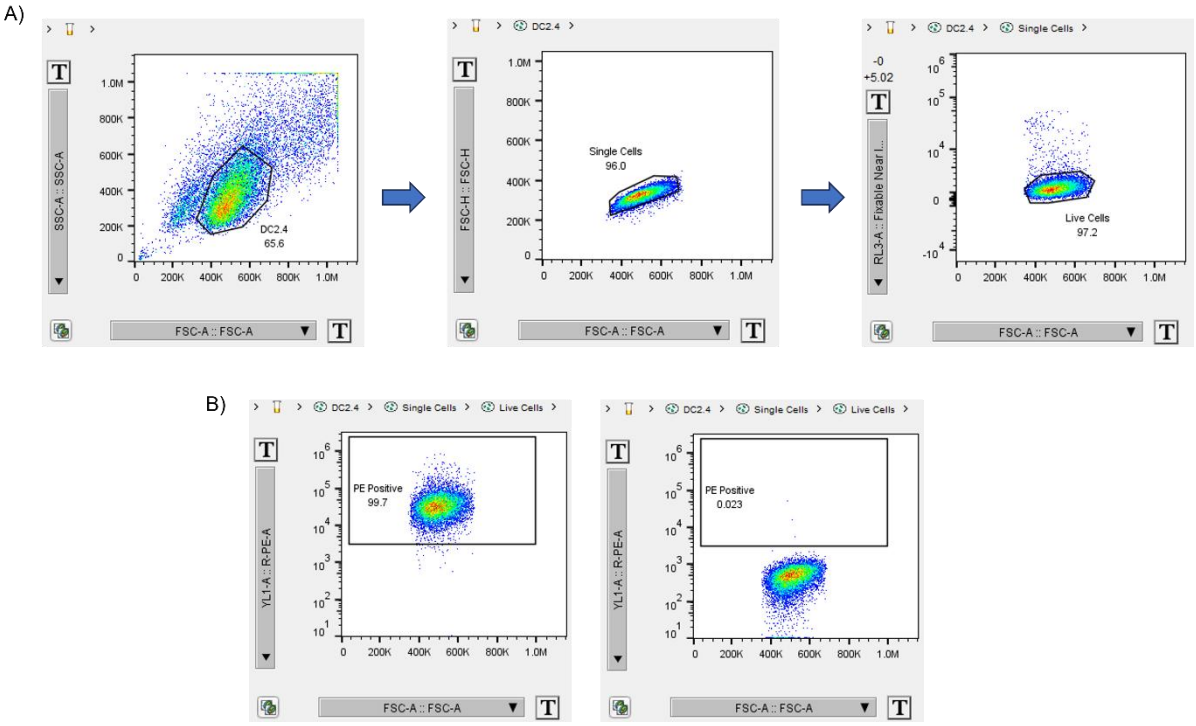


Figure 2.1 Representative Gating Strategy for a Typical Flow Cytometry Experiment on DC2.4 Cells Using an Anti-SIINFEKL/H-2Kb PE Antibody
(A) DC2.4 cells were gated around the cell population by FSC-A/SSC-A to exclude debris. FSC-A/FSC-H selected singlets. Near-IR fixable live/dead stain was used to select live cells. **(B)** Following the gating strategy of (A), a PE gate was created from SIINFEKL peptide and SIINFEKL/H-2Kb PE monoclonal antibody treated cells, which showed strong PE positivity, compared with SIINFEKL peptide isotype-treated cells, which represented the background.

2.6.4 B3Z *LacZ* Antigen Cross-Presentation Assay With Peptides and Proteins

DC2.4 cells were counted and seeded into a 96-well round-bottomed plate at 40,000 cells/well in 50 µL of complete media with 1x penicillin/streptomycin (#15140-122, Gibco) and incubated at 37°C, 5% CO_2 for 2 hours. In cathepsin S siRNA knockdown studies, the cathepsin S siRNA knockdown cells, unrelated siRNA knockdown cells, and wildtype DC2.4 cells were seeded in separate wells. For inhibitor studies, inhibitors were added to cell culture media during cell seeding and peptide pulsing at the concentrations stated (Table 2.7). Protein and peptide samples were diluted in cell culture media to form a 2x concentration curve depending on the experimental range. For inhibitor studies, peptides were diluted in culture media containing the respective inhibitors (Table 2.7).

Table 2.7 Inhibitor Concentrations for B3Z Assay	
Inhibitor	**Concentrations**
Amiloride	1 mM
Brefeldin A	17.8 nM (1x, 5µg/mL)
Chloroquine	10 µM
Cytochalasin D	5 µM
Dynasore	30 µM
Epoxomicin	10 nM
Leucine homophenylalanine vinyl sulphone (LHVS)	10 nM & 100 nM
MG-132	100 nM

After 2 hours of incubation, 50 µl of the 2x concentration curves were added in triplicate to the 50 µl of DC2.4 culture to 1x concentration. A SIINFEKL concentration curve was used as a positive control. A “no peptide/protein” control well was used to establish the background. DMSO only was used as a vehicle control for the inhibitors. Cultures were incubated for 4 hours with the peptide at 37°C, 5% CO_2.

After 4 hours, plates containing cells and peptides were centrifuged at 400 x g for 5 minutes, and the media was removed. Cells were washed twice with 120 µl of DPBS by gently pipetting to remove peptides and inhibitors. For brefeldin A (#420601, Biolegend), DC2.4 cells required fixing in 100 µl of 4% formalin for 15 minutes. Formalin was removed, and gently fixed cells were washed thrice with 200 µl of DPBS. B3Z cells were counted and seeded at 40,000 cells/well in 100 µl of complete RPMI with 1x penicillin/streptomycin in media per well to the DC2.4 plates and incubated overnight at 37°C, 5% CO_2.

The following day, the cells were harvested by centrifugation at 300 x g for 5 minutes, and the media was removed. Cells were washed with 200 µl of DPBS with centrifugation. 12mL/plate of chlorophenol red-β-D-galactopyranoside (CPRG) lysis buffer (Appendix II) was prepared. 100 µl of CPRG lysis buffer was added to each well and was incubated at 37°C for 4 hours. Plates were measured at an absorbance of 570 nm with 650 nm as background reference on the Varioskan LUX multimode

microplate reader. Absorbance values were obtained by subtracting the 650 nm reading from the 570nm reading. Using GraphPad Prism software, absorbance concentration curves were used to create four-parameter logistic non-linear regression dose-response curves. From this, the log(ED_{50}) values are calculated. The maximum response was calculated by normalised repeats to create four-parameter logistic non-linear regression dose-response curves against their non-treated control well counterparts.

2.6.5 B3Z *LacZ* Antigen Cross-Presentation Assay With OVA Beads

OVA beads were vortexed to homogenise and aliquoted into centrifuge tubes to the desired concentration. For the cathepsin S siRNA experiment, beads were centrifuged and resuspended at 10 mg/mL in DC2.4 media (Materials and Methods 2.2.1). Beads were serially diluted from 10 mg/mL stock in 1:2 increments across 12 wells to give a dose curve from 10 mg/mL (“neat”) to 24.4 µg/mL (1:4096). Beads were added to wells containing DC2.4 cells that had either been transfected with cathepsin S siRNA, unrelated siRNA, or untransfected (Materials and Methods 2.5.3).

For endocytosis and proteasome inhibition experiments, beads were diluted 1:4 and 1:8 in complete media with or without inhibition, as described (Materials and Methods 2.6.4). Beads were incubated with cells for 4 hours before being removed by pipette and washed with 200 µl of DPBS four times. Cells were fixed in 100 µl of 4% formalin for 15 minutes. Formalin was removed, and fixed cells were washed thoroughly with 200 µl four times. The assay proceeded to B3Z co-culture and CPRG assay (Materials and Methods 2.6.4).

2.7 Statistical Tests

Statistical analysis was conducted using GraphPad Prism software. A two-tailed unpaired t-test was performed when comparing two sample datasets. Comparisons between three or more samples were performed by ordinary one-way analysis of variance (ANOVA) with either Bonferroni's, Dunnett's or Tukey's post hoc multiple comparisons tests as appropriate. Graphical data is presented as mean or median with error bars for standard deviation (±SD). All assays that underwent statistical analysis had at least three independent replications. P values are classified into the following categories: ns - $p>0.05$, * - $p\leq0.05$, ** - $p\leq0.01$, *** - $p\leq0.001$, ****- $p\leq0.0001$.

3 Expression and Functional Assessment of OVA-ROP as a Model ROP

3.1 Introduction

ROPs have demonstrated the ability to stimulate an immune response *in vivo,* leading to tumour regression in mouse models (Cai et al., 2017; Zhang et al., 2023). However, the process by which ROPs are cross-presented is not fully understood. An OVA model ROP was designed to study the pathways.

OVA is a commonly used, mildly immunogenic model antigen with well-defined mouse $CD4^+$ and $CD8^+$ epitopes (Karandikar et al., 2019; Rotzschke et al., 1991). The primary $CD4^+$ epitope sequence is the 17-mer ISQAVHAAHAEINEAGR (Sun et al., 2010), with the primary $CD8^+$ epitope the 9-mer SIINFEKL (Dersh et al., 2019). Many commercially available tools are used to study SIINFEKL epitope presentation by MHC-I molecules, including TCR-like monoclonal antibodies (mAb) specific to SIINFEKL presented on H-2Kb (e.g. 25-D1.16) (Porgador et al., 1997), OVA-specific transgenic mice (e.g. OT-1), and T cell hybridoma cells lines (e.g. B3Z) engineered with a TCR specific for SIINFEKL/H-2Kb (Hogquist et al., 1994; Karttunen et al., 1992).

OVA is a foreign antigen and is readily recognised by the immune system. Its native immunogenicity, topped with its well-characterised epitopes, makes it a valuable model for immunotherapy studies. For example, mouse B16 melanoma cells are often engineered to express OVA (B16-OVA) as a tumour antigen analogue (Brown et al., 2001; Vianello et al., 2006; Ya et al., 2015). One lab used gold nanoparticles as a vehicle for an OVA peptide cancer vaccine model coupled with B16-OVA-expressing tumours (Almeida et al., 2015). Their nanoparticle system was revealed to be more beneficial than soluble OVA in prophylactic and therapeutic settings (Almeida et al.,

2015). Another group demonstrated the versatility of OVA to validate their peptide-coated oncolytic virus strategy, which they term PeptiENV (Ylosmaki et al., 2018). The researchers used cholesterol-containing moieties to conjugate OVA to an oncolytic virus. They demonstrated antigen cross-presentation of the OVA $CD8^+$ SIINFEKL epitope and anti-tumour efficacy in a B16-OVA syngeneic mouse model (Ylosmaki et al., 2018). The anti-tumour effect was from the oncolytic virus's direct killing of the tumour cells and immune activation through the conjugated OVA peptide (Ylosmaki et al., 2018).

As SIINFEKL-specific tools are readily available, using OVA as a model antigen to study the mechanisms of ROP cross-presentation was a practical starting point. With a model, we can understand the factors influencing cross-presentation and how to manipulate ROPs to enhance their functionality. To couple with OVA-ROP, a suitable antigen cross-presenting cell line was necessary for *in vitro* study.

DC2.4 cells are a mouse DC cell line that displays typical mouse DC morphology and cell surface expression markers, including H-2Kb MHC-I and I-A(d) MHC-II molecules, necessary for antigen cross-presentation and presentation, respectively (Neefjes et al., 2011). DC2.4 expresses costimulatory molecules B7-1 (CD80) and B7-2 (CD86) required for T cell activation (Alegre et al., 2001; Gong et al., 2011), and DEC-205, a PAMP receptor (Shrimpton et al., 2009). Therefore, DC2.4 is a capable cell line for the study of ROP cross-presentation in a controlled and repeatable manner.

ROPs comprise a long chain of overlapping peptides derived from a tumour antigen, with a linker between the overlapping regions designed to be cleaved by cathepsin S, a cysteine protease associated with antigen presentation and the vacuolar pathway of cross-presentation (Bertholet et al., 2006; Shen et al., 2004). By creating an

overlapping polypeptide, ROPs break self-tolerance by covering all the epitopes from the original protein but without the structural or sequence homology (Cai et al., 2017; Zhang et al., 2023).

However, as ROPs are an artificial chain of overlapping peptides, they have no native structure. This lack of structure makes them prone to aggregation, which adds additional challenges to their expression and purification, particularly in mammalian expression systems. As such, *E. coli* expression was chosen for ROP production for its rapid growth rate and high expression yields (Baeshen et al., 2015). The risk for proteins in *E. coli* is overexpression, which can break the refolding and export machinery, leading to aggregation into insoluble masses known as inclusion bodies (Taylor et al., 1986). Fortunately, there are established methods of processing and purifying recombinant proteins from inclusion bodies, which will be discussed further in this chapter. Historically, many approved recombinant therapeutic proteins, including insulin, interferons, and hormones, were successfully isolated from inclusion bodies (Graumann & Premstaller, 2006). However, using *E. coli* as an expression system for recombinant protein therapeutics is no longer as common as mammalian expression (Walsh, 2018).

Expressing the ROP is one challenge; the other is establishing whether it is readily internalised, where it is localised, and whether ROPs offer a unique localisation pattern compared to native OVA protein. By conjugating fluorophores to OVA-ROP and OVA and examining them using confocal microscopy, we can determine the effectiveness of DC2.4 uptake of ROP and its localisation. Of importance is whether the proteins are localised in specific compartments of the cells. For instance, lysosomes can be visualized using probes that selectively stain acidic organelles, such as LysoTracker or pHrodo. The cells retain these probes, and their fluorescence intensity correlates

with pH (Chazotte, 2011; Lindner et al., 2020). By combining OVA-ROP conjugation with dyes for lysosomal compartments, we can elucidate the localisation of ROP in DC2.4 cells and whether they escape the lysosome into the cytosol, a crucial component of the cytosolic pathway of antigen cross-presentation (Kovacsovics-Bankowski & Rock, 1995).

Complete endosomal escape into the cytosol would not be beneficial for studying the importance of cross-presentation through the vacuolar pathway. However, complete endosomal escape is unlikely, as cross-presentation is rare compared to digestion for MHC-II antigen presentation, with one study describing the yield to be 0.0011% for 0.8 µm OVA microspheres and 0.0024% for 3 µm OVA microspheres (Mant et al., 2012).

In this chapter, we will explore the expression and purification of OVA-ROP and use this ROP model to study its localisation and cross-presentation potential. With the creation of a model ROP, model cell lines, and analysis tools like TCR-like antibodies, unravelling the pathways and mechanisms of ROP cross-presentation becomes possible.

3.1.1 Chapter Aims

- Establish a robust *E. coli* expression system for OVA-ROP as a model antigen for ROPs.
- Purify OVA-ROP to a high degree for *in vitro* cross-presentation studies on DC2.4 cells.
- Determine whether DC2.4 cells can uptake OVA-ROP and its localisation within the cells.
- Detect OVA-ROP cross-presentation by TCR-like antibody flow cytometry assay measuring the SIINFEKL contained within the sequence of OVA-ROP.

3.1.2 Hypothesis

- OVA-ROP can be expressed and purified from *E. coli*, internalised, and cross-presented by DC2.4 cells.

3.2 Results

3.2.1 OVA-ROP is Overexpressed in *E. coli* and Forms Inclusion Bodies

OVA-ROP was expressed in *E. coli* for its ease and high yield (amino acid sequence in Table 2.2; Materials and Methods 2.1.7). Four constructs were selected for expression and purification purposes: pNIC28-Bsa4, which contains an N-terminal 6xHis-tag for affinity chromatography; pNIC-MBP2-LIC, containing the maltose binding protein (MBP) solubility tag and 6xHis-tag; pNIC-CTH0, containing a C-terminal 6xHis-tag; and pSUMO-LIC, having the removable SUMO protein solubility tag. Complete DNA sequences can be found in Appendix III.

OVA-ROP gene was synthesised and cloned out of its holding vector by PCR (Figure 3.1A) using primers designed for ligation-independent cloning method into the four constructs (Appendix III). OVA-ROP was cloned into the four vectors and was sequenced to confirm the insertion of the gene. All four OVA-ROP constructs were transformed into Rosetta (DE3) competent *E. coli* and expressed highly from Bsa4, MBP2 and SUMO constructs but not from CTH0, observed from total cell lysates of overexpressed *E. coli* (Figure 3.1B, Lanes 1-4). All four ROP constructs were not observable in the soluble fraction of lysed *E. coli* cells (Figure 3.1B, Lanes 5-8). However, upon purification of the soluble fraction, small quantities of the correct molecular weight were observed (Figure 3.1C). Together, this shows that expression was high in *E. coli*, but most of the protein was not expressed as soluble ROP and formed inclusion bodies within the cells.

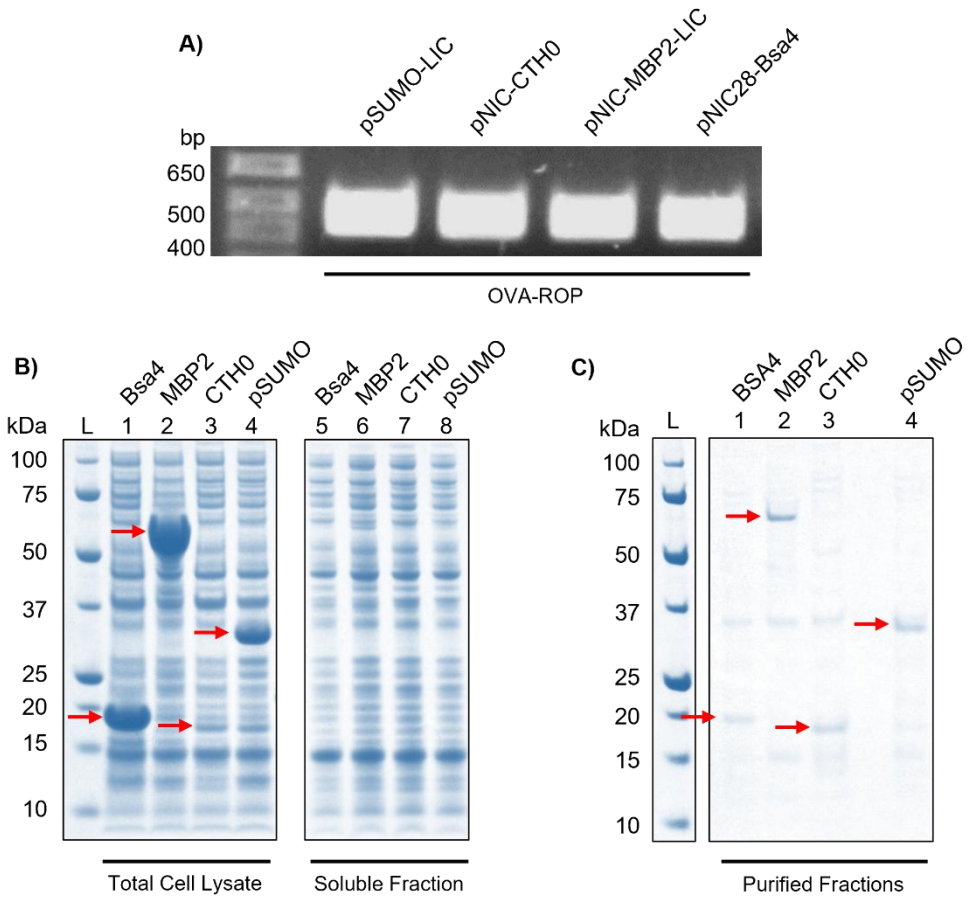


Figure 3.1 Expression of OVA-ROP in *E. coli*
OVA-ROP was cloned into four constructs by LIC and expressed in Rosetta (DE3) competent *E. coli* expression system. **(A)** DNA inserts for OVA-ROP cloned by PCR for insertion by LIC into four vectors (pSUMO-LIC, pNIC-CTH0, pNIC-MBP2-LIC and pNIC28-Bsa4). **(B)** Test expression of OVA-ROP in Rosetta *E. coli* by SDS-PAGE. The presence of tagged OVA-ROP at the correct molecular weight. Arrows highlight ROP bands. *Lanes 1-4:* total cell lysates of OVA-ROP expression in four constructs were tested. *Lanes 5-8:* soluble expression fraction of OVA-ROP for each construct. **(C)** SDS-PAGE analysis of OVA-ROP purification for the four constructs from soluble expression fractions showing the presence of tagged OVA-ROP at the correct molecular weight. Red arrows highlight ROP bands.

3.2.2 Guanidine Solubilises OVA-ROP From Inclusion Bodies

The pellets obtained after cell lysis needed to be solubilised using chaotropic agents to disaggregate the OVA-ROP inclusion body. A 6 M GuHCl and 8 M urea test was performed at two different pHs to determine the optimal condition for solubilising OVA-ROP. GuHCl at pH 7.4 and 5.0 solubilised better than urea at either pH (Figure 3.2A). The difference is further evident from the urea tubes producing a turbid solution from partial solubilisation (Figure 3.2B, top), compared with the clear tubes of the GuHCl

solubilised samples (Figure 3.2B, bottom). GuHCl-solubilised OVA-ROP was purified by nickel affinity chromatography at both pH 5.0 and 7.4, with yield in comparable volumes being more significant for pH 7.4 due to pH being in the optimal range for nickel resin binding (Figure 3.2C).

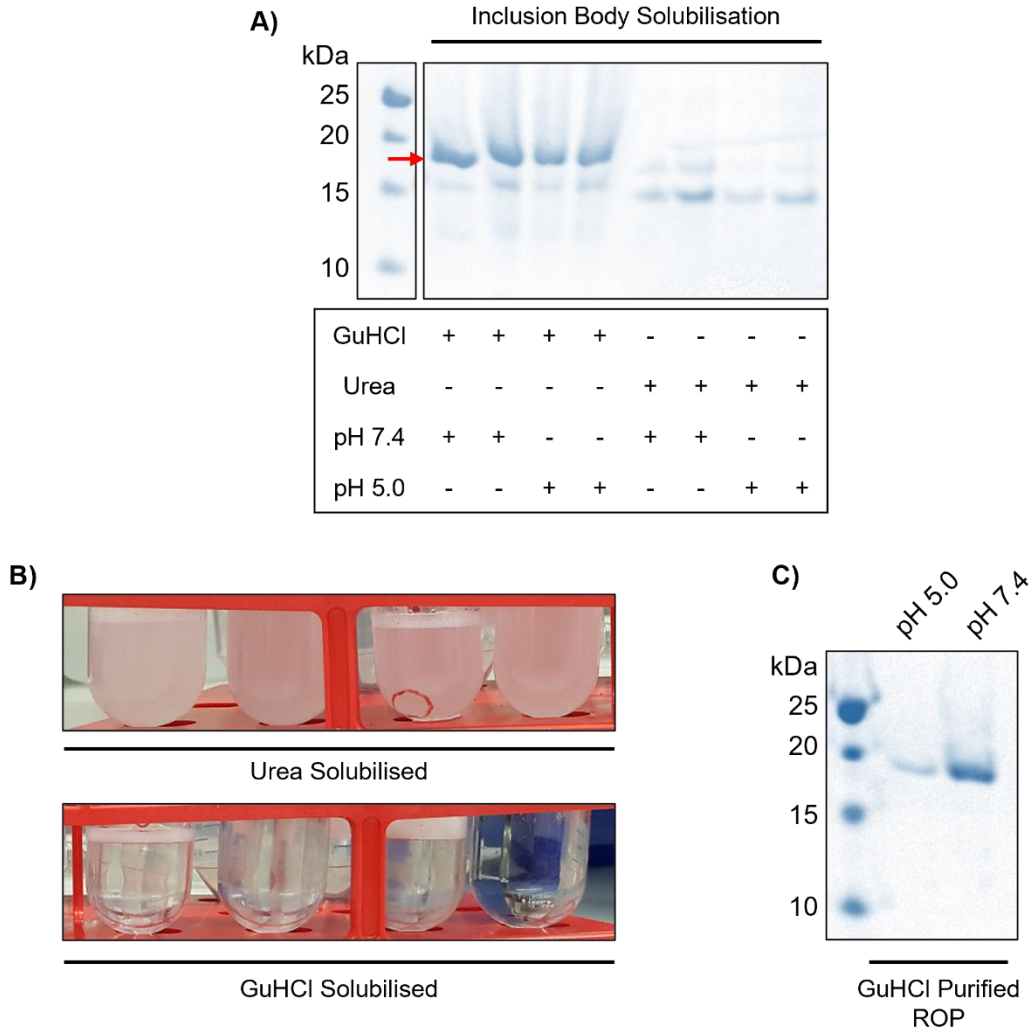


Figure 3.2 Solubilisation and Purification of OVA-ROP From Inclusion Bodies
OVA-ROP expressed in *E. coli* as an insoluble inclusion body pellet. The inclusion body pellet was solubilised by 6 M GuHCl and 8 M urea. **(A)** SDS-PAGE analysis of OVA-ROP inclusion body pellets from pNIC28-Bsa4 expression construct resuspended in 6 M GuHCl or 8 M urea at pH 5.0 or 7.4. Arrow designates the molecular weight of soluble OVA-ROP. **(B)** Representative examples of solubilisation of OVA-ROP in 8 M urea compared to 6 M GuHCl. **(C)** 6 M GuHCl solubilised OVA-ROP was purified by nickel affinity chromatography at pH 5.0 and 7.4.

3.2.3 Buffer and Additive Refolding Screen of OVA-ROP

After purification of OVA-ROP, GuHCl was removed in a process known as refolding to allow for compatibility with downstream processes, including cellular assays for antigen cross-presentation analysis. The OVA-ROP was subjected to four different strategies to establish the best for maintaining OVA-ROP in solution. ‘Fast dilution’ involved diluting the ROP dropwise into 20x the volume of refolding buffer, rapidly reducing the GuHCl concentration and its chaotropic effects. ‘Slow dilution’ was performed by dropwise addition of buffer to OVA-ROP stock to slowly reduce the concentration of GuHCl, subjecting the ROP to intermediate GuHCl concentrations. On-column refolding was a process by which the concentration of GuHCl was reduced either sequentially with stepwise reductions in concentration (e.g., 6 M, 4 M, 2 M, 1 M) or by a gradient concentration reduction on a fast protein liquid chromatography (FPLC) machine. Finally, dialysis involved aliquoting OVA-ROP into a dialysis cassette or tube, adding it to a large volume of refolding buffer and relying upon differences in osmotic pressure to diffuse the GuHCl over several hours, with buffer changes every two hours.

All four methods were evaluated for OVA-ROP, with the dilution methods including 0.5 M Arg-Glu as a refolding and solubility enhancer (Figure 3.3A). SDS-PAGE revealed that none of the methods produced soluble OVA-ROP in meaningful quantities and overwhelmingly precipitated (Figure 3.3B). The precipitation occurred regardless of the presence of the Arg-Glu, which did not affect the solubility of OVA-ROP.

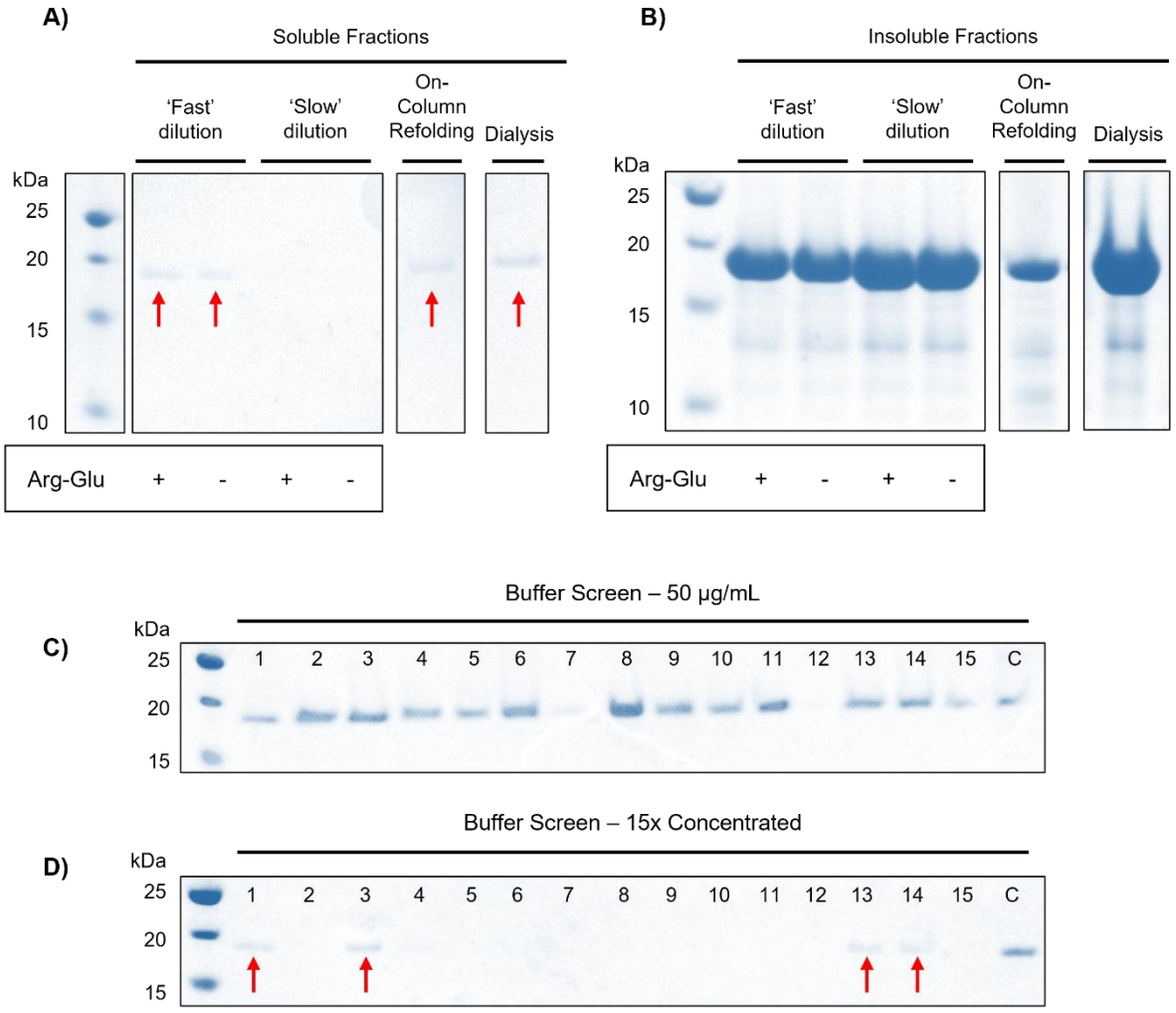
It was apparent that the conditions required for OVA-ROP to be soluble after the removal of GuHCl remain to be established. A buffer screen was necessary to discover the pH, salt concentration and additives required for OVA-ROP to be soluble. The commercial kit consisted of fifteen buffers of different pH, ionic strength, and additives

(Appendix II - QuickFold Protein Refolding Kit). OVA-ROP was diluted from 1 mg/mL stock to 50 µg/mL in each buffer, and samples of each test were run on SDS-PAGE. All buffers, except for buffers 7 and 12, could sustain OVA-ROP in solution at low concentrations (Figure 3.3C). Upon concentrating OVA-ROP 15-fold to test stability at higher concentrations, only four buffers displayed a potential to maintain the solubility of OVA-ROP: buffers 1, 3, 13 and 14 (Figure 3.3D). The buffer composition was cross-referenced, with 0.75 M GuHCl and 0.5% Triton X-100 detergent being the shared additives. From the buffer screen, detergents were the most promising additive to enhance the solubility of OVA-ROP, but the bands were still quite faint, suggesting only partial solubility.

A screen to determine the optimal detergent to promote maximum solubility of OVA-ROP was performed by diluting 1 mg/mL stock of OVA-ROP to 50 µg/mL in buffers containing one of three detergents at 0.1%, 0.5% and 1.0% concentration. The detergents were DDM, which has a neutral charge; CHAPS, which is zwitterionic; and sarkosyl, which is anionic. Equal volumes of each detergent screen sample were run on SDS-PAGE to compare solubility. DDM and sarkosyl showed better solubility than CHAPS at all concentrations assessed (Figure 3.3E). DDM and sarkosyl solubilised samples were concentrated twenty-fold by centrifugal concentrators to determine solubility at higher ROP concentrations. Sarkosyl maintained solubility even at higher concentrations of OVA-ROP (Figure 3.3F). However, it was unclear how effective DDM was at higher concentrations of OVA-ROP as the SDS-PAGE was incompatible with the DDM concentration present, resulting in a smearing of the bands (Appendix I – Figure 7.1).

The sarkosyl concentration was assessed to evaluate whether it concentrated with the OVA-ROP. Sarkosyl becomes turbid in acidic conditions proportional to its

concentration, which can be measured at an absorbance of 405 nm. A standard curve of known sarkosyl concentrations ranging from 0% to 0.025% was produced, and a sigmoidal four-parameter logistic curve was generated (Figure 3.3G). The sarkosyl concentration was diluted at 1:200 and 1:500 to within range of the standard curve, and the concentration was interpolated. OVA-ROP refolded and concentrated from 0.5% sarkosyl refolding buffer showed a final average concentration of around 4.54% sarkosyl in a 1 mg/mL concentrated stock of OVA-ROP (Figure 3.3G), proving that the sarkosyl was concentrating with the OVA-ROP using this method.



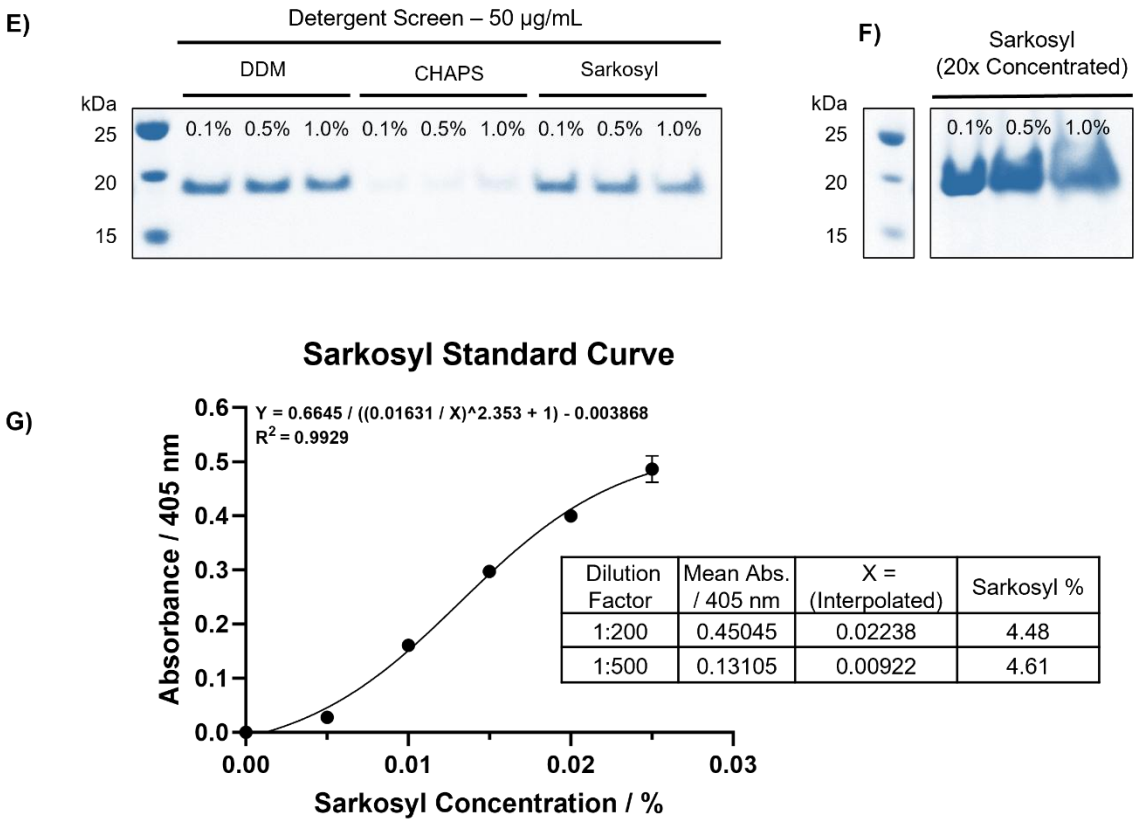


Figure 3.3 Screening OVA-ROP for Optimal Solubility Conditions
A solubility screen of OVA-ROP in various buffers with different refolding techniques was adopted. **(A)** SDS-PAGE analysis of soluble fractions of OVA-ROP diluted 20-fold to 50 µg/mL following 'fast' dilution, 'slow' dilution with and without 50 mM Arg-Glu mix (1:1), along with on-column refolding, and dialysis refolding methods. **(B)** SDS-PAGE analysis of insoluble material from fast dilution, slow dilution, on-column refolding, and dialysis refolding methods. **(C)** SDS-PAGE analysis of OVA-ROP buffer screen with QuickFold buffer refolding kit (Appendix II) by 'fast' dilution method with 6 M GuHCl as soluble control (C) **(D)** SDS-PAGE analysis of buffer screen following 15x concentration by volume. Arrows designate buffers displaying bands of soluble fractions. Concentrated OVA-ROP in 6 M GuHCl was used as soluble control (C) **(E)** SDS-PAGE analysis of detergent screen of OVA-ROP diluted by 'fast' dilution twenty-fold to 50 µg/mL in DDM, CHAPS and sarkosyl at 0.1%, 0.5% and 1.0%. **(F)** SDS-PAGE analysis of sarkosyl solubilised OVA-ROP concentrated twenty-fold from original 0.1%, 0.5% and 1.0% detergent screen. **(G)** Sarkosyl turbidity concentration assay. A standard curve was generated using GraphPad Prism's sigmoidal four-parameter logistic curve equation. Equation and R^2 value for curve displayed. OVA-ROP sarkosyl concentration of twenty-fold concentrated detergent screen interpolated from 1:200 and 1:500.

3.2.4 Sarkosyl Directly Solubilises OVA-ROP From Inclusion Bodies

As the current sarkosyl-solubilised OVA-ROP was incompatible with downstream processes, an alternative method was adopted for OVA-ROP solubilisation using sarkosyl directly. Sarkosyl, being mildly chaotropic, solubilised OVA-ROP directly from inclusion body pellets at 1% and 10% concentration in HEPES buffer, bypassing the

need for GuHCl (Figure 3.4A, left). Sarkosyl-solubilised OVA-ROP at 1% and 10% was diluted to 0.25% sarkosyl to allow for compatibility with nickel resin columns for purification and was purified successfully (Figure 3.4A, right). However, sample concentration was necessary as eluted ROP concentrations were only 0.15 and 0.16 mg/mL of OVA-ROP in 0.25% sarkosyl buffer for 1% and 10% solubilised samples, respectively. 1% was concentrated 11-fold, while 10% was concentrated 7.5-fold, both to a volume of 0.6 mL.

The sarkosyl concentration was measured by a turbidimetric assay using a sarkosyl standard curve (Figure 3.4B). The interpolation showed a concentration of 1.16% for the “1%” OVA-ROP and 0.71% sarkosyl for the “10%” OVA-ROP (Figure 3.4B), showing that the sarkosyl continued to concentrate with the OVA-ROP even at concentrations below sarkosyl’s critical micelle concentration (CMC) value of ~0.4%.

As sarkosyl was concentrated with OVA-ROP, It was necessary to avoid using concentration steps completely and purify OVA-ROP at the highest concentration with the lowest sarkosyl concentration possible. Further optimisations of the purification processes using smaller elution volumes and selective fractionation from nickel resin allowed for OVA-ROP solubilisation at 1% and elution from the nickel resin column at 0.1% sarkosyl at a concentration of 1.18 mg/mL (Figure 3.4C), confirmed by BCA assay (Appendix I – Figure 7.2). Attempts to lower the sarkosyl concentration by dialyses led to complete precipitation of the ROP (not shown).

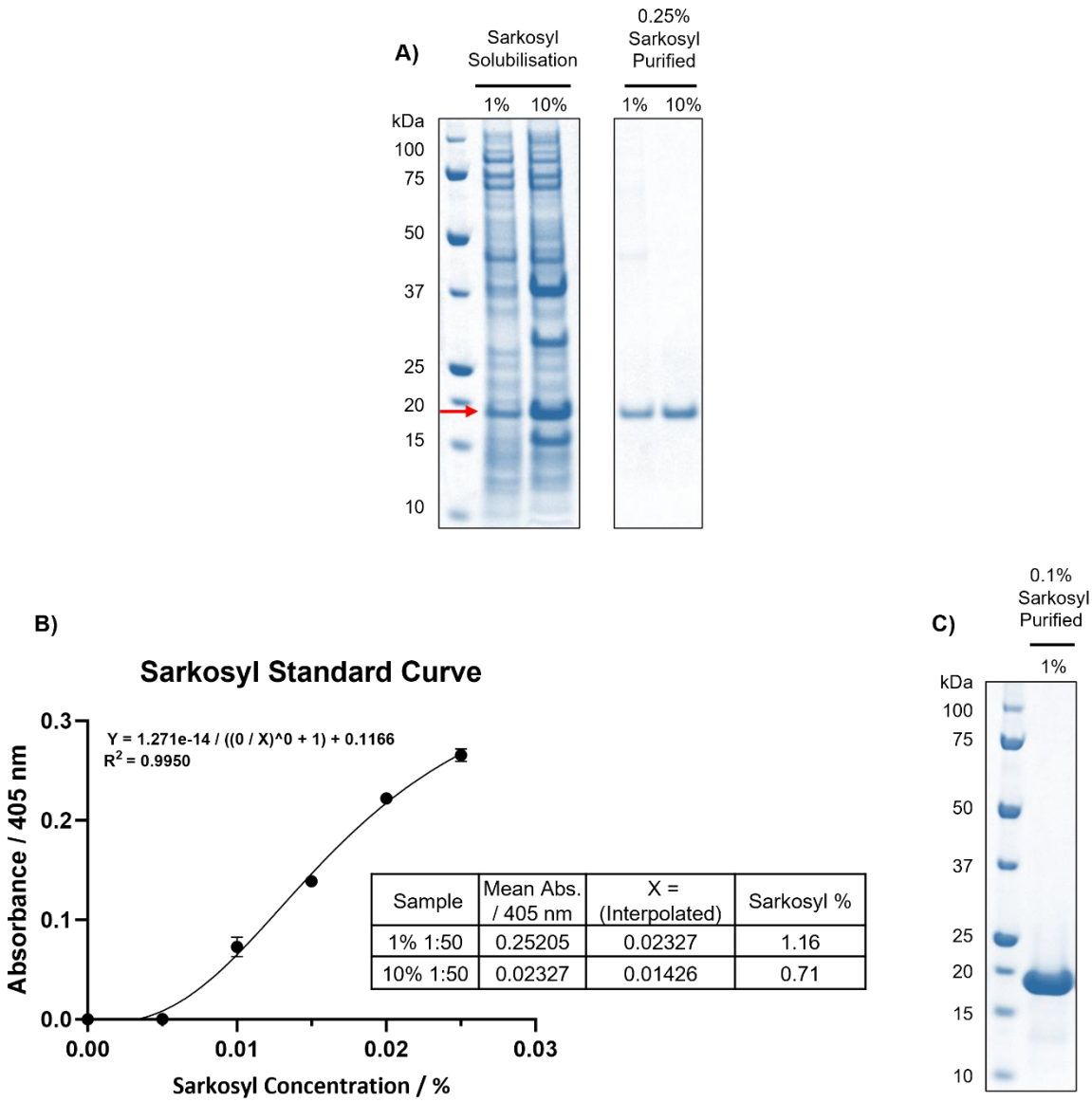


Figure 3.4 Sarkosyl as a Direct Solubilisation Reagent for OVA-ROP Inclusion Bodies
Sarkosyl was used to solubilise OVA-ROP directly from inclusion bodies. **(A)** SDS-PAGE analysis of OVA-ROP sarkosyl solubilisation and purification. *Left*: sarkosyl solubilisation of OVA-ROP inclusion body pellets by 1% or 10% sarkosyl in 50 mM HEPES pH 7.4, 500 mM NaCl, 10 mM imidazole, 10% glycerol buffer. Arrow designates a band corresponding to OVA-ROP molecular weight. *Right*: OVA-ROP was diluted to 0.25% in HEPES buffer from 1% and 10% solubilisation and purified by nickel resin affinity chromatography. **(B)** Sarkosyl turbidity concentration assay. A standard curve was generated using GraphPad Prism's sigmoidal four-parameter logistic curve calculation. Equation and R^2 value for curve displayed. Sarkosyl concentration from 0.25% purification of 1% and 10% concentrated 11-fold and 7.5-fold, respectively. Samples were diluted 1:50 and interpolated from the standard curve. **(C)** SDS-PAGE analysis of 0.1% sarkosyl purified OVA-ROP from 1% solubilisation.

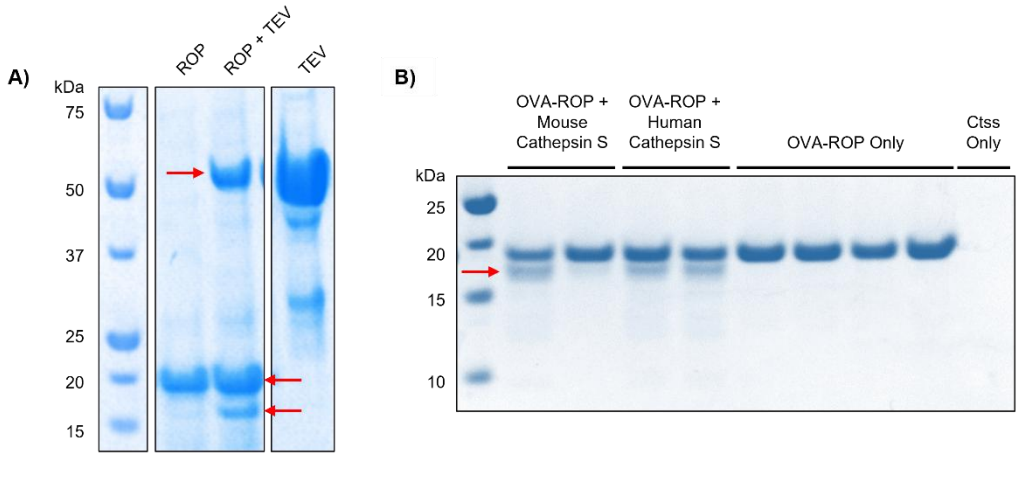
3.2.5 Proteolytic Cleavage of OVA-ROP With TEV and Cathepsin S

The N-terminal 6xHis-tag contained in the TEV sequence linker of pNIC28-Bsa4 was maintained on the ROP for purification. However, since it is no longer needed, the removal of the tag was attempted by TEV protease digestion overnight at 4°C. The goal was to maximise the digestion of the TEV linker while maintaining protein stability.

An equal mass of pre- and post-digestion OVA-ROP was run on SDS-PAGE to analyse the degree of tag removal. The SDS-PAGE analysis showed a smaller molecular-weight band in the TEV-digested wells (Figure 3.5A), which aligned with the drop in molecular weight associated with the 6xHis-tag removal at a mass of 2.35 kDa. However, most OVA-ROP was still in tagged form compared to the no enzyme control lane (Figure 3.5A). The likelihood is that the sarkosyl was causing significant disruption to the TEV activity, inhibiting its ability to digest the TEV linker. As the tag was unlikely to disrupt antigen cross-presentation assay, the tagged version of OVA-ROP was maintained.

OVA-ROP was assessed with recombinant mouse and human cathepsin S protease in a pH 6.5 buffer mixture to observe whether the OVA-ROP was recognised by cathepsin S (Figure 3.5B). In the mouse cathepsin S test, one out of two replicates displayed partial cleavage by cathepsin S after overnight incubation (Figure 3.5B). At the same time, human cathepsin S also showed partial cleavage in both replicate samples (Figure 3.5B). The partial cleavage is likely due to the sarkosyl concentration interfering with the protease activity. The ~17 kDa band observed in the protease-treated samples was excised from the gel and confirmed to be an OVA-ROP digestion product by tryptic digest tandem mass spectrometry with a Mascot MOWSE score of 473 within the CMD database containing the OVA-ROP sequence (QQ01OVAAGGA-

C001) (Figure 3.5C), and score of 167 for its parent protein OVA on the Swiss-Prot database (Figure 3.5C), with a score of >50 (p≤0.05) considered a significant match.



C)

Sample code	Database	Mascot Score	Title
AS1 QQ01OVAGGA-C001	CMD constructs	473	QQ01OVAGGA-c001
	Swiss-Prot sequences (top 5)	167	**Ovalbumin** OS=Gallus gallus GN=SERPINB14 PE=1 SV=2
		162	Trypsin OS=Sus scrofa PE=1 SV=1
		105	TRYPSIN OS=SUS SCROFA PE=1 SV=1
		74	ANIONIC TRYPSIN-1 OS=RATTUS NORVEGICUS GN=PRSS1 PE=1 SV=1
		71	Glutamine--fructose-6-phosphate aminotransferase [isomerizin

Figure 3.5 Proteolytic Activity of TEV Protease and Cathepsin S on OVA-ROP
OVA-ROP purified at 1.18 mg/mL in 0.1% sarkosyl was subjected to digestion by TEV and cathepsin S proteases. **(A)** SDS-PAGE analysis of ROP, ROP with TEV protease and TEV alone. *Top arrow*: TEV protease. *Middle arrow*: undigested tagged OVA-ROP. *Bottom arrow:* OVA-ROP TEV protease digestion product. **(B)** SDS-PAGE analysis of ROP digested with mouse and human cathepsin S. OVA-ROP and cathepsin S (ctss only) was used as a control. Arrow designates cathepsin S product band excised for tandem mass spectrometry analysis. **(C)** Tryptic digest tandem mass spectrometry analysis of band extracted from *Figure 3.5B (red arrow);* Mascot MOWSE score from CMD database and top 5 Swiss-Prot database sequences. Mascot Score >50 is considered a significant match (P≤0.05).

3.2.6 Sarkosyl-Formulated OVA-ROP is Tolerated by DC2.4 cells in Low Concentrations

An MTS cell viability assay was performed on DC2.4 cells with sarkosyl and OVA-ROP to ensure that the final preparation of OVA-ROP was compatible with biological systems. MTS assay showed that sarkosyl alone was tolerated to a concentration of 0.008%, with an increase in the concentration to 0.01% leading to a rapid reduction in cell viability (Figure 3.6A). A follow-up was performed with a concentration of OVA-

ROP between 50 and 100 µg/mL to precisely target the maximum tolerated concentration for OVA-ROP, representing a sarkosyl concentration of 0.007% to 0.014% (Figure 3.6B). DC2.4 tolerated sarkosyl-solubilised OVA-ROP up to 80 µg/mL (0.011% sarkosyl) before dropping under 90% viability (Figure 3.6B). From the MTS assays, the maximum concentration of OVA-ROP was fixed at 50 µg/mL (0.007% sarkosyl; 2.7 µM ROP concentration) to maintain maximum survivability of DC2.4 in the assay while giving a workable concentration for antigen cross-presentation studies.

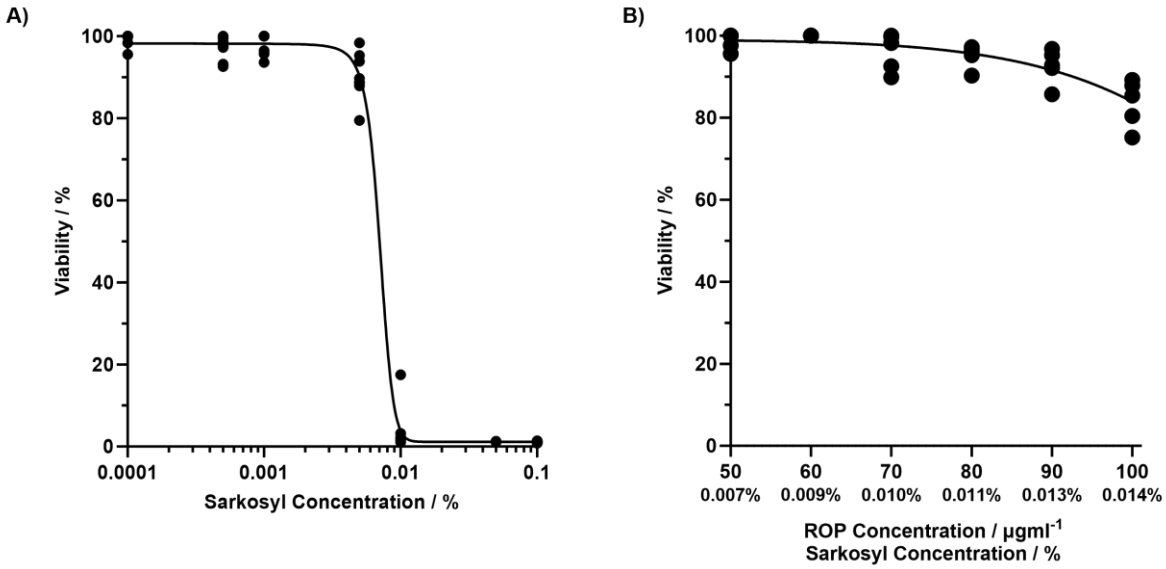


Figure 3.6 Testing Sarkosyl and OVA-ROP Cytotoxicity on DC2.4 cells by MTS assay
Sarkosyl and OVA-ROP purified with 0.1% sarkosyl were tested on DC2.4 cells. **(A)** MTS assay plot displaying viability of DC2.4 cells versus sarkosyl concentration. Graph created in GraphPad Prism software. **(B)** MTS assay plot of DC2.4 viability with increasing OVA-ROP concentration. Corresponding sarkosyl concentration with OVA-ROP is displayed below each OVA-ROP concentration. The graph was created in GraphPad Prism software.

3.2.7 Visualising the Internalisation and Localisation of OVA-ROP in DC2.4 Cells

After confirming the tolerance of DC2.4 cells to sarkosyl-solubilised OVA-ROP, the uptake of OVA-ROP by DC2.4 cells was examined before determining its cross-presentation capacity. Confocal microscopy was used to compare OVA-ROP uptake to OVA by conjugating OVA-ROP and OVA with sarkosyl (OVA-sarkosyl) to Alexa488 NHS ester, with pre-conjugated OVA-Alexa488 as a control. Along with the conjugated proteins, DC2.4 cells were stained with LysoTracker Red, which stains the lysosome of cells, to establish whether the OVA-ROP and OVA were compartmentalised in the lysosomal structures. The Alexa488-conjugated OVA-ROP, OVA-sarkosyl, and OVA at an equimolar concentration (2.7 μM) were incubated with the DC2.4 cells pre-stained with LysoTracker Red for 1 hour and fixed with formalin. Zeiss Z10 40x objective confocal microscopy imaging showed that OVA-ROP, OVA-sarkosyl, and OVA were successfully internalised by DC2.4 (Figure 3.7A), with OVA-ROP, OVA-sarkosyl, and OVA localised within the lysosome. However, OVA-ROP was more diffuse than OVA in the cell interior. A 63x (40x for OVA-sarkosyl) objective image was captured to observe OVA, OVA-sarkosyl, and OVA-ROP in more detail, along with DAPI nuclei staining (Figure 3.7B). The image reveals the diffuse nature of OVA-ROP within DC2.4 cells, potentially indicating a distinct processing pathway compared to OVA control, which is more concentrated around the lysosomal compartments. However, OVA-sarkosyl also displays a diffuse localisation, indicating that sarkosyl may be responsible for this pattern.

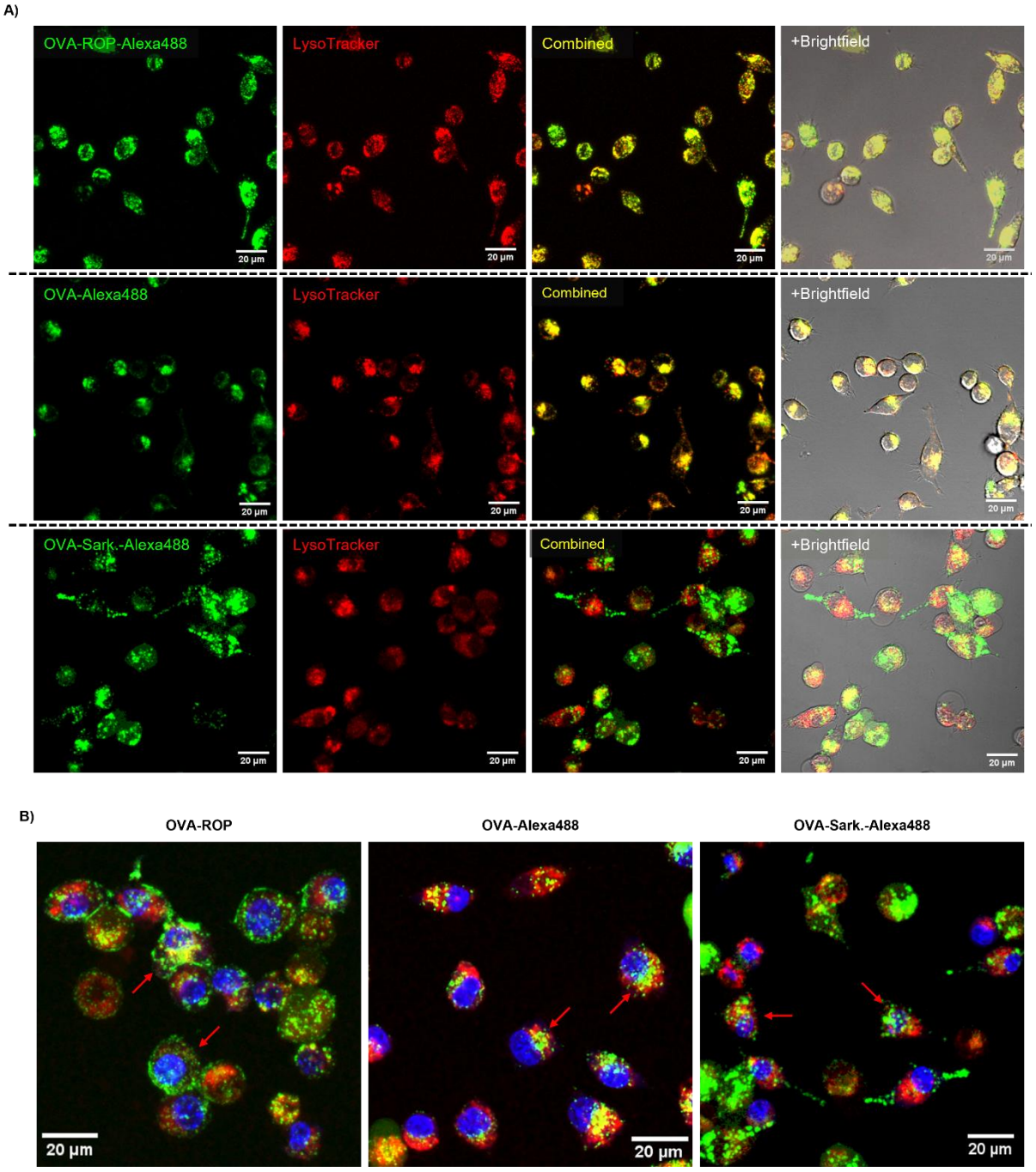


Figure 3.7 Confocal Microscopy of OVA and OVA-ROP in DC2.4 Cells
Confocal microscopy images of OVA-ROP-Alexa488, OVA-Alexa488 control and OVA-Sarkosl-Alexa488 (OVA-Sark.-Alexa488) within DC2.4 cells stained with LysoTracker red. **(A)** Zeiss Z10 40x/1.3 oil objective confocal microscope images of OVA-ROP-Alexa488, OVA-Alexa488 control, OVA-Sark.-Alexa488 conjugates only, LysoTracker red only, combination OVA/OVA-ROP with LysoTracker red, and brightfield combined image. Images were processed in ImageJ software using z-stack maximum projection and exclusion of top and bottom cell surfaces. **(B)** Zeiss Z10 63x/1.4 oil (40x/1.3 oil for OVA-Sark.) objective confocal microscope image of DC2.4 cells stained with LysoTracker red and OVA-ROP-Alexa488, OVA-Alexa488 control and OVA-Sark.-Alexa488 conjugates. The nuclei were stained with DAPI. Images were processed in ImageJ using z-stack maximum projection and exclusion of top and bottom cell surfaces. Arrows indicate cells of interest that show diffuse OVA-Sark. and ROP or localised OVA-Alexa488 control.

3.2.8 OVA-ROP is Cross-Presented by DC2.4 Cells

After demonstrating the uptake of OVA-ROP by DC2.4 cells, the next step was to determine if the cells could process and cross-present OVA-ROP. 50 µg/mL (2.7 µM) of OVA-ROP was incubated with DC2.4 for 4, 8 and 16 hours and stained with SIINFEKL/H-2Kb TCR-like mAb with PE fluorescent conjugation. In a preliminary test of the incubation period for OVA-ROP cross-presentation, 4 and 8 hours were the optimal times, with 16 hours barely above the background signal (Figure 3.8A). The effect could be attributed to the degradation of the ROP or the impact of sarkosyl on the cells after long-term exposure. From this, 4- and 8-hour incubations were adopted for OVA-ROP. They exhibited a significant increase in median fluorescence for 4 and 8 hours compared with the untreated control wells (Figure 3.8B), showing the cross-presentation of OVA-ROP. An example histogram (Figure 3.8C) shows the shift in fluorescence intensity between untreated and treated wells at 4 and 8 hours and the SIINFEKL positive control.

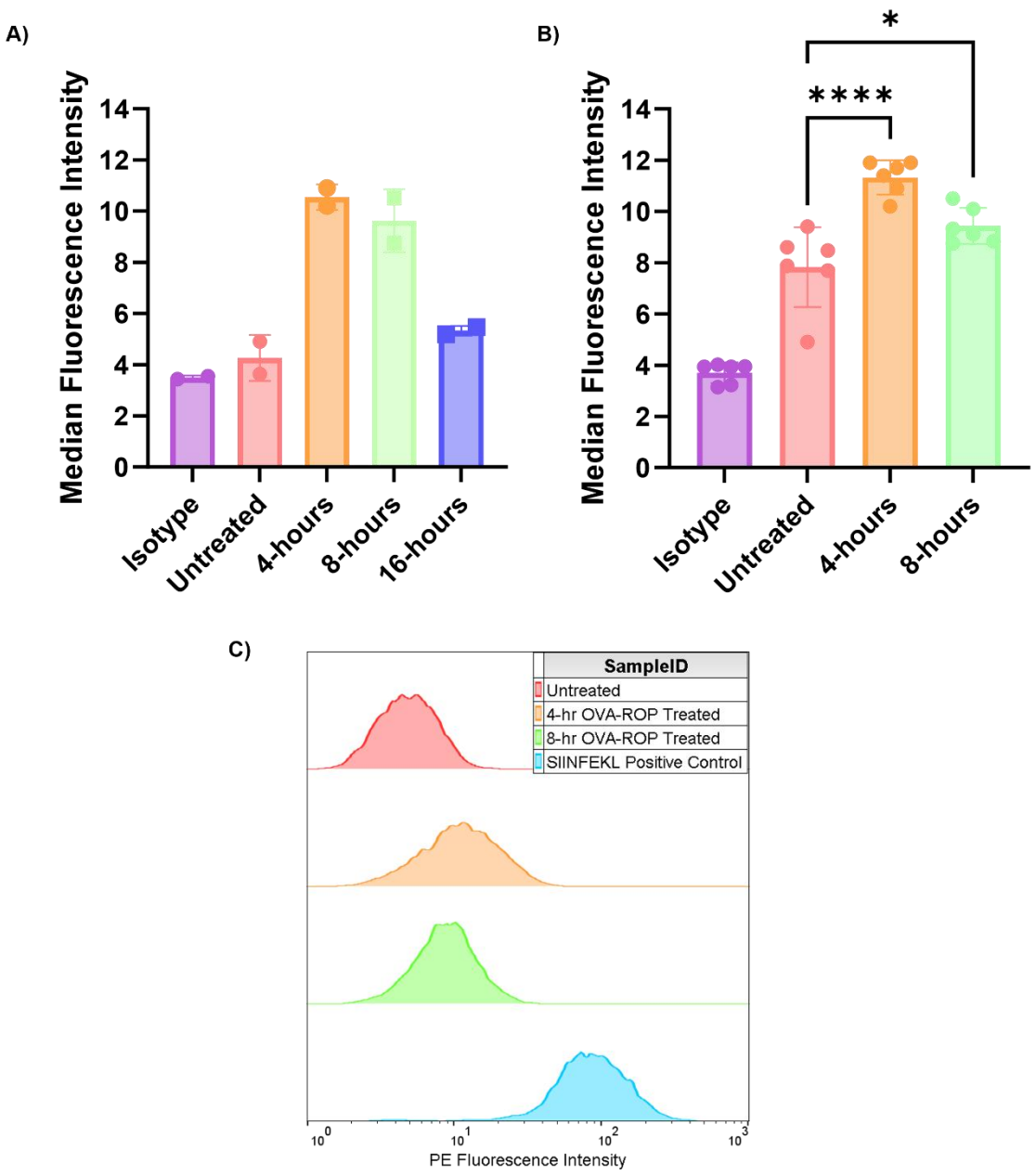


Figure 3.8 OVA-ROP Cross-Presentation Analysis by T Cell Receptor-Like Antibody
OVA-ROP cross-presentation was assessed by flow cytometry using SIINFEKL/H-2Kb TCR-like monoclonal antibody (25-D1.16). **(A)** Preliminary test of OVA-ROP cross-presentation in DC2.4 cells stained with 25-D1.16 PE mAb after 4-, 8- or 16-hours incubation of OVA-ROP (median ±SD; n=2). Untreated cells are used as background control. Graphs created in GraphPad Prism. **(B)** OVA-ROP cross-presentation in DC2.4 cells stained with 25-D1.16 PE mAb after 4- and 8-hours incubation compared to untreated cells (median ±SD; n=6). An isotype control was used to quantify non-specific binding. Graphs and statistics were performed in GraphPad Prism using ordinary one-way ANOVA with Bonferroni's post hoc multiple comparisons test (*** - p≤0.001, ****- p≤0.0001). **(C)** Representative histogram of PE Fluorescence intensity for OVA-ROP and 4- and 8-hour incubation compared with untreated and SIINFEKL peptide positive control.

3.3 Discussion

ROPs are artificial polypeptides with no native structure, making them challenging to express and purify in a soluble state. Four different constructs were used to help in OVA-ROPs purification, solubility, or both. Three out of the four constructs were high expressers. However, none produced a high yield in a soluble form, indicating that the solubility tags were not strong enough to prevent the formation of inclusion bodies. As OVA-ROP was produced in inclusion bodies, chaotropic agents were necessary to disaggregate the insoluble masses.

GuHCl was initially used for this purpose and solubilised the inclusion bodies well, but initial refolding tests did not reveal a solution that stabilised OVA-ROP. A buffer screen was performed to discover the optimal buffer and included various pH levels, ionic strengths, and additives such as KCl, arginine, Triton X-100, and EDTA (AthenaES, 2020). Cross-referencing the composition of the buffers that promoted solubility revealed that they all contained 0.75M GuHCl and 0.5% Triton X-100 in common.

The use of detergents in refolding was promising and was investigated further with three different detergents: DDM, CHAPS and sarkosyl. CHAPS failed to promote solubility, but sarkosyl and DDM did preserve solubility at lower concentrations. However, DDM was seen to concentrate intensely on the ROP and was challenging to remove, so sarkosyl was considered the best candidate.

A turbidimetric assay assessed the concentration of sarkosyl-refolded ROP to be too high to allow for testing on cells, so direct solubilisation methods were investigated. ROP was directly solubilised by sarkosyl from the inclusion body, and through purification optimisations, it was possible to elute ROP with sarkosyl to 1.18 mg/mL at 0.1% sarkosyl.

Cleavage of the TEV tag was attempted, but sarkosyl inhibition of the TEV protease prevented its effective removal. Likewise, its presence also hindered cathepsin S, but a 17 kDa product was confirmed to be an OVA-ROP derivative by gel-band tryptic digest mass spectrometry. Finally, the toxicity was assessed by MTS and tolerated by the DC2.4 at the target 50 µg/mL, demonstrated an ability to be internalised by DC2.4 cells and was cross-presented successfully.

Producing soluble proteins is often preferable to the time-consuming isolation and refolding from inclusion bodies. The MBP and SUMO solubility tags were incorporated into the expression scheme to promote soluble expression of ROP. MBP is a highly soluble *E. coli* protein that aids in the solubility of its conjugation partner (Kapust & Waugh, 1999). In comparison, SUMO is a eukaryotic protein, which again acts as a solubility enhancer and chaperone to aid protein solubilisation and refolding and is removable by SUMO protease (Marblestone et al., 2006). SUMO protease is highly specific and cleaves at the end of the SUMO tag sequence, leaving no residues upstream from the target ROP sequence (Reverter & Lima, 2004). The lack of successful soluble expression with either of these tags led to them being discontinued in favour of the N-terminal 6xHis-tag to refocus on solubilisation and purification from inclusion bodies.

Although not preferred, producing proteins as inclusion bodies has its benefits. Inclusion bodies provide better protection from protease degradation and are relatively homogenous, consisting mainly of the recombinant protein of interest, which makes purification simpler (Kumar, 2011; Singh et al., 2015). As inclusion bodies are relatively pure, this can reduce the need for several purification steps. Nonetheless, nickel resin affinity chromatography was still necessary to increase the purity to an acceptable degree (>90%).

Chaotropic agents are needed to solubilise inclusion bodies by denaturing their aggregated structure. Urea and GuHCl are the two most used chaotropic agents, but both have advantages and disadvantages. For example, urea is non-ionic and is compatible with SDS-PAGE analysis but does tend to spontaneously degrade into ammonia and cyanate over time, which can potentially damage proteins through carbamoylation (Lippincott & Apostol, 1999). Urea's damaging degradation products necessitate fresh buffer preparation and constant low-temperature control of solutions and protein to slow the spontaneous decomposition of urea (Hagel et al., 1971).

GuHCl is 2 to 2.5 times more potent than urea as a solubilising agent (Dempsey et al., 2005). However, it is also strongly ionic, making it incompatible with SDS-PAGE analysis (Funderburgh & Prakash, 1996), producing smeary bands on the gel. A method to avoid this is by ethanol precipitating the protein, leaving the ethanol-soluble GuHCl in the solution (Pepinsky, 1991). After precipitation, the protein is solubilised in an SDS-PAGE loading buffer and was adopted later in the project. From both the SDS-PAGE analysis and the clarity of solutions following their addition, GuHCl was significantly more potent at solubilising than urea for OVA-ROP. The inability of urea to solubilise OVA-ROP may point to its inherent insolubility, requiring the more potent GuHCl to enable solubilisation.

For naturally occurring proteins, removing GuHCl is needed to enable the protein to fold into its native structure, a process known as refolding (Vallejo & Rinas, 2004). ROPs do not have a native structure, so refolding is not a wholly accurate term. Regardless, the process is the same, with similar precautions needed to maintain solubility and minimise aggregation. Refolding is an empirical process, with a protein's hydrophobicity, charge and the buffer's ionic strength, pH and additives determining

whether refolding succeeds or fails (Burgess, 2009; Singh et al., 2015; Vallejo & Rinas, 2004; Yamaguchi & Miyazaki, 2014).

Along with the buffer, determining the technique to permit refolding is essential. With dilution, on-column refolding, and dialysis being the primary methods, with 50% of reported experiments in the REFOLD database being dilution refolding, 33% through dialysis, and around 12% through column refolding methods (Chow et al., 2006). 50 mM Arg-Glu was included in the dilution experiments, as it can enhance the maximum concentration of soluble proteins by up to 8.7-fold and prevent aggregation (Golovanov et al., 2004). However, the inclusion of Arg-Glu did not significantly increase the solubility of OVA-ROP. Although all the methods adopted led to substantial precipitation, ‘fast’ dilution was preferred, as it allowed for rapid screening of suitable buffers by observing turbidity through absorbance readings at 600 nm.

The fast dilution method was implemented into the buffer screen to determine the optimal buffers and additives rapidly. Low-concentration GuHCl was highlighted as it has been demonstrated to enhance the refolding of proteins by preventing incorrectly folded intermediates from forming and promoting the correct, more stable structure (Tsumoto et al., 2003). Triton X-100 was another additive, but ultimately, it was not used due to its potentially endocrine-disrupting degradation products, which could impact mice during *in vivo* studies (Luo et al., 2020), so other detergents were examined.

The detergent screen revealed sarkosyl as a good candidate due to its wide use in the solubilisation and refolding of inclusion bodies (Frankel et al., 1991; Tao et al., 2010). DDM was discounted as it was considerably more challenging to remove than sarkosyl due to its lower CMC of 0.17 mM (0.0087%) (Dezi et al., 2013) compared with

sarkosyl's CMC of ~13-14 mM (~0.4%) (Tseng et al., 2016). DDM also has a much larger micelle size of ~70-74 kDa (Strop & Brunger, 2005) than sarkosyl's reported 0.6 kDa micelle size (Chisnall et al., 2014).

The CMC is the concentration where the surfactant begins aggregating to form micelles (Perinelli et al., 2020). The CMC and micelle size for DDM means it forms micelle at a 100-fold lower concentration than sarkosyl and is 80-fold larger. The combination of DDM's CMC and micelle size makes its removal through dialysis difficult, inevitably leading to it concentrating along with the protein. However, CMC values are only accurate in pure water, with CMC dropping with increasing ionic strength of the buffer (Tseng et al., 2016). Therefore, careful consideration of the concentration of sarkosyl and the molecular weight cut-offs is necessary to avoid concentrating the sarkosyl with the ROP.

Sarkosyl is insoluble at low pH levels, resulting in a turbid solution proportional to its concentration and can be measured at an absorbance of 405 nm in a turbidimetric assay (Kurucz et al., 1995). Even at a starting concentration of nearly half of the stated CMC of sarkosyl (~14 mM; ~0.4%), sarkosyl concentrated with the OVA-ROP. The concentrating effect may be due to the ionic strength of the buffer affecting the CMC or the sarkosyl associating with the protein to form a mixed micelle, which is not removable by dialysis (Chisnall et al., 2014).

Detergents such as sarkosyl are amphiphilic surfactants; their primary function is to allow the mixture of hydrophobic molecules such as lipids with water. As such, they disrupt the lipid bilayer found around all cells, damage or kill cells, and are often used in cell lysis buffers (Brown & Audet, 2008). Therefore, it was crucial to control the final concentration of sarkosyl in ROP preparation. Sarkosyl has been shown to have mild

solubilising effects on inclusion bodies (Burgess, 1996), with concentrations of up to 10% used with up to 95% protein recovery (Massiah et al., 2016). Unfortunately, dialysis tests proved that OVA-ROP relied on sarkosyl to maintain solubility in an aqueous buffer.

The maintenance of OVA-ROP necessitating sarkosyl was problematic, with the partial cleavage of the TEV protease during the attempted tag-removal step indicative of an inhibitory effect of the sarkosyl on the protease. Although tag removal was not necessary for OVA-ROP, the incomplete cleavage was a concern for compatibility with the cathepsin S and antigen cross-presentation assays.

Cathepsin S is a crucial protease in antigen presentation and the vacuolar pathway of cross-presentation (Shen et al., 2004). OVA-ROP has been engineered to contain an LRMK linker sequence, a known cleavage site of cathepsin S derived from the invariant chain (Ruckrich et al., 2006). However, the cathepsin protease family is promiscuous in its proteolytic activity (Wilkinson et al., 2015), so cleavage could occur at other sites within the ROP sequence. Attempts to elucidate potential cathepsin S cleavage sites have been explored before, with one study examining a series of 4-6 amino acid linkers finding that LLSVGG was a strong linker for enhancing cross-presentation (Rabu et al., 2019). Only partial cleavage was observed with cathepsin S on OVA-ROP, likely because of sarkosyl inhibition of the protease. Whether this was random or specific cleavage was unclear. However, it was the first indication that cathepsin S processed OVA-ROP and evidence of a propensity for the vacuolar pathway of cross-presentation.

The MTS assay used to assess sarkosyl's toxicity measures cell proliferation and metabolic activity through their ability to reduce tetrazolium compounds to formazan,

which is directly proportional to the number of living cells (Cory et al., 1991). However, although sarkosyl did not hinder the metabolic activity of the DC2.4 cells at low concentrations, there is a potential that other unobserved effects may have occurred. For example, one study examined permeabilisation from low concentrations of Triton X-100 with cell-impermeable ferrocyanide molecules (Koley & Bard, 2010). In the study, at low Triton X-100 concentrations, the HeLa cells were still viable but displayed permeability for ferrocyanide molecules (Koley & Bard, 2010). Therefore, sarkosyl may enhance OVA-ROP uptake through permeabilisation, potentially giving a false impression of its immunogenicity.

Sarkosyl permeabilisation may be evident from the confocal microscopy cellular uptake study with LysoTracker Red combined with OVA-ROP-Alexa488 and OVA-Alexa488. Upon entry, the trafficking of proteins to the endosome-lysosome pathway is an essential first step in the processing of antigens for presentation and cross-presentation (Watts, 2012). To demonstrate this trafficking, LysoTracker was used to stain the acidic lysosomal compartments of the cells (Chazotte, 2011). The diffuse nature of OVA-ROP, compared to the lysosome-concentrated OVA, could potentially be indicative of a greater degree of lysosomal escape with OVA-ROP compared to OVA, as endosome-to-cytosol export is a crucial process in the TAP-dependent antigen cross-presentation pathway (Kovacsovics-Bankowski & Rock, 1995). However, membrane permeabilisation by sarkosyl may have increased the uptake and dispersal of the ROP within the cells by facilitating its escape. OVA-sarkosyl Alexa488 conjugate, which was formulated with an equal concentration of sarkosyl to ROP, also had a diffuse localisation, adding to the evidence of membrane permeabilisation rather than an inherent benefit of OVA-ROP in escaping the endosome.

If permeabilisation had affected cellular localisation, it did not appear to hinder the cross-presentation of OVA-ROP through DC2.4 with the TCR-like antibody. The cross-presentation of OVA-ROP has been demonstrated with the SIINFEKL/H-2Kb antibody in a previous study and showed an increase in fluorescent intensity of approximately 17.6% over the untreated samples (Cai et al., 2017). The newly generated ROP showed a 44% increase in median fluorescence intensity compared to the untreated samples. However, the treatment time for the ROP presented in the paper was 13 hours (Cai et al., 2017), compared to 4 hours for the new OVA-ROP, with longer incubations proving detrimental. This discrepancy may be attributable to a difference in design, sequence, or buffer formulation between the two ROPs, especially with the inclusion of sarkosyl. One outstanding question is how OVA-ROP compares to OVA, which will be evaluated in a cell-based assay in chapter four.

Studying subtle nuances with inhibitors or enhancers that affect antigen cross-presentation in further assays with the narrow range of fluorescent intensity of OVA-ROP would be challenging, especially when compared to SIINFEKL, which had around 1000-fold greater fluorescence intensity than OVA-ROP. However, SIINFEKL is a “ready-to-go” peptide, requires no processing, and can bind directly to MHC-I, bypassing the antigen cross-presentation machinery (Eisen et al., 2012). Therefore, SIINFEKL peptide is a valuable tool as a positive control for antibody recognition and binding but not for antigen cross-presentation.

3.4 Conclusion

As an artificial polypeptide, ROP is a challenging molecule to produce in a soluble state and forms inclusion bodies, even with conjugation to solubility-enhancing tags. For successful purification and refolding, sarkosyl was needed to solubilise these masses. However, OVA-ROP was found to be dependent on sarkosyl to maintain its solubility. Although not ideal for the downstream process, sarkosyl-solubilised OVA-ROP was tolerated by DC2.4 enough to determine its localisation upon internalisation and perform tests on its ability to be cross-presented with a TCR-like antibody. The next objective is to investigate how we can improve the design of OVA-ROP to increase solubility and antigenicity to allow for further studies into the mechanisms involved in antigen cross-presentation.

4 Alternative ROP and Peptide Formulation Strategies

4.1 Introduction

As demonstrated in the preceding chapter, OVA-ROP was successfully produced and purified from *E. coli* cells but relied on the anionic detergent sarkosyl to maintain its solubility. Although OVA-ROP was cross-presented, the study was limited by sarkosyl, which, in concentrations exceeding 0.01%, was toxic to DC2.4 cells. Furthermore, while the antigen cross-presentation of OVA-ROP was significant, it remained low, constraining the scope for investigating cross-presentation pathways. This chapter explores fusions with targeting domains for binding to DCs to address the challenges related to OVA-ROP solubility and antigenicity.

The approximately 50 kDa fragment crystallisation (Fc) domain of the IgG antibody plays a crucial role in binding to Fc-receptors on macrophages, DCs, and B lymphocytes to regulate the immune response and induce endocytosis (Leserman et al., 1980; Mellman & Plutner, 1984). The high-affinity FcγRs are particularly interesting, as their engagement triggers endocytosis and enhances cross-presentation in DCs. (Regnault et al., 1999). The Fc domain has been demonstrated to increase the solubility of associated fusion partners and prolong their half-life in serum (Jazayeri & Carroll, 2012). Therefore, combining Fc-tags with peptides and proteins can augment their antigenicity and bolster solubility.

The activation potential of IgG is subject to influence by its subtype, as Fc receptors can be either excitatory or inhibitory and display varying affinities for specific IgG subtypes (Bournazos et al., 2020; Bruhns et al., 2009). For example, the mouse IgG2a (mIgG2a) Fc subtype has a high binding affinity to all excitatory FcγRs (I, III and IV) and low affinity for the inhibitory FcγRIIB (Bruhns, 2012). Consequently, mIgG2a

exhibits an activation-to-inhibition ratio of 69, in contrast to a ratio of 0.1 for mouse IgG1 (Nimmerjahn & Ravetch, 2005), indicating a potential to elicit a pronounced immunostimulatory response. In humans, IgG 1, 3 and 4 all show high affinity for the excitatory FcγRI and lower affinity for inhibitory FcγRIIB (Bruhns, 2012).

Even considering the IgG subtype, monomeric Fc-tagged fusions exhibit poor immunogenicity, primarily attributed to the FcRn recycling pathway. FcRn is an Fc-binding receptor located within the endosomes of cells. It binds to antibodies after internalisation by FcγR and plays a crucial role in immune regulation by facilitating the trafficking of IgG molecules through cells (Hulett & Hogarth, 1998; Pyzik et al., 2019). Studies have shown that the FcRn is essential in the recycling of monomeric IgG, which contributes to the prolonged serum half-life of IgG antibodies (Qiao et al., 2008; Roopenian et al., 2003; Wani et al., 2006). The FcRn receptor enables the continuous circulation of monomeric IgG until it binds to its specific antigen epitope and joins with other antibodies to form an IC. The IC cross-links with multiple Fc receptors, increasing signalling, internalisation, and antigen presentation (den Haan & Bevan, 2002; Rafiq et al., 2002; Weflen et al., 2013).

Fc-tags cannot cross-link multiple Fc-receptors, as they do not contain the fragment-antigen binding (Fab) domain to bind to antigens and allow them to form ICs. Since ICs cannot form from Fc fusions, preventing interference with the uptake and cross-presentation of Fc-fusion tags involves reducing or eliminating FcγR binding. For example, a mutation at asparagine 297 has been shown to remove a glycosylation site and cause a significant decrease in FcγR binding (Bolt et al., 1993). Some modifications are receptor-specific, such as glycine 237 to alanine and glutamine 318 to alanine, which display a reduction in binding to FcγRII (Lund et al., 1992). Other mutations, such as glycine 236 to arginine and leucine 328 to arginine, are more

general and decrease binding to all FcγR (Horton et al., 2010). These mutations result in the Fc-tag primarily functioning for solubility and purification, losing its immunogenic benefits. The second approach involves diminishing FcRn activity on the Fc-tag by mutations in regions associated with FcRn binding. Modifications to isoleucine 253 and histidine 310 and 435 have been shown to eliminate the FcRn binding and lead to a reduction in recycling but reduce the half-life of the fusion protein *in vivo* (Kim et al., 1999).

An alternative approach to circumvent the FcRn recycling pathway and enhance Fc-receptor cross-linking is the formation of hexameric IgG structures (Mekhaiel et al., 2011; Qureshi et al., 2017; Rowley et al., 2018). Hexameric IgGs are created by engineering the polymerising IgM tailpiece to the C-terminus of IgG (Mekhaiel et al., 2011; Rowley et al., 2018). A single-point mutation at position 309 (EU Numbering) from glutamine to cysteine (Q309C), a residue found at the hinge region between the constant heavy $(CH)_2$ and CH_3 domains of Fc, stabilises this multimerisation through a disulphide bond between neighbouring Fc-domains (Mekhaiel et al., 2011; Rowley et al., 2018). The formation of an Fc hexamer has the potential to facilitate the cross-linking of multiple FcγRs, thereby enhancing receptor-mediated endocytosis, uptake, and protection from recycling pathways (den Haan & Bevan, 2002; Rafiq et al., 2002; Weflen et al., 2013). Consequently, a hexameric Fc fusion may be more immunogenic than its monomeric counterpart.

So far, most of the therapeutic potential of hexameric-Fc has been in treating autoimmune diseases by blocking FcγR-mediated functions and promoting their internalisation and degradation (Qureshi et al., 2017). One study utilising human IgG1 Fc hexamers suppressed acute and chronic arthritis in mouse models by blocking the FcγR and inhibiting the classical complement pathway more efficiently than the

monomeric Fc (Spirig et al., 2018). These effects were achieved at doses ten times lower than those typically used in traditional intravenous immunoglobulin (IVIG) therapy (Spirig et al., 2018).

In cancer vaccine research, Fc-fusions have commonly utilised monomeric Fc for stability and purification while intentionally diminishing immunogenic potential by introducing mutations that abolish Fc-receptor binding. In one study, a vaccine consisting of an XCL1 DC chemokine conjugated to a mutant Fc and an OVA epitope SLP showed a significant increase in the CTL response and anti-tumour immunity in B16-OVA tumour models, compared to OVA SLP or OVA SLP with XCL1 co-administered (Botelho et al., 2019; Crozat et al., 2010; Dorner et al., 2002). This effect was despite the mutant Fc being engineered to prevent FcγR binding (Botelho et al., 2019).

Another strategy examined an oncolytic adenovirus armed with an Fc-fused signal regulatory protein α (SIRPα) (Huang et al., 2020). SIRPα is an inhibitory receptor on macrophages that interacts with CD47, a cancer-overexpressed self-recognition molecule that provides a “do not eat me” signal to inhibit macrophage phagocytosis (Huang et al., 2020; Oldenborg et al., 2000). In a study using *in vivo* mouse tumour xenograft models, treatment with the oncolytic virus inhibited the growth of CD47-positive ovarian cancer by combining the oncolytic virus’s direct tumour cell killing with the blockade of CD47 by SIRPα-Fc (Huang et al., 2020). In the study, the Fc tag was included primarily for detection purposes in immunofluorescence assays to evaluate SIRPα-Fc expression and its binding to CD47 on cancer cells (Huang et al., 2020).

In the clinic, aflibercept is a VEGF receptor-Fc fusion approved by the FDA in 2012 in combination with folinic acid, fluorouracil, and irinotecan (FOLFIRI) chemotherapy

treatment regime against metastatic colorectal cancer (Regeneron Pharmaceuticals, 2012). Aflibercept acts as a decoy receptor for VEGF, preventing tumour growth by inhibiting angiogenesis (Holash et al., 2002).

In addition to the broader targeting of Fc-receptors on various immune cells, DCs feature motifs that are either exclusive to them or found in higher quantities than other immune cells. These motifs can be targeted to augment DC-specific uptake and processing. For example, DEC-205 is a PAMP receptor found on the cell surface of DCs and in low levels on macrophages, B cells and T cells (Kato et al., 2006). It is an endocytic receptor, with PAMP binding leading to internalisation and antigen presentation (Jiang et al., 1995). By targeting antigens to DEC-205, there is a potential to augment cross-presentation and T cell-mediated immune responses, surpassing the effects of using the antigen alone. One group successfully demonstrated enhanced antigen presentation by targeting DEC-205 with an anti-DEC-205 scFv fused to the cancer-testis antigen MAGE-A3 (Birkholz et al., 2010). The study found a larger MHC-II restricted antigen presentation than pulsing the DC cells with the MAGE-A3 alone, demonstrating a platform for targeting DEC-205 with scFvs (Birkholz et al., 2010).

scFvs are one of the smallest subtypes of antibodies, only containing the antigen recognition sites of the heavy and light chain linked together with a small flexible linker (Huston et al., 1988). ScFvs can be expressed in mammalian cells and *E. coli,* with examples in *E. coli* targeting liver, breast, and B-cell malignancies (Ji et al., 2016; Mikiewicz et al., 2020; Yu et al., 2014). Only a limited number of *E. coli*-expressed scFv constructs have received clinical approval, with a notable example being brolucizumab. Brolucizumab gained approval from the FDA in 2019 to treat neovascular age-related macular degeneration and was isolated and refolded from *E. coli* inclusion bodies (European Medicines Agency, 2019; Novartis, 2019).

Unlike scFvs, mammalian expression is necessary for Fc-tags due to their specific cytosolic conditions essential for proper disulphide bond formation, which are not present in the reducing cytoplasm of *E. coli* (Derman & Beckwith, 1991). In *E. coli*, disulphide bond formation primarily occurs in the periplasm by disulphide bond (Dsb) catalysing proteins. However, transporting the proteins to the periplasm can lead to limited expression yields (Berkmen, 2012; De Geyter et al., 2016).

For this chapter, a fusion protein was created by combining a mIgG2a Fc with a truncated OVA-ROP (tOVA-ROP) to target excitatory FcγRI receptors on the mouse DC2.4 cell line. The truncation of ROP aimed to minimise steric hindrance that might obstruct Fc fusion formation and FcγR binding and improve the likelihood of achieving soluble expression. Following monomer expression, the study will explore the potential for inducing multimerisation of mIgG2a Fc by adding the IgM tailpiece and the glutamine to cysteine mutation at position 94, equivalent to position 309 (Mekhaiel et al., 2011; Rowley et al., 2018). The goal is to assess the feasibility of generating IC-like structures to facilitate the cross-linking of FcγR, thereby promoting enhanced uptake and circumventing FcRn recycling (den Haan & Bevan, 2002; Rafiq et al., 2002; Weflen et al., 2013).

This chapter will explore two potential scFv constructs targeting DEC-205 featuring distinct antigen epitopes. The first will be an anti-mouse DEC-205 scFv (NLDC-145) (Demangel et al., 2005; Swiggard et al., 1995), conjugated to the $CD4^+$ (ISQAVHAAHAEINEAGR) and $CD8^+$ (SIINFEKL) minimal epitopes as a precursor to a DEC-205 scFv ROP conjugate (Rotzschke et al., 1991; Shimonkevitz et al., 1984). The second is an anti-human DEC-205 scFv (MG38-3) (Birkholz et al., 2010; Guo et al., 2000), conjugated to HLA-$A2^+$ epitopes from NY-ESO-1 $CD4^+$ 80-109 sequence

and the known $CD8^+$ epitope (SLLMWITQC) from NY-ESO-1 (Gnjatic et al., 2003; Jager et al., 2000).

NY-ESO-1 is a human cancer-testis antigen primarily expressed in germ-line cells but exhibits upregulation in a range of primary and metastatic solid tumours, including but not limited to breast, ovarian, melanoma, neuroblastoma, and prostate cancer (Aung et al., 2014; Fossa et al., 2004; Jungbluth et al., 2001; Odunsi et al., 2003; Rodolfo et al., 2003). NY-ESO-1 was selected as a model cancer antigen to investigate the potential anti-tumour therapeutic effects of a DEC-205 targeting approach in human models and will serve as a proof-of-concept for a cancer antigen targeting ROP fusion.

Previously, flow cytometry was employed with the SIINFEKL/H-2Kb TCR-like monoclonal antibody to assess cross-presentation levels from OVA-ROP. However, it did not provide insight into the impact of $CD8^+$ T cell activation on the immune system. The B3Z T cell hybridoma, equipped with a sensitive TCR specific to SIINFEKL/H-2Kb and the *LacZ* gene under the nuclear factor of activated T cells (NFAT) promoter of IL-2 addresses these issues (Karttunen et al., 1992). As a cell-based assay, it is more physiologically relevant and will be used to measure cross-presentation and model T-cell activation.

These studies will highlight the potential of developing a targeted strategy using an Fc-tag or scFv fusion specifically designed for uptake by DCs. When combined with ROPs and peptides, this approach can potentially enhance presentation capabilities more effectively than when these components are used alone.

4.1.1 Chapter Aims

- Clone tOVA-ROP into the pFUSE vector to create an Fc-fusion ROP to improve solubility and antigenicity.
- Implement the IgM tailpiece and Q94C mutations to the pFUSE Fc-tag construct to induce hexamerisation.
- Evaluate the antigenicity of tOVA-ROP-Fc compared to OVA-ROP using the B3Z *LacZ* CPRG Assay to measure antigen cross-presentation.
- Clone and express an anti-DEC-205 OVA and NY-ESO-1 scFv fusions to assess the viability of a DC-targeting peptide cancer vaccine.

4.1.2 Hypotheses

- The inclusion of Fc-tag enhances the solubility and antigenicity compared to OVA-ROP alone.
- Mutations in the Fc-tag will enable multimeric IgG formation and IC-like structures.
- Anti-DEC-205-OVA and -NY-ESO-1 scFv fusions can be expressed and display enhanced uptake and antigenicity compared to non-targeted peptides.

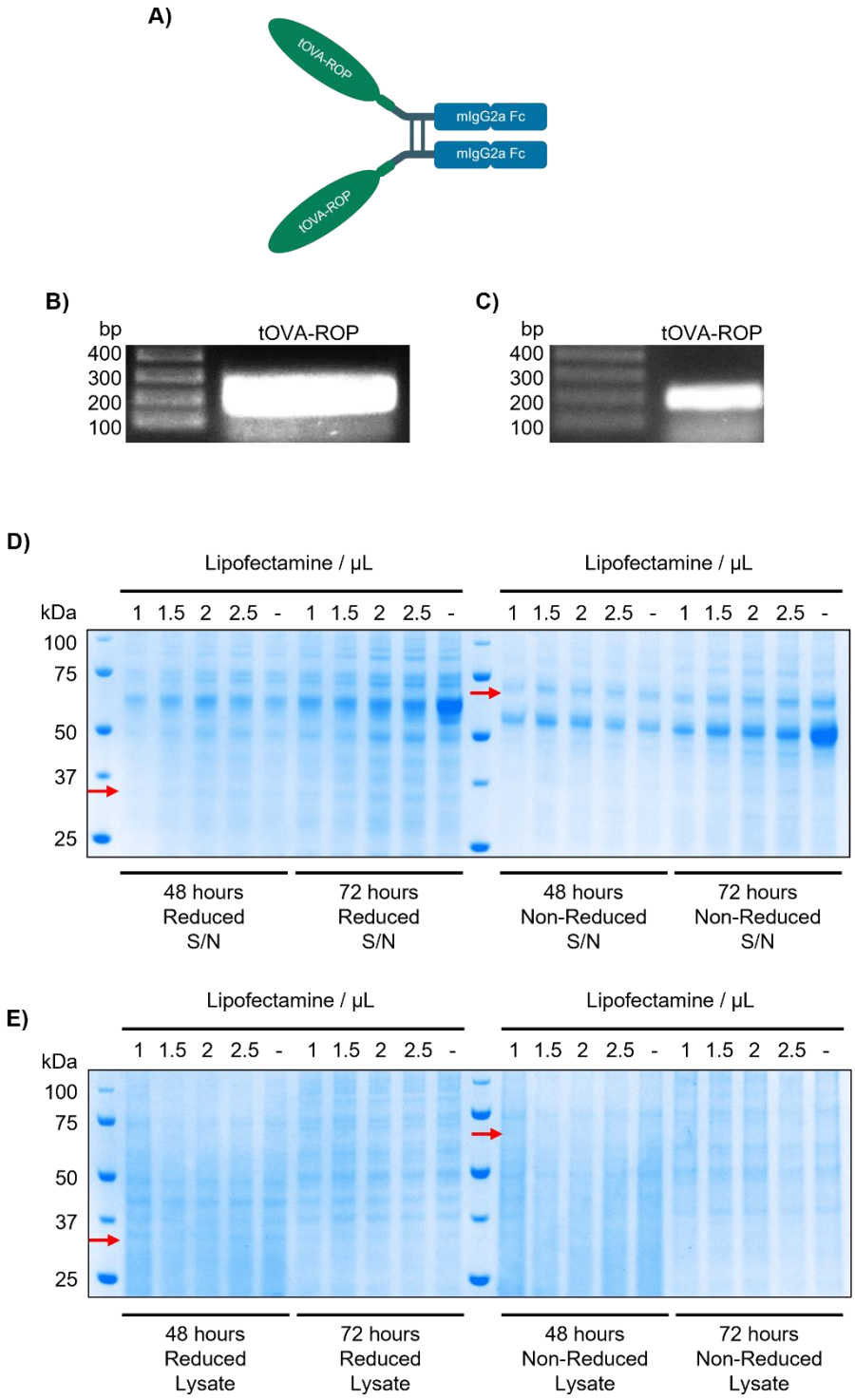
4.2 Results

4.2.1 tOVA-ROP-Fc Fusions are Expressed in Mammalian Cells

An OVA-ROP fusion with an Fc-tag was investigated to eliminate OVA-ROP dependency on sarkosyl. The pFUSE vector, containing the mIgG2a Fc with an IL-2 secretion signal sequence, was used for the fusion. For the Fc-fusion, the tOVA-ROP sequence (Table 2.2; Materials and Methods 2.1.7) was conjugated to the Fc-tag (Figure 4.1A). The tOVA-ROP gene was amplified from the synthesised gene fragment by tOVA-Fc-fwd and tOVA-Fc-rev primers (Appendix III). The gene fragment was synthesised with a 5' EcoRI and 3' BglII cleavage site for ligation into the pFUSE vector (Figure 4.1B). The vector and insert were double digested with EcoRI and BglII restriction enzymes and ligated together by T4 ligase. Successful ligation of tOVA-ROP into pFUSE (pFUSE-tOVA-ROP) was confirmed by PCR colony screen with the same primers used for PCR amplification and transformed into Mach1 *E. coli* cells for construct expression (Figure 4.1C).

The tOVA-ROP-Fc construct was transiently transfected for mammalian expression in HEK293 cells. The tOVA-ROP-Fc protein was transfected with 2 µg pFUSE-tOVA-ROP DNA and four lipofectamine volumes (1, 1.5, 2.0 and 2.5 µl) to find the optimal expression ratio. After three days of culturing, the tOVA-ROP-Fc culture supernatant and cells were harvested and lysed with RIPA buffer, and the supernatant was concentrated 20x by centrifugal concentrators. Reduced and non-reduced SDS-PAGE analysis saw no observable bands in the concentrated supernatant (S/N) (Figure 4.1D) or lysate (Figure 4.1E) at any DNA to LFA ratios assessed compared to the no DNA control transfection, showing poor expression of tOVA-ROP-Fc. Western blot analysis was performed using a goat anti-mouse mIgG2a Fc-specific HRP-conjugated antibody to ascertain whether expression was occurring. tOVA-ROP-Fc was detectable in the

supernatant (Figure 4.1F) and lysate (Figure 4.1G) by reduced and non-reduced loading on a western blot. The reduced and non-reduced loading showed that the Fc was forming into the complete tOVA-ROP-Fc homodimer. The western blot proved that tOVA-ROP-Fc expression was occurring at low yields, requiring further optimisation.



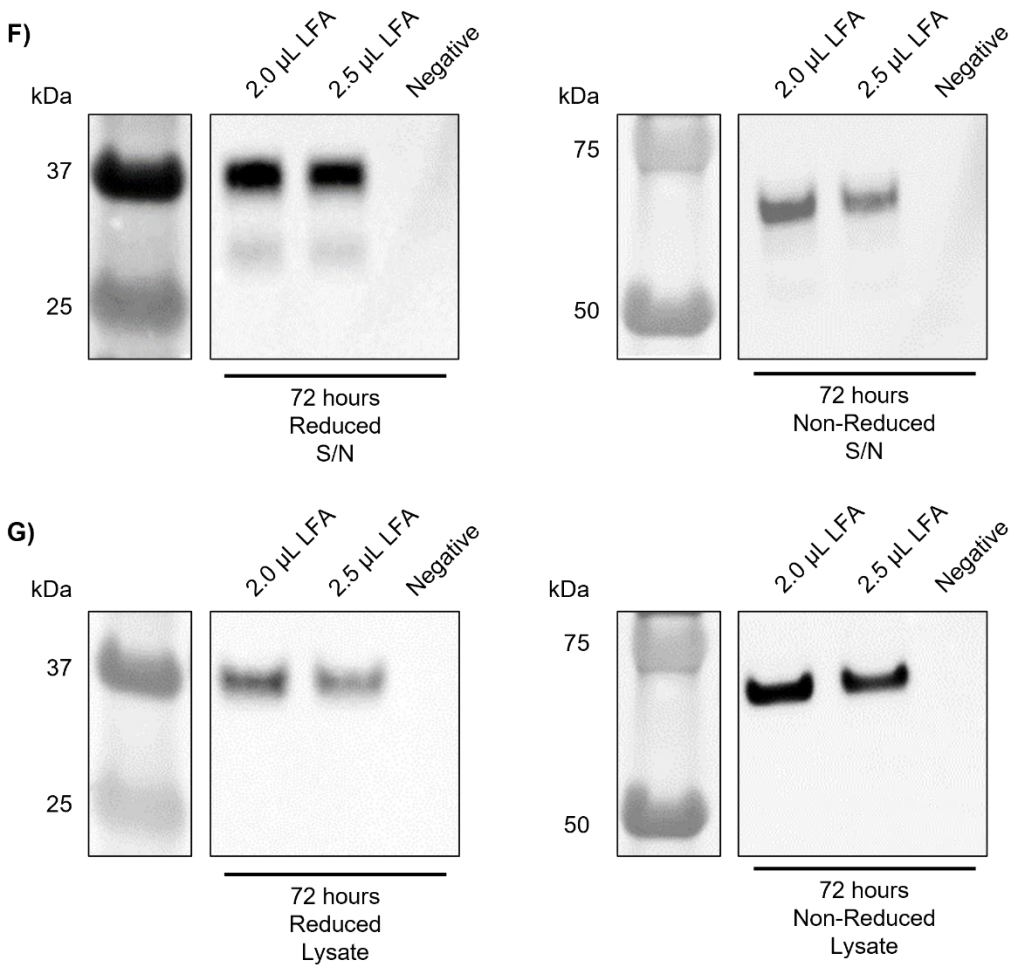


Figure 4.1 tOVA-ROP Fc-fusion Protein Expression in HEK293 Cells
The tOVA-ROP gene fragment was cloned into the pFUSE-mIgG2a-Fc2 vector containing Fc-tag and IL-2 signal sequence and transiently transfected into HEK293 cells. **(A)** Schematic of tOVA-ROP mIgG2a Fc homodimer. Image made in Biorender.com. **(B)** 1.5% agarose gel electrophoresis of PCR amplification products (50 µl) of tOVA-ROP gene from gene fragment by tOVA-FC-fwd and tOVA-Fc-rev primers. **(C)** 0.75% agarose gel electrophoresis of PCR colony screen (20 µl) of pFUSE-tOVA-ROP transfection and selection of colonies from overnight culturing of Mach1 cells. **(D)** SDS-PAGE analysis of 20x concentrated reduced and non-reduced supernatant (S/N) of harvested HEK293 (samples normalised by original culture volume, 10 µl loading) 48- and 72-hours post-transfection with pFUSE-tOVA-ROP with 2 µg of DNA and a range of lipofectamine volumes (1, 1.5, 2, 2, 2.5 µL). No DNA transfection with 2.5 µL LFA was used as a negative control (-). Red arrows designating the expected molecular weight of tOVA-ROP-Fc as a reduced monomer (33.4 kDa) or non-reduced homodimer (66.8 kDa). **(E)** SDS-PAGE analysis of reduced and non-reduced cell pellet lysate (5 µl) of HEK293 48- and 72-hours post-transfection with pFUSE-tOVA-ROP with 2 µg of DNA and a range of lipofectamine volumes (1, 1.5, 2, 2, 2.5 µL). No DNA transfection with 2.5 µL LFA was used as a negative control (-). **(F)** Western Blot analysis using goat anti-mouse mIgG2a Fc-specific HRP-conjugated antibody on 20x concentrated reduced and non-reduced HEK293 supernatant (S/N) (normalised by original volume) samples at 72-hour harvest, with 2 and 2.5 µl LFA (lipofectamine) and 2 µg of the pFUSE-tOVA-ROP construct. A no DNA transfection with 2.5 µl LFA was used as a control (-). Developed using ECL HRP substrate. **(G)** Western Blot analysis using goat anti-mouse mIgG2a Fc-specific HRP-conjugated antibody on reduced and non-reduced HEK293 cell lysate samples (5 µl) at 72-hour harvests, with 2 and 2.5 µl LFA (LFA) and 2 µg of the pFUSE-tOVA-ROP construct. No DNA Transfection with 2.5 µl as a control (-). Blot developed using ECL substrate.

4.2.2 tOVA-ROP-Fc is Purifiable From Mammalian Cell Pellets and Displays a Propensity to Cross-Present

Expression of tOVA-ROP-Fc was transferred from HEK293 to Expi293F suspension culture cells for larger-scale expression (250 mL) and to optimise production yield. The goal was to improve productivity and obtain a suitable yield for purification and further analysis. Expi293F cells were transfected with the pFUSE-tOVA-ROP 1:3 and 1:6 DNA:PEI ratio and incubated for five days. SDS-PAGE analysis evaluated the expression levels and differences between the 1:3 and 1:6 ratios. It showed no discernible expression five days after transfection in tests with the 1:3 ratio (Figure 4.2A) and the 1:6 DNA:PEI ratio (Figure 4.2B). From the gel, the change in ratios and the expression system did not appear to have affected yield.

As expression may have occurred at low levels, purification was performed on the 250 mL of the tOVA-ROP-Fc transfected Expi293F supernatant by protein A affinity capture to concentrate any protein present. Following elution from protein A and analysis of elution fractions by SDS-PAGE, no yield of tOVA-ROP-Fc was observed in either the reduced or non-reduced samples (Figure 4.2A-B), suggesting that the fusion of the tOVA-ROP sequence to Fc may disrupt expression or secretion because of an inherent instability linked to the tOVA-ROP.

To further analyse whether the Expi293F were expressing tOVA-ROP-Fc, a western blot analysis was performed on the samples, which revealed that most of the tOVA-ROP-Fc was found within the pellet and not the supernatant. This localisation was apparent through a reduced (Figure 4.2C) and non-reduced (Figure 4.2D) western blot showing the homodimer and monomeric forms of tOVA-ROP-Fc in higher concentrations within the pellet. Analysis of material purified through protein A affinity capture on western blot revealed evidence of small quantities of purified material and

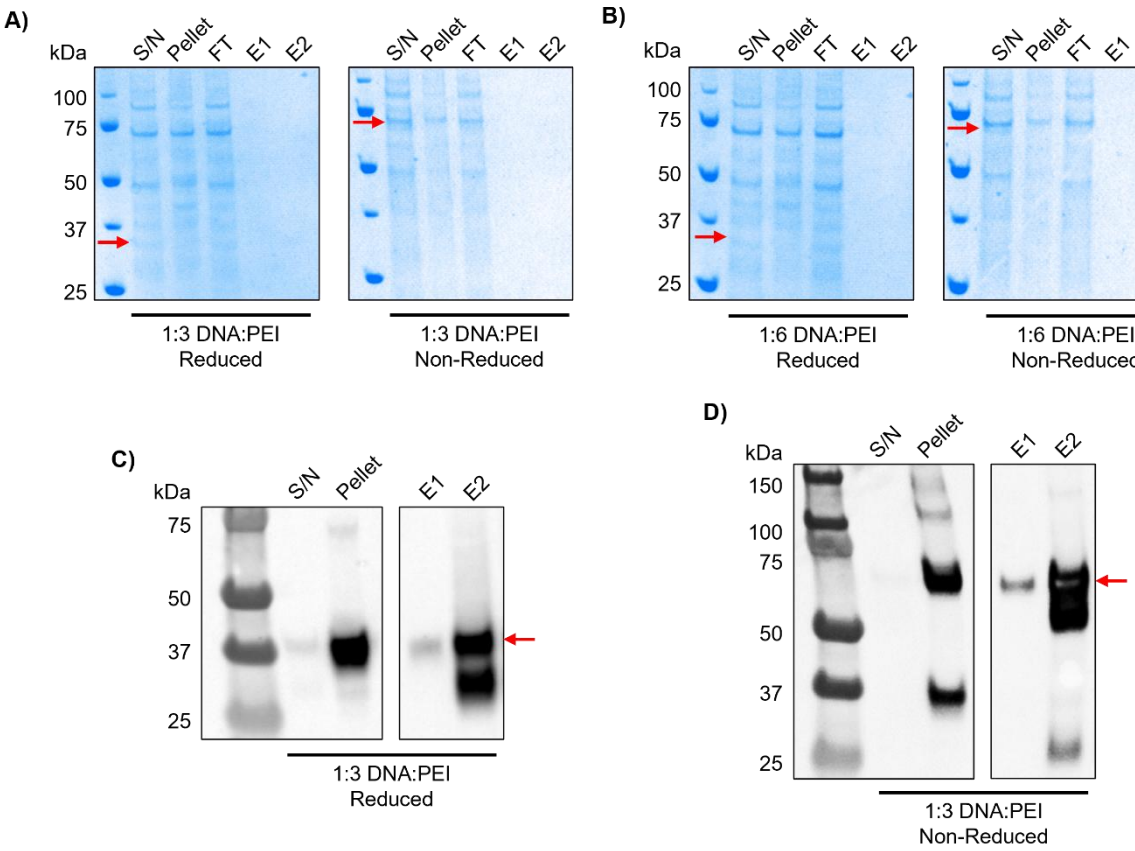
an unknown second band in reduced (Figure 4.2C) and non-reduced (Figure 4.2D) western blot images. Together, this shows that tOVA-ROP-Fc was poorly expressed, with most of the protein not being secreted and trapped within the cells despite the IL-2 secretion signal sequence, providing further evidence of tOVA-ROPs instability with the Fc fusion partner.

From the western blot images of Expi293F cells, most of the tOVA-ROP-Fc produced was not being secreted but was present in the cell pellet (Figure 4.2C-D). Pellets were resuspended in DPBS and pulse sonicated to lyse the cells. The lysate was clarified by centrifugation and filtration before protein A affinity chromatography purification to isolate and purify tOVA-ROP-Fc. Eluates from tOVA-ROP-Fc purification were run on SDS-PAGE and were present at high purity (Figure 4.2E-F). Notably, the IL-2 signal sequence was present due to a lack of secretion, changing the molecular weight from 33.4 kDa to 35.6 kDa. The six eluates were combined, concentrated by centrifugal concentrators, and measured by BCA assay (Appendix I – Figure 7.3) to a 91.8 µg/mL concentration, yielding 40 µg from approximately $1.41x10^9$ cells. A 0.5 µg sample was taken for SDS-PAGE analysis to confirm purity. The combined tOVA-ROP-Fc eluate fraction showed a high purity level and was stable in solution (Figure 4.2E-F).

To evaluate the antigenicity of tOVA-ROP-Fc compared to OVA-ROP and OVA, a B3Z antigen-cross presentation assay was performed (Materials and Methods 2.6.4). B3Z cells contain a TCR specific to H-2Kb/SIINFEKL with β-galactosidase expression under the NFAT promoter of IL-2, with the enzyme activity measurable by CPRG assay and proportional to cross-presentation activity. CPRG is a galactoside analogue hydrolysed from the yellow-coloured CPRG to galactose and the chromophore chlorophenol red, measurable by spectrophotometry. 500 nM of OVA, OVA-ROP and tOVA-ROP-Fc were pulsed on DC2.4 cells in culture for six hours before co-culturing

the DC2.4 cells with the B3Z cells overnight. SIINFEKL peptide was used as a positive control, and the B3Z assay was developed using CPRG and measured after six hours of incubation. tOVA-ROP-Fc and OVA produced a small signal over the background (Figure 4.2G), whereas OVA-ROP alone did not have a signal at the concentration assessed. Due to the small yield of tOVA-ROP-Fc, repeats and higher concentration tests were not viable.

Based on this limited study, there were indications that tOVA-ROP-Fc was slightly antigenic and potentially more effective than OVA and OVA-ROP at equivalent concentrations. However, due to the low yield of tOVA-ROP-Fc, it was impossible to conclude without repeated statistical testing.



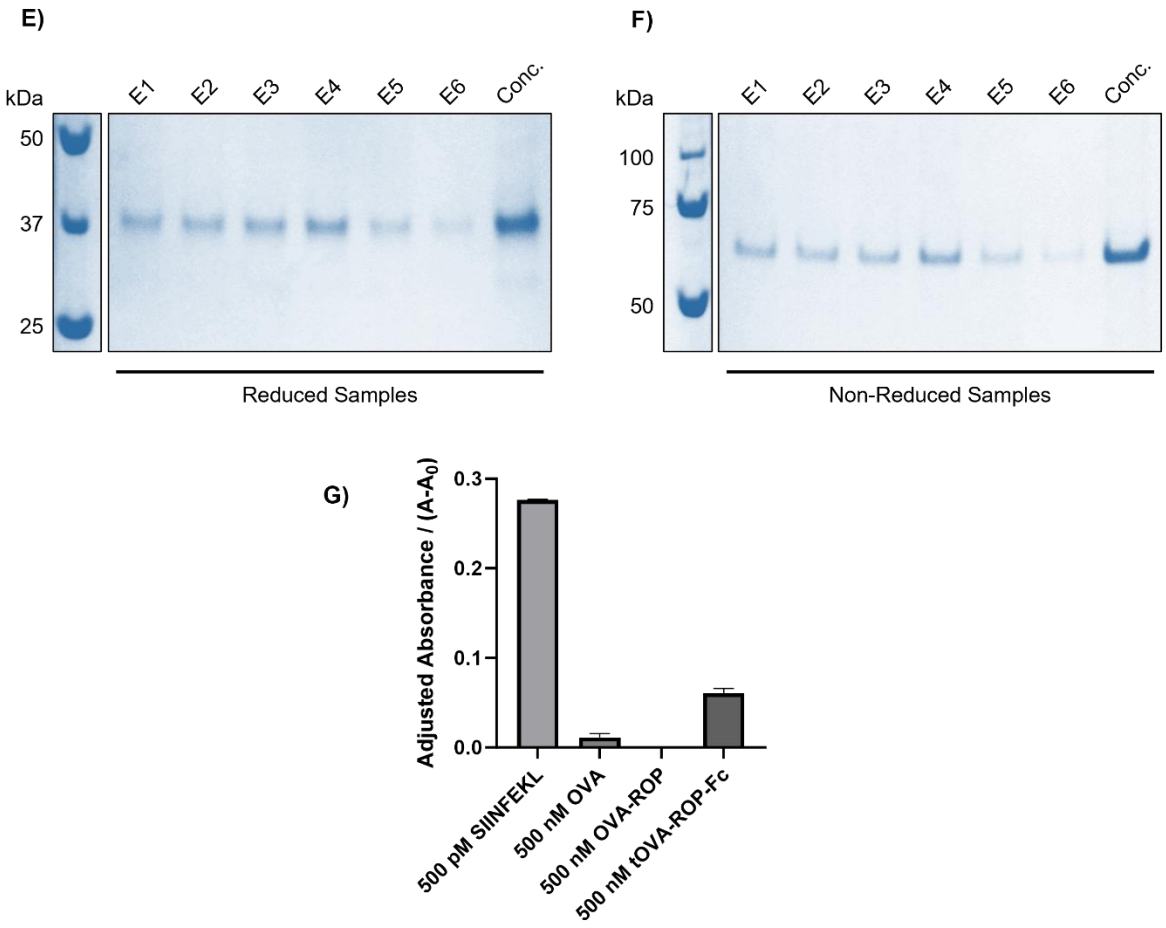


Figure 4.2 Purification and Antigenicity Assessment of tOVA-ROP-Fc
Expression was transferred to Expi293F cell culture for expression, purification, and antigenicity testing. **(A)** Reduced and non-reduced SDS-PAGE analysis of Expi293F cell culture expression and purification five days post-transfection with a DNA:PEI ratio of 1:3. Gel lanes showing protein content of supernatant (S/N, 5 µl), cell pellet (1 µl) and protein A column unbound flowthrough (F/T, 5 µl). tOVA-ROP-Fc protein A purified and eluted from the column as 800 µl fractions with 200 µl of neutralising 1 M TRIS-HCl pH 8.0, shown by elution fraction 1 (E1) and elution fraction 2 (E2). Red arrows designating the expected molecular weight of tOVA-ROP-Fc as a reduced monomer (33.4 kDa) or non-reduced homodimer (66.8 kDa). **(B)** SDS-PAGE analysis as in Figure 4.2A, but with a 1:6 DNA:PEI ratio. **(C)** Western Blot analysis using goat anti-mouse mIgG2a Fc-specific HRP-conjugated antibody on reduced Expi293F cell culture expression and purification five days post-transfection with a DNA:PEI ratio of 1:3. Western blot showing protein content of supernatant (S/N 5 µl), cell pellet (1 µl) and elution fractions (5 µl) from protein A purification. Red arrows designating the expected molecular weight of tOVA-ROP-Fc**. (D)** Non-reduced western blot of samples in Figure 4.2C. **(E)** Reducing SDS-PAGE analysis of protein A purified tOVA-ROP-Fc from Expi293F cell lysate, eluted into six fractions of 800 µl (E1-E6) with 200 µl neutralising 1 M TRIS-HCL pH 8.0. 10 µl loaded for E1 to E6. Analysis also of combined and concentrated E1-E6 eluate (500 ng loaded) fractions (Conc.) **(F)** Non-reducing SDS-PAGE of samples in Figure 4.2E. **(G)** B3Z CPRG assay test of tOVA-ROP-Fc compared to equimolar concentrations of OVA-ROP and OVA. 500 pM SIINFEKL was used as a positive control for the assay. Adjusted absorbance was calculated by subtracting absorbance values at 570 nm from reference absorbance values at 650 nm from all samples, then subtracting no protein/peptide negative control well values from the sample. Data shows mean ±SD.

4.2.3 The Inclusion of IgM Tailpiece Sequence and Q94C Mutation Can Induce Multimerisation of Fc-Tags

As a proof of concept, the tOVA-ROP-Fc was cross-presented but displayed a poor expression yield. In its present state, the homodimer tOVA-ROP-Fc is unlikely to provoke additional immune responses because of the lack of FcγR cross-linking and the inherent mechanisms facilitating the transport of homodimer immunoglobulin back out of cells via FcRn. To enhance Fc-tag efficacy and its ability to cross-link FcγR, the Fc-tag was modified through mutagenesis on the pFUSE vector to add the IgM tailpiece and the Q94C stabilising mutation. The mutation enhances the formation of hexameric structures composed of six homodimers, each carrying twelve conjugated fusion proteins. This configuration can potentially be more immunogenic than the individual Fc homodimer components (Figure 4.3A).

Before expressing the hexameric Fc with a fusion partner, it was crucial to ascertain whether the mutations induced the formation of hexameric structures. Additionally, identifying whether the previously observed low expression with pFUSE was attributable to the fusion partner was an essential step in the process (Figure 4.3A). The IgM tailpiece sequence (Table 2.2; Materials and Methods 2.1.7) was inserted using mutagenic primers (Appendix III) through site-directed mutagenesis (Figure 4.3B). After confirming the sequence was inserted, a Q94C mutagenesis (amino acid sequence in Table 2.2; Materials and Methods 2.1.7) was performed and sequenced for complete mutagenesis.

The pFUSE-Fc, mFc-IgM, and mFc_{QC}-IgM constructs were transiently transfected into Expi293F cells and purified from the supernatant by protein A affinity chromatography. Comparing a single Fc subunit expression to a hexameric expression of pFUSE-Fc without a fusion partner provides a baseline for future tOVA-ROP fusion comparison.

The protein A chromatography eluate was estimated by spectrophotometry at 280 nm absorbance using a calculated extinction coefficient of 32805 $M^{-1}cm^{-1}$ for pFUSE-Fc (26.3 kDa) and 35410 $M^{-1}cm^{-1}$ for mFc-IgM, and mFc_{QC}-IgM (28.2 kDa) (Figure 4.3C).

The 1 mL fractions were combined, and the yield was estimated by spectrophotometry, indicating an estimated yield of 5.79 mg at 0.97 mg/mL for the pFUSE-Fc and 5.97 mg at 1.49 mg/mL for the mFc-IgM (Figure 4.3C). The introduction of the Q94C mutation led to a significant drop in the estimated yield to around 0.67 mg at 0.33 mg/mL, suggesting that the introduced mutation strongly impacted cell expression (Figure 4.3C).

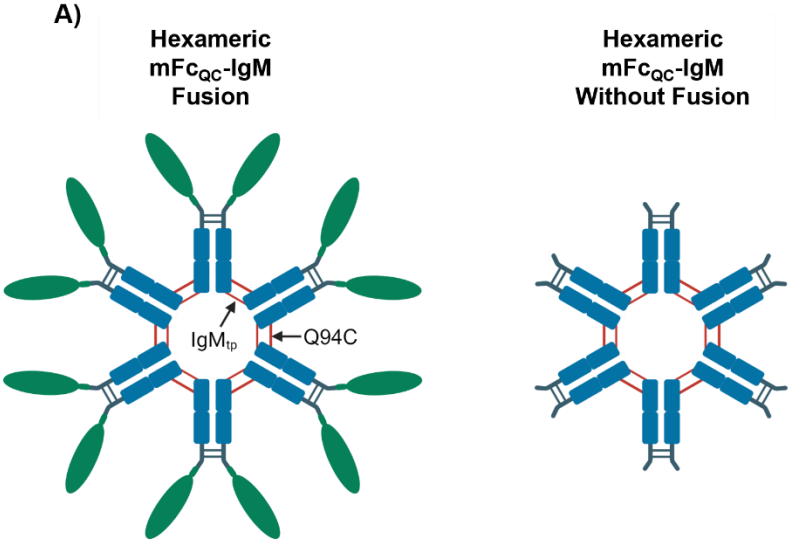
A total of 2 µg of each sample was loaded on an SDS-PAGE, with the pFUSE-Fc, mFc-IgM, and mFc_{QC}-IgM samples easily detectable by SDS-PAGE (Figure 4.3D-E), unlike the expression of tOVA-ROP-Fc described previously. The higher expression suggests that the persistently low yield of tOVA-ROP-Fc resulted from the fusion partner. Therefore, the fusion of the Fc-tag did not provide the ROP with stability. Observations from the reduced gel showed that the eluates of homodimer Fc were highly pure (Figure 4.3D), with no multimerisation observed, due to the disruption of the disulphide bonds in the tailpiece and those introduced as a stabilising mutation at Q94C. The non-reduced gel, loaded with an equal quantity of protein (2 µg), revealed higher molecular weight bands upon introduction of the IgM tailpiece-only mutation tags. These bands corresponded to molecular weights consistent with the dimerisation of the homodimer Fc-tag (Figure 4.3E).

With the inclusion of the stabilising Q94C mutation, the additional disulphide bond saw molecular weight bands corresponding to the size of dimers, trimers, and pentamers emerge (Figure 4.3E). Regardless of the introduction of the tailpiece or Q94C

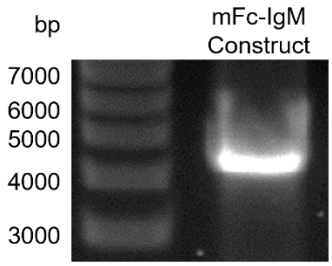
mutation, most of the Fc was found as a homodimer, indicating a preference for the structurally simpler homodimer or an inherent instability with each additional polymerisation step.

The successful expression of pFUSE-Fc highlighted the direct influence of tOVA-ROP on lower expression yields. Given the low expression levels observed for multimeric Fc without a fusion partner and the poor expression of tOVA-ROP-Fc, it is evident that producing a hexameric tOVA-ROP-Fc in its current configuration was not feasible.

A)



B)



C)

pFUSE-Fc		
Fraction	**A280**	**mg/mL**
E1	2.71	2.18
E2	1.98	1.59
E3	1.29	1.04
E4	0.58	0.47
E5	0.35	0.28
E6	0.24	0.19
Average		**0.965**

mFc-IgM		
Fraction	**A280**	**mg/mL**
E1	5.44	4.33
E2	1.36	1.08
E3	0.42	0.33
E4	0.24	0.19
Average		**1.492**

mFcQC-IgM		
Fraction	**A280**	**mg/mL**
E1	0.66	0.53
E2	0.19	0.15
Average		**0.336**

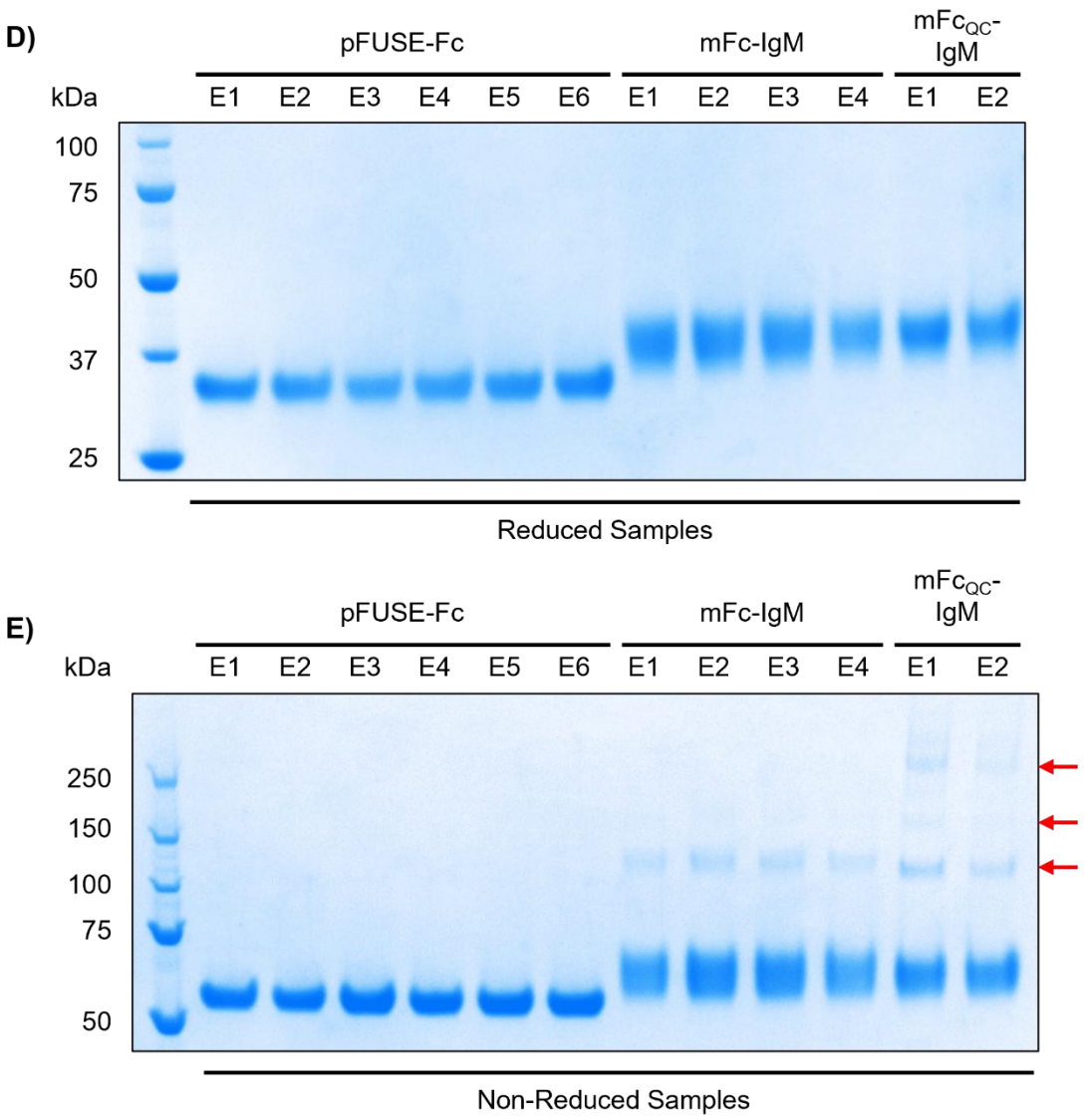


Figure 4.3 Multimerisation of mFc-IgM and mFc$_{QC}$-IgM Constructs
Empty pFUSE-Fc, mFc-IgM, and mFc$_{QC}$-IgM were cloned and transiently expressed in Expi293F cells. **(A)** The schematic of hexameric IgG shows the location of additional disulphide bonds (red) from the IgM tailpiece and Q94C mutations. Hexamer is shown with and without an associated fusion partner. **(B)** 1% agarose gel electrophoresis of PCR mutagenesis (10 µl) for insertion of IgM tailpiece into pFUSE-mIgG2a-Fc2 vector by Q5 mutagenesis using mutagenic primers. The band at 4.5 kb corresponds to the molecular weight for the complete construct. **(C)** Table of elution concentrations from protein A affinity purification of pFUSE-Fc, mFc-IgM, and mFc$_{QC}$-IgM from harvested Expi293F supernatant five days post-transfection (DNA:PEI 1:3). Absorbance 280 nm was measured on a Nanodrop and converted to mg/mL using the Beer-Lambert equation and calculated extinction coefficients of 32805 $M^{-1}cm^{-1}$ for pFUSE-Fc (26.3 kDa) and 35410 $M^{-1}cm^{-1}$ for mFc-IgM, and mFc$_{QC}$-IgM (28.2 kDa) **(D)** Reducing SDS-PAGE of protein A affinity purified pFUSE-Fc, mFc-IgM, and mFc$_{QC}$-IgM. 2 µg loaded. **(E)** Non-reducing SDS-PAGE of protein A affinity purified pFUSE-Fc, mFc-IgM, and mFc$_{QC}$-IgM as in figure 4.3C. Ascending red arrows designating banding of approximate size for dimer (112.8 kDa) and trimer (169.2 kDa). The third arrow indicates a potentially higher molecular weight multimer above the ladder's maximum predicted to be a pentamer (282 kDa).

4.2.4 OVA Epitope DEC-205 scFv Fusion is Expressed, Purified and Refolded From *E. coli*

OVA-ROP and tOVA-ROP have been challenging to express, even with the aid of Fc-tag. As a result, alternative strategies involving smaller subunits with the potential for multimerisation were explored to enhance antigen cross-presentation efficacy. A proposed approach links an anti-DEC-205 scFv to OVA $CD4^+$ and $CD8^+$ epitopes using a flexible (GGGS) linker to target the DEC-205 cell surface receptor found on DCs (amino acid sequence in Table 2.2; Materials and Methods 2.1.7) (Figure 4.4A). An Avitag was incorporated to facilitate the biotinylation of the fusion protein, enabling the analysis of the molecule via streptavidin conjugation. Additionally, Avitag can induce multimerisation by taking advantage of streptavidin's four biotin-binding sites (Figure 4.4A).

OVA-DEC-205 scFv was modified to include a SUMO fusion protein for cytoplasmic expression or a pelB sequence for periplasmic expression in *E. coli*. OVA-DEC-205 scFv and pelB-OVA-DEC-205 scFv constructs were generated by PCR amplifying their gene fragments using mutagenic primers (Appendix III). These constructs were then cloned into the pSUMO and pNIC-CTH0 vectors, respectively. The successful cloning was verified through PCR colony screening (Figure 4.4B) and by sequencing the complete constructs. Both constructs were transformed into a Rosetta (DE3) *E. coli* expression system and induced overnight. The analysis of the periplasmic expression showed no detectable expression of OVA-DEC-205 scFv (Figure 4.4C). The periplasmic compartment was dialysed to prepare for nickel affinity chromatography purification despite lacking a clear band. Purifying the dialysed periplasmic lysate did not result in the purification of OVA-DEC-205 scFv due to poor expression (Figure 4.4C).

SUMO was employed to facilitate robust expression and enhance the solubility of the scFv during the refolding process. The SUMO-tagged scFv exhibited strong expression in total cell lysates (Figure 4.4D) but was notably absent in the lysate of *E. coli* (Figure 4.4D). Upon analysis of the pellet, it was evident that OVA-DEC-205 scFv had aggregated and formed inclusion bodies (Figure 4.4D). The SUMO-tagged OVA-DEC-205 scFv inclusion body was solubilised by GuHCl buffer (Materials and Methods 2.4.3) and was purified successfully by nickel affinity chromatography (Figure 4.4E).

Following purification, the SUMO-tagged DEC-205-OVA-scFv was refolded by dialysis using OVA-DEC-205 refolding buffer (Materials and Methods 2.4.4). It remained soluble after multiple rounds of dialysis into 50 mM TRIS-HCl pH 8.0, 150 mM NaCl buffer (Figure 4.4E). The SUMO-tagged OVA-DEC-205 scFv was concentrated from 5 mL to 1.9 mL using centrifugal concentrators, and its concentration was determined by measuring the absorbance at 280 nm, with a calculated mass of 44.42 kDa and extinction coefficient of 69,705 $M^{-1}cm^{-1}$, resulting in a concentration of 1.22 mg/mL (totalling 2.32 mg). This analysis indicates that the scFv had formed inclusion bodies, was solubilised effectively by GuHCl, and remained soluble after refolding at higher concentrations than achievable with OVA-ROP or tOVA-ROP-Fc.

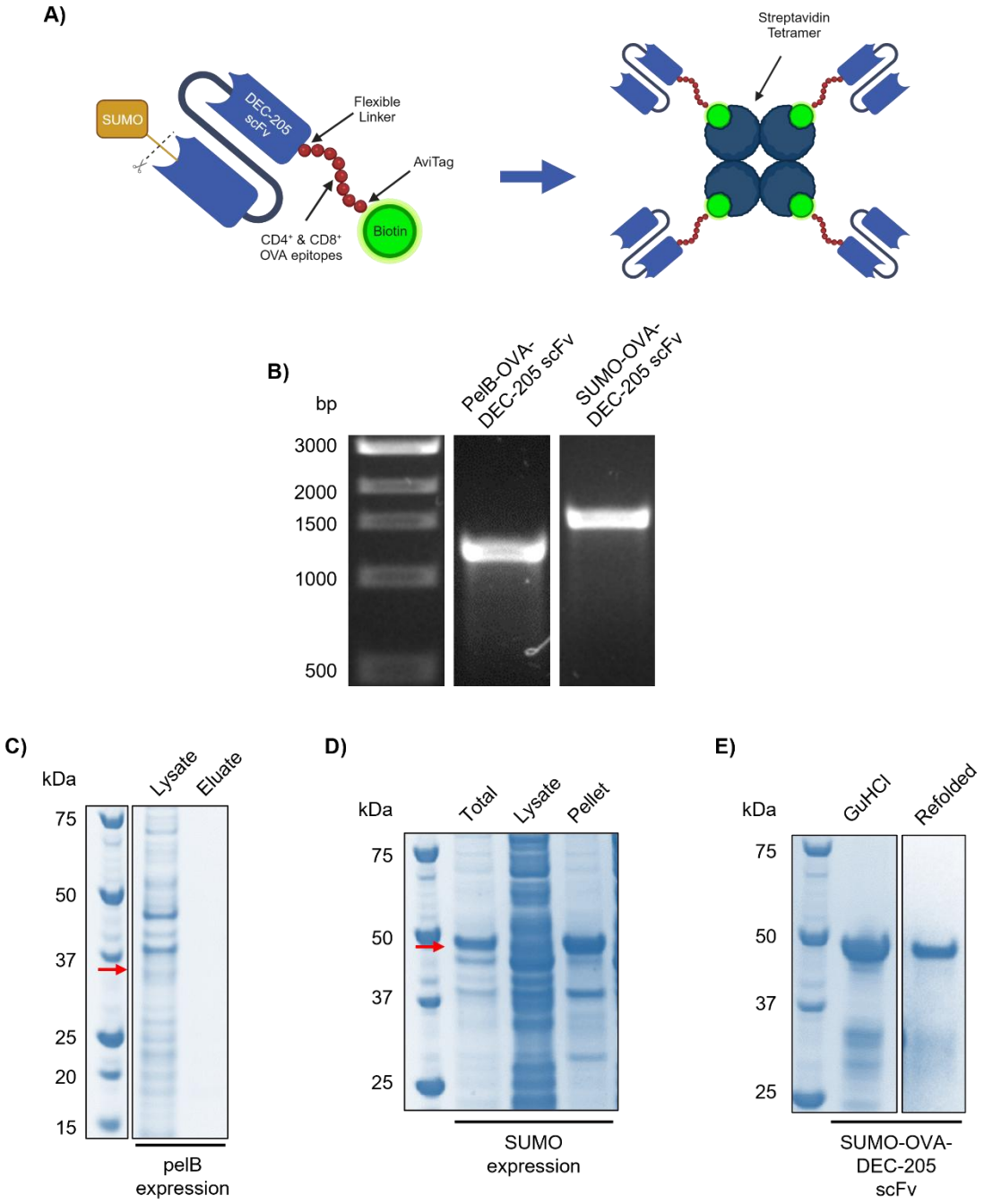


Figure 4.4 Expression and Purification of OVA-DEC-205 scFv Fusion in *E. coli*
OVA-DEC-205 scFv was cloned into pelB and SUMO constructs for periplasmic and cytoplasmic expression, respectively. **(A)** Schematic of OVA-DEC-205 scFv with SUMO protease tag as a monomer and tetramer unit conjugated to streptavidin. **(B)** 1.5% agarose gel electrophoresis of PCR colony screen (10 µl) using mutagenic primers (Appendix III) for pelB-OVA-DEC-205 scFv gene insertion into pNIC-CTH0 vector and OVA-DEC-205 scFv into pSUMO-LIC vector to produce SUMO-OVA-DEC-205 scFv. **(C)** SDS-PAGE analysis of pelB-OVA-DEC-205 scFv expression in *E. coli* lysate and elution from nickel resin affinity chromatography. Lysate diluted 1:500 with 10 µl loading. Eluate loaded neat with 10 µl loading. The red arrow indicates the expected molecular weight of OVA-DEC-205 scFv (33.6 kDa). **(D)** SDS-PAGE analysis of SUMO-OVA-DEC-205 scFv expression from total cell lysates (Total), soluble lysate, and cell lysis pellet. 1:50 dilution, 10 µl loaded. The red arrow indicates the expected molecular weight of the SUMO-tagged OVA-DEC-205 scFv (44.4 kDa). **(E)** SDS-PAGE analysis of SUMO-OVA-DEC-205 scFv solubilised in GuHCl (10 µl (~5 µg) loading by ethanol precipitation method (Materials and Methods 2.3.1)), and refolded scFv (2 µg) following dialysis in scFv refolding followed by 50 mM TRIS-HCl pH 8.0, 150 mM NaCl buffer.

4.2.5 SUMO Tag Removal From OVA-DEC-205 scFv Leads to Precipitation of the Fusion Protein

After refolding the SUMO-tagged OVA-DEC-205, the next step involved the removal of the SUMO tag. The removal was performed using SUMO proteases at various weight-to-weight (w/w) ratios with the scFv. TCEP reducing agent was added to facilitate the protease's catalytic activity. Cleavage of the SUMO tag from the OVA-DEC-205 scFv was successful for all the ratios evaluated (Figure 4.5A). However, the SUMO tag removal from the scFv resulted in the protein precipitating (Figure 4.5A).

A reducing agent is essential for optimal SUMO protease activity but may potentially harm the scFv stability by disrupting disulphide bonds. Therefore, the buffer was modified in the subsequent attempts with either no additional reducing agent or glutathione redox reaction (GSH/GSSG) as an alternative to TCEP to preserve the integrity of the disulphide bonds. GSH/GSSG and no additional reducing agent digests showed partial cleavage of the SUMO-tag and a small quantity of OVA-DEC-205 scFv in the solution, with most of it precipitating shortly after (Figure 4.5B). Therefore, the precipitation indicates that the instability was not caused by reducing agents but by misfolding or instability of the scFv maintained solely by SUMO.

As a small quantity of cleaved product was present in the solution following digestion of the SUMO tag, the cleaved SUMO tag and uncleaved products were removed by nickel affinity chromatography, by the 6xHis-tag present on the SUMO-tag and the SUMO protease. Unfortunately, the unbound column flowthrough did not contain the cleaved DEC-205 scFv (Figure 4.5C). Analysing the eluate, little of the scFv was present, with the majority remaining bound to the column (Figure 4.5C). Considering the available evidence, the scFv underwent precipitation on the column. The precipitation could be attributed to potential misfolding or dependence on SUMO for

maintaining its solubility. The selected OVA-epitope fusion might have introduced structural instability, so further optimisation of the fusion partner sequence is required to facilitate the production of a soluble scFv fusion protein.

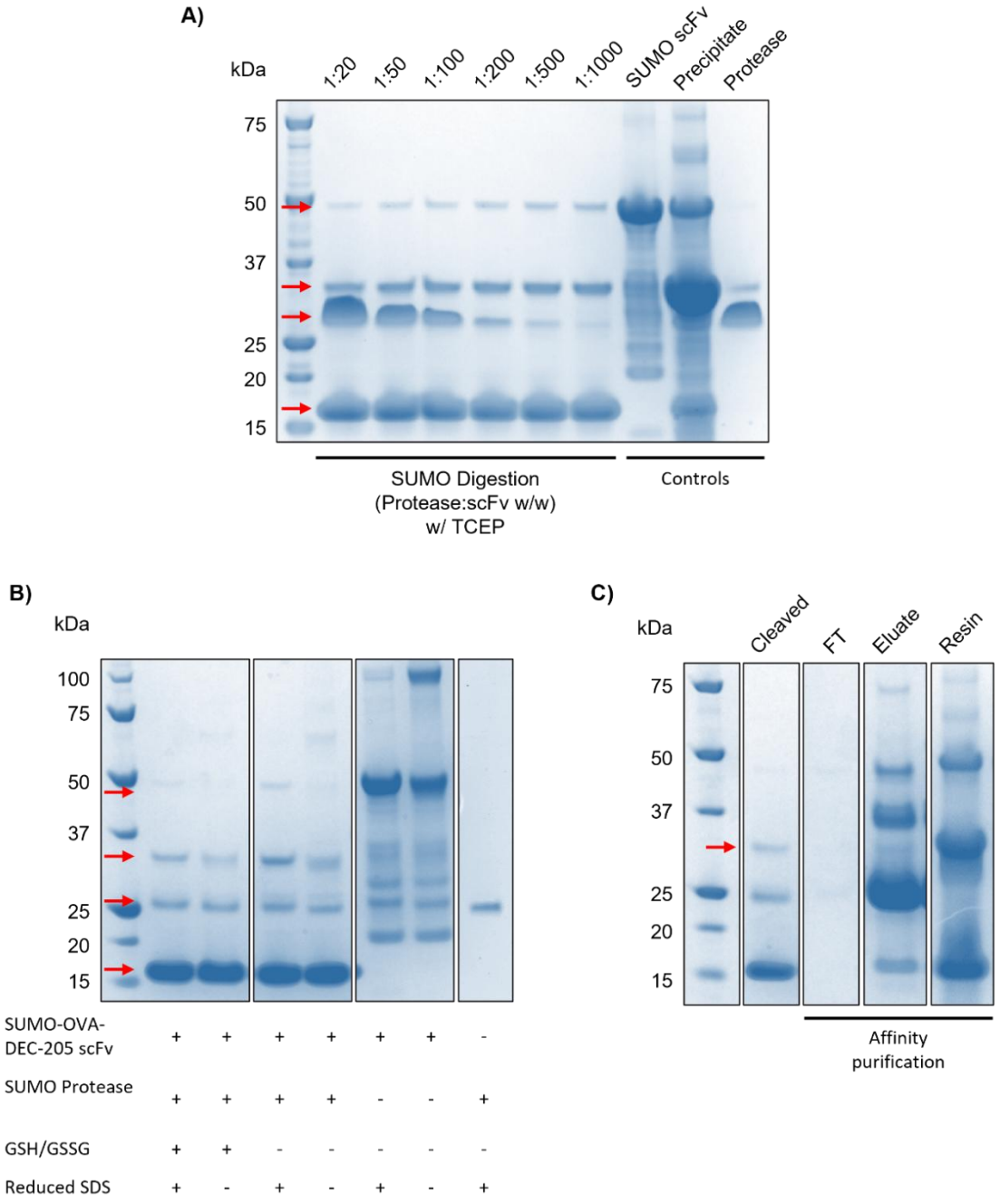


Figure 4.5 SUMO-Tag Removal From OVA-DEC-205 scFv by SUMO Protease
The SUMO tag was removed from OVA-DEC-205 scFv to allow for complete scFv activity and to prevent interference. **(A)** Reduced SDS-PAGE analysis of SUMO protease digest experiment (100 µg in 100 µl; 5 µl loaded). SUMO protease was added with 1 mM TCEP and tested at a range of protease-to-protein w/w ratios. Un-cleaved scFv (SUMO scFv) and protease-only controls were included. Precipitated material was also included for identification. Red arrows indicate in descending order: SUMO-OVA-DEC-205 scFv (un-cleaved; 44.4 kDa), OVA-DEC-205 (cleaved; 31.9 kDa), SUMO protease (28.2 kDa) and SUMO (cleaved tag; 12.6 kDa; runs at ~16-17 kDa on gel). **(B)** SDS-PAGE analysis of SUMO protease activity on SUMO-OVA-DEC-205 scFv (100 µg in 100 µl; 1:100 w/w; 5 µl loaded) with and without the presence of 3 mM/0.3 mM GSH/GSSG redox pair as a replacement for TCEP. Samples were reduced and non-reduced to identify misfolds. 2 µg SUMO-OVA-DEC-205 scFv (un-cleaved) and 1 µl SUMO protease only (1:1000 w/w) were included as controls for band identification. **(C)** SDS-PAGE analysis of nickel affinity negative purified OVA-DEC-205 scFv. Samples of cleaved product (5 µl), column flowthrough (10 µl), and eluate (10 µl) were collected and analysed, along with 5 µl of resin boiled with 10 µl SDS buffer to detect material on the column after elution.

4.2.6 NY-ESO-1 Epitope DEC-205 scFv Fusion is Expressed, Purified and Refolded From *E. coli*

Concurrently, an alternative anti-DEC-205 scFv fusion system was assessed as a substitute for OVA. The system consisted of $CD4^+$ and $CD8^+$ epitopes derived from the cancer testis-antigen NY-ESO-1. The NY-ESO-1 epitope region comprised 39 amino acids fused to an anti-human DEC-205 scFv with a flexible $(GGGS)_3$ linker and Avitag for future multimerisation (amino acid sequence in Table 2.2; Materials and Methods 2.1.7).

The NY-ESO-1-DEC-205 scFv (NYE-DEC-205 scFv) was cloned identically to OVA-DEC-205 scFv for periplasmic (pelB) and cytoplasmic (SUMO) expression with the same primers (Appendix III). PelB- and SUMO-NYE-DEC-205 scFv were expressed in Rosetta (DE3) *E. coli* cells. SDS-PAGE analysis of the lysed cells revealed that no observed band was present at the exact molecular weight for periplasmic expression (34.1 kDa) (Figure 4.6A); however, bands at around 37-38 kDa encouraged nickel resin affinity chromatography. Eluates from the chromatography displayed no purified NYE-DEC-205 scFv (Figure 4.6A), showing deficient expression of the scFv in the periplasmic space.

The expression focus shifted to SUMO-tagged NYE-DEC-205 scFv, with SDS-PAGE analysis demonstrating substantial expression in the total cell lysate, comprising soluble and insoluble fractions (Figure 4.6B). However, when analysing the soluble lysate, there was no evident band at the anticipated molecular weight (46.6 kDa) (Figure 4.6B). Further pellet examination indicated that the SUMO-NYE-DEC-205 scFv was forming an inclusion body. SUMO-NYE-DEC-205 scFv was solubilised by GuHCl and purified using a nickel resin column (Figure 4.6C). The scFv was

successfully refolded using the scFv refolding buffer (Materials and Methods 2.4.4) and then dialysed into a 50 mM TRIS-HCl pH 8.0, 150 mM NaCl buffer (Figure 4.6C).

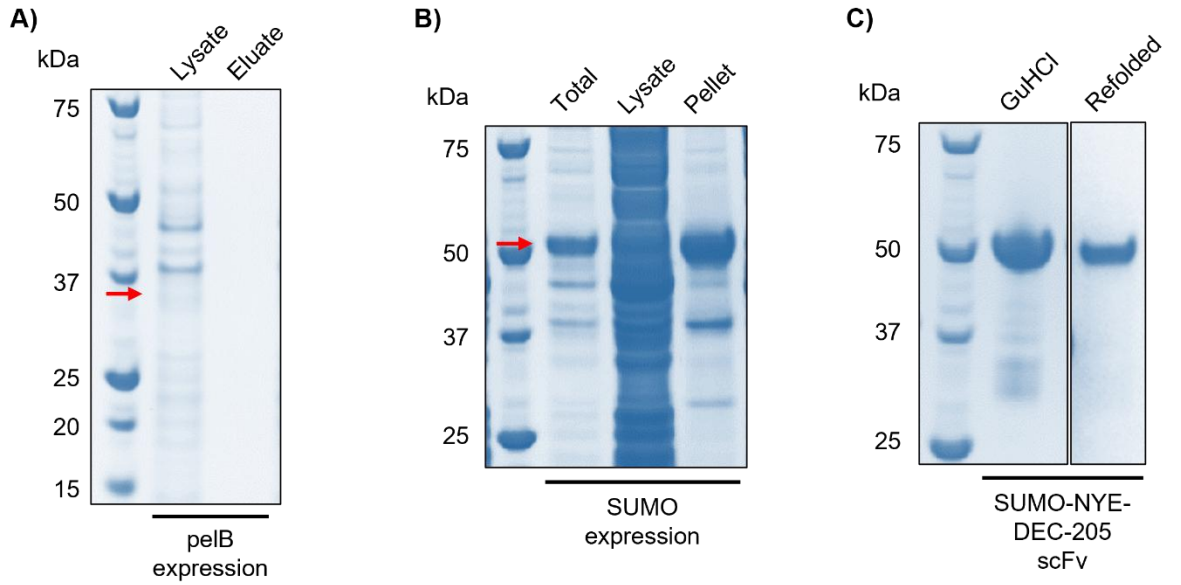


Figure 4.6 Expression and Purification of NYE-DEC-205 scFv Fusion in *E. coli*
NYE-DEC-205 scFv expressed in periplasmic and cytoplasmic compartments of *E. coli* **(A)** SDS-PAGE analysis of periplasmic lysis (lysate diluted 1:500 with 10 µl loading) with TSE buffer (Materials and Methods 2.4.3) and eluate of periplasmic compartment with nickel affinity chromatography (10 µl). The red arrow designates the expected molecular weight of NYE-DEC-205 scFv (34.1 kDa). **(B)** SDS-PAGE analysis of SUMO-tagged NYE-DEC-205 total cell lysates (soluble + insoluble), lysate (soluble), and pellet (insoluble) expression. Diluted 1:50, 10 µl loaded. Red arrow indicating SUMO-DEC-205 scFv expression. **(C)** SDS-PAGE analysis of SUMO-tagged NYE-DEC-205 scFv inclusion body solubilised and purified by nickel resin chromatography in 6 M GuHCl (10 µl (~5 µg) loading by ethanol precipitation method) and SUMO-tagged NYE-DEC-205 scFv following refolding (2 µg).

4.2.7 SUMO Tag Removal From NY-ESO-1 DEC-205 scFv Leads to Precipitation of the Fusion Protein

The next step for SUMO-tagged NYE-DEC-205 scFv was tag removal by SUMO protease. Various SUMO protease to scFv concentration ratios were assessed, using 100 µg of protein and 1 mM TCEP for each digestion. Removing the tag resulted in most of the scFv fusion precipitating out of the solution (Figure 4.6D). The process of removing the tag from SUMO-NYE-DEC-205 scFv proceeded by employing the GSH/GSSG redox reaction or by omitting the use of any additional reducing agent. This investigation aimed to determine whether NYE-DEC-205 scFv, like SUMO-OVA-

DEC-205 scFv, precipitated due to the reducing agents required for SUMO-tag removal or misfolding. Most of the NYE-DEC-205 scFv precipitated upon tag removal with GSH/GSSG redox reaction or with no additional reducing agents (Figure 4.6).

Purification was performed on the remaining NYE-DEC-205 scFv by nickel affinity chromatography (Figure 4.7F). The cleaved product was passed through a nickel resin to capture any remaining SUMO-tag, SUMO protease, and uncleaved SUMO-NYE-DEC-205 scFv. The flowthrough from the nickel resin demonstrated that these components had bound successfully but also removed the cleaved NYE-DEC-205 scFv (Figure 4.7F). Examination of the eluate and the resin revealed that the cleaved product was firmly and irreversibly bound to the column resin due to the instability and precipitation of the NYE-DEC-205 scFv (Figure 4.7F). The data suggests that the DEC-205 scFv molecule exhibits inherent instability in its structure. This instability could be attributed to misfolding or the introduction of conjugates that disrupt its structure, leading to a loss of its ability to fold appropriately and maintain solubility.

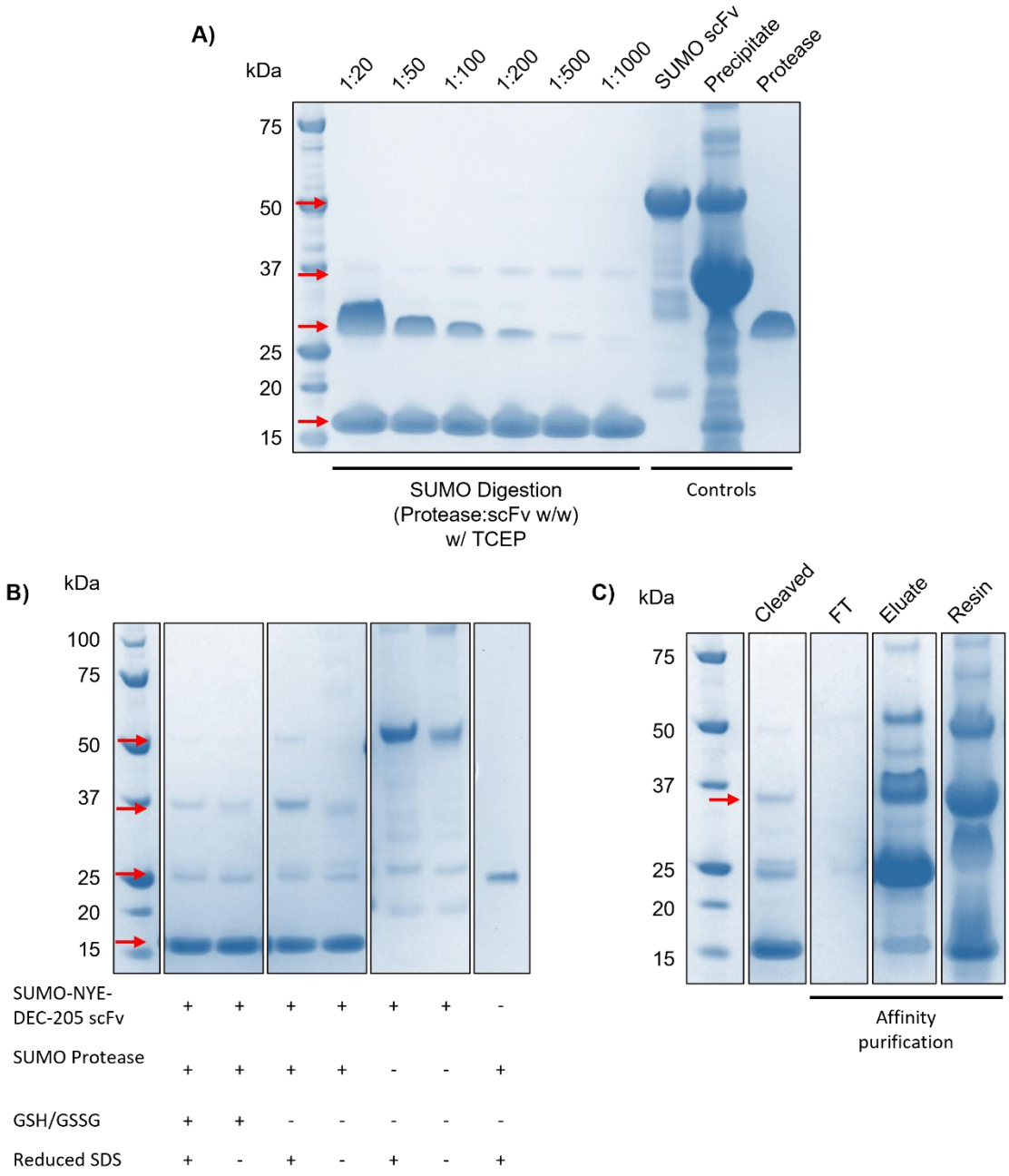


Figure 4.7 SUMO-Tag Removal From NYE-DEC-205 scFv by SUMO Protease
SUMO protease was used to remove the SUMO-tag from NYE-DEC-205 scFv. **(A)** SDS-PAGE analysis of SUMO protease digestion with 1 mM TCEP at a range of protease:scFv ratios (100 µg digest in 100 µl, 5 µl loaded). 5 µg un-cleaved SUMO-NYE-DEC-205 scFv (SUMO-scFv) and SUMO protease only loaded as a control. Precipitated material from SUMO protease digest was included to elucidate composition. Red arrows indicate in descending order: SUMO-NYE-DEC-205 scFv (un-cleaved; 46.6 kDa; runs at ~50 kDa), NYE-DEC-205 (cleaved; 34.1 kDa), SUMO protease (28.2 kDa) and SUMO (cleaved tag; 12.6 kDa; runs at ~16-17 kDa). **(B)** SDS-PAGE analysis of SUMO protease digestion (100 µg digest in 100 µl; 5 µl loaded) with and without 3 mM/0.3mM GSG/GSSG redox. Samples loaded reduced and non-reduced. 2 µg uncleaved NYE-DEC-205 scFv and SUMO only loaded as controls. Red arrow order as indicated in (A). **(C)** SDS-PAGE analysis of cleaved NYE-DEC-205 scFv passed through negative selection nickel affinity chromatography. Cleaved sample (5 µl), flowthrough (unbound, 10 µl) fraction and elution fraction (bound, 10 µl) loaded along with a 5 µl sample of resin resuspended in 10 µl SDS loading buffer for irreversibly bound material. Red arrow designating cleaved NYE-DEC-205 scFv.

4.3 Discussion

Fusing a truncated version of OVA-ROP to an Fc-tag was explored as a potential method of improving its solubility and immunogenicity. However, the tOVA-ROP-Fc fusion protein was secreted minimally in HEK293 and Expi293F cells, with the protein only observable by western blot in the supernatant and the majority remaining within the cells. Small quantities of tOVA-ROP-Fc were purified from the cell pellet to evaluate its antigenicity. A pilot B3Z assay was performed on tOVA-ROP-Fc with OVA-ROP and OVA. The experiment was performed once in duplicate due to the yields. However, it did show a small signal, with tOVA-ROP-Fc appearing to outperform OVA and OVA-ROP at equimolar concentrations.

As a proof of concept, the IgM tailpiece and the Q94C mutation in the Fc-tag were incorporated to assess the viability of producing multimeric IC-like structures. The multimerisation was initially expressed without a fusion partner before introducing additional partners that could hinder multimerisation. The pFUSE-Fc, mFc-IgM, and mFc_{QC}-IgM were all expressed and secreted by the Expi293F cells. Non-reduced SDS-PAGE analysis revealed low quantities of dimers, trimers, and pentamers, indicating that multimerisation occurred. However, each successive multimerisation led to increasingly lower amounts, especially when compared to the monomeric Fc band present on the gel.

In the tOVA-ROP-Fc study, the main destabilising element was the tOVA-ROP. As a result, alternative fusion formulations were explored. A fusion of an anti-mouse DEC-205 scFv and OVA epitopes was chosen as a proof-of-concept instead of using complex overlapping peptides. Additionally, the anti-human DEC-205 scFv was paired with NY-ESO-1. The expression of DEC-205 scFv was in an *E. coli* expression system

with SUMO N-terminal tag for cytosolic expression and pelB signal sequence for periplasmic expression, an oxidative environment that encourages disulphide bond formation (Dewi et al., 2016). The expression of pelB was notably absent, with no recoverable or purifiable scFv. In contrast, SUMO exhibited high expression levels but primarily formed inclusion bodies.

In contrast to previous attempts at OVA-ROP refolding, the SUMO-tagged OVA-DEC-205 scFv and NYE-DEC-205 scFv fusions appeared successful, requiring only a few additives to aid in the refolding process. Efforts to eliminate the tag were undertaken using the GSH/GSSG system, but the scFv proved to be unstable without the solubilising SUMO tag.

Overall, combining tOVA-ROP with Fc-tag was partly successful. The Fc-fusion system demonstrated that it was mildly capable of expressing tOVA-ROP-Fc, with the protein not being secreted, despite the inclusion of the IL-2 signal sequence, a commonly used secretion signal sequence for recombinant proteins (Stern et al., 2007; Zhang et al., 2005). The lack of supernatant expression and accumulation in the cell pellet suggests either an instability with the protein or a problem with its secretion, potentially attributable to its misfolding.

Unlike *E. coli*, mammalian cells do not accumulate misfolded proteins as they are readily degraded through proteasome and lysosome pathways (Buchberger et al., 2010). The cytoplasmic disulphide bond in *E. coli* (CyDisCo) strain was proposed as an alternative expression system for tOVA-ROP-Fc in *E. coli*. This strain has been specifically engineered to express the essential for respiration and vegetative growth protein 1 (Erv1p) to catalyse disulphide bond formation and DsbC to catalyse its isomerisation (Gaciarz et al., 2016; Hatahet et al., 2010). CyDisCo has been

demonstrated to express soluble antibody fragments in *E. coli* (Gaciarz et al., 2016; Hatahet et al., 2010). Ultimately, *E. coli* expression was not pursued due to the optimised Fc constructs for mammalian expression and the attempt to avoid disaggregating and refolding from inclusion bodies if the modified strain did not successfully fold the fusion. As demonstrated, the Fc tag alone was easily expressed. Therefore, the challenges with the fusion were unlikely to be attributed to a problem with mammalian expression and more to the folding with the fusion.

Despite the poor secretion for the Fc-fusion, it was purified from the cell pellet but with the IL-2 sequence still attached. One potential solution would be eliminating the IL-2 sequence through mutagenesis during the cloning stages. However, since the Fc-tag was placed at the C-terminus, leaving the IL-2 sequence attached would primarily affect the N-terminal section of the OVA sequence and was unlikely to affect its immunogenicity.

Interestingly, when examining the immunogenicity of tOVA-ROP-Fc against OVA-ROP, OVA-ROP consistently failed to produce a signal in the B3Z assay, unlike in the previous chapter with the flow cytometry assay. The preparation of OVA-ROP at the concentration examined was within the sarkosyl tolerance seen with DC2.4. Therefore, sarkosyl may interfere with the cell assay, potentially through the permeabilisation effect discussed previously or another instability of the OVA-ROP within the co-culture assay (Koley & Bard, 2010). However, what was observed was a potential enhancement with the Fc-fusion, possibly attributable to excitatory Fc-receptor binding or the lack of interference from sarkosyl. However, the low yield for OVA-ROP-Fc hindered the possibility of conducting repetitions with various concentrations and assessing statistical significance. Coupled with the limited response observed in the

B3Z assay, it became impractical to pursue further analysis as a potential candidate for an enhanced ROP.

The problem did not lie in the expression of the Fc, as the unconjugated Fc exhibited high expression, suggesting that tOVA-ROP was the source of the issue. However, when attempts were made to multimerise the Fc-tag, there were diminishing returns for every additional polymerisation. Interestingly, the band for IgM tailpiece mutation is “fuzzy” compared with the much clearer wildtype band; this is likely due to glycosylation of the IgM tailpiece, as IgM are heavily glycosylated molecules and the addition of the 18-amino acid tailpiece adds an asparagine molecule known to be a site for N-linked glycosylation (Arnold et al., 2005). The IgM tailpiece-only bands in the non-reduced gel displayed evidence of dimerisation, which can be attributed to the formation of disulphide bonds at cysteine-575 within the IgM tailpiece (Arnold et al., 2005). This disulphide bond is strong enough for dimer formation but cannot maintain larger multimers without the additional disulphide bond created with the Q94C mutation.

Nevertheless, separating the multimeric from the monomeric would require high culture volumes and considerable purification to separate the multimers by size (Mekhaiel et al., 2011), with each successive downstream process reducing the total yield. On top of that, the multimeric expression is without a fusion partner, which would be significantly detrimental to the expression yields of multimers and, depending on its size and the length of the linker, could interfere with their formation by steric hindrance between the monomers. As the multimers’ yields only comprised a small portion of the total expression, with the majority being monomeric, further optimisations would need to be investigated. Nevertheless, adding a fusion partner would exacerbate the poor multimeric yields.

Generating a smaller and simpler system with epitopes fused to an scFv proved challenging for both the OVA and NY-ESO-1 systems. NY-ESO-1 was explored to produce a model for studying a human cancer antigen. Like OVA, NY-ESO-1 has extensively characterised HLA-A2-restricted $CD8^+$ epitope (Jager et al., 1998; Zeng et al., 2002) and the availability of tools for assessing its presentation on MHC-I, such as the HLA-$A2^+$ NY-ESO-1 TCR (1G4) Jurkat reporter cell line (Jager et al., 1998; Li et al., 2005; Zeng et al., 2002). The 1G4-Jurkat cells have also been engineered to express luciferase under the NFAT promoter upon HLA-TCR (1G4) binding (BPS Bioscience), allowing detection of NY-ESO-1 presentation on primary HLA-$A2^+$ antigen-presenting cells or cell lines such as THP-1 cells (Jager et al., 1998; Zeng et al., 2002). This system establishes itself as an alternative human model for studying peptide and ROP cancer vaccines.

The refolding of the scFv initially looked promising with the SUMO-tag, as it remained soluble with the aid of GSH/GSSG and L-arginine. Glutathione redox, composed of a 10:1 ratio of reduced glutathione (GSH) to oxidised glutathione (GSSG), has been shown to catalyse the formation of disulphide bonds (S. S. Wang et al., 2006). Meanwhile, arginine is commonly used as a refolding additive because of its hydrophilic and positive charge through its guanidinium group, which prevents aggregation by binding to negatively charged areas and exposed hydrophobic regions on proteins (Arakawa et al., 2007; Chen et al., 2008).

Despite this, the solubility of both scFv fusions was reliant on SUMO, with the fusion protein's instability potentially being due to numerous factors, such as the fusion sequence, inadequate refolding buffers or methods, or the formation of incorrect disulphide bonds. Correctly forming these bonds is essential to maintain protein stability, and any wrong confirmation may have caused the scFv instability upon

SUMO tag removal. Unfortunately, removing SUMO was unavoidable as its size can have unintended consequences on scFv confirmation and biological activity (Arnau et al., 2006; Sun et al., 2012).

Had the refolding been successful, the objective was to first visualise scFv binding to DEC-205 through its Avitag, a sequence derived from chicken egg white avidin protein with a strong affinity for biotin (Kay et al., 2009). The Avitag would have allowed for the detection of the molecule on and in cells through streptavidin-conjugated fluorophores, with streptavidin's interaction and binding affinity to biotin being very high, creating one of the strongest non-covalent bonds in nature (Laitinen et al., 2006). The biotinylation also functioned as a potential multimerisation platform for forming multiple valency complexes through free streptavidin and its four biotin-binding sites (Kipriyanov et al., 1996).

Using streptavidin as a scaffold for multimerisation has been developed for many purposes; the most widely used is the generation of MHC-tetramers, designed to analyse antigen-specific TCRs on cells (Altman et al., 1996). The low avidity and high off-rate of monomeric soluble MHCs made them impractical to study MHC-TCR interactions, so the MHC-tetramer was developed by conjugation to streptavidin through biotin, leading to increased stability and avidity compared to the monomer (Altman et al., 1996).

Therapeutic uses for streptavidin tetramers include a multimer for selective detection and expansion of CAR-T cells using four extracellular domains of human CD19 fused with streptavidin (Lian et al., 2022). A few studies have also examined the use of streptavidin tetramers in immunotherapy, including linking anti-CD20 antibodies to

streptavidin for the treatment of non-Hodgkin lymphoma and a fusion with CD40L for targeting the immune checkpoint (Kilinc et al., 2006; Pagel et al., 2006).

4.4 Conclusion

OVA-ROP and its derivatives still proved challenging molecules to express, purify, and maintain in a soluble format. Some success was observed using tOVA-ROP-Fc and B3Z assay, but the poor yield limited the number of experiments needed to assess significance. Attempts to produce multimeric structures with the tailpiece and Q94C mutation were partially successful, with signs of multimerisation. However, the vast majority were still homodimers and would require considerable optimisation and downstream processing to produce significant concentrations for testing. Creating scFv fusions in *E. coli* cells initially seemed promising, with the SUMO version appearing to refold. Ultimately, the cleavage of SUMO resulted in its instability, which caused the scFv fusion to precipitate out of the solution.

A distinct approach is required to deepen our understanding of the underlying mechanisms of antigen cross-presentation routing, particularly the influence of the cathepsin S cleavage site. For the next chapter, smaller synthetic peptides will be used as a substitute for ROP to elucidate how peptide cancer vaccines are transported within cells and the significance of the vacuolar pathway in antigen cross-presentation.

5 Uncovering the Role of the Cathepsin S Sensitive Linker in Antigen Cross-Presentation

5.1 Introduction

In previous chapters, OVA-ROP and its derivatives were investigated as potential models for studying the LRMK cleavage site in antigen cross-presentation. The tOVA-ROP-Fc displayed a propensity for cross-presentation. However, issues around the expression of tOVA-ROP-Fc prevented further investigations. On the other hand, the scFv fusions expressed well but were difficult to maintain in solution after tag removal. In the following study, synthetic peptides will be investigated as an alternative model to elucidate the contribution of the cathepsin S linker in cross-presentation without reliance on recombinant protein expression.

Synthetic peptides are made cell-free to an exact size and specification with modifications, such as unnatural amino acids, that are not possible recombinantly (Wang et al., 2022). Synthesised peptides are considerably smaller than the 143 amino acid OVA-ROP but still require uptake and processing, as they are not short enough to bind to MHC-I directly (Khan et al., 2007). However, peptides do not fully represent larger, more complex molecules like OVA-ROP and may bypass specific processes or progress through them quickly (Rosalia et al., 2013).

Synthetic peptides are helpful tools that offer valuable insights into peptide internalisation, processing and presentation. The primary internalisation mechanisms in DCs are phagocytosis, macropinocytosis, dynamin-dependent endocytosis (clathrin-mediated and clathrin-independent), and dynamin-independent endocytosis (Rennick et al., 2021). The overall contribution of these entry mechanisms can be observed using chemical inhibitors.

Amiloride, a widely used macropinocytosis inhibitor, inhibits the Na^+/H^+ exchange and lowers submembrane pH (Koivusalo et al., 2010). Cytochalasin D targets phagocytosis and macropinocytosis through the depolymerisation of F-actin (Casella et al., 1981; Ting-Beall et al., 1995). Finally, dynasore inhibits the guanosine triphosphate hydrolase (GTPase) activity of dynamin and consequently blocks dynamin-dependent uptake, such as clathrin-mediated endocytosis (Kirchhausen et al., 2008). Their specific actions on various cellular processes will offer a clearer picture of the peptide uptake dynamics and their presentation to discern which pathways are essential for cross-presentation.

For instance, mannose receptor-mediated endocytosis directs antigens towards early endosomes with a higher pH, steering away from degradation via the lysosomal pathway often associated with macropinocytosis (Burgdorf et al., 2007; Rauen et al., 2014). On the other hand, cross-presentation through the phagocytosis pathway is a time-dependent mechanism, where Rab27a regulates phagosome pH via NOX2, leading to a less acidic environment and promoting cross-presentation (Burgdorf et al., 2008; Jancic et al., 2007). Over time, the phagosomes reacidify, reducing cross-presentation and increasing digestion, resulting in improved MHC-II presentation (Burgdorf et al., 2008; Jancic et al., 2007). Therefore, rapid endosomal escape is imperative for the cytosolic cross-presentation pathway via phagocytosis.

Upon escape into the cytosol, proteins undergo digestion by the proteasome (Burgdorf et al., 2008; Kloetzel, 2001; Kovacsovics-Bankowski & Rock, 1995). Subsequently, they are imported into the ER through the TAP protein, loaded onto MHC-I and transported to the cell surface (Burgdorf et al., 2008; Joffre et al., 2012; Kovacsovics-Bankowski & Rock, 1995). Various inhibitors can be used to investigate the involvement of the cytosolic pathway.

One method by which specialised cross-presenting DCs mediate cross-presentation is through deacidification of their endosomes. For example, the $CD8^+$ DC subtype in mice and the cDC1 subtype in humans exhibit high efficiency in cross-presentation, partly attributable to their less acidic endosomes (Savina et al., 2009; Segura et al., 2013). Deacidification prevents the rapid degradation of proteins, providing more time for export from the endosome to the cytosol and leading to higher cross-presentation efficiency (Accapezzato et al., 2005; Delamarre et al., 2006; Garulli et al., 2008). Chemical inhibitors such as chloroquine inhibit the acidification of the endosomes and have been shown to enhance cross-presentation (Accapezzato et al., 2005; Savarino et al., 2003). Therefore, chloroquine can demonstrate whether endosome deacidification and escape are paramount for the cross-presentation of the peptides.

Upon endosomal escape, proteins are processed by the proteasome before transportation into the ER. Many studies have thoroughly documented the inhibitory effects of compounds like MG-132 and epoxomicin on the proteasome, which leads to a decrease in antigen cross-presentation (Duvallet et al., 2016; Imai et al., 2005; Mant et al., 2012; Menager et al., 2014). MG-132 is a reversible inhibitor of the 26S proteasome complex (Lee & Goldberg, 1996), and epoxomicin is a specific and irreversible inhibitor of the 20S subunit of the proteasome (Meng et al., 1999). By inhibiting the proteasome, the overall contribution of the cytosolic pathway in contrast to the proteasome-independent vacuolar pathway can be uncovered, explaining how differences in peptide sequences may affect processing.

Following proteasomal degradation, peptides are imported into the ER by TAP, loaded onto MHC-I, and exported to the cell surface (Burgdorf et al., 2008; Kovacsovics-Bankowski & Rock, 1995). However, evidence, especially within the vacuolar pathway, indicates that some MHC molecules originate from recycling endosomes (Basha et

al., 2012; Di Pucchio et al., 2008; Nair-Gupta et al., 2014). The export mechanism of MHC-I molecules can be analysed by employing brefeldin A, a protein transport inhibitor known to prevent extracellular delivery of newly synthesised MHC to the cell surface (Fujiwara et al., 1988; Yewdell & Bennink, 1989). Therefore, it can help discern whether peptide loading arises through the ER-Golgi network or recycling endosomes.

MHC export inhibition can also discern whether peptides can bind directly to empty MHC-I on the cell surface. In normal physiological conditions, empty MHC-I molecules on the cell surface are quickly removed (Ljunggren et al., 1990; Schumacher et al., 1990). Nevertheless, evidence suggests that at sub-33°C, MHC-I can be retained on the cell surface and stabilised by binding to MHC-I-specific peptides (Ljunggren et al., 1990; Schumacher et al., 1990). SIINFEKL peptide is a prime example, as it is a “ready-to-go” peptide at the correct size for empty MHC-I on the cell surface, bypassing the intracellular machinery and giving a false impression of its efficiency at being processed by the DCs.

The vacuolar pathway is principally TAP and proteasome-independent and is mediated by the cysteine protease cathepsin S within the endosomal compartment (Shen et al., 2004). Therefore, to examine the contribution of the proteasome-dependent cytosolic pathway to the vacuolar pathway, inhibition of cathepsin S needs to occur. Cathepsin S inhibition can be achieved through chemical inhibition or gene knockdown. Chemical inhibition is quick and relatively simple with LHVS, a potent cell-permeable and irreversible pan-cathepsin inhibitor (Palmer et al., 1995). However, LHVS is non-selective and will bind and inhibit cathepsin B, L and S subtypes at different concentrations, with many of these cathepsins involved in processing antigens (Palmer et al., 1995; Riese & Chapman, 2000; Riese et al., 1996; Shen et al., 2004). Although LHVS is pan-cathepsin, it does exhibit a higher affinity for

cathepsin S than B and L (Palmer et al., 1995; Riese et al., 1996). Therefore, LHVS can be made specific to cathepsin S by controlling the concentration.

Unlike LHVS, siRNA is engineered to reduce or eliminate gene expression specifically. One advantage is that gene knockdown can be measured and quantified through qPCR or western blot analysis techniques, making it possible to quantify changes in expression levels. The disadvantage is that effective siRNA knockdown is difficult in some cells and is not always complete (Campeau & Gobeil, 2011). Nevertheless, combined with chemical inhibition, it can be valuable in furthering evidence on the effect of cathepsin S inhibition.

Many of the inhibitors mentioned have been valuable tools in investigating cross-presentation pathways. One group found that TAP-deficient murine DCs incubated at 26°C showed increased cell surface MHC-I that could fully present phagocytosed antigens but failed to present soluble ones (Merzougui et al., 2011). The group then used MG-132 and epoxomicin in the TAP knockout cells at 37°C and 26°C and found that they both significantly reduced antigen cross-presentation in TAP knockout and wildtype models equally at either temperature (Merzougui et al., 2011). At the same time, they found that inhibition of cathepsin S by LHVS reduced cross-presentation by 80% in both the wildtype and TAP knockout models, suggesting that their OVA-based antigen system required the proteasome and cathepsin S intact to function (Merzougui et al., 2011).

The authors used this experiment in part to propose a new model for a distinct protease-dependent, TAP-independent mechanism for phagocytosed antigens through an unknown transporter of protease-digested peptides from the ER to a

discrete compartment for loading onto MHC-I molecules recycled from the cell surface (Merzougui et al., 2011).

The inhibition study underscores two principles. Firstly, it emphasises the presence of substantial redundancy and intersecting pathways in cross-presentation and the adaptability and robustness of the immune system, ensuring effective antigen cross-presentation. Secondly, it demonstrates how inhibitors can be used to uncover how antigens are processed. Thirdly, it demonstrates that the method of entry and an antigen's form as either a soluble antigen or as a particle can profoundly impact the cross-presentation process. Specifically, in the context of the endosome-to-cytosol pathway, peptides derived from soluble proteins typically exhibit ERAP-independence and undergo processing within the endosome. This process involves TAP-mediated import and subsequent trimming facilitated by IRAP (Burgdorf et al., 2008; Saveanu et al., 2009). Whereas peptides from particulate antigens tend to be processed by both ERAP and IRAP in the ER and the endosome in a TAP-dependent manner (Burgdorf et al., 2008; Saveanu et al., 2009).

For this study, three peptides were synthesised: the "cathepsin S (ctss) peptide", which contains the whole LRMKLPKP motif derived from a known cathepsin S cleavage site, followed by the OVA $CD8^+$ epitope SIINFEKL. The second peptide, referred to as "mutant peptide", has a double point mutation of the fourth residue, lysine to aspartic acid (K → D), and the fifth residue, leucine to proline (L → P). The mutation rationale was adapted from research by Lützner & Kalbacher, which showed that acidic amino acids in the P1 position and proline at P1' were unfavourable for cathepsin S cleavage (Lützner & Kalbacher, 2008). The final peptide is the "scrambled peptide", which contains an identical amino acid composition to the ctss peptide but with the residues preceding the SIINFEKL epitope in random order. The reasoning was to determine

whether the amino acid sequence or the LRMK site contributed to the cross-presentation of the ctss peptide. All three peptides contain hydrophilic arginine residues at the N- and C-terminus of the sequence to aid in peptide solubility (Kyte & Doolittle, 1982).

The synthetic peptides used in this study have been designed to investigate the contribution of cathepsin S through the LRMK site to cross-presentation, compared to peptides that contain disruptions to the cleavage site. The aim is to discover the specificity of the site, along with the contribution of the amino acid composition and order in cross-presentation. The synthetic peptides will be combined with LHVS and siRNA inhibition to provide a two-pronged approach to maximise the potential for cathepsin S inhibition. The peptides will also be combined with inhibitors of cell internalisation, antigen processing and export to determine whether the LRMK site influences their processing independent of cathepsin S cleavage. The synthetic peptides will provide valuable insight into this motif's importance and further our understanding of its significance in ROP cross-presentation.

Comparing the synthetic peptides and the various inhibitors to a control peptide is challenging, as the minimal size of SIINFEKL renders it unsuitable as a control for cross-presentation. A larger and more complex control is needed to validate different pathways of cross-presentation and the inhibitors employed. A particulate-based OVA-conjugated latex bead system was proposed to validate the inhibitors and compare soluble and particulate-based antigens in DC2.4 cells. Nevertheless, it is essential to recognize that OVA beads may undergo processing through pathways distinct from those of soluble synthetic peptides. These differences must be considered when interpreting the experimental data and drawing conclusions. However, OVA-

conjugated beads will still provide valuable insight to validate the cross-presentation experiments.

5.1.1 Chapter Aims

- Investigate the impact of the ER-to-Golgi secretion network on the ctss, mutant and scrambled synthetic peptides.
- Determine the preferred route of entry of the peptides into DC2.4 cells, differentiating between peptides with and without the cathepsin S cleavage site.
- Evaluate the contribution of the endosome-to-cytosol and vacuolar pathways in peptide antigen cross-presentation.
- Investigate the influence of the vacuolar pathway mediated by cathepsin S on antigen cross-presentation efficiency for the peptides through chemical inhibition and siRNA knockdown.
- Use OVA-conjugated beads to elucidate differences in antigen cross-presentation between particulate and peptide-based systems.

5.1.2 Hypotheses

- The entry and processing of the peptides differs depending on their sequence and the inclusion of the LRMK sequence.
- The synthetic peptides exhibit differences in cross-presentation when comparing the cathepsin S-sensitive LRMK and disrupted LRMK sequences.
- Cathepsin S knockdown significantly affects the antigen cross-presentation of the LRMK-containing peptide over those that do not.
- Differences in inhibition profiles are observable with the soluble vs. particulate-based antigen systems.

5.2 Results

5.2.1 Brefeldin A Partially Inhibits MHC-I Export of the Synthetic Peptides

The protein transport inhibitor brefeldin A was used to evaluate the influence of exporting MHC-I via the ER and Golgi on the cross-presentation of three synthetic peptides: ctss, mutant, and scrambled peptide (sequences in Table 2.5, Materials and Methods 2.5.1). The aim was to determine whether the linker's inclusion affected the peptides' routing through the ER-to-Golgi network.

The B3Z CPRG cross-presentation assay was used with DC2.4 cells for the peptides, using SIINFEKL as a positive assay control. DMSO-only vehicle control was included, from 0.05% in a two-fold series, to ensure that the DMSO used to dissolve the peptides did not exert any activating effects on the assay. A concentration curve for SIINFEKL control peptide and each synthetic peptide was created across twelve concentrations with a two-fold dilution series starting at 2000 nM (4000 pM for SIINFEKL) (Materials and Methods 2.6.4). DC2.4 Cells were treated with or without brefeldin A for 2 hours before adding peptides for 4 hours with or without further inhibition. Cells were fixed and co-cultured overnight with B3Z cells before progressing to CPRG assay.

Dose-response curves were created from the B3Z assay by normalising the data and plotting on a variable slope four-parameter non-linear regression. Each peptide with and without inhibition was compared on dose-response curves (Figure 5.1A-D) to show whether brefeldin A affected the potency and efficacy of the peptides. Inhibition with brefeldin A saw a rightwards shift in the dose-response curves for SIINFEKL, ctss peptide, mutant peptide, and scrambled peptide (Figure 5.1A-D). The curves also reduced the maximum response for the ctss peptide, mutant, and scrambled peptides (Figure 5.1A-D), indicating that the brefeldin A had functioned to inhibit peptide

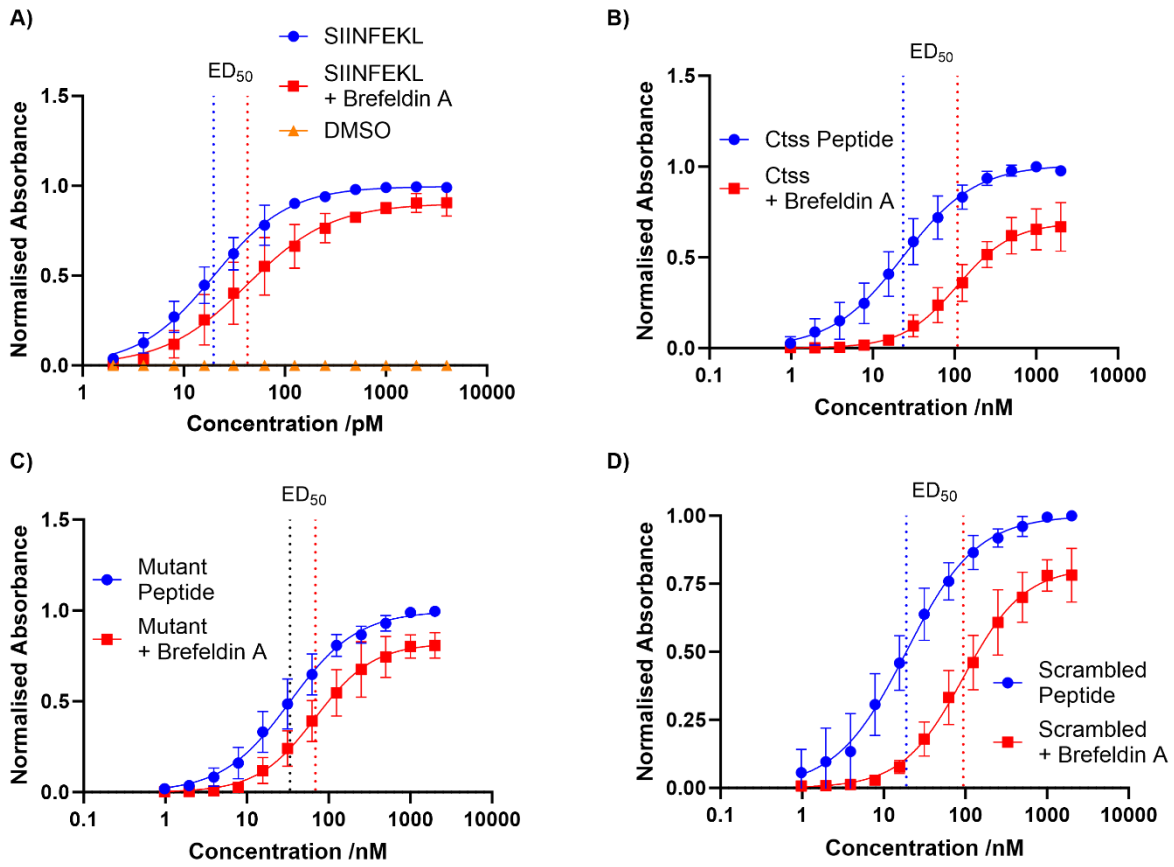
processing. DMSO vehicle control produced no signal above the background (Figure 5.1A).

The logarithmic median effective dose ($log(ED_{50})$) and the maximum response for each peptide were calculated from non-linear regression to quantify the change from inhibition. SIINFEKL peptide saw no significant difference in the $log(ED_{50})$ with inhibition compared to without (Figure 5.1E), indicating that SIINFEKL was not reliant on MHC-I export through the Golgi for its presentation. The $log(ED_{50})$ for ctss and scrambled peptide showed a significant increase, indicating decreased potency and a dependency on MHC-I export via the ER and Golgi (Figure 5.1F). However, although the mutant peptide saw a rise in the $log(ED_{50})$, it was not significant ($P=0.065$), indicating that the potency of the peptides was unaffected by brefeldin A when compared to ctss and scrambled peptides.

The $log(ED_{50})$ value is not the only variable when considering whether inhibition has occurred, with the maximum response equally important. The maximum response was normalised between repeats for comparison and showed that the SIINFEKL maximum response did not significantly change with the inhibition of brefeldin A (Figure 5.1G). There were no significant changes in the efficacy or potency of SIINFEKL after the administration of brefeldin A. Potentially due to the size of SIINFEKL, which allows for a high affinity binding to MHC-I or avoidance of the antigen cross-presentation machinery.

When comparing the ctss, mutant and scrambled peptides, a significant drop in the maximum response was observed (Figure 5.1G), signifying that the brefeldin A inhibition was significantly reducing peptide presentation and required ER and Golgi-dependent export and processing by the DC2.4 cells.

The maximum response of the ctss peptide decreased more significantly than that of the mutant peptide but not the scrambled peptide, indicating that the amino acid substitutions in the mutant peptide have more of an impact on the efficacy of the peptides through this pathway than the inclusion of LRMK. The similarities between the ctss peptide and the scrambled peptide with identical amino acid composition further support this conclusion. As the inhibition was incomplete for the peptides, more investigations into peptide processing and pathways were required.



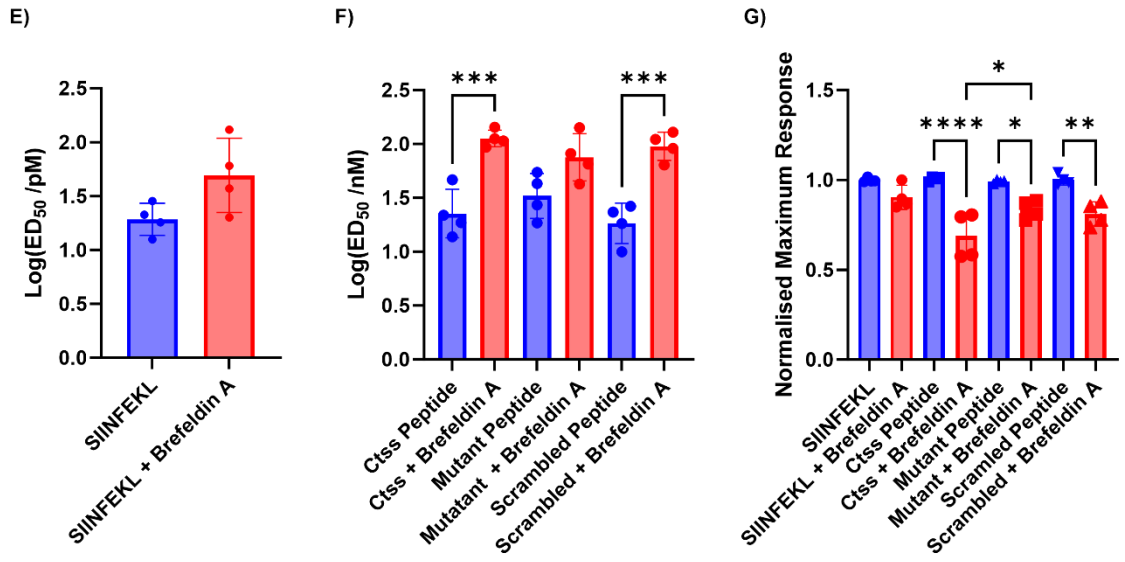


Figure 5.1 Inhibition of Peptide Cross-Presentation by MHC-I Export Blockade
DC2.4 cells were treated with 1x brefeldin A (5 µg/mL) to inhibit their MHC-I export, followed by synthetic peptide pulsing. A twelve-point two-fold dilution series with and without 1x brefeldin A was generated from data of B3Z CPRG absorbance readings and normalised against maximum absorbance of non-inhibited cells (n=4). The four-parameter logistic (4PL) regression dose-response curve was generated from normalised means (±SD). Coloured dotted lines represent ED50 values for each. **(A)** Curves generated for SIINFEKL control peptide diluted from 4000 pM to 2 pM, along with DMSO vehicle control in two-fold dilution series from 0.05%. Curves from 2000 nM to 0.98 nM for **(B)** ctss peptide, **(C)** mutant peptide, and **(D)** scrambled peptide. **(E)** Log(ED50) calculated from dose-response curves for SIINFEKL comparing non-inhibited to brefeldin A treated cells. Data represents mean log(ED50) ±SD. **(F)** Log(ED50) for ctss, mutant and scrambled peptide. **(G)** Normalised maximum response calculated by normalising top value from 4PL regression dose-response of inhibited cells against non-inhibited cells. Data represents the mean top value for each experiment ±SD. Significance calculated for SIINFEKL by an unpaired t-test (n=4; ns - p>0.05) and from ordinary one-way ANOVA with Bonferroni's post hoc multiple comparisons test for all other synthetic peptides (n=4; ns - p>0.05, * - p≤0.05, ** - p≤0.01, *** - p≤0.001, ****- p≤0.0001.) For clarity comparisons with p>0.05 (ns) not shown on graphs.

5.2.2 Endocytosis Inhibition of DC2.4 Cells Reveals Unexpected Enhancement of SIINFEKL Potency

The next focus was on understanding the preferred entry pathways of SIINFEKL into the cells to understand whether it bypasses internalisation. The peptides were evaluated with three different endocytosis inhibitors (Table 5.1).

Table 5.1 Endocytosis Inhibitors

Inhibitor Name	Effect
Amiloride	Inhibits macropinocytosis by inhibiting Na^+/H^+ exchange and lowering submembrane pH
Cytochalasin D	Inhibits phagocytosis and macropinocytosis by depolymerisation of F-actin
Dynasore	Inhibits dynamin- and clathrin-mediated endocytosis by inhibiting the GTPase activity of dynamin

DC2.4 cells were treated with amiloride, cytochalasin D or dynasore for two hours before the addition of the peptide dilution series for 4 hours with continued inhibition before proceeding with co-culture with B3Z and CPRG assay comparing against cells without inhibition. Data was normalised and plotted as a dose-response curve for the SIINFEKL control peptide.

The SIINFEKL dose-response curve with amiloride inhibition resembled the untreated SIINFEKL curve (Figure 5.2A), suggesting that the macropinocytosis pathway was not contributing to SIINFEKL's uptake. Conversely, inhibiting with cytochalasin D led to a noticeable leftward and upward shift in the dose-response curve (Figure 5.2B). Since cytochalasin D affects both macropinocytosis and phagocytosis, this could indicate that inhibition of phagocytosis or alternative mechanisms of cytochalasin D may be altering the cross-presentation environment. Dynasore also induced a change for SIINFEKL, resulting in a faster-rising but flatter dose-response curve (Figure 5.2C). This augmentation suggests that either dynamin-dependent endocytosis plays a role or, like cytochalasin D, off-target effects influence the cross-presentation environment for SIINFEKL.

The log(ED_{50}) and maximum response were calculated from the dose-response curves. Cytochalasin D and dynasore saw a significant shift in the log(ED_{50}) value compared to the uninhibited control, while amiloride made no meaningful change (Figure 5.2D). Comparing the maximum responses, neither amiloride, cytochalasin D or dynasore significantly differed in the maximum response (Figure 5.2E). The lack of change provides evidence of SIINFEKL as a direct binder, not affected by inhibition of endocytosis pathways and entering the cells efficiently. Together with the brefeldin A data, this provides evidence of SIINFEKL as an unsuitable control for cross-presentation.

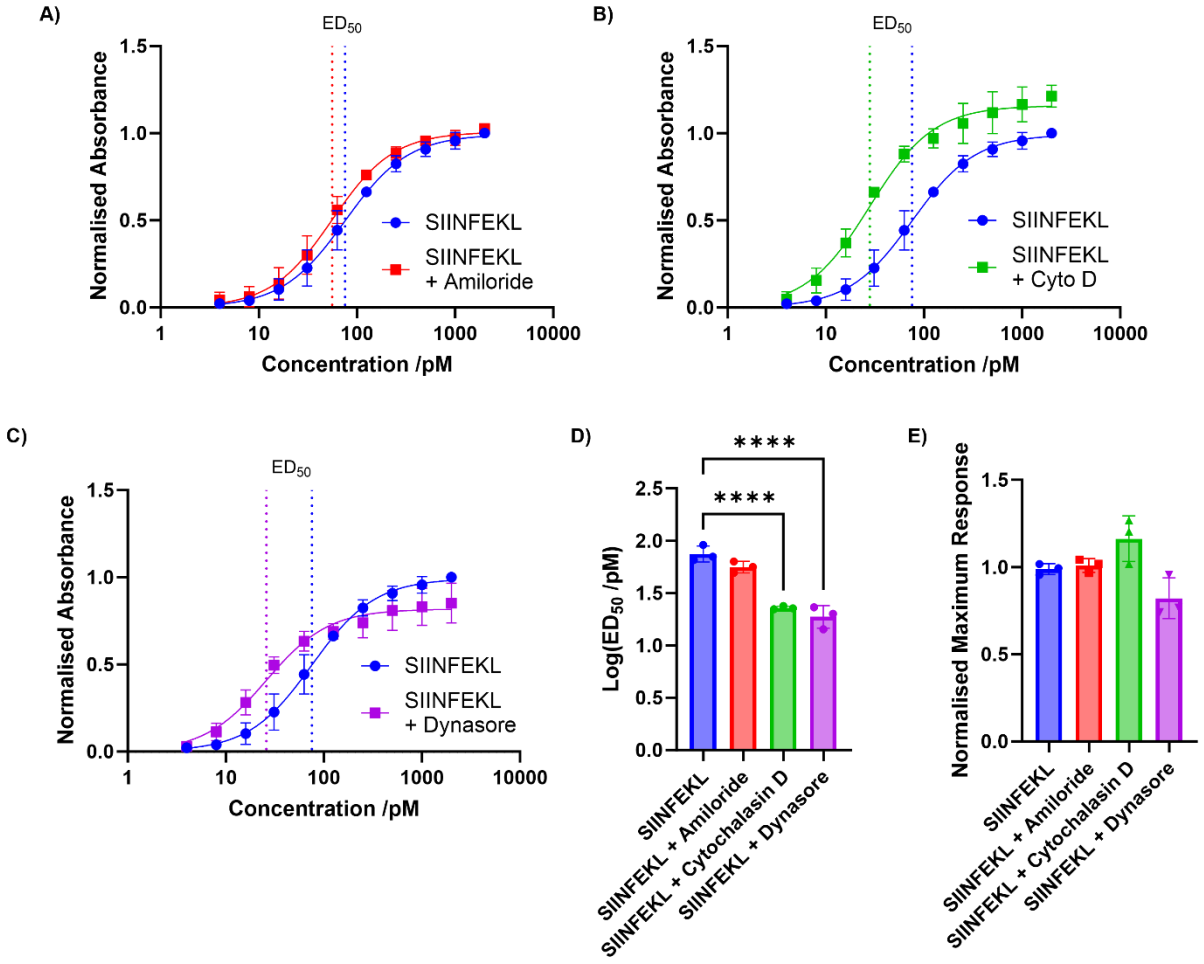


Figure 5.2 SIINFEKL Peptide MHC-I Presentation With Endocytosis Inhibitors
DC2.4 cells pulsed with SIINFEKL peptide with and without 1 mM amiloride, 5 µM cytochalasin D (Cyto D) or 30 µM dynasore. Data generated from B3Z CPRG absorbance readings and normalised against maximum absorbance of non-inhibited cells (n=3). The 4PL regression dose-response curve was generated from the normalised means (±SD). SIINFEKL control peptide was diluted from 2000 pM to 5 pM across a twelve-point two-fold dilution series with and without cell treatment with **(A)** amiloride, **(B)** cytochalasin D, and **(C)** dynasore. Coloured dotted lines represent ED50 values for each. **(D)** Log(ED50) calculated from dose-response curves for SIINFEKL peptide with and without amiloride, cytochalasin D and dynasore inhibition (n=3). **(E)** Normalised maximum response calculated by normalising top value from 4PL regression dose-response of amiloride, cytochalasin D and dynasore-inhibited cells against non-inhibited cells. Data represents the mean top value for each experiment ±SD (n=3). Significance was calculated from ordinary one-way ANOVA with Dunnett's post hoc multiple comparisons test against non-inhibited cells (ns - $p>0.05$, **** - $p\leq 0.0001$). For clarity, graphs do not show comparisons with $p>0.05$ (ns).

5.2.3 Endocytosis Inhibition Shows Similar Internalisation Profiles Between the Synthetic Peptides

Turning attention to the ctss, mutant, and scrambled peptides, endocytosis inhibitors were used to observe differences between sequences and their role in antigen cross-presentation. As some of these inhibitors have overlapping effects, a single inhibitor

and combination test was performed to fully elucidate potential entry routes that may enhance these peptides' cross-presentation. Also, an MTS assay was performed to evaluate the potential toxicity of the inhibitors on their own and in combination. All inhibitors displayed mild toxicity, except for the combination of amiloride and dynasore, which saw a drop to 44.2% viability, and all three in combination led to a significant decrease to around 16.5% (Appendix I – Figure 7.4). Consequently, these two conditions were excluded from the datasets.

The peptides were evaluated with and without inhibitors, with all monotreatment and combinations assessed with a concentration curve across a two-fold dilution series. The data was normalised and presented as a dose-response curve. Amiloride saw a rightwards shift in the dose-response curve for ctss, mutant, and scrambled peptides (Figure 5.3A-C), indicating an inhibitory effect on the peptides, albeit to a lesser extent with the mutant peptide compared to ctss and scrambled. On the other hand, cytochalasin D showed a leftward shift in all three peptides, indicating an increase in potency (Figure 5.3D-F). Finally, dynasore saw no real change in the curves, following closely with the uninhibited ctss, mutant and scrambled peptide (Appendix I – Figure 7.5), indicating a negligible effect by dynamin-dependent endocytosis on peptide uptake.

With the combination studies, the mixture of amiloride and cytochalasin D for all three peptides reverted the dose-response curve to the same as non-treated cells, reversing the inhibition caused by amiloride and the enhancement of cytochalasin D (Figure 5.3G-I). This reversal could be a consequence of the compounding effect of these two inhibitors on the DC2.4 cells, as they both impact macropinocytosis. Finally, the combination of cytochalasin D and dynasore yielded the same outcome as cytochalasin D monotreatment for all tested peptides (Appendix I – Figure 7.5),

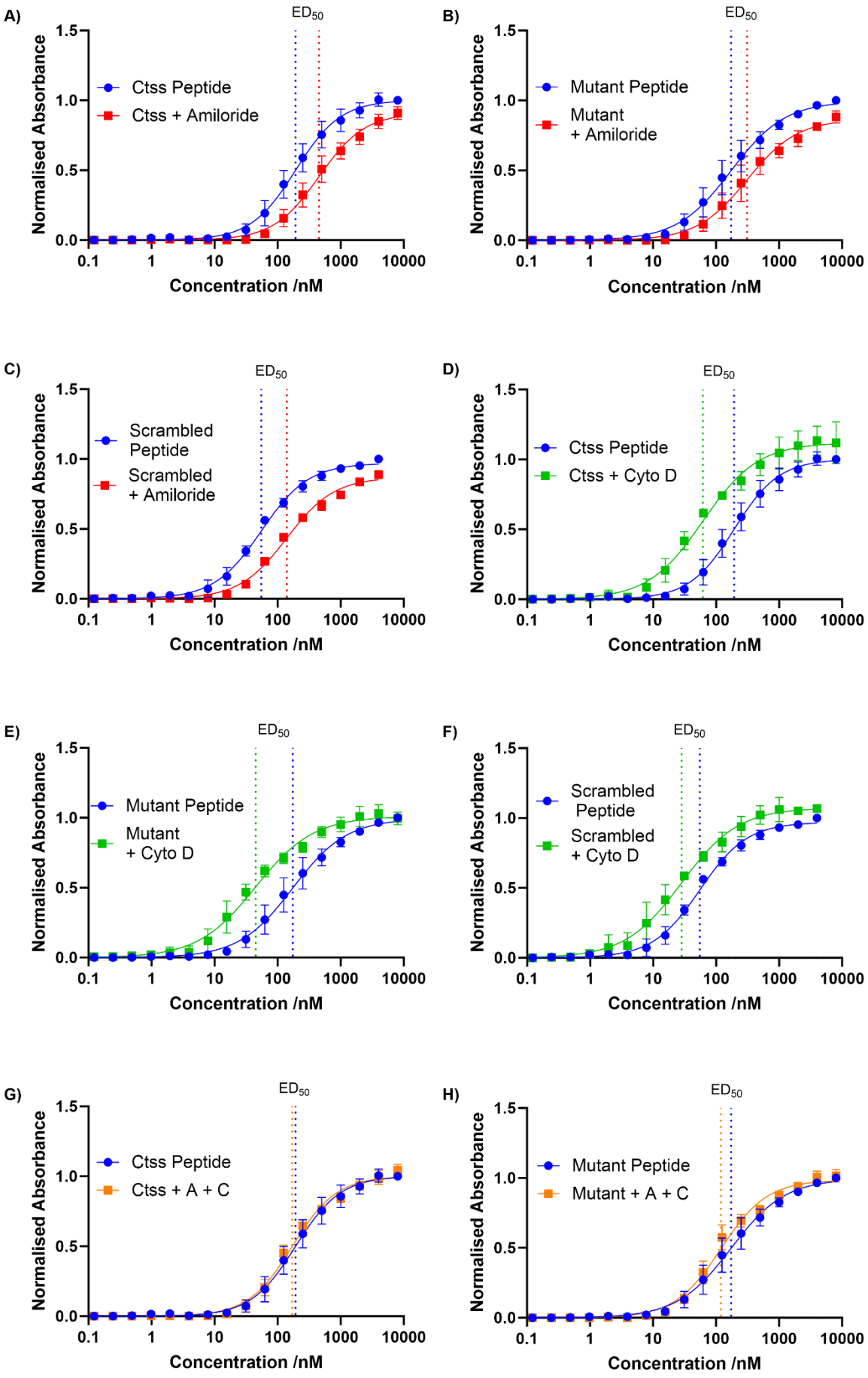
showing that cytochalasin D's enhancement was not because of an increased utilisation of clathrin-mediated endocytosis or other dynamin-dependent mechanisms.

By evaluating the log(ED_{50}) and maximum responses for the peptides, a contrast between the peptides was observed, with ctss peptide displaying a significant increase in the log(ED_{50}) from amiloride, along with a significant decrease with cytochalasin D and combination cytochalasin D and dynasore treatment (Figure 5.3J). Interestingly, dynasore alone did not lead to a significant shift, unlike SIINFEKL, implying that clathrin-mediated endocytosis was not an essential pathway for this peptide. The reversal observed with the dose-response curve with amiloride with cytochalasin D was confirmed through the log(ED_{50}), displaying no notable change in the potency between treated and untreated (Figure 5.3J). Unlike the ctss peptide, the mutant peptide did not show a significant increase in the log(ED_{50}) compared to the untreated but did see the same significant decrease with the use of cytochalasin D either alone or in combination (Figure 5.3K). Finally, the scrambled peptide showed the most similarity with the ctss peptide, seeing an increase in the log(ED_{50}), with a decrease with cytochalasin D alone or in combination (Figure 5.3L).

The changes in the ctss peptide appear to be only with potency, as there was no significant change in the normalised maximum response between the untreated and any treated or combination-treated cells (Figure 5.3M). Interestingly, although there was no significant shift in the log(ED_{50}) with the mutant peptide, there was a significant decrease in the normalised maximum response (Figure 5.3N), indicating that the efficacy was affected. However, the potency of the peptide was not. The results demonstrate how macropinocytosis may be a substantial entry pathway for the mutant peptide and that a combination of maximum response and log(ED_{50}) is essential to understanding changes in peptide dynamics. A drop was observed in the maximum

response for scrambled with amiloride. However, this was not enough to be significant (P= 0.0502), with no significance observed for any other inhibitor or combination (Figure 5.3O).

Overall, all three peptides displayed similar changes in antigen cross-presentation with the inhibitors. This similarity implies that the ctss peptide with the LRMK site did not affect the entry route compared to the mutant or scrambled peptide. All peptides were processed partly through macropinocytosis shown through amiloride inhibition, and dynasore did not appear to have any significant effect on the antigen cross-presentation of the peptides, ruling out clathrin-mediated endocytosis as a route of entry into the DC2.4 cells for these peptides. The contrast between cytochalasin D and amiloride is unusual since they both affect macropinocytosis. Interestingly, the scrambled peptide, which had the same amino acid composition as ctss but rearranged, was more potent than in all these experiments. The reasons for this are unknown, but it could indicate that the LRMK site may be routing the peptides through to the vacuolar pathway, which may be less efficient at cross-presentation than the cytosolic pathway.


A)
ED50
Normalised Absorbance
Concentration /nM
Ctss Peptide
Ctss + Amiloride
B)
ED50
Normalised Absorbance
Concentration /nM
Mutant Peptide
Mutant
+ Amiloride
C)
ED50
Normalised Absorbance
Concentration /nM
Scrambled
Peptide
Scrambled
+ Amiloride
D)
ED50
Normalised Absorbance
Concentration /nM
Ctss Peptide
Ctss + Cyto D
E)
ED50
Normalised Absorbance
Concentration /nM
Mutant Peptide
Mutant
+ Cyto D
F)
ED50
Normalised Absorbance
Concentration /nM
Scrambled
Peptide
Scrambled
+ Cyto D
G)
ED50
Normalised Absorbance
Concentration /nM
Ctss Peptide
Ctss + A + C
H)
ED50
Normalised Absorbance
Concentration /nM
Mutant Peptide
Mutant + A + C

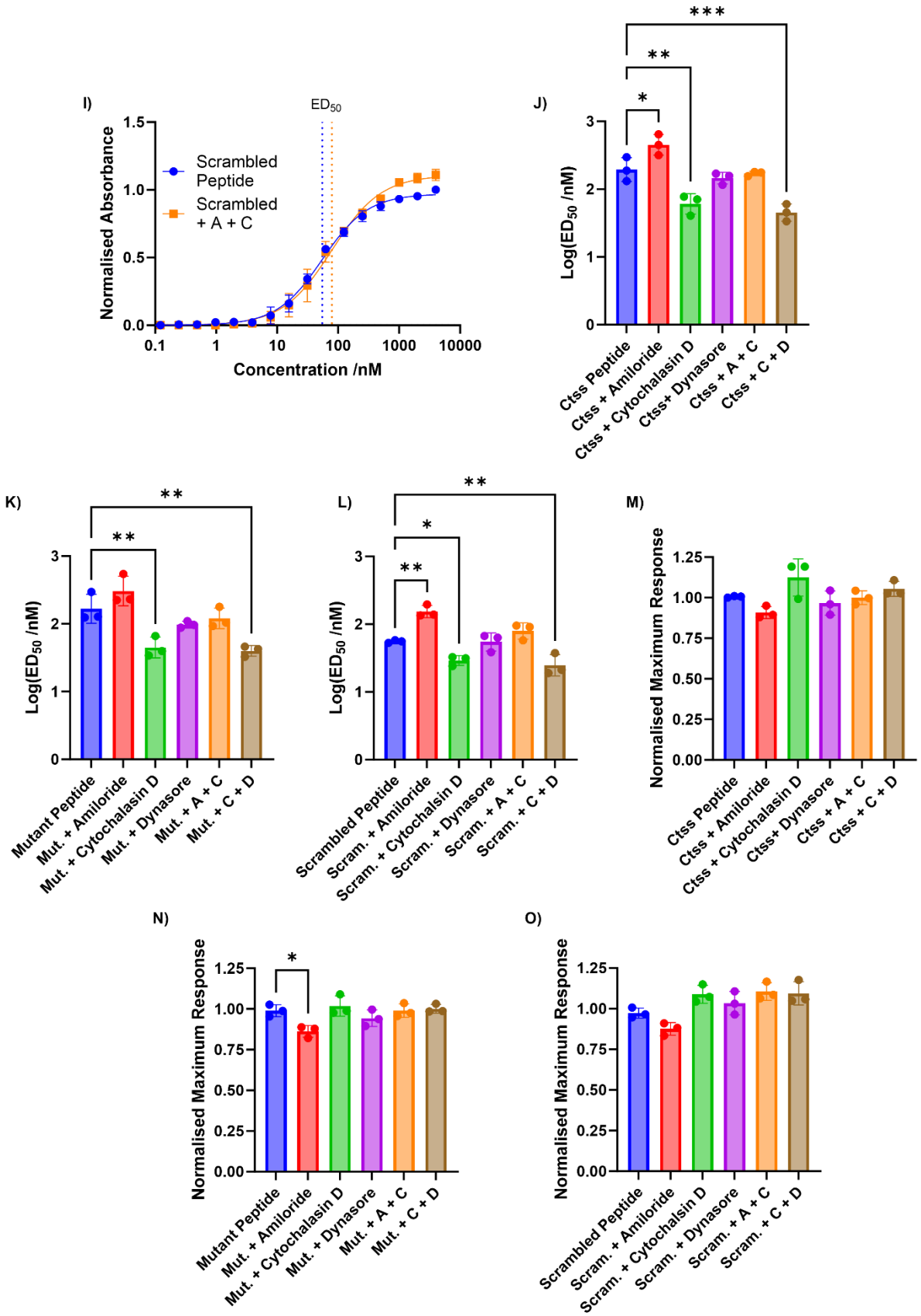

I)
ED50
Normalised Absorbance
Scrambled Peptide
Scrambled + A + C
Concentration /nM
J)
Log(ED50 /nM)
Ctss Peptide
Ctss + Amiloride
Ctss + Cytochalasin D
Ctss+ Dynasore
Ctss + A + C
Ctss + C + D
K)
Log(ED50 /nM)
Mutant Peptide
Mut. + Amiloride
Mut. + Cytochalasin D
Mut. + Dynasore
Mut. + A + C
Mut. + C + D
L)
Log(ED50 /nM)
Scrambled Peptide
Scram. + Amiloride
Scram. + Cytochalasin D
Scram. + Dynasore
Scram. + A + C
Scram. + C + D
M)
Normalised Maximum Response
N)
Normalised Maximum Response
O)
Normalised Maximum Response

Figure 5.3 Cross-Presentation of Synthetic Peptides With Endocytosis Inhibition
DC2.4 cells were pulsed with synthetic peptides under inhibition by 1 mM amiloride, 5 µM cytochalasin D, 30 µM dynasore or a combination thereof. Pulsed DC2.4 co-cultured with B3Z and CPRG assay developed. Data generated from B3Z CPRG absorbance readings and normalised against maximum absorbance of non-inhibited cells (n=3). The 4PL regression curve was generated from normalised means (±SD). Coloured dotted lines represent ED_{50} values for each. Ctss and mutant peptides were diluted from 8000 nM to 61 pM and scrambled from 4000 nM to 30.5 pM across an 18-point two-fold dilution series. **(A)** ctss peptide with (w/) amiloride **(B)** mutant peptide w/ amiloride; **(C)** scrambled peptide w/ amiloride. **(D)** ctss peptide w/ cyto D; **(E)** mutant peptide w/ cyto D; **(F)** scrambled peptide w/ cyto D. **(G)** ctss peptide w/ amiloride and cyto D; **(H)** mutant peptide w/ amiloride and cyto D; **(I)** scrambled peptide w/ amiloride and cyto D. **(J)** Log(ED_{50}) calculated from dose-response curves with and without amiloride, cytochalasin D, dynasore, amiloride and cytochalasin D combination or cytochalasin D and dynasore combination inhibition (n=3) for ctss peptide; **(K)** mutant peptide, and **(L)** scrambled peptide. **(M)** Normalised maximum response calculated by normalising top values from 4PL regression dose-response of amiloride, cytochalasin D and dynasore inhibited cells against non-inhibited cells for ctss peptide; **(N)** mutant peptide; **(O)** scrambled peptide. Data represents the mean top values for each experiment ±SD (n=3). Significance was calculated from ordinary one-way ANOVA with Dunnett's post hoc multiple comparisons test (n=3; ns - p>0.05 * - p≤0.05, ** - p≤0.01, *** - p≤0.001). For clarity, graphs do not show comparisons with p>0.05 (ns). Additional dose-response curves can be found in Appendix I – Figure 7.5.

5.2.4 Proteasome and Cathepsin S Inhibition Reveals Differences in Processing of the Synthetic Peptides

Comprehending the intracellular processing of peptides before their MHC-I binding and subsequent export to the cell surface is paramount. Next, the investigation considered whether the peptides are presented through the endosome-to-proteasome or the vacuolar pathway using various inhibitors (Table 5.2).

Table 5.2 Proteasome, Endosome and Protease Inhibitors

Inhibitor Name	Effect
Chloroquine	Inhibitor of endosome acidification, which enhances cross-presentation
Epoxomicin	Inhibitor of the 20S subunit of the proteasome, which inhibits cytosolic antigen cross-presentation
LHVS	Pan-cathepsin inhibitor, which inhibits vacuolar antigen cross-presentation
MG-132	Inhibitor of the 26S subunit of the proteasome, which inhibits cytosolic antigen cross-presentation

An MTS assay was performed with the four compounds, with MG-132, epoxomicin, and chloroquine found to be well-tolerated by the cells up to 150 nM, 15 nM, and 10 µM, respectively (Appendix I – Figure 7.6). LHVS exhibited no detectable toxicity up to 1 µM (not shown), a concentration significantly exceeding the level required for effective cathepsin S inhibition.

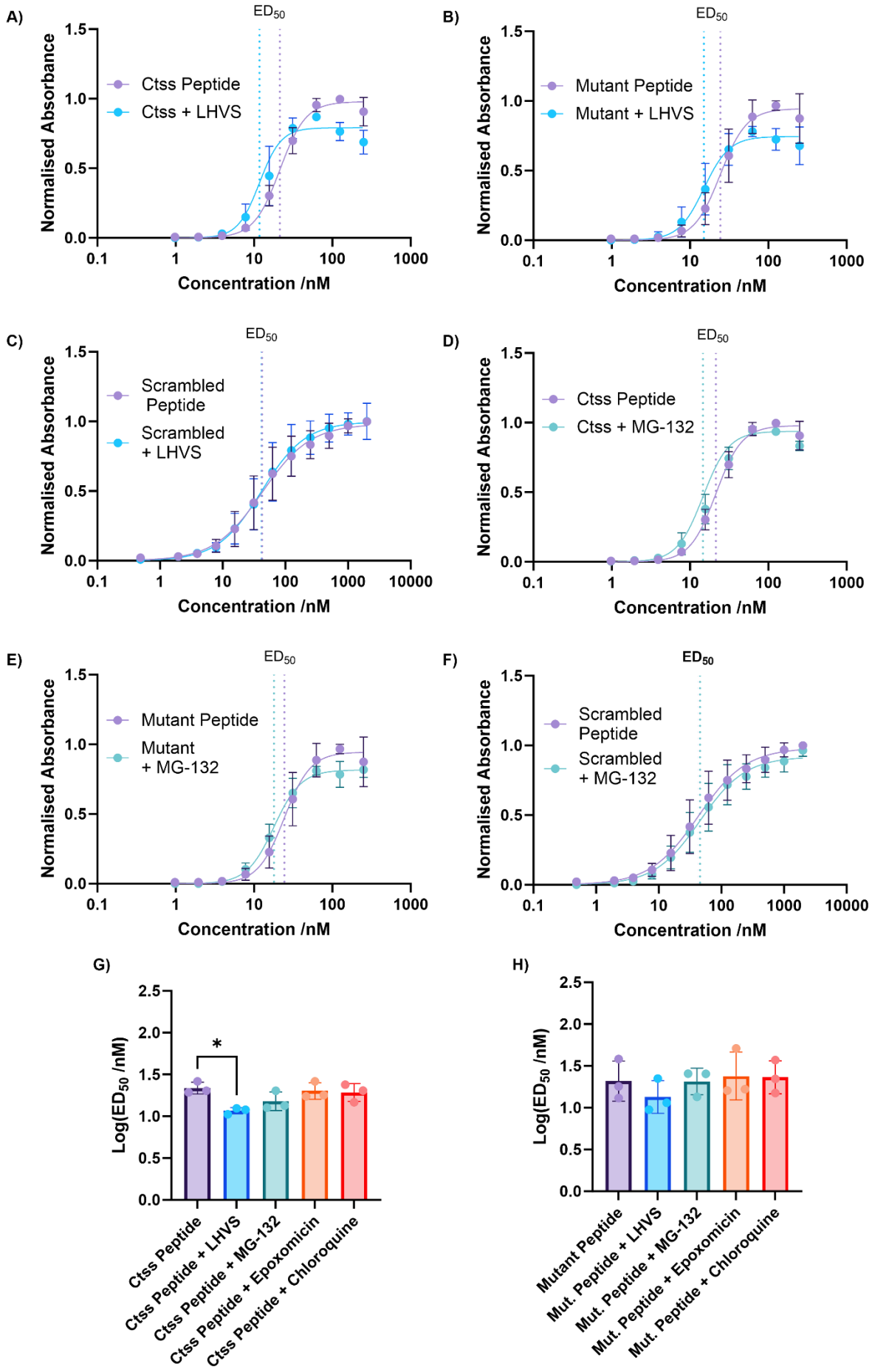
Inhibitor treatments were performed on DC2.4 cells for two hours before adding peptides under treatment for another four hours and co-cultured in B3Z assay overnight. SIINFEKL is not a reasonable control for peptide processing, so it was used as a positive control without inhibition. Data was collected to form dose-response curves.

LHVS inhibition on the ctss peptide showed a sharper rise but plateau lower than the untreated (Figure 5.4A), indicating that potency at lower doses was increased. Overall, the efficacy was decreased, likely due to the inhibition of cathepsin S. For the mutant peptide, there was a similar shift leftwards in the curve with a plateau lower than the mutant peptide on LHVS-treated cells (Figure 5.4B). The scrambled peptide was unaffected by LHVS, displaying overlapping curves with the untreated control (Figure 5.4C). For MG-132 treatment, ctss broadly matched the non-treated cells (Figure 5.4D), but for the mutant peptide, there was a lower plateau of the curves with MG-132 compared to non-treated cells (Figure 5.4E). Scrambled peptide still proved to be resistant to inhibition, with the MG-132 curve broadly matching that of untreated cells (Figure 5.4F). For all three peptides, epoxomicin and chloroquine-treated cells equalled the non-treated cells (Appendix I – Figure 7.7).

The ctss peptide log(ED_{50}) showed a significant decrease for LHVS, with no change for MG-132, epoxomicin and chloroquine (Figure 5.4G). The lower log(ED_{50}) for LHVS may be due to the peptide being preferentially shuttled through the cytosolic pathway at these concentrations, with the limiting factor not being the vacuolar pathway. For the mutant peptide, the log(ED_{50}) calculations revealed no significant change in the potency of the peptides with any of the inhibitors (Figure 5.4H). Finally, the log(ED_{50}) for the scrambled peptide was calculated, showing no significant change for the scrambled peptide with any of the inhibitors (Figure 5.4I).

The normalised maximum response saw a significant decrease for LHVS compared to untreated cells for ctss peptide, with no change seen with MG-132, epoxomicin or chloroquine (Figure 5.4J). LHVS inhibition revealed processing of the ctss peptide through the vacuolar pathway mediated by cathepsin S, as demonstrated by the reduction in ctss peptide cross-presentation (Figure 5.4J). Although no change in potency through log(ED_{50}) was observed for the mutant peptide, it did show a significant decrease in efficacy with cell treatment of LHVS (Figure 5.4K), indicating that this peptide was also processed partly by cathepsin S. None of the other inhibitors influenced the mutant peptide, with MG-132 failing to reach significance (P= 0.086) (Figure 5.4K). The scrambled peptide showed no change in maximum response with any of the inhibitors, suggesting a lower affinity for cathepsin S or a proteasome-independent mechanism (Figure 5.4L).

These results suggest that cathepsin S is a critical protease in processing the ctss and mutant peptides but not for the scrambled peptide. The similarities between ctss and mutant peptides are despite the mutant peptide having a disrupted cathepsin S cleavage site, which could indicate the promiscuity of cathepsin S recognition. LHVS did not affect scrambled peptides despite having the same composition, which suggests that the LRMK sequence is vital for cleavage by cathepsin S. The absence of proteasome inhibition with MG-132 and epoxomicin may point to proteasome-independent processing or a requirement for higher concentrations. Similarly, the ineffectiveness of chloroquine could be attributed to a low concentration, an alkali endo-lysosome system, or rapid escape of the peptides from the endosomes. Unfortunately, based on the MTS viability assay results, increasing the concentrations of MG-132, epoxomicin, and chloroquine was not feasible.


A)
ED50
Normalised Absorbance
Ctss Peptide
Ctss + LHVS
Concentration /nM
B)
ED50
Normalised Absorbance
Mutant Peptide
Mutant + LHVS
Concentration /nM
C)
ED50
Normalised Absorbance
Scrambled Peptide
Scrambled + LHVS
Concentration /nM
D)
ED50
Normalised Absorbance
Ctss Peptide
Ctss + MG-132
Concentration /nM
E)
ED50
Normalised Absorbance
Mutant Peptide
Mutant + MG-132
Concentration /nM
F)
ED50
Normalised Absorbance
Scrambled Peptide
Scrambled + MG-132
Concentration /nM
G)
Log(ED50 /nM)
*
Ctss Peptide
Ctss Peptide + LHVS
Ctss Peptide + MG-132
Ctss Peptide + Epoxomicin
Ctss Peptide + Chloroquine
H)
Log(ED50 /nM)
Mutant Peptide
Mut. Peptide + LHVS
Mut. Peptide + MG-132
Mut. Peptide + Epoxomicin
Mut. Peptide + Chloroquine

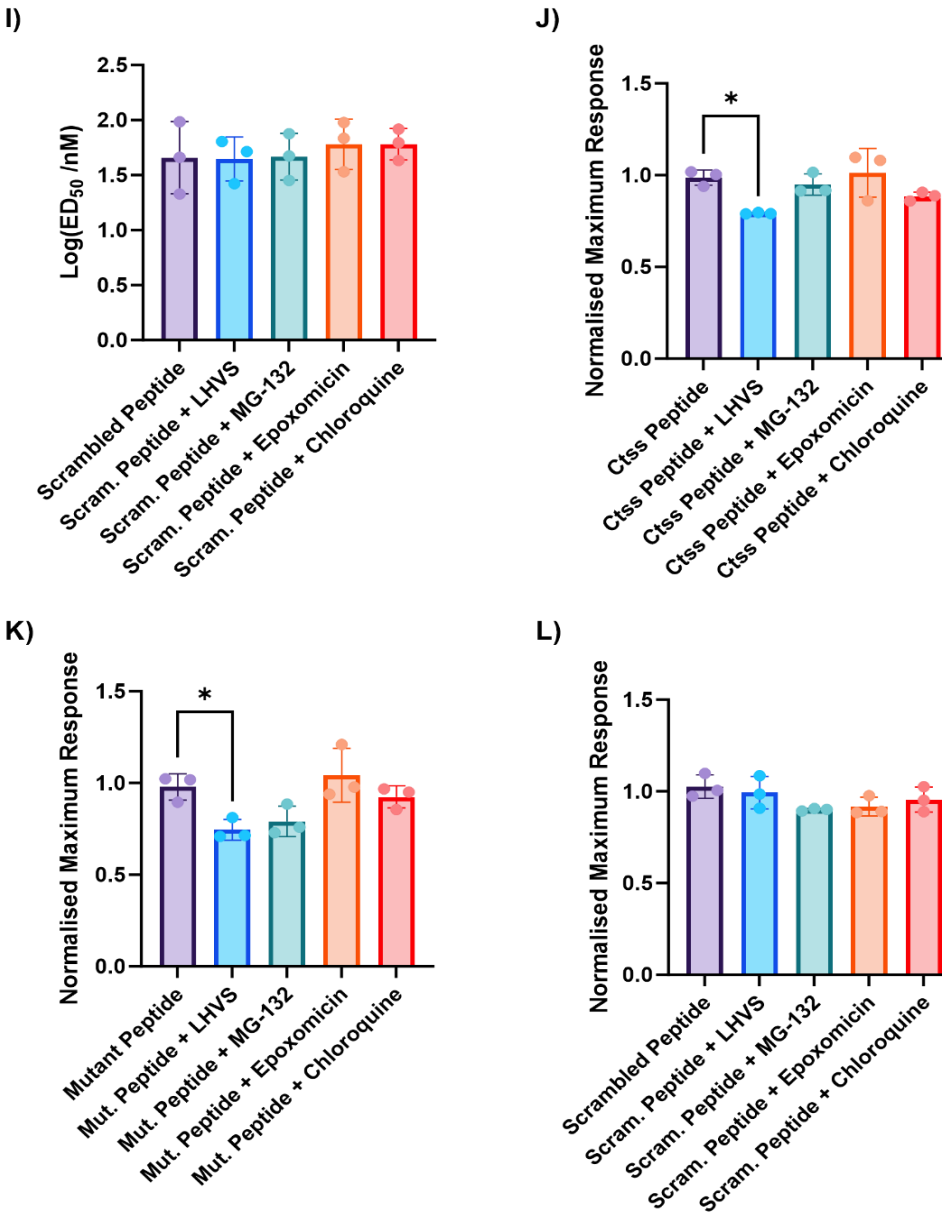


Figure 5.4 Cross-Presentation Profile of Synthetic Peptides With Cathepsin S, Proteasome, and Endosome Acidification Inhibitors.
DC2.4 cells were subjected to 10 nM LHVS, 100 nM MG-132, 10 nM epoxomicin, or 10 µM chloroquine and pulsed with synthetic peptides. Pulsed DC2.4 co-cultured with B3Z and CPRG assay developed. Data generated from B3Z CPRG absorbance readings and normalised against maximum absorbance of non-inhibited cells (n=3). 4PL regression dose-response curve generated from normalised means (±SD) by two-fold dilution series of peptide diluted from 250 nM to 0.98 nM for ctss and mutant, and 2000 to 0.48 nM for scrambled with and without cell treatment for **(A)** ctss peptide w/ LHVS; **(B)** mutant peptide w/ LHVS; **(C)** scrambled peptide w/ LHVS **(D)** ctss peptide w/ MG-132; **(E)** mutant peptide w/ MG-132; **(F)** scrambled peptide w/ MG-132. **(G)** Log(ED_{50}) calculated from dose-response curves of LHVS, MG-132, epoxomicin or chloroquine treated cells against untreated cells (n=3; Mean ±SD) for ctss peptide; **(H)** mutant peptide; **(I)** scrambled peptide. **(J)** Normalised maximum response of ctss peptide calculated by normalising top value from 4PL regression dose-response curve of LHVS, MG-132, epoxomicin or chloroquine inhibition cells against non-inhibited cells for ctss peptide; **(K)** mutant peptide; **(L)** scrambled peptide. Data represents the mean top value for each experiment ±SD (n=3). Significance was calculated from ordinary one-way ANOVA with Dunnett's post hoc multiple comparisons test (n=3; ns - $p>0.05$ * - $p\leq0.05$). For clarity, graphs do not show comparisons with $p>0.05$ (ns). Additional dose-response curves can be found in Appendix I – Figure 7.7

5.2.5 High Concentration LHVS Demonstrates Further Inhibition of Cross-Presentation

As LHVS was tolerated by the cells up to micromolar concentrations, LHVS was studied further at 10x the concentration of the previous experiment to ascertain any further inhibitory effects on the peptides that may involve cathepsin digestion. A two-fold serial dilution dose-response curve was generated from the B3Z CPRG assay readout. The difference with the ctss peptide was stark, with a significant rightwards shift in the curve and a lower plateau, indicating reduced potency and efficacy (Figure 5.5A). Comparable results were seen with mutant peptide and scrambled peptide with LHVS but to a lesser extent than ctss peptide (Figure 5.5B-C).

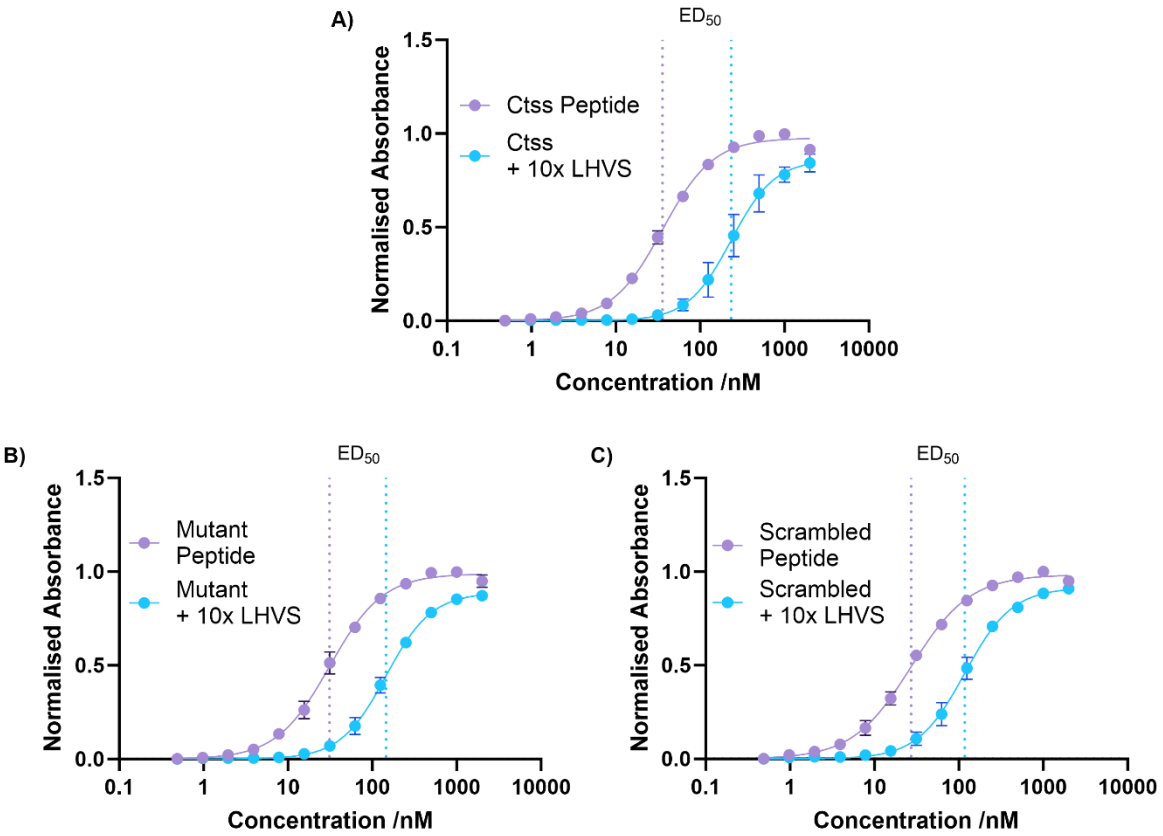
The log(ED_{50}) values and normalised maximum response were derived from the dose-response curves. For the ctss, mutant and scrambled peptide, a significant rise in the log(ED_{50}) was observed with the LHVS treatment compared to without, indicating a significant reduction in potency from LHVS inhibition (Figure 5.5D).

Comparing the peptides with untreated DC2.4 cells, which displayed broadly similar log(ED_{50}) (Figure 5.5E), we can clarify whether the inhibition of cathepsin S through LHVS had a more substantial effect on one peptide over the others. The ctss peptide showed a significant increase in the log(ED_{50}) compared to mutant and scrambled, and when scrambled and mutant were compared against one another (Figure 5.5E). The differences indicate that the ctss peptide was more affected by the inhibition of cathepsin S than mutant or scrambled.

Overall, the normalised maximum response was significantly decreased for the ctss, mutant and scrambled peptides compared to their untreated counterparts (Figure

5.5F), which shows that the LHVS at 100 nM inhibited cross-presentation by affecting potency and efficacy simultaneously.

Comparing the maximum responses between peptides, although there was no significant difference between the ctss and mutant peptide, there was a significant worsening of the normalised maximum response when compared to the scrambled peptide (Figure 5.5G), pointing to an increased inhibition with the inclusion of LRMK and therefore a more considerable reliance of cathepsin S cleavage. As the concentration was high, other cathepsins could also be inhibited, which may affect the processing of the peptides.



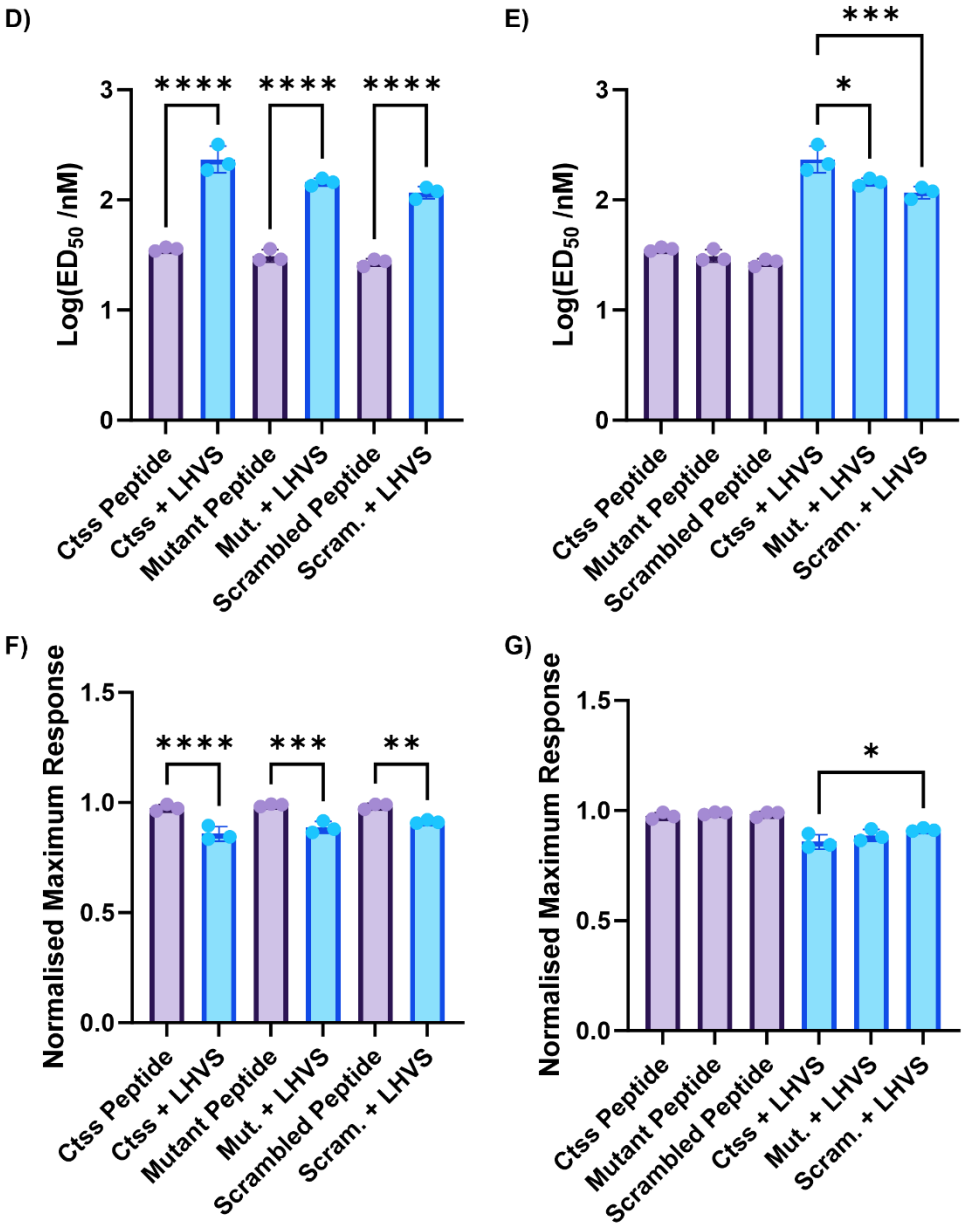


Figure 5.5 Effect of Higher LHVS Concentration on Synthetic Peptide Cross-Presentation
DC2.4 cells treated with 100 nM (10x) LHVS followed two hours later with synthetic peptides. Pulsed DC2.4 co-cultured with B3Z and CPRG assay developed. Data generated from B3Z CPRG absorbance readings and normalised against maximum absorbance of non-inhibited cells (n=3). 4PL regression dose-response curve generated from normalised means (±SD) by two-fold dilution series of peptide diluted from 2000 to 0.49 nM for **(A)** ctss peptide; **(B)** mutant peptide; and **(C)** scrambled peptide. **(D)** Log(ED_{50}) calculated from dose-response curves with and without 10x LHVS against untreated cells (n=3; Mean ±SD) for ctss, mutant, and scrambled peptide, and **(E)** Log(ED_{50}) comparison between ctss, mutant and scrambled peptide. **(F)** Normalised maximum response calculated by normalising top value from 4PL regression dose-response curve of 10x LHVS inhibited cells against non-inhibited cells for ctss, mutant, and scrambled peptide; **(G)** Normalised maximum response comparing between ctss, mutant and scrambled peptide. Significance was calculated from ordinary one-way ANOVA with Bonferroni's post hoc multiple comparisons test (n=3; ns - $p>0.05$ * - $p\leq0.05$, ** - $p\leq0.01$, *** - $p\leq0.001$, **** - $p\leq0.0001$). For clarity, graphs do not show comparisons with $p>0.05$ (ns).

5.2.6 OVA Beads With Inhibitors Uncovers Differences Between Particulate and Soluble Antigen Processing

The efficacy of SIINFEKL as a positive control for antigen cross-presentation was questionable because of its ability to bind directly to MHC-I without processing by cross-presentation pathways. Therefore, an alternative model was necessary.

OVA-conjugated latex beads were used as a cross-presentation control to validate the potency of inhibitory drugs on antigen cross-presentation in DC2.4 cells. OVA was conjugated to 3 µm carboxyl-modified latex beads through free amines on OVA (Materials and Methods 2.5.2). A BCA assay was performed to assess the solution of OVA before and after conjugation to calculate the bound mass. The bound mass was determined to be 0.26 µg/10^6 beads or approximately 175 µg of OVA per milligram of beads (Appendix I – Figure 7.8).

DC2.4 cells were treated with 125 µg of beads with and without inhibition, followed by B3Z co-culture and CPRG assay. Cytochalasin D and amiloride in this assay showed a decrease in cross-presentation (Figure 5.6). Amiloride and cytochalasin D inhibit macropinocytosis, so the beads are likely processed through these pathways. Phagocytosis is also inhibited by cytochalasin D and is likely involved in its uptake because of the bead's large size. Counterintuitively, dynasore exhibited an increase in cross-presentation (Figure 5.6). It is possible that inhibiting this specific route led to increased peptide uptake through alternative pathways like phagocytosis, potentially benefiting cross-presentation for the OVA beads. Alternatively, off-target effects from dynasore inhibition might have contributed to this unexpected outcome.

Of the two proteasome inhibitors, MG-132 treatment saw a significant decrease, showing that the beads' processing was proteasome-dependent and processed by the

cytosolic pathway (Figure 5.6). However, treatment with epoxomicin did not result in a significant difference in absorbance, possibly due to inadequate inhibitor concentration (Figure 5.6). Brefeldin A treatment also saw a significant decrease in absorbance, adding to evidence of a proteasome-dependent and ER-Golgi export through the cytosolic pathway (Figure 5.6). Interestingly, chloroquine did not show a significant increase (Figure 5.6), which leads to more creditability to either an alkali endosomal compartment or an inadequate chloroquine concentration limited by the cell viability of the DC2.4 cells. LHVS treatment, which occurred at the original 10 nM concentration, saw a significant decrease in cross-presentation, suggesting that the beads were also processed by cathepsin S through the vacuolar pathway (Figure 5.6). Some of these inhibitors had demonstrated to have no function on the synthetic peptides. However, the OVA beads show that the functionality of the inhibitors is intact in DC2.4 cells.

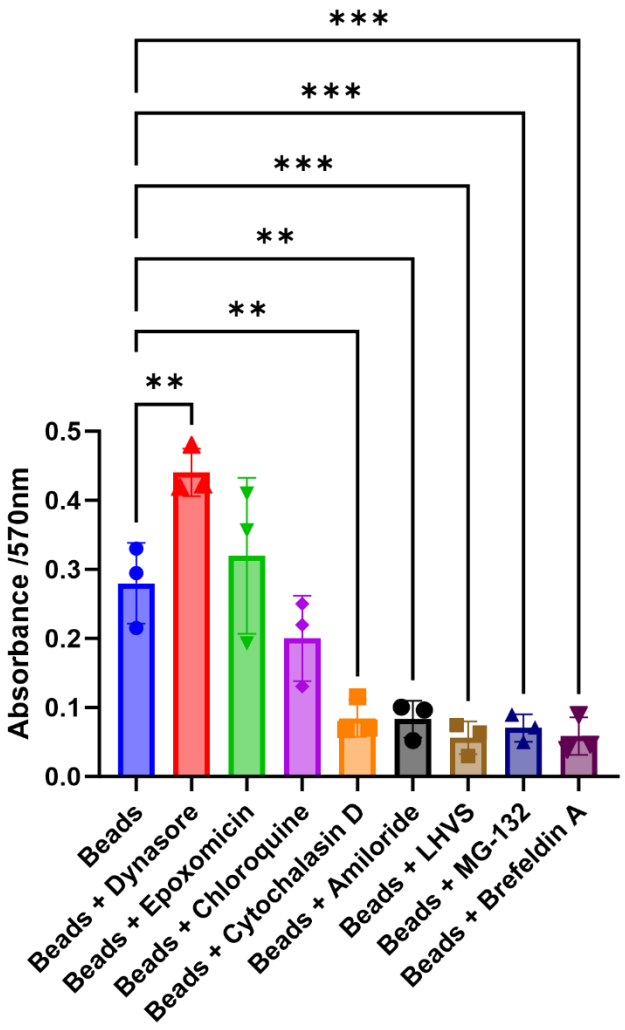


Figure 5.6 Cross-Presentation of OVA Beads With Inhibitors
DC2.4 cells treated with and without inhibition from 30 µM dynasore, 10 nM epoxomicin, 10 µM chloroquine, 5 µM cytochalasin D, 1 mM amiloride, 10 nM LHVS, 100 nM MG-132 and 5 µg/mL brefeldin A pulsed with 125 µg beads. Pulsed DC2.4 fixed and co-cultured with B3Z for CPRG assay developed with absorbance readings at 570nm after background subtraction. Graphs show mean absorbance ±SD error. Significance was calculated from ordinary one-way ANOVA with Dunnett's post hoc multiple comparisons test (n=3; ns - $p>0.05$, ** - $p\leq0.01$, *** - $p\leq0.001$). For clarity, comparisons with $p>0.05$ (ns) are not displayed on graphs.

5.2.7 Cathepsin S Knockdown Differentiates the LRMK-Containing Peptide in Antigen Cross-Presentation

As LHVS has pan-cathepsin activity, there was no guarantee that even at the lower concentration, it was specific to cathepsin S, so an alternative approach was necessary. siRNA knockdown was proposed to achieve a more specific knockdown of cathepsin S, allowing an investigation into the precise impact of cathepsin S on peptide processing and presentation.

The DC2.4 cells were transfected with 25 (1x) or 50 (2x) pmol of mouse cathepsin S siRNA via lipid transfection. Along with the siRNA, a non-specific scrambled siRNA was used as a transfection control, non-transfected DC2.4 as a negative control for comparison of knockdown efficiency, and fluorescein-conjugated siRNA as a transfection efficiency control (Appendix I – Figure 7.9) (Materials and Methods 2.5.3).

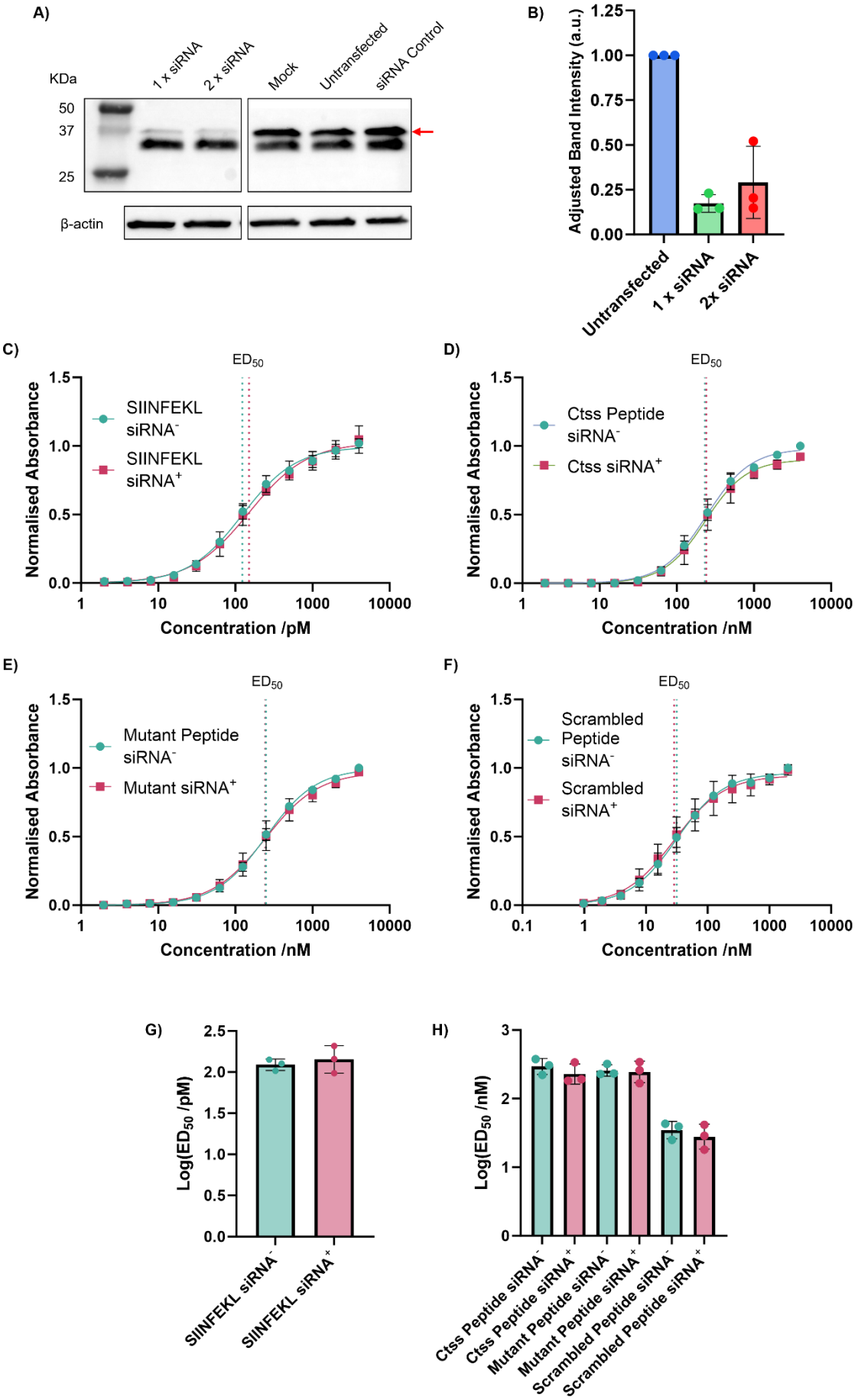
Western blot analysis was performed to validate the knockdown of the cathepsin S compared to wild-type cells (Figure 5.7A). Two bands were present in the western blot analysis using the polyclonal antibody, with the siRNA treatment consistently downregulating the upper band, which was the correct molecular weight for pro-cathepsin S (36.4 kDa). Band intensity analysis normalised to β-actin expression revealed a consistent knockdown of the top band of up to 82% compared to the DC2.4 cells treated with the scrambled sequence negative control siRNA (Figure 5.7B). In contrast, the unknown lower band showed only minor knockdown (Appendix I – Figure 7.10).

The cells treated with the siRNA were assessed by B3Z assay to analyse the effect of cathepsin S knockdown on the antigen cross-presentation of ctss, mutant and scrambled peptide, and SIINFEKL as a control peptide. The DC2.4 cells were treated 72 hours post-siRNA transfection and pulsed with the peptides under a two-fold dilution series for four hours before washing away and incubating with the B3Z cells and proceeding with the B3Z CPRG assay. From the B3Z assay, the dose-response curves were generated and normalised.

The SIINFEKL-treated cells had dose-response curves identical to their untransfected counterpart (Figure 5.7C). The ctss peptide saw a similar curve profile to the untransfected cells but had a lower maximum (Figure 5.7D), potentially indicating an

effect of cathepsin S knockdown on this peptide. In the case of siRNA knockdown involving scrambled and mutant peptides in DC2.4 cells, the resulting curve profile resembled that of untransfected cells (Figure 5.7E-F). This observation indicated a minimal effect on the cross-presentation of these two peptides following cathepsin S knockdown.

The log(ED_{50}) and normalised maximum response were calculated from the dose-response curves. Examining the log(ED_{50}) for SIINFEKL, no notable change was observed between the siRNA-treated and untreated cells (Figure 5.7G); likewise, the log(ED_{50}) for ctss, mutant and scrambled was maintained with siRNA treatment (Figure 5.7H). With the normalised maximum response, no significant difference was observed for SIINFEKL (Figure 5.7I), meaning no overall effect from cathepsin S knockdown. However, with the synthetic peptides, differences were observed with the normalised maximum response. For the ctss peptide, a significant decrease was observed, which was not apparent for mutant or scrambled peptide (Figure 5.7J). Together, this points to slight inhibition occurring with the cross-presentation of the LRMK-containing ctss peptide, which was not observed in the mutant or scrambled, providing evidence of the role of cathepsin S in the cross-presenting efficacy of the ctss peptide.


A)
KDa
1 x siRNA
2 x siRNA
Mock
Untransfected
siRNA Control
50
37
25
β-actin
B)
Adjusted Band Intensity (a.u.)
1.25
1.00
0.75
0.50
0.25
0.00
Untransfected
1 x siRNA
2x siRNA
C)
ED50
Normalised Absorbance
SIINFEKL siRNA-
SIINFEKL siRNA+
Concentration /pM
D)
ED50
Normalised Absorbance
Ctss Peptide siRNA-
Ctss siRNA+
Concentration /nM
E)
ED50
Normalised Absorbance
Mutant Peptide siRNA-
Mutant siRNA+
Concentration /nM
F)
ED50
Normalised Absorbance
Scrambled Peptide siRNA-
Scrambled siRNA+
Concentration /nM
G)
Log(ED50 /pM)
SIINFEKL siRNA-
SIINFEKL siRNA+
H)
Log(ED50 /nM)
Ctss Peptide siRNA-
Ctss Peptide siRNA+
Mutant Peptide siRNA-
Mutant Peptide siRNA+
Scrambled Peptide siRNA-
Scrambled Peptide siRNA+

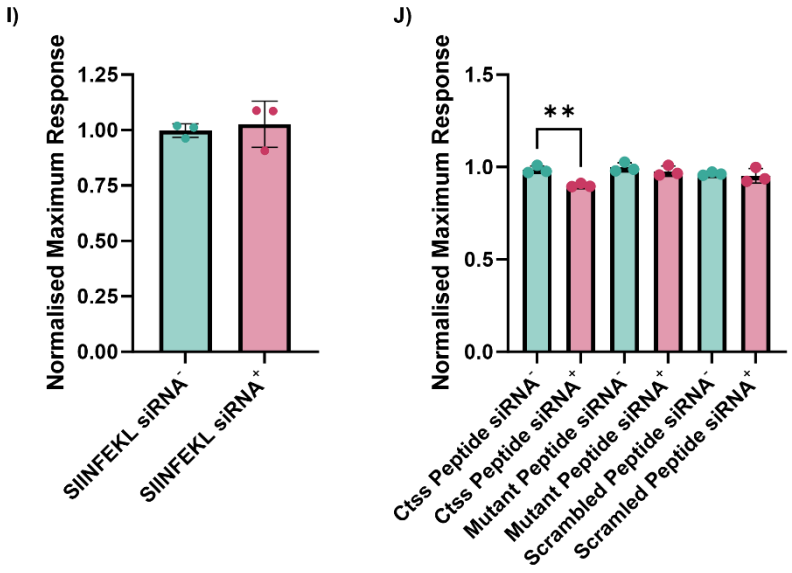


Figure 5.7 Cross-Presentation of Synthetic Peptides With Cathepsin S siRNA Knockdown
DC2.4 cells were subjected to siRNA knockdown followed by pulsing with peptides 72 hours post-knockdown. **(A)** Western blot image showing 20 µg DC2.4 lysate of 1x siRNA (25 pmol) and 2 x siRNA (50 pmol) knockdown versus mock (RNAiMAX only), untransfected and siRNA negative control DC2.4 lysate. β-actin was used as a housekeeping gene for band intensity analysis. The red arrow indicates the molecular weight band for pro-cathepsin S (36.4 kDa). **(B)** Band intensity analysis was performed in ImageJ by band peak analysis, taking the area under the curve of bands from western blot images. Intensity normalised and adjusted against β-actin expression for each lane. Graph showing Mean ±SD (n=3). **(C)** siRNA knockdown ($siRNA^+$) and wildtype ($siRNA^-$) DC2.4/B3Z CPRG assay generated 4PL regression dose-response curves from means (±SD) by dilution series of peptide diluted from 4000 to 2 pM for SIINFEKL and 4000 to 0.98 nM for **(D)** ctss peptide; **(E)** mutant peptide; and **(F)** scrambled peptide. Data generated from B3Z CPRG absorbance readings and normalised against maximum absorbance of $siRNA^-$ cells (n=3). **(G)** Log(ED_{50}) calculated from dose-response curves of $siRNA^+$ against $siRNA^-$ cells (n=3; Mean ±SD) for SIINFEKL peptide and **(H)** ctss, mutant and scrambled peptides. **(I)** Normalised maximum response of the peptides was calculated by normalising top value from 4PL regression dose-response curve of $siRNA^+$ cells against $siRNA^-$ cells for SIINFEKL peptide, and **(J)** ctss, mutant and scrambled peptide. Significance was calculated for SIINFEKL by unpaired t-test (n=3; ns – p>0.05). The significance for ctss, mutant and scrambled was calculated by ordinary one-way ANOVA with Bonferroni's post hoc multiple comparisons tests (n=3; ns - p>0.05, ** - p≤0.01). For clarity, graphs do not show comparisons with p>0.05 (ns).

5.2.8 Cathepsin S Knockdown Validates a Crucial Role of the Vacuolar Pathway in the Cross-Presentation of OVA Beads

OVA-conjugated beads were evaluated with siRNA knockdown to determine if reduced cross-presentation was unique to the ctss peptide. A dilution series of the OVA-conjugated bead created a dose-response curve (Materials and Methods 2.6.5). The dose-response curve shows a similar trajectory except towards the higher bead concentrations, where the siRNA knockdown cells showed a lower plateau than the untreated cells (Figure 5.8A). Calculating the log(ED_{50}) and a normalised maximum

response with and without treatment of DC2.4 cells with cathepsin S siRNA showed no significant change with the log(ED_{50}) (Figure 5.8B). However, it did show a significant decrease within the normalised maximum response (Figure 5.8C), indicating reduced cross-presentation from siRNA knockdown of cathepsin S, providing evidence of the role of the vacuolar pathway in cross-presentation of OVA-conjugated beads.

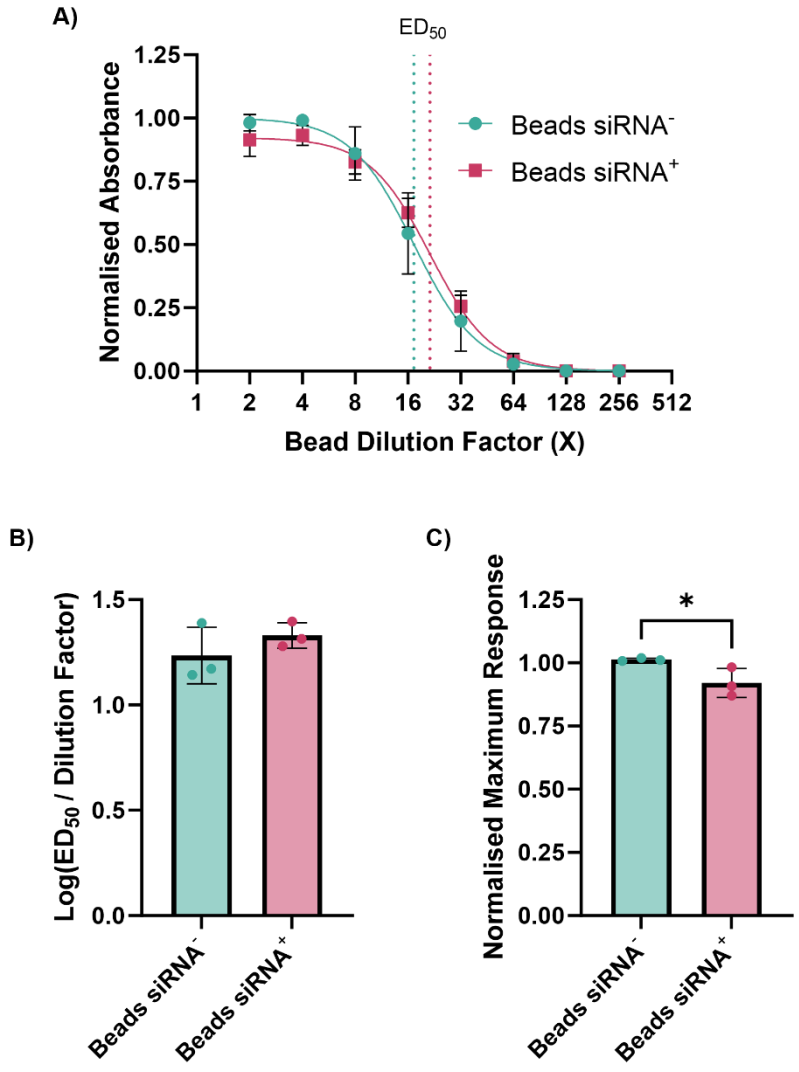


Figure 5.8 Cross-Presentation of OVA beads With Cathepsin S siRNA Knockdown
DC2.4 cells were subjected to siRNA knockdown and pulsing with OVA-conjugated 72 hours post-knockdown. Pulsed DC2.4 fixed and co-cultured with B3Z for CPRG assay. Data generated from B3Z CPRG absorbance readings and normalised against maximum absorbance of $siRNA^-$ cells (n=3). **(A)** 4PL regression dose-response curve generated from normalised means (±SD error) by two-fold bead dilution series from stock. **(B)** Log(ED_{50}) calculated from bead dose-response curves of $siRNA^+$ against $siRNA^-$ cells (n=3; Mean ±SD). **(C)** Normalised maximum response of beads calculated by normalising top value from 4PL regression dose-response curve of $siRNA^+$ cells against $siRNA^-$ cells. Significance was calculated using an unpaired t-test (n=3; ns - $p>0.05$, * - $p\leq0.05$).

5.3 Discussion

In this chapter, synthetic peptides were used to delve deeper into the nuances of antigen cross-presentation and the cathepsin S-sensitive LRMK linker found between the overlapping sequences of ROP. Overall, the three synthetic peptides displayed similarities in their processing, appearing to be internalised through similar pathways, with no discernible differences between the peptides using amiloride, cytochalasin D and dynasore.

Similarly, the peptides were unaffected by proteasome or endosome acidification inhibitors. However, the bead study confirmed that MG-132 was functional, but epoxomicin and chloroquine were not at the concentrations used. Brefeldin A, which inhibits Golgi export, reduced but did not completely inhibit the export of MHC-I and cross-presentation on the three peptides, potentially suggesting an alternative export mechanism for the peptides not via the Golgi export machinery.

With LHVS inhibition, ctss and mutant peptide were significantly inhibited but scrambled was not, suggesting that the LRMK-containing site was contributing to cross-presentation via cathepsin S and the vacuolar pathway, as the scrambled peptide, which contains the same amino acid composition, was not affected. The effect on the mutant peptide suggests that cathepsin S binding and cleavage were not interrupted by the mutations, indicating recognition and cleavage promiscuity of cathepsin S. The siRNA knockdown was demonstrated to knockdown cathepsin S expression, with a consistent reduction in one of the two bands observed. The knockdown demonstrated a small but significant reduction in the cross-presentation of the ctss peptide, which was not present for the mutant or scrambled. Therefore, this

provides evidence for the role of cathepsin S in processing the ctss peptide through its LRMK site.

The OVA beads delivered a robust control for antigen cross-presentation and validated many inhibitors at the concentrations used. For example, MG-132 inhibited the bead cross-presentation but not the peptides, suggesting that the peptide processing was proteasome-independent. Cytochalasin D and amiloride also significantly reduced cross-presentation of the beads, whereas only amiloride decreased it in the peptides, while cytochalasin D had the opposite effect. The results demonstrate that inhibition occurred through the phagocytic and macropinocytic pathways for the particulate antigen. Finally, the beads showed reduced cross-presentation with siRNA knockdown, which was only shared with the ctss peptide. The peptide and bead experiments demonstrate the crucial, but not fundamental, contribution of cathepsin S and the vacuolar pathway of cross-presentation.

Currently, there is no consensus on the contribution of each pathway to total antigen cross-presentation. However, it is thought that the cytosolic pathway is the more dominant of the two (Joffre et al., 2012; Palmowski et al., 2006). Therefore, the internalisation, processing and presentation methods must be uncovered to understand the effect of peptide composition and the LRMK cleavage site on peptide and ROP routing through the two pathways.

Upon examination of the entry route of the peptides with inhibitors, a consistent enhancement of cross-presentation by cytochalasin D for the synthetic peptides was observed. In contrast, amiloride reduced the antigen cross-presentation of all three peptides. Amiloride inhibits macropinocytosis, while cytochalasin D inhibits both macropinocytosis and phagocytosis. The overlapping inhibition by amiloride and

cytochalasin D shows that the peptides are predominantly taken into the cells via the pinocytic pathway. This observation aligns with the literature, demonstrating that peptides and proteins internalised by macropinocytosis can access MHC-I pathways (Ackerman & Cresswell, 2003).

Dynamin-dependent endocytosis primarily relies on receptor-mediated processes. For instance, the uptake of mannosylated proteins through the mannose receptor is clathrin-dependent, as is the internalisation through DEC-205, a type 1 C-type lectin receptor present on DCs that recognises markers of dying or dead cells (Burgdorf et al., 2007; Shrimpton et al., 2009; Tel et al., 2011). Since the peptides were not engineered to present substrates for receptor binding, the inhibition of dynamin-dependent endocytosis using dynasore had no impact on their uptake. Why SIINFEKL displayed enhanced efficacy by dynasore, whereas the synthetic peptides did not, remains unknown but could be attributable to the difference in their processing needs.

The role of cytochalasin D in the literature appears to contradict the rise observed with the synthetic peptides, as many experiments demonstrate a tendency for the inhibition of cross-presentation with cytochalasin D (Menager et al., 2014; Pouniotis et al., 2006; Prato et al., 2005). However, some labs have observed an increase in internalisation with cytochalasin D. For instance, one group used dextran and a cell-penetrating peptide tag consisting of eight arginine residues conjugated to enhanced GFP and saw an increase in uptake in A431 skin epithelial cell line when treated with 10 µM of cytochalasin D, which was not seen with enhanced GFP alone (He et al., 2018). The authors speculated that cytochalasin D may be causing tubulations and invaginations of plasma membranes by reducing cortical tension of the membrane, leading to increased permeance of macromolecules (He et al., 2018).

Other evidence for the off-target effects of cytochalasin D comes from increased intracellular folate through cytochalasin D, which disrupts actin and increases folic acid receptors on the cell surface (Lewis et al., 1998). The established precedent for disruption to cortical tension in the membrane may clarify how DC2.4 cells treated with cytochalasin D exhibit enhanced uptake of peptides, resulting in a more pronounced potency as evidenced by the shift in the curves. Notably, there is no change in the overall efficacy with treatment, but that may be due to assay saturation.

With the inclusion of both amiloride and cytochalasin D co-administration, the effect of either amiloride or cytochalasin D alone is completely reversed. As cytotoxic effects were ruled out, this could be a compounding effect of two inhibitors, as they both function to inhibit macropinocytosis, with the higher degree of inhibition compensating for the enhancement caused by cytochalasin D's changes to the membrane. Cells may compensate for this inhibition by using alternative uptake routes that are more advantageous for cross-presentation, as suggested by the heightened response observed with cytochalasin D. This response is reversed when amiloride is co-administered. Overall, the internalisation route does not exhibit any discernible effect on cross-presentation between the three peptides, suggesting that the LRMK site does not affect internalisation.

Upon internalisation, inhibition of the proteasome offered an insight into the processing required by synthetic peptides and the degree to which endosomal-to-cytosolic escape occurs. The toxicity of MG-132 and epoxomicin limited their application in the DC2.4 cells assessed. However, several papers have successfully used MG-132 at 1 μM and epoxomicin at 50 nM in cross-presentation studies with DC2.4 (Ito et al., 2014; Mant et al., 2012). One study successfully used MG-132 to inhibit the processing of their F37A peptide at concentrations as low as 20 nM (Mant et al., 2012). This discrepancy

in toxicity and efficacy may be due to the specific conditions in which the DC2.4 cells were subjected to inhibition, a deviation in the sensitivity over time, or the synthetic peptides being processed in a proteasome-independent manner.

Chloroquine was used to investigate whether an enhancement in cross-presentation could be attained by its impact on endosome deacidification. However, this effect was not observed, possibly due to the concentration utilised, which has been reported to be up to 100 µM in other studies demonstrating the desired outcome (Shakushiro et al., 2004). Still, other studies have also shown an enhancement of cross-presentation at 10 µM, the concentration used here (Mant et al., 2012). Alternatively, the peptides may rapidly pass through the endosome membrane, whereby chloroquine's desired effect would not be observed.

Partial inhibition was also seen with brefeldin A, even at 5 µg/mL, a commonly used concentration that has been demonstrated to be inhibitory in DC2.4 cells (Isnard et al., 2020; Shakushiro et al., 2004; Zhang et al., 2023). The incomplete inhibition may result from assay saturation, which is adjustable by varying the ratio of B3Z and DC2.4 cells. Alternatively, the peptides may be associated with MHC-I through pathways not reliant on ER-Golgi export, such as MHC-I recycling pathways or the cathepsin S-dependent vacuolar pathway (Basha et al., 2012; Di Pucchio et al., 2008; Nair-Gupta et al., 2014).

Turning our attention to cathepsin S inhibition through LHVS, changes in the mutant peptide compared to the ctss peptide did not appear to prevent its cleavage, despite the aspartic acid and proline substitutions being considered unfavourable for cathepsin S cleavage (Lützner & Kalbacher, 2008). The cleavage in the mutant peptide may indicate promiscuity within the cathepsin protease family, as they lack a specific recognition motif but have preferred residue patterns (Lützner & Kalbacher, 2008;

Wilkinson et al., 2015). The lack of inhibition for a scrambled peptide with the same amino acid composition as the ctss peptide gives evidence of a preferential but not specific cleavage motif. Overall, the inhibition observed was only partial, suggesting that the inhibition of cathepsin S cleavage was not the limiting factor in their cross-presentation, indirectly indicating processing through the cytosolic pathway.

Increasing the LHVS concentration, the enhanced cleavage of all three peptides demonstrates that the pan-cathepsin nature of LHVS may inhibit multiple cathepsin subtypes at this higher concentration. Cathepsin B, L and S are all involved in the antigen presentation pathways (Cruz-Leal et al., 2018; Hsieh et al., 2002; Zhang et al., 2000). However, cathepsin B, D, and L inhibition in mice has no observable effect on antigen cross-presentation (Shen et al., 2004). Hence, the higher degree of inhibition observed could be attributed to a disparity in cathepsin S affinity for the scrambled peptide, which is only evident at higher concentrations.

Another possibility is that the LHVS concentration was inadequate for a thorough inhibition of cathepsin S in DC2.4 cells. Supporting this is one study with DC2.4 lysates using LHVS and probing cathepsins with the cysteine protease probe JPM-565 (Bogyo et al., 2000). The probe binds to the same site as LHVS and was found to bind in concentrations up to 1 μM LHVS for cathepsin S and B (Bogyo et al., 2000). The study potentially signifies that the original LHVS concentration was insufficient for cathepsin S in the DC2.4 cell line. However, caution must be taken as this experiment was performed in lysates rather than live cells. Nevertheless, between the two concentrations of LHVS used, there is evidence of substantial worsening of the ctss peptide cross-presentation compared to the mutant and scrambled sequences.

Knockdown of cathepsin S siRNA addressed the specificity concern of LHVS. However, one challenge was the availability and specificity of antibodies for mouse cathepsin S. The cathepsin S siRNA western blot antibody used for this assay was polyclonal, which has advantages in terms of sensitivity for the protein from multiple epitope binding but comes at the disadvantage of cross-reactivity. The problem of cross-reactivity is likely evident with this cathepsin S antibody, as it consistently showed two bands. The lower band is speculated to be another pro-cathepsin subtype, such as L or K, which have an estimated molecular weight of 35.8 kDa and 35.1 kDa and share 52% and 56% homology similarity of sequence compared to cathepsin S (Altschul et al., 1990; UniProt, 2023). However, it cannot be ruled out that the lower band may be an isoform of cathepsin S, explaining why the observed effect of the knockdown with the ctss peptide was minor and non-existent for the mutant peptide.

Protein-level quantification was prioritised for assessing knockdown to ensure that the functional protein levels were sufficiently low to investigate their impact on the peptides and beads. However, in subsequent studies, additionally incorporating gene-level analyses would be advantageous to quantify the knockdown comprehensively. Nevertheless, the siRNA knockdown of cathepsin S proved that the vacuolar pathway processed the LRMK-containing ctss peptide, which was not replicated in alternative sequences or controls.

Along with peptides, OVA-conjugated beads were used to validate the inhibitors and cathepsin S knockdown and to demonstrate differences between particulate and soluble antigens. The beads were 3 µm in size, so macropinocytosis and phagocytosis were the most likely entry method, as macropinosomes can vary from 0.2 to 5.0 microns, and the optimal uptake range for phagosomes is between 2.0 to 3.0 microns (Champion et al., 2008; Lim & Gleeson, 2011; Swanson & Watts, 1995). Therefore,

inhibition from cytochalasin D and amiloride eliminates the most probable entry mechanisms used by the beads (Beletskii et al., 2005; Guermonprez et al., 2003; Koivusalo et al., 2010). On the other hand, when DC2.4 cells were subjected to dynasore treatment, an unexpected augmentation in antigen cross-presentation for the beads was observed. At first, this was theorised to be a potential rerouting of pathways favouring cross-presentation. Nevertheless, it is essential to note that clathrin-mediated endocytosis has a maximum size of approximately 0.2 microns (Burgdorf et al., 2006; Rejman et al., 2004). Therefore, it is not a viable uptake pathway for the OVA beads. Thus, the increased cross-presentation with dynasore suggests that it may exert additional effects on the cell, contributing to the apparent enhancement in cross-presentation.

One of the additional effects of dynasore is its ability to inhibit V-ATPase (Sakai et al., 2010). V-ATPase is a proton pump which contributes to the acidification of the lysosome during its maturation, leading to the activation of lysosomal proteases (Embgenbroich & Burgdorf, 2018; Liberman et al., 2014). A hallmark of efficient cross-presenting DCs is their alkali endosome and lysosomal compartments, regulated by NOX2 NADPH oxidase and V-ATPase (Mantegazza et al., 2008; Savina et al., 2009; Segura et al., 2013). The apparent increase in cross-presentation of OVA-conjugated beads may result from the inhibition of V-ATPase, leading to higher pH endosomes, less protease digestion and escape into the cytosol, enhancing cross-presentation.

However, the same effect was not observed with chloroquine, which also deacidifies the lysosomal and endosomal compartments. This contradiction could indicate an inadequate concentration of chloroquine in the cells for inhibition to occur or another off-target effect of dynasore. For example, studies have demonstrated that dynasore influences cholesterol homeostasis, leading to the accumulation of cholesterol in the

ER and inducing Golgi vesiculation (Girard et al., 2011; Grimmer et al., 2005; Robinet et al., 2006), which could alter the dynamics of cross-presentation.

The bead study also validated MG-132, which exhibited cross-presentation inhibition for beads but not peptides. This observation suggests that the bead processing was proteasome-dependent, while the peptides were not due to the differences in size or processing between peptides and particles. However, epoxomicin failed to change bead processing and, therefore, was confirmed to not be functional at the concentration evaluated.

Although the OVA beads were proteasome-dependent, cathepsin S also participated in their cross-presentation, confirming an existing study that showed that cathepsin S was strongly associated with the processing of three-micron beads and likely processed OVA through the vacuolar pathway (Mant et al., 2012). However, there is a discrepancy between the effects observed with LHVS and the cathepsin S knockdown through siRNA. The reduction in cross-presentation from LHVS for the beads was considerable, contrasting with the slight decline from the siRNA knockdown. This variance with beads could stem from differences in the experimental setup, either from examining a single LHVS concentration compared to the dose-response curves for the peptides or the overall inefficiency of the siRNA knockdown.

Overall, it is essential to consider that in untreated cells, the potency of the ctss peptide was lower than that for the scrambled peptide despite the presence of the LRMK site. This lower potency is consistent even though both ctss and the scrambled peptide share an identical overall composition, suggesting that the amino acid composition combined with their order is more crucial in determining the efficiency of peptide cross-presentation. Overall, including the LRMK cathepsin S sensitive linker did contribute

to the cross-presentation of the peptides, which is evident from its partial inhibition. Nevertheless, it only represents a modest fall in the maximum response, demonstrating that it is not the only factor in its cross-presentation.

5.4 Conclusion

Synthetic peptides and OVA-conjugated beads provided two contrasting methods of studying the intricacies of internalisation, processing, and cross-presentation pathways. Overall, the peptides resisted many of the inhibitors used in this process, while in contrast, the beads were susceptible, demonstrating the differences in how DCs process beads and small peptides. The study also revealed that some inhibitors, such as cytochalasin D and dynasore, can unexpectedly enhance cross-presentation under certain circumstances. These unanticipated results may be due to the rerouting of peptides through alternative, more conducive cross-presentation pathways, evidenced by the amiloride reversal. However, it could also be from the off-target effects discussed. More research is needed to understand this phenomenon.

LHVS and the siRNA knockdown decreased the cross-presentation of the LRMK-containing ctss and mutant peptides. In the same study, the scrambled peptide did not display inhibition by LHVS but was more potent overall. Therefore, the peptide's sequence composition and residue order influence its ability to cross-present. Thus, the overall design of the peptide is equally as crucial as the LMRK in developing an efficacious peptide vaccine. These observations are accurate for peptides, as they are far more likely to be affected by nuances in the sequences than proteins or ROPs. All other factors being constant, the LRMK site demonstrated its role as a contributing factor in peptide cross-presentation and, consequently, as part of ROPs repertoire of cross-presentation.

6 Final Discussion

6.1 Thesis Overview

ROP cross-presentation is not a fully understood process, with the LRMK site thought to contribute to ROP cross-presentation through cathepsin S in the vacuolar pathway. To study ROPs in greater detail, a model ROP was needed. OVA is a commonly used mildly immunogenic protein with well-characterised $CD4^+$ and $CD8^+$ epitopes (Karandikar et al., 2019; Rotzschke et al., 1991), making it a prime candidate for studying cancer vaccine strategies and cross-presentation.

OVA-ROP was developed as a model ROP to study cross-presentation and understand its mechanisms. OVA-ROP was successfully produced in *E. coli* as an insoluble inclusion body and solubilised using GuHCl (Figure 3.2) but was difficult to remove while maintaining solubility. After extensive testing, sarkosyl was the prime candidate for maintaining ROP solubility and was used to directly solubilise OVA-ROP without relying on GuHCl (Figure 3.4).

However, OVA-ROP relied on the anionic detergent sarkosyl to maintain its solubility, with removal leading to complete precipitation. Keeping sarkosyl in solution during cellular testing was necessary to assess OVA-ROP's antigenicity despite potential toxicity. Having evaluated OVA-ROP sarkosyl toxicity on DC2.4, a maximum concentration was established that would allow DC2.4 cells to be evaluated with OVA-ROP without compromising the integrity of the cells (Figure 3.6). The question was whether OVA-ROP in the presence of sarkosyl could elicit a response in DC2.4 cells. Using an anti-H-2Kb/SIINFEKL PE antibody, OVA-ROP displayed a modest ability to cross-present (Figure 3.8). However, cross-presentation was limited, with the range

between the background and ROP detection not being broad enough to study entry pathways, processing, and the contribution of the LRMK site to cross-presentation.

Alternative sequences and expression strategies were developed to overcome issues with OVA-ROP. The first was to create a truncated version of OVA-ROP with an Fc tag to improve solubility by producing a smaller, less complex ROP coupled with the highly soluble Fc region from IgG. Despite attempts to improve the stability of the protein through the truncation of OVA-ROP and the inclusion of the Fc domain, the protein remained unstable. After harvest from the Expi293F cells, most of the tOVA-ROP-Fc was within the cells, with only a small amount extractable (Figure 4.2).

The reporter assay for antigen cross-presentation was switched from an anti-H-2Kb/SIINFEKL antibody to a more physiologically relevant cell-based assay using the B3Z T cell hybridoma. B3Z contains a TCR specific to SIINFEKL in the context of H-2Kb. It has been engineered to contain the *LacZ* gene, expressing β-galactosidase, under the NFAT promoter of IL-2, activated upon TCR binding and measurable by a CPRG assay (Karttunen et al., 1992).

Although only produced in small quantities, tOVA-ROP-Fc was compared to OVA-ROP and OVA in the B3Z assay. The experiments suggested that tOVA-ROP-Fc was more efficacious than OVA-ROP and OVA in immune activation response. However, its minimal activation and limited yields made it unsuitable for further study to elucidate LRMK and its role in enhancing cross-presentation (Figure 4.2).

From the prior experiments, it was clear that immunogenicity was limited, so other potential tag and fusion methods were sought to improve cross-presentation, potentially benefiting future ROPs. One of the methods examined was inducing Fc-tag multimerisation and forming IC-like structures. These structures increase the cross-

linking of Fc receptors, leading to enhanced antigen uptake and shielding associated antigens from degradation and improved antigen presentation and cross-presentation (den Haan & Bevan, 2002; Rafiq et al., 2002; Weflen et al., 2013). Multimerisation was achieved by mutating the tailpiece of IgM onto the Fc-tag with an additional point mutation in the Fc-tag, adding a disulphide bond to stabilise the structure (Figure 4.3). However, the yields from the Fc-multimerisation without any additional epitopes were low. There were diminishing returns on expression yield with increasing multimer formation, which fusion partners would exacerbate.

Another method trialled was to conjugate an anti-mouse DEC-205 scFv to OVA epitopes to target DC2.4 and to enhance targeted cellular uptake and cross-presentation, with the knowledge feeding back to applications with a targeted ROP approach. The production of the scFv fusion initially looked promising, with the SUMO-expressed anti-DEC-205 OVA fusion maintaining solubility after refolding (Figure 4.4). However, removing the SUMO tag resulted in precipitation (Figure 4.5). Either the scFv fusion relied on SUMO for its solubility or the buffer or process of refolding was incorrect, leading to an unstable or incorrectly folded structure. Equally, including the OVA epitopes contributed to its instability.

It was challenging to produce OVA-ROP, its derivatives, and minimal epitope scFv fusion in a soluble state. Therefore, an alternative model antigen system was explored with NY-ESO-1 epitopes. NY-ESO-1 is a human melanoma antigen with well-defined $CD8^+$ epitope sequences (Jager et al., 2000). NY-ESO-1 epitopes were fused to an anti-human DEC-205 scFv, and similarly, the expression was initially successful but ended with precipitation of the fusion protein upon removal of the SUMO-tag (Figure 4.6 & 4.7).

After determining that OVA-ROP and its derivatives were unsuitable for analysing the effect of the LRMK site on cathepsin S-mediated cross-presentation, synthetic peptides were explored. Three synthetic peptides were created to investigate the function of the LRMK site in antigen uptake, processing, and export in DC2.4 cells. The ctss peptide contained the entire LRMK sequence. The mutant peptide had two amino acid substitutions at the P1' and P1 sites in the sequence to disrupt cathepsin S cleavage. The scrambled peptide had the same amino acid composition as the ctss peptide but with a scrambled sequence upstream of the SIINFEKL sequence. The scrambled sequence was to determine whether the cleavage sequence or the overall composition was the determining factor in efficient antigen cross-presentation.

All three peptides behaved similarly, with only subtle differences distinguishing them. Brefeldin A inhibition saw reductions in all three peptides to different extents, with the ctss and scrambled peptides behaving similarly in potency and efficacy reduction. The similarities suggest that the cathepsin S cleavage site was not involved in routing the peptide through different export mechanisms (Figure 5.1). Although the mutant peptide saw a shift in the curve, indicating a reduction in potency, the overall efficacy was maintained, adding more evidence that the LRMK site was unlikely to affect the export mechanism (Figure 5.1).

The trend continued with the endocytosis inhibitors, which broadly displayed similar profiles for ctss peptide and scrambled peptide for amiloride, cytochalasin D and dynasore inhibition. Mutant peptide again showed a subtle discrepancy, with the amiloride potency not being significantly affected, but the maximum response or efficacy was reduced (Figure 5.3). However, one of the most surprising effects was with cytochalasin D, which showed increased potency for the peptides (Figure 5.3). The reason for this is not understood but is thought to be an off-target effect.

Overall, the study on the inhibitors of cross-presentation revealed that proteasome inhibition through MG-132 had no significant effect on any of the three peptides. However, LHVS, a pan-cathepsin inhibitor with nanomolar affinity for cathepsin S (Palmer et al., 1995), showed a notable decrease in potency and efficacy for the ctss peptide. Additionally, it demonstrated a reduction in effectiveness for the mutant peptide (Figure 5.4). The observation showed that the LRMK site contributes to the cross-presentation of these peptides, as only the scrambled peptide did not exhibit any changes in cross-presentation when subjected to LHVS inhibition. Additionally, cathepsin S showed binding promiscuity, as evidenced by the LHVS-induced reduction with the mutant peptide, which was synthesised with unfavourable amino acids in its sequence to limit its cleavage. However, caution must be exercised due to LHVS's pan-cathepsin activity, which can disrupt alternative cathepsin subtypes and reduce peptide processing. The potential pan-cathepsin effect was observed when the dose was increased to 100 nM, which caused a significant decrease in antigen cross-presentation for all three peptides, regardless of the presence of the LRMK site. (Figure 5.5).

As SIINFEKL was not an adequate control for cross-presentation, OVA-conjugated beads were deployed to elucidate whether the inhibitors at the concentration were functional and to operate as a control for cross-presentation. Overall, the OVA beads differed from soluble peptides, highlighting differences in cross-presentation between soluble and particulate systems (Figure 5.6). However, the beads provided insight into the chemical inhibition that appeared non-functional for soluble peptides. For example, the processing of these synthetic peptides was concluded to be proteasome-independent as MG-132 strongly affected the beads but not the peptides at equal inhibitor concentrations.

siRNA knockdown was investigated to address the shortcomings of the chemical inhibition strategy. The siRNA knockdown was broadly successful, with the top band on the western blot consistently decreasing with cathepsin S siRNA treatment (Figure 5.7). However, doubts continued on the reliability of the data due to the persistence of the lower band, which is speculated to be either another cathepsin subtype or an alternative form of cathepsin S. Regardless, the siRNA knockdown saw a significant decrease in the cross-presentation of the beads.

It should be noted that the strength of inhibition with LHVS on the beads was significant, while only minor in the siRNA knockdown study (Figure 5.7). This observation is potentially due to the size and routing of the particulate versus the soluble antigen and the general contribution of the vacuolar and cytosolic pathways. Furthermore, it could point to more evidence of inefficiency in siRNA knockdown compared to LHVS.

SiRNA knockdown within the peptide study showed a significant reduction of ctss peptide that was not seen with the mutant or scrambled peptide, suggesting that the LRMK site played a role in the cross-presentation of the ctss peptide (Figure 5.7). This ctss peptide-exclusive observation was only with siRNA knockdown, not with LHVS, as seen for the reduction of mutant peptide cross-presentation with LHVS but not siRNA. There are two possible reasons for the observed difference. Firstly, the siRNA knockdown might not have been efficient, as evidenced by the slight decrease, which was not observable in the mutant peptide. Secondly, LHVS may have additional inhibitory effects that contribute to the efficiency of their cross-presentation.

6.2 Thesis Discussion

ROPs were developed to incorporate multiple overlapping epitopes of a cancer antigen into a single polypeptide chain. The rationale is twofold: first, it aims to produce a single-chain molecule that benefits from better batch-to-batch quality control compared to multiple, smaller peptides that would require individual assessment (Cai et al., 2017). Second, it aims to create a polypeptide chain with lower homology to the original antigen to avoid problems associated with self-recognition and immune tolerance (Cai et al., 2017). Breaking immune tolerance is one of the biggest challenges with peptide vaccines, as T cells that recognise self-antigens are quickly eliminated as part of central tolerance mechanisms (Xing & Hogquist, 2012).

The other defining feature of an ROP is the cathepsin S cleavage motif engineered between the overlapping regions. This motif is based on the cleavage sequence of the CLIP on the invariant chain, which is cleaved off MHC-II during antigen presentation by cathepsin S to allow for peptide association (Riese et al., 1996). Cathepsin S also participates in the vacuolar pathway of antigen cross-presentation (Riese et al., 1996). Although recent studies with survivin-ROP in melanoma models have shown strong cross-presentation (Zhang et al., 2023), a complete understanding of cathepsin S's contribution to ROP cross-presentation was unknown.

OVA-ROP was designed to be a model ROP for antigen cross-presentation studies to understand the role of cathepsin S in ROP cross-presentation, validate the pathways involved, and help develop future, more efficacious ROPs. ROPs are artificial polypeptides lacking a native structure. As a result, they are unlikely to be produced successfully in mammalian cells, as misfolded or unfolded proteins are quickly eliminated from cells through the ubiquitin-proteasome system or autophagy

processes (Ciechanover & Kwon, 2015). However, *E. coli* accumulates misfolded proteins into large insoluble masses known as inclusion bodies (Carrio & Villaverde, 2005). Inclusion bodies isolate the protein from the rest of the subcellar material in *E. coli* and act as a rudimentary purification step, as inclusion bodies are often made up of mostly the recombinant protein of interest (Singh et al., 2015). One drawback of insoluble masses is that they can be challenging to refold into a configuration that encourages solubility. Despite this, ROPs are created in *E. coli* cells due to their cost-effectiveness and high yields.

Producing a stable form of OVA-ROP was challenging due to the hydrophobic nature of OVA, which comprises around 50% hydrophobic residues (Li-Chan, 1989). The overlapping nature of ROPs further complicates the matter, as depending on where the overlaps are, their formulation can increase the concentration of hydrophobic residues. Because of this, sarkosyl was necessary to maintain the solubility of OVA-ROP but limited its application in cells due to it proving harmful to the integrity of DC2.4 cells at high concentrations. Consequently, cross-presentation was possible but limited, posing a challenge for studies investigating different inhibitors, requiring a more comprehensive range of concentrations.

Many groups have used synthetic long peptides to produce cancer peptide vaccines, including for HPV-16 expressing tumours, p53 in metastatic colon cancer, and survivin (Onodi et al., 2018; Speetjens et al., 2009; Zwaveling et al., 2002). Being synthetic, it avoids the issues associated with the recombinant expression but comes at an increased cost and limited yield. Therefore, the attractiveness of producing a polypeptide from *E. coli* is evident compared to the synthetic route.

While various groups have formulated peptide-based cancer vaccines through recombinant technology, many vaccines are designed as fusion proteins incorporating small epitopes rather than larger peptides or proteins. This approach avoids compromising the fusion protein's structure, formation, and yield. One study showed that fusing peptides to transthyretin, a transport protein for the thyroid hormone thyroxine and retinol, showed a 90-fold increase in immunogenicity for its associated peptide (Mehta et al., 2020). Another study mentioned previously is the XCL1 fused with an OVA SLP with a mutated Fc tag, which showed a significant immunogenic response in B16-OVA mouse models (Botelho et al., 2019).

The success of these fusion studies inspired the production of tOVA-ROP-Fc and anti-DEC-205 scFv OVA fusion proteins. These alternatives comprise $CD4^+$ and $CD8^+$ epitopes derived from the OVA protein sequence and served as a proof of concept for a targeted strategy. Establishing the fusions as a stable and reliable method of producing peptide cancer vaccines could then be applied to augment ROP immunogenicity or solubility. For tOVA-ROP-Fc, the change also came from the expression system from *E. coli* to the Expi293F mammalian cell line. The idea was that producing proteins successfully and in a soluble form would make it easier to isolate and purify them from cells without relying on the solubilisation of inclusion bodies and refolding steps of *E. coli*. However, tOVA-ROP-Fc was only obtained in small quantities from the mammalian cells, with the low yield posing a challenge, limiting the amount of observable cross-presentation.

The limited expression was disappointing as Fc-tags have been used to produce vaccines in various anti-cancer therapeutics. One such example is a study that showed a WN peptide-Fc fusion composed of a twelve amino acid peptide, which binds to numerous cancer cell types, combined with an Fc tag that attaches to FcγRs

on immune cells (Mobergslien et al., 2016). The dual action brings cancer and immune cells into proximity, activating the immune cells, which can act on the tumour cells and prevent their growth (Mobergslien et al., 2016). Another example is CUE-101, an E7-pHLA-IL2-Fc fusion protein designed to expand HPV E7-specific $CD8^+$ T cell populations (Quayle et al., 2020). The Fc has been mutated to prevent Fc receptor binding but still preserve neonatal receptor binding, making it a scaffold for the vaccine strategy (Quayle et al., 2020). With these two examples, there is precedent for various use cases for Fc fusion proteins in anti-cancer therapeutics.

The B3Z assay on tOVA-ROP-Fc did demonstrate that including an Fc domain improved the cross-presentation over OVA-ROP. However, the poor OVA-ROP cross-presentation was likely from the sarkosyl hampering its uptake and cross-presentation. In any case, including an Fc-tag has vast potential in the context of next-generation ROP technologies.

The anti-DEC-205 scFv fusions were designed as a targeted system for a peptide-cancer vaccine as an alternative to the passive ROP strategy. They were intended to demonstrate the feasibility of targeting antigens to the cell surface of DCs, with the technology feeding into ROP design strategies. The fusion was created with a minimalistic epitope approach to demonstrate its feasibility before incorporating destabilising elements such as an ROP. Many other groups have also taken an antigen-targeted approach and successfully shown efficacy in cancer therapy. One study used an anti-epidermal growth factor receptor (EGFR) scFv fused with an anti-cancer lytic peptide ZXR2, to target EGFR-expressing tumours for membrane lysis by ZXR2 (Zhang et al., 2023).

Conversely, a different approach has been taken by a group that utilises a cancer-specific cell-penetrating peptide to direct and deliver an anti-mutant KRAS scFv to mutated KRAS tumours (Lim et al., 2013). The strategy demonstrated increased apoptosis in a KRAS mutant HCT116 human colorectal carcinoma cell line (Lim et al., 2013). Together, these results exhibit that scFv fusions deserve more investigation into their application in the context of a DC targeting ROP for more specific uptake and increased cross-presentation.

The hurdle to overcome with the DEC-205 scFv system was removing the SUMO tag, which destabilised and precipitated the fusion protein. The sequences for the mouse and human DEC-205 scFv were compiled from existing sequences (Birkholz et al., 2010; Demangel et al., 2005), so the reason was unclear and could be from destabilisation caused by the fusion partner or incorrect folding that was exposed when the SUMO tag was removed. For this experiment to succeed, the scFv design and its associated epitopes must be carefully considered along with its expression system. Although *E. coli* was used to express scFvs, the mammalian system offers advantages, including post-translational modifications and cytosolic disulphide bond formation.

After examining OVA-ROP and fusion proteins, the question of the ROP cathepsin S cleavage motifs' contribution to cross-presentation was unanswered. Synthetic peptides have effectively been used to study cross-presentation. One study looked at SLPs for Melan-A and found that they were proteasome-dependent and were processed through the cytosolic pathway involving TAP and the ERAD-related p97 protein (Menager et al., 2014). Another study contradicts this, showing that long peptides composed of HLA-A2-restricted peptides of melanoma antigens gp100 and melanoma antigen recognized by T cells 1 (MART1) were proteasome-independent,

relied upon the vacuolar pathway, and bound to MHC-I via a peptide exchange mechanism in vesicles away from the ER (Ma et al., 2016). Finally, in a recent study, the HLA-A1-restricted peptides from the MAGE-A3 antigen were principally vacuolar in their cross-presentation but still displayed a TAP dependency (Ma et al., 2019). Collectively, these three papers glimpse the intricate, redundant, and overlapping mechanisms involved in antigen cross-presentation. Conducting studies on this topic, as we have demonstrated, can aid in comprehending cross-presentation and how distinct peptides, proteins, and particulate systems are impacted by it.

One constraint of this study is that OVA-ROP contains the minimal LRMK motif, while the ctss synthetic peptide has the complete LRMKLPKP sequence. The deviation was intended to optimise recognition and maximise cathepsin S response to elucidate its effect on cross-presentation via the vacuolar pathway. Then, from this baseline, discover which amino acids are essential for optimal binding. It is important to note that it is still unknown whether the inclusion of the minimal LRMK site contributes to cleavage by cathepsin S for cross-presentation. However, by demonstrating first that the entire sequence is recognised by cathepsin S, further research can lead to a new ROP design with the entire sequence or further studies on the minimal LRMK site compared to the full-length sequence.

Using inhibitors with the synthetic peptides produced contradictory results, specifically with cytochalasin D. It was believed that inhibiting macropinocytosis and phagocytosis with cytochalasin D would hinder peptide uptake and cross-presentation. However, the opposite was observed. On the other hand, amiloride, which inhibits macropinocytosis, showed a decrease in cross-presentation, suggesting macropinocytosis participates in the processing of the peptides. It was then assumed that cytochalasin D inhibition may upregulate an alternative pathway. However,

inhibition of other mechanisms of uptake involving receptors, such as clathrin-mediated or dynamin-dependent, were not affected by their inhibition by dynasore or in combination with cytochalasin D. Also, the synthetic peptides do not have additional modifications like mannosylation that would assist in binding to receptors such as DEC-205 or the mannose receptor for their uptake (Shrimpton et al., 2009; Tel et al., 2011). Complicating things further, the combination of cytochalasin D and amiloride saw the cross-presentation revert to the uninhibited baseline.

Since cytochalasin D is known to inhibit macropinocytosis, the difference observed between the enhanced cross-presentation response of cytochalasin D and diminished response with amiloride and the complete reversal of their respective responses with combination treatment can only be explained by an off-target effect of cytochalasin D. Only a few studies have shown that cytochalasin D may have alternative effects, including the study that speculated the change in cholesterol in the cell membranes caused by cytochalasin D might be causing tubulations and invaginations of the membrane (He et al., 2018). These disruptions could allow the peptide to penetrate the membrane and enter the cytosol, where the proteasome machinery for cross-presentation is located (He et al., 2018). However, this phenomenon is not fully understood and warrants further investigation.

In studying the role of cathepsin S, chemical inhibition and genetic knockdown were considered to maximise the potential for exposing the role of cathepsin S in processing the synthetic peptides for cross-presentation. The inconsistency between the chemical inhibition via LHVS and the gene knockdown via siRNA validated this approach with the observed differences, particularly between the mutant peptide, which displayed a reduction in cross-presentation under LHVS inhibition but not under siRNA

knockdown. The differences in observation are thought to be from the inefficiency of the siRNA knockdown.

The focus of the siRNA knockdown quantification was by western blot. However, this system was imperfect due to the dual banding, which is believed to be from another subtype of cathepsin. The second band may also represent a different form of cathepsin S, which occurs in three forms: preproprotein of around 38.5 kDa, proprotein of about 36 kDa, and a mature protein of approximately 24 kDa (Smyth et al., 2022). Knockdown of the precursor cathepsin S was observed in siRNA-treated cells compared to wild-type cells, as confirmed by western blot analysis. However, to rigorously evaluate this knockdown, examining the protein levels within the cells and verifying the genetic knockdown using qPCR would be beneficial.

Ultimately, the choice to prioritise protein-level expression was driven by the understanding that protein levels are crucial for the digestion of peptides, offering a more direct measure than relying solely on relative gene expression levels. Although further evidence of cathepsin S knockdown would have been provided by looking at gene expression levels, a reduction in the cross-presentation of the ctss peptide with siRNA was observed, even with incomplete knockdown. The mutant peptide only decreased with LHVS inhibition, indicating the importance of the LRMK site being fully intact for cross-presentation. Together, these findings provide evidence for the significance of the LRMK site in cross-presentation. Furthermore, as considerable cross-presentation still occurs under the influence of siRNA knockdown or LHVS, the cross-presentation was not exclusively through the vacuolar pathway. Therefore, although the LRMK site contributes to the cross-presentation of synthetic peptides and ROP, it is not the only factor determining cross-presentation efficiency.

Future studies would apply what we have learnt to aid in the design of ROP, including the complete LRMK sequence and comparisons between the shortened and full length. Studies would investigate the LRMK system with the larger, different model ROP and with a protein and particulate-based system to compare the relative changes in antigen cross-presentation that occur with the inclusion of the cathepsin S linker.

Alternative approaches for the cathepsin S knockdown would also be considered, utilising CRISPR/Cas9 technology to remove cathepsin S entirely from the DC2.4 cells and other cell models. Other proteins worth considering for knockout include TAP, which is integral for the cytosolic pathway and, in combination with cathepsin S knockdown, will delve deeper into our understanding of the general contribution of peptides and ROPs through the cytosolic and vacuolar pathways.

None of the inhibitors used in the assay showed complete knockdown, which may be attributable to assay saturation. Therefore, in future studies, changes in cell ratio between DC2.4 and B3Z would be investigated, with a higher B3Z ratio perhaps revealing changes not observable with the current assay set-up. Other cell lines, such as THP-1 monocyte and Jurkat cell lines, would also be considered in studying human-based epitope peptides and ROPs. There is also the potential to examine more physiologically relevant models by extracting T cells and differentiating monocytes from human blood, or by using H-2Kb/SIINFEKL specific OT I TCR transgenic mice.

Future studies would also look at the intriguing role of cytochalasin D and dynasore in peptide and particulate uptake, especially given the observed enhancement of antigen cross-presentation. Finally, we would explore how the antigen composition of ROP and additional tags and fusions enhance its solubility and immunogenicity to augment cross-presentation.

6.3 Thesis Conclusion

ROP vaccines aim to avoid self-recognition and maximise the number of epitopes through their overlapping sequence and the cathepsin S-sensitive linker. However, further research was needed to understand its ability to cross-present and the role of the LRMK site. OVA-ROP was designed as a model ROP to understand the fundamental pathways of entry, processing, and presentation by DCs. However, the challenge was producing it in a form that allowed for the tests required to answer these questions, necessitating the need for synthetic peptides to understand the contribution of LRMK. While not a complete substitute for ROP, the ctss peptide containing the LRMK motif was processed by cathepsin S. Consequently, this study offers additional insights into the potential role of the motif in directing ROPs to the vacuolar pathway of antigen cross-presentation. Synthetic peptides also raised more questions on the entry of peptides into cells, especially with the counterintuitive effects observed.

The comparisons between peptide and OVA bead uptake demonstrate the complexity of cross-presentation from their uptake to cell-surface presentation on MHC-I. Cross-presentation is not conducted by a single mechanism but rather by multiple redundant and adaptable pathways and systems. Overall, the significance of the vacuolar pathway mediated by cathepsin S cannot be overstated. However, the contribution of the LRMK site is only one piece of the puzzle, with the overall design and composition of ROP and peptides equally important. Designing peptides for efficacious immunogenicity is still empirical, involving diverse designs, formulations, and sequence libraries. This process is also the case for ROPs, where the sequence can be altered dramatically by changing the length of overlaps and sequence lengths. Therefore, the LRMK motif and its capacity for cross-presentation is one of many essential tools for creating effective cancer vaccines.

References

Abbas, A. K., Murphy, K. M., & Sher, A. (1996). Functional diversity of helper T lymphocytes. *Nature*, *383*(6603), 787-793. https://doi.org/10.1038/383787a0

Abiko, K., Matsumura, N., Hamanishi, J., Horikawa, N., Murakami, R., Yamaguchi, K., Yoshioka, Y., Baba, T., Konishi, I., & Mandai, M. (2015). IFN-gamma from lymphocytes induces PD-L1 expression and promotes progression of ovarian cancer. *Br J Cancer*, *112*(9), 1501-1509. https://doi.org/10.1038/bjc.2015.101

Accapezzato, D., Visco, V., Francavilla, V., Molette, C., Donato, T., Paroli, M., Mondelli, M. U., Doria, M., Torrisi, M. R., & Barnaba, V. (2005). Chloroquine enhances human CD8+ T cell responses against soluble antigens in vivo. *J Exp Med*, *202*(6), 817-828. https://doi.org/10.1084/jem.20051106

Ackerman, A. L., & Cresswell, P. (2003). Regulation of MHC class I transport in human dendritic cells and the dendritic-like cell line KG-1. *J Immunol*, *170*(8), 4178-4188. https://doi.org/10.4049/jimmunol.170.8.4178

Ackerman, A. L., Giodini, A., & Cresswell, P. (2006). A role for the endoplasmic reticulum protein retrotranslocation machinery during crosspresentation by dendritic cells. *Immunity*, *25*(4), 607-617. https://doi.org/10.1016/j.immuni.2006.08.017

Aderem, A., & Underhill, D. M. (1999). Mechanisms of phagocytosis in macrophages. *Annu Rev Immunol*, *17*, 593-623. https://doi.org/10.1146/annurev.immunol.17.1.593

Agadjanyan, M. G., Ghochikyan, A., Petrushina, I., Vasilevko, V., Movsesyan, N., Mkrtichyan, M., Saing, T., & Cribbs, D. H. (2005). Prototype Alzheimer's disease vaccine using the immunodominant B cell epitope from beta-amyloid and promiscuous T cell epitope pan HLA DR-binding peptide. *J Immunol*, *174*(3), 1580-1586. https://doi.org/10.4049/jimmunol.174.3.1580

Ahmad, A. S., Ormiston-Smith, N., & Sasieni, P. D. (2015). Trends in the lifetime risk of developing cancer in Great Britain: comparison of risk for those born from 1930 to 1960. *Br J Cancer*, *112*(5), 943-947. https://doi.org/10.1038/bjc.2014.606

Akbar, S. M., Inaba, K., & Onji, M. (1996). Upregulation of MHC class II antigen on dendritic cells from hepatitis B virus transgenic mice by interferon-gamma: abrogation of immune response defect to a T-cell-dependent antigen. *Immunology*, *87*(4), 519-527. https://doi.org/10.1046/j.1365-2567.1996.516576.x

Alegre, M. L., Frauwirth, K. A., & Thompson, C. B. (2001). T-cell regulation by CD28 and CTLA-4. *Nat Rev Immunol*, *1*(3), 220-228. https://doi.org/10.1038/35105024

Alexander, J., del Guercio, M. F., Frame, B., Maewal, A., Sette, A., Nahm, M. H., & Newman, M. J. (2004). Development of experimental carbohydrate-conjugate vaccines composed of Streptococcus pneumoniae capsular polysaccharides and the universal helper T-lymphocyte epitope (PADRE). *Vaccine*, *22*(19), 2362-2367. https://doi.org/10.1016/j.vaccine.2003.11.061

Almand, B., Clark, J. I., Nikitina, E., van Beynen, J., English, N. R., Knight, S. C., Carbone, D. P., & Gabrilovich, D. I. (2001). Increased production of immature myeloid cells in cancer patients: a mechanism of immunosuppression in cancer. *J Immunol*, *166*(1), 678-689. https://doi.org/10.4049/jimmunol.166.1.678

Almeida, J. P. M., Lin, A. Y., Figueroa, E. R., Foster, A. E., & Drezek, R. A. (2015). In vivo gold nanoparticle delivery of peptide vaccine induces anti-tumor immune response in prophylactic and therapeutic tumor models. *Small*, *11*(12), 1453-1459. https://doi.org/10.1002/smll.201402179

Altman, J. D., Moss, P. A., Goulder, P. J., Barouch, D. H., McHeyzer-Williams, M. G., Bell, J. I., McMichael, A. J., & Davis, M. M. (1996). Phenotypic analysis of antigen-specific T lymphocytes. *Science*, *274*(5284), 94-96. https://doi.org/10.1126/science.274.5284.94

Altschul, S. F., Gish, W., Miller, W., Myers, E. W., & Lipman, D. J. (1990). Basic local alignment search tool. *J Mol Biol*, *215*(3), 403-410. https://doi.org/10.1016/S0022-2836(05)80360-2

Ambrosini, G., Adida, C., & Altieri, D. C. (1997). A novel anti-apoptosis gene, survivin, expressed in cancer and lymphoma. *Nat Med*, *3*(8), 917-921. https://doi.org/10.1038/nm0897-917

Anand, U., Dey, A., Chandel, A. K. S., Sanyal, R., Mishra, A., Pandey, D. K., De Falco, V., Upadhyay, A., Kandimalla, R., Chaudhary, A., Dhanjal, J. K., Dewanjee, S., Vallamkondu, J., & Perez de la Lastra, J. M. (2023). Cancer chemotherapy and beyond: Current status, drug candidates,

associated risks and progress in targeted therapeutics. *Genes Dis*, *10*(4), 1367-1401. https://doi.org/10.1016/j.gendis.2022.02.007

Andtbacka, R. H., Kaufman, H. L., Collichio, F., Amatruda, T., Senzer, N., Chesney, J., Delman, K. A., Spitler, L. E., Puzanov, I., Agarwala, S. S., Milhem, M., Cranmer, L., Curti, B., Lewis, K., Ross, M., Guthrie, T., Linette, G. P., Daniels, G. A., Harrington, K., . . . Coffin, R. S. (2015). Talimogene Laherparepvec Improves Durable Response Rate in Patients With Advanced Melanoma. *J Clin Oncol*, *33*(25), 2780-2788. https://doi.org/10.1200/JCO.2014.58.3377

Arakawa, T., Ejima, D., Tsumoto, K., Obeyama, N., Tanaka, Y., Kita, Y., & Timasheff, S. N. (2007). Suppression of protein interactions by arginine: a proposed mechanism of the arginine effects. *Biophys Chem*, *127*(1-2), 1-8. https://doi.org/10.1016/j.bpc.2006.12.007

Araki, N., Johnson, M. T., & Swanson, J. A. (1996). A role for phosphoinositide 3-kinase in the completion of macropinocytosis and phagocytosis by macrophages. *J Cell Biol*, *135*(5), 1249-1260. https://doi.org/10.1083/jcb.135.5.1249

Arase, H., Arase, N., & Saito, T. (1996). Interferon gamma production by natural killer (NK) cells and NK1.1+ T cells upon NKR-P1 cross-linking. *J Exp Med*, *183*(5), 2391-2396. https://doi.org/10.1084/jem.183.5.2391

Arnau, J., Lauritzen, C., Petersen, G. E., & Pedersen, J. (2006). Current strategies for the use of affinity tags and tag removal for the purification of recombinant proteins. *Protein Expr Purif*, *48*(1), 1-13. https://doi.org/10.1016/j.pep.2005.12.002

Arnold, J. N., Wormald, M. R., Suter, D. M., Radcliffe, C. M., Harvey, D. J., Dwek, R. A., Rudd, P. M., & Sim, R. B. (2005). Human serum IgM glycosylation: identification of glycoforms that can bind to mannan-binding lectin. *J Biol Chem*, *280*(32), 29080-29087. https://doi.org/10.1074/jbc.M504528200

AthenaES. (2020). *QuickFold™ Protein Refolding Kit Application Manual Version 2.2*

Aung, P. P., Liu, Y. C., Ballester, L. Y., Robbins, P. F., Rosenberg, S. A., & Lee, C. C. (2014). Expression of New York esophageal squamous cell carcinoma-1 in primary and metastatic melanoma. *Hum Pathol*, *45*(2), 259-267. https://doi.org/10.1016/j.humpath.2013.05.029

Bachem, A., Guttler, S., Hartung, E., Ebstein, F., Schaefer, M., Tannert, A., Salama, A., Movassaghi, K., Opitz, C., Mages, H. W., Henn, V., Kloetzel, P. M., Gurka, S., & Kroczek, R. A. (2010). Superior antigen cross-presentation and XCR1 expression define human CD11c+CD141+ cells as homologues of mouse CD8+ dendritic cells. *J Exp Med*, *207*(6), 1273-1281. https://doi.org/10.1084/jem.20100348

Baeshen, M. N., Al-Hejin, A. M., Bora, R. S., Ahmed, M. M., Ramadan, H. A., Saini, K. S., Baeshen, N. A., & Redwan, E. M. (2015). Production of Biopharmaceuticals in E. coli: Current Scenario and Future Perspectives. *J Microbiol Biotechnol*, *25*(7), 953-962. https://doi.org/10.4014/jmb.1412.12079

Bailey, A. L., & Cullis, P. R. (1997). Membrane fusion with cationic liposomes: effects of target membrane lipid composition. *Biochemistry*, *36*(7), 1628-1634. https://doi.org/10.1021/bi961173x

Baker, K., Qiao, S. W., Kuo, T. T., Aveson, V. G., Platzer, B., Andersen, J. T., Sandlie, I., Chen, Z., de Haar, C., Lencer, W. I., Fiebiger, E., & Blumberg, R. S. (2011). Neonatal Fc receptor for IgG (FcRn) regulates cross-presentation of IgG immune complexes by CD8-CD11b+ dendritic cells. *Proc Natl Acad Sci U S A*, *108*(24), 9927-9932. https://doi.org/10.1073/pnas.1019037108

Bangs Laboratories Inc. (2013). *Covalent Coupling*. https://www.bangslabs.com/sites/default/files/imce/docs/TechNote%20205%20Web.pdf

Barry, K. C., Hsu, J., Broz, M. L., Cueto, F. J., Binnewies, M., Combes, A. J., Nelson, A. E., Loo, K., Kumar, R., Rosenblum, M. D., Alvarado, M. D., Wolf, D. M., Bogunovic, D., Bhardwaj, N., Daud, A. I., Ha, P. K., Ryan, W. R., Pollack, J. L., Samad, B., . . . Krummel, M. F. (2018). A natural killer-dendritic cell axis defines checkpoint therapy-responsive tumor microenvironments. *Nat Med*, *24*(8), 1178-1191. https://doi.org/10.1038/s41591-018-0085-8

Barry, M., & Bleackley, R. C. (2002). Cytotoxic T lymphocytes: all roads lead to death. *Nat Rev Immunol*, *2*(6), 401-409. https://doi.org/10.1038/nri819

Baselga, J., Tripathy, D., Mendelsohn, J., Baughman, S., Benz, C. C., Dantis, L., Sklarin, N. T., Seidman, A. D., Hudis, C. A., Moore, J., Rosen, P. P., Twaddell, T., Henderson, I. C., & Norton, L. (1996). Phase II study of weekly intravenous recombinant humanized anti-p185HER2 monoclonal

antibody in patients with HER2/neu-overexpressing metastatic breast cancer. *J Clin Oncol*, *14*(3), 737-744. https://doi.org/10.1200/JCO.1996.14.3.737

Basha, G., Omilusik, K., Chavez-Steenbock, A., Reinicke, A. T., Lack, N., Choi, K. B., & Jefferies, W. A. (2012). A CD74-dependent MHC class I endolysosomal cross-presentation pathway. *Nat Immunol*, *13*(3), 237-245. https://doi.org/10.1038/ni.2225

Beatty, G., & Paterson, Y. (2001). IFN-gamma-dependent inhibition of tumor angiogenesis by tumor-infiltrating CD4+ T cells requires tumor responsiveness to IFN-gamma. *J Immunol*, *166*(4), 2276-2282. https://doi.org/10.4049/jimmunol.166.4.2276

Beckman, E. M., Porcelli, S. A., Morita, C. T., Behar, S. M., Furlong, S. T., & Brenner, M. B. (1994). Recognition of a lipid antigen by CD1-restricted alpha beta+ T cells. *Nature*, *372*(6507), 691-694. https://doi.org/10.1038/372691a0

Beletskii, A., Cooper, M., Sriraman, P., Chiriac, C., Zhao, L., Abbot, S., & Yu, L. (2005). High-throughput phagocytosis assay utilizing a pH-sensitive fluorescent dye. *Biotechniques*, *39*(6), 894-897. https://doi.org/10.2144/000112001

Bennett, S. R., Carbone, F. R., Karamalis, F., Miller, J. F., & Heath, W. R. (1997). Induction of a CD8+ cytotoxic T lymphocyte response by cross-priming requires cognate CD4+ T cell help. *J Exp Med*, *186*(1), 65-70. https://doi.org/10.1084/jem.186.1.65

Berkmen, M. (2012). Production of disulfide-bonded proteins in Escherichia coli. *Protein Expr Purif*, *82*(1), 240-251. https://doi.org/10.1016/j.pep.2011.10.009

Berneman, Z. N., Gastl, G., Gangji, D., van Camp, B., Jochmans, K., Aulitzky, W., Flament, J., Peetermans, M. E., & Huber, C. (1986). Treatment of hairy-cell leukemia with recombinant alpha 2-interferon. *Eur J Cancer Clin Oncol*, *22*(8), 987-990. https://doi.org/10.1016/0277-5379(86)90066-0

Bertholet, S., Goldszmid, R., Morrot, A., Debrabant, A., Afrin, F., Collazo-Custodio, C., Houde, M., Desjardins, M., Sher, A., & Sacks, D. (2006). Leishmania antigens are presented to CD8+ T cells by a transporter associated with antigen processing-independent pathway in vitro and in vivo. *J Immunol*, *177*(6), 3525-3533. https://doi.org/10.4049/jimmunol.177.6.3525

Beum, P. V., Lindorfer, M. A., Beurskens, F., Stukenberg, P. T., Lokhorst, H. M., Pawluczkowycz, A. W., Parren, P. W., van de Winkel, J. G., & Taylor, R. P. (2008). Complement activation on B lymphocytes opsonized with rituximab or ofatumumab produces substantial changes in membrane structure preceding cell lysis. *J Immunol*, *181*(1), 822-832. https://doi.org/10.4049/jimmunol.181.1.822

Beury, D. W., Parker, K. H., Nyandjo, M., Sinha, P., Carter, K. A., & Ostrand-Rosenberg, S. (2014). Cross-talk among myeloid-derived suppressor cells, macrophages, and tumor cells impacts the inflammatory milieu of solid tumors. *J Leukoc Biol*, *96*(6), 1109-1118. https://doi.org/10.1189/jlb.3A0414-210R

Bezu, L., Kepp, O., Cerrato, G., Pol, J., Fucikova, J., Spisek, R., Zitvogel, L., Kroemer, G., & Galluzzi, L. (2018). Trial watch: Peptide-based vaccines in anticancer therapy. *Oncoimmunology*, *7*(12), e1511506. https://doi.org/10.1080/2162402X.2018.1511506

Bijker, M. S., van den Eeden, S. J., Franken, K. L., Melief, C. J., van der Burg, S. H., & Offringa, R. (2008). Superior induction of anti-tumor CTL immunity by extended peptide vaccines involves prolonged, DC-focused antigen presentation. *Eur J Immunol*, *38*(4), 1033-1042. https://doi.org/10.1002/eji.200737995

Billadeau, D. D., & Leibson, P. J. (2002). ITAMs versus ITIMs: striking a balance during cell regulation. *J Clin Invest*, *109*(2), 161-168. https://doi.org/10.1172/JCI14843

Binnewies, M., Mujal, A. M., Pollack, J. L., Combes, A. J., Hardison, E. A., Barry, K. C., Tsui, J., Ruhland, M. K., Kersten, K., Abushawish, M. A., Spasic, M., Giurintano, J. P., Chan, V., Daud, A. I., Ha, P., Ye, C. J., Roberts, E. W., & Krummel, M. F. (2019). Unleashing Type-2 Dendritic Cells to Drive Protective Antitumor CD4(+) T Cell Immunity. *Cell*, *177*(3), 556-571 e516. https://doi.org/10.1016/j.cell.2019.02.005

Birkholz, K., Schwenkert, M., Kellner, C., Gross, S., Fey, G., Schuler-Thurner, B., Schuler, G., Schaft, N., & Dorrie, J. (2010). Targeting of DEC-205 on human dendritic cells results in efficient MHC class II-restricted antigen presentation. *Blood*, *116*(13), 2277-2285. https://doi.org/10.1182/blood-2010-02-268425

Bogyo, M., Verhelst, S., Bellingard-Dubouchaud, V., Toba, S., & Greenbaum, D. (2000). Selective targeting of lysosomal cysteine proteases with radiolabeled electrophilic substrate analogs. *Chem Biol*, *7*(1), 27-38. https://doi.org/10.1016/s1074-5521(00)00061-2

Bolt, S., Routledge, E., Lloyd, I., Chatenoud, L., Pope, H., Gorman, S. D., Clark, M., & Waldmann, H. (1993). The generation of a humanized, non-mitogenic CD3 monoclonal antibody which retains in vitro immunosuppressive properties. *Eur J Immunol*, *23*(2), 403-411. https://doi.org/10.1002/eji.1830230216

Bonifaz, L., Bonnyay, D., Mahnke, K., Rivera, M., Nussenzweig, M. C., & Steinman, R. M. (2002). Efficient targeting of protein antigen to the dendritic cell receptor DEC-205 in the steady state leads to antigen presentation on major histocompatibility complex class I products and peripheral CD8+ T cell tolerance. *J Exp Med*, *196*(12), 1627-1638. https://doi.org/10.1084/jem.20021598

Booth, J. W., Kim, M. K., Jankowski, A., Schreiber, A. D., & Grinstein, S. (2002). Contrasting requirements for ubiquitylation during Fc receptor-mediated endocytosis and phagocytosis. *EMBO J*, *21*(3), 251-258. https://doi.org/10.1093/emboj/21.3.251

Borrego, F., Ulbrecht, M., Weiss, E. H., Coligan, J. E., & Brooks, A. G. (1998). Recognition of human histocompatibility leukocyte antigen (HLA)-E complexed with HLA class I signal sequence-derived peptides by CD94/NKG2 confers protection from natural killer cell-mediated lysis. *J Exp Med*, *187*(5), 813-818. https://doi.org/10.1084/jem.187.5.813

Botelho, N. K., Tschumi, B. O., Hubbell, J. A., Swartz, M. A., Donda, A., & Romero, P. (2019). Combination of Synthetic Long Peptides and XCL1 Fusion Proteins Results in Superior Tumor Control. *Front Immunol*, *10*, 294. https://doi.org/10.3389/fimmu.2019.00294

Bottcher, J. P., Bonavita, E., Chakravarty, P., Blees, H., Cabeza-Cabrerizo, M., Sammicheli, S., Rogers, N. C., Sahai, E., Zelenay, S., & Reis e Sousa, C. (2018). NK Cells Stimulate Recruitment of cDC1 into the Tumor Microenvironment Promoting Cancer Immune Control. *Cell*, *172*(5), 1022-1037 e1014. https://doi.org/10.1016/j.cell.2018.01.004

Bournazos, S., Gupta, A., & Ravetch, J. V. (2020). The role of IgG Fc receptors in antibody-dependent enhancement. *Nat Rev Immunol*, *20*(10), 633-643. https://doi.org/10.1038/s41577-020-00410-0

Boutilier, A. J., & Elsawa, S. F. (2021). Macrophage Polarization States in the Tumor Microenvironment. *Int J Mol Sci*, *22*(13). https://doi.org/10.3390/ijms22136995

Bridgeman, J. S., Ladell, K., Sheard, V. E., Miners, K., Hawkins, R. E., Price, D. A., & Gilham, D. E. (2014). CD3zeta-based chimeric antigen receptors mediate T cell activation via cis- and trans-signalling mechanisms: implications for optimization of receptor structure for adoptive cell therapy. *Clin Exp Immunol*, *175*(2), 258-267. https://doi.org/10.1111/cei.12216

Brocker, T., & Karjalainen, K. (1995). Signals through T cell receptor-zeta chain alone are insufficient to prime resting T lymphocytes. *J Exp Med*, *181*(5), 1653-1659. https://doi.org/10.1084/jem.181.5.1653

Brown, D. M., Fisher, T. L., Wei, C., Frelinger, J. G., & Lord, E. M. (2001). Tumours can act as adjuvants for humoral immunity. *Immunology*, *102*(4), 486-497. https://doi.org/10.1046/j.1365-2567.2001.01213.x

Brown, G. D. (2006). Dectin-1: a signalling non-TLR pattern-recognition receptor. *Nat Rev Immunol*, *6*(1), 33-43. https://doi.org/10.1038/nri1745

Brown, J. M., & Wilson, W. R. (2004). Exploiting tumour hypoxia in cancer treatment. *Nat Rev Cancer*, *4*(6), 437-447. https://doi.org/10.1038/nrc1367

Brown, R. B., & Audet, J. (2008). Current techniques for single-cell lysis. *J R Soc Interface*, *5 Suppl 2*(Suppl 2), S131-138. https://doi.org/10.1098/rsif.2008.0009.focus

Brudno, J. N., Maric, I., Hartman, S. D., Rose, J. J., Wang, M., Lam, N., Stetler-Stevenson, M., Salem, D., Yuan, C., Pavletic, S., Kanakry, J. A., Ali, S. A., Mikkilineni, L., Feldman, S. A., Stroncek, D. F., Hansen, B. G., Lawrence, J., Patel, R., Hakim, F., . . . Kochenderfer, J. N. (2018). T Cells Genetically Modified to Express an Anti-B-Cell Maturation Antigen Chimeric Antigen Receptor Cause Remissions of Poor-Prognosis Relapsed Multiple Myeloma. *J Clin Oncol*, *36*(22), 2267-2280. https://doi.org/10.1200/JCO.2018.77.8084

Bruhns, P. (2012). Properties of mouse and human IgG receptors and their contribution to disease models. *Blood*, *119*(24), 5640-5649. https://doi.org/10.1182/blood-2012-01-380121

Bruhns, P., Iannascoli, B., England, P., Mancardi, D. A., Fernandez, N., Jorieux, S., & Daeron, M. (2009). Specificity and affinity of human Fcgamma receptors and their polymorphic variants for human IgG subclasses. *Blood*, *113*(16), 3716-3725. https://doi.org/10.1182/blood-2008-09-179754

Buchberger, A., Bukau, B., & Sommer, T. (2010). Protein quality control in the cytosol and the endoplasmic reticulum: brothers in arms. *Mol Cell*, *40*(2), 238-252. https://doi.org/10.1016/j.molcel.2010.10.001

Bulbake, U., Doppalapudi, S., Kommineni, N., & Khan, W. (2017). Liposomal Formulations in Clinical Use: An Updated Review. *Pharmaceutics*, *9*(2). https://doi.org/10.3390/pharmaceutics9020012

Burgdorf, S., Kautz, A., Bohnert, V., Knolle, P. A., & Kurts, C. (2007). Distinct pathways of antigen uptake and intracellular routing in CD4 and CD8 T cell activation. *Science*, *316*(5824), 612-616. https://doi.org/10.1126/science.1137971

Burgdorf, S., Lukacs-Kornek, V., & Kurts, C. (2006). The mannose receptor mediates uptake of soluble but not of cell-associated antigen for cross-presentation. *J Immunol*, *176*(11), 6770-6776. https://doi.org/10.4049/jimmunol.176.11.6770

Burgdorf, S., Scholz, C., Kautz, A., Tampe, R., & Kurts, C. (2008). Spatial and mechanistic separation of cross-presentation and endogenous antigen presentation. *Nat Immunol*, *9*(5), 558-566. https://doi.org/10.1038/ni.1601

Burgess, R. R. (1996). Purification of overproduced Escherichia coli RNA polymerase sigma factors by solubilizing inclusion bodies and refolding from Sarkosyl. *Methods Enzymol*, *273*, 145-149. https://doi.org/10.1016/s0076-6879(96)73014-8

Burgess, R. R. (2009). Refolding solubilized inclusion body proteins. *Methods Enzymol*, *463*, 259-282. https://doi.org/10.1016/S0076-6879(09)63017-2

Burnet, F. M. (1970). The concept of immunological surveillance. *Prog Exp Tumor Res*, *13*, 1-27. https://doi.org/10.1159/000386035

Burnet, M. (1957). Cancer: a biological approach. III. Viruses associated with neoplastic conditions. IV. Practical applications. *Br Med J*, *1*(5023), 841-847. https://doi.org/10.1136/bmj.1.5023.841

Burstein, N. A., & Law, L. W. (1971). Neonatal thymectomy and non-viral mammary tumours in mice. *Nature*, *231*(5303), 450-452. https://doi.org/10.1038/231450a0

Cafri, G., Gartner, J. J., Zaks, T., Hopson, K., Levin, N., Paria, B. C., Parkhurst, M. R., Yossef, R., Lowery, F. J., Jafferji, M. S., Prickett, T. D., Goff, S. L., McGowan, C. T., Seitter, S., Shindorf, M. L., Parikh, A., Chatani, P. D., Robbins, P. F., & Rosenberg, S. A. (2020). mRNA vaccine-induced neoantigen-specific T cell immunity in patients with gastrointestinal cancer. *J Clin Invest*, *130*(11), 5976-5988. https://doi.org/10.1172/JCI134915

Cai, L., Zhang, J., Zhu, R., Shi, W., Xia, X., Edwards, M., Finch, W., Coombs, A., Gao, J., Chen, K., Owen, S., Jiang, S., & Lu, W. (2017). Protective cellular immunity generated by cross-presenting recombinant overlapping peptide proteins. *Oncotarget*, *8*(44), 76516-76524. https://doi.org/10.18632/oncotarget.20407

Caminschi, I., Proietto, A. I., Ahmet, F., Kitsoulis, S., Shin Teh, J., Lo, J. C., Rizzitelli, A., Wu, L., Vremec, D., van Dommelen, S. L., Campbell, I. K., Maraskovsky, E., Braley, H., Davey, G. M., Mottram, P., van de Velde, N., Jensen, K., Lew, A. M., Wright, M. D., . . . Lahoud, M. H. (2008). The dendritic cell subtype-restricted C-type lectin Clec9A is a target for vaccine enhancement. *Blood*, *112*(8), 3264-3273. https://doi.org/10.1182/blood-2008-05-155176

Campeau, E., & Gobeil, S. (2011). RNA interference in mammals: behind the screen. *Brief Funct Genomics*, *10*(4), 215-226. https://doi.org/10.1093/bfgp/elr018

Cancer Research UK. (2023). *Cancer Statistics for the UK*. Retrieved November 2023 from https://www.cancerresearchuk.org/health-professional/cancer-statistics-for-the-uk

Carrio, M. M., & Villaverde, A. (2005). Localization of chaperones DnaK and GroEL in bacterial inclusion bodies. *J Bacteriol*, *187*(10), 3599-3601. https://doi.org/10.1128/JB.187.10.3599-3601.2005

Casella, J. F., Flanagan, M. D., & Lin, S. (1981). Cytochalasin D inhibits actin polymerization and induces depolymerization of actin filaments formed during platelet shape change. *Nature*, *293*(5830), 302-305. https://doi.org/10.1038/293302a0

Cebrian, I., Visentin, G., Blanchard, N., Jouve, M., Bobard, A., Moita, C., Enninga, J., Moita, L. F., Amigorena, S., & Savina, A. (2011). Sec22b regulates phagosomal maturation and antigen crosspresentation by dendritic cells. *Cell*, *147*(6), 1355-1368. https://doi.org/10.1016/j.cell.2011.11.021

Cella, M., Scheidegger, D., Palmer-Lehmann, K., Lane, P., Lanzavecchia, A., & Alber, G. (1996). Ligation of CD40 on dendritic cells triggers production of high levels of interleukin-12 and enhances T cell stimulatory capacity: T-T help via APC activation. *J Exp Med*, *184*(2), 747-752. https://doi.org/10.1084/jem.184.2.747

Champion, J. A., Walker, A., & Mitragotri, S. (2008). Role of particle size in phagocytosis of polymeric microspheres. *Pharm Res*, *25*(8), 1815-1821. https://doi.org/10.1007/s11095-008-9562-y

Chan, T., Sami, A., El-Gayed, A., Guo, X., & Xiang, J. (2006). HER-2/neu-gene engineered dendritic cell vaccine stimulates stronger HER-2/neu-specific immune responses compared to DNA vaccination. *Gene Ther*, *13*(19), 1391-1402. https://doi.org/10.1038/sj.gt.3302797

Chang, C. C., Pirozzi, G., Wen, S. H., Chung, I. H., Chiu, B. L., Errico, S., Luongo, M., Lombardi, M. L., & Ferrone, S. (2015). Multiple structural and epigenetic defects in the human leukocyte antigen class I antigen presentation pathway in a recurrent metastatic melanoma following immunotherapy. *J Biol Chem*, *290*(44), 26562-26575. https://doi.org/10.1074/jbc.M115.676130

Chazotte, B. (2011). Labeling lysosomes in live cells with LysoTracker. *Cold Spring Harb Protoc*, *2011*(2), pdb prot5571. https://doi.org/10.1101/pdb.prot5571

Cheever, M. A., & Higano, C. S. (2011). PROVENGE (Sipuleucel-T) in prostate cancer: the first FDA-approved therapeutic cancer vaccine. *Clin Cancer Res*, *17*(11), 3520-3526. https://doi.org/10.1158/1078-0432.CCR-10-3126

Chen, J., Liu, Y., Wang, Y., Ding, H., & Su, Z. (2008). Different effects of L-arginine on protein refolding: suppressing aggregates of hydrophobic interaction, not covalent binding. *Biotechnol Prog*, *24*(6), 1365-1372. https://doi.org/10.1002/btpr.93

Chen, X., Du, Y., Hu, Q., & Huang, Z. (2017). Tumor-derived CD4+CD25+regulatory T cells inhibit dendritic cells function by CTLA-4. *Pathol Res Pract*, *213*(3), 245-249. https://doi.org/10.1016/j.prp.2016.12.008

Chesney, J., Puzanov, I., Collichio, F., Singh, P., Milhem, M. M., Glaspy, J., Hamid, O., Ross, M., Friedlander, P., Garbe, C., Logan, T. F., Hauschild, A., Lebbe, C., Chen, L., Kim, J. J., Gansert, J., Andtbacka, R. H. I., & Kaufman, H. L. (2018). Randomized, Open-Label Phase II Study Evaluating the Efficacy and Safety of Talimogene Laherparepvec in Combination With Ipilimumab Versus Ipilimumab Alone in Patients With Advanced, Unresectable Melanoma. *J Clin Oncol*, *36*(17), 1658-1667. https://doi.org/10.1200/JCO.2017.73.7379

Chisnall, B., Johnson, C., Kulaberoglu, Y., & Chen, Y. W. (2014). Insoluble protein purification with sarkosyl: facts and precautions. *Methods Mol Biol*, *1091*, 179-186. https://doi.org/10.1007/978-1-62703-691-7_12

Chow, M. K., Amin, A. A., Fulton, K. F., Fernando, T., Kamau, L., Batty, C., Louca, M., Ho, S., Whisstock, J. C., Bottomley, S. P., & Buckle, A. M. (2006). The REFOLD database: a tool for the optimization of protein expression and refolding. *Nucleic Acids Res*, *34*(Database issue), D207-212. https://doi.org/10.1093/nar/gkj080

Chua, T. C., Saxena, A., Liauw, W., Kokandi, A., & Morris, D. L. (2010). Systematic review of randomized and nonrandomized trials of the clinical response and outcomes of neoadjuvant systemic chemotherapy for resectable colorectal liver metastases. *Ann Surg Oncol*, *17*(2), 492-501. https://doi.org/10.1245/s10434-009-0781-1

Church, A. K., VanDerMeid, K. R., Baig, N. A., Baran, A. M., Witzig, T. E., Nowakowski, G. S., & Zent, C. S. (2016). Anti-CD20 monoclonal antibody-dependent phagocytosis of chronic lymphocytic leukaemia cells by autologous macrophages. *Clin Exp Immunol*, *183*(1), 90-101. https://doi.org/10.1111/cei.12697

Ciechanover, A., & Kwon, Y. T. (2015). Degradation of misfolded proteins in neurodegenerative diseases: therapeutic targets and strategies. *Exp Mol Med*, *47*(3), e147. https://doi.org/10.1038/emm.2014.117

ClinicalTrials.gov. (2023). National Library of Medicine (USA). Retrieved 10th November from www.clinicaltrials.gov

Cohn, L., Chatterjee, B., Esselborn, F., Smed-Sorensen, A., Nakamura, N., Chalouni, C., Lee, B. C., Vandlen, R., Keler, T., Lauer, P., Brockstedt, D., Mellman, I., & Delamarre, L. (2013). Antigen delivery to early endosomes eliminates the superiority of human blood BDCA3+ dendritic cells at cross presentation. *J Exp Med*, *210*(5), 1049-1063. https://doi.org/10.1084/jem.20121251

Cole, K. E., Strick, C. A., Paradis, T. J., Ogborne, K. T., Loetscher, M., Gladue, R. P., Lin, W., Boyd, J. G., Moser, B., Wood, D. E., Sahagan, B. G., & Neote, K. (1998). Interferon-inducible T cell alpha

chemoattractant (I-TAC): a novel non-ELR CXC chemokine with potent activity on activated T cells through selective high affinity binding to CXCR3. *J Exp Med*, *187*(12), 2009-2021. https://doi.org/10.1084/jem.187.12.2009

Coley, W. B. (1991). The treatment of malignant tumors by repeated inoculations of erysipelas. With a report of ten original cases. 1893. *Clin Orthop Relat Res*(262), 3-11. https://www.ncbi.nlm.nih.gov/pubmed/1984929

Collin, M., & Bigley, V. (2018). Human dendritic cell subsets: an update. *Immunology*, *154*(1), 3-20. https://doi.org/10.1111/imm.12888

Collins, A. V., Brodie, D. W., Gilbert, R. J., Iaboni, A., Manso-Sancho, R., Walse, B., Stuart, D. I., van der Merwe, P. A., & Davis, S. J. (2002). The interaction properties of costimulatory molecules revisited. *Immunity*, *17*(2), 201-210. https://doi.org/10.1016/s1074-7613(02)00362-x

Collison, L. W., Workman, C. J., Kuo, T. T., Boyd, K., Wang, Y., Vignali, K. M., Cross, R., Sehy, D., Blumberg, R. S., & Vignali, D. A. (2007). The inhibitory cytokine IL-35 contributes to regulatory T-cell function. *Nature*, *450*(7169), 566-569. https://doi.org/10.1038/nature06306

Connor, J., Yatvin, M. B., & Huang, L. (1984). pH-sensitive liposomes: acid-induced liposome fusion. *Proc Natl Acad Sci U S A*, *81*(6), 1715-1718. https://doi.org/10.1073/pnas.81.6.1715

Conrad, C., Gregorio, J., Wang, Y. H., Ito, T., Meller, S., Hanabuchi, S., Anderson, S., Atkinson, N., Ramirez, P. T., Liu, Y. J., Freedman, R., & Gilliet, M. (2012). Plasmacytoid dendritic cells promote immunosuppression in ovarian cancer via ICOS costimulation of Foxp3(+) T-regulatory cells. *Cancer Res*, *72*(20), 5240-5249. https://doi.org/10.1158/0008-5472.CAN-12-2271

Constant, S. L., & Bottomly, K. (1997). Induction of Th1 and Th2 CD4+ T cell responses: the alternative approaches. *Annu Rev Immunol*, *15*, 297-322. https://doi.org/10.1146/annurev.immunol.15.1.297

Copland, M. J., Baird, M. A., Rades, T., McKenzie, J. L., Becker, B., Reck, F., Tyler, P. C., & Davies, N. M. (2003). Liposomal delivery of antigen to human dendritic cells. *Vaccine*, *21*(9-10), 883-890. https://doi.org/10.1016/s0264-410x(02)00536-4

Corrales, L., Glickman, L. H., McWhirter, S. M., Kanne, D. B., Sivick, K. E., Katibah, G. E., Woo, S. R., Lemmens, E., Banda, T., Leong, J. J., Metchette, K., Dubensky, T. W., Jr., & Gajewski, T. F. (2015). Direct Activation of STING in the Tumor Microenvironment Leads to Potent and Systemic Tumor Regression and Immunity. *Cell Rep*, *11*(7), 1018-1030. https://doi.org/10.1016/j.celrep.2015.04.031

Corthay, A., Skovseth, D. K., Lundin, K. U., Rosjo, E., Omholt, H., Hofgaard, P. O., Haraldsen, G., & Bogen, B. (2005). Primary antitumor immune response mediated by CD4+ T cells. *Immunity*, *22*(3), 371-383. https://doi.org/10.1016/j.immuni.2005.02.003

Cory, A. H., Owen, T. C., Barltrop, J. A., & Cory, J. G. (1991). Use of an aqueous soluble tetrazolium/formazan assay for cell growth assays in culture. *Cancer Commun*, *3*(7), 207-212. https://doi.org/10.3727/095535491820873191

Creelan, B. C., Wang, C., Teer, J. K., Toloza, E. M., Yao, J., Kim, S., Landin, A. M., Mullinax, J. E., Saller, J. J., Saltos, A. N., Noyes, D. R., Montoya, L. B., Curry, W., Pilon-Thomas, S. A., Chiappori, A. A., Tanvetyanon, T., Kaye, F. J., Thompson, Z. J., Yoder, S. J., . . . Antonia, S. J. (2021). Tumor-infiltrating lymphocyte treatment for anti-PD-1-resistant metastatic lung cancer: a phase 1 trial. *Nat Med*, *27*(8), 1410-1418. https://doi.org/10.1038/s41591-021-01462-y

Cromme, F. V., Airey, J., Heemels, M. T., Ploegh, H. L., Keating, P. J., Stern, P. L., Meijer, C. J., & Walboomers, J. M. (1994). Loss of transporter protein, encoded by the TAP-1 gene, is highly correlated with loss of HLA expression in cervical carcinomas. *J Exp Med*, *179*(1), 335-340. https://doi.org/10.1084/jem.179.1.335

Croop, J. M., Raymond, M., Haber, D., Devault, A., Arceci, R. J., Gros, P., & Housman, D. E. (1989). The three mouse multidrug resistance (mdr) genes are expressed in a tissue-specific manner in normal mouse tissues. *Mol Cell Biol*, *9*(3), 1346-1350. https://doi.org/10.1128/mcb.9.3.1346-1350.1989

Crozat, K., Guiton, R., Contreras, V., Feuillet, V., Dutertre, C. A., Ventre, E., Vu Manh, T. P., Baranek, T., Storset, A. K., Marvel, J., Boudinot, P., Hosmalin, A., Schwartz-Cornil, I., & Dalod, M. (2010). The XC chemokine receptor 1 is a conserved selective marker of mammalian cells homologous to mouse CD8alpha+ dendritic cells. *J Exp Med*, *207*(6), 1283-1292. https://doi.org/10.1084/jem.20100223

Cruz-Leal, Y., Grubaugh, D., Nogueira, C. V., Lopetegui-Gonzalez, I., Del Valle, A., Escalona, F., Laborde, R. J., Alvarez, C., Fernandez, L. E., Starnbach, M. N., Higgins, D. E., & Lanio, M. E. (2018). The Vacuolar Pathway in Macrophages Plays a Major Role in Antigen Cross-Presentation Induced by the Pore-Forming Protein Sticholysin II Encapsulated Into Liposomes. *Front Immunol*, *9*, 2473. https://doi.org/10.3389/fimmu.2018.02473

Cui, Y. L., Li, H. K., Zhou, H. Y., Zhang, T., & Li, Q. (2013). Correlations of tumor-associated macrophage subtypes with liver metastases of colorectal cancer. *Asian Pac J Cancer Prev*, *14*(2), 1003-1007. https://doi.org/10.7314/apjcp.2013.14.2.1003

Curiel, T. J., Cheng, P., Mottram, P., Alvarez, X., Moons, L., Evdemon-Hogan, M., Wei, S., Zou, L., Kryczek, I., Hoyle, G., Lackner, A., Carmeliet, P., & Zou, W. (2004). Dendritic cell subsets differentially regulate angiogenesis in human ovarian cancer. *Cancer Res*, *64*(16), 5535-5538. https://doi.org/10.1158/0008-5472.CAN-04-1272

Curtsinger, J. M., & Mescher, M. F. (2010). Inflammatory cytokines as a third signal for T cell activation. *Curr Opin Immunol*, *22*(3), 333-340. https://doi.org/10.1016/j.coi.2010.02.013

Dallabona, M., Sarubbo, S., Merler, S., Corsini, F., Pulcrano, G., Rozzanigo, U., Barbareschi, M., & Chioffi, F. (2017). Impact of mass effect, tumor location, age, and surgery on the cognitive outcome of patients with high-grade gliomas: a longitudinal study. *Neurooncol Pract*, *4*(4), 229-240. https://doi.org/10.1093/nop/npw030

Daniels, M. A., & Jameson, S. C. (2000). Critical role for CD8 in T cell receptor binding and activation by peptide/major histocompatibility complex multimers. *J Exp Med*, *191*(2), 335-346. https://doi.org/10.1084/jem.191.2.335

Davila, M. L., Riviere, I., Wang, X., Bartido, S., Park, J., Curran, K., Chung, S. S., Stefanski, J., Borquez-Ojeda, O., Olszewska, M., Qu, J., Wasielewska, T., He, Q., Fink, M., Shinglot, H., Youssif, M., Satter, M., Wang, Y., Hosey, J., . . . Brentjens, R. (2014). Efficacy and toxicity management of 19-28z CAR T cell therapy in B cell acute lymphoblastic leukemia. *Sci Transl Med*, *6*(224), 224ra225. https://doi.org/10.1126/scitranslmed.3008226

de Bruin, E. C., McGranahan, N., Mitter, R., Salm, M., Wedge, D. C., Yates, L., Jamal-Hanjani, M., Shafi, S., Murugaesu, N., Rowan, A. J., Gronroos, E., Muhammad, M. A., Horswell, S., Gerlinger, M., Varela, I., Jones, D., Marshall, J., Voet, T., Van Loo, P., . . . Swanton, C. (2014). Spatial and temporal diversity in genomic instability processes defines lung cancer evolution. *Science*, *346*(6206), 251-256. https://doi.org/10.1126/science.1253462

De Geyter, J., Tsirigotaki, A., Orfanoudaki, G., Zorzini, V., Economou, A., & Karamanou, S. (2016). Protein folding in the cell envelope of Escherichia coli. *Nat Microbiol*, *1*(8), 16107. https://doi.org/10.1038/nmicrobiol.2016.107

Delamarre, L., Couture, R., Mellman, I., & Trombetta, E. S. (2006). Enhancing immunogenicity by limiting susceptibility to lysosomal proteolysis. *J Exp Med*, *203*(9), 2049-2055. https://doi.org/10.1084/jem.20052442

Demangel, C., Zhou, J., Choo, A. B., Shoebridge, G., Halliday, G. M., & Britton, W. J. (2005). Single chain antibody fragments for the selective targeting of antigens to dendritic cells. *Mol Immunol*, *42*(8), 979-985. https://doi.org/10.1016/j.molimm.2004.09.034

den Haan, J. M., & Bevan, M. J. (2002). Constitutive versus activation-dependent cross-presentation of immune complexes by CD8(+) and CD8(-) dendritic cells in vivo. *J Exp Med*, *196*(6), 817-827. https://doi.org/10.1084/jem.20020295

den Haan, J. M., Lehar, S. M., & Bevan, M. J. (2000). CD8(+) but not CD8(-) dendritic cells cross-prime cytotoxic T cells in vivo. *J Exp Med*, *192*(12), 1685-1696. https://doi.org/10.1084/jem.192.12.1685

Derman, A. I., & Beckwith, J. (1991). Escherichia coli alkaline phosphatase fails to acquire disulfide bonds when retained in the cytoplasm. *J Bacteriol*, *173*(23), 7719-7722. https://doi.org/10.1128/jb.173.23.7719-7722.1991

Dersh, D., Yewdell, J. W., & Wei, J. (2019). A SIINFEKL-Based System to Measure MHC Class I Antigen Presentation Efficiency and Kinetics. *Methods Mol Biol*, *1988*, 109-122. https://doi.org/10.1007/978-1-4939-9450-2_9

Dezi, M., Di Cicco, A., Bassereau, P., & Levy, D. (2013). Detergent-mediated incorporation of transmembrane proteins in giant unilamellar vesicles with controlled physiological contents. *Proc Natl Acad Sci U S A*, *110*(18), 7276-7281. https://doi.org/10.1073/pnas.1303857110

Dhodapkar, K. M., Krasovsky, J., Williamson, B., & Dhodapkar, M. V. (2002). Antitumor monoclonal antibodies enhance cross-presentation ofcCellular antigens and the generation of myeloma-specific killer T cells by dendritic cells. *J Exp Med*, *195*(1), 125-133. https://doi.org/10.1084/jem.20011097

Di Pucchio, T., Chatterjee, B., Smed-Sorensen, A., Clayton, S., Palazzo, A., Montes, M., Xue, Y., Mellman, I., Banchereau, J., & Connolly, J. E. (2008). Direct proteasome-independent cross-presentation of viral antigen by plasmacytoid dendritic cells on major histocompatibility complex class I. *Nat Immunol*, *9*(5), 551-557. https://doi.org/10.1038/ni.1602

Diao, L., & Meibohm, B. (2013). Pharmacokinetics and pharmacokinetic-pharmacodynamic correlations of therapeutic peptides. *Clin Pharmacokinet*, *52*(10), 855-868. https://doi.org/10.1007/s40262-013-0079-0

Diaz-Montero, C. M., Salem, M. L., Nishimura, M. I., Garrett-Mayer, E., Cole, D. J., & Montero, A. J. (2009). Increased circulating myeloid-derived suppressor cells correlate with clinical cancer stage, metastatic tumor burden, and doxorubicin-cyclophosphamide chemotherapy. *Cancer Immunol Immunother*, *58*(1), 49-59. https://doi.org/10.1007/s00262-008-0523-4

Diedrich, G., Bangia, N., Pan, M., & Cresswell, P. (2001). A role for calnexin in the assembly of the MHC class I loading complex in the endoplasmic reticulum. *J Immunol*, *166*(3), 1703-1709. https://doi.org/10.4049/jimmunol.166.3.1703

Dighe, A. S., Richards, E., Old, L. J., & Schreiber, R. D. (1994). Enhanced in vivo growth and resistance to rejection of tumor cells expressing dominant negative IFN gamma receptors. *Immunity*, *1*(6), 447-456. https://doi.org/10.1016/1074-7613(94)90087-6

Dikov, M. M., Oyama, T., Cheng, P., Takahashi, T., Takahashi, K., Sepetavec, T., Edwards, B., Adachi, Y., Nadaf, S., Daniel, T., Gabrilovich, D. I., & Carbone, D. P. (2001). Vascular endothelial growth factor effects on nuclear factor-kappaB activation in hematopoietic progenitor cells. *Cancer Res*, *61*(5), 2015-2021. https://www.ncbi.nlm.nih.gov/pubmed/11280761

Dingjan, I., Verboogen, D. R., Paardekooper, L. M., Revelo, N. H., Sittig, S. P., Visser, L. J., Mollard, G. F., Henriet, S. S., Figdor, C. G., Ter Beest, M., & van den Bogaart, G. (2016). Lipid peroxidation causes endosomal antigen release for cross-presentation. *Sci Rep*, *6*, 22064. https://doi.org/10.1038/srep22064

Dolen, Y., Gileadi, U., Chen, J. L., Valente, M., Creemers, J. H. A., Van Dinther, E. A. W., van Riessen, N. K., Jager, E., Hruby, M., Cerundolo, V., Diken, M., Figdor, C. G., & de Vries, I. J. M. (2021). PLGA Nanoparticles Co-encapsulating NY-ESO-1 Peptides and IMM60 Induce Robust CD8 and CD4 T Cell and B Cell Responses. *Front Immunol*, *12*, 641703. https://doi.org/10.3389/fimmu.2021.641703

Dorner, B. G., Dorner, M. B., Zhou, X., Opitz, C., Mora, A., Guttler, S., Hutloff, A., Mages, H. W., Ranke, K., Schaefer, M., Jack, R. S., Henn, V., & Kroczek, R. A. (2009). Selective expression of the chemokine receptor XCR1 on cross-presenting dendritic cells determines cooperation with CD8+ T cells. *Immunity*, *31*(5), 823-833. https://doi.org/10.1016/j.immuni.2009.08.027

Dorner, B. G., Scheffold, A., Rolph, M. S., Huser, M. B., Kaufmann, S. H., Radbruch, A., Flesch, I. E., & Kroczek, R. A. (2002). MIP-1alpha, MIP-1beta, RANTES, and ATAC/lymphotactin function together with IFN-gamma as type 1 cytokines. *Proc Natl Acad Sci U S A*, *99*(9), 6181-6186. https://doi.org/10.1073/pnas.092141999

Dranoff, G., Jaffee, E., Lazenby, A., Golumbek, P., Levitsky, H., Brose, K., Jackson, V., Hamada, H., Pardoll, D., & Mulligan, R. C. (1993). Vaccination with irradiated tumor cells engineered to secrete murine granulocyte-macrophage colony-stimulating factor stimulates potent, specific, and long-lasting anti-tumor immunity. *Proc Natl Acad Sci U S A*, *90*(8), 3539-3543. https://doi.org/10.1073/pnas.90.8.3539

Driessen, C., Bryant, R. A., Lennon-Dumenil, A. M., Villadangos, J. A., Bryant, P. W., Shi, G. P., Chapman, H. A., & Ploegh, H. L. (1999). Cathepsin S controls the trafficking and maturation of MHC class II molecules in dendritic cells. *J Cell Biol*, *147*(4), 775-790. https://doi.org/10.1083/jcb.147.4.775

Driessen, C., Lennon-Dumenil, A. M., & Ploegh, H. L. (2001). Individual cathepsins degrade immune complexes internalized by antigen-presenting cells via Fcgamma receptors. *Eur J Immunol*, *31*(5), 1592-1601. https://doi.org/10.1002/1521-4141(200105)31:5<1592::AID-IMMU1592>3.0.CO;2-K

Druker, B. J., Sawyers, C. L., Kantarjian, H., Resta, D. J., Reese, S. F., Ford, J. M., Capdeville, R., & Talpaz, M. (2001). Activity of a specific inhibitor of the BCR-ABL tyrosine kinase in the blast

crisis of chronic myeloid leukemia and acute lymphoblastic leukemia with the Philadelphia chromosome. *N Engl J Med*, *344*(14), 1038-1042. https://doi.org/10.1056/NEJM200104053441402

Dunn, G. P., Bruce, A. T., Ikeda, H., Old, L. J., & Schreiber, R. D. (2002). Cancer immunoediting: from immunosurveillance to tumor escape. *Nat Immunol*, *3*(11), 991-998. https://doi.org/10.1038/ni1102-991

Duvallet, E., Boulpicante, M., Yamazaki, T., Daskalogianni, C., Prado Martins, R., Baconnais, S., Manoury, B., Fahraeus, R., & Apcher, S. (2016). Exosome-driven transfer of tumor-associated Pioneer Translation Products (TA-PTPs) for the MHC class I cross-presentation pathway. *Oncoimmunology*, *5*(9), e1198865. https://doi.org/10.1080/2162402X.2016.1198865

Dzionek, A., Fuchs, A., Schmidt, P., Cremer, S., Zysk, M., Miltenyi, S., Buck, D. W., & Schmitz, J. (2000). BDCA-2, BDCA-3, and BDCA-4: three markers for distinct subsets of dendritic cells in human peripheral blood. *J Immunol*, *165*(11), 6037-6046. https://doi.org/10.4049/jimmunol.165.11.6037

Ehrlich, P. (1908). Ueber den jetzigen Stand der Karzinomforschung. *Ned. Tijdschr. Genees*, *5*, 273-290.

Eilber, F., Giuliano, A., Eckardt, J., Patterson, K., Moseley, S., & Goodnight, J. (1987). Adjuvant chemotherapy for osteosarcoma: a randomized prospective trial. *Journal of Clinical Oncology*, *5*(1), 21-26. https://doi.org/10.1200/jco.1987.5.1.21

Eisen, H. N., Hou, X. H., Shen, C., Wang, K., Tanguturi, V. K., Smith, C., Kozyrytska, K., Nambiar, L., McKinley, C. A., Chen, J., & Cohen, R. J. (2012). Promiscuous binding of extracellular peptides to cell surface class I MHC protein. *Proc Natl Acad Sci U S A*, *109*(12), 4580-4585. https://doi.org/10.1073/pnas.1201586109

Embgenbroich, M., & Burgdorf, S. (2018). Current Concepts of Antigen Cross-Presentation. *Front Immunol*, *9*, 1643. https://doi.org/10.3389/fimmu.2018.01643

European Medicines Agency. (2019). *Bevou (Assessment Report)*. https://www.ema.europa.eu/en/documents/assessment-report/beovu-epar-public-assessment-report_en.pdf

Falk, K., Rotzschke, O., Stevanovic, S., Jung, G., & Rammensee, H. G. (1994). Pool sequencing of natural HLA-DR, DQ, and DP ligands reveals detailed peptide motifs, constraints of processing, and general rules. *Immunogenetics*, *39*(4), 230-242. https://doi.org/10.1007/BF00188785

Fang, H., Ang, B., Xu, X., Huang, X., Wu, Y., Sun, Y., Wang, W., Li, N., Cao, X., & Wan, T. (2014). TLR4 is essential for dendritic cell activation and anti-tumor T-cell response enhancement by DAMPs released from chemically stressed cancer cells. *Cell Mol Immunol*, *11*(2), 150-159. https://doi.org/10.1038/cmi.2013.59

Farina, A. R., Masciulli, M. P., Tacconelli, A., Cappabianca, L., De Santis, G., Gulino, A., & Mackay, A. R. (2002). All-trans-retinoic acid induces nuclear factor kappaB activation and matrix metalloproteinase-9 expression and enhances basement membrane invasivity of differentiation-resistant human SK-N-BE 9N neuroblastoma Cells. *Cell Growth Differ*, *13*(8), 343-354. https://www.ncbi.nlm.nih.gov/pubmed/12193473

Fontenot, J. D., Gavin, M. A., & Rudensky, A. Y. (2003). Foxp3 programs the development and function of CD4+CD25+ regulatory T cells. *Nat Immunol*, *4*(4), 330-336. https://doi.org/10.1038/ni904

Foote, J. B., Kok, M., Leatherman, J. M., Armstrong, T. D., Marcinkowski, B. C., Ojalvo, L. S., Kanne, D. B., Jaffee, E. M., Dubensky, T. W., Jr., & Emens, L. A. (2017). A STING Agonist Given with OX40 Receptor and PD-L1 Modulators Primes Immunity and Reduces Tumor Growth in Tolerized Mice. *Cancer Immunol Res*, *5*(6), 468-479. https://doi.org/10.1158/2326-6066.CIR-16-0284

Forloni, M., Albini, S., Limongi, M. Z., Cifaldi, L., Boldrini, R., Nicotra, M. R., Giannini, G., Natali, P. G., Giacomini, P., & Fruci, D. (2010). NF-kappaB, and not MYCN, regulates MHC class I and endoplasmic reticulum aminopeptidases in human neuroblastoma cells. *Cancer Res*, *70*(3), 916-924. https://doi.org/10.1158/0008-5472.CAN-09-2582

Forster, R., Schubel, A., Breitfeld, D., Kremmer, E., Renner-Muller, I., Wolf, E., & Lipp, M. (1999). CCR7 coordinates the primary immune response by establishing functional microenvironments in secondary lymphoid organs. *Cell*, *99*(1), 23-33. https://doi.org/10.1016/s0092-8674(00)80059-8

Fossa, A., Berner, A., Fossa, S. D., Hernes, E., Gaudernack, G., & Smeland, E. B. (2004). NY-ESO-1 protein expression and humoral immune responses in prostate cancer. *Prostate*, *59*(4), 440-447. https://doi.org/10.1002/pros.20025

Fotoran, W. L., Santangelo, R., de Miranda, B. N. M., Irvine, D. J., & Wunderlich, G. (2017). DNA-Loaded Cationic Liposomes Efficiently Function as a Vaccine against Malarial Proteins. *Mol Ther Methods Clin Dev*, *7*, 1-10. https://doi.org/10.1016/j.omtm.2017.08.004

Frankel, S., Sohn, R., & Leinwand, L. (1991). The use of sarkosyl in generating soluble protein after bacterial expression. *Proc Natl Acad Sci U S A*, *88*(4), 1192-1196. https://doi.org/10.1073/pnas.88.4.1192

Freeman, G. J., Long, A. J., Iwai, Y., Bourque, K., Chernova, T., Nishimura, H., Fitz, L. J., Malenkovich, N., Okazaki, T., Byrne, M. C., Horton, H. F., Fouser, L., Carter, L., Ling, V., Bowman, M. R., Carreno, B. M., Collins, M., Wood, C. R., & Honjo, T. (2000). Engagement of the PD-1 immunoinhibitory receptor by a novel B7 family member leads to negative regulation of lymphocyte activation. *J Exp Med*, *192*(7), 1027-1034. https://doi.org/10.1084/jem.192.7.1027

Frey, B., Rubner, Y., Kulzer, L., Werthmoller, N., Weiss, E. M., Fietkau, R., & Gaipl, U. S. (2014). Antitumor immune responses induced by ionizing irradiation and further immune stimulation. *Cancer Immunol Immunother*, *63*(1), 29-36. https://doi.org/10.1007/s00262-013-1474-y

Fujiwara, T., Oda, K., Yokota, S., Takatsuki, A., & Ikehara, Y. (1988). Brefeldin A causes disassembly of the Golgi complex and accumulation of secretory proteins in the endoplasmic reticulum. *J Biol Chem*, *263*(34), 18545-18552. https://www.ncbi.nlm.nih.gov/pubmed/3192548

Funderburgh, J. L., & Prakash, S. (1996). SDS-polyacrylamide gel electrophoretic analysis of proteins in the presence of guanidinium hydrochloride. *Biotechniques*, *20*(3), 376-378. https://doi.org/10.2144/19962003376

Gaciarz, A., Veijola, J., Uchida, Y., Saaranen, M. J., Wang, C., Horkko, S., & Ruddock, L. W. (2016). Systematic screening of soluble expression of antibody fragments in the cytoplasm of E. coli. *Microb Cell Fact*, *15*, 22. https://doi.org/10.1186/s12934-016-0419-5

Gargett, T., Yu, W., Dotti, G., Yvon, E. S., Christo, S. N., Hayball, J. D., Lewis, I. D., Brenner, M. K., & Brown, M. P. (2016). GD2-specific CAR T Cells Undergo Potent Activation and Deletion Following Antigen Encounter but can be Protected From Activation-induced Cell Death by PD-1 Blockade. *Mol Ther*, *24*(6), 1135-1149. https://doi.org/10.1038/mt.2016.63

Garulli, B., Stillitano, M. G., Barnaba, V., & Castrucci, M. R. (2008). Primary CD8+ T-cell response to soluble ovalbumin is improved by chloroquine treatment in vivo. *Clin Vaccine Immunol*, *15*(10), 1497-1504. https://doi.org/10.1128/CVI.00166-08

Gerlinger, M., Rowan, A. J., Horswell, S., Math, M., Larkin, J., Endesfelder, D., Gronroos, E., Martinez, P., Matthews, N., Stewart, A., Tarpey, P., Varela, I., Phillimore, B., Begum, S., McDonald, N. Q., Butler, A., Jones, D., Raine, K., Latimer, C., . . . Swanton, C. (2012). Intratumor heterogeneity and branched evolution revealed by multiregion sequencing. *N Engl J Med*, *366*(10), 883-892. https://doi.org/10.1056/NEJMoa1113205

Geurtsen, J., Driessen, N. N., & Appelmelk, B. J. (2010). Chapter 34 - Mannose–fucose recognition by DC-SIGN. In O. Holst, P. J. Brennan, M. v. Itzstein, & A. P. Moran (Eds.), *Microbial Glycobiology* (pp. 673-695). Academic Press. https://doi.org/https://doi.org/10.1016/B978-0-12-374546-0.00034-1

Ghaffari, A., Peterson, N., Khalaj, K., Vitkin, N., Robinson, A., Francis, J. A., & Koti, M. (2018). STING agonist therapy in combination with PD-1 immune checkpoint blockade enhances response to carboplatin chemotherapy in high-grade serous ovarian cancer. *Br J Cancer*, *119*(4), 440-449. https://doi.org/10.1038/s41416-018-0188-5

Gnjatic, S., Atanackovic, D., Jager, E., Matsuo, M., Selvakumar, A., Altorki, N. K., Maki, R. G., Dupont, B., Ritter, G., Chen, Y. T., Knuth, A., & Old, L. J. (2003). Survey of naturally occurring CD4+ T cell responses against NY-ESO-1 in cancer patients: correlation with antibody responses. *Proc Natl Acad Sci U S A*, *100*(15), 8862-8867. https://doi.org/10.1073/pnas.1133324100

Golovanov, A. P., Hautbergue, G. M., Wilson, S. A., & Lian, L. Y. (2004). A simple method for improving protein solubility and long-term stability. *J Am Chem Soc*, *126*(29), 8933-8939. https://doi.org/10.1021/ja049297h

Gong, Y. B., Huang, Y. F., Li, Y., Han, G. C., Li, Y. R., Wang, D. J., Du, G. P., Yu, J. F., & Song, J. (2011). Experimental study of the mechanism of tolerance induction in dexamethasone-treated dendritic cells. *Med Sci Monit*, *17*(5), BR125-131. https://doi.org/10.12659/msm.881758

Gorbachev, A. V., Kobayashi, H., Kudo, D., Tannenbaum, C. S., Finke, J. H., Shu, S., Farber, J. M., & Fairchild, R. L. (2007). CXC chemokine ligand 9/monokine induced by IFN-gamma production by tumor cells is critical for T cell-mediated suppression of cutaneous tumors. *J Immunol*, *178*(4), 2278-2286. https://doi.org/10.4049/jimmunol.178.4.2278

Gou, S., Wang, S., Liu, W., Chen, G., Zhang, D., Du, J., Yan, Z., Wang, H., Zhai, W., Sui, X., Wu, Y., Qi, Y., & Gao, Y. (2021). Adjuvant-free peptide vaccine targeting Clec9a on dendritic cells can induce robust antitumor immune response through Syk/IL-21 axis. *Theranostics*, *11*(15), 7308-7321. https://doi.org/10.7150/thno.56406

Grabosch, S., Bulatovic, M., Zeng, F., Ma, T., Zhang, L., Ross, M., Brozick, J., Fang, Y., Tseng, G., Kim, E., Gambotto, A., Elishaev, E., R, P. E., & Vlad, A. M. (2019). Cisplatin-induced immune modulation in ovarian cancer mouse models with distinct inflammation profiles. *Oncogene*, *38*(13), 2380-2393. https://doi.org/10.1038/s41388-018-0581-9

Graham, D. B., Stephenson, L. M., Lam, S. K., Brim, K., Lee, H. M., Bautista, J., Gilfillan, S., Akilesh, S., Fujikawa, K., & Swat, W. (2007). An ITAM-signaling pathway controls cross-presentation of particulate but not soluble antigens in dendritic cells. *J Exp Med*, *204*(12), 2889-2897. https://doi.org/10.1084/jem.20071283

Grant, G. A., & Miller, J. F. (1965). Effect of neonatal thymectomy on the induction of sarcomata in C57 BL mice. *Nature*, *205*(976), 1124-1125. https://doi.org/10.1038/2051124a0

Graumann, K., & Premstaller, A. (2006). Manufacturing of recombinant therapeutic proteins in microbial systems. *Biotechnol J*, *1*(2), 164-186. https://doi.org/10.1002/biot.200500051

Grever, M. R., Abdel-Wahab, O., Andritsos, L. A., Banerji, V., Barrientos, J., Blachly, J. S., Call, T. G., Catovsky, D., Dearden, C., Demeter, J., Else, M., Forconi, F., Gozzetti, A., Ho, A. D., Johnston, J. B., Jones, J., Juliusson, G., Kraut, E., Kreitman, R. J., . . . Falini, B. (2017). Consensus guidelines for the diagnosis and management of patients with classic hairy cell leukemia. *Blood*, *129*(5), 553-560. https://doi.org/10.1182/blood-2016-01-689422

Groh, V., Wu, J., Yee, C., & Spies, T. (2002). Tumour-derived soluble MIC ligands impair expression of NKG2D and T-cell activation. *Nature*, *419*(6908), 734-738. https://doi.org/10.1038/nature01112

Gross, A., Hashimoto, C., Sticht, H., & Eichler, J. (2015). Synthetic Peptides as Protein Mimics. *Front Bioeng Biotechnol*, *3*, 211. https://doi.org/10.3389/fbioe.2015.00211

Grotzke, J. E., Kozik, P., Morel, J. D., Impens, F., Pietrosemoli, N., Cresswell, P., Amigorena, S., & Demangel, C. (2017). Sec61 blockade by mycolactone inhibits antigen cross-presentation independently of endosome-to-cytosol export. *Proc Natl Acad Sci U S A*, *114*(29), E5910-E5919. https://doi.org/10.1073/pnas.1705242114

Guan, H. H., Budzynski, W., Koganty, R. R., Krantz, M. J., Reddish, M. A., Rogers, J. A., Longenecker, B. M., & Samuel, J. (1998). Liposomal formulations of synthetic MUC1 peptides: effects of encapsulation versus surface display of peptides on immune responses. *Bioconjug Chem*, *9*(4), 451-458. https://doi.org/10.1021/bc970183n

Guermonprez, P., Saveanu, L., Kleijmeer, M., Davoust, J., Van Endert, P., & Amigorena, S. (2003). ER-phagosome fusion defines an MHC class I cross-presentation compartment in dendritic cells. *Nature*, *425*(6956), 397-402. https://doi.org/10.1038/nature01911

Guiducci, C., Vicari, A. P., Sangaletti, S., Trinchieri, G., & Colombo, M. P. (2005). Redirecting in vivo elicited tumor infiltrating macrophages and dendritic cells towards tumor rejection. *Cancer Res*, *65*(8), 3437-3446. https://doi.org/10.1158/0008-5472.CAN-04-4262

Gul, N., Babes, L., Siegmund, K., Korthouwer, R., Bogels, M., Braster, R., Vidarsson, G., ten Hagen, T. L., Kubes, P., & van Egmond, M. (2014). Macrophages eliminate circulating tumor cells after monoclonal antibody therapy. *J Clin Invest*, *124*(2), 812-823. https://doi.org/10.1172/JCI66776

Guo, M., Gong, S., Maric, S., Misulovin, Z., Pack, M., Mahnke, K., Nussenzweig, M. C., & Steinman, R. M. (2000). A monoclonal antibody to the DEC-205 endocytosis receptor on human dendritic cells. *Hum Immunol*, *61*(8), 729-738. https://doi.org/10.1016/s0198-8859(00)00144-0

Hack, K., Reilly, L., Proby, C., Fleming, C., Leigh, I., & Foerster, J. (2012). Wnt5a inhibits the CpG oligodeoxynucleotide-triggered activation of human plasmacytoid dendritic cells. *Clin Exp Dermatol*, *37*(5), 557-561. https://doi.org/10.1111/j.1365-2230.2012.04362.x

Hagel, P., Gerding, J. J., Fieggen, W., & Bloemendal, H. (1971). Cyanate formation in solutions of urea. I. Calculation of cyanate concentrations at different temperature and pH. *Biochim Biophys Acta*, *243*(3), 366-373. https://doi.org/10.1016/0005-2795(71)90003-1

Hall, E. J., & Giaccia, A. J. (2006). *Radiobiology for the Radiologist* (Vol. 6). Philadelphia.

Hamid, O., Robert, C., Daud, A., Hodi, F. S., Hwu, W. J., Kefford, R., Wolchok, J. D., Hersey, P., Joseph, R. W., Weber, J. S., Dronca, R., Gangadhar, T. C., Patnaik, A., Zarour, H., Joshua, A. M., Gergich, K., Elassaiss-Schaap, J., Algazi, A., Mateus, C., . . . Ribas, A. (2013). Safety and tumor responses with lambrolizumab (anti-PD-1) in melanoma. *N Engl J Med*, *369*(2), 134-144. https://doi.org/10.1056/NEJMoa1305133

Han, N., Zhang, Z., Liu, S., Ow, A., Ruan, M., Yang, W., & Zhang, C. (2017). Increased tumor-infiltrating plasmacytoid dendritic cells predicts poor prognosis in oral squamous cell carcinoma. *Arch Oral Biol*, *78*, 129-134. https://doi.org/10.1016/j.archoralbio.2017.02.012

Hanahan, D. (2022). Hallmarks of Cancer: New Dimensions. *Cancer Discov*, *12*(1), 31-46. https://doi.org/10.1158/2159-8290.CD-21-1059

Hanahan, D., & Weinberg, R. A. (2000). The hallmarks of cancer. *Cell*, *100*(1), 57-70. https://doi.org/10.1016/s0092-8674(00)81683-9

Hanahan, D., & Weinberg, R. A. (2011). Hallmarks of cancer: the next generation. *Cell*, *144*(5), 646-674. https://doi.org/10.1016/j.cell.2011.02.013

Hao, Q., & Tang, H. (2018). Interferon-gamma and Smac mimetics synergize to induce apoptosis of lung cancer cells in a TNFalpha-independent manner. *Cancer Cell Int*, *18*, 84. https://doi.org/10.1186/s12935-018-0579-y

Harding, C. V., & Song, R. (1994). Phagocytic processing of exogenous particulate antigens by macrophages for presentation by class I MHC molecules. *J Immunol*, *153*(11), 4925-4933. https://www.ncbi.nlm.nih.gov/pubmed/7963555

Harjunpaa, A., Junnikkala, S., & Meri, S. (2000). Rituximab (anti-CD20) therapy of B-cell lymphomas: direct complement killing is superior to cellular effector mechanisms. *Scand J Immunol*, *51*(6), 634-641. https://doi.org/10.1046/j.1365-3083.2000.00745.x

Hatahet, F., Nguyen, V. D., Salo, K. E., & Ruddock, L. W. (2010). Disruption of reducing pathways is not essential for efficient disulfide bond formation in the cytoplasm of E. coli. *Microb Cell Fact*, *9*, 67. https://doi.org/10.1186/1475-2859-9-67

He, L., Sayers, E. J., Watson, P., & Jones, A. T. (2018). Contrasting roles for actin in the cellular uptake of cell penetrating peptide conjugates. *Sci Rep*, *8*(1), 7318. https://doi.org/10.1038/s41598-018-25600-8

Hegde, P. S., Karanikas, V., & Evers, S. (2016). The Where, the When, and the How of Immune Monitoring for Cancer Immunotherapies in the Era of Checkpoint Inhibition. *Clin Cancer Res*, *22*(8), 1865-1874. https://doi.org/10.1158/1078-0432.CCR-15-1507

Heger, L., Hatscher, L., Liang, C., Lehmann, C. H. K., Amon, L., Luhr, J. J., Kaszubowski, T., Nzirorera, R., Schaft, N., Dorrie, J., Irrgang, P., Tenbusch, M., Kunz, M., Socher, E., Autenrieth, S. E., Purbojo, A., Sirbu, H., Hartmann, A., Alexiou, C., . . . Dudziak, D. (2023). XCR1 expression distinguishes human conventional dendritic cell type 1 with full effector functions from their immediate precursors. *Proc Natl Acad Sci U S A*, *120*(33), e2300343120. https://doi.org/10.1073/pnas.2300343120

Henriques, S. T., Quintas, A., Bagatolli, L. A., Homble, F., & Castanho, M. A. (2007). Energy-independent translocation of cell-penetrating peptides occurs without formation of pores. A biophysical study with pep-1. *Mol Membr Biol*, *24*(4), 282-293. https://doi.org/10.1080/09687860601142936

Hermann, C., van Hateren, A., Trautwein, N., Neerincx, A., Duriez, P. J., Stevanovic, S., Trowsdale, J., Deane, J. E., Elliott, T., & Boyle, L. H. (2015). TAPBPR alters MHC class I peptide presentation by functioning as a peptide exchange catalyst. *Elife*, *4*. https://doi.org/10.7554/eLife.09617

Herskovic, A., Martz, K., al-Sarraf, M., Leichman, L., Brindle, J., Vaitkevicius, V., Cooper, J., Byhardt, R., Davis, L., & Emami, B. (1992). Combined chemotherapy and radiotherapy compared with radiotherapy alone in patients with cancer of the esophagus. *N Engl J Med*, *326*(24), 1593-1598. https://doi.org/10.1056/NEJM199206113262403

Heufler, C., Koch, F., Stanzl, U., Topar, G., Wysocka, M., Trinchieri, G., Enk, A., Steinman, R. M., Romani, N., & Schuler, G. (1996). Interleukin-12 is produced by dendritic cells and mediates T helper 1 development as well as interferon-gamma production by T helper 1 cells. *Eur J Immunol*, *26*(3), 659-668. https://doi.org/10.1002/eji.1830260323

Hewlett, L. J., Prescott, A. R., & Watts, C. (1994). The coated pit and macropinocytic pathways serve distinct endosome populations. *J Cell Biol*, *124*(5), 689-703. https://doi.org/10.1083/jcb.124.5.689

Higgins, C. F. (1992). ABC transporters: from microorganisms to man. *Annu Rev Cell Biol*, *8*, 67-113. https://doi.org/10.1146/annurev.cb.08.110192.000435

Hilf, N., Kuttruff-Coqui, S., Frenzel, K., Bukur, V., Stevanovic, S., Gouttefangeas, C., Platten, M., Tabatabai, G., Dutoit, V., van der Burg, S. H., Thor Straten, P., Martinez-Ricarte, F., Ponsati, B., Okada, H., Lassen, U., Admon, A., Ottensmeier, C. H., Ulges, A., Kreiter, S., . . . Wick, W. (2019). Actively personalized vaccination trial for newly diagnosed glioblastoma. *Nature*, *565*(7738), 240-245. https://doi.org/10.1038/s41586-018-0810-y

Hogquist, K. A., Jameson, S. C., Heath, W. R., Howard, J. L., Bevan, M. J., & Carbone, F. R. (1994). T cell receptor antagonist peptides induce positive selection. *Cell*, *76*(1), 17-27. https://doi.org/10.1016/0092-8674(94)90169-4

Holash, J., Davis, S., Papadopoulos, N., Croll, S. D., Ho, L., Russell, M., Boland, P., Leidich, R., Hylton, D., Burova, E., Ioffe, E., Huang, T., Radziejewski, C., Bailey, K., Fandl, J. P., Daly, T., Wiegand, S. J., Yancopoulos, G. D., & Rudge, J. S. (2002). VEGF-Trap: a VEGF blocker with potent antitumor effects. *Proc Natl Acad Sci U S A*, *99*(17), 11393-11398. https://doi.org/10.1073/pnas.172398299

Honey, K., Nakagawa, T., Peters, C., & Rudensky, A. (2002). Cathepsin L regulates CD4+ T cell selection independently of its effect on invariant chain: a role in the generation of positively selecting peptide ligands. *J Exp Med*, *195*(10), 1349-1358. https://doi.org/10.1084/jem.20011904

Horton, H. M., Bernett, M. J., Peipp, M., Pong, E., Karki, S., Chu, S. Y., Richards, J. O., Chen, H., Repp, R., Desjarlais, J. R., & Zhukovsky, E. A. (2010). Fc-engineered anti-CD40 antibody enhances multiple effector functions and exhibits potent in vitro and in vivo antitumor activity against hematologic malignancies. *Blood*, *116*(16), 3004-3012. https://doi.org/10.1182/blood-2010-01-265280

Houde, M., Bertholet, S., Gagnon, E., Brunet, S., Goyette, G., Laplante, A., Princiotta, M. F., Thibault, P., Sacks, D., & Desjardins, M. (2003). Phagosomes are competent organelles for antigen cross-presentation. *Nature*, *425*(6956), 402-406. https://doi.org/10.1038/nature01912

Hsieh, C. S., deRoos, P., Honey, K., Beers, C., & Rudensky, A. Y. (2002). A role for cathepsin L and cathepsin S in peptide generation for MHC class II presentation. *J Immunol*, *168*(6), 2618-2625. https://doi.org/10.4049/jimmunol.168.6.2618

Hu, C. E., Gan, J., Zhang, R. D., Cheng, Y. R., & Huang, G. J. (2011). Up-regulated myeloid-derived suppressor cell contributes to hepatocellular carcinoma development by impairing dendritic cell function. *Scand J Gastroenterol*, *46*(2), 156-164. https://doi.org/10.3109/00365521.2010.516450

Hu, L., Zhu, M., Shen, Y., Zhong, Z., & Wu, B. (2021). The prognostic value of intratumoral and peritumoral tumor-infiltrating FoxP3+Treg cells in of pancreatic adenocarcinoma: a meta-analysis. *World J Surg Oncol*, *19*(1), 300. https://doi.org/10.1186/s12957-021-02420-1

Hu, R., Wei, W., Mian, A., Gonter-Aubin, K., Kabel, C., Mato, A., Stephens, D. M., Hanlon, A., Khajavian, S., Shadman, M., Brander, D., Madanat, Y., Park, J. H., Tallman, M., Pinilla-Ibarz, J., & Hill, B. T. (2022). Treatment outcomes with purine nucleoside analog alone or with rituximab for hairy cell leukemia at first relapse. *Eur J Haematol*, *108*(5), 379-382. https://doi.org/10.1111/ejh.13744

Hu, Z., Leet, D. E., Allesoe, R. L., Oliveira, G., Li, S., Luoma, A. M., Liu, J., Forman, J., Huang, T., Iorgulescu, J. B., Holden, R., Sarkizova, S., Gohil, S. H., Redd, R. A., Sun, J., Elagina, L., Giobbie-Hurder, A., Zhang, W., Peter, L., . . . Ott, P. A. (2021). Personal neoantigen vaccines induce persistent memory T cell responses and epitope spreading in patients with melanoma. *Nat Med*, *27*(3), 515-525. https://doi.org/10.1038/s41591-020-01206-4

Huang, B., Pan, P. Y., Li, Q., Sato, A. I., Levy, D. E., Bromberg, J., Divino, C. M., & Chen, S. H. (2006). Gr-1+CD115+ immature myeloid suppressor cells mediate the development of tumor-induced T regulatory cells and T-cell anergy in tumor-bearing host. *Cancer Res*, *66*(2), 1123-1131. https://doi.org/10.1158/0008-5472.CAN-05-1299

Huang, Y., Lv, S. Q., Liu, P. Y., Ye, Z. L., Yang, H., Li, L. F., Zhu, H. L., Wang, Y., Cui, L. Z., Jiang, D. Q., Hao, F. Y., Xu, H. M., Jin, H. J., & Qian, Q. J. (2020). A SIRPalpha-Fc fusion protein enhances the antitumor effect of oncolytic adenovirus against ovarian cancer. *Mol Oncol*, *14*(3), 657-668. https://doi.org/10.1002/1878-0261.12628

Huang, Y. H., Zhu, C., Kondo, Y., Anderson, A. C., Gandhi, A., Russell, A., Dougan, S. K., Petersen, B. S., Melum, E., Pertel, T., Clayton, K. L., Raab, M., Chen, Q., Beauchemin, N., Yazaki, P. J.,

Pyzik, M., Ostrowski, M. A., Glickman, J. N., Rudd, C. E., . . . Blumberg, R. S. (2015). CEACAM1 regulates TIM-3-mediated tolerance and exhaustion. *Nature*, *517*(7534), 386-390. https://doi.org/10.1038/nature13848

Huang, Z. Y., Barreda, D. R., Worth, R. G., Indik, Z. K., Kim, M. K., Chien, P., & Schreiber, A. D. (2006). Differential kinase requirements in human and mouse Fc-gamma receptor phagocytosis and endocytosis. *J Leukoc Biol*, *80*(6), 1553-1562. https://doi.org/10.1189/jlb.0106019

Hughes, E. A., & Cresswell, P. (1998). The thiol oxidoreductase ERp57 is a component of the MHC class I peptide-loading complex. *Curr Biol*, *8*(12), 709-712. https://doi.org/10.1016/s0960-9822(98)70278-7

Hulett, M. D., & Hogarth, P. M. (1998). The second and third extracellular domains of FcgammaRI (CD64) confer the unique high affinity binding of IgG2a. *Mol Immunol*, *35*(14-15), 989-996. https://doi.org/10.1016/s0161-5890(98)00069-8

Idusogie, E. E., Presta, L. G., Gazzano-Santoro, H., Totpal, K., Wong, P. Y., Ultsch, M., Meng, Y. G., & Mulkerrin, M. G. (2000). Mapping of the C1q binding site on rituxan, a chimeric antibody with a human IgG1 Fc. *J Immunol*, *164*(8), 4178-4184. https://doi.org/10.4049/jimmunol.164.8.4178

Ikehara, S., Pahwa, R. N., Fernandes, G., Hansen, C. T., & Good, R. A. (1984). Functional T cells in athymic nude mice. *Proc Natl Acad Sci U S A*, *81*(3), 886-888. https://doi.org/10.1073/pnas.81.3.886

Imai, J., Hasegawa, H., Maruya, M., Koyasu, S., & Yahara, I. (2005). Exogenous antigens are processed through the endoplasmic reticulum-associated degradation (ERAD) in cross-presentation by dendritic cells. *Int Immunol*, *17*(1), 45-53. https://doi.org/10.1093/intimm/dxh184

Isnard, S., Hatton, E., Guillerme, J.-B., & Hosmalin, A. (2020). Chapter Eighteen - Monitoring antigen cross-presentation by human dendritic cells purified from peripheral blood. In L. Galluzzi & N.-P. Rudqvist (Eds.), *Methods in Enzymology* (Vol. 635, pp. 283-305). Academic Press. https://doi.org/https://doi.org/10.1016/bs.mie.2020.01.004

Ito, M., Hayashi, K., Adachi, E., Minamisawa, T., Homma, S., Koido, S., & Shiba, K. (2014). Combinatorial contextualization of peptidic epitopes for enhanced cellular immunity. *PLoS One*, *9*(10), e110425. https://doi.org/10.1371/journal.pone.0110425

Ito, S., Okano, S., Morita, M., Saeki, H., Tsutsumi, S., Tsukihara, H., Nakashima, Y., Ando, K., Imamura, Y., Ohgaki, K., Oki, E., Kitao, H., Mimori, K., & Maehara, Y. (2016). Expression of PD-L1 and HLA Class I in Esophageal Squamous Cell Carcinoma: Prognostic Factors for Patient Outcome. *Ann Surg Oncol*, *23*(Suppl 4), 508-515. https://doi.org/10.1245/s10434-016-5376-z

Ito, T., Kanzler, H., Duramad, O., Cao, W., & Liu, Y. J. (2006). Specialization, kinetics, and repertoire of type 1 interferon responses by human plasmacytoid predendritic cells. *Blood*, *107*(6), 2423-2431. https://doi.org/10.1182/blood-2005-07-2709

Itoh, N., Yonehara, S., Ishii, A., Yonehara, M., Mizushima, S., Sameshima, M., Hase, A., Seto, Y., & Nagata, S. (1991). The polypeptide encoded by the cDNA for human cell surface antigen Fas can mediate apoptosis. *Cell*, *66*(2), 233-243. https://doi.org/10.1016/0092-8674(91)90614-5

Jager, E., Chen, Y. T., Drijfhout, J. W., Karbach, J., Ringhoffer, M., Jager, D., Arand, M., Wada, H., Noguchi, Y., Stockert, E., Old, L. J., & Knuth, A. (1998). Simultaneous humoral and cellular immune response against cancer-testis antigen NY-ESO-1: definition of human histocompatibility leukocyte antigen (HLA)-A2-binding peptide epitopes. *J Exp Med*, *187*(2), 265-270. https://doi.org/10.1084/jem.187.2.265

Jager, E., Nagata, Y., Gnjatic, S., Wada, H., Stockert, E., Karbach, J., Dunbar, P. R., Lee, S. Y., Jungbluth, A., Jager, D., Arand, M., Ritter, G., Cerundolo, V., Dupont, B., Chen, Y. T., Old, L. J., & Knuth, A. (2000). Monitoring CD8 T cell responses to NY-ESO-1: correlation of humoral and cellular immune responses. *Proc Natl Acad Sci U S A*, *97*(9), 4760-4765. https://doi.org/10.1073/pnas.97.9.4760

Jahanafrooz, Z., Baradaran, B., Mosafer, J., Hashemzaei, M., Rezaei, T., Mokhtarzadeh, A., & Hamblin, M. R. (2020). Comparison of DNA and mRNA vaccines against cancer. *Drug Discov Today*, *25*(3), 552-560. https://doi.org/10.1016/j.drudis.2019.12.003

James, J. S., & Dubs, G. (1997). FDA approves new kind of lymphoma treatment. Food and Drug Administration. *AIDS Treat News*(No 284), 2-3. https://www.ncbi.nlm.nih.gov/pubmed/11364912

Jancic, C., Savina, A., Wasmeier, C., Tolmachova, T., El-Benna, J., Dang, P. M., Pascolo, S., Gougerot-Pocidalo, M. A., Raposo, G., Seabra, M. C., & Amigorena, S. (2007). Rab27a regulates

phagosomal pH and NADPH oxidase recruitment to dendritic cell phagosomes. *Nat Cell Biol*, *9*(4), 367-378. https://doi.org/10.1038/ncb1552

Janeway, C. A., Jr. (1992). The T cell receptor as a multicomponent signalling machine: CD4/CD8 coreceptors and CD45 in T cell activation. *Annu Rev Immunol*, *10*, 645-674. https://doi.org/10.1146/annurev.iy.10.040192.003241

Jazayeri, J. A., & Carroll, G. J. (2012). Half-Life Extension by Fusion to the Fc Region. In *Therapeutic Proteins* (pp. 157-188). https://doi.org/https://doi.org/10.1002/9783527644827.ch9

Ji, X., Shen, Y., Sun, H., & Gao, X. (2016). A novel anti-alpha-fetoprotein single-chain variable fragment displays anti-tumor effects in HepG2 cells as a single agent or in combination with paclitaxel. *Tumour Biol*, *37*(8), 10085-10096. https://doi.org/10.1007/s13277-016-4803-x

Jiang, S., Song, R., Popov, S., Mirshahidi, S., & Ruprecht, R. M. (2006). Overlapping synthetic peptides as vaccines. *Vaccine*, *24*(37-39), 6356-6365. https://doi.org/10.1016/j.vaccine.2006.04.070

Jiang, W., Swiggard, W. J., Heufler, C., Peng, M., Mirza, A., Steinman, R. M., & Nussenzweig, M. C. (1995). The receptor DEC-205 expressed by dendritic cells and thymic epithelial cells is involved in antigen processing. *Nature*, *375*(6527), 151-155. https://doi.org/10.1038/375151a0

Joffre, O. P., Segura, E., Savina, A., & Amigorena, S. (2012). Cross-presentation by dendritic cells. *Nat Rev Immunol*, *12*(8), 557-569. https://doi.org/10.1038/nri3254

Jorgovanovic, D., Song, M., Wang, L., & Zhang, Y. (2020). Roles of IFN-gamma in tumor progression and regression: a review. *Biomark Res*, *8*, 49. https://doi.org/10.1186/s40364-020-00228-x

Jung, H. I., Jeong, D., Ji, S., Ahn, T. S., Bae, S. H., Chin, S., Chung, J. C., Kim, H. C., Lee, M. S., & Baek, M. J. (2017). Overexpression of PD-L1 and PD-L2 Is Associated with Poor Prognosis in Patients with Hepatocellular Carcinoma. *Cancer Res Treat*, *49*(1), 246-254. https://doi.org/10.4143/crt.2016.066

Jungbluth, A. A., Chen, Y. T., Stockert, E., Busam, K. J., Kolb, D., Iversen, K., Coplan, K., Williamson, B., Altorki, N., & Old, L. J. (2001). Immunohistochemical analysis of NY-ESO-1 antigen expression in normal and malignant human tissues. *Int J Cancer*, *92*(6), 856-860. https://doi.org/10.1002/ijc.1282

Kagi, D., Vignaux, F., Ledermann, B., Burki, K., Depraetere, V., Nagata, S., Hengartner, H., & Golstein, P. (1994). Fas and perforin pathways as major mechanisms of T cell-mediated cytotoxicity. *Science*, *265*(5171), 528-530. https://doi.org/10.1126/science.7518614

Kantoff, P. W., Higano, C. S., Shore, N. D., Berger, E. R., Small, E. J., Penson, D. F., Redfern, C. H., Ferrari, A. C., Dreicer, R., Sims, R. B., Xu, Y., Frohlich, M. W., Schellhammer, P. F., & Investigators, I. S. (2010). Sipuleucel-T immunotherapy for castration-resistant prostate cancer. *N Engl J Med*, *363*(5), 411-422. https://doi.org/10.1056/NEJMoa1001294

Kaplan, D. H., Shankaran, V., Dighe, A. S., Stockert, E., Aguet, M., Old, L. J., & Schreiber, R. D. (1998). Demonstration of an interferon gamma-dependent tumor surveillance system in immunocompetent mice. *Proc Natl Acad Sci U S A*, *95*(13), 7556-7561. https://doi.org/10.1073/pnas.95.13.7556

Kapust, R. B., & Waugh, D. S. (1999). Escherichia coli maltose-binding protein is uncommonly effective at promoting the solubility of polypeptides to which it is fused. *Protein Sci*, *8*(8), 1668-1674. https://doi.org/10.1110/ps.8.8.1668

Karandikar, S. H., Sidney, J., Sette, A., Selby, M. J., Korman, A. J., & Srivastava, P. K. (2019). New epitopes in ovalbumin provide insights for cancer neoepitopes. *JCI Insight*, *5*(8). https://doi.org/10.1172/jci.insight.127882

Karsten, C. M., Pandey, M. K., Figge, J., Kilchenstein, R., Taylor, P. R., Rosas, M., McDonald, J. U., Orr, S. J., Berger, M., Petzold, D., Blanchard, V., Winkler, A., Hess, C., Reid, D. M., Majoul, I. V., Strait, R. T., Harris, N. L., Kohl, G., Wex, E., . . . Kohl, J. (2012). Anti-inflammatory activity of IgG1 mediated by Fc galactosylation and association of FcgammaRIIB and dectin-1. *Nat Med*, *18*(9), 1401-1406. https://doi.org/10.1038/nm.2862

Karttunen, J., Sanderson, S., & Shastri, N. (1992). Detection of rare antigen-presenting cells by the lacZ T-cell activation assay suggests an expression cloning strategy for T-cell antigens. *Proc Natl Acad Sci U S A*, *89*(13), 6020-6024. https://doi.org/10.1073/pnas.89.13.6020

Karyampudi, L., Lamichhane, P., Scheid, A. D., Kalli, K. R., Shreeder, B., Krempski, J. W., Behrens, M. D., & Knutson, K. L. (2014). Accumulation of memory precursor CD8 T cells in regressing tumors following combination therapy with vaccine and anti-PD-1 antibody. *Cancer Res*, *74*(11), 2974-2985. https://doi.org/10.1158/0008-5472.CAN-13-2564

Kato, M., McDonald, K. J., Khan, S., Ross, I. L., Vuckovic, S., Chen, K., Munster, D., MacDonald, K. P., & Hart, D. N. (2006). Expression of human DEC-205 (CD205) multilectin receptor on leukocytes. *Int Immunol*, *18*(6), 857-869. https://doi.org/10.1093/intimm/dxl022

Kay, B. K., Thai, S., & Volgina, V. V. (2009). High-throughput biotinylation of proteins. *Methods Mol Biol*, *498*, 185-196. https://doi.org/10.1007/978-1-59745-196-3_13

Keler, T., Halk, E., Vitale, L., O'Neill, T., Blanset, D., Lee, S., Srinivasan, M., Graziano, R. F., Davis, T., Lonberg, N., & Korman, A. (2003). Activity and safety of CTLA-4 blockade combined with vaccines in cynomolgus macaques. *J Immunol*, *171*(11), 6251-6259. https://doi.org/10.4049/jimmunol.171.11.6251

Keskin, D. B., Anandappa, A. J., Sun, J., Tirosh, I., Mathewson, N. D., Li, S., Oliveira, G., Giobbie-Hurder, A., Felt, K., Gjini, E., Shukla, S. A., Hu, Z., Li, L., Le, P. M., Allesoe, R. L., Richman, A. R., Kowalczyk, M. S., Abdelrahman, S., Geduldig, J. E., . . . Reardon, D. A. (2019). Neoantigen vaccine generates intratumoral T cell responses in phase Ib glioblastoma trial. *Nature*, *565*(7738), 234-239. https://doi.org/10.1038/s41586-018-0792-9

Khan, S., Bijker, M. S., Weterings, J. J., Tanke, H. J., Adema, G. J., van Hall, T., Drijfhout, J. W., Melief, C. J., Overkleeft, H. S., van der Marel, G. A., Filippov, D. V., van der Burg, S. H., & Ossendorp, F. (2007). Distinct uptake mechanisms but similar intracellular processing of two different toll-like receptor ligand-peptide conjugates in dendritic cells. *J Biol Chem*, *282*(29), 21145-21159. https://doi.org/10.1074/jbc.M701705200

Kiessler, M., Plesca, I., Sommer, U., Wehner, R., Wilczkowski, F., Muller, L., Tunger, A., Lai, X., Rentsch, A., Peuker, K., Zeissig, S., Seifert, A. M., Seifert, L., Weitz, J., Bachmann, M., Bornhauser, M., Aust, D., Baretton, G., & Schmitz, M. (2021). Tumor-infiltrating plasmacytoid dendritic cells are associated with survival in human colon cancer. *J Immunother Cancer*, *9*(3). https://doi.org/10.1136/jitc-2020-001813

Kilinc, M. O., Mukundan, L., Yolcu, E. S., Singh, N. P., Suttles, J., & Shirwan, H. (2006). Generation of a multimeric form of CD40L with potent immunostimulatory activity using streptavidin as a chaperon. *Exp Mol Pathol*, *80*(3), 252-261. https://doi.org/10.1016/j.yexmp.2005.12.004

Kim, J. K., Firan, M., Radu, C. G., Kim, C. H., Ghetie, V., & Ward, E. S. (1999). Mapping the site on human IgG for binding of the MHC class I-related receptor, FcRn. *Eur J Immunol*, *29*(9), 2819-2825. https://doi.org/10.1002/(SICI)1521-4141(199909)29:09<2819::AID-IMMU2819>3.0.CO;2-6

Kipriyanov, S. M., Little, M., Kropshofer, H., Breitling, F., Gotter, S., & Dubel, S. (1996). Affinity enhancement of a recombinant antibody: formation of complexes with multiple valency by a single-chain Fv fragment-core streptavidin fusion. *Protein Eng*, *9*(2), 203-211. https://doi.org/10.1093/protein/9.2.203

Kirchhausen, T., Macia, E., & Pelish, H. E. (2008). Use of dynasore, the small molecule inhibitor of dynamin, in the regulation of endocytosis. *Methods Enzymol*, *438*, 77-93. https://doi.org/10.1016/S0076-6879(07)38006-3

Klein, G. (1966). Tumor antigens. *Annual Reviews in Microbiology*, *20*(1), 223-252.

Kloetzel, P. M. (2001). Antigen processing by the proteasome. *Nat Rev Mol Cell Biol*, *2*(3), 179-187. https://doi.org/10.1038/35056572

Koebel, C. M., Vermi, W., Swann, J. B., Zerafa, N., Rodig, S. J., Old, L. J., Smyth, M. J., & Schreiber, R. D. (2007). Adaptive immunity maintains occult cancer in an equilibrium state. *Nature*, *450*(7171), 903-907. https://doi.org/10.1038/nature06309

Kohlhapp, F. J., & Kaufman, H. L. (2016). Molecular Pathways: Mechanism of Action for Talimogene Laherparepvec, a New Oncolytic Virus Immunotherapy. *Clin Cancer Res*, *22*(5), 1048-1054. https://doi.org/10.1158/1078-0432.CCR-15-2667

Koivusalo, M., Welch, C., Hayashi, H., Scott, C. C., Kim, M., Alexander, T., Touret, N., Hahn, K. M., & Grinstein, S. (2010). Amiloride inhibits macropinocytosis by lowering submembranous pH and preventing Rac1 and Cdc42 signaling. *J Cell Biol*, *188*(4), 547-563. https://doi.org/10.1083/jcb.200908086

Koley, D., & Bard, A. J. (2010). Triton X-100 concentration effects on membrane permeability of a single HeLa cell by scanning electrochemical microscopy (SECM). *Proc Natl Acad Sci U S A*, *107*(39), 16783-16787. https://doi.org/10.1073/pnas.1011614107

Kono, K., Igawa, T., & Takagishi, T. (1997). Cytoplasmic delivery of calcein mediated by liposomes modified with a pH-sensitive poly(ethylene glycol) derivative. *Biochim Biophys Acta*, *1325*(2), 143-154. https://doi.org/10.1016/s0005-2736(96)00244-1

Koopmann, J. O., Albring, J., Huter, E., Bulbuc, N., Spee, P., Neefjes, J., Hammerling, G. J., & Momburg, F. (2000). Export of antigenic peptides from the endoplasmic reticulum intersects with retrograde protein translocation through the Sec61p channel. *Immunity*, *13*(1), 117-127. https://doi.org/10.1016/s1074-7613(00)00013-3

Koshizuka, T., Kawaguchi, Y., & Nishiyama, Y. (2005). Herpes simplex virus type 2 membrane protein UL56 associates with the kinesin motor protein KIF1A. *J Gen Virol*, *86*(Pt 3), 527-533. https://doi.org/10.1099/vir.0.80633-0

Kovacsovics-Bankowski, M., & Rock, K. L. (1995). A phagosome-to-cytosol pathway for exogenous antigens presented on MHC class I molecules. *Science*, *267*(5195), 243-246. https://doi.org/10.1126/science.7809629

Krause, A., Guo, H. F., Latouche, J. B., Tan, C., Cheung, N. K., & Sadelain, M. (1998). Antigen-dependent CD28 signaling selectively enhances survival and proliferation in genetically modified activated human primary T lymphocytes. *J Exp Med*, *188*(4), 619-626. https://doi.org/10.1084/jem.188.4.619

Kuehnemuth, B., Piseddu, I., Wiedemann, G. M., Lauseker, M., Kuhn, C., Hofmann, S., Schmoeckel, E., Endres, S., Mayr, D., Jeschke, U., & Anz, D. (2018). CCL1 is a major regulatory T cell attracting factor in human breast cancer. *BMC Cancer*, *18*(1), 1278. https://doi.org/10.1186/s12885-018-5117-8

Kuhn, I., Harden, P., Bauzon, M., Chartier, C., Nye, J., Thorne, S., Reid, T., Ni, S., Lieber, A., Fisher, K., Seymour, L., Rubanyi, G. M., Harkins, R. N., & Hermiston, T. W. (2008). Directed evolution generates a novel oncolytic virus for the treatment of colon cancer. *PLoS One*, *3*(6), e2409. https://doi.org/10.1371/journal.pone.0002409

Kumar, D. (2011). 2.54 - Protein Refolding/Renaturation. In M. Moo-Young (Ed.), *Comprehensive Biotechnology (Second Edition)* (pp. 765-784). Academic Press. https://doi.org/https://doi.org/10.1016/B978-0-08-088504-9.00136-7

Kurbacher, C. M., Kurbacher, J. A., Cramer, E. M., Rhiem, K., Mallman, P. K., Reichelt, R., Reinhold, U., Stier, U., & Cree, I. A. (2005). Continuous low-dose GM-CSF as salvage therapy in refractory recurrent breast or female genital tract carcinoma. *Oncology (Williston Park)*, *19*(4 Suppl 2), 23-26. https://www.ncbi.nlm.nih.gov/pubmed/15934497

Kurucz, I., Titus, J. A., Jost, C. R., & Segal, D. M. (1995). Correct disulfide pairing and efficient refolding of detergent-solubilized single-chain Fv proteins from bacterial inclusion bodies. *Mol Immunol*, *32*(17-18), 1443-1452. https://doi.org/10.1016/0161-5890(95)00105-0

Kushwah, R., & Hu, J. (2011). Complexity of dendritic cell subsets and their function in the host immune system. *Immunology*, *133*(4), 409-419. https://doi.org/10.1111/j.1365-2567.2011.03457.x

Kusmartsev, S., Nefedova, Y., Yoder, D., & Gabrilovich, D. I. (2004). Antigen-specific inhibition of CD8+ T cell response by immature myeloid cells in cancer is mediated by reactive oxygen species. *J Immunol*, *172*(2), 989-999. https://doi.org/10.4049/jimmunol.172.2.989

Kvistborg, P., Shu, C. J., Heemskerk, B., Fankhauser, M., Thrue, C. A., Toebes, M., van Rooij, N., Linnemann, C., van Buuren, M. M., Urbanus, J. H., Beltman, J. B., Thor Straten, P., Li, Y. F., Robbins, P. F., Besser, M. J., Schachter, J., Kenter, G. G., Dudley, M. E., Rosenberg, S. A., . . . Schumacher, T. N. (2012). TIL therapy broadens the tumor-reactive CD8(+) T cell compartment in melanoma patients. *Oncoimmunology*, *1*(4), 409-418. https://doi.org/10.4161/onci.18851

Kyte, J., & Doolittle, R. F. (1982). A simple method for displaying the hydropathic character of a protein. *J Mol Biol*, *157*(1), 105-132. https://doi.org/10.1016/0022-2836(82)90515-0

Labani-Motlagh, A., Ashja-Mahdavi, M., & Loskog, A. (2020). The Tumor Microenvironment: A Milieu Hindering and Obstructing Antitumor Immune Responses. *Front Immunol*, *11*, 940. https://doi.org/10.3389/fimmu.2020.00940

Labidi-Galy, S. I., Treilleux, I., Goddard-Leon, S., Combes, J. D., Blay, J. Y., Ray-Coquard, I., Caux, C., & Bendriss-Vermare, N. (2012). Plasmacytoid dendritic cells infiltrating ovarian cancer are associated with poor prognosis. *Oncoimmunology*, *1*(3), 380-382. https://doi.org/10.4161/onci.18801

Laheru, D., Lutz, E., Burke, J., Biedrzycki, B., Solt, S., Onners, B., Tartakovsky, I., Nemunaitis, J., Le, D., Sugar, E., Hege, K., & Jaffee, E. (2008). Allogeneic granulocyte macrophage colony-

stimulating factor-secreting tumor immunotherapy alone or in sequence with cyclophosphamide for metastatic pancreatic cancer: a pilot study of safety, feasibility, and immune activation. *Clin Cancer Res*, *14*(5), 1455-1463. https://doi.org/10.1158/1078-0432.CCR-07-0371

Laitinen, O. H., Hytonen, V. P., Nordlund, H. R., & Kulomaa, M. S. (2006). Genetically engineered avidins and streptavidins. *Cell Mol Life Sci*, *63*(24), 2992-3017. https://doi.org/10.1007/s00018-006-6288-z

Lauber, K., Bohn, E., Krober, S. M., Xiao, Y. J., Blumenthal, S. G., Lindemann, R. K., Marini, P., Wiedig, C., Zobywalski, A., Baksh, S., Xu, Y., Autenrieth, I. B., Schulze-Osthoff, K., Belka, C., Stuhler, G., & Wesselborg, S. (2003). Apoptotic cells induce migration of phagocytes via caspase-3-mediated release of a lipid attraction signal. *Cell*, *113*(6), 717-730. https://doi.org/10.1016/s0092-8674(03)00422-7

Le Naour, J., Zitvogel, L., Galluzzi, L., Vacchelli, E., & Kroemer, G. (2020). Trial watch: STING agonists in cancer therapy. *Oncoimmunology*, *9*(1), 1777624. https://doi.org/10.1080/2162402X.2020.1777624

Le, X. F., Claret, F. X., Lammayot, A., Tian, L., Deshpande, D., LaPushin, R., Tari, A. M., & Bast, R. C., Jr. (2003). The role of cyclin-dependent kinase inhibitor p27Kip1 in anti-HER2 antibody-induced G1 cell cycle arrest and tumor growth inhibition. *J Biol Chem*, *278*(26), 23441-23450. https://doi.org/10.1074/jbc.M300848200

Leach, D. R., Krummel, M. F., & Allison, J. P. (1996). Enhancement of antitumor immunity by CTLA-4 blockade. *Science*, *271*(5256), 1734-1736. https://doi.org/10.1126/science.271.5256.1734

Lechardeur, D., Verkman, A. S., & Lukacs, G. L. (2005). Intracellular routing of plasmid DNA during non-viral gene transfer. *Adv Drug Deliv Rev*, *57*(5), 755-767. https://doi.org/10.1016/j.addr.2004.12.008

Lee, D. H., & Goldberg, A. L. (1996). Selective inhibitors of the proteasome-dependent and vacuolar pathways of protein degradation in Saccharomyces cerevisiae. *J Biol Chem*, *271*(44), 27280-27284. https://doi.org/10.1074/jbc.271.44.27280

Lee, H. J., Kim, Y. A., Sim, C. K., Heo, S. H., Song, I. H., Park, H. S., Park, S. Y., Bang, W. S., Park, I. A., Lee, M., Lee, J. H., Cho, Y. S., Chang, S., Jung, J., Kim, J., Lee, S. B., Kim, S. Y., Lee, M. S., & Gong, G. (2017). Expansion of tumor-infiltrating lymphocytes and their potential for application as adoptive cell transfer therapy in human breast cancer. *Oncotarget*, *8*(69), 113345-113359. https://doi.org/10.18632/oncotarget.23007

Lee, P. T., Benlagha, K., Teyton, L., & Bendelac, A. (2002). Distinct functional lineages of human V(alpha)24 natural killer T cells. *J Exp Med*, *195*(5), 637-641. https://doi.org/10.1084/jem.20011908

Lemos, H., Ou, R., McCardle, C., Lin, Y., Calver, J., Minett, J., Chadli, A., Huang, L., & Mellor, A. L. (2020). Overcoming resistance to STING agonist therapy to incite durable protective antitumor immunity. *J Immunother Cancer*, *8*(2). https://doi.org/10.1136/jitc-2020-001182

Leserman, L. D., Weinstein, J. N., Blumenthal, R., & Terry, W. D. (1980). Receptor-mediated endocytosis of antibody-opsonized liposomes by tumor cells. *Proc Natl Acad Sci U S A*, *77*(7), 4089-4093. https://doi.org/10.1073/pnas.77.7.4089

Lewis, C. M., Smith, A. K., & Kamen, B. A. (1998). Receptor-mediated folate uptake is positively regulated by disruption of the actin cytoskeleton. *Cancer Res*, *58*(14), 2952-2956. https://www.ncbi.nlm.nih.gov/pubmed/9679952

Li-Chan, E. (1989). Biochemical basis for the properties of egg white. *Crit. Rev. Poulty Biol.*, *2*, 21-58.

Li, A. M., Hucks, G. E., Dinofia, A. M., Seif, A. E., Teachey, D. T., Baniewicz, D., Callahan, C., Fasano, C., McBride, B., Gonzalez, V., Nazimuddin, F., Porter, D. L., Lacey, S. F., June, C. H., Grupp, S. A., & Maude, S. L. (2018). Checkpoint Inhibitors Augment CD19-Directed Chimeric Antigen Receptor (CAR) T Cell Therapy in Relapsed B-Cell Acute Lymphoblastic Leukemia. *Blood*, *132*(Supplement 1), 556-556. https://doi.org/10.1182/blood-2018-99-112572

Li, J., Lin, W., Chen, H., Xu, Z., Ye, Y., & Chen, M. (2020). Dual-target IL-12-containing nanoparticles enhance T cell functions for cancer immunotherapy. *Cell Immunol*, *349*, 104042. https://doi.org/10.1016/j.cellimm.2020.104042

Li, M. O., Wan, Y. Y., Sanjabi, S., Robertson, A. K., & Flavell, R. A. (2006). Transforming growth factor-beta regulation of immune responses. *Annu Rev Immunol*, *24*, 99-146. https://doi.org/10.1146/annurev.immunol.24.021605.090737

Li, Y., Moysey, R., Molloy, P. E., Vuidepot, A. L., Mahon, T., Baston, E., Dunn, S., Liddy, N., Jacob, J., Jakobsen, B. K., & Boulter, J. M. (2005). Directed evolution of human T-cell receptors with picomolar affinities by phage display. *Nat Biotechnol*, *23*(3), 349-354. https://doi.org/10.1038/nbt1070

Lian, H., Jiang, J., Wang, Y., Yu, X., Zheng, R., Long, J., Zhou, M., Zhou, S., Wei, C., Zhao, A., & Gao, J. (2022). A novel multimeric sCD19-streptavidin fusion protein for functional detection and selective expansion of CD19-targeted CAR-T cells. *Cancer Med*, *11*(15), 2978-2989. https://doi.org/10.1002/cam4.4657

Liberman, R., Bond, S., Shainheit, M. G., Stadecker, M. J., & Forgac, M. (2014). Regulated assembly of vacuolar ATPase is increased during cluster disruption-induced maturation of dendritic cells through a phosphatidylinositol 3-kinase/mTOR-dependent pathway. *J Biol Chem*, *289*(3), 1355-1363. https://doi.org/10.1074/jbc.M113.524561

Lim, J. P., & Gleeson, P. A. (2011). Macropinocytosis: an endocytic pathway for internalising large gulps. *Immunol Cell Biol*, *89*(8), 836-843. https://doi.org/10.1038/icb.2011.20

Lim, K. J., Sung, B. H., Shin, J. R., Lee, Y. W., Kim, D. J., Yang, K. S., & Kim, S. C. (2013). A cancer specific cell-penetrating peptide, BR2, for the efficient delivery of an scFv into cancer cells. *PLoS One*, *8*(6), e66084. https://doi.org/10.1371/journal.pone.0066084

Lindner, B., Burkard, T., & Schuler, M. (2020). Phagocytosis assays with different pH-sensitive fluorescent particles and various readouts. *Biotechniques*, *68*(5), 245-250. https://doi.org/10.2144/btn-2020-0003

Lippincott, J., & Apostol, I. (1999). Carbamylation of cysteine: a potential artifact in peptide mapping of hemoglobins in the presence of urea. *Anal Biochem*, *267*(1), 57-64. https://doi.org/10.1006/abio.1998.2970

Liu, B. L., Robinson, M., Han, Z. Q., Branston, R. H., English, C., Reay, P., McGrath, Y., Thomas, S. K., Thornton, M., Bullock, P., Love, C. A., & Coffin, R. S. (2003). ICP34.5 deleted herpes simplex virus with enhanced oncolytic, immune stimulating, and anti-tumour properties. *Gene Ther*, *10*(4), 292-303. https://doi.org/10.1038/sj.gt.3301885

Liu, B. R., Huang, Y. W., Winiarz, J. G., Chiang, H. J., & Lee, H. J. (2011). Intracellular delivery of quantum dots mediated by a histidine- and arginine-rich HR9 cell-penetrating peptide through the direct membrane translocation mechanism. *Biomaterials*, *32*(13), 3520-3537. https://doi.org/10.1016/j.biomaterials.2011.01.041

Liu, C., Yang, M., Zhang, D., Chen, M., & Zhu, D. (2022). Clinical cancer immunotherapy: Current progress and prospects. *Front Immunol*, *13*, 961805. https://doi.org/10.3389/fimmu.2022.961805

Liu, G., Rui, W., Zheng, H., Huang, D., Yu, F., Zhang, Y., Dong, J., Zhao, X., & Lin, X. (2020). CXCR2-modified CAR-T cells have enhanced trafficking ability that improves treatment of hepatocellular carcinoma. *Eur J Immunol*, *50*(5), 712-724. https://doi.org/10.1002/eji.201948457

Liu, Z., Zhou, H., Wang, W., Fu, Y. X., & Zhu, M. (2016). A novel dendritic cell targeting HPV16 E7 synthetic vaccine in combination with PD-L1 blockade elicits therapeutic antitumor immunity in mice. *Oncoimmunology*, *5*(6), e1147641. https://doi.org/10.1080/2162402X.2016.1147641

Ljunggren, H. G., & Karre, K. (1990). In search of the 'missing self': MHC molecules and NK cell recognition. *Immunol Today*, *11*(7), 237-244. https://doi.org/10.1016/0167-5699(90)90097-s

Ljunggren, H. G., Stam, N. J., Ohlen, C., Neefjes, J. J., Hoglund, P., Heemels, M. T., Bastin, J., Schumacher, T. N., Townsend, A., Karre, K., & et al. (1990). Empty MHC class I molecules come out in the cold. *Nature*, *346*(6283), 476-480. https://doi.org/10.1038/346476a0

Lo, U. G., Bao, J., Cen, J., Yeh, H. C., Luo, J., Tan, W., & Hsieh, J. T. (2019). Interferon-induced IFIT5 promotes epithelial-to-mesenchymal transition leading to renal cancer invasion. *Am J Clin Exp Urol*, *7*(1), 31-45. https://www.ncbi.nlm.nih.gov/pubmed/30906803

Loercher, A. E., Nash, M. A., Kavanagh, J. J., Platsoucas, C. D., & Freedman, R. S. (1999). Identification of an IL-10-Producing HLA-DR-Negative Monocyte Subset in the Malignant Ascites of Patients with Ovarian Carcinoma That Inhibits Cytokine Protein Expression and Proliferation of Autologous T Cells1. *The Journal of Immunology*, *163*(11), 6251-6260. https://doi.org/10.4049/jimmunol.163.11.6251

Löffler, A., Kufer, P., Lutterbüse, R., Zettl, F., Daniel, P. T., Schwenkenbecher, J. M., Riethmüller, G., Dörken, B., & Bargou, R. C. (2000). A recombinant bispecific single-chain antibody, CD19 ×

CD3, induces rapid and high lymphoma-directed cytotoxicity by unstimulated T lymphocytes. *Blood*, *95*(6), 2098-2103. https://doi.org/https://doi.org/10.1182/blood.V95.6.2098

Lorentzen, C. L., Haanen, J. B., Met, O., & Svane, I. M. (2022). Clinical advances and ongoing trials on mRNA vaccines for cancer treatment. *Lancet Oncol*, *23*(10), e450-e458. https://doi.org/10.1016/S1470-2045(22)00372-2

Lu, C., Redd, P. S., Lee, J. R., Savage, N., & Liu, K. (2016). The expression profiles and regulation of PD-L1 in tumor-induced myeloid-derived suppressor cells. *Oncoimmunology*, *5*(12), e1247135. https://doi.org/10.1080/2162402X.2016.1247135

Lu, Y., Yang, W., Qin, C., Zhang, L., Deng, J., Liu, S., & Qin, Z. (2009). Responsiveness of stromal fibroblasts to IFN-gamma blocks tumor growth via angiostasis. *J Immunol*, *183*(10), 6413-6421. https://doi.org/10.4049/jimmunol.0901073

Lund, J., Pound, J. D., Jones, P. T., Duncan, A. R., Bentley, T., Goodall, M., Levine, B. A., Jefferis, R., & Winter, G. (1992). Multiple binding sites on the CH2 domain of IgG for mouse Fc gamma R11. *Mol Immunol*, *29*(1), 53-59. https://doi.org/10.1016/0161-5890(92)90156-r

Luo, N., Nixon, M. J., Gonzalez-Ericsson, P. I., Sanchez, V., Opalenik, S. R., Li, H., Zahnow, C. A., Nickels, M. L., Liu, F., Tantawy, M. N., Sanders, M. E., Manning, H. C., & Balko, J. M. (2018). DNA methyltransferase inhibition upregulates MHC-I to potentiate cytotoxic T lymphocyte responses in breast cancer. *Nat Commun*, *9*(1), 248. https://doi.org/10.1038/s41467-017-02630-w

Luo, W., Hickman, D., Keykhosravani, M., Wilson, J., Fink, J., Huang, L., Chen, D., & O'Donnell, S. (2020). Identification and characterization of a Triton X-100 replacement for virus inactivation. *Biotechnol Prog*, *36*(6), e3036. https://doi.org/10.1002/btpr.3036

Luster, A. D., & Ravetch, J. V. (1987). Biochemical characterization of a gamma interferon-inducible cytokine (IP-10). *J Exp Med*, *166*(4), 1084-1097. https://doi.org/10.1084/jem.166.4.1084

Luther, S. A., Tang, H. L., Hyman, P. L., Farr, A. G., & Cyster, J. G. (2000). Coexpression of the chemokines ELC and SLC by T zone stromal cells and deletion of the ELC gene in the plt/plt mouse. *Proc Natl Acad Sci U S A*, *97*(23), 12694-12699. https://doi.org/10.1073/pnas.97.23.12694

Lützner, N., & Kalbacher, H. (2008). Quantifying cathepsin S activity in antigen presenting cells using a novel specific substrate. *J Biol Chem*, *283*(52), 36185-36194. https://doi.org/10.1074/jbc.M806500200

Lyman, G. H., Dale, D. C., Friedberg, J., Crawford, J., & Fisher, R. I. (2004). Incidence and predictors of low chemotherapy dose-intensity in aggressive non-Hodgkin's lymphoma: a nationwide study. *J Clin Oncol*, *22*(21), 4302-4311. https://doi.org/10.1200/JCO.2004.03.213

Ma, W., Stroobant, V., Heirman, C., Sun, Z., Thielemans, K., Mulder, A., van der Bruggen, P., & Van den Eynde, B. J. (2019). The Vacuolar Pathway of Long Peptide Cross-Presentation Can Be TAP Dependent. *J Immunol*, *202*(2), 451-459. https://doi.org/10.4049/jimmunol.1800353

Ma, W., Zhang, Y., Vigneron, N., Stroobant, V., Thielemans, K., van der Bruggen, P., & Van den Eynde, B. J. (2016). Long-Peptide Cross-Presentation by Human Dendritic Cells Occurs in Vacuoles by Peptide Exchange on Nascent MHC Class I Molecules. *J Immunol*, *196*(4), 1711-1720. https://doi.org/10.4049/jimmunol.1501574

Maccomb, W. S., & Fletcher, G. H. (1957). Planned combination of surgery and radiation in treatment of advanced primary head and neck cancers. *Am J Roentgenol Radium Ther Nucl Med*, *77*(3), 397-414. https://www.ncbi.nlm.nih.gov/pubmed/13403033

Mach, N., Gillessen, S., Wilson, S. B., Sheehan, C., Mihm, M., & Dranoff, G. (2000). Differences in dendritic cells stimulated in vivo by tumors engineered to secrete granulocyte-macrophage colony-stimulating factor or Flt3-ligand. *Cancer Res*, *60*(12), 3239-3246. https://www.ncbi.nlm.nih.gov/pubmed/10866317

Macon-Lemaitre, L., & Triebel, F. (2005). The negative regulatory function of the lymphocyte-activation gene-3 co-receptor (CD223) on human T cells. *Immunology*, *115*(2), 170-178. https://doi.org/10.1111/j.1365-2567.2005.02145.x

Maeurer, M. J., Gollin, S. M., Storkus, W. J., Swaney, W., Karbach, J., Martin, D., Castelli, C., Salter, R., Knuth, A., & Lotze, M. T. (1996). Tumor escape from immune recognition: loss of HLA-A2 melanoma cell surface expression is associated with a complex rearrangement of the short arm of chromosome 6. *Clin Cancer Res*, *2*(4), 641-652. https://www.ncbi.nlm.nih.gov/pubmed/9816214

Maleckar, J. R., & Sherman, L. A. (1987). The composition of the T cell receptor repertoire in nude mice. *J Immunol*, *138*(11), 3873-3876. https://www.ncbi.nlm.nih.gov/pubmed/2953792

Maleno, I., Aptsiauri, N., Cabrera, T., Gallego, A., Paschen, A., Lopez-Nevot, M. A., & Garrido, F. (2011). Frequent loss of heterozygosity in the beta2-microglobulin region of chromosome 15 in primary human tumors. *Immunogenetics*, *63*(2), 65-71. https://doi.org/10.1007/s00251-010-0494-4

Maleno, I., Lopez-Nevot, M. A., Cabrera, T., Salinero, J., & Garrido, F. (2002). Multiple mechanisms generate HLA class I altered phenotypes in laryngeal carcinomas: high frequency of HLA haplotype loss associated with loss of heterozygosity in chromosome region 6p21. *Cancer Immunol Immunother*, *51*(7), 389-396. https://doi.org/10.1007/s00262-002-0296-0

Maloney, D. G., Grillo-Lopez, A. J., White, C. A., Bodkin, D., Schilder, R. J., Neidhart, J. A., Janakiraman, N., Foon, K. A., Liles, T. M., Dallaire, B. K., Wey, K., Royston, I., Davis, T., & Levy, R. (1997). IDEC-C2B8 (Rituximab) anti-CD20 monoclonal antibody therapy in patients with relapsed low-grade non-Hodgkin's lymphoma. *Blood*, *90*(6), 2188-2195. https://www.ncbi.nlm.nih.gov/pubmed/9310469

Maloney, D. G., Smith, B., & Rose, A. (2002). Rituximab: Mechanism of action and resistance. *Semin Oncol*, *29*(1S2), 2-9. https://doi.org/10.1053/sonc.2002.30156

Manolova, V., Flace, A., Bauer, M., Schwarz, K., Saudan, P., & Bachmann, M. F. (2008). Nanoparticles target distinct dendritic cell populations according to their size. *Eur J Immunol*, *38*(5), 1404-1413. https://doi.org/10.1002/eji.200737984

Manoury, B., Hewitt, E. W., Morrice, N., Dando, P. M., Barrett, A. J., & Watts, C. (1998). An asparaginyl endopeptidase processes a microbial antigen for class II MHC presentation. *Nature*, *396*(6712), 695-699. https://doi.org/10.1038/25379

Mant, A., Chinnery, F., Elliott, T., & Williams, A. P. (2012). The pathway of cross-presentation is influenced by the particle size of phagocytosed antigen. *Immunology*, *136*(2), 163-175. https://doi.org/10.1111/j.1365-2567.2012.03558.x

Mantegazza, A. R., Savina, A., Vermeulen, M., Perez, L., Geffner, J., Hermine, O., Rosenzweig, S. D., Faure, F., & Amigorena, S. (2008). NADPH oxidase controls phagosomal pH and antigen cross-presentation in human dendritic cells. *Blood*, *112*(12), 4712-4722. https://doi.org/10.1182/blood-2008-01-134791

Marblestone, J. G., Edavettal, S. C., Lim, Y., Lim, P., Zuo, X., & Butt, T. R. (2006). Comparison of SUMO fusion technology with traditional gene fusion systems: enhanced expression and solubility with SUMO. *Protein Sci*, *15*(1), 182-189. https://doi.org/10.1110/ps.051812706

Martinez, F. O., & Gordon, S. (2014). The M1 and M2 paradigm of macrophage activation: time for reassessment. *F1000Prime Rep*, *6*, 13. https://doi.org/10.12703/P6-13

Massarelli, E., William, W., Johnson, F., Kies, M., Ferrarotto, R., Guo, M., Feng, L., Lee, J. J., Tran, H., Kim, Y. U., Haymaker, C., Bernatchez, C., Curran, M., Zecchini Barrese, T., Rodriguez Canales, J., Wistuba, I., Li, L., Wang, J., van der Burg, S. H., . . . Glisson, B. (2019). Combining Immune Checkpoint Blockade and Tumor-Specific Vaccine for Patients With Incurable Human Papillomavirus 16-Related Cancer: A Phase 2 Clinical Trial. *JAMA Oncol*, *5*(1), 67-73. https://doi.org/10.1001/jamaoncol.2018.4051

Massiah, M. A., Wright, K. M., & Du, H. (2016). Obtaining Soluble Folded Proteins from Inclusion Bodies Using Sarkosyl, Triton X-100, and CHAPS: Application to LB and M9 Minimal Media. *Curr Protoc Protein Sci*, *84*, 6 13 11-16 13 24. https://doi.org/10.1002/0471140864.ps0613s84

McAdam, A. J., Schweitzer, A. N., & Sharpe, A. H. (1998). The role of B7 co-stimulation in activation and differentiation of CD4+ and CD8+ T cells. *Immunol Rev*, *165*, 231-247. https://doi.org/10.1111/j.1600-065x.1998.tb01242.x

Medina-Echeverz, J., Haile, L. A., Zhao, F., Gamrekelashvili, J., Ma, C., Metais, J. Y., Dunbar, C. E., Kapoor, V., Manns, M. P., Korangy, F., & Greten, T. F. (2014). IFN-gamma regulates survival and function of tumor-induced CD11b+ Gr-1high myeloid derived suppressor cells by modulating the anti-apoptotic molecule Bcl2a1. *Eur J Immunol*, *44*(8), 2457-2467. https://doi.org/10.1002/eji.201444497

Mehta, N. K., Pradhan, R. V., Soleimany, A. P., Moynihan, K. D., Rothschilds, A. M., Momin, N., Rakhra, K., Mata-Fink, J., Bhatia, S. N., Wittrup, K. D., & Irvine, D. J. (2020). Pharmacokinetic tuning of protein-antigen fusions enhances the immunogenicity of T-cell vaccines. *Nat Biomed Eng*, *4*(6), 636-648. https://doi.org/10.1038/s41551-020-0563-4

Mekhaiel, D. N., Czajkowsky, D. M., Andersen, J. T., Shi, J., El-Faham, M., Doenhoff, M., McIntosh, R. S., Sandlie, I., He, J., Hu, J., Shao, Z., & Pleass, R. J. (2011). Polymeric human Fc-fusion proteins with modified effector functions. *Sci Rep*, *1*, 124. https://doi.org/10.1038/srep00124

Mellman, I., & Plutner, H. (1984). Internalization and degradation of macrophage Fc receptors bound to polyvalent immune complexes. *J Cell Biol*, *98*(4), 1170-1177. https://doi.org/10.1083/jcb.98.4.1170

Mempel, T. R., Henrickson, S. E., & Von Andrian, U. H. (2004). T-cell priming by dendritic cells in lymph nodes occurs in three distinct phases. *Nature*, *427*(6970), 154-159. https://doi.org/10.1038/nature02238

Menager, J., Ebstein, F., Oger, R., Hulin, P., Nedellec, S., Duverger, E., Lehmann, A., Kloetzel, P. M., Jotereau, F., & Guilloux, Y. (2014). Cross-presentation of synthetic long peptides by human dendritic cells: a process dependent on ERAD component p97/VCP but Not sec61 and/or Derlin-1. *PLoS One*, *9*(2), e89897. https://doi.org/10.1371/journal.pone.0089897

Meng, L., Mohan, R., Kwok, B. H., Elofsson, M., Sin, N., & Crews, C. M. (1999). Epoxomicin, a potent and selective proteasome inhibitor, exhibits in vivo antiinflammatory activity. *Proc Natl Acad Sci U S A*, *96*(18), 10403-10408. https://doi.org/10.1073/pnas.96.18.10403

Meraz, I. M., Savage, D. J., Segura-Ibarra, V., Li, J., Rhudy, J., Gu, J., & Serda, R. E. (2014). Adjuvant cationic liposomes presenting MPL and IL-12 induce cell death, suppress tumor growth, and alter the cellular phenotype of tumors in a murine model of breast cancer. *Mol Pharm*, *11*(10), 3484-3491. https://doi.org/10.1021/mp5002697

Merzougui, N., Kratzer, R., Saveanu, L., & van Endert, P. (2011). A proteasome-dependent, TAP-independent pathway for cross-presentation of phagocytosed antigen. *EMBO Rep*, *12*(12), 1257-1264. https://doi.org/10.1038/embor.2011.203

Mieog, J. S., van der Hage, J. A., & van de Velde, C. J. (2007). Neoadjuvant chemotherapy for operable breast cancer. *Br J Surg*, *94*(10), 1189-1200. https://doi.org/10.1002/bjs.5894

Mikiewicz, D., Lukasiewicz, N., Zielinski, M., Cecuda-Adamczewska, V., Bierczynska-Krzysik, A., Romanik-Chruscielewska, A., & Kesik-Brodacka, M. (2020). Bacterial expression and characterization of an anti-CD22 single-chain antibody fragment. *Protein Expr Purif*, *170*, 105594. https://doi.org/10.1016/j.pep.2020.105594

Mittal, D., Gubin, M. M., Schreiber, R. D., & Smyth, M. J. (2014). New insights into cancer immunoediting and its three component phases--elimination, equilibrium and escape. *Curr Opin Immunol*, *27*, 16-25. https://doi.org/10.1016/j.coi.2014.01.004

Mizukami, Y., Kono, K., Kawaguchi, Y., Akaike, H., Kamimura, K., Sugai, H., & Fujii, H. (2008). CCL17 and CCL22 chemokines within tumor microenvironment are related to accumulation of Foxp3+ regulatory T cells in gastric cancer. *Int J Cancer*, *122*(10), 2286-2293. https://doi.org/10.1002/ijc.23392

Mobergslien, A., Peng, Q., Vasovic, V., & Sioud, M. (2016). Cancer cell-binding peptide fused Fc domain activates immune effector cells and blocks tumor growth. *Oncotarget*, *7*(46), 75940-75953. https://doi.org/10.18632/oncotarget.12445

Montagne, F., Guisier, F., Venissac, N., & Baste, J. M. (2021). The Role of Surgery in Lung Cancer Treatment: Present Indications and Future Perspectives-State of the Art. *Cancers (Basel)*, *13*(15). https://doi.org/10.3390/cancers13153711

Morita, M., Motoki, K., Akimoto, K., Natori, T., Sakai, T., Sawa, E., Yamaji, K., Koezuka, Y., Kobayashi, E., & Fukushima, H. (1995). Structure-activity relationship of alpha-galactosylceramides against B16-bearing mice. *J Med Chem*, *38*(12), 2176-2187. https://doi.org/10.1021/jm00012a018

Mosmann, T. R., & Coffman, R. L. (1989). TH1 and TH2 cells: different patterns of lymphokine secretion lead to different functional properties. *Annu Rev Immunol*, *7*, 145-173. https://doi.org/10.1146/annurev.iy.07.040189.001045

Mosser, D. M., & Edwards, J. P. (2008). Exploring the full spectrum of macrophage activation. *Nat Rev Immunol*, *8*(12), 958-969. https://doi.org/10.1038/nri2448

Munshi, N. C., Anderson, L. D., Jr., Shah, N., Madduri, D., Berdeja, J., Lonial, S., Raje, N., Lin, Y., Siegel, D., Oriol, A., Moreau, P., Yakoub-Agha, I., Delforge, M., Cavo, M., Einsele, H., Goldschmidt, H., Weisel, K., Rambaldi, A., Reece, D., . . . San-Miguel, J. (2021). Idecabtagene Vicleucel in Relapsed and Refractory Multiple Myeloma. *N Engl J Med*, *384*(8), 705-716. https://doi.org/10.1056/NEJMoa2024850

Murciano-Goroff, Y. R., Warner, A. B., & Wolchok, J. D. (2020). The future of cancer immunotherapy: microenvironment-targeting combinations. *Cell Res*, *30*(6), 507-519. https://doi.org/10.1038/s41422-020-0337-2

Muul, L. M., Spiess, P. J., Director, E. P., & Rosenberg, S. A. (1987). Identification of specific cytolytic immune responses against autologous tumor in humans bearing malignant melanoma. *J Immunol*, *138*(3), 989-995.

Nair-Gupta, P., Baccarini, A., Tung, N., Seyffer, F., Florey, O., Huang, Y., Banerjee, M., Overholtzer, M., Roche, P. A., Tampe, R., Brown, B. D., Amsen, D., Whiteheart, S. W., & Blander, J. M. (2014). TLR signals induce phagosomal MHC-I delivery from the endosomal recycling compartment to allow cross-presentation. *Cell*, *158*(3), 506-521. https://doi.org/10.1016/j.cell.2014.04.054

Natori, T., Morita, M., Akimoto, K., & Koezuka, Y. (1994). Agelasphins, novel antitumor and immunostimulatory cerebrosides from the marine sponge Agelas mauritianus. *Tetrahedron*, *50*(9), 2771-2784. https://doi.org/https://doi.org/10.1016/S0040-4020(01)86991-X

Neefjes, J., Jongsma, M. L., Paul, P., & Bakke, O. (2011). Towards a systems understanding of MHC class I and MHC class II antigen presentation. *Nat Rev Immunol*, *11*(12), 823-836. https://doi.org/10.1038/nri3084

Newman, N. B., Sidhu, M. K., Baby, R., Moss, R. A., Nissenblatt, M. J., Chen, T., Lu, S. E., & Jabbour, S. K. (2016). Long-Term Bone Marrow Suppression During Postoperative Chemotherapy in Rectal Cancer Patients After Preoperative Chemoradiation Therapy. *Int J Radiat Oncol Biol Phys*, *94*(5), 1052-1060. https://doi.org/10.1016/j.ijrobp.2015.12.374

Nicolai, C. J., Wolf, N., Chang, I. C., Kirn, G., Marcus, A., Ndubaku, C. O., McWhirter, S. M., & Raulet, D. H. (2020). NK cells mediate clearance of CD8(+) T cell-resistant tumors in response to STING agonists. *Sci Immunol*, *5*(45). https://doi.org/10.1126/sciimmunol.aaz2738

Nie, Y., Yang, G., Song, Y., Zhao, X., So, C., Liao, J., Wang, L. D., & Yang, C. S. (2001). DNA hypermethylation is a mechanism for loss of expression of the HLA class I genes in human esophageal squamous cell carcinomas. *Carcinogenesis*, *22*(10), 1615-1623. https://doi.org/10.1093/carcin/22.10.1615

Nimmerjahn, F., & Ravetch, J. V. (2005). Divergent immunoglobulin g subclass activity through selective Fc receptor binding. *Science*, *310*(5753), 1510-1512. https://doi.org/10.1126/science.1118948

Novartis. (2019). *BEOVU (prescribing information)*. https://www.accessdata.fda.gov/drugsatfda_docs/label/2019/761125s000lbl.pdf

O'Shaughnessy, J. (2005). Extending survival with chemotherapy in metastatic breast cancer. *The oncologist*, *10*(S3), 20-29.

Odunsi, K., Jungbluth, A. A., Stockert, E., Qian, F., Gnjatic, S., Tammela, J., Intengan, M., Beck, A., Keitz, B., Santiago, D., Williamson, B., Scanlan, M. J., Ritter, G., Chen, Y. T., Driscoll, D., Sood, A., Lele, S., & Old, L. J. (2003). NY-ESO-1 and LAGE-1 cancer-testis antigens are potential targets for immunotherapy in epithelial ovarian cancer. *Cancer Res*, *63*(18), 6076-6083. https://www.ncbi.nlm.nih.gov/pubmed/14522938

Okita, R., Maeda, A., Shimizu, K., Nojima, Y., Saisho, S., & Nakata, M. (2017). PD-L1 overexpression is partially regulated by EGFR/HER2 signaling and associated with poor prognosis in patients with non-small-cell lung cancer. *Cancer Immunol Immunother*, *66*(7), 865-876. https://doi.org/10.1007/s00262-017-1986-y

Oldenborg, P. A., Zheleznyak, A., Fang, Y. F., Lagenaur, C. F., Gresham, H. D., & Lindberg, F. P. (2000). Role of CD47 as a marker of self on red blood cells. *Science*, *288*(5473), 2051-2054. https://doi.org/10.1126/science.288.5473.2051

Onodi, F., Maherzi-Mechalikh, C., Mougel, A., Ben Hamouda, N., Taboas, C., Gueugnon, F., Tran, T., Nozach, H., Marcon, E., Gey, A., Terme, M., Bouzidi, A., Maillere, B., Kerzerho, J., Tartour, E., & Tanchot, C. (2018). High Therapeutic Efficacy of a New Survivin LSP-Cancer Vaccine Containing CD4(+) and CD8(+) T-Cell Epitopes. *Front Oncol*, *8*, 517. https://doi.org/10.3389/fonc.2018.00517

Osborn, M. J., McElmurry, R. T., Lees, C. J., DeFeo, A. P., Chen, Z. Y., Kay, M. A., Naldini, L., Freeman, G., Tolar, J., & Blazar, B. R. (2011). Minicircle DNA-based gene therapy coupled with immune modulation permits long-term expression of alpha-L-iduronidase in mice with mucopolysaccharidosis type I. *Mol Ther*, *19*(3), 450-460. https://doi.org/10.1038/mt.2010.249

Ostrand-Rosenberg, S., & Sinha, P. (2009). Myeloid-derived suppressor cells: linking inflammation and cancer. *J Immunol*, *182*(8), 4499-4506. https://doi.org/10.4049/jimmunol.0802740

Ott, P. A., Hu, Z., Keskin, D. B., Shukla, S. A., Sun, J., Bozym, D. J., Zhang, W., Luoma, A., Giobbie-Hurder, A., Peter, L., Chen, C., Olive, O., Carter, T. A., Li, S., Lieb, D. J., Eisenhaure, T., Gjini, E., Stevens, J., Lane, W. J., . . . Wu, C. J. (2017). An immunogenic personal neoantigen vaccine for patients with melanoma. *Nature*, *547*(7662), 217-221. https://doi.org/10.1038/nature22991

Outzen, H. C., Custer, R. P., Eaton, G. J., & Prehn, R. T. (1975). Spontaneous and induced tumor incidence in germfree "nude" mice. *J Reticuloendothel Soc*, *17*(1), 1-9. https://www.ncbi.nlm.nih.gov/pubmed/1089790

Pagel, J. M., Lin, Y., Hedin, N., Pantelias, A., Axworthy, D., Stone, D., Hamlin, D. K., Wilbur, D. S., & Press, O. W. (2006). Comparison of a tetravalent single-chain antibody-streptavidin fusion protein and an antibody-streptavidin chemical conjugate for pretargeted anti-CD20 radioimmunotherapy of B-cell lymphomas. *Blood*, *108*(1), 328-336. https://doi.org/10.1182/blood-2005-11-4327

Palmer, J. T., Rasnick, D., Klaus, J. L., & Bromme, D. (1995). Vinyl sulfones as mechanism-based cysteine protease inhibitors. *J Med Chem*, *38*(17), 3193-3196. https://doi.org/10.1021/jm00017a002

Palmowski, M. J., Gileadi, U., Salio, M., Gallimore, A., Millrain, M., James, E., Addey, C., Scott, D., Dyson, J., Simpson, E., & Cerundolo, V. (2006). Role of immunoproteasomes in cross-presentation. *J Immunol*, *177*(2), 983-990. https://doi.org/10.4049/jimmunol.177.2.983

Pan, Y., Yu, Y., Wang, X., & Zhang, T. (2020). Tumor-Associated Macrophages in Tumor Immunity. *Front Immunol*, *11*, 583084. https://doi.org/10.3389/fimmu.2020.583084

Pantano, F., Berti, P., Guida, F. M., Perrone, G., Vincenzi, B., Amato, M. M., Righi, D., Dell'aquila, E., Graziano, F., Catalano, V., Caricato, M., Rizzo, S., Muda, A. O., Russo, A., Tonini, G., & Santini, D. (2013). The role of macrophages polarization in predicting prognosis of radically resected gastric cancer patients. *J Cell Mol Med*, *17*(11), 1415-1421. https://doi.org/10.1111/jcmm.12109

Pardo, J., Balkow, S., Anel, A., & Simon, M. M. (2002). Granzymes are essential for natural killer cell-mediated and perf-facilitated tumor control. *Eur J Immunol*, *32*(10), 2881-2887. https://doi.org/10.1002/1521-4141(2002010)32:10<2881::AID-IMMU2881>3.0.CO;2-K

Paris, F., Fuks, Z., Kang, A., Capodieci, P., Juan, G., Ehleiter, D., Haimovitz-Friedman, A., Cordon-Cardo, C., & Kolesnick, R. (2001). Endothelial apoptosis as the primary lesion initiating intestinal radiation damage in mice. *Science*, *293*(5528), 293-297. https://doi.org/10.1126/science.1060191

Paz, I., Sachse, M., Dupont, N., Mounier, J., Cederfur, C., Enninga, J., Leffler, H., Poirier, F., Prevost, M. C., Lafont, F., & Sansonetti, P. (2010). Galectin-3, a marker for vacuole lysis by invasive pathogens. *Cell Microbiol*, *12*(4), 530-544. https://doi.org/10.1111/j.1462-5822.2009.01415.x

Pedersen, M. H., Hood, B. L., Beck, H. C., Conrads, T. P., Ditzel, H. J., & Leth-Larsen, R. (2017). Downregulation of antigen presentation-associated pathway proteins is linked to poor outcome in triple-negative breast cancer patient tumors. *Oncoimmunology*, *6*(5), e1305531. https://doi.org/10.1080/2162402X.2017.1305531

Pepinsky, R. B. (1991). Selective precipitation of proteins from guanidine hydrochloride-containing solutions with ethanol. *Anal Biochem*, *195*(1), 177-181. https://doi.org/10.1016/0003-2697(91)90315-k

Perinelli, D. R., Cespi, M., Lorusso, N., Palmieri, G. F., Bonacucina, G., & Blasi, P. (2020). Surfactant Self-Assembling and Critical Micelle Concentration: One Approach Fits All? *Langmuir*, *36*(21), 5745-5753. https://doi.org/10.1021/acs.langmuir.0c00420

Peters, P. J., Borst, J., Oorschot, V., Fukuda, M., Krahenbuhl, O., Tschopp, J., Slot, J. W., & Geuze, H. J. (1991). Cytotoxic T lymphocyte granules are secretory lysosomes, containing both perforin and granzymes. *J Exp Med*, *173*(5), 1099-1109. https://doi.org/10.1084/jem.173.5.1099

Petrillo, M., Zannoni, G. F., Martinelli, E., Pedone Anchora, L., Ferrandina, G., Tropeano, G., Fagotti, A., & Scambia, G. (2015). Polarisation of Tumor-Associated Macrophages toward M2 Phenotype Correlates with Poor Response to Chemoradiation and Reduced Survival in Patients with Locally Advanced Cervical Cancer. *PLoS One*, *10*(9), e0136654. https://doi.org/10.1371/journal.pone.0136654

Pooley, J. L., Heath, W. R., & Shortman, K. (2001). Cutting edge: intravenous soluble antigen is presented to CD4 T cells by CD8- dendritic cells, but cross-presented to CD8 T cells by CD8+ dendritic cells. *J Immunol*, *166*(9), 5327-5330. https://doi.org/10.4049/jimmunol.166.9.5327

Porgador, A., Yewdell, J. W., Deng, Y., Bennink, J. R., & Germain, R. N. (1997). Localization, quantitation, and in situ detection of specific peptide-MHC class I complexes using a monoclonal antibody. *Immunity*, *6*(6), 715-726. https://doi.org/10.1016/s1074-7613(00)80447-1

Pouget, J. P., Frelon, S., Ravanat, J. L., Testard, I., Odin, F., & Cadet, J. (2002). Formation of modified DNA bases in cells exposed either to gamma radiation or to high-LET particles. *Radiat Res*, *157*(5), 589-595. https://doi.org/10.1667/0033-7587(2002)157[0589:fomdbi]2.0.co;2

Pouniotis, D. S., Apostolopoulos, V., & Pietersz, G. A. (2006). Penetratin tandemly linked to a CTL peptide induces anti-tumour T-cell responses via a cross-presentation pathway. *Immunology*, *117*(3), 329-339. https://doi.org/10.1111/j.1365-2567.2005.02304.x

Powell, K., Marquart, J., Olivier, T., & Prasad, V. (2022). The role of surgery in metastatic cancer: the case for a pragmatic tumor-agnostic randomized trial. *Future Oncol*, *18*(36), 3955-3959. https://doi.org/10.2217/fon-2022-0840

Prato, S., Maxwell, T., Pinzon-Charry, A., Schmidt, C. W., Corradin, G., & Lopez, J. A. (2005). MHC class I-restricted exogenous presentation of a synthetic 102-mer malaria vaccine polypeptide. *Eur J Immunol*, *35*(3), 681-689. https://doi.org/10.1002/eji.200425771

Propper, D. J., Chao, D., Braybrooke, J. P., Bahl, P., Thavasu, P., Balkwill, F., Turley, H., Dobbs, N., Gatter, K., Talbot, D. C., Harris, A. L., & Ganesan, T. S. (2003). Low-dose IFN-gamma induces tumor MHC expression in metastatic malignant melanoma. *Clin Cancer Res*, *9*(1), 84-92. https://www.ncbi.nlm.nih.gov/pubmed/12538455

Przepiorka, D., Ko, C. W., Deisseroth, A., Yancey, C. L., Candau-Chacon, R., Chiu, H. J., Gehrke, B. J., Gomez-Broughton, C., Kane, R. C., Kirshner, S., Mehrotra, N., Ricks, T. K., Schmiel, D., Song, P., Zhao, P., Zhou, Q., Farrell, A. T., & Pazdur, R. (2015). FDA Approval: Blinatumomab. *Clin Cancer Res*, *21*(18), 4035-4039. https://doi.org/10.1158/1078-0432.CCR-15-0612

Pulendran, B., Smith, J. L., Caspary, G., Brasel, K., Pettit, D., Maraskovsky, E., & Maliszewski, C. R. (1999). Distinct dendritic cell subsets differentially regulate the class of immune response in vivo. *Proc Natl Acad Sci U S A*, *96*(3), 1036-1041. https://doi.org/10.1073/pnas.96.3.1036

Pyzik, M., Sand, K. M. K., Hubbard, J. J., Andersen, J. T., Sandlie, I., & Blumberg, R. S. (2019). The Neonatal Fc Receptor (FcRn): A Misnomer? *Front Immunol*, *10*, 1540. https://doi.org/10.3389/fimmu.2019.01540

Qiao, S. W., Kobayashi, K., Johansen, F. E., Sollid, L. M., Andersen, J. T., Milford, E., Roopenian, D. C., Lencer, W. I., & Blumberg, R. S. (2008). Dependence of antibody-mediated presentation of antigen on FcRn. *Proc Natl Acad Sci U S A*, *105*(27), 9337-9342. https://doi.org/10.1073/pnas.0801717105

Quayle, S. N., Girgis, N., Thapa, D. R., Merazga, Z., Kemp, M. M., Histed, A., Zhao, F., Moreta, M., Ruthardt, P., Hulot, S., Nelson, A., Kraemer, L. D., Beal, D. R., Witt, L., Ryabin, J., Soriano, J., Haydock, M., Spaulding, E., Ross, J. F., . . . Simcox, M. E. (2020). CUE-101, a Novel E7-pHLA-IL2-Fc Fusion Protein, Enhances Tumor Antigen-Specific T-Cell Activation for the Treatment of HPV16-Driven Malignancies. *Clin Cancer Res*, *26*(8), 1953-1964. https://doi.org/10.1158/1078-0432.CCR-19-3354

Quesada, J. R., Hersh, E. M., Manning, J., Reuben, J., Keating, M., Schnipper, E., Itri, L., & Gutterman, J. U. (1986). Treatment of hairy cell leukemia with recombinant alpha-interferon. *Blood*, *68*(2), 493-497. https://www.ncbi.nlm.nih.gov/pubmed/3730612

Quesada, J. R., Reuben, J., Manning, J. T., Hersh, E. M., & Gutterman, J. U. (1984). Alpha interferon for induction of remission in hairy-cell leukemia. *N Engl J Med*, *310*(1), 15-18. https://doi.org/10.1056/NEJM198401053100104

Qureshi, O. S., Rowley, T. F., Junker, F., Peters, S. J., Crilly, S., Compson, J., Eddleston, A., Bjorkelund, H., Greenslade, K., Parkinson, M., Davies, N. L., Griffin, R., Pither, T. L., Cain, K., Christodoulou, L., Staelens, L., Ward, E., Tibbitts, J., Kiessling, A., . . . Humphreys, D. P. (2017). Multivalent Fcgamma-receptor engagement by a hexameric Fc-fusion protein triggers Fcgamma-receptor internalisation and modulation of Fcgamma-receptor functions. *Sci Rep*, *7*(1), 17049. https://doi.org/10.1038/s41598-017-17255-8

Raber, P., Ochoa, A. C., & Rodriguez, P. C. (2012). Metabolism of L-arginine by myeloid-derived suppressor cells in cancer: mechanisms of T cell suppression and therapeutic perspectives. *Immunol Invest*, *41*(6-7), 614-634. https://doi.org/10.3109/08820139.2012.680634

Raber, P. L., Thevenot, P., Sierra, R., Wyczechowska, D., Halle, D., Ramirez, M. E., Ochoa, A. C., Fletcher, M., Velasco, C., Wilk, A., Reiss, K., & Rodriguez, P. C. (2014). Subpopulations of myeloid-derived suppressor cells impair T cell responses through independent nitric oxide-related pathways. *Int J Cancer*, *134*(12), 2853-2864. https://doi.org/10.1002/ijc.28622

Rabu, C., Rangan, L., Florenceau, L., Fortun, A., Charpentier, M., Dupre, E., Paolini, L., Beauvillain, C., Dupel, E., Latouche, J. B., Adotevi, O., Labarriere, N., & Lang, F. (2019). Cancer vaccines: designing artificial synthetic long peptides to improve presentation of class I and class II T cell epitopes by dendritic cells. *Oncoimmunology*, *8*(4), e1560919. https://doi.org/10.1080/2162402X.2018.1560919

Radosavljevic, M., Cuillerier, B., Wilson, M. J., Clement, O., Wicker, S., Gilfillan, S., Beck, S., Trowsdale, J., & Bahram, S. (2002). A cluster of ten novel MHC class I related genes on human chromosome 6q24.2-q25.3. *Genomics*, *79*(1), 114-123. https://doi.org/10.1006/geno.2001.6673

Rafiq, K., Bergtold, A., & Clynes, R. (2002). Immune complex-mediated antigen presentation induces tumor immunity. *J Clin Invest*, *110*(1), 71-79. https://doi.org/10.1172/JCI15640

Ramos-Casals, M., Brahmer, J. R., Callahan, M. K., Flores-Chavez, A., Keegan, N., Khamashta, M. A., Lambotte, O., Mariette, X., Prat, A., & Suarez-Almazor, M. E. (2020). Immune-related adverse events of checkpoint inhibitors. *Nat Rev Dis Primers*, *6*(1), 38. https://doi.org/10.1038/s41572-020-0160-6

Ramos, C. A., Rouce, R., Robertson, C. S., Reyna, A., Narala, N., Vyas, G., Mehta, B., Zhang, H., Dakhova, O., Carrum, G., Kamble, R. T., Gee, A. P., Mei, Z., Wu, M. F., Liu, H., Grilley, B., Rooney, C. M., Heslop, H. E., Brenner, M. K., . . . Dotti, G. (2018). In Vivo Fate and Activity of Second- versus Third-Generation CD19-Specific CAR-T Cells in B Cell Non-Hodgkin's Lymphomas. *Mol Ther*, *26*(12), 2727-2737. https://doi.org/10.1016/j.ymthe.2018.09.009

Ratikan, J. A., Sayre, J. W., & Schaue, D. (2013). Chloroquine engages the immune system to eradicate irradiated breast tumors in mice. *Int J Radiat Oncol Biol Phys*, *87*(4), 761-768. https://doi.org/10.1016/j.ijrobp.2013.07.024

Rauen, J., Kreer, C., Paillard, A., van Duikeren, S., Benckhuijsen, W. E., Camps, M. G., Valentijn, A. R., Ossendorp, F., Drijfhout, J. W., Arens, R., & Burgdorf, S. (2014). Enhanced cross-presentation and improved CD8+ T cell responses after mannosylation of synthetic long peptides in mice. *PLoS One*, *9*(8), e103755. https://doi.org/10.1371/journal.pone.0103755

Ravetch, J. V., & Bolland, S. (2001). IgG Fc receptors. *Annu Rev Immunol*, *19*, 275-290. https://doi.org/10.1146/annurev.immunol.19.1.275

Reff, M. E., Carner, K., Chambers, K. S., Chinn, P. C., Leonard, J. E., Raab, R., Newman, R. A., Hanna, N., & Anderson, D. R. (1994). Depletion of B cells in vivo by a chimeric mouse human monoclonal antibody to CD20. *Blood*, *83*(2), 435-445. https://www.ncbi.nlm.nih.gov/pubmed/7506951

Regeneron Pharmaceuticals. (2012). *ZALTRAP (Prescribing Information)*. https://www.accessdata.fda.gov/drugsatfda_docs/label/2012/125418s000lbl.pdf

Regnault, A., Lankar, D., Lacabanne, V., Rodriguez, A., Thery, C., Rescigno, M., Saito, T., Verbeek, S., Bonnerot, C., Ricciardi-Castagnoli, P., & Amigorena, S. (1999). Fcgamma receptor-mediated induction of dendritic cell maturation and major histocompatibility complex class I-restricted antigen presentation after immune complex internalization. *J Exp Med*, *189*(2), 371-380. https://doi.org/10.1084/jem.189.2.371

Rejman, J., Oberle, V., Zuhorn, I. S., & Hoekstra, D. (2004). Size-dependent internalization of particles via the pathways of clathrin- and caveolae-mediated endocytosis. *Biochem J*, *377*(Pt 1), 159-169. https://doi.org/10.1042/BJ20031253

Ren, L., Yu, Y., Wang, L., Zhu, Z., Lu, R., & Yao, Z. (2016). Hypoxia-induced CCL28 promotes recruitment of regulatory T cells and tumor growth in liver cancer. *Oncotarget*, *7*(46), 75763-75773. https://doi.org/10.18632/oncotarget.12409

Rennick, J. J., Johnston, A. P. R., & Parton, R. G. (2021). Key principles and methods for studying the endocytosis of biological and nanoparticle therapeutics. *Nat Nanotechnol*, *16*(3), 266-276. https://doi.org/10.1038/s41565-021-00858-8

Riese, R. J., & Chapman, H. A. (2000). Cathepsins and compartmentalization in antigen presentation. *Curr Opin Immunol*, *12*(1), 107-113. https://doi.org/10.1016/s0952-7915(99)00058-8

Riese, R. J., Wolf, P. R., Bromme, D., Natkin, L. R., Villadangos, J. A., Ploegh, H. L., & Chapman, H. A. (1996). Essential role for cathepsin S in MHC class II-associated invariant chain processing and peptide loading. *Immunity*, *4*(4), 357-366. https://doi.org/10.1016/s1074-7613(00)80249-6

Rockwell, S., Dobrucki, I. T., Kim, E. Y., Marrison, S. T., & Vu, V. T. (2009). Hypoxia and radiation therapy: past history, ongoing research, and future promise. *Curr Mol Med*, *9*(4), 442-458. https://doi.org/10.2174/156652409788167087

Rodolfo, M., Luksch, R., Stockert, E., Chen, Y. T., Collini, P., Ranzani, T., Lombardo, C., Dalerba, P., Rivoltini, L., Arienti, F., Fossati-Bellani, F., Old, L. J., Parmiani, G., & Castelli, C. (2003). Antigen-specific immunity in neuroblastoma patients: antibody and T-cell recognition of NY-ESO-1 tumor antigen. *Cancer Res*, *63*(20), 6948-6955. https://www.ncbi.nlm.nih.gov/pubmed/14583496

Rojas, L. A., Sethna, Z., Soares, K. C., Olcese, C., Pang, N., Patterson, E., Lihm, J., Ceglia, N., Guasp, P., Chu, A., Yu, R., Chandra, A. K., Waters, T., Ruan, J., Amisaki, M., Zebboudj, A., Odgerel, Z., Payne, G., Derhovanessian, E., . . . Balachandran, V. P. (2023). Personalized RNA neoantigen vaccines stimulate T cells in pancreatic cancer. *Nature*, *618*(7963), 144-150. https://doi.org/10.1038/s41586-023-06063-y

Romee, R., Foley, B., Lenvik, T., Wang, Y., Zhang, B., Ankarlo, D., Luo, X., Cooley, S., Verneris, M., Walcheck, B., & Miller, J. (2013). NK cell CD16 surface expression and function is regulated by a disintegrin and metalloprotease-17 (ADAM17). *Blood*, *121*(18), 3599-3608. https://doi.org/10.1182/blood-2012-04-425397

Romero, I., Garrido, C., Algarra, I., Chamorro, V., Collado, A., Garrido, F., & Garcia-Lora, A. M. (2018). MHC Intratumoral Heterogeneity May Predict Cancer Progression and Response to Immunotherapy. *Front Immunol*, *9*, 102. https://doi.org/10.3389/fimmu.2018.00102

Roopenian, D. C., Christianson, G. J., Sproule, T. J., Brown, A. C., Akilesh, S., Jung, N., Petkova, S., Avanessian, L., Choi, E. Y., Shaffer, D. J., Eden, P. A., & Anderson, C. L. (2003). The MHC class I-like IgG receptor controls perinatal IgG transport, IgG homeostasis, and fate of IgG-Fc-coupled drugs. *J Immunol*, *170*(7), 3528-3533. https://doi.org/10.4049/jimmunol.170.7.3528

Rosalia, R. A., Quakkelaar, E. D., Redeker, A., Khan, S., Camps, M., Drijfhout, J. W., Silva, A. L., Jiskoot, W., van Hall, T., van Veelen, P. A., Janssen, G., Franken, K., Cruz, L. J., Tromp, A., Oostendorp, J., van der Burg, S. H., Ossendorp, F., & Melief, C. J. (2013). Dendritic cells process synthetic long peptides better than whole protein, improving antigen presentation and T-cell activation. *Eur J Immunol*, *43*(10), 2554-2565. https://doi.org/10.1002/eji.201343324

Rosenberg, S. A., Lotze, M. T., Muul, L. M., Leitman, S., Chang, A. E., Ettinghausen, S. E., Matory, Y. L., Skibber, J. M., Shiloni, E., Vetto, J. T., & et al. (1985). Observations on the systemic administration of autologous lymphokine-activated killer cells and recombinant interleukin-2 to patients with metastatic cancer. *N Engl J Med*, *313*(23), 1485-1492. https://doi.org/10.1056/NEJM198512053132327

Rosenberg, S. A., Lotze, M. T., Yang, J. C., Aebersold, P. M., Linehan, W. M., Seipp, C. A., & White, D. E. (1989). Experience with the use of high-dose interleukin-2 in the treatment of 652 cancer patients. *Ann Surg*, *210*(4), 474-484; discussion 484-475. https://doi.org/10.1097/00000658-198910000-00008

Rosenberg, S. A., Yang, J. C., Sherry, R. M., Kammula, U. S., Hughes, M. S., Phan, G. Q., Citrin, D. E., Restifo, N. P., Robbins, P. F., Wunderlich, J. R., Morton, K. E., Laurencot, C. M., Steinberg, S. M., White, D. E., & Dudley, M. E. (2011). Durable complete responses in heavily pretreated patients with metastatic melanoma using T-cell transfer immunotherapy. *Clin Cancer Res*, *17*(13), 4550-4557. https://doi.org/10.1158/1078-0432.CCR-11-0116

Rossi, M., Carboni, S., Di Berardino-Besson, W., Riva, E., Santiago-Raber, M. L., Belnoue, E., & Derouazi, M. (2021). STING Agonist Combined to a Protein-Based Cancer Vaccine Potentiates Peripheral and Intra-Tumoral T Cell Immunity. *Front Immunol*, *12*, 695056. https://doi.org/10.3389/fimmu.2021.695056

Rotzschke, O., Falk, K., Stevanovic, S., Jung, G., Walden, P., & Rammensee, H. G. (1991). Exact prediction of a natural T cell epitope. *Eur J Immunol*, *21*(11), 2891-2894. https://doi.org/10.1002/eji.1830211136

Rowley, T. F., Peters, S. J., Aylott, M., Griffin, R., Davies, N. L., Healy, L. J., Cutler, R. M., Eddleston, A., Pither, T. L., Sopp, J. M., Zaccheo, O., Fossati, G., Cain, K., Ventom, A. M., Hailu, H., Ward, E. J., Sherington, J., Brennan, F. R., Fallah-Arani, F., & Humphreys, D. P. (2018). Engineered

hexavalent Fc proteins with enhanced Fc-gamma receptor avidity provide insights into immune-complex interactions. *Commun Biol*, *1*, 146. https://doi.org/10.1038/s42003-018-0149-9

Rubens, R. D., Sexton, S., Tong, D., Winter, P. J., Knight, R. K., & Hayward, J. L. (1980). Combined chemotherapy and radiotherapy for locally advanced breast cancer. *Eur J Cancer (1965)*, *16*(3), 351-356. https://doi.org/10.1016/0014-2964(80)90352-7

Ruckrich, T., Brandenburg, J., Cansier, A., Muller, M., Stevanovic, S., Schilling, K., Wiederanders, B., Beck, A., Melms, A., Reich, M., Driessen, C., & Kalbacher, H. (2006). Specificity of human cathepsin S determined by processing of peptide substrates and MHC class II-associated invariant chain. *Biol Chem*, *387*(10-11), 1503-1511. https://doi.org/10.1515/BC.2006.188

Saccani, A., Schioppa, T., Porta, C., Biswas, S. K., Nebuloni, M., Vago, L., Bottazzi, B., Colombo, M. P., Mantovani, A., & Sica, A. (2006). p50 nuclear factor-kappaB overexpression in tumor-associated macrophages inhibits M1 inflammatory responses and antitumor resistance. *Cancer Res*, *66*(23), 11432-11440. https://doi.org/10.1158/0008-5472.CAN-06-1867

Sadat Tabatabaei Mirakabad, F., Nejati-Koshki, K., Akbarzadeh, A., Yamchi, M. R., Milani, M., Zarghami, N., Zeighamian, V., Rahimzadeh, A., Alimohammadi, S., Hanifehpour, Y., & Joo, S. W. (2014). PLGA-based nanoparticles as cancer drug delivery systems. *Asian Pac J Cancer Prev*, *15*(2), 517-535. https://doi.org/10.7314/apjcp.2014.15.2.517

Saeland, E., van Vliet, S. J., Backstrom, M., van den Berg, V. C., Geijtenbeek, T. B., Meijer, G. A., & van Kooyk, Y. (2007). The C-type lectin MGL expressed by dendritic cells detects glycan changes on MUC1 in colon carcinoma. *Cancer Immunol Immunother*, *56*(8), 1225-1236. https://doi.org/10.1007/s00262-006-0274-z

Sakai, H., Moriura, Y., Notomi, T., Kawawaki, J., Ohnishi, K., & Kuno, M. (2010). Phospholipase C-dependent Ca2+-sensing pathways leading to endocytosis and inhibition of the plasma membrane vacuolar H+-ATPase in osteoclasts. *Am J Physiol Cell Physiol*, *299*(3), C570-578. https://doi.org/10.1152/ajpcell.00486.2009

Sarkar, K., Kruhlak, M. J., Erlandsen, S. L., & Shaw, S. (2005). Selective inhibition by rottlerin of macropinocytosis in monocyte-derived dendritic cells. *Immunology*, *116*(4), 513-524. https://doi.org/10.1111/j.1365-2567.2005.02253.x

Sato, E., Olson, S. H., Ahn, J., Bundy, B., Nishikawa, H., Qian, F., Jungbluth, A. A., Frosina, D., Gnjatic, S., Ambrosone, C., Kepner, J., Odunsi, T., Ritter, G., Lele, S., Chen, Y. T., Ohtani, H., Old, L. J., & Odunsi, K. (2005). Intraepithelial CD8+ tumor-infiltrating lymphocytes and a high CD8+/regulatory T cell ratio are associated with favorable prognosis in ovarian cancer. *Proc Natl Acad Sci U S A*, *102*(51), 18538-18543. https://doi.org/10.1073/pnas.0509182102

Savarino, A., Boelaert, J. R., Cassone, A., Majori, G., & Cauda, R. (2003). Effects of chloroquine on viral infections: an old drug against today's diseases? *Lancet Infect Dis*, *3*(11), 722-727. https://doi.org/10.1016/s1473-3099(03)00806-5

Saveanu, L., Carroll, O., Lindo, V., Del Val, M., Lopez, D., Lepelletier, Y., Greer, F., Schomburg, L., Fruci, D., Niedermann, G., & van Endert, P. M. (2005). Concerted peptide trimming by human ERAP1 and ERAP2 aminopeptidase complexes in the endoplasmic reticulum. *Nat Immunol*, *6*(7), 689-697. https://doi.org/10.1038/ni1208

Saveanu, L., Carroll, O., Weimershaus, M., Guermonprez, P., Firat, E., Lindo, V., Greer, F., Davoust, J., Kratzer, R., Keller, S. R., Niedermann, G., & van Endert, P. (2009). IRAP identifies an endosomal compartment required for MHC class I cross-presentation. *Science*, *325*(5937), 213-217. https://doi.org/10.1126/science.1172845

Savina, A., Jancic, C., Hugues, S., Guermonprez, P., Vargas, P., Moura, I. C., Lennon-Dumenil, A. M., Seabra, M. C., Raposo, G., & Amigorena, S. (2006). NOX2 controls phagosomal pH to regulate antigen processing during crosspresentation by dendritic cells. *Cell*, *126*(1), 205-218. https://doi.org/10.1016/j.cell.2006.05.035

Savina, A., Peres, A., Cebrian, I., Carmo, N., Moita, C., Hacohen, N., Moita, L. F., & Amigorena, S. (2009). The small GTPase Rac2 controls phagosomal alkalinization and antigen crosspresentation selectively in CD8(+) dendritic cells. *Immunity*, *30*(4), 544-555. https://doi.org/10.1016/j.immuni.2009.01.013

Savoldo, B., Ramos, C. A., Liu, E., Mims, M. P., Keating, M. J., Carrum, G., Kamble, R. T., Bollard, C. M., Gee, A. P., Mei, Z., Liu, H., Grilley, B., Rooney, C. M., Heslop, H. E., Brenner, M. K., & Dotti, G. (2011). CD28 costimulation improves expansion and persistence of chimeric antigen receptor-modified T cells in lymphoma patients. *J Clin Invest*, *121*(5), 1822-1826. https://doi.org/10.1172/JCI46110

Schaue, D., Ratikan, J. A., Iwamoto, K. S., & McBride, W. H. (2012). Maximizing tumor immunity with fractionated radiation. *Int J Radiat Oncol Biol Phys*, *83*(4), 1306-1310. https://doi.org/10.1016/j.ijrobp.2011.09.049

Schietinger, A., Philip, M., Krisnawan, V. E., Chiu, E. Y., Delrow, J. J., Basom, R. S., Lauer, P., Brockstedt, D. G., Knoblaugh, S. E., Hammerling, G. J., Schell, T. D., Garbi, N., & Greenberg, P. D. (2016). Tumor-Specific T Cell Dysfunction Is a Dynamic Antigen-Driven Differentiation Program Initiated Early during Tumorigenesis. *Immunity*, *45*(2), 389-401. https://doi.org/10.1016/j.immuni.2016.07.011

Schreibelt, G., Klinkenberg, L. J., Cruz, L. J., Tacken, P. J., Tel, J., Kreutz, M., Adema, G. J., Brown, G. D., Figdor, C. G., & de Vries, I. J. (2012). The C-type lectin receptor CLEC9A mediates antigen uptake and (cross-)presentation by human blood BDCA3+ myeloid dendritic cells. *Blood*, *119*(10), 2284-2292. https://doi.org/10.1182/blood-2011-08-373944

Schrors, B., Lubcke, S., Lennerz, V., Fatho, M., Bicker, A., Wolfel, C., Derigs, P., Hankeln, T., Schadendorf, D., Paschen, A., & Wolfel, T. (2017). HLA class I loss in metachronous metastases prevents continuous T cell recognition of mutated neoantigens in a human melanoma model. *Oncotarget*, *8*(17), 28312-28327. https://doi.org/10.18632/oncotarget.16048

Schumacher, T. N., Heemels, M. T., Neefjes, J. J., Kast, W. M., Melief, C. J., & Ploegh, H. L. (1990). Direct binding of peptide to empty MHC class I molecules on intact cells and in vitro. *Cell*, *62*(3), 563-567. https://doi.org/10.1016/0092-8674(90)90020-f

Schuster, S. J., Bishop, M. R., Tam, C. S., Waller, E. K., Borchmann, P., McGuirk, J. P., Jaeger, U., Jaglowski, S., Andreadis, C., Westin, J. R., Fleury, I., Bachanova, V., Foley, S. R., Ho, P. J., Mielke, S., Magenau, J. M., Holte, H., Van Besien, K., Kersten, M. J., . . . Maziarz, R. T. (2017). Primary Analysis of Juliet: A Global, Pivotal, Phase 2 Trial of CTL019 in Adult Patients with Relapsed or Refractory Diffuse Large B-Cell Lymphoma. *Blood*, *130*(Supplement 1), 577-577. https://doi.org/10.1182/blood.V130.Suppl_1.577.577

Schuster, S. J., Bishop, M. R., Tam, C. S., Waller, E. K., Borchmann, P., McGuirk, J. P., Jager, U., Jaglowski, S., Andreadis, C., Westin, J. R., Fleury, I., Bachanova, V., Foley, S. R., Ho, P. J., Mielke, S., Magenau, J. M., Holte, H., Pantano, S., Pacaud, L. B., . . . Investigators, J. (2019). Tisagenlecleucel in Adult Relapsed or Refractory Diffuse Large B-Cell Lymphoma. *N Engl J Med*, *380*(1), 45-56. https://doi.org/10.1056/NEJMoa1804980

Schwartz, R. H. (2003). T cell anergy. *Annu Rev Immunol*, *21*, 305-334. https://doi.org/10.1146/annurev.immunol.21.120601.141110

Screpanti, V., Wallin, R. P., Ljunggren, H. G., & Grandien, A. (2001). A central role for death receptor-mediated apoptosis in the rejection of tumors by NK cells. *J Immunol*, *167*(4), 2068-2073. https://doi.org/10.4049/jimmunol.167.4.2068

Sebzda, E., Wallace, V. A., Mayer, J., Yeung, R. S., Mak, T. W., & Ohashi, P. S. (1994). Positive and negative thymocyte selection induced by different concentrations of a single peptide. *Science*, *263*(5153), 1615-1618. https://doi.org/10.1126/science.8128249

Segars, J. H., Nagata, T., Bours, V., Medin, J. A., Franzoso, G., Blanco, J. C., Drew, P. D., Becker, K. G., An, J., Tang, T., & et al. (1993). Retinoic acid induction of major histocompatibility complex class I genes in NTera-2 embryonal carcinoma cells involves induction of NF-kappa B (p50-p65) and retinoic acid receptor beta-retinoid X receptor beta heterodimers. *Mol Cell Biol*, *13*(10), 6157-6169. https://doi.org/10.1128/mcb.13.10.6157-6169.1993

Segura, E., Durand, M., & Amigorena, S. (2013). Similar antigen cross-presentation capacity and phagocytic functions in all freshly isolated human lymphoid organ-resident dendritic cells. *J Exp Med*, *210*(5), 1035-1047. https://doi.org/10.1084/jem.20121103

Selenko, N., Majdic, O., Jager, U., Sillaber, C., Stockl, J., & Knapp, W. (2002). Cross-priming of cytotoxic T cells promoted by apoptosis-inducing tumor cell reactive antibodies? *J Clin Immunol*, *22*(3), 124-130. https://doi.org/10.1023/a:1015463811683

Serwold, T., Gonzalez, F., Kim, J., Jacob, R., & Shastri, N. (2002). ERAAP customizes peptides for MHC class I molecules in the endoplasmic reticulum. *Nature*, *419*(6906), 480-483. https://doi.org/10.1038/nature01074

Shakushiro, K., Yamasaki, Y., Nishikawa, M., & Takakura, Y. (2004). Efficient scavenger receptor-mediated uptake and cross-presentation of negatively charged soluble antigens by dendritic cells. *Immunology*, *112*(2), 211-218. https://doi.org/10.1111/j.1365-2567.2004.01871.x

Shankaran, V., Ikeda, H., Bruce, A. T., White, J. M., Swanson, P. E., Old, L. J., & Schreiber, R. D. (2001). IFNgamma and lymphocytes prevent primary tumour development and shape tumour immunogenicity. *Nature*, *410*(6832), 1107-1111. https://doi.org/10.1038/35074122

Shen, L., Sigal, L. J., Boes, M., & Rock, K. L. (2004). Important role of cathepsin S in generating peptides for TAP-independent MHC class I crosspresentation in vivo. *Immunity*, *21*(2), 155-165. https://doi.org/10.1016/j.immuni.2004.07.004

Shen, Z., Zhou, S., Wang, Y., Li, R. L., Zhong, C., Liang, C., & Sun, Y. (2010). Higher intratumoral infiltrated Foxp3+ Treg numbers and Foxp3+/CD8+ ratio are associated with adverse prognosis in resectable gastric cancer. *J Cancer Res Clin Oncol*, *136*(10), 1585-1595. https://doi.org/10.1007/s00432-010-0816-9

Shimonkevitz, R., Colon, S., Kappler, J. W., Marrack, P., & Grey, H. M. (1984). Antigen recognition by H-2-restricted T cells. II. A tryptic ovalbumin peptide that substitutes for processed antigen. *J Immunol*, *133*(4), 2067-2074. https://www.ncbi.nlm.nih.gov/pubmed/6332146

Shrikant, P., Khoruts, A., & Mescher, M. F. (1999). CTLA-4 blockade reverses CD8+ T cell tolerance to tumor by a CD4+ T cell- and IL-2-dependent mechanism. *Immunity*, *11*(4), 483-493. https://doi.org/10.1016/s1074-7613(00)80123-5

Shrimpton, R. E., Butler, M., Morel, A. S., Eren, E., Hue, S. S., & Ritter, M. A. (2009). CD205 (DEC-205): a recognition receptor for apoptotic and necrotic self. *Mol Immunol*, *46*(6), 1229-1239. https://doi.org/10.1016/j.molimm.2008.11.016

Shukla, S. A., Rooney, M. S., Rajasagi, M., Tiao, G., Dixon, P. M., Lawrence, M. S., Stevens, J., Lane, W. J., Dellagatta, J. L., Steelman, S., Sougnez, C., Cibulskis, K., Kiezun, A., Hacohen, N., Brusic, V., Wu, C. J., & Getz, G. (2015). Comprehensive analysis of cancer-associated somatic mutations in class I HLA genes. *Nat Biotechnol*, *33*(11), 1152-1158. https://doi.org/10.1038/nbt.3344

Sidney, J., del Guercio, M. F., Southwood, S., Engelhard, V. H., Appella, E., Rammensee, H. G., Falk, K., Rotzschke, O., Takiguchi, M., Kubo, R. T., & et al. (1995). Several HLA alleles share overlapping peptide specificities. *J Immunol*, *154*(1), 247-259. https://www.ncbi.nlm.nih.gov/pubmed/7527812

Siebenkas, C., Chiappinelli, K. B., Guzzetta, A. A., Sharma, A., Jeschke, J., Vatapalli, R., Baylin, S. B., & Ahuja, N. (2017). Inhibiting DNA methylation activates cancer testis antigens and expression of the antigen processing and presentation machinery in colon and ovarian cancer cells. *PLoS One*, *12*(6), e0179501. https://doi.org/10.1371/journal.pone.0179501

Simpson, J. A., Al-Attar, A., Watson, N. F., Scholefield, J. H., Ilyas, M., & Durrant, L. G. (2010). Intratumoral T cell infiltration, MHC class I and STAT1 as biomarkers of good prognosis in colorectal cancer. *Gut*, *59*(7), 926-933. https://doi.org/10.1136/gut.2009.194472

Singh, A., Upadhyay, V., Upadhyay, A. K., Singh, S. M., & Panda, A. K. (2015). Protein recovery from inclusion bodies of Escherichia coli using mild solubilization process. *Microb Cell Fact*, *14*, 41. https://doi.org/10.1186/s12934-015-0222-8

Sisirak, V., Faget, J., Gobert, M., Goutagny, N., Vey, N., Treilleux, I., Renaudineau, S., Poyet, G., Labidi-Galy, S. I., Goddard-Leon, S., Durand, I., Le Mercier, I., Bajard, A., Bachelot, T., Puisieux, A., Puisieux, I., Blay, J. Y., Menetrier-Caux, C., Caux, C., & Bendriss-Vermare, N. (2012). Impaired IFN-alpha production by plasmacytoid dendritic cells favors regulatory T-cell expansion that may contribute to breast cancer progression. *Cancer Res*, *72*(20), 5188-5197. https://doi.org/10.1158/0008-5472.CAN-11-3468

Sittig, S. P., Bakdash, G., Weiden, J., Skold, A. E., Tel, J., Figdor, C. G., de Vries, I. J., & Schreibelt, G. (2016). A Comparative Study of the T Cell Stimulatory and Polarizing Capacity of Human Primary Blood Dendritic Cell Subsets. *Mediators Inflamm*, *2016*, 3605643. https://doi.org/10.1155/2016/3605643

Smyth, P., Sasiwachirangkul, J., Williams, R., & Scott, C. J. (2022). Cathepsin S (CTSS) activity in health and disease - A treasure trove of untapped clinical potential. *Molecular Aspects of Medicine*, *88*, 101106. https://doi.org/https://doi.org/10.1016/j.mam.2022.101106

Song, M., Ping, Y., Zhang, K., Yang, L., Li, F., Zhang, C., Cheng, S., Yue, D., Maimela, N. R., Qu, J., Liu, S., Sun, T., Li, Z., Xia, J., Zhang, B., Wang, L., & Zhang, Y. (2019). Low-Dose IFNgamma Induces Tumor Cell Stemness in Tumor Microenvironment of Non-Small Cell Lung Cancer. *Cancer Res*, *79*(14), 3737-3748. https://doi.org/10.1158/0008-5472.CAN-19-0596

Song, R., & Harding, C. V. (1996). Roles of proteasomes, transporter for antigen presentation (TAP), and beta 2-microglobulin in the processing of bacterial or particulate antigens via an alternate class I MHC processing pathway. *The Journal of Immunology*, *156*(11), 4182-4190. https://doi.org/10.4049/jimmunol.156.11.4182

Southwood, S., Sidney, J., Kondo, A., del Guercio, M. F., Appella, E., Hoffman, S., Kubo, R. T., Chesnut, R. W., Grey, H. M., & Sette, A. (1998). Several common HLA-DR types share largely overlapping peptide binding repertoires. *J Immunol*, *160*(7), 3363-3373. https://www.ncbi.nlm.nih.gov/pubmed/9531296

Speetjens, F. M., Kuppen, P. J., Welters, M. J., Essahsah, F., Voet van den Brink, A. M., Lantrua, M. G., Valentijn, A. R., Oostendorp, J., Fathers, L. M., Nijman, H. W., Drijfhout, J. W., van de Velde, C. J., Melief, C. J., & van der Burg, S. H. (2009). Induction of p53-specific immunity by a p53 synthetic long peptide vaccine in patients treated for metastatic colorectal cancer. *Clin Cancer Res*, *15*(3), 1086-1095. https://doi.org/10.1158/1078-0432.CCR-08-2227

Spiliotis, E. T., Manley, H., Osorio, M., Zuniga, M. C., & Edidin, M. (2000). Selective export of MHC class I molecules from the ER after their dissociation from TAP. *Immunity*, *13*(6), 841-851. https://doi.org/10.1016/s1074-7613(00)00081-9

Spirig, R., Campbell, I. K., Koernig, S., Chen, C. G., Lewis, B. J. B., Butcher, R., Muir, I., Taylor, S., Chia, J., Leong, D., Simmonds, J., Scotney, P., Schmidt, P., Fabri, L., Hofmann, A., Jordi, M., Spycher, M. O., Cattepoel, S., Brasseit, J., . . . Zuercher, A. W. (2018). rIgG1 Fc Hexamer Inhibits Antibody-Mediated Autoimmune Disease via Effects on Complement and FcgammaRs. *J Immunol*, *200*(8), 2542-2553. https://doi.org/10.4049/jimmunol.1701171

Spolski, R., & Leonard, W. J. (2014). Interleukin-21: a double-edged sword with therapeutic potential. *Nat Rev Drug Discov*, *13*(5), 379-395. https://doi.org/10.1038/nrd4296

Spranger, S., Dai, D., Horton, B., & Gajewski, T. F. (2017). Tumor-Residing Batf3 Dendritic Cells Are Required for Effector T Cell Trafficking and Adoptive T Cell Therapy. *Cancer Cell*, *31*(5), 711-723 e714. https://doi.org/10.1016/j.ccell.2017.04.003

Srivastava, P., Paluch, B. E., Matsuzaki, J., James, S. R., Collamat-Lai, G., Taverna, P., Karpf, A. R., & Griffiths, E. A. (2015). Immunomodulatory action of the DNA methyltransferase inhibitor SGI-110 in epithelial ovarian cancer cells and xenografts. *Epigenetics*, *10*(3), 237-246. https://doi.org/10.1080/15592294.2015.1017198

Staehli, F., Ludigs, K., Heinz, L. X., Seguin-Estevez, Q., Ferrero, I., Braun, M., Schroder, K., Rebsamen, M., Tardivel, A., Mattmann, C., MacDonald, H. R., Romero, P., Reith, W., Guarda, G., & Tschopp, J. (2012). NLRC5 deficiency selectively impairs MHC class I- dependent lymphocyte killing by cytotoxic T cells. *J Immunol*, *188*(8), 3820-3828. https://doi.org/10.4049/jimmunol.1102671

Stamper, C. C., Zhang, Y., Tobin, J. F., Erbe, D. V., Ikemizu, S., Davis, S. J., Stahl, M. L., Seehra, J., Somers, W. S., & Mosyak, L. (2001). Crystal structure of the B7-1/CTLA-4 complex that inhibits human immune responses. *Nature*, *410*(6828), 608-611. https://doi.org/10.1038/35069118

Stark, B., Andreae, F., Mosgoeller, W., Edetsberger, M., Gaubitzer, E., Koehler, G., & Prassl, R. (2008). Liposomal vasoactive intestinal peptide for lung application: protection from proteolytic degradation. *Eur J Pharm Biopharm*, *70*(1), 153-164. https://doi.org/10.1016/j.ejpb.2008.04.015

Stephens, A. J., Burgess-Brown, N. A., & Jiang, S. (2021). Beyond Just Peptide Antigens: The Complex World of Peptide-Based Cancer Vaccines. *Front Immunol*, *12*, 696791. https://doi.org/10.3389/fimmu.2021.696791

Sterner, R. C., & Sterner, R. M. (2021). CAR-T cell therapy: current limitations and potential strategies. *Blood Cancer J*, *11*(4), 69. https://doi.org/10.1038/s41408-021-00459-7

Stifter, K., Krieger, J., Ruths, L., Gout, J., Mulaw, M., Lechel, A., Kleger, A., Seufferlein, T., Wagner, M., & Schirmbeck, R. (2020). IFN-gamma treatment protocol for MHC-I(lo)/PD-L1(+) pancreatic tumor cells selectively restores their TAP-mediated presentation competence and CD8 T-cell priming potential. *J Immunother Cancer*, *8*(2). https://doi.org/10.1136/jitc-2020-000692

Strauss, L., Bergmann, C., Szczepanski, M., Gooding, W., Johnson, J. T., & Whiteside, T. L. (2007). A unique subset of CD4+CD25highFoxp3+ T cells secreting interleukin-10 and transforming growth factor-beta1 mediates suppression in the tumor microenvironment. *Clin Cancer Res*, *13*(15 Pt 1), 4345-4354. https://doi.org/10.1158/1078-0432.CCR-07-0472

Strop, P., & Brunger, A. T. (2005). Refractive index-based determination of detergent concentration and its application to the study of membrane proteins. *Protein Sci*, *14*(8), 2207-2211. https://doi.org/10.1110/ps.051543805

Stutman, O. (1974). Tumor development after 3-methylcholanthrene in immunologically deficient athymic-nude mice. *Science*, *183*(4124), 534-536. https://doi.org/10.1126/science.183.4124.534

Subklewe, M., von Bergwelt-Baildon, M., & Humpe, A. (2019). Chimeric Antigen Receptor T Cells: A Race to Revolutionize Cancer Therapy. *Transfus Med Hemother*, *46*(1), 15-24. https://doi.org/10.1159/000496870

Suh, W. K., Cohen-Doyle, M. F., Fruh, K., Wang, K., Peterson, P. A., & Williams, D. B. (1994). Interaction of MHC class I molecules with the transporter associated with antigen processing. *Science*, *264*(5163), 1322-1326. https://doi.org/10.1126/science.8191286

Sul, J., Blumenthal, G. M., Jiang, X., He, K., Keegan, P., & Pazdur, R. (2016). FDA Approval Summary: Pembrolizumab for the Treatment of Patients With Metastatic Non-Small Cell Lung Cancer Whose Tumors Express Programmed Death-Ligand 1. *Oncologist*, *21*(5), 643-650. https://doi.org/10.1634/theoncologist.2015-0498

Sun, L. Z., Elsayed, S., Aasen, T. B., Van Do, T., Aardal, N. P., Florvaag, E., & Vaali, K. (2010). Comparison between ovalbumin and ovalbumin peptide 323-339 responses in allergic mice: humoral and cellular aspects. *Scand J Immunol*, *71*(5), 329-335. https://doi.org/10.1111/j.1365-3083.2010.02382.x

Sun, W., Xie, J., Lin, H., Mi, S., Li, Z., Hua, F., & Hu, Z. (2012). A combined strategy improves the solubility of aggregation-prone single-chain variable fragment antibodies. *Protein Expr Purif*, *83*(1), 21-29. https://doi.org/10.1016/j.pep.2012.02.006

Swanson, J. A., & Watts, C. (1995). Macropinocytosis. *Trends Cell Biol*, *5*(11), 424-428. https://doi.org/10.1016/s0962-8924(00)89101-1

Swenerton, K. D., Legha, S. S., Smith, T., Hortobagyi, G. N., Gehan, E. A., Yap, H.-Y., Gutterman, J. U., & Blumenschein, G. R. (1979). Prognostic Factors in Metastatic Breast Cancer Treated with Combination Chemotherapy1. *Cancer Research*, *39*(5), 1552-1562.

Swiggard, W. J., Mirza, A., Nussenzweig, M. C., & Steinman, R. M. (1995). DEC-205, a 205-kDa protein abundant on mouse dendritic cells and thymic epithelium that is detected by the monoclonal antibody NLDC-145: purification, characterization, and N-terminal amino acid sequence. *Cell Immunol*, *165*(2), 302-311. https://doi.org/10.1006/cimm.1995.1218

Taieb, J., & Gallois, C. (2020). Adjuvant Chemotherapy for Stage III Colon Cancer. *Cancers (Basel)*, *12*(9). https://doi.org/10.3390/cancers12092679

Takada, A., Yoshida, S., Kajikawa, M., Miyatake, Y., Tomaru, U., Sakai, M., Chiba, H., Maenaka, K., Kohda, D., Fugo, K., & Kasahara, M. (2008). Two novel NKG2D ligands of the mouse H60 family with differential expression patterns and binding affinities to NKG2D. *J Immunol*, *180*(3), 1678-1685. https://doi.org/10.4049/jimmunol.180.3.1678

Takahashi, T., Tagami, T., Yamazaki, S., Uede, T., Shimizu, J., Sakaguchi, N., Mak, T. W., & Sakaguchi, S. (2000). Immunologic self-tolerance maintained by CD25(+)CD4(+) regulatory T cells constitutively expressing cytotoxic T lymphocyte-associated antigen 4. *J Exp Med*, *192*(2), 303-310. https://doi.org/10.1084/jem.192.2.303

Tamm, I., Wang, Y., Sausville, E., Scudiero, D. A., Vigna, N., Oltersdorf, T., & Reed, J. C. (1998). IAP-family protein survivin inhibits caspase activity and apoptosis induced by Fas (CD95), Bax, caspases, and anticancer drugs. *Cancer Res*, *58*(23), 5315-5320. https://www.ncbi.nlm.nih.gov/pubmed/9850056

Tan, M. C., Goedegebuure, P. S., Belt, B. A., Flaherty, B., Sankpal, N., Gillanders, W. E., Eberlein, T. J., Hsieh, C. S., & Linehan, D. C. (2009). Disruption of CCR5-dependent homing of regulatory T cells inhibits tumor growth in a murine model of pancreatic cancer. *J Immunol*, *182*(3), 1746-1755. https://doi.org/10.4049/jimmunol.182.3.1746

Tang, D., Kang, R., Coyne, C. B., Zeh, H. J., & Lotze, M. T. (2012). PAMPs and DAMPs: signal 0s that spur autophagy and immunity. *Immunol Rev*, *249*(1), 158-175. https://doi.org/10.1111/j.1600-065X.2012.01146.x

Tao, H., Liu, W., Simmons, B. N., Harris, H. K., Cox, T. C., & Massiah, M. A. (2010). Purifying natively folded proteins from inclusion bodies using sarkosyl, Triton X-100, and CHAPS. *Biotechniques*, *48*(1), 61-64. https://doi.org/10.2144/000113304

Taylor, G., Hoare, M., Gray, D. R., & Marston, F. A. O. (1986). Size and Density of Protein Inclusion Bodies. *Bio/Technology*, *4*(6), 553-557. https://doi.org/10.1038/nbt0686-553

Tekguc, M., Wing, J. B., Osaki, M., Long, J., & Sakaguchi, S. (2021). Treg-expressed CTLA-4 depletes CD80/CD86 by trogocytosis, releasing free PD-L1 on antigen-presenting cells. *Proc Natl Acad Sci U S A*, *118*(30). https://doi.org/10.1073/pnas.2023739118

Tel, J., Benitez-Ribas, D., Hoosemans, S., Cambi, A., Adema, G. J., Figdor, C. G., Tacken, P. J., & de Vries, I. J. (2011). DEC-205 mediates antigen uptake and presentation by both resting and activated human plasmacytoid dendritic cells. *Eur J Immunol*, *41*(4), 1014-1023. https://doi.org/10.1002/eji.201040790

Timke, C., Winnenthal, H. S., Klug, F., Roeder, F. F., Bonertz, A., Reissfelder, C., Rochet, N., Koch, M., Tjaden, C., Buechler, M. W., Debus, J., Werner, J., Beckhove, P., Weitz, J., & Huber, P. E. (2011). Randomized controlled phase I/II study to investigate immune stimulatory effects by low dose radiotherapy in primarily operable pancreatic cancer. *BMC Cancer*, *11*, 134. https://doi.org/10.1186/1471-2407-11-134

Ting-Beall, H. P., Lee, A. S., & Hochmuth, R. M. (1995). Effect of cytochalasin D on the mechanical properties and morphology of passive human neutrophils. *Ann Biomed Eng*, *23*(5), 666-671. https://doi.org/10.1007/BF02584463

Tohme, S., Simmons, R. L., & Tsung, A. (2017). Surgery for Cancer: A Trigger for Metastases. *Cancer Res*, *77*(7), 1548-1552. https://doi.org/10.1158/0008-5472.CAN-16-1536

Townsend, D. M., & Tew, K. D. (2003). The role of glutathione-S-transferase in anti-cancer drug resistance. *Oncogene*, *22*(47), 7369-7375. https://doi.org/10.1038/sj.onc.1206940

Trapani, J. A., Jans, P., Smyth, M. J., Froelich, C. J., Williams, E. A., Sutton, V. R., & Jans, D. A. (1998). Perforin-dependent nuclear entry of granzyme B precedes apoptosis, and is not a consequence of nuclear membrane dysfunction. *Cell Death Differ*, *5*(6), 488-496. https://doi.org/10.1038/sj.cdd.4400373

Traynor, K. (2011). Ipilimumab approved for metastatic melanoma. *Am J Health Syst Pharm*, *68*(9), 768. https://doi.org/10.2146/news110025

Tseng, T. S., Wang, S. H., Chang, T. W., Wei, H. M., Wang, Y. J., Tsai, K. C., Liao, Y. D., & Chen, C. (2016). Sarkosyl-Induced Helical Structure of an Antimicrobial Peptide GW-Q6 Plays an Essential Role in the Binding of Surface Receptor OprI in Pseudomonas aeruginosa. *PLoS One*, *11*(10), e0164597. https://doi.org/10.1371/journal.pone.0164597

Tsumoto, K., Ejima, D., Kumagai, I., & Arakawa, T. (2003). Practical considerations in refolding proteins from inclusion bodies. *Protein Expr Purif*, *28*(1), 1-8. https://doi.org/10.1016/s1046-5928(02)00641-1

U'Ren, L., Kedl, R., & Dow, S. (2006). Vaccination with liposome--DNA complexes elicits enhanced antitumor immunity. *Cancer Gene Ther*, *13*(11), 1033-1044. https://doi.org/10.1038/sj.cgt.7700982

Ukkonen, P., Lewis, V., Marsh, M., Helenius, A., & Mellman, I. (1986). Transport of macrophage Fc receptors and Fc receptor-bound ligands to lysosomes. *J Exp Med*, *163*(4), 952-971. https://doi.org/10.1084/jem.163.4.952

UniProt, C. (2023). UniProt: the Universal Protein Knowledgebase in 2023. *Nucleic Acids Res*, *51*(D1), D523-D531. https://doi.org/10.1093/nar/gkac1052

Vallejo, L. F., & Rinas, U. (2004). Strategies for the recovery of active proteins through refolding of bacterial inclusion body proteins. *Microb Cell Fact*, *3*(1), 11. https://doi.org/10.1186/1475-2859-3-11

van den Berg, J. H., Heemskerk, B., van Rooij, N., Gomez-Eerland, R., Michels, S., van Zon, M., de Boer, R., Bakker, N. A. M., Jorritsma-Smit, A., van Buuren, M. M., Kvistborg, P., Spits, H., Schotte, R., Mallo, H., Karger, M., van der Hage, J. A., Wouters, M., Pronk, L. M., Geukes Foppen, M. H., . . . Haanen, J. (2020). Tumor infiltrating lymphocytes (TIL) therapy in metastatic melanoma: boosting of neoantigen-specific T cell reactivity and long-term follow-up. *J Immunother Cancer*, *8*(2). https://doi.org/10.1136/jitc-2020-000848

van den Broek, M. E., Kagi, D., Ossendorp, F., Toes, R., Vamvakas, S., Lutz, W. K., Melief, C. J., Zinkernagel, R. M., & Hengartner, H. (1996). Decreased tumor surveillance in perforin-deficient mice. *J Exp Med*, *184*(5), 1781-1790. https://doi.org/10.1084/jem.184.5.1781

van Endert, P. M., Tampe, R., Meyer, T. H., Tisch, R., Bach, J. F., & McDevitt, H. O. (1994). A sequential model for peptide binding and transport by the transporters associated with antigen processing. *Immunity*, *1*(6), 491-500. https://doi.org/10.1016/1074-7613(94)90091-4

Varypataki, E. M., Silva, A. L., Barnier-Quer, C., Collin, N., Ossendorp, F., & Jiskoot, W. (2016). Synthetic long peptide-based vaccine formulations for induction of cell mediated immunity: A comparative study of cationic liposomes and PLGA nanoparticles. *J Control Release*, *226*, 98-106. https://doi.org/10.1016/j.jconrel.2016.02.018

Vassilakos, A., Cohen-Doyle, M. F., Peterson, P. A., Jackson, M. R., & Williams, D. B. (1996). The molecular chaperone calnexin facilitates folding and assembly of class I histocompatibility molecules. *EMBO J*, *15*(7), 1495-1506. https://www.ncbi.nlm.nih.gov/pubmed/8612572

Vianello, F., Papeta, N., Chen, T., Kraft, P., White, N., Hart, W. K., Kircher, M. F., Swart, E., Rhee, S., Palu, G., Irimia, D., Toner, M., Weissleder, R., & Poznansky, M. C. (2006). Murine B16 melanomas expressing high levels of the chemokine stromal-derived factor-1/CXCL12 induce tumor-specific T cell chemorepulsion and escape from immune control. *J Immunol*, *176*(5), 2902-2914. https://doi.org/10.4049/jimmunol.176.5.2902

Villani, A. C., Satija, R., Reynolds, G., Sarkizova, S., Shekhar, K., Fletcher, J., Griesbeck, M., Butler, A., Zheng, S., Lazo, S., Jardine, L., Dixon, D., Stephenson, E., Nilsson, E., Grundberg, I., McDonald, D., Filby, A., Li, W., De Jager, P. L., . . . Hacohen, N. (2017). Single-cell RNA-seq reveals new types of human blood dendritic cells, monocytes, and progenitors. *Science*, *356*(6335). https://doi.org/10.1126/science.aah4573

Vita, R., Mahajan, S., Overton, J. A., Dhanda, S. K., Martini, S., Cantrell, J. R., Wheeler, D. K., Sette, A., & Peters, B. (2019). The Immune Epitope Database (IEDB): 2018 update. *Nucleic Acids Res*, *47*(D1), D339-D343. https://doi.org/10.1093/nar/gky1006

von Delwig, A., Hilkens, C. M., Altmann, D. M., Holmdahl, R., Isaacs, J. D., Harding, C. V., Robertson, H., McKie, N., & Robinson, J. H. (2006). Inhibition of macropinocytosis blocks antigen presentation of type II collagen in vitro and in vivo in HLA-DR1 transgenic mice. *Arthritis Res Ther*, *8*(4), R93. https://doi.org/10.1186/ar1964

Vulcano, M., Dusi, S., Lissandrini, D., Badolato, R., Mazzi, P., Riboldi, E., Borroni, E., Calleri, A., Donini, M., Plebani, A., Notarangelo, L., Musso, T., & Sozzani, S. (2004). Toll receptor-mediated regulation of NADPH oxidase in human dendritic cells. *J Immunol*, *173*(9), 5749-5756. https://doi.org/10.4049/jimmunol.173.9.5749

Walsh, G. (2018). Biopharmaceutical benchmarks 2018. *Nat Biotechnol*, *36*(12), 1136-1145. https://doi.org/10.1038/nbt.4305

Walunas, T. L., Lenschow, D. J., Bakker, C. Y., Linsley, P. S., Freeman, G. J., Green, J. M., Thompson, C. B., & Bluestone, J. A. (1994). CTLA-4 can function as a negative regulator of T cell activation. *Immunity*, *1*(5), 405-413. https://doi.org/10.1016/1074-7613(94)90071-x

Wang, L., Wang, N., Zhang, W., Cheng, X., Yan, Z., Shao, G., Wang, X., Wang, R., & Fu, C. (2022). Therapeutic peptides: current applications and future directions. *Signal Transduct Target Ther*, *7*(1), 48. https://doi.org/10.1038/s41392-022-00904-4

Wang, S. S., Chang, C. K., Peng, M. J., & Liu, H. S. (2006). Effect of Glutathione Redox System on Lysozyme Refolding in Size Exclusion Chromatography. *Food and Bioproducts Processing*, *84*(1), 18-27. https://doi.org/10.1205/fbp.05141

Wang, Z., Hong, J., Sun, W., Xu, G., Li, N., Chen, X., Liu, A., Xu, L., Sun, B., & Zhang, J. Z. (2006). Role of IFN-gamma in induction of Foxp3 and conversion of CD4+ CD25- T cells to CD4+ Tregs. *J Clin Invest*, *116*(9), 2434-2441. https://doi.org/10.1172/JCI25826

Wang, Z., Marincola, F. M., Rivoltini, L., Parmiani, G., & Ferrone, S. (1999). Selective histocompatibility leukocyte antigen (HLA)-A2 loss caused by aberrant pre-mRNA splicing in 624MEL28 melanoma cells. *J Exp Med*, *190*(2), 205-215. https://doi.org/10.1084/jem.190.2.205

Wani, M. A., Haynes, L. D., Kim, J., Bronson, C. L., Chaudhury, C., Mohanty, S., Waldmann, T. A., Robinson, J. M., & Anderson, C. L. (2006). Familial hypercatabolic hypoproteinemia caused by deficiency of the neonatal Fc receptor, FcRn, due to a mutant beta2-microglobulin gene. *Proc Natl Acad Sci U S A*, *103*(13), 5084-5089. https://doi.org/10.1073/pnas.0600548103

Watts, C. (2012). The endosome-lysosome pathway and information generation in the immune system. *Biochim Biophys Acta*, *1824*(1), 14-21. https://doi.org/10.1016/j.bbapap.2011.07.006

Weflen, A. W., Baier, N., Tang, Q. J., Van den Hof, M., Blumberg, R. S., Lencer, W. I., & Massol, R. H. (2013). Multivalent immune complexes divert FcRn to lysosomes by exclusion from recycling sorting tubules. *Mol Biol Cell*, *24*(15), 2398-2405. https://doi.org/10.1091/mbc.E13-04-0174

Wiertz, E. J., Tortorella, D., Bogyo, M., Yu, J., Mothes, W., Jones, T. R., Rapoport, T. A., & Ploegh, H. L. (1996). Sec61-mediated transfer of a membrane protein from the endoplasmic reticulum to the proteasome for destruction. *Nature*, *384*(6608), 432-438. https://doi.org/10.1038/384432a0

Wilkinson, R. D., Williams, R., Scott, C. J., & Burden, R. E. (2015). Cathepsin S: therapeutic, diagnostic, and prognostic potential. *Biol Chem*, *396*(8), 867-882. https://doi.org/10.1515/hsz-2015-0114

Williams, B. B., Wall, M., Miao, R. Y., Williams, B., Bertoncello, I., Kershaw, M. H., Mantamadiotis, T., Haber, M., Norris, M. D., Gautam, A., Darcy, P. K., & Ramsay, R. G. (2008). Induction of T cell-mediated immunity using a c-Myb DNA vaccine in a mouse model of colon cancer. *Cancer Immunol Immunother*, *57*(11), 1635-1645. https://doi.org/10.1007/s00262-008-0497-2

Wolf, E., Hofmeister, R., Kufer, P., Schlereth, B., & Baeuerle, P. A. (2005). BiTEs: bispecific antibody constructs with unique anti-tumor activity. *Drug Discov Today*, *10*(18), 1237-1244. https://doi.org/10.1016/S1359-6446(05)03554-3

Wyld, L., Audisio, R. A., & Poston, G. J. (2015). The evolution of cancer surgery and future perspectives. *Nat Rev Clin Oncol*, *12*(2), 115-124. https://doi.org/10.1038/nrclinonc.2014.191

Wylie, B., Ong, F., Belhoul-Fakir, H., Priebatsch, K., Bogdawa, H., Stirnweiss, A., Watt, P., Cunningham, P., Stone, S. R., & Waithman, J. (2021). Targeting Cross-Presentation as a Route to Improve the Efficiency of Peptide-Based Cancer Vaccines. *Cancers (Basel)*, *13*(24). https://doi.org/10.3390/cancers13246189

Xie, C. B., Jane-Wit, D., & Pober, J. S. (2020). Complement Membrane Attack Complex: New Roles, Mechanisms of Action, and Therapeutic Targets. *Am J Pathol*, *190*(6), 1138-1150. https://doi.org/10.1016/j.ajpath.2020.02.006

Xing, Y., & Hogquist, K. A. (2012). T-cell tolerance: central and peripheral. *Cold Spring Harb Perspect Biol*, *4*(6). https://doi.org/10.1101/cshperspect.a006957

Ya, Z., Hailemichael, Y., Overwijk, W., & Restifo, N. P. (2015). Mouse model for pre-clinical study of human cancer immunotherapy. *Curr Protoc Immunol*, *108*, 20 21 21-20 21 43. https://doi.org/10.1002/0471142735.im2001s108

Yakes, F. M., Chinratanalab, W., Ritter, C. A., King, W., Seelig, S., & Arteaga, C. L. (2002). Herceptin-induced inhibition of phosphatidylinositol-3 kinase and Akt Is required for antibody-mediated effects on p27, cyclin D1, and antitumor action. *Cancer Res*, *62*(14), 4132-4141. https://www.ncbi.nlm.nih.gov/pubmed/12124352

Yamaguchi, H., & Miyazaki, M. (2014). Refolding techniques for recovering biologically active recombinant proteins from inclusion bodies. *Biomolecules*, *4*(1), 235-251. https://doi.org/10.3390/biom4010235

Yamamoto, K., Venida, A., Yano, J., Biancur, D. E., Kakiuchi, M., Gupta, S., Sohn, A. S. W., Mukhopadhyay, S., Lin, E. Y., Parker, S. J., Banh, R. S., Paulo, J. A., Wen, K. W., Debnath, J., Kim, G. E., Mancias, J. D., Fearon, D. T., Perera, R. M., & Kimmelman, A. C. (2020). Autophagy promotes immune evasion of pancreatic cancer by degrading MHC-I. *Nature*, *581*(7806), 100-105. https://doi.org/10.1038/s41586-020-2229-5

Yamauchi, Y., Safi, S., Blattner, C., Rathinasamy, A., Umansky, L., Juenger, S., Warth, A., Eichhorn, M., Muley, T., Herth, F. J. F., Dienemann, H., Platten, M., Beckhove, P., Utikal, J., Hoffmann, H., & Umansky, V. (2018). Circulating and Tumor Myeloid-derived Suppressor Cells in Resectable Non-Small Cell Lung Cancer. *Am J Respir Crit Care Med*, *198*(6), 777-787. https://doi.org/10.1164/rccm.201708-1707OC

Yang, I., Kremen, T. J., Giovannone, A. J., Paik, E., Odesa, S. K., Prins, R. M., & Liau, L. M. (2004). Modulation of major histocompatibility complex Class I molecules and major histocompatibility complex-bound immunogenic peptides induced by interferon-alpha and interferon-gamma treatment of human glioblastoma multiforme. *J Neurosurg*, *100*(2), 310-319. https://doi.org/10.3171/jns.2004.100.2.0310

Yewdell, J. W., & Bennink, J. R. (1989). Brefeldin A specifically inhibits presentation of protein antigens to cytotoxic T lymphocytes. *Science*, *244*(4908), 1072-1075. https://doi.org/10.1126/science.2471266

Yin, Y., Boesteanu, A. C., Binder, Z. A., Xu, C., Reid, R. A., Rodriguez, J. L., Cook, D. R., Thokala, R., Blouch, K., McGettigan-Croce, B., Zhang, L., Konradt, C., Cogdill, A. P., Panjwani, M. K., Jiang,

S., Migliorini, D., Dahmane, N., Posey, A. D., Jr., June, C. H., . . . Johnson, L. A. (2018). Checkpoint Blockade Reverses Anergy in IL-13Ralpha2 Humanized scFv-Based CAR T Cells to Treat Murine and Canine Gliomas. *Mol Ther Oncolytics*, *11*, 20-38. https://doi.org/10.1016/j.omto.2018.08.002

Ylosmaki, E., Malorzo, C., Capasso, C., Honkasalo, O., Fusciello, M., Martins, B., Ylosmaki, L., Louna, A., Feola, S., Paavilainen, H., Peltonen, K., Hukkanen, V., Viitala, T., & Cerullo, V. (2018). Personalized Cancer Vaccine Platform for Clinically Relevant Oncolytic Enveloped Viruses. *Mol Ther*, *26*(9), 2315-2325. https://doi.org/10.1016/j.ymthe.2018.06.008

Yokoyama, W. M., & Kim, S. (2006). Licensing of natural killer cells by self-major histocompatibility complex class I. *Immunol Rev*, *214*, 143-154. https://doi.org/10.1111/j.1600-065X.2006.00458.x

Yu, F., Wang, Y., Xiao, Y., He, Y., Luo, C., Duan, D., Li, C., Xu, S., & Xiang, T. (2014). RP215 single chain fragment variable and single domain recombinant antibodies induce cell cycle arrest at G0/G1 phase in breast cancer. *Mol Immunol*, *59*(1), 100-109. https://doi.org/10.1016/j.molimm.2014.01.007

Zamani, P., Teymouri, M., Nikpoor, A. R., Navashenaq, J. G., Gholizadeh, Z., Darban, S. A., & Jaafari, M. R. (2020). Nanoliposomal vaccine containing long multi-epitope peptide E75-AE36 pulsed PADRE-induced effective immune response in mice TUBO model of breast cancer. *Eur J Cancer*, *129*, 80-96. https://doi.org/10.1016/j.ejca.2020.01.010

Zehner, M., Chasan, A. I., Schuette, V., Embgenbroich, M., Quast, T., Kolanus, W., & Burgdorf, S. (2011). Mannose receptor polyubiquitination regulates endosomal recruitment of p97 and cytosolic antigen translocation for cross-presentation. *Proc Natl Acad Sci U S A*, *108*(24), 9933-9938. https://doi.org/10.1073/pnas.1102397108

Zehner, M., Marschall, A. L., Bos, E., Schloetel, J. G., Kreer, C., Fehrenschild, D., Limmer, A., Ossendorp, F., Lang, T., Koster, A. J., Dubel, S., & Burgdorf, S. (2015). The translocon protein Sec61 mediates antigen transport from endosomes in the cytosol for cross-presentation to CD8(+) T cells. *Immunity*, *42*(5), 850-863. https://doi.org/10.1016/j.immuni.2015.04.008

Zeng, G., Li, Y., El-Gamil, M., Sidney, J., Sette, A., Wang, R. F., Rosenberg, S. A., & Robbins, P. F. (2002). Generation of NY-ESO-1-specific CD4+ and CD8+ T cells by a single peptide with dual MHC class I and class II specificities: a new strategy for vaccine design. *Cancer Res*, *62*(13), 3630-3635. https://www.ncbi.nlm.nih.gov/pubmed/12097265

Zhang, H., Han, G., Liu, H., Chen, J., Ji, X., Zhou, F., Zhou, Y., & Xie, C. (2011). The development of classically and alternatively activated macrophages has different effects on the varied stages of radiation-induced pulmonary injury in mice. *J Radiat Res*, *52*(6), 717-726. https://doi.org/10.1269/jrr.11054

Zhang, T., Maekawa, Y., Hanba, J., Dainichi, T., Nashed, B. F., Hisaeda, H., Sakai, T., Asao, T., Himeno, K., Good, R. A., & Katunuma, N. (2000). Lysosomal cathepsin B plays an important role in antigen processing, while cathepsin D is involved in degradation of the invariant chain inovalbumin-immunized mice. *Immunology*, *100*(1), 13-20. https://doi.org/10.1046/j.1365-2567.2000.00000.x

Zhang, Y., Apilado, R., Coleman, J., Ben-Sasson, S., Tsang, S., Hu-Li, J., Paul, W. E., & Huang, H. (2001). Interferon gamma stabilizes the T helper cell type 1 phenotype. *J Exp Med*, *194*(2), 165-172. https://doi.org/10.1084/jem.194.2.165

Zhang, Y., Zhou, Y., Gong, M., Zhang, Q., Zheng, Q., Shen, Y., Lu, W., & Jiang, S. (2023). Survivin-Based Recombinant Overlapping Peptides Induce T Lymphocyte Cytotoxicity and Prolong the Survival in In Vivo Melanoma Model. *Advanced Therapeutics*, *n/a*(n/a), 2300253. https://doi.org/https://doi.org/10.1002/adtp.202300253

Zhang, Z., Tongchusak, S., Mizukami, Y., Kang, Y. J., Ioji, T., Touma, M., Reinhold, B., Keskin, D. B., Reinherz, E. L., & Sasada, T. (2011). Induction of anti-tumor cytotoxic T cell responses through PLGA-nanoparticle mediated antigen delivery. *Biomaterials*, *32*(14), 3666-3678. https://doi.org/10.1016/j.biomaterials.2011.01.067

Zhao, M. Z., Sun, Y., Jiang, X. F., Liu, L., Liu, L., & Sun, L. X. (2019). Promotion on NLRC5 upregulating MHC-I expression by IFN-gamma in MHC-I-deficient breast cancer cells. *Immunol Res*, *67*(6), 497-504. https://doi.org/10.1007/s12026-019-09111-w

Zilberberg, J., Friedman, T. M., Dranoff, G., & Korngold, R. (2011). Treatment with GM-CSF secreting myeloid leukemia cell vaccine prior to autologous-BMT improves the survival of leukemia-

challenged mice. *Biol Blood Marrow Transplant*, *17*(3), 330-340. https://doi.org/10.1016/j.bbmt.2010.09.020

Zom, G. G., Willems, M., Khan, S., van der Sluis, T. C., Kleinovink, J. W., Camps, M. G. M., van der Marel, G. A., Filippov, D. V., Melief, C. J. M., & Ossendorp, F. (2018). Novel TLR2-binding adjuvant induces enhanced T cell responses and tumor eradication. *J Immunother Cancer*, *6*(1), 146. https://doi.org/10.1186/s40425-018-0455-2

Zou, W., Machelon, V., Coulomb-L'Hermin, A., Borvak, J., Nome, F., Isaeva, T., Wei, S., Krzysiek, R., Durand-Gasselin, I., Gordon, A., Pustilnik, T., Curiel, D. T., Galanaud, P., Capron, F., Emilie, D., & Curiel, T. J. (2001). Stromal-derived factor-1 in human tumors recruits and alters the function of plasmacytoid precursor dendritic cells. *Nat Med*, *7*(12), 1339-1346. https://doi.org/10.1038/nm1201-1339

Zwaveling, S., Ferreira Mota, S. C., Nouta, J., Johnson, M., Lipford, G. B., Offringa, R., van der Burg, S. H., & Melief, C. J. (2002). Established human papillomavirus type 16-expressing tumors are effectively eradicated following vaccination with long peptides. *J Immunol*, *169*(1), 350-358. https://doi.org/10.4049/jimmunol.169.1.350

7 Appendices

7.1 Appendix I – Supplementary Results

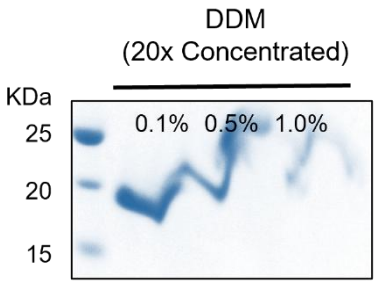
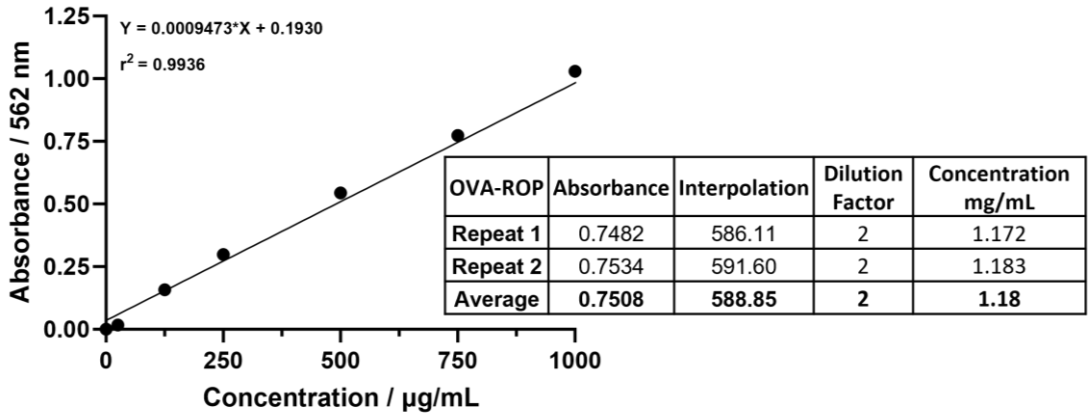
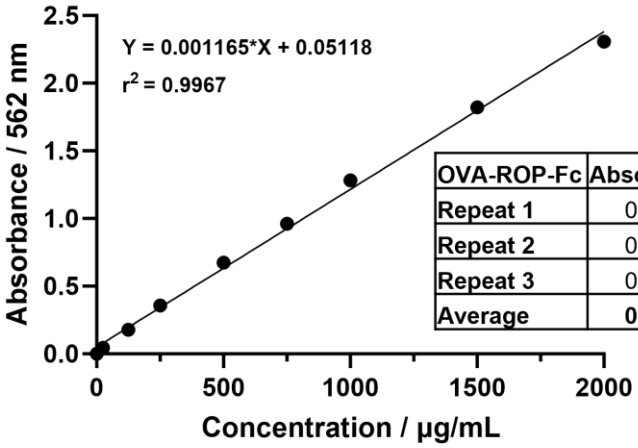


Figure 7.1 DDM Concentration in OVA-ROP Detergent Screen
SDS-PAGE analysis of DDM solubilised OVA-ROP concentrated twenty-fold from the original 0.1%, 0.5% and 1.0% detergent screen.



OVA-ROP	Absorbance	Interpolation	Dilution Factor	Concentration mg/mL
Repeat 1	0.7482	586.11	2	1.172
Repeat 2	0.7534	591.60	2	1.183
Average	**0.7508**	**588.85**	**2**	**1.18**

Figure 7.2 OVA-ROP Concentration Determination by BCA Assay
Concentration determination of OVA-ROP by BCA Assay. Concentration of undiluted OVA-ROP-Fc calculated from interpolation of BCA assay standard curve. Linear regression and interpolation calculations were performed using GraphPad Prism software.



OVA-ROP-Fc	Absorbance	Interpolation / µg/mL
Repeat 1	0.2352	91.6
Repeat 2	0.2323	89.1
Repeat 3	0.2389	94.8
Average	**0.2355**	**91.8**

Figure 7.3 tOVA-ROP-Fc Concentration Determination by BCA Assay
Concentration determination of OVA-ROP-Fc by BCA Assay. Concentration of undiluted OVA-ROP-Fc calculated from interpolation of BCA assay standard curve. Linear regression and interpolation calculations were performed using GraphPad Prism software.

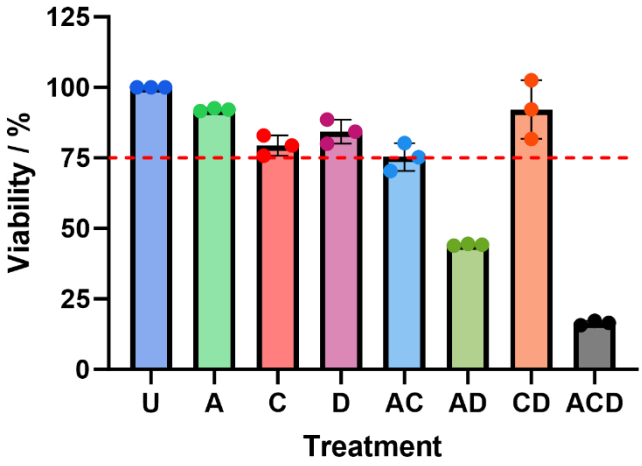


Figure 7.4 DC2.4 MTS Cytotoxicity Assessment of Endocytosis Inhibitors
MTS viability assay on untreated DC2.4 cells (U) compared to 1 mM amiloride (A), 5 µM cytochalasin D (C), 30 µM dynasore (D), or a combination of amiloride and cytochalasin (AC), amiloride and dynasore (AD), cytochalasin D and dynasore (CD), and combination of all three (ACD). The red line indicates the cut-off for viability at 75%, with AD and ACD excluded from testing.

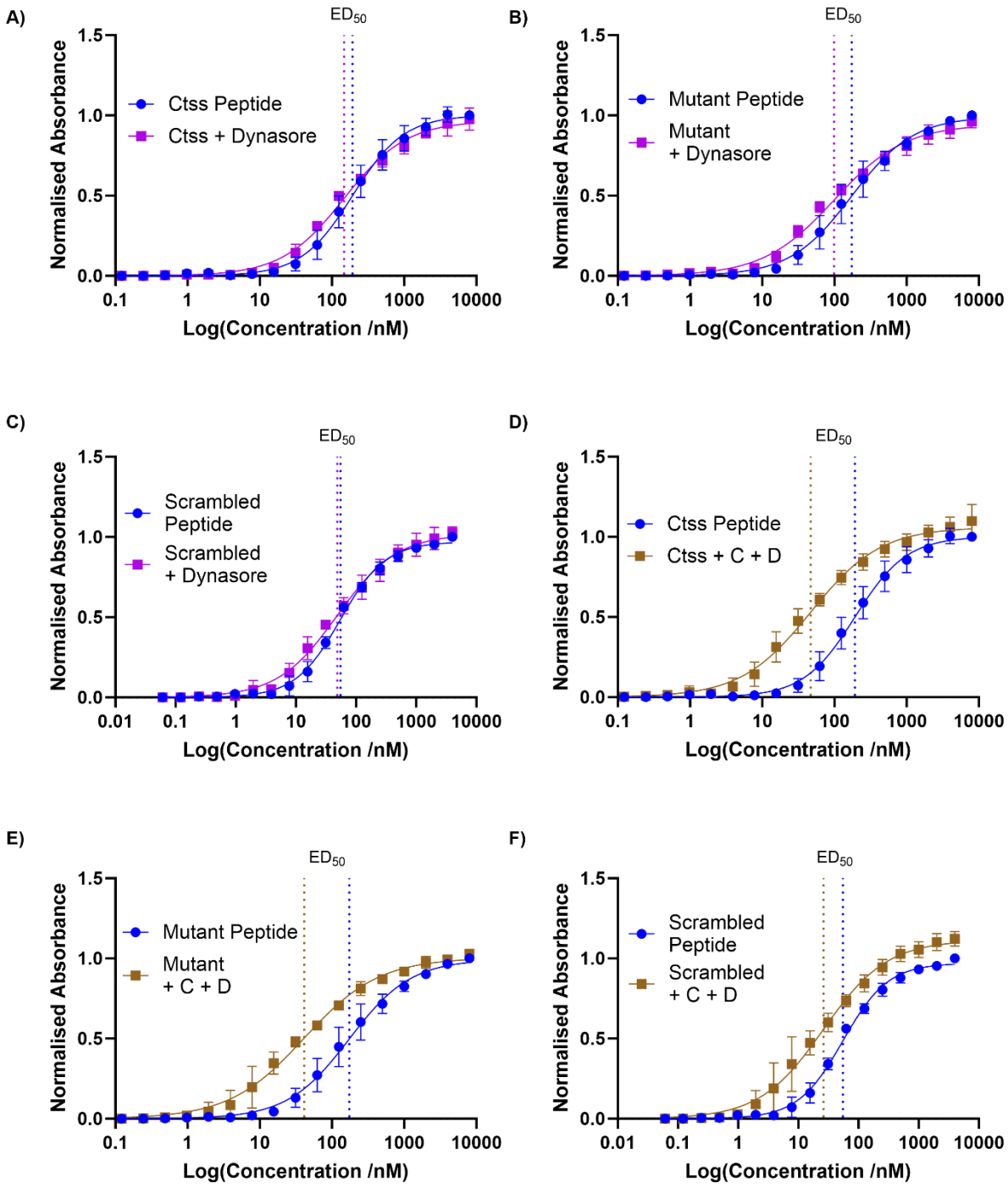


Figure 7.5 B3Z Assay Dose-Response Curves of Dynasore and Cytochalasin D With Dynasore
DC2.4 cells were pulsed with synthetic peptides under inhibition by 30 μM dynasore or combined with 5 μM cytochalasin D. Pulsed DC2.4 co-cultured with B3Z and CPRG assay developed. Data generated from B3Z CPRG absorbance readings and normalised against maximum absorbance of non-inhibited cells (n=3). 4PL regression curve generated from normalised means (±SD). Coloured dotted lines represent ED50 values for each. Peptides were diluted from 8000 nM to 61 pM across an 18-point two-fold dilution series. Peptides diluted with and without cell treatment with dynasore for **(A)** ctss peptide, **(B)** mutant peptide, and **(C)** scrambled peptide. Peptides diluted with and without combination treatment of cells with dynasore and cytochalasin D for **(D)** Ctss peptide, **(E)** mutant peptide, **(F)** scrambled peptide.

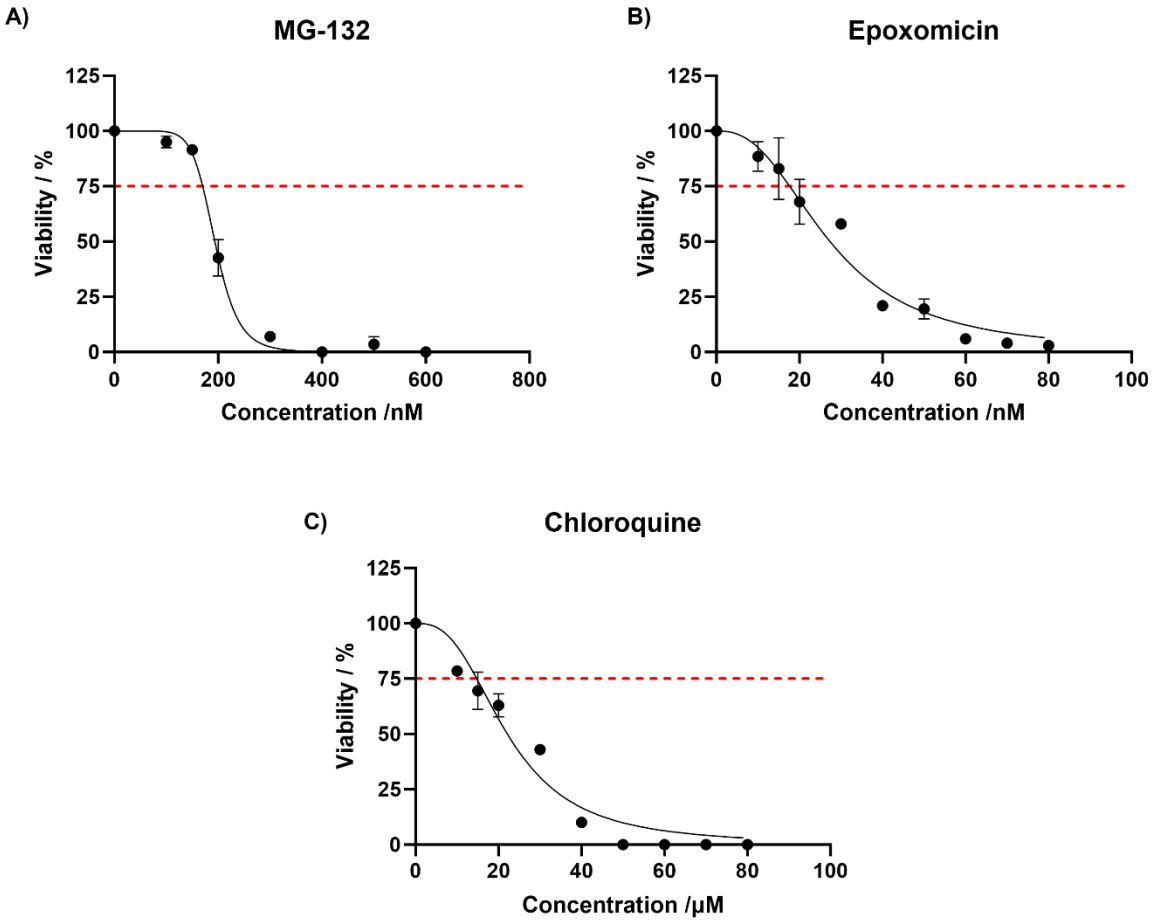


Figure 7.6 DC2.4 MTS Cytotoxicity Assessment of Proteasome and Endosome Inhibitors
MTS viability dose-response curves for DC2.4 cells treated with **(A)** MG-132, **(B)** epoxomicin and **(C)** chloroquine. The viability threshold represented by the red line is set to 75% viability. Viabilities above the line are considered tolerable to cells.

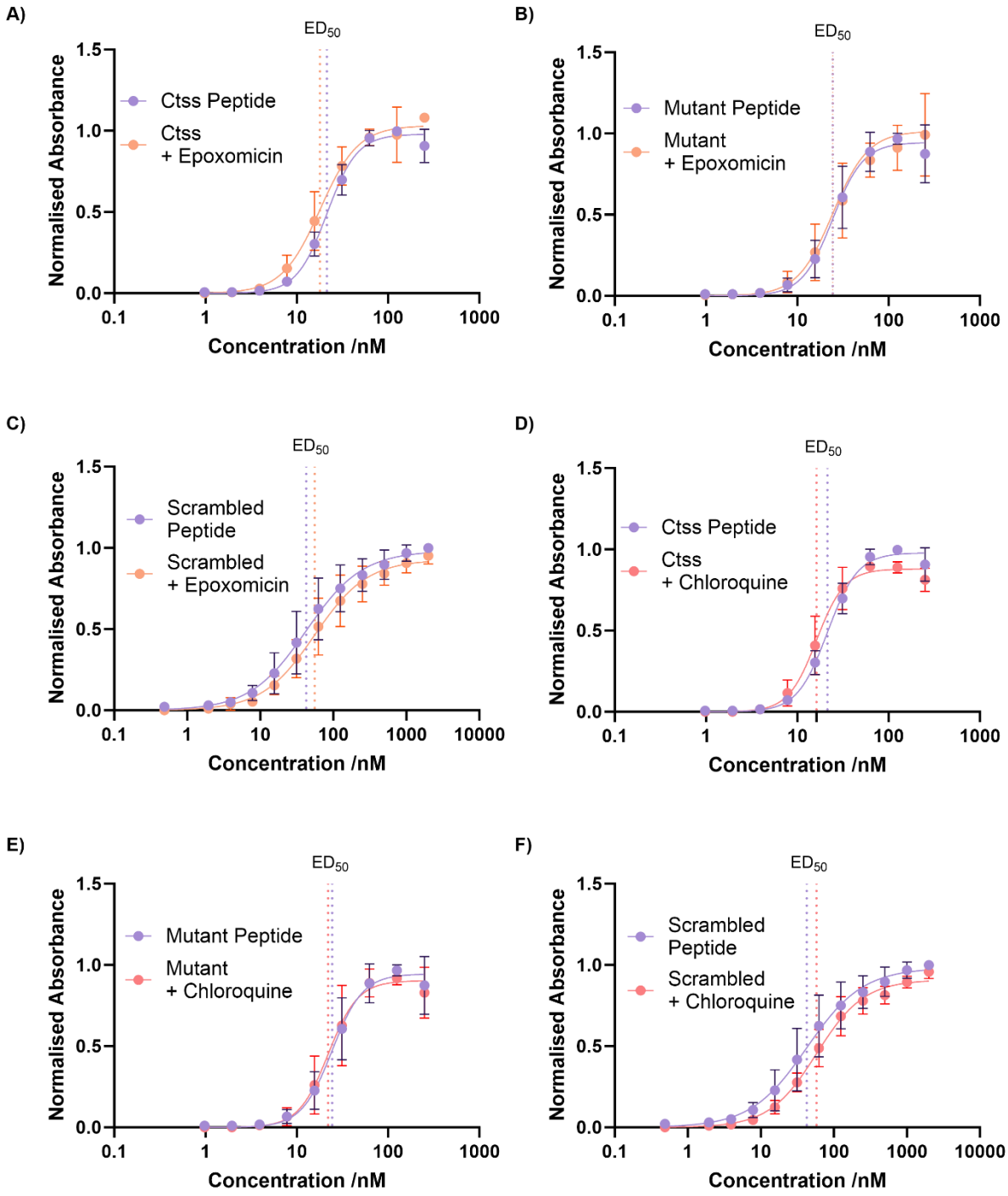
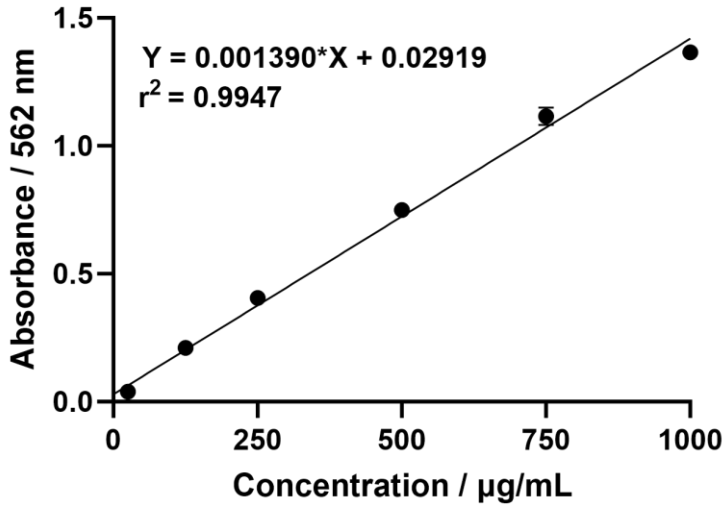


Figure 7.7 B3Z Assay Dose-Response Curves of Epoxomicin and Chloroquine
DC2.4 cells were pulsed with synthetic peptides under inhibition by 10 nM epoxomicin or 10 µM chloroquine. Pulsed DC2.4 co-cultured with B3Z and CPRG assay developed. Data generated from B3Z CPRG absorbance readings and normalised against maximum absorbance of non-inhibited cells (n=3). The four-parameter logistic (4PL) regression curve was generated from normalised means (±SD). Coloured dotted lines represent ED50 values for each. Peptide diluted with and without cell treatment with epoxomicin for **(A)** ctss peptide from 250 nM to 0.98 nM; **(B)** mutant peptide from 250 nM to 0.98 nM; **(C)** scrambled peptide from 2000 to 0.48 nM.



OVA	Absorbance	Dilution Factor	Concentration / mg/mL	Mass / mg
Before	0.7228	2	0.998	4.991
After	0.4799	1	0.3243	3.243

Conjugated Mass / mg	1.748
Total Beads	6.75×10^9
µg/10^6 beads	0.26
OVA µg/mg of beads	175

Figure 7.8 Measuring the Yield of OVA Conjugated to Latex Beads Using a BCA Assay
The concentration of OVA solution before and after bead conjugation was measured by BCA Assay to determine bound mass. The concentration of OVA concentrations before and after conjugation was calculated by interpolating the BCA assay standard curve. Linear regression and interpolation calculations were performed using GraphPad Prism software. Concentration and volume were used to determine the total mass in solution, with the differences being the conjugated mass. Using the certificate of analysis (Thermo Fisher), the total number of beads and, therefore, the mass per million and per milligram was calculated.

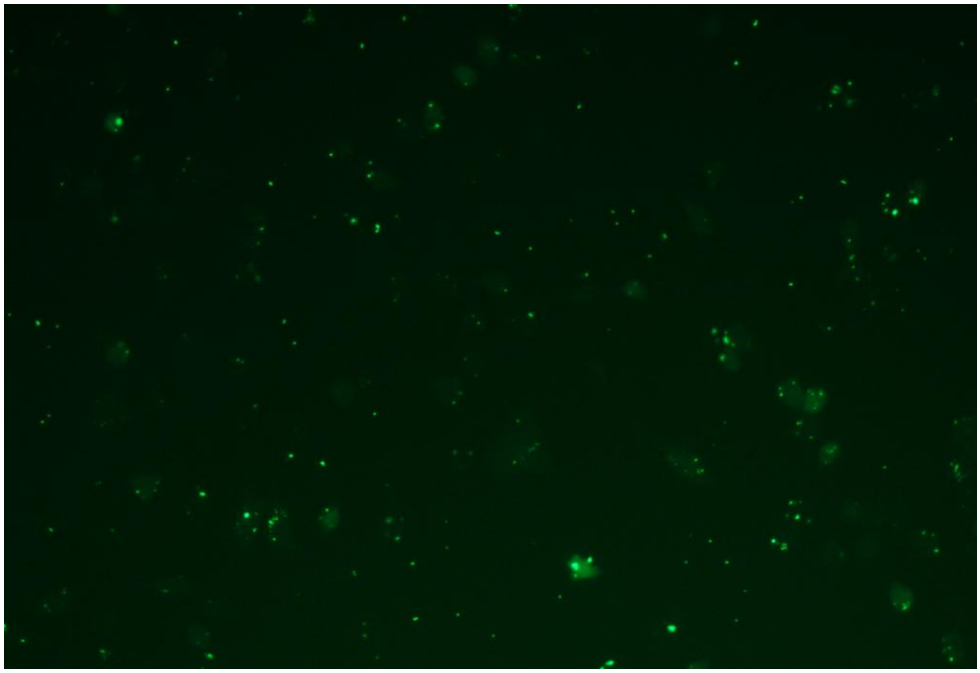


Figure 7.9 Fluorescein-Conjugated siRNA Transfection Control
DC2.4 cells transfected with fluorescein-conjugated siRNA as a positive control for transfection. Imaged six hours post-transfection using a Zeiss Axiovert 25 fluorescent microscope under blue light with a green filter.

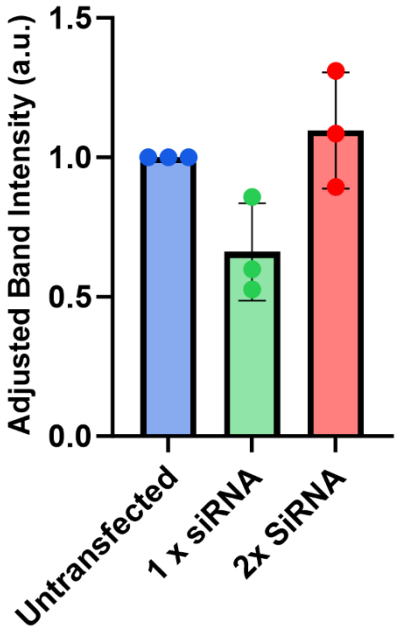


Figure 7.10 siRNA Knockdown Band Intensity Analysis of Second Band
Band intensity analysis of second lower band on cathepsin S western blot. Analysis was performed in ImageJ by band peak analysis, taking the area under the curve of bands from western blot images. Intensity normalised and adjusted against β-actin expression for each lane. Graph showing Mean ±SD of n=3.

7.2 Appendix II – Buffer & Media List

Name	Composition (#Product, Company)
1 x TAE buffer	40 mM Tris Base 20 mM glacial acetic acid (#A0400BP17, Fisher Scientific) 1mM EDTA sodium salt (#E5134-50G, Sigma-Aldrich)
Low salt LB/LB agar (1L)	10 g tryptone (#TRP03, Formedium) 5 g yeast Extract (#YEA03, Formedium) 5 g sodium chloride (15 g agar)
E. coli lysis buffer	50 mM HEPES (#H3375, Sigma-Aldrich) pH 8.0 500 mM NaCl 10% glycerol 10 mM imidazole 0.5 mg/mL lysozyme (#89833, Pierce) 50 Units Benzonase 1 x cOmplete protease inhibitor cocktail (#11697498001, Roche) 0.1% DDM 1 mM magnesium sulphate (#10316240, Fisher Scientific) 0.5 mM Tris(2-carboxyethyl)phosphine (TCEP, #M02624, Fluorochem)
Wash buffer	50 mM HEPES pH 8.0 500 mM sodium chloride 10% glycerol 25 mM imidazole 0.5 mM TCEP
Elution buffer	50 mM HEPES pH 8.0 500 mM sodium chloride 10% glycerol 500 mM imidazole 0.5 mM TCEP
IB wash buffer	50 mM HEPES pH 8.0 500 mM sodium chloride 10% glycerol 10 mM imidazole
Urea pH 7.5 buffer	8 M urea (#U5128, Sigma-Aldrich) 50 mM HEPES pH 7.5 500 mM sodium chloride 10% glycerol 10 mM imidazole
Urea pH 5.0 buffer	8 M urea 50 mM sodium acetate pH 5.0 500 mM sodium chloride 10% glycerol 10 mM imidazole
GuHCl pH 7.5 buffer	6 M guanidine hydrochloride (#50950, Sigma-Aldrich) 50 mM HEPES pH 7.5 500 mM sodium chloride 10% glycerol 10 mM imidazole
GuHCl pH 5.0 buffer	6 M guanidine hydrochloride 50 mM sodium acetate pH 5.0 500 mM sodium chloride

	10% glycerol 10 mM imidazole
GuHCl wash buffer	6 M guanidine hydrochloride 50 mM HEPES pH 7.5 500 mM sodium chloride 10% glycerol 25 mM imidazole
GuHCl elution buffer	6 M guanidine hydrochloride 50 mM HEPES pH 7.5 500 mM sodium chloride 10% glycerol 500 mM imidazole
ROP refolding buffer	50 mM HEPES pH 7.4 500 mM sodium chloride 10% glycerol
4 M, 2 M, 1 M, and 0 M GuHCl pH 7.5 buffer	4 M/2 M/1 M/0 M guanidine hydrochloride 50 mM HEPES pH 7.5 500 mM sodium chloride 10% glycerol 10 mM imidazole
Detergent screen buffer	50 mM HEPES pH 8.0 300 mM sodium chloride 10% glycerol
0.1%/1%/5%/10% sarkosyl buffer	0.1%/1%/5%/10% (v/v) sarkosyl 50 mM HEPES pH 8.0 500 mM sodium chloride 10% glycerol 10 mM imidazole 0.5 mM TCEP
Sarkosyl binding buffer	0.25% (v/v) sarkosyl 50 mM HEPES pH 8.0 500 mM sodium chloride 10% glycerol 10 mM imidazole 0.5 mM TCEP
Sarkosyl wash buffer	0.25% (v/v) sarkosyl 50 mM HEPES pH 8.0 500 mM sodium chloride 10% glycerol 25 mM imidazole 0.5 mM TCEP
Sarkosyl elution buffer	0.25% (v/v) Sarkosyl 50 mM HEPES pH 8.0 500 mM sodium chloride 10% glycerol 500 mM imidazole 0.5 mM TCEP
ROP dialysis buffer	50 mM HEPES pH 8.0 10% glycerol 300 mM sodium chloride
10x phosphate binding buffer	0.67 M sodium phosphate dibasic (#S7907, Sigma-Aldrich) 0.33 M sodium phosphate monobasic (#71505, Sigma-Aldrich) adjusted to pH 7.2 with 5 M sodium hydroxide (#S8055, Sigma-Aldrich)

TSE buffer	50 mM TRIS-HCl pH 8.0 20% sucrose 1 mM EDTA 1 x cOmplete protease inhibitor cocktail
SUMO lysis buffer	50 mM TRIS-HCl pH 8.0 150 mM sodium chloride 0.1% DDM 10 mM imidazole 1 x (50U) Benzonase 1 mM magnesium sulphate 1x cOmplete protease inhibitor
SUMO wash buffer	50 mM TRIS-HCl pH 8.0 150 mM sodium chloride 25 mM imidazole
scFv refolding buffer	50 mM TRIS-HCl pH 8.0 150 mM sodium chloride 0.5 M L-arginine 0.1 mM oxidised glutathione (GSSG, #SC-29093, Chemcruz) 1 mM reduced glutathione (GSH, #101814, MP Biomedicals) 1 mM EDTA
scFv dilution buffer	50 mM TRIS-HCl pH 8.0 150 mM sodium chloride
SUMO protease reduced master mix	41.5 µl of scFv dilution buffer 1 mM TCEP
SUMO protease redox master mix	41.5 µl of scFv dilution buffer 0.1 mM GSSG 1 mM GSH
Tag binding buffer	50 mM TRIS-HCl pH 8.0 150 mM sodium chloride 10 mM imidazole
Tag wash buffer	50 mM TRIS-HCl pH 8.0 150 mM sodium chloride 25mM imidazole
Tag elution buffer	50 mM TRIS-HCl pH 8.0 150 mM sodium chloride 500 mM imidazole
Blocking buffer	5% (w/v) skimmed milk powder (#70166, Millipore) 1 x DPBS 0.1% TWEEN-20
Conjugation sarkosyl buffer	0.1% sarkosyl 50 mM HEPES pH 8.0 300 mM sodium chloride 10% glycerol
CPRG lysis buffer	150 µM CPRG (#10884308001, Roche) 5 mM DTT 0.125% (v/v) octylphenoxy poly(ethyleneoxy)ethanol, (IGEPAL CA-630, #I3021, Sigma Aldrich) 9 mM magnesium chloride ($MgCl_2$, #M2393, Sigma-Aldrich) in 1x PBS

QuickFold Protein Refolding Kit (AthenaES, USA) Buffer list

	Composition
Buffer 1	50 mM MES pH 6.0, 9.6 mM NaCl, 0.4 mM potassium chloride (KCl), 2 mM MgCl2, 2 mM calcium chloride (CaCl2), 0.75 M guanidine HCl, 0.5% Triton X-100, 1 mM DTT
Buffer 2	50 mM MES pH 6.0, 9.6 mM NaCl, 0.4 mM KCl, 2 mM MgCl2, 2 mM CaCl2, 0.5 M arginine, 0.05% polyethylene glycol 3,550, 1 mM GSH, 0.1 mM GSSH
Buffer 3	50 mM MES pH 6.0, 9.6 mM NaCl, 0.4 mM KCl, 1mM EDTA, 0.4 M sucrose, 0.75 M guanidine HCl, 0.5% Triton X-100, 0.05% polyethylene glycol 3, 550, 1 mM DTT
Buffer 4	50 mM MES pH 6.0, 240 mM NaCl, 10 mM KCl, 2 mM MgCl2, 2 mM CaCl2, 0.75 M guanidine HCl, 1 mM DTT
Buffer 5	50 mM MES pH 6.0, 240 mM NaCl, 10 mM KCl, 1 mM EDTA, 0.4 M sucrose, 0.75 M guanidine HCl, 1 mM DTT
Buffer 6	50 mM MES pH 6.0, 240 mM NaCl, 10 mM KCl, 1 mM EDTA, 0.5 M arginine, 0.4 M sucrose, 0.5% Triton X-100, 0.05% polyethylene glycol 3,550, 1 mM GSH, 0.1 mM GSSH
Buffer 7	50 mM MES pH 6.0, 240 mM NaCl, 10 mM KCl, 2 mM MgCl2, 2 mM CaCl2, 0.75 M guanidine HCl, 0.05% polyethylene glycol 3,550, 1 mM DTT
Buffer 8	50 mM Tris-Cl pH 8.5, 9.6 mM NaCl, 0.4 mM KCl, 2 mM MgCl2, 2 mM CaCl2, 0.5 M arginine, 0.4 M sucrose, 0.75 M guanidine HCl, 1 mM GSH, 0.1 mM GSSH
Buffer 9	50 mM Tris-Cl pH 8.5, 9.6 mM NaCl, 0.4 mM KCl, 1 mM EDTA, 0.5 M arginine, 0.75 M guanidine HCl, 0.05% polyethylene glycol 3,550, 1 mM DTT
Buffer 10	50 mM Tris-Cl pH 8.5, 9.6 mM NaCl, 0.4 mM KCl, 2 mM MgCl2, 2 mM CaCl2, 0.5 M arginine, 0.4 M sucrose, 0.75 M guanidine HCl, 1 mM GSH, 0.1 mM GSSH
Buffer 11	50 mM Tris-Cl pH 8.5, 9.6 mM NaCl, 0.4 mM KCl, 1 mM EDTA, 0.5% Triton X-100, 1 mM DTT
Buffer 12	50 mM Tris-Cl pH 8.5, 240 mM NaCl, 10 mM KCl, 1 mM EDTA, 0.05% polyethylene glycol 3,550, 1 mM GSH, 0.1 mM GSSH
Buffer 13	50 mM Tris-Cl pH 8.5, 240 mM NaCl, 10 mM KCl, 1 mM EDTA, 0.5 M arginine, 0.75 M guanidine HCl, 0.5% Triton X-100, 1 mM DTT
Buffer 14	50 mM Tris-Cl pH 8.5, 240 mM NaCl, 10 mM KCl, 2 mM MgCl2, 2 mM CaCl2, 0.5 M arginine, 0.4 M sucrose, 0.75 M guanidine HCl, 0.5% Triton X-100, 0.05% polyethylene glycol 3,550, 1 mM GSH, 0.1 mM GSSH
Buffer 15	50 mM Tris-Cl pH 8.5, 240 mM NaCl, 10 mM KCl, 1 mM EDTA, 2 mM MgCl2, 2 mM CaCl2, 0.4 M sucrose, 1 mM DTT

7.3 Appendix III – DNA and Protein Sequences

Primer Name	Description	Sequence
pLIC-Fwd	LIC vector sequencing forward primer	TGTGAGCGGATAACAATTCC
pLIC-Rev	LIC vector sequencing Reverse primer	AGCAGCCAACTCAGCTTCC
Bsa4/MBP2-OR-Fwd	OVA-ROP LIC forward primer for pNIC28-Bsa4 and pNIC-MBP2-LIC	TACTTCCAATCCATGAGCATGCTGGTTCTGCT
Bsa4/MBP2-OR-Rev	OVA-ROP LIC reverse primer for pNIC28-Bsa4 and pNIC-MBP2-LIC	TATCCACCTTTACTGTTAACGACCTGCTTCATTAATTTCGG
CTH0-OR-Fwd	OVA-ROP LIC forward primer for pNIC-CTH0	TTAAGAAGGAGATATACTATGAGCATGCTGGTTCTGCTGCC
CTH0-OR-Rev	OVA-ROP LIC reverse primer for pNIC-CTH0	GATTGGAAGTAGAGGTTCTCTGCACGACCTGCTTCATTAATTTC
SUMO-OR-Fwd	OVA-ROP LIC forward primer for pSUMO-LIC	ACCAGGAGCAAACGGGAGGTATGAGCATGCTGGTTCTG
SUMO-OR-Rev	OVA-ROP LIC reverse Primer for pSUMO-LIC	CAGACCGCCACCGCTTTAACGACCTGCTTCATTAATTTC
pFUSE-tOR-Fwd	Forward primer for amplification of tOVA-ROP for pFUSE insertion	TTGTCACGAATTCGATGCCCGATGAGGTGTCC
pFUSE-tOR-Rev	Reverse primer for amplification of tOVA-ROP for pFUSE insertion	TCTGGGAGATCTGACTTTGATCTTCCGTTCTT
Mu IgM Q5 mutagenesis-Fwd	Forward mutagenesis primer for insertion of mouse IgM tailpiece to end of IgG Fc	ATGAGCGACACCGGCGGCACATGTTACTGAGCTCAGCTAGCTGGC
Mu IgM Q5 mutagenesis-Rev	Reverse mutagenesis primer for insertion of mouse IgM tailpiece to end of IgG Fc	GATCAGGGACACGTTGTACAGTGTGGGTTTACCCGGAGTCCGGGA
Q94C Mutagenesis-Fwd	Forward mutagenesis primer for substitution of glutamine to cysteine at position 94 on Fc-tag	CCCCATCTGCCACCAGGACTGGATGAGTGGC
Q94C Mutagenesis-Rev	Reverse mutagenesis primer for substitution of glutamine to cysteine at position 94 on Fc-tag	TGGTGGCAGATGGGGAGGGCACTGACC
Fc-Seq Rev	Fc tag sequencing reverse primer	TCCCCCTGAACCTGAAACAT
pNIC-CTH0-DEC-Fwd	OVA and NY-ESO-1 DEC-205 scFv fusion LIC forward primer for pNIC-CTH0	TTAAGAAGGAGATATACTATGAAATATCTGCTGCCGACC
pNIC-CTH0-DEC-Rev	OVA and NY-ESO-1 DEC-205 scFv fusion LIC reverse primer for pNIC-CTH0	GATTGGAAGTAGAGGTTCTCTGCTTATTCGTGCCATTCGATTTTCTGG
pSUMO-OVA-DEC-Fwd	OVA-DEC-205 scFv fusion LIC forward primer for pSUMO-LIC	ACCAGGAGCAAACGGGAGGTGAAGTTAAACTGCAGCAGAG

pSUMO-NYE-DEC-Fwd	NY-ESO-1-scFv fusion LIC forward primer for pSUMO-LIC	ACCAGGAGCAAACGGGAGGTGAAG TTCAGCTGCAGCAGAG
pSUMO-DEC-Rev	OVA and NY-ESO-1 DEC-205 scFv fusion LIC forward primer for pSUMO-LIC	CAGACCGCCACCGCTTTATTCGTGC CATTCGATTTTCTGG

Ovalbumin Protein Sequence – 42.9 kDa (ε –31,775 $M^{-1}cm^{-1}$)

$CD8^+$ epitope, **$CD4^+$ epitope**

MGSIGAASMEFCFDVFKELKVHHANENIFYCPIAIMSALAMVYLGAKDSTRTQINKVVRFDKL
PGFGDSIEAQCGTSVNVHSSLRDILNQITKPNDVYSFSLASRLYAEERYPILPEYLQCVKELY
RGGLEPINFQTAADQARELINSWVESQTNGIIRNVLQPSSVDSQTAMVLVNAIVFKGLWEKA
FKDEDTQAMPFRVTEQESKPVQMMYQIGLFRVASMASEKMKILELPFASGTMSMLVLLPDE
VSGLEQLE**SIINFEKL**TEWTSSNVMEERKIKVYLPRMKMEEKYNLTSVLMAMGITDVFSSSA
NLSGISSAESLK**ISQAVHAAHAEINEAGR**EVVGSAEAGVDAASVSEEFRADHPFLFCIKHIAT
NAVLFFGRCVSP

SUMO-OVA-DEC-205 scFv fusion protein sequence – 44.42 kDa (ε – 69,705 $M^{-1}cm^{-1}$) – anti-mouse DEC-205 scFv sequence (NLDC-145) (Demangel et al., 2005; Swiggard et al., 1995)

$CD8^+$ epitope, **$CD4^+$ epitope**, **$(G_4S)_3$ linker**, **AviTag**

MCSSHHHHHHGSGSGSDQEAKPSTEDLGDKKEGEYIKLKVIGQDSSEIHFKVKMTTHLKKL
KESYCQRQGVPMNSLRFLFEGQRIADNHTPKELGMEEEDVIEVYQEQTGGSS**GGGGSGG
GGSGGGGS**DIQMTQSPSFLSTSLGNSITITCHASQNIKGWLAWYQQKSGNAPQLLIYKASS
LQSGVPSRFSGSGSGTDYIFTISNLQPEDIATYYCQHYQSFPWTFGGGTKLEIKRAA**GGGG
SGGGGSGGGGS**SIINFEKL**ISQAVHAAHAEINEAGR**GLNDIFEAQKIEWHE**

SUMO-NY-ESO-205 scFv fusion protein sequence – 46.6 kDa (ε – 62715 $M^{-1}cm^{-1}$) – anti-human DEC-205 scFv sequence (MG38-3) (Birkholz et al., 2010; Guo et al., 2000)

$CD8^+$ epitope, **$CD4^+$ epitope**, **$(G_4S)_3$ linker**, **AviTag**

MCSSHHHHHHGSGSGSDQEAKPSTEDLGDKKEGEYIKLKVIGQDSSEIHFKVKMTTHLKKL
KESYCQRQGVPMNSLRFLFEGQRIADNHTPKELGMEEEDVIEVYQEQTGGEVQLQQSGPV
LVKPGASVKMSCKASGNTFTDSFMHWMKQSHGKSLEWIGIINPYNGGTSYNQKFKGKATLT
VDKSSSTAYMELNSLTSEDSAVYYCARNGVRYYFDYWGQGTTLTVSSASGA**GGGGSGGG
GSGGGGS**AAQPAMADYKQAVVTQESALTTSPGETVTLTCRSSTGAVTISNYANWVQEKPD
HLFTGLIGGTNNRAPGVPARFSGSLIGDKAALTITGAQTEDEAIYFCALWYNNQFIFGSGTKV
TVL**GGGGSGGGGSGGGGS**ARGPESRLLEFYLAMPFATPMEAELARRSL**SLLMWITQCGL
NDIFEAQKIEWHE**

SUMO tag

MCSSHHHHHHGSGSGSDQEAKPSTEDLGDKKEGEYIKLKVIGQDSSEIHFKVKMTTHLKKL
KESYCQRQGVPMNSLRFLFEGQRIADNHTPKELGMEEEDVIEVYQEQTGG

MBP2 tag

MKIEEGKLVIWINGDKGYNGLAEVGKKFEKDTGIKVTVEHPDKLEEKFPQVAATGDGPDIIFW
AHDRFGGYAQSGLLAEITPDKAFQDKLYPFTWDAVRYNGKLIAYPIAVEALSLIYNKDLLPNP
PKTWEEIPALDKELKAKGKSALMFNLQEPYFTWPLIAADGGYAFKYENGKYDIKDVGVDNA
GAKAGLTFLVDLIKNKHMNADTDYSIAEAAFNKGETAMTINGPWAWSNIDTSKVNYGVTVLP
TFKGQPSKPFVGVLSAGINAASPNKELAKEFLENYLLTDEGLEAVNKDKPLGAVALKSYEEE
LAKDPRIAATMENAQKGEIMPNIPQMSAFWYAVRTAVINAASGRQTVDEALKDAQTNSGGS
HHHHHHSSGVDLGTENLYFQS

C-terminal (CTH0) 6xHis TEV tag

ENLYFQSHHHHHH

N-terminal (Bsa4) 6xHis TEV tag

MHHHHHHSSGVDLGTENLYFQS

PelB Signal Sequence with 6x His-tag and TEV site

KYLLPTAAAGLLLLAAQPAMAHHHHHHENLYFQS

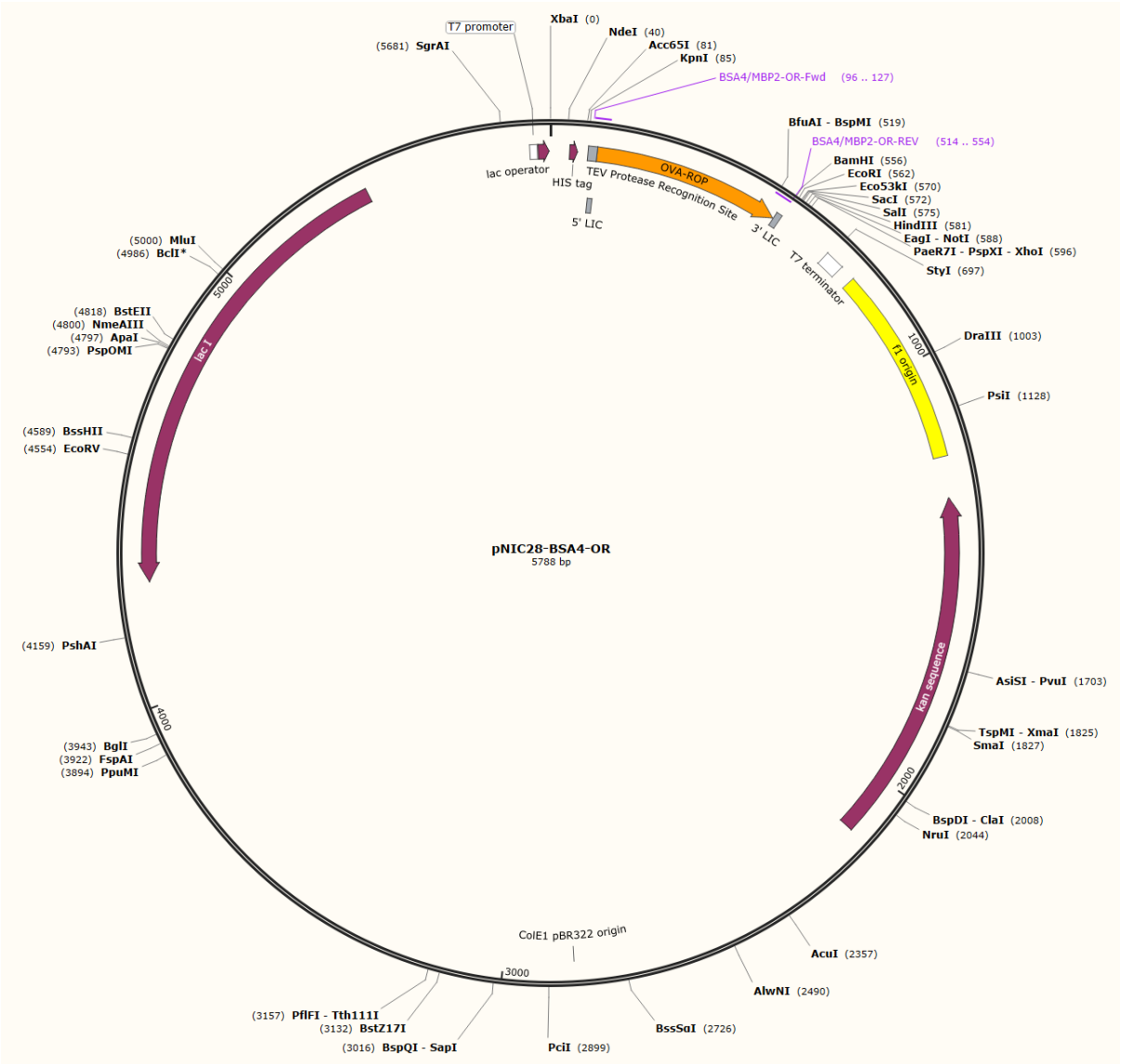
G/S Linker

GGGGSGGGGSGGGGS

AviTag™

GLNDIFEAQKIEWHE

pNIC28-Bsa4-OR (OVA-ROP) Construct Map

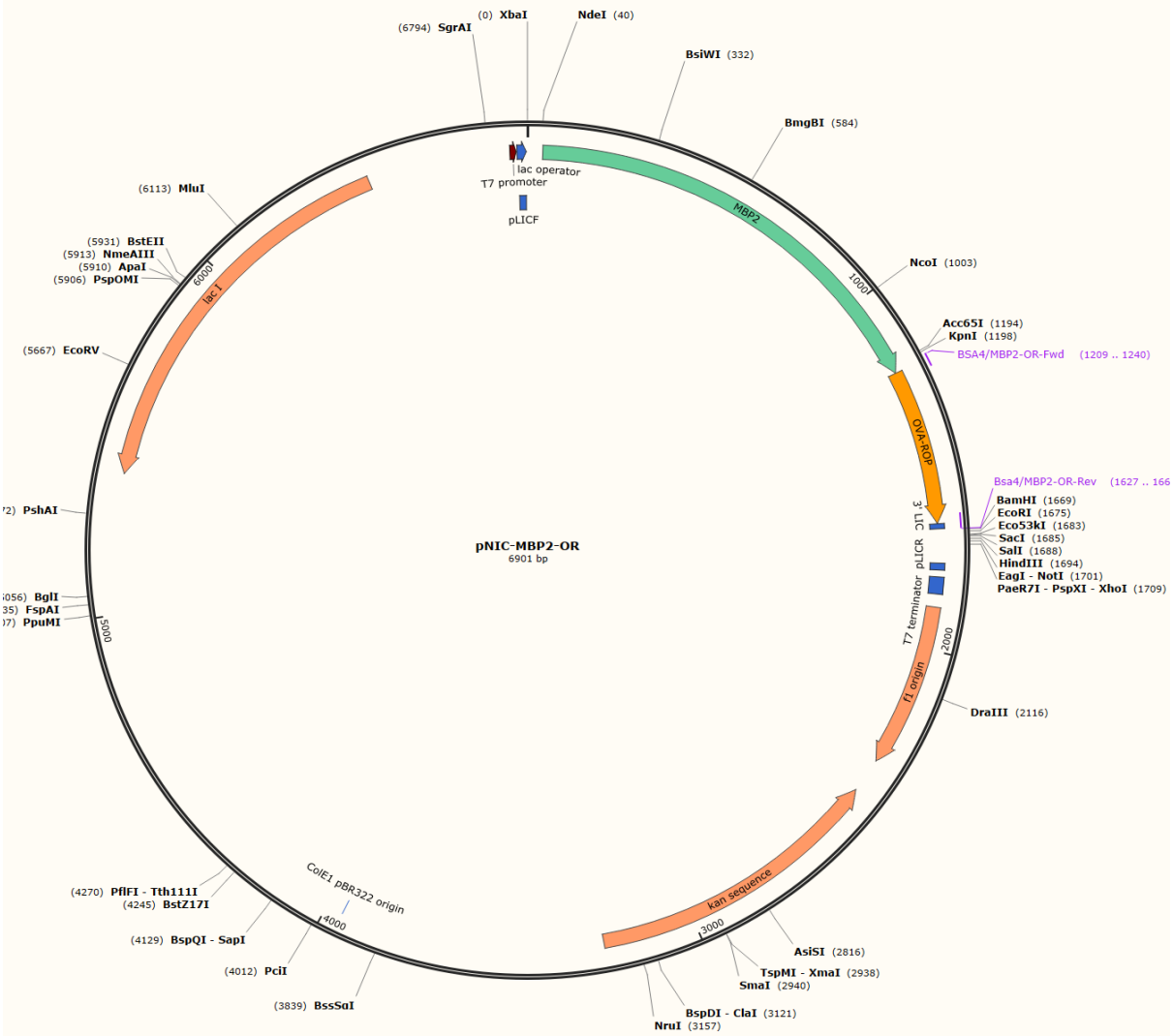


pNIC28-Bsa4-OR (OVA-ROP) Construct DNA Sequence – Bold highlights OVA-ROP Gene

ctagaaataattttgtttaactttaagaaggagatatacatatgcaccatcatcatcatcattcttctggtgtagatctgggtaccgaga
acctgtacttccaatcc**atgagcatgctggttctgctgccggatgaagttagcggtctggaacagctggaaagcattatca**
attttgaaaaactgaccgaatggaccagcagcaatgttatggaactgcgtatgaaaacagaatggacctcaagtaatgt
gatggaagaacgcaaaatcaaagtgtatctgcctcgcatgaaaatggaagagaaatataacctgaccagcgttctgat
ggccctgcggatgaaaaaatacaatctgacctcagtgctgatggcaatgggtattaccgatgtttttagcagcagcgca
aatctgagcggtattagcagcgcagaaagcctgaaaattagtctgcgcatgaagattagctcagccgaatcactgaaa
atttcacaggcagttcatgcagcacatgccgaaattaatgaagcaggtcgttaacagtaaaggtggatacggatccgaatt
cgagctccgtcgacaagcttgcggccgcactcgagcaccaccaccaccaccactgagatccggctgctaacaaagcccgaa
aggaagctgagttggctgctgccaccgctgagcaataactagcataaccccttggggcctctaaacgggtcttgaggggttttttg
ctgaaaggaggaactatatccggattggcgaatgggacgcgccctgtagcggcgcattaagcgcggcgggtgtggtggttacg
cgcagcgtgaccgctacacttgccagcgccctagcgcccgctcctttcgctttcttcccttcctttctcgccacgttcgccggctttccc
cgtcaagctctaaatcgggggctccctttagggttccgatttagtgctttacggcacctcgaccccaaaaaacttgattagggtgatg
gttcacgtagtgggccatcgccctgatagacggtttttcgccctttgacgttggagtccacgttctttaatagtggactcttgttccaaac
tggaacaacactcaaccctatctcggtctattcttttgatttataagggattttgccgatttcggcctattggttaaaaaatgagctgattt
aacaaaaatttaacgcgaattttaacaaaatattaacgtttacaatttcaggtggcacttttcggggaaatgtgcgcggaacccta
tttgtttatttttctaaatacattcaaatatgtatccgctcatgaattaattcttagaaaaactcatcgagcatcaaatgaaactgcaattt
attcatatcaggattatcaataccatatttttgaaaaagccgtttctgtaatgaaggagaaaactcaccgaggcagttccataggat
ggcaagatcctggtatcggtctgcgattccgactcgtccaacatcaatacaacctattaatttcccctcgtcaaaaataaggttatca
agtgagaaatcaccatgagtgacgactgaatccggtgagaatggcaaaagtttatgcatttctttccagacttgttcaacaggcca
gccattacgctcgtcatcaaaatcactcgcatcaaccaaaccgttattcattcgtgattgcgcctgagcgagacgaaatacgcgat
cgctgttaaaaggacaattacaaacaggaatcgaatgcaaccggcgcaggaacactgccagcgcatcaacaatattttcacct
gaatcaggatattcttctaatacctggaatgctgttttcccggggatcgcagtggtgagtaaccatgcatcatcaggagtacggata
aaatgcttgatggtcggaagaggcataaattccgtcagccagtttagtctgaccatctcatctgtaacatcattggcaacgctacctt
tgccatgtttcagaaacaactctggcgcatcgggcttcccatacaatcgatagattgtcgcacctgattgcccgacattatcgcgag
cccatttatacccatataaatcagcatccatgttggaatttaatcgcggcctagagcaagacgtttcccgttgaatatggctcataac
acccccttgtattactgtttatgtaagcagacagttttattgttcatgaccaaaatcccttaacgtgagttttcgttccactgagcgtcaga
ccccgtagaaaagatcaaaggatcttcttgagatcctttttttctgcgcgtaatctgctgcttgcaaacaaaaaaaccaccgctacc
agcggtggtttgtttgccggatcaagagctaccaactctttttccgaaggtaactggcttcagcagagcgcagataccaaatactgt
ccttctagtgtagccgtagttaggccaccacttcaagaactctgtagcaccgcctacatacctcgctctgctaatcctgttaccagtg
gctgctgccagtggcgataagtcgtgtcttaccgggttggactcaagacgatagttaccggataaggcgcagcggtcgggctga
acgggggttcgtgcacacagcccagcttggagcgaacgacctacaccgaactgagatacctacagcgtgagctatgagaa
agcgccacgcttcccgaagggagaaaggcggacaggtatccggtaagcggcagggtcggaacaggagagcgcacgagg
gagcttccagggggaaacgcctggtatctttatagtcctgtcgggtttcgccacctctgacttgagcgtcgatttttgtgatgctcgtca
ggggggcggagcctatggaaaaacgccagcaacgcggccttttacggttcctggccttttgctggccttttgctcacatgttctttcc
tgcgttatcccctgattctgtggataaccgtattaccgcctttgagtgagctgataccgctcgccgcagccgaacgaccgagcgca
gcgagtcagtgagcgaggaagcggaagagcgcctgatgcggtattttctccttacgcatctgtgcggtatttcacaccgcatatat
ggtgcactctcagtacaatctgctctgatgccgcatagttaagccagtatacactccgctatcgctacgtgactgggtcatggctgc
gccccgacacccgccaacacccgctgacgcgccctgacgggcttgtctgctcccggcatccgcttacagacaagctgtgaccg
tctccgggagctgcatgtgtcagaggttttcaccgtcatcaccgaaacgcgcgaggcagctgcggtaaagctcatcagcgtggtc
gtgaagcgattcacagatgtctgcctgttcatccgcgtccagctcgttgagtttctccagaagcgttaatgtctggcttctgataaagc
gggccatgttaagggcggttttttcctgtttggtcactgatgcctccgtgtaagggggatttctgttcatgggggtaatgataccgatga
aacgagagaggatgctcacgatacgggttactgatgatgaacatgcccggttactggaacgttgtgagggtaaacaactggcg
gtatggatgcggcgggaccagagaaaaatcactcagggtcaatgccagcgcttcgttaatacagatgtaggtgttccacagggt
agccagcagcatcctgcgatgcagatccggaacataatggtgcagggcgctgacttccgcgtttccagactttacgaaacacgg
aaaccgaagaccattcatgttgttgctcaggtcgcagacgttttgcagcagcagtcgcttcacgttcgctcgcgtatcggtgattcatt
ctgctaaccagtaaggcaaccccgccagcctagccgggtcctcaacgacaggagcacgatcatgcgcacccgtggggccgc
catgccggcgataatggcctgcttctcgccgaaacgtttggtggcgggaccagtgacgaaggcttgagcgagggcgtgcaaga
ttccgaataccgcaagcgacaggccgatcatcgtcgcgctccagcgaaagcggtcctcgccgaaaatgacccagagcgctgc
cggcacctgtcctacgagttgcatgataaagaagacagtcataagtgcggcgacgatagtcatgccccgcgcccaccggaag
gagctgactgggttgaaggctctcaagggcatcggtcgagatcccggtgcctaatgagtgagctaacttacattaattgcgttgcg
ctcactgcccgctttccagtcgggaaacctgtcgtgccagctgcattaatgaatcggccaacgcgcggggagaggcggtttgcgt
attgggcgccagggtggtttttctttcaccagtgagacgggcaacagctgattgcccttcaccgcctggccctgagagagttgcag

caagcggtccacgctggtttgccccagcaggcgaaaatcctgtttgatggtggttaacggcgggatataacatgagctgtcttcgg
tatcgtcgtatcccactaccgagatatccgcaccaacgcgcagcccggactcggtaatggcgcgcattgcgcccagcgccatct
gatcgttggcaaccagcatcgcagtgggaacgatgccctcattcagcatttgcatggtttgttgaaaaccggacatggcactcca
gtcgccttcccgttccgctatcggctgaatttgattgcgagtgagatatttatgccagccagccagacgcagacgcgccgagaca
gaacttaatgggcccgctaacagcgcgatttgctggtgacccaatgcgaccagatgctccacgcccagtcgcgtaccgtcttcat
gggagaaaataatactgttgatgggtgtctggtcagagacatcaagaaataacgccggaacattagtgcaggcagcttccaca
gcaatggcatcctggtcatccagcggatagttaatgatcagcccactgacgcgttgcgcgagaagattgtgcaccgccgctttac
aggcttcgacgccgcttcgttctaccatcgacaccaccacgctggcacccagttgatcggcgcgagatttaatcgccgcgacaat
ttgcgacggcgcgtgcagggccagactggaggtggcaacgccaatcagcaacgactgtttgcccgccagttgttgtgccacgc
ggttgggaatgtaattcagctccgccatcgccgcttccacttttcccgcgttttcgcagaaacgtggctggcctggttcaccacgcg
ggaaacggtctgataagagacaccggcatactctgcgacatcgtataacgttactggtttcacattcaccaccctgaattgactctc
ttccgggcgctatcatgccataccgcgaaaggttttgcgccattcgatggtgtccgggatctcgacgctctcccttatgcgactcctg
cattaggaagcagcccagtagtaggttgaggccgttgagcaccgccgccgcaaggaatggtgcatgcaaggagatggcgcc
caacagtcccccggccacggggcctgccaccatacccacgccgaaacaagcgctcatgagcccgaagtggcgagcccgat
cttccccatcggtgatgtcggcgatataggcgccagcaaccgcacctgtggcgccggtgatgccggccacgatgcgtccggcgt
agaggatcgagatctcgatcccgcgaaattaatacgactcactataggggaattgtgagcggataacaattcccct

pNIC28-MBP2-OR (OVA-ROP) Construct Sequence Map



pNIC28-MBP2-OR DNA Sequence - **Bold** highlights OVA-ROP Gene

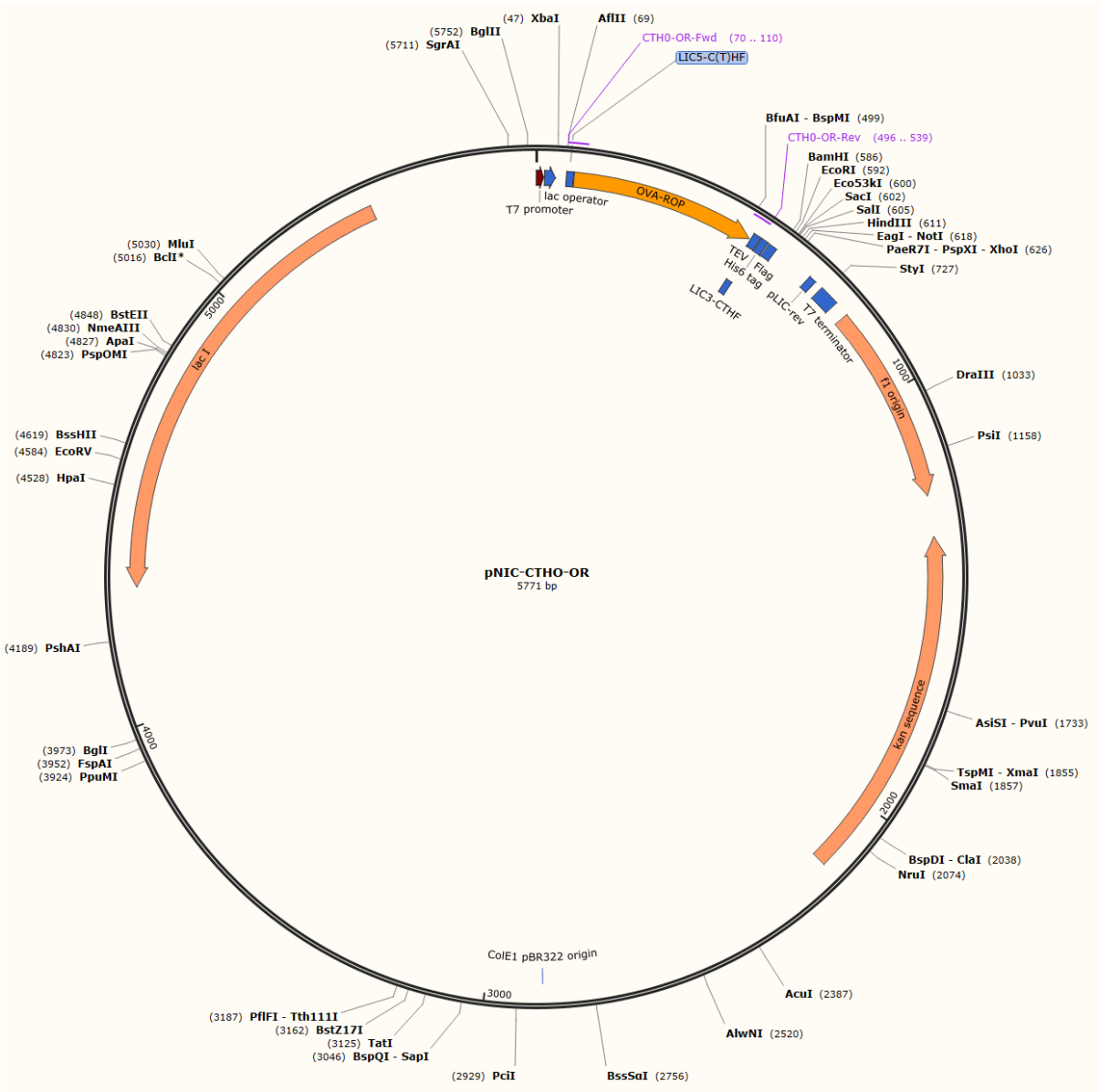
ctagaaataattttgtttaactttaagaaggagatatacatatgaaaatcgaagaaggtaaactggtaatctggattaacggcgata
aaggctataacggcctagctgaagtcggtaagaaattcgagaaagataccggaattaaagtcaccgttgagcatccggataaa
ctggaagagaaattcccacaggttgcggcaactggcgatggccctgacattatcttctgggcacacgaccgctttggtggctacg
ctcaatctggcctgttggctgaaatcaccccggacaaagcgttccaggacaagctgtatccgtttacctgggatgccgtacgttac
aacggcaagctgattgcttacccgatcgctgttgaagcgttatcgctgatttataacaaagatctgctgccgaacccgccaaaaac
ctgggaagagatcccggcgctggataaagaactgaaagcgaaaggtaagagcgcgctgatgttcaacctgcaagaaccgta
cttcacctggccgctgattgctgctgacggggttatgcgttcaagtatgaaaacggcaagtacgacattaaagacgtgggcgtg
gataacgctggcgcgaaagcgggtctgaccttcctggttgacctgattaaaaacaaacacatgaatgcagacaccgattactcc
atcgcagaagctgcctttaataaaggcgaaacagcgatgaccatcaacggcccgtgggcatggtccaacatcgacaccagca
aagtgaattatggtgtaacggtactgccgaccttcaagggtcaaccatccaaaccgttcgttggcgtgctgagcgcaggtattaac
gccgccagtccgaacaaagagctggcaaaagagttcctcgaaaactatctgctgactgatgaaggtctggaagcggttaataa
agacaaaccgctgggtgccgtagcgctgaagtcttacgaggaagagttggcgaaagatccacgtattgccgccaccatggaa
aacgcccagaaaggtgaaatcatgccgaacatcccgcagatgtccgctttctggtatgccgtgcgtactgcggtgatcaacgcc
gccagcggtcgtcagactgtcgatgaagccctgaaagacgcgcagactaattcgggcggctctcaccaccatcatcatcactctt
ctggcgtggatctgggtaccgagaacctgtacttccaatcc**atgagcatgctggttctgctgccggatgaagttagcggtctg**
gaacagctggaaagcattatcaattttgaaaaactgaccgaatggaccagcagcaatgttatggaactgcgtatgaaa
acagaatggacctcaagtaatgtgatggaagaacgcaaaatcaaagtgtatctgcctcgcatgaaaatggaagagaa
atataacctgaccagcgttctgatggccctgcggatgaaaaaatacaatctgacctcagtgctgatggcaatgggtatt
accgatgtttttagcagcagcgcaaatctgagcggtattagcagcgcagaaagcctgaaaattagtctgcgcatgaag
attagctcagccgaatcactgaaaatttcacaggcagttcatgcagcacatgccgaaattaatgaagcaggtcgttaac
agtaaaggtggatacggatccgaattcgagctccgtcgacaagcttgcggccgcactcgagcaccaccaccaccaccactga
gatccggctgctaacaaagcccgaaaggaagctgagttggctgctgccaccgctgagcaataactagcataacccctttggggc
ctctaaacgggtcttgaggggttttttgctgaaaggaggaactatatccggattggcgaatgggacgcgccctgtagcggcgcatt
aagcgcggcgggtgtggtggttacgcgcagcgtgaccgctacacttgccagcgccctagcgcccgctcctttcgctttcttcccttc
ctttctcgccacgttcgccggctttccccgtcaagctctaaatcgggggctccctttagggttccgatttagtgctttacggcacctcga
ccccaaaaaacttgattagggtgatggttcacgtagtgggccatcgccctgatagacggtttttcgccctttgacgttggagtccacg
ttctttaatagtggactcttgttccaaactggaacaacactcaaccctatctcggtctattcttttgatttataagggattttgccgatttcg
gcctattggttaaaaaatgagctgatttaacaaaaatttaacgcgaattttaacaaaatattaacgtttacaatttcaggtggcacttttt
cggggaaatgtgcgcggaacccctatttgtttatttttctaaatacattcaaatatgtatccgctcatgaattaattcttagaaaaactc
atcgagcatcaaatgaaactgcaatttattcatatcaggattatcaataccatatttttgaaaaagccgtttctgtaatgaaggagaa
aactcaccgaggcagttccataggatggcaagatcctggtatcggtctgcgattccgactcgtccaacatcaatacaacctattaa
tttcccctcgtcaaaaataaggttatcaagtgagaaatcaccatgagtgacgactgaatccggtgagaatggcaaaagtttatgc
atttctttccagacttgttcaacaggccagccattacgctcgtcatcaaaatcactcgcatcaaccaaaccgttattcattcgtgattgc
gcctgagcgagacgaaatacgcgatcgctgttaaaaggacaattacaaacaggaatcgaatgcaaccggcgcaggaacact
gccagcgcatcaacaatattttcacctgaatcaggatattcttctaatacctggaatgctgttttcccggggatcgcagtggtgagta
accatgcatcatcaggagtacggataaaatgcttgatggtcggaagaggcataaattccgtcagccagtttagtctgaccatctca
tctgtaacatcattggcaacgctacctttgccatgtttcagaaacaactctggcgcatcgggcttcccatacaatcgatagattgtcg
cacctgattgcccgacattatcgcgagcccatttatacccatataaatcagcatccatgttggaatttaatcgcggcctagagcaag
acgtttcccgttgaatatggctcataacacccttgtattactgtttatgtaagcagacagttttattgttcatgaccaaaatcccttaac
gtgagttttcgttccactgagcgtcagaccccgtagaaaagatcaaaggatcttcttgagatccttttttttctgcgcgtaatctgctgctt
gcaaacaaaaaaaccaccgctaccagcggtggtttgtttgccggatcaagagctaccaactctttttccgaaggtaactggcttca
gcagagcgcagataccaaatactgtccttctagtgtagccgtagttaggccaccacttcaagaactctgtagcaccgcctacata
cctcgctctgctaatcctgttaccagtggctgctgccagtggcgataagtcgtgtcttaccgggttggactcaagacgatagttaccg
gataaggcgcagcggtcgggctgaacgggggttcgtgcacacagcccagcttggagcgaacgacctacaccgaactgag
atacctacagcgtgagctatgagaaagcgccacgcttcccgaagggagaaaggcggacaggtatccggtaagcggcagggt
cggaacaggagagcgcacgagggagcttccagggggaaacgcctggtatctttatagtcctgtcgggtttcgccacctctgactt
gagcgtcgatttttgtgatgctcgtcaggggggcggagcctatggaaaaacgccagcaacgcggccttttacggttcctggccttt
tgctggccttttgctcacatgttctttcctgcgttatcccctgattctgtggataaccgtattaccgcctttgagtgagctgataccgctcgc
cgcagccgaacgaccgagcgcagcgagtcagtgagcgaggaagcggaagagcgcctgatgcggtattttctccttacgcatct
gtgcggtatttcacaccgcatatatggtgcactctcagtacaatctgctctgatgccgcatagttaagccagtatacactccgctatc
gctacgtgactgggtcatggctgcgccccgacacccgccaacacccgctgacgcgccctgacgggcttgtctgctcccggcatc
cgcttacagacaagctgtgaccgtctccgggagctgcatgtgtcagaggttttcaccgtcatcaccgaaacgcgcgaggcagct
gcggtaaagctcatcagcgtggtcgtgaagcgattcacagatgtctgcctgttcatccgcgtccagctcgttgagtttctccagaag
cgttaatgtctggcttctgataaagcgggccatgttaagggcggttttttcctgtttggtcactgatgcctccgtgtaagggggatttctgt
tcatgggggtaatgataccgatgaaacgagagaggatgctcacgatacgggttactgatgatgaacatgcccggttactggaac

gttgtgagggtaaacaactggcggtatggatgcggcgggaccagagaaaaatcactcagggtcaatgccagcgcttcgttaat
acagatgtaggtgttccacagggtagccagcagcatcctgcgatgcagatccggaacataatggtgcagggcgctgacttccg
cgtttccagactttacgaaacacggaaaccgaagaccattcatgttgttgctcaggtcgcagacgttttgcagcagcagtcgcttca
cgttcgctcgcgtatcggtgattcattctgctaaccagtaaggcaaccccgccagcctagccgggtcctcaacgacaggagcac
gatcatgcgcacccgtggggccgccatgccggcgataatggcctgcttctcgccgaaacgtttggtggcgggaccagtgacga
aggcttgagcgagggcgtgcaagattccgaataccgcaagcgacaggccgatcatcgtcgcgctccagcgaaagcggtcctc
gccgaaaatgacccagagcgctgccggcacctgtcctacgagttgcatgataaagaagacagtcataagtgcggcgacgata
gtcatgccccgcgcccaccggaaggagctgactgggttgaaggctctcaagggcatcggtcgagatcccggtgcctaatgagt
gagctaacttacattaattgcgttgcgctcactgcccgctttccagtcgggaaacctgtcgtgccagctgcattaatgaatcggcca
acgcgcggggagaggcggtttgcgtattgggcgccagggtggtttttcttttcaccagtgagacgggcaacagctgattgcccttc
accgcctggccctgagagagttgcagcaagcggtccacgctggtttgccccagcaggcgaaaatcctgtttgatggtggttaacg
gcgggatataacatgagctgtcttcggtatcgtcgtatcccactaccgagatatccgcaccaacgcgcagcccggactcggtaat
ggcgcgcattgcgcccagcgccatctgatcgttggcaaccagcatcgcagtgggaacgatgccctcattcagcatttgcatggttt
gttgaaaaccggacatggcactccagtcgccttcccgttccgctatcggctgaatttgattgcgagtgagatatttatgccagccag
ccagacgcagacgcgccgagacagaacttaatgggcccgctaacagcgcgatttgctggtgacccaatgcgaccagatgctc
cacgcccagtcgcgtaccgtcttcatgggagaaaataatactgttgatgggtgtctggtcagagacatcaagaaataacgccgg
aacattagtgcaggcagcttccacagcaatggcatcctggtcatccagcggatagttaatgatcagcccactgacgcgttgcgcg
agaagattgtgcaccgccgctttacaggcttcgacgccgcttcgttctaccatcgacaccaccacgctggcacccagttgatcgg
cgcgagatttaatcgccgcgacaatttgcgacggcgcgtgcagggccagactggaggtggcaacgccaatcagcaacgactg
tttgcccgccagttgttgtgccacgcggttgggaatgtaattcagctccgccatcgccgcttccacttttcccgcgttttcgcagaaac
gtggctggcctggttcaccacgcgggaaacggtctgataagagacaccggcatactctgcgacatcgtataacgttactggtttc
acattcaccaccctgaattgactctcttccgggcgctatcatgccataccgcgaaaggttttgcgccattcgatggtgtccgggatct
cgacgctctcccttatgcgactcctgcattaggaagcagcccagtagtaggttgaggccgttgagcaccgccgccgcaaggaat
ggtgcatgcaaggagatggcgcccaacagtcccccggccacggggcctgccaccatacccacgccgaaacaagcgctcat
gagcccgaagtggcgagcccgatcttccccatcggtgatgtcggcgatataggcgccagcaaccgcacctgtggcgccggtga
tgccggccacgatgcgtccggcgtagaggatcgagatctcgatcccgcgaaattaatacgactcactatagggaattgtgagc
ggataacaattcccct

pNIC-CTH0-OR (OVA-ROP) Sequence Map

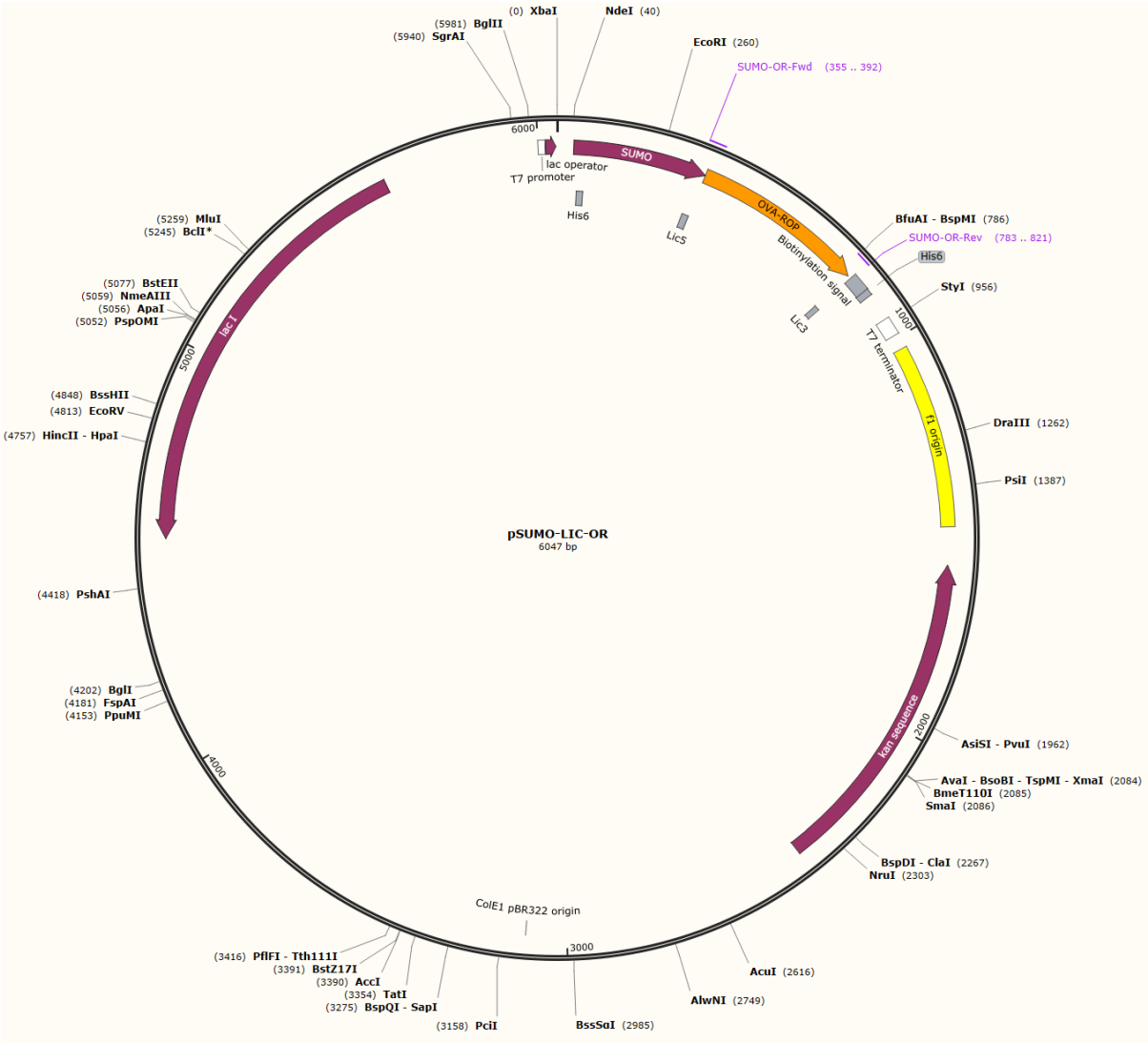
pNIC-CTH0-OR (OVA-ROP) DNA Sequence – **Bold** Highlights OVA-ROP Gene

taatacgactcactatagggaattgtgagcggataacaattcccctctagaaataattttgtttaaccttaagaaggagatatact**a**
tgagcatgctggttctgctgccggatgaagttagcggtctggaacagctggaaagcattatcaatttttgaaaaactgacc
gaatggaccagcagcaatgttatggaactgcgtatgaaaacagaatggacctcaagtaatgtgatggaagaacgcaa
aatcaaagtgtatctgcctcgcatgaaaatggaagagaaatataacctgaccagcgttctgatggccctgcggatgaa
aaaatacaatctgacctcagtgctgatggcaatgggtattaccgatgtttttagcagcagcgcaaatctgagcggtatta
gcagcgcagaaagcctgaaaattagtctgcgcatgaagattagctcagccgaatcactgaaaatttcacaggcagttc
atgcagcacatgccgaaattaatgaagcaggtcgtgcagagaacctctacttccaatcgcaccatcatcaccaccattgata
caaggatgacgacgataagtgaggatccgaattcgagctccgtcgacaagcttgcggccgcactcgagcaccaccaccacca
ccactgagatccggctgctaacaaagcccgaaaggaagctgagttggctgctgccaccgctgagcaataactagcataaccc
cttggggcctctaaacgggtcttgaggggttttttgctgaaaggaggaactatatccggattggcgaatgggacgcgccctgtagc
ggcgcattaagcgcggcgggtgtggtggttacgcgcagcgtgaccgctacacttgccagcgccctagcgcccgctcctttcgcttt
cttcccttcctttctcgccacgttcgccggctttccccgtcaagctctaaatcgggggctccctttagggttccgatttagtgctttacggc
acctcgaccccaaaaaacttgattagggtgatggttcacgtagtgggccatcgccctgatagacggtttttcgccctttgacgttgga
gtccacgttctttaatagtggactcttgttccaaactggaacaacactcaaccctatctcggtctattcttttgatttataagggattttgcc
gatttcggcctattggttaaaaaatgagctgatttaacaaaaatttaacgcgaattttaacaaaatattaacgtttacaatttcaggtg
gcacttttcggggaaatgtgcgcggaacccctatttgtttatttttctaaatacattcaaatatgtatccgctcatgaattaattcttagaa



aaactcatcgagcatcaaatgaaactgcaatttattcatatcaggattatcaataccatatttttgaaaaagccgtttctgtaatgaag
gagaaaactcaccgaggcagttccataggatggcaagatcctggtatcggtctgcgattccgactcgtccaacatcaatacaac
ctattaatttcccctcgtcaaaaataaggttatcaagtgagaaatcaccatgagtgacgactgaatccggtgagaatggcaaaag
tttatgcatttctttccagacttgttcaacaggccagccattacgctcgtcatcaaaatcactcgcatcaaccaaaccgttattcattcgt
gattgcgcctgagcgagacgaaatacgcgatcgctgttaaaaggacaattacaaacaggaatcgaatgcaaccggcgcagg
aacactgccagcgcatcaacaatattttcacctgaatcaggatattcttctaatacctggaatgctgttttcccggggatcgcagtggt
gagtaaccatgcatcatcaggagtacggataaaatgcttgatggtcggaagaggcataaattccgtcagccagtttagtctgacc
atctcatctgtaacatcattggcaacgctacctttgccatgtttcagaaacaactctggcgcatcgggcttcccatacaatcgataga
ttgtcgcacctgattgcccgacattatcgcgagcccatttatacccatataaatcagcatccatgttggaatttaatcgcggcctaga
gcaagacgtttcccgttgaatatggctcataacacccttgtattactgtttatgtaagcagacagttttattgttcatgaccaaaatcc
cttaacgtgagttttcgttccactgagcgtcagaccccgtagaaaagatcaaaggatcttcttgagatcctttttttctgcgcgtaatct
gctgcttgcaaacaaaaaaaccaccgctaccagcggtggtttgtttgccggatcaagagctaccaactctttttccgaaggtaact
ggcttcagcagagcgcagataccaaatactgtccttctagtgtagccgtagttaggccaccacttcaagaactctgtagcaccgc
ctacatacctcgctctgctaatcctgttaccagtggctgctgccagtggcgataagtcgtgtcttaccgggttggactcaagacgata
gttaccggataaggcgcagcggtcgggctgaacgggggttcgtgcacacagcccagcttggagcgaacgacctacaccga
actgagatacctacagcgtgagctatgagaaagcgccacgcttcccgaagggagaaaggcggacaggtatccggtaagcgg
cagggtcggaacaggagagcgcacgagggagcttccagggggaaacgcctggtatctttatagtcctgtcgggtttcgccacct
ctgacttgagcgtcgatttttgtgatgctcgtcaggggggcggagcctatggaaaaacgccagcaacgcggccttttacggttcct
ggccttttgctggccttttgctcacatgttctttcctgcgttatcccctgattctgtggataaccgtattaccgcctttgagtgagctgatac
cgctcgccgcagccgaacgaccgagcgcagcgagtcagtgagcgaggaagcggaagagcgcctgatgcggtattttctcctt
acgcatctgtgcggtatttcacaccgcatatatggtgcactctcagtacaatctgctctgatgccgcatagttaagccagtatacact
ccgctatcgctacgtgactgggtcatggctgcgccccgacacccgccaacacccgctgacgcgccctgacgggcttgtctgctc
ccggcatccgcttacagacaagctgtgaccgtctccgggagctgcatgtgtcagaggttttcaccgtcatcaccgaaacgcgcga
ggcagctgcggtaaagctcatcagcgtggtcgtgaagcgattcacagatgtctgcctgttcatccgcgtccagctcgttgagtttctc
cagaagcgttaatgtctggcttctgataaagcgggccatgttaagggcggttttttcctgtttggtcactgatgcctccgtgtaagggg
gatttctgttcatgggggtaatgataccgatgaaacgagagaggatgctcacgatacgggttactgatgatgaacatgcccggtta
ctggaacgttgtgagggtaaacaactggcggtatggatgcggcgggaccagagaaaaatcactcagggtcaatgccagcgct
tcgttaatacagatgtaggtgttccacagggtagccagcagcatcctgcgatgcagatccggaacataatggtgcagggcgctg
acttccgcgtttccagactttacgaaacacggaaaccgaagaccattcatgttgttgctcaggtcgcagacgttttgcagcagcagt
cgcttcacgttcgctcgcgtatcggtgattcattctgctaaccagtaaggcaaccccgccagcctagccgggtcctcaacgacag
gagcacgatcatgcgcacccgtggggccgccatgccggcgataatggcctgcttctcgccgaaacgtttggtggcgggaccag
tgacgaaggcttgagcgagggcgtgcaagattccgaataccgcaagcgacaggccgatcatcgtcgcgctccagcgaaagc
ggtcctcgccgaaaatgacccagagcgctgccggcacctgtcctacgagttgcatgataaagaagacagtcataagtgcggcg
acgatagtcatgccccgcgcccaccggaaggagctgactgggttgaaggctctcaagggcatcggtcgagatcccggtgccta
atgagtgagctaacttacattaattgcgttgcgctcactgcccgctttccagtcgggaaacctgtcgtgccagctgcattaatgaatc
ggccaacgcgcggggagaggcggtttgcgtattgggcgccagggtggtttttcttttcaccagtgagacgggcaacagctgattg
cccttcaccgcctggccctgagagagttgcagcaagcggtccacgctggtttgccccagcaggcgaaaatcctgtttgatggtgg
ttaacggcgggatataacatgagctgtcttcggtatcgtcgtatcccactaccgagatatccgcaccaacgcgcagcccggactc
ggtaatggcgcgcattgcgcccagcgccatctgatcgttggcaaccagcatcgcagtgggaacgatgccctcattcagcatttgc
atggtttgttgaaaaccggacatggcactccagtcgccttcccgttccgctatcggctgaatttgattgcgagtgagatatttatgcca
gccagccagacgcagacgcgccgagacagaacttaatgggcccgctaacagcgcgatttgctggtgacccaatgcgaccag
atgctccacgcccagtcgcgtaccgtcttcatgggagaaaataatactgttgatgggtgtctggtcagagacatcaagaaataac
gccggaacattagtgcaggcagcttccacagcaatggcatcctggtcatccagcggatagttaatgatcagcccactgacgcgtt
gcgcgagaagattgtgcaccgccgctttacaggcttcgacgccgcttcgttctaccatcgacaccaccacgctggcacccagttg
atcggcgcgagatttaatcgccgcgacaatttgcgacggcgcgtgcagggccagactggaggtggcaacgccaatcagcaac
gactgtttgcccgccagttgttgtgccacgcggttgggaatgtaattcagctccgccatcgccgcttccacttttcccgcgttttcgca
gaaacgtggctggcctggttcaccacgcgggaaacggtctgataagagacaccggcatactctgcgacatcgtataacgttact
ggtttcacattcaccaccctgaattgactctcttccgggcgctatcatgccataccgcgaaaggttttgcgccattcgatggtgtccgg
gatctcgacgctctcccttatgcgactcctgcattaggaagcagcccagtagtaggttgaggccgttgagcaccgccgccgcaag
gaatggtgcatgcaaggagatggcgcccaacagtcccccggccacggggcctgccaccatacccacgccgaaacaagcgc
tcatgagcccgaagtggcgagcccgatcttccccatcggtgatgtcggcgatataggcgccagcaaccgcacctgtggcgccg
gtgatgccggccacgatgcgtccggcgtagaggatcgagatctcgatcccgcgaaat

pSUMO-LIC-OR (OVA-ROP) Construct Sequence Map

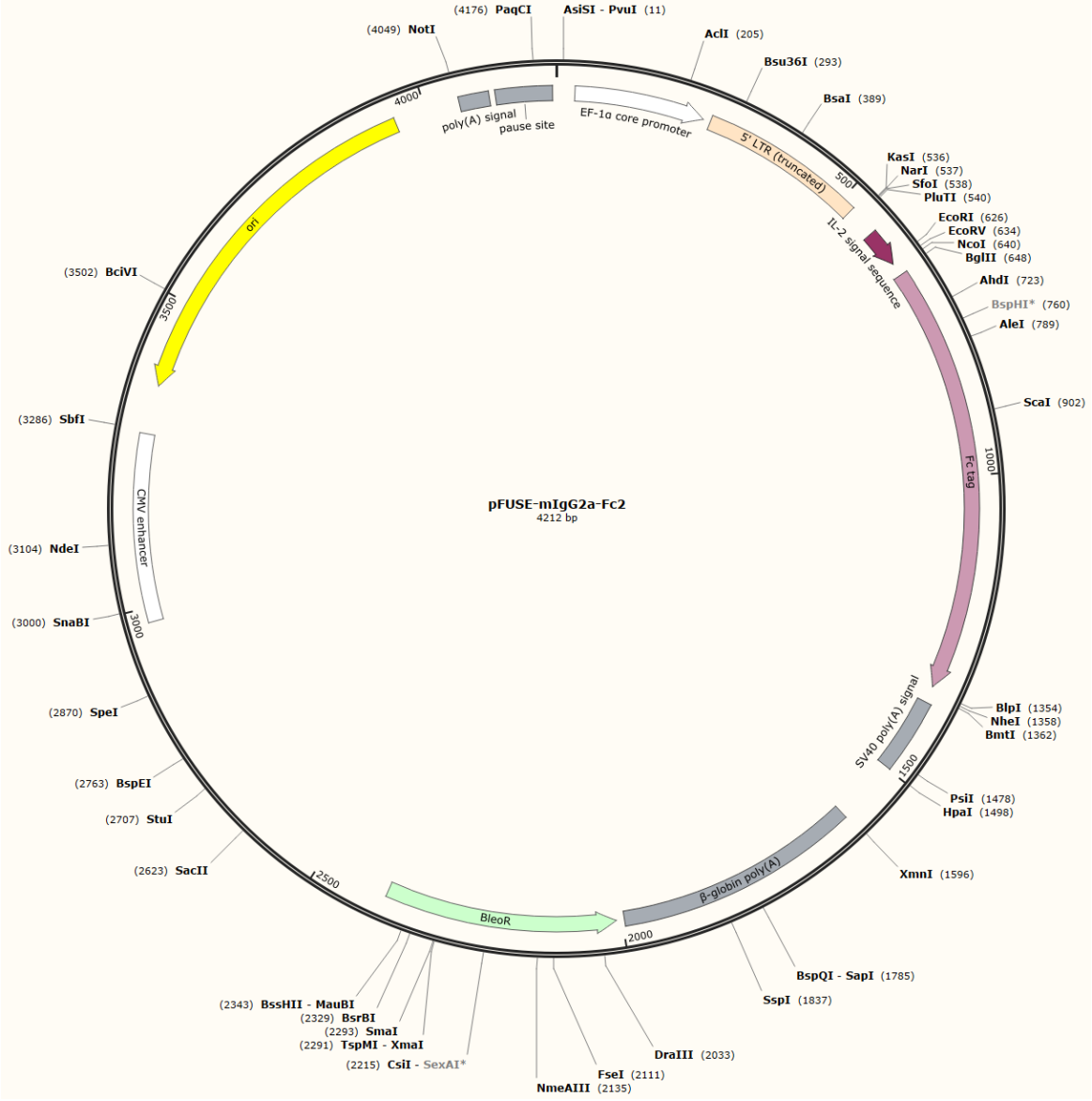


pSUMO-LIC-OR (OVA-ROP) DNA Sequence – **Bold** highlights OVA-ROP gene

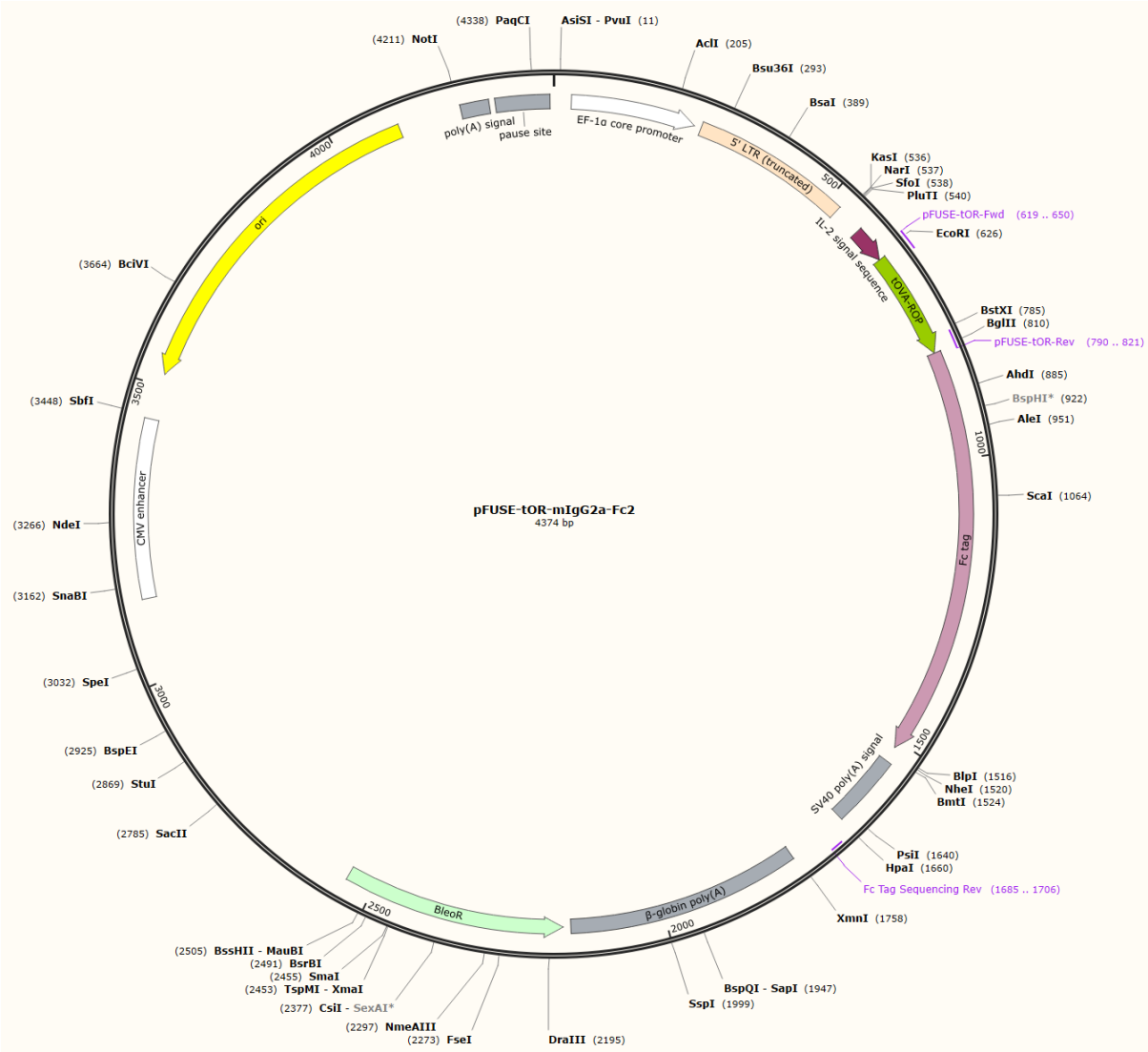
ctagaaataattttgtttaactttaagaaggagatatacatatgtgcagcagccatcatcatcatcacggcagcggcagcggct
ctgaccaggaggcaaaaccttcaactgaggacttgggggataagaaggaaggtgaatatattaaactcaaagtcattggacag
gatagcagtgagattcacttcaaagtgaaaatgacaacacatctcaagaaactcaaagaatcatactgtcaaagacagggtgtt
ccaatgaattcactcaggtttctctttgagggtcagagaattgctgataatcatactccaaaagaactgggaatggaggaagaag
atgtgattgaagtttaccaggagcaaacgggaggt**atgagcatgctggttctgctgccggatgaagttagcggtctggaac**
agctggaaagcattatcaattttgaaaaactgaccgaatggaccagcagcaatgttatggaactgcgtatgaaaacag
aatggacctcaagtaatgtgatggaagaacgcaaaatcaaagtgtatctgcctcgcatgaaaatggaagagaaatata
acctgaccagcgttctgatggccctgcggatgaaaaaatacaatctgacctcagtgctgatggcaatgggtattaccga
tgtttttagcagcagcgcaaatctgagcggtattagcagcgcagaaagcctgaaaattagtctgcgcatgaagattagc
tcagccgaatcactgaaaatttcacaggcagttcatgcagcacatgccgaaattaatgaagcaggtcgttaaagcggtg
gcggtctgaacgacatcttcgaggctcagaaaatcgaatggcacgaacaccaccaccaccaccactgagatccggctgctaa
caaagcccgaaaggaagctgagttggctgctgccaccgctgagcaataactagcataacccctttggggcctctaaacgggtctt
gaggggttttttgctgaaaggaggaactatatccggattggcgaatgggacgcgccctgtagcggcgcattaagcgcggcgggt
gtggtggttacgcgcagcgtgaccgctacacttgccagcgccctagcgcccgctcctttcgctttcttcccttcctttctcgccacgttc
gccggctttccccgtcaagctctaaatcgggggctcccttagggttccgatttagtgctttacggcacctcgaccccaaaaaacttg
attagggtgatggttcacgtagtgggccatcgccctgatagacggtttttcgccctttgacgttggagtccacgttctttaatagtggac
tcttgttccaaactggaacaacactcaaccctatctcggtctattcttttgatttataagggattttgccgatttcggcctattggttaaaa
aatgagctgatttaacaaaaatttaacgcgaattttaacaaaatattaacgtttacaatttcaggtggcacttttcggggaaatgtgc
gcggaacccctatttgtttatttttctaaatacattcaaatatgtatccgctcatgaattaattcttagaaaaactcatcgagcatcaaat
gaaactgcaatttattcatatcaggattatcaataccatatttttgaaaaagccgtttctgtaatgaaggagaaaactcaccgaggc
agttccataggatggcaagatcctggtatcggtctgcgattccgactcgtccaacatcaatacaacctattaatttcccctcgtcaaa
aataaggttatcaagtgagaaatcaccatgagtgacgactgaatccggtgagaatggcaaaagtttatgcatttctttccagacttg
ttcaacaggccagccattacgctcgtcatcaaaatcactcgcatcaaccaaaccgttattcattcgtgattgcgcctgagcgagac
gaaatacgcgatcgctgttaaaaggacaattacaaacaggaatcgaatgcaaccggcgcaggaacactgccagcgcatcaa
caatattttcacctgaatcaggatattcttctaatacctggaatgctgttttcccggggatcgcagtggtgagtaaccatgcatcatca
ggagtacggataaaatgcttgatggtcggaagaggcataaattccgtcagccagtttagtctgaccatctcatctgtaacatcattg
gcaacgctacctttgccatgtttcagaaacaactctggcgcatcgggcttcccatacaatcgatagattgtcgcacctgattgcccg
acattatcgcgagcccatttatacccatataaatcagcatccatgttggaatttaatcgcggcctagagcaagacgtttcccgttgaa
tatggctcataacacccttgtattactgtttatgtaagcagacagttttattgttcatgaccaaaatcccttaacgtgagttttcgttcca
ctgagcgtcagaccccgtagaaaagatcaaaggatcttcttgagatcctttttttctgcgcgtaatctgctgcttgcaaacaaaaaa
accaccgctaccagcggtggtttgtttgccggatcaagagctaccaactctttttccgaaggtaactggcttcagcagagcgcaga
taccaaatactgtccttctagtgtagccgtagttaggccaccacttcaagaactctgtagcaccgcctacatacctcgctctgctaat
cctgttaccagtggctgctgccagtggcgataagtcgtgtcttaccgggttggactcaagacgatagttaccggataaggcgcag
cggtcgggctgaacgggggttcgtgcacacagcccagcttggagcgaacgacctacaccgaactgagatacctacagcgtg
agctatgagaaagcgccacgcttcccgaagggagaaaggcggacaggtatccggtaagcggcagggtcggaacaggaga
gcgcacgagggagcttccagggggaaacgcctggtatctttatagtcctgtcgggtttcgccacctctgacttgagcgtcgatttttgt
gatgctcgtcaggggggcggagcctatggaaaaacgccagcaacgcggccttttacggttcctggccttttgctggccttttgctc
acatgttctttcctgcgttatcccctgattctgtggataaccgtattaccgcctttgagtgagctgataccgctcgccgcagccgaacg
accgagcgcagcgagtcagtgagcgaggaagcggaagagcgcctgatgcggtattttctccttacgcatctgtgcggtatttcac
accgcatatatggtgcactctcagtacaatctgctctgatgccgcatagttaagccagtatacactccgctatcgctacgtgactgg
gtcatggctgcgccccgacacccgccaacacccgctgacgcgccctgacgggcttgtctgctcccggcatccgcttacagaca
agctgtgaccgtctccgggagctgcatgtgtcagaggttttcaccgtcatcaccgaaacgcgcgaggcagctgcggtaaagctc
atcagcgtggtcgtgaagcgattcacagatgtctgcctgttcatccgcgtccagctcgttgagtttctccagaagcgttaatgtctggc
ttctgataaagcgggccatgttaagggcggttttttcctgtttggtcactgatgcctccgtgtaagggggatttctgttcatgggggtaat
gataccgatgaaacgagagaggatgctcacgatacgggttactgatgatgaacatgcccggttactggaacgttgtgagggtaa
acaactggcggtatggatgcggcgggaccagagaaaaatcactcagggtcaatgccagcgcttcgttaatacagatgtaggtg
ttccacagggtagccagcagcatcctgcgatgcagatccggaacataatggtgcagggcgctgacttccgcgtttccagacttta
cgaaacacggaaaccgaagaccattcatgttgttgctcaggtcgcagacgttttgcagcagcagtcgcttcacgttcgctcgcgta
tcggtgattcattctgctaaccagtaaggcaaccccgccagcctagccgggtcctcaacgacaggagcacgatcatgcgcacc
cgtggggccgccatgccggcgataatggcctgcttctcgccgaaacgtttggtggcgggaccagtgacgaaggcttgagcgag
ggcgtgcaagattccgaataccgcaagcgacaggccgatcatcgtcgcgctccagcgaaagcggtcctcgccgaaaatgacc
cagagcgctgccggcacctgtcctacgagttgcatgataaagaagacagtcataagtgcggcgacgatagtcatgccccgcgc
ccaccggaaggagctgactgggttgaaggctctcaagggcatcggtcgagatcccggtgcctaatgagtgagctaacttacatt

aattgcgttgcgctcactgcccgctttccagtcgggaaacctgtcgtgccagctgcattaatgaatcggccaacgcgcggggaga
ggcggtttgcgtattgggcgccagggtggtttttctttcaccagtgagacgggcaacagctgattgcccttcaccgcctggccctga
gagagttgcagcaagcggtccacgctggtttgccccagcaggcgaaaatcctgtttgatggtggttaacggcgggatataacatg
agctgtcttcggtatcgtcgtatcccactaccgagatatccgcaccaacgcgcagcccggactcggtaatggcgcgcattgcgcc
cagcgccatctgatcgttggcaaccagcatcgcagtgggaacgatgccctcattcagcatttgcatggtttgttgaaaaccggaca
tggcactccagtcgccttcccgttccgctatcggctgaatttgattgcgagtgagatatttatgccagccagccagacgcagacgc
gccgagacagaacttaatgggcccgctaacagcgcgatttgctggtgacccaatgcgaccagatgctccacgcccagtcgcgt
accgtcttcatgggagaaaataatactgttgatgggtgtctggtcagagacatcaagaaataacgccggaacattagtgcaggc
agcttccacagcaatggcatcctggtcatccagcggatagttaatgatcagcccactgacgcgttgcgcgagaagattgtgcacc
gccgctttacaggcttcgacgccgcttcgttctaccatcgacaccaccacgctggcacccagttgatcggcgcgagatttaatcgc
cgcgacaatttgcgacggcgcgtgcagggccagactggaggtggcaacgccaatcagcaacgactgtttgcccgccagttgtt
gtgccacgcggttgggaatgtaattcagctccgccatcgccgcttccacttttcccgcgttttcgcagaaacgtggctggcctggttc
accacgcgggaaacggtctgataagagacaccggcatactctgcgacatcgtataacgttactggtttcacattcaccaccctga
attgactctcttccgggcgctatcatgccataccgcgaaaggttttgcgccattcgatggtgtccgggatctcgacgctctcccttatg
cgactcctgcattaggaagcagcccagtagtaggttgaggccgttgagcaccgccgccgcaaggaatggtgcatgcaaggag
atggcgcccaacagtcccccggccacggggcctgccaccatacccacgccgaaacaagcgctcatgagcccgaagtggcg
agcccgatcttccccatcggtgatgtcggcgatataggcgccagcaaccgcacctgtggcgccggtgatgccggccacgatgc
gtccggcgtagaggatcgagatctcgatcccgcgaaattaatacgactcactataggggaattgtgagcggataacaattcccct

pFUSE-mIgG2a-Fc2 Vector Sequence Map



pFUSE-tOR-mIgG2a-Fc2 Vector Sequence Map

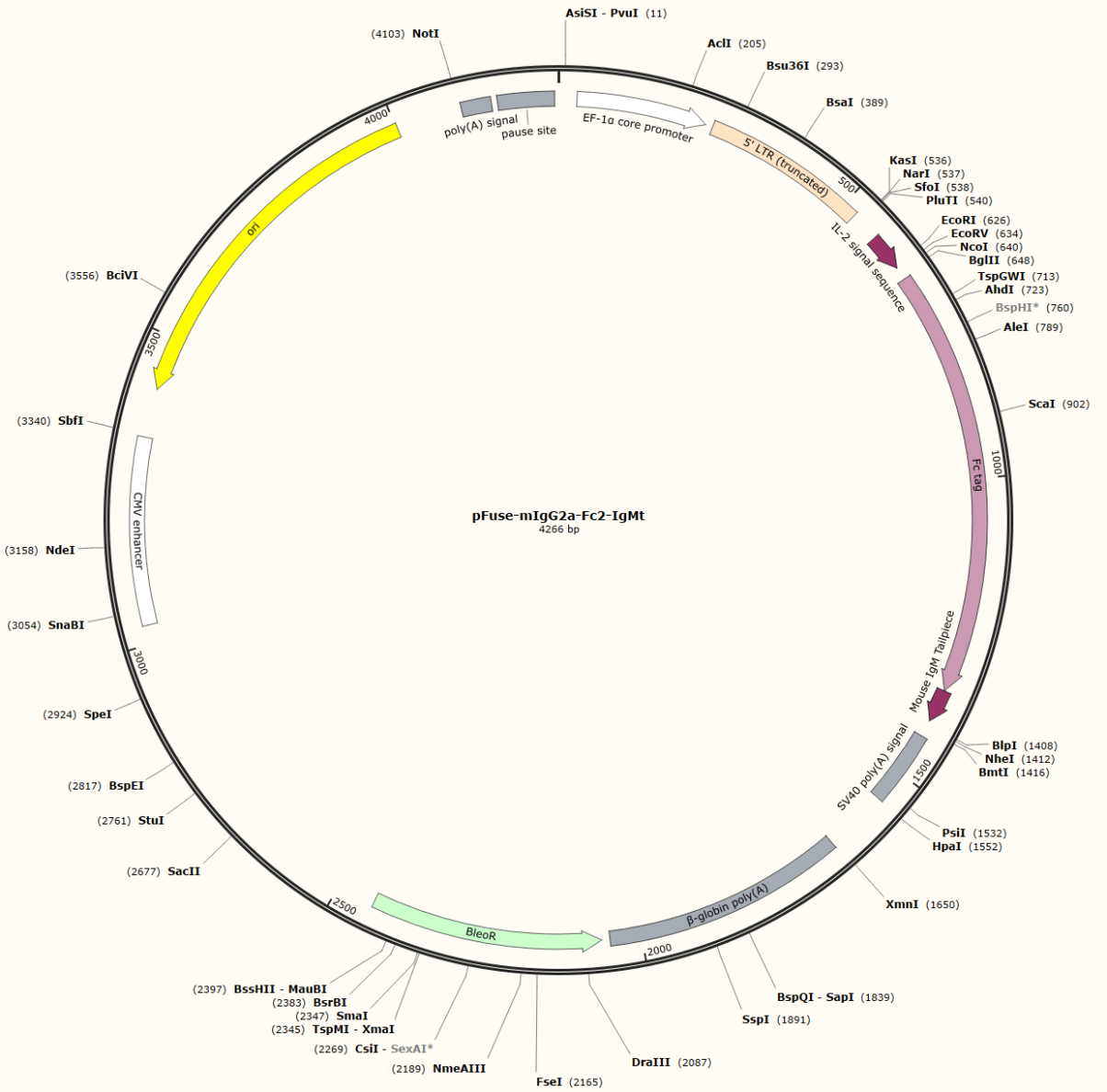


pFUSE-tOR-mIgG2a-Fc2 DNA Sequence – **Bold** is tOVA-ROP, underlined is Fc Tag

ggatctgcgatcgctccggtgcccgtcagtgggcagagcgcacatcgcccacagtccccgagaagttgggggggagggtcgg
caattgaacgggtgcctagagaaggtggcgcggggtaaactgggaaagtgatgtcgtgtactggctccgccttttcccgagggt
gggggagaaccgtatataagtgcagtagtcgccgtgaacgttcttttcgcaacgggtttgccgccagaacacagctgaagcttc
gaggggctcgcatctctccttcacgcgcccgccgccctacctgaggccgccatccacgccggttgagtcgcgttctgccgcctcc
cgcctgtggtgcctcctgaactgcgtccgccgtctaggtaagtttaaagctcaggtcgagaccgggcctttgtccggcgctcccttg
gagcctacctagactcagccggctctccacgctttgcctgaccctgcttgctcaactctacgtctttgtttcgttttctgttctgcgccgtta
cagatccaagctgtgaccggcgcctacctgagatcaccggcgaaggagggccaccatgtacaggatgcaactcctgtcttgca
ttgcactaagtcttgcacttgtcacgaattcg**atgcccgatgaggtgtccggcctggaacagctggaatccatcatcaacttc
gagaagctgaccgagtggaccagcagcctgagaatgaagctgcccaagcctgagagcatcatcaattttgaaaagc
tcacggaatggaccagctccaacgtgatggaagaacggaagatcaaagtcagatct**cccagagggcccacaatcaag
ccctgtcctccatgcaaatgcccagcacctaacctcttgggtggaccatccgtcttcatcttccctccaaagatcaaggatgtactca
tgatctccctgagccccatagtcacatgtgtggtggtggatgtgagcgaggatgacccagatgtccagatcagctggtttgtgaac
aacgtggaagtacacacagctcagacacaaacccatagagaggattacaacagtactctccgggtggtcagtgccctccccat
ccagcaccaggactggatgagtggcaaggagttcaaatgcaaggtcaacaacaaagacctcccagcgcccatcgagagaa
ccatctcaaaacccaaagggtcagtaagagctccacaggtatatgtcttgcctccaccagaagaagagatgactaagaaaca
ggtcactctgacctgcatggtcacagacttcatgcctgaagacatttacgtggagtggaccaacaacgggaaaacagagctaa
actacaagaacactgaaccagtcctggactctgatggttcttacttcatgtacagcaagctgagagtggaaaagaagaactggg

tggaaagaaatagctactcctgttcagtggtccacgagggtctgcacaatcaccacacgactaagagcttctcccggactccgg
gtaaatgagctcagctagctggccagacatgataagatacattgatgagtttggacaaaccacaactagaatgcagtgaaaaa
aatgctttatttgtgaaatttgtgatgctattgctttatttgtaaccattataagctgcaataaacaagttaacaacaacaattgcattcatt
ttatgtttcaggttcaggggggaggtgtgggaggtttttttaaagcaagtaaaacctctacaaatgtggtatggaattaattctaaaatac
agcatagcaaaactttaacctccaaatcaagcctctacttgaatccttttctgagggatgaataaggcataggcatcaggggctgtt
gccaatgtgcattagctgtttgcagcctcaccttctttcatggagtttaagatatagtgtattttcccaaggtttgaactagctcttcatttct
ttatgttttaaatgcactgacctcccacattccctttttagtaaaatattcagaaataatttaaatacatcattgcaatgaaaataaatgtt
ttttattaggcagaatccagatgctcaaggcccttcataatatcccccagtttagtagttggacttagggaacaaaggaacctttaat
agaaattggacagcaagaaagcgagcttctagcttatcctcagtcctgctcctctgccacaaagtgcacgcagttgccggccgg
gtcgcgcagggcgaactcccgcccccacggctgctcgccgatctcggtcatggccggcccggaggcgtcccggaagttcgtgg
acacgacctccgaccactcggcgtacagctcgtccaggccgcgcacccacacccaggccagggtgttgtccggcaccacctg
gtcctggaccgcgctgatgaacagggtcacgtcgtcccggaccacaccggcgaagtcgtcctccacgaagtcccgggagaac
ccgagccggtcggtccagaactcgaccgctccggcgacgtcgcgcgcggtgagcaccggaacggcactggtcaacttggcc
atgatggctcctcctgtcaggagaggaaagagaagaaggttagtacaattgctatagtgagttgtattatactatgcagatatacta
tgccaatgattaattgtcaaactagggctgcagggttcatagtgccacttttcctgcactgccccatctcctgcccacccttcccagg
catagacagtcagtgacttaccaaactcacaggagggagaaggcagaagcttgagacagacccgcgggaccgccgaactg
cgaggggacgtggctagggcggcttcttttatggtgcgccggccctcggaggcagggcgctcggggaggcctagcggccaatc
tgcggtggcaggaggcggggccgaaggccgtgcctgaccaatccggagcacataggagtctcagccccccgccccaaagc
aaggggaagtcacgcgcctgtagcgccagcgtgttgtgaaatgggggcttgggggggttggggccctgactagtcaaaacaa
actcccattgacgtcaatggggtggagacttggaaatccccgtgagtcaaaccgctatccacgcccattgatgtactgccaaaac
cgcatcatcatggtaatagcgatgactaatacgtagatgtactgccaagtaggaaagtcccataaggtcatgtactgggcataat
gccaggcgggccatttaccgtcattgacgtcaataggggggcgtacttggcatatgatacacttgatgtactgccaagtgggcagttt
accgtaaatactccacccattgacgtcaatggaaagtccctattggcgttactatgggaacatacgtcattattgacgtcaatgggc
gggggtcgttgggcggtcagccaggcgggccatttaccgtaagttatgtaacgcctgcaggttaattaagaacatgtgagcaaa
aggccagcaaaaggccaggaaccgtaaaaaggccgcgttgctggcgtttttccataggctccgccccccctgacgagcatcaca
aaaatcgacgctcaagtcagaggtggcgaaacccgacaggactataaagataccaggcgtttcccccctggaagctccctcgtg
cgctctcctgttccgaccctgccgcttaccggatacctgtccgcctttctcccttcgggaagcgtggcgctttctcatagctcacgctgt
aggtatctcagttcggtgtaggtcgttcgctccaagctgggctgtgtgcacgaacccccccgttcagcccgaccgctgcgccttatcc
ggtaactatcgtcttgagtccaacccggtaagacacgacttatcgccactggcagcagccactggtaacaggattagcagagcg
aggtatgtaggcggtgctacagagttcttgaagtggtggcctaactacggctacactagaagaacagtatttggtatctgcgctctg
ctgaagccagttaccttcggaaaaagagttggtagctcttgatccggcaaacaaaccaccgctggtagcggtggtttttttgtttgca
agcagcagattacgcgcagaaaaaaaggatctcaagaagatcctttgatcttttctacggggtctgacgctcagtggaacgaaa
actcacgttaagggattttggtcatggctagttaattaacatttaaatcagcggccgcaataaaatatctttattttcattacatctgtgtg
ttggttttttgtgtgaatcgtaactaacatacgctctccatcaaaacaaaacgaaacaaaacaaactagcaaaataggctgtcccc
agtgcaagtgcaggtgccagaacatttctctatcgaa

pFUSE-mIgG2a-Fc2-IgMt and pFUSE-mIgG2a-Fc2-IgMt-Q94C Vector Map

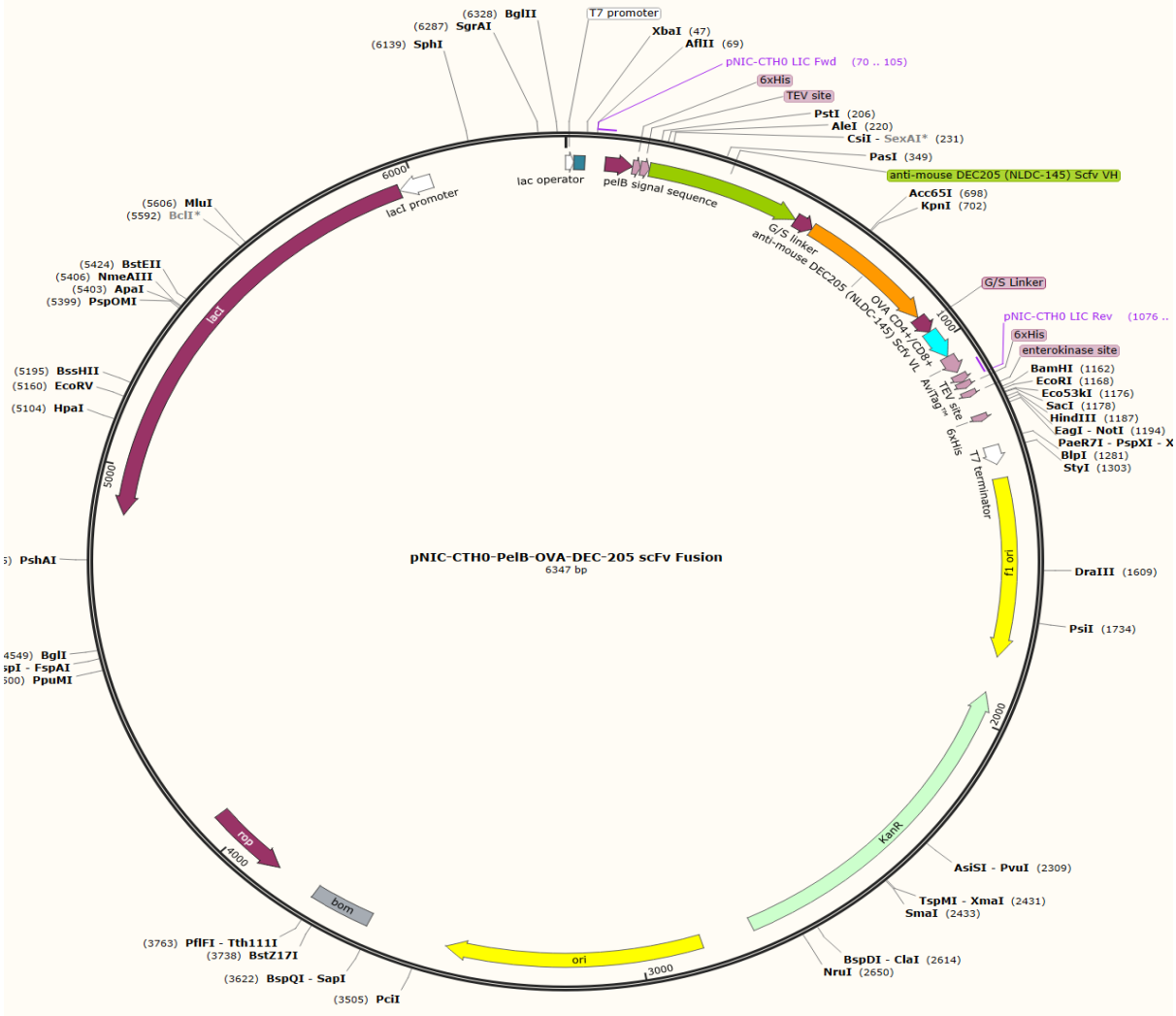


pFUSE-mIgG2a-Fc2-IgMt/IgM-Q94C DNA Sequence – **Bold** Highlights IgM tailpiece, underlined is Fc Tag, **Bold Underlined** highlights the Q94C mutation site (**cag** in non-mutant)

ggatctgcgatcgctccggtgcccgtcagtgggcagagcgcacatcgcccacagtccccgagaagttgggggggagggtcgg
caattgaacgggtgcctagagaaggtggcgcggggtaaactgggaaagtgatgtcgtgtactggctccgccttttcccgagggt
gggggagaaccgtatataagtgcagtagtcgccgtgaacgttctttttcgcaacgggtttgccgccagaacacagctgaagcttc
gaggggctcgcatctctccttcacgcgcccgccgccctacctgaggccgccatccacgccggttgagtcgcgttctgccgcctcc
cgcctgtggtgcctcctgaactgcgtccgccgtctaggtaagtttaaagctcaggtcgagaccgggcctttgtccggcgctcccttg
gagcctacctagactcagccggctctccacgctttgcctgaccctgcttgctcaactctacgtctttgtttcgttttctgttctgcgccgtta
cagatccaagctgtgaccggcgcctacctgagatcaccggcgaaggagggccaccatgtacaggatgcaactcctgtcttgca
ttgcactaagtcttgcacttgtcacgaattcgatatcggccatggttagatctcccagagggcccacaatcaagccctgtcctccatg
caaatgcccagcacctaacctcttgggtggaccatccgtcttcatcttccctccaaagatcaaggatgtactcatgatctccctgag
ccccatagtcacatgtgtggtggtggatgtgagcgaggatgacccagatgtccagatcagctggtttgtgaacaacgtggaagta
cacacagctcagacacaaacccatagagaggattacaacagtactctccgggtggtcagtgccctccccatc**tgc**caccaccc
catctgccaccaggactggatgagtggcaaggagttcaaatgcaaggtcaacaacaaagacctcccagcgcccatcgagag
aaccatctcaaaacccaaagggtcagtaagagctccacaggtatatgtcttgcctccaccagaagaagagatgactaagaaa

caggtcactctgacctgcatggtcacagacttcatgcctgaagacatttacgtggagtggaccaacaacgggaaaacagagct
aaactacaagaacactgaaccagtcctggactctgatggttcttacttcatgtacagcaagctgagagtggaaaagaagaactg
ggtggaaagaaatagctactcctgttcagtggtccacgagggtctgcacaatcaccacacgactaagagcttctcccggactcc
gggtaaa**cccacactgtacaacgtgtccctgatcatgagcgacaccggcggcacatgttactga**gctcagctagctggc
cagacatgataagatacattgatgagtttggacaaaccacaactagaatgcagtgaaaaaaatgctttatttgtgaaatttgtgatg
ctattgctttatttgtaaccattataagctgcaataaacaagttaacaacaacaattgcattcattttatgtttcaggttcaggggaggt
gtgggaggttttttaaagcaagtaaaacctctacaaatgtggtatggaattaattctaaaatacagcatagcaaaactttaacctcc
aaatcaagcctctacttgaatccttttctgagggatgaataaggcataggcatcaggggctgttgccaatgtgcattagctgtttgca
gcctcaccttctttcatggagtttaagatatagtgtattttcccaaggtttgaactagctcttcatttctttatgttttaaatgcactgacctcc
cacattccctttttagtaaaatattcagaaataatttaaatacatcattgcaatgaaaataaatgtttttttattaggcagaatccagatgc
tcaaggcccttcataatatcccccagtttagtagttggacttagggaacaaaggaacctttaatagaaattggacagcaagaaag
cgagcttctagcttatcctcagtcctgctcctctgccacaaagtgcacgcagttgccggccgggtcgcgcagggcgaactcccgc
ccccacggctgctcgccgatctcggtcatggccggcccggaggcgtcccggaagttcgtggacacgacctccgaccactcggc
gtacagctcgtccaggccgcgcacccacacccaggccagggtgttgtccggcaccacctggtcctggaccgcgctgatgaaca
gggtcacgtcgtcccggaccacaccggcgaagtcgtcctccacgaagtcccgggagaacccgagccggtcggtccagaact
cgaccgctccggcgacgtcgcgcgcggtgagcaccggaacggcactggtcaacttggccatgatggctcctcctgtcaggaga
ggaaagagaagaaggttagtacaattgctatagtgagttgtattatactatgcagatatactatgccaatgattaattgtcaaactag
ggctgcagggttcatagtgccacttttcctgcactgccccatctcctgcccaccctttcccaggcatagacagtcagtgacttaccaa
actcacaggagggagaaggcagaagcttgagacagacccgcgggaccgccgaactgcgaggggacgtggctagggcgg
cttcttttatggtgcgccggccctcggaggcagggcgctcggggaggcctagcggccaatctgcggtggcaggaggcggggcc
gaaggccgtgcctgaccaatccggagcacataggagtctcagccccccgccccaaagcaaggggaagtcacgcgcctgtag
cgccagcgtgttgtgaaatgggggcttgggggggttggggccctgactagtcaaaacaaactcccattgacgtcaatggggtgg
agacttggaaatccccgtgagtcaaaccgctatccacgcccattgatgtactgccaaaaccgcatcatcatggtaatagcgatga
ctaatacgtagatgtactgccaagtaggaaagtcccataaggtcatgtactgggcataatgccaggcgggccatttaccgtcattg
acgtcaataggggggcgtacttggcatatgatacacttgatgtactgccaagtgggcagtttaccgtaaatactccacccattgacgt
caatggaaagtccctattggcgttactatgggaacatacgtcattattgacgtcaatgggcgggggtcgttgggcggtcagccag
gcgggccatttaccgtaagttatgtaacgcctgcaggttaattaagaacatgtgagcaaaaggccagcaaaaggccaggaacc
gtaaaaaggccgcgttgctggcgtttttccataggctccgccccctgacgagcatcacaaaaatcgacgctcaagtcagaggt
ggcgaaacccgacaggactataaagataccaggcgtttccccctggaagctccctcgtgcgctctcctgttccgaccctgccgctt
accggatacctgtccgcctttctcccttcgggaagcgtggcgctttctcatagctcacgctgtaggtatctcagttcggtgtaggtcgtt
cgctccaagctgggctgtgtgcacgaaccccccgttcagcccgaccgctgcgccttatccggtaactatcgtcttgagtccaaccc
ggtaagacacgacttatcgccactggcagcagccactggtaacaggattagcagagcgaggtatgtaggcggtgctacagagt
tcttgaagtggtggcctaactacggctacactagaagaacagtatttggtatctgcgctctgctgaagccagttaccttcggaaaaa
gagttggtagctcttgatccggcaaacaaaccaccgctggtagcggtggttttttgtttgcaagcagcagattacgcgcagaaaa
aaaggatctcaagaagatcctttgatcttttctacggggtctgacgctcagtggaacgaaaactcacgttaagggattttggtcatg
gctagttaattaacatttaaatcagcggccgcaataaaatatctttatttcattacatctgtgtgttggttttttgtgtgaatcgtaactaac
atacgctctccatcaaaacaaaacgaaacaaaacaaactagcaaaataggctgtccccagtgcaagtgcaggtgccagaac
atttctctatcgaa

pNIC-CTH0-PelB-OVA-DEC-205 scFv Fusion Construct Sequence Map



pNIC-CTH0-PelB-OVA-DEC-205 scFv Fusion DNA Sequence –

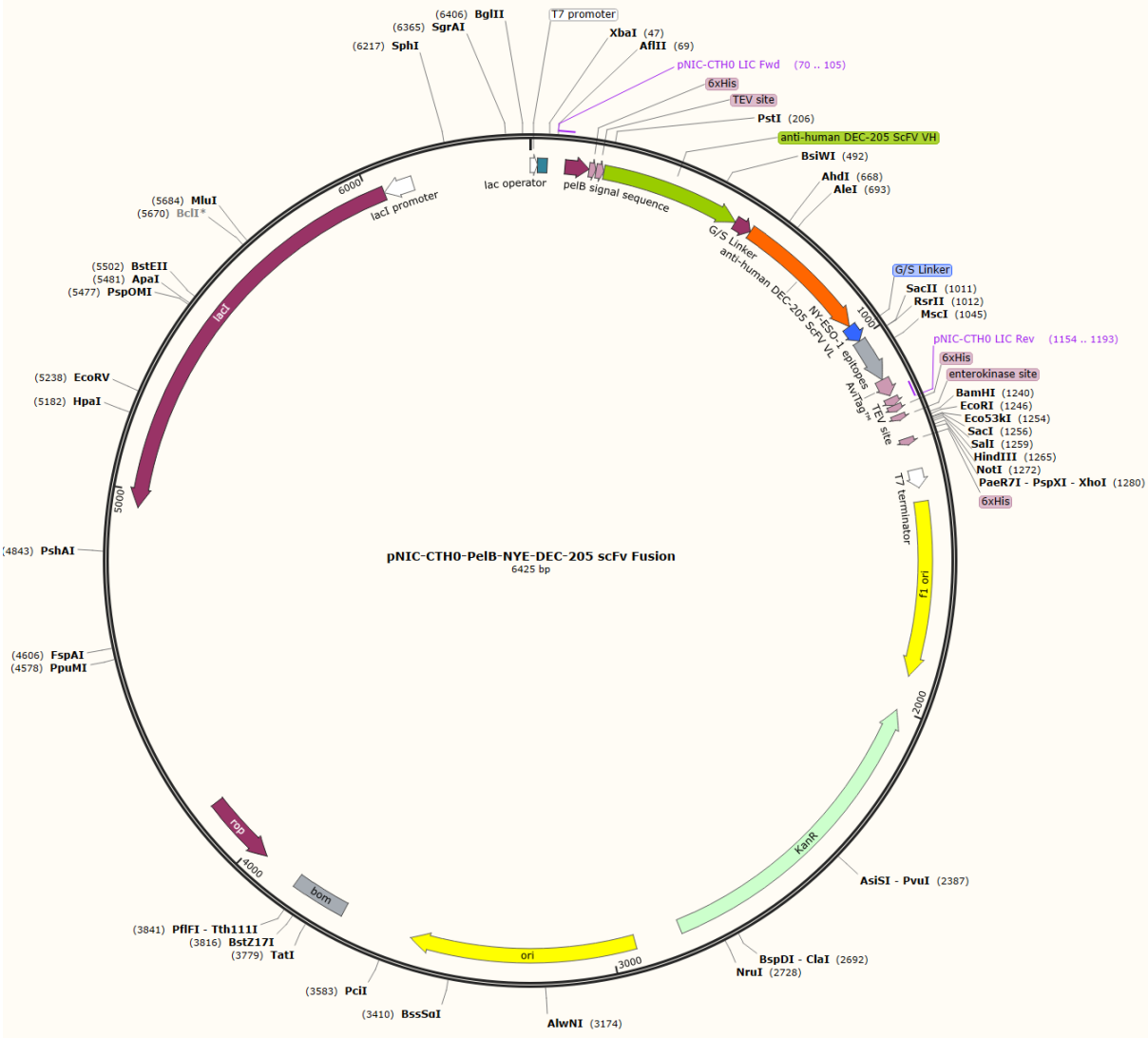
PelB+6xHis+TEV
DEC-205 scFv VH
G/S Linker
DEC-205 scFv VL
OVA Epitopes
Avitag

taatacgactcactatagggaattgtgagcggataacaattcccctctagaaataattttgtttaaccttaagaaggagatatacta
tgaaatatctgctgccgaccgcagcagcgggtctgctgctgctggcagcacagcctgcaatggcacatcatcatcatcaccatga
aaacctgtattttcagagcgaagttaaactgcagcagagcggcactgaagtggtcaaacctggtgcttctgtgaaattatcctgta
aagcgagcggttatatttttacgtcctacgacatagactgggtacgtcagacccccgaacaggggctggagtggattggctggatt
ttccctggggaggggtcgactgagtacaatgagaaattcaaggggagagccacgttgtcggttgataagtcaagttctaccgcct
atatggaattgactagactgacctccgaggactcagcagtctatttctgtgctcgcggcgattactaccgccggtactttgacttatgg
ggtcaaggaaccacagtaacagtcagttcggaggaggcggaagcggcggaggaggaagcggtgggggaggatctgata
ttcaaatgacccaatcaccctctttcttatccacgagcttaggcaacagcatcacgataacttgtcatgcctcgcaaaacattaaag
gctggctggcatggtaccaacaaaagtctggtaacgcaccccaacttcttatctataaggccagtagcttgcagtccggggtgcc
cagccgttttagtggttcaggctccgggaccgactacattttcacaataagcaacttacagccagaagatatagcgacgtactact
gtcaacattaccagtccttcccgtggaccttcggaggcgggactaaattggagatcaaaagagcagccggcggaggggttcc
ggtggaggtggtagtggaggaggcgggagt**tccatcattaattttgagaagttgatttcccaagcggtacacgccgcgcac**

gcagaaataaatgaagcggggagagggctgaacgacatatttgaagcccagaaaatcgaatggcacgaataagcagag
aacctctacttccaatcgcaccatcatcaccaccattgatacaaggatgacgacgataagtgaggatccgaattcgagctccgtc
gacaagcttgcggccgcactcgagcaccaccaccaccaccactgagatccggctgctaacaaagcccgaaaggaagctga
gttggctgctgccaccgctgagcaataactagcataaccccttggggcctctaaacgggtcttgaggggttttttgctgaaaggag
gaactatatccggattggcgaatgggacgcgccctgtagcggcgcattaagcgcggcgggtgtggtggttacgcgcagcgtga
ccgctacacttgccagcgccctagcgcccgctcctttcgctttcttcccttcctttctcgccacgttcgccggctttccccgtcaagctct
aaatcgggggctcccttttagggttccgatttagtgctttacggcacctcgaccccaaaaaacttgattagggtgatggttcacgtagt
gggccatcgccctgatagacggtttttcgccctttgacgttggagtccacgttctttaatagtggactcttgttccaaactggaacaac
actcaaccctatctcggtctattcttttgatttataagggattttgccgatttcggcctattggttaaaaaatgagctgatttaacaaaaat
ttaacgcgaattttaacaaaatattaacgtttacaatttcaggtggcacttttcggggaaatgtgcgcggaacccctatttgtttatttttc
taaatacattcaaatatgtatccgctcatgaattaattcttagaaaaactcatcgagcatcaaatgaaactgcaatttattcatatcag
gattatcaataccatatttttgaaaaagccgtttctgtaatgaaggagaaaactcaccgaggcagttccataggatggcaagatcc
tggtatcggtctgcgattccgactcgtccaacatcaatacaacctattaatttcccctcgtcaaaaataaggttatcaagtgagaaat
caccatgagtgacgactgaatccggtgagaatggcaaaagtttatgcatttctttccagacttgttcaacaggccagccattacgct
cgtcatcaaaatcactcgcatcaaccaaaccgttattcattcgtgattgcgcctgagcgagacgaaatacgcgatcgctgttaaaa
ggacaattacaaacaggaatcgaatgcaaccggcgcaggaacactgccagcgcatcaacaatattttcacctgaatcaggat
attcttctaatacctggaatgctgttttcccggggatcgcagtggtgagtaaccatgcatcatcaggagtacggataaaatgcttgat
ggtcggaagaggcataaattccgtcagccagtttagtctgaccatctcatctgtaacatcattggcaacgctacctttgccatgtttca
gaaacaactctggcgcatcgggcttcccatacaatcgatagattgtcgcacctgattgcccgacattatcgcgagcccatttatacc
catataaatcagcatccatgttggaatttaatcgcggcctagagcaagacgtttcccgttgaatatggctcataacacccttgtatt
actgtttatgtaagcagacagttttattgttcatgaccaaaatcccttaacgtgagttttcgttccactgagcgtcagaccccgtagaa
aagatcaaaggatcttcttgagatcctttttttctgcgcgtaatctgctgcttgcaaacaaaaaaaccaccgctaccagcggtggttt
gtttgccggatcaagagctaccaactctttttccgaaggtaactggcttcagcagagcgcagataccaaatactgtccttctagtgta
gccgtagttaggccaccacttcaagaactctgtagcaccgcctacatacctcgctctgctaatcctgttaccagtggctgctgccag
tggcgataagtcgtgtcttaccgggttggactcaagacgatagttaccggataaggcgcagcggtcgggctgaacgggggttc
gtgcacacagcccagcttggagcgaacgacctacaccgaactgagatacctacagcgtgagctatgagaaagcgccacgctt
cccgaagggagaaaggcggacaggtatccggtaagcggcagggtcggaacaggagagcgcacgagggagcttccaggg
ggaaacgcctggtatctttatagtcctgtcgggtttcgccacctctgacttgagcgtcgatttttgtgatgctcgtcaggggggcggag
cctatggaaaaacgccagcaacgcggccttttacggttcctggccttttgctggccttttgctcacatgttctttcctgcgttatcccctg
attctgtggataaccgtattaccgcctttgagtgagctgataccgctcgccgcagccgaacgaccgagcgcagcgagtcagtga
gcgaggaagcggaagagcgcctgatgcggtattttctccttacgcatctgtgcggtatttcacaccgcatatatggtgcactctcagt
acaatctgctctgatgccgcatagttaagccagtatacactccgctatcgctacgtgactgggtcatggctgcgccccgacacccg
ccaacacccgctgacgcgccctgacgggcttgtctgctcccggcatccgcttacagacaagctgtgaccgtctccgggagctgc
atgtgtcagaggttttcaccgtcatcaccgaaacgcgcgaggcagctgcggtaaagctcatcagcgtggtcgtgaagcgattca
cagatgtctgcctgttcatccgcgtccagctcgttgagtttctccagaagcgttaatgtctggcttctgataaagcgggccatgttaag
ggcggttttttcctgtttggtcactgatgcctccgtgtaagggggatttctgttcatgggggtaatgataccgatgaaacgagagagg
atgctcacgatacgggttactgatgatgaacatgcccggttactggaacgttgtgagggtaaacaactggcggtatggatgcggc
gggaccagagaaaaatcactcagggtcaatgccagcgcttcgttaatacagatgtaggtgttccacagggtagccagcagcat
cctgcgatgcagatccggaacataatggtgcagggcgctgacttccgcgtttccagactttacgaaacacggaaaccgaagac
cattcatgttgttgctcaggtcgcagacgttttgcagcagcagtcgcttcacgttcgctcgcgtatcggtgattcattctgctaaccagt
aaggcaaccccgccagcctagccgggtcctcaacgacaggagcacgatcatgcgcacccgtggggccgccatgccggcga
taatggcctgcttctcgccgaaacgtttggtggcgggaccagtgacgaaggcttgagcgagggcgtgcaagattccgaataccg
caagcgacaggccgatcatcgtcgcgctccagcgaaagcggtcctcgccgaaaatgacccagagcgctgccggcacctgtc
ctacgagttgcatgataaagaagacagtcataagtgcggcgacgatagtcatgccccgcgcccaccggaaggagctgactgg
gttgaaggctctcaagggcatcggtcgagatcccggtgcctaatgagtgagctaacttacattaattgcgttgcgctcactgcccgc
tttccagtcgggaaacctgtcgtgccagctgcattaatgaatcggccaacgcgcggggagaggcggtttgcgtattgggcgcca
gggtggtttttctttcaccagtgagacgggcaacagctgattgcccttcaccgcctggccctgagagagttgcagcaagcggtcc
acgctggtttgccccagcaggcgaaaatcctgtttgatggtggttaacggcgggatataacatgagctgtcttcggtatcgtcgtatc
ccactaccgagatatccgcaccaacgcgcagcccggactcggtaatggcgcgcattgcgcccagcgccatctgatcgttggca
accagcatcgcagtgggaacgatgccctcattcagcatttgcatggtttgttgaaaaccggacatggcactccagtcgccttcccg
ttccgctatcggctgaatttgattgcgagtgagatatttatgccagccagccagacgcagacgcgccgagacagaacttaatggg
cccgctaacagcgcgatttgctggtgacccaatgcgaccagatgctccacgcccagtcgcgtaccgtcttcatgggagaaaata
atactgttgatgggtgtctggtcagagacatcaagaaataacgccggaacattagtgcaggcagcttccacagcaatggcatcct
ggtcatccagcggatagttaatgatcagcccactgacgcgttgcgcgagaagattgtgcaccgccgctttacaggcttcgacgcc
gcttcgttctaccatcgacaccaccacgctggcacccagttgatcggcgcgagatttaatcgccgcgacaatttgcgacggcgcg

tgcagggccagactggaggtggcaacgccaatcagcaacgactgtttgcccgccagttgttgtgccacgcggttgggaatgtaa
ttcagctccgccatcgccgcttccactttttcccgcgttttcgcagaaacgtggctggcctggttcaccacgcgggaaacggtctgat
aagagacaccggcatactctgcgacatcgtataacgttactggtttcacattcaccaccctgaattgactctcttccgggcgctatca
tgccataccgcgaaaggttttgcgccattcgatggtgtccgggatctcgacgctctcccttatgcgactcctgcattaggaagcagc
ccagtagtaggttgaggccgttgagcaccgccgccgcaaggaatggtgcatgcaaggagatggcgcccaacagtcccccgg
ccacggggcctgccaccatacccacgccgaaacaagcgctcatgagcccgaagtggcgagcccgatcttccccatcggtgat
gtcggcgatataggcgccagcaaccgcacctgtggcgccggtgatgccggccacgatgcgtccggcgtagaggatcgagatc
tcgatcccgcgaaat

pNIC-CTH0-PelB-NYE-DEC-205 scFv Fusion Construct Sequence Map



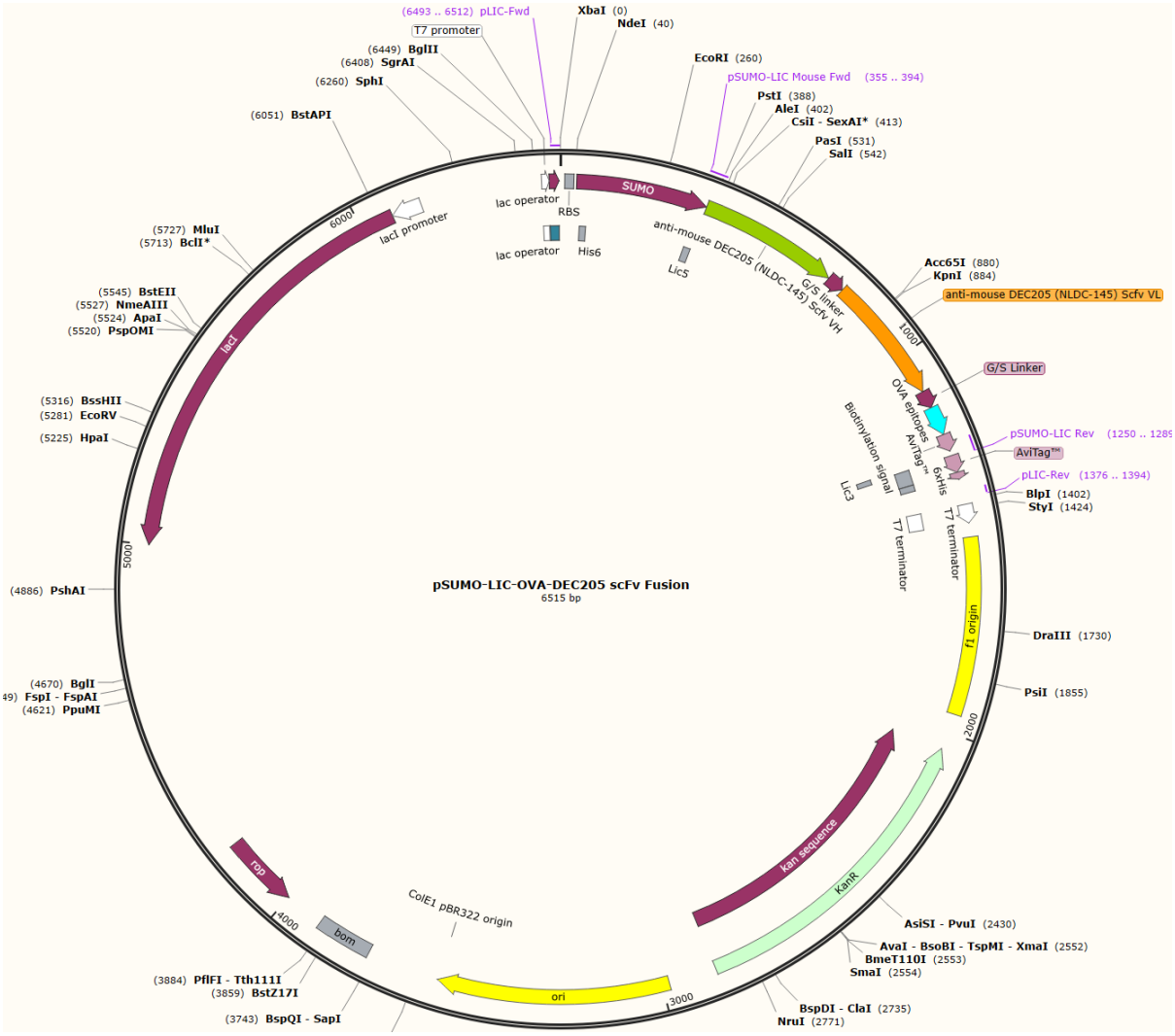
pNIC-CTH0-PelB-NYE-DEC-205 scFv Fusion DNA Sequence

PelB+6xHis+TEV
DEC-205 scFv VH
G/S Linker
DEC-205 scFv VL
NY-ESO-1 Epitopes
Avitag

taatacgactcactatagggaattgtgagcggataacaattcccctctagaaataattttgtttaaccttaagaaggagatatacta
tgaaatatctgctgccgaccgcagcagcgggtctgctgctgctggcagcacagcctgcaatggcacatcatcatcatcaccatga
aaacctgtattttcagagcgaagttcagctgcagcagagcggtccagtgctggtcaagccaggtgcgagcgtgaaaatgtcgtg
caaggcatctggtaatacctttacagattcatttatgcactggatgaagcagtcccatgggaagagcctggaatggataggtattat
taatccttacaatgggggtacttcatacaatcagaagtttaaggggaaagccacgttgacagtggataaaagttcgtcaacagca
tatatggaactgaactctttaacctccgaagactcggccgtttattactgcgcacgtaatggcgtacgctattatttcgactattggggt
cagggaactactctgacagtatcatcggcatcaggagccggtggtgggggtagcggaggaggggggagcggtggaggcggt
agcgctgcacaaccggccatggcggattataagcaagctgtagtgacccaggagtccgccctgaccaccagtccaggcgaa
accgtcacacttacgtgccgctcctcaacgggagccgtgactatcagcaactacgcaaactgggtgcaagaaaaacccgatca
cctgttcacagggttgattggaggtactaacaaccgtgccccgggtgttcctgcgcgcttcagtgggagtctgatcggagataagg
cggccttaaccataacaggagcgcagactgaagatgaagccatctacttctgtgccttgtggtacaacaaccaattcatctttggtt
caggaaccaaggtcacagttcttggaggcggtggctcaggggggaggtggttcaggtggcggaggctcagcccgcggaccg
gagagtcggctgctggaattttatctggccatgccatttgccacaccgatggaagccgagttggcacggcgcagcttat
cccttctgatgtggatcacgcagtgcggtctgaatgatatttttgaagcccagaaaatcgaatggcacgaataagcagagaa
cctctacttccaatcgcaccatcatcaccaccattgatacaaggatgacgacgataagtgaggatccgaattcgagctccgtcga
caagcttgcggccgcactcgagcaccaccaccaccaccactgagatccggctgctaacaaagcccgaaaggaagctgagtt
ggctgctgccaccgctgagcaataactagcataacccctttggggcctctaaacgggtcttgaggggttttttgctgaaaggagga
actatatccggattggcgaatgggacgcgccctgtagcggcgcattaagcgcggcgggtgtggtggttacgcgcagcgtgacc
gctacacttgccagcgccctagcgcccgctcctttcgctttcttcccttcctttctcgccacgttcgccggctttccccgtcaagctctaa
atcgggggctcccttttagggttccgatttagtgctttacggcacctcgaccccaaaaaacttgattagggtgatggttcacgtagtgg
gccatcgccctgatagacggtttttcgccctttgacgttggagtccacgttctttaatagtggactcttgttccaaactggaacaacact
caaccctatctcggtctattcttttgatttataagggattttgccgatttcggcctattggttaaaaaatgagctgatttaacaaaaattta
acgcgaattttaacaaaatattaacgtttacaatttcaggtggcacttttcggggaaatgtgcgcggaacccctatttgtttatttttcta
aatacattcaaatatgtatccgctcatgaattaattcttagaaaaactcatcgagcatcaaatgaaactgcaatttattcatatcagg
attatcaataccatatttttgaaaaagccgtttctgtaatgaaggagaaaactcaccgaggcagttccataggatggcaagatcct
ggtatcggtctgcgattccgactcgtccaacatcaatacaacctattaatttcccctcgtcaaaaataaggttatcaagtgagaaatc
accatgagtgacgactgaatccggtgagaatggcaaaagtttatgcatttctttccagacttgttcaacaggccagccattacgctc
gtcatcaaaatcactcgcatcaaccaaaccgttattcattcgtgattgcgcctgagcgagacgaaatacgcgatcgctgttaaaa
ggacaattacaaacaggaatcgaatgcaaccggcgcaggaacactgccagcgcatcaacaatattttcacctgaatcaggat
attcttctaatacctggaatgctgttttcccggggatcgcagtggtgagtaaccatgcatcatcaggagtacggataaaatgcttgat
ggtcggaagaggcataaattccgtcagccagtttagtctgaccatctcatctgtaacatcattggcaacgctacctttgccatgtttca
gaaacaactctggcgcatcgggcttcccatacaatcgatagattgtcgcacctgattgcccgacattatcgcgagcccatttatacc
catataaatcagcatccatgttggaatttaatcgcggcctagagcaagacgtttcccgttgaatatggctcataacacccttgtatt
actgtttatgtaagcagacagttttattgttcatgaccaaaatcccttaacgtgagttttcgttccactgagcgtcagaccccgtagaa
aagatcaaaggatcttcttgagatcctttttttctgcgcgtaatctgctgcttgcaaacaaaaaaaccaccgctaccagcggtggttt
gtttgccggatcaagagctaccaactctttttccgaaggtaactggcttcagcagagcgcagataccaaatactgtccttctagtgta
gccgtagttaggccaccacttcaagaactctgtagcaccgcctacatacctcgctctgctaatcctgttaccagtggctgctgccag
tggcgataagtcgtgtcttaccgggttggactcaagacgatagttaccggataaggcgcagcggtcgggctgaacgggggttc
gtgcacacagcccagcttggagcgaacgacctacaccgaactgagatacctacagcgtgagctatgagaaagcgccacgctt
cccgaagggagaaaggcggacaggtatccggtaagcggcagggtcggaacaggagagcgcacgagggagcttccaggg
ggaaacgcctggtatctttatagtcctgtcgggtttcgccacctctgacttgagcgtcgatttttgtgatgctcgtcaggggggcggag
cctatggaaaaacgccagcaacgcggccttttacggttcctggccttttgctggccttttgctcacatgttctttcctgcgttatcccctg
attctgtggataaccgtattaccgcctttgagtgagctgataccgctcgccgcagccgaacgaccgagcgcagcgagtcagtga
gcgaggaagcggaagagcgcctgatgcggtattttctccttacgcatctgtgcggtatttcacaccgcatatatggtgcactctcagt
acaatctgctctgatgccgcatagttaagccagtatacactccgctatcgctacgtgactgggtcatggctgcgccccgacacccg
ccaacacccgctgacgcgccctgacgggcttgtctgctcccggcatccgcttacagacaagctgtgaccgtctccgggagctgc
atgtgtcagaggttttcaccgtcatcaccgaaacgcgcgaggcagctgcggtaaagctcatcagcgtggtcgtgaagcgattca
cagatgtctgcctgttcatccgcgtccagctcgttgagtttctccagaagcgttaatgtctggcttctgataaagcgggccatgttaag
ggcggttttttcctgtttggtcactgatgcctccgtgtaagggggatttctgttcatgggggtaatgataccgatgaaacgagagagg
atgctcacgatacgggttactgatgatgaacatgcccggttactggaacgttgtgagggtaaacaactggcggtatggatgcggc
gggaccagagaaaaatcactcagggtcaatgccagcgcttcgttaatacagatgtaggtgttccacagggtagccagcagcat
cctgcgatgcagatccggaacataatggtgcagggcgctgacttccgcgtttccagactttacgaaacacggaaaccgaagac
cattcatgttgttgctcaggtcgcagacgttttgcagcagcagtcgcttcacgttcgctcgcgtatcggtgattcattctgctaaccagt
aaggcaaccccgccagcctagccgggtcctcaacgacaggagcacgatcatgcgcacccgtggggccgccatgccggcga
taatggcctgcttctcgccgaaacgtttggtggcgggaccagtgacgaaggcttgagcgagggcgtgcaagattccgaataccg

caagcgacaggccgatcatcgtcgcgctccagcgaaagcggtcctcgccgaaaatgacccagagcgctgccggcacctgtc
ctacgagttgcatgataaagaagacagtcataagtgcggcgacgatagtcatgccccgcgcccaccggaaggagctgactgg
gttgaaggctctcaagggcatcggtcgagatcccggtgcctaatgagtgagctaacttacattaattgcgttgcgctcactgcccgc
tttccagtcgggaaacctgtcgtgccagctgcattaatgaatcggccaacgcgcggggagaggcggtttgcgtattgggcgcca
gggtggtttttctttcaccagtgagacgggcaacagctgattgcccttcaccgcctggccctgagagagttgcagcaagcggtcc
acgctggtttgccccagcaggcgaaaatcctgtttgatggtggttaacggcgggatataacatgagctgtcttcggtatcgtcgtatc
ccactaccgagatatccgcaccaacgcgcagcccggactcggtaatggcgcgcattgcgcccagcgccatctgatcgttggca
accagcatcgcagtgggaacgatgccctcattcagcatttgcatggtttgttgaaaaccggacatggcactccagtcgccttcccg
ttccgctatcggctgaatttgattgcgagtgagatatttatgccagccagccagacgcagacgcgccgagacagaacttaatggg
cccgctaacagcgcgatttgctggtgacccaatgcgaccagatgctccacgcccagtcgcgtaccgtcttcatgggagaaaata
atactgttgatgggtgtctggtcagagacatcaagaaataacgccggaacattagtgcaggcagcttccacagcaatggcatcct
ggtcatccagcggatagttaatgatcagcccactgacgcgttgcgcgagaagattgtgcaccgccgctttacaggcttcgacgcc
gcttcgttctaccatcgacaccaccacgctggcacccagttgatcggcgcgagatttaatcgccgcgacaatttgcgacggcgcg
tgcagggccagactggaggtggcaacgccaatcagcaacgactgtttgcccgccagttgttgtgccacgcggttgggaatgtaa
ttcagctccgccatcgccgcttccacttttcccgcgttttcgcagaaacgtggctggcctggttcaccacgcgggaaacggtctgat
aagagacaccggcatactctgcgacatcgtataacgttactggtttcacattcaccaccctgaattgactctcttccgggcgctatca
tgccataccgcgaaaggttttgcgccattcgatggtgtccgggatctcgacgctctcccttatgcgactcctgcattaggaagcagc
ccagtagtaggttgaggccgttgagcaccgccgccgcaaggaatggtgcatgcaaggagatggcgcccaacagtcccccgg
ccacggggcctgccaccatacccacgccgaaacaagcgctcatgagcccgaagtggcgagcccgatcttccccatcggtgat
gtcggcgatataggcgccagcaaccgcacctgtggcgccggtgatgccggccacgatgcgtccggcgtagaggatcgagatc
tcgatcccgcgaaat

pSUMO-LIC-OVA-DEC-205 scFv Fusion Construct Sequence Map



pSUMO-LIC-OVA-DEC-205 scFv Fusion DNA Sequence

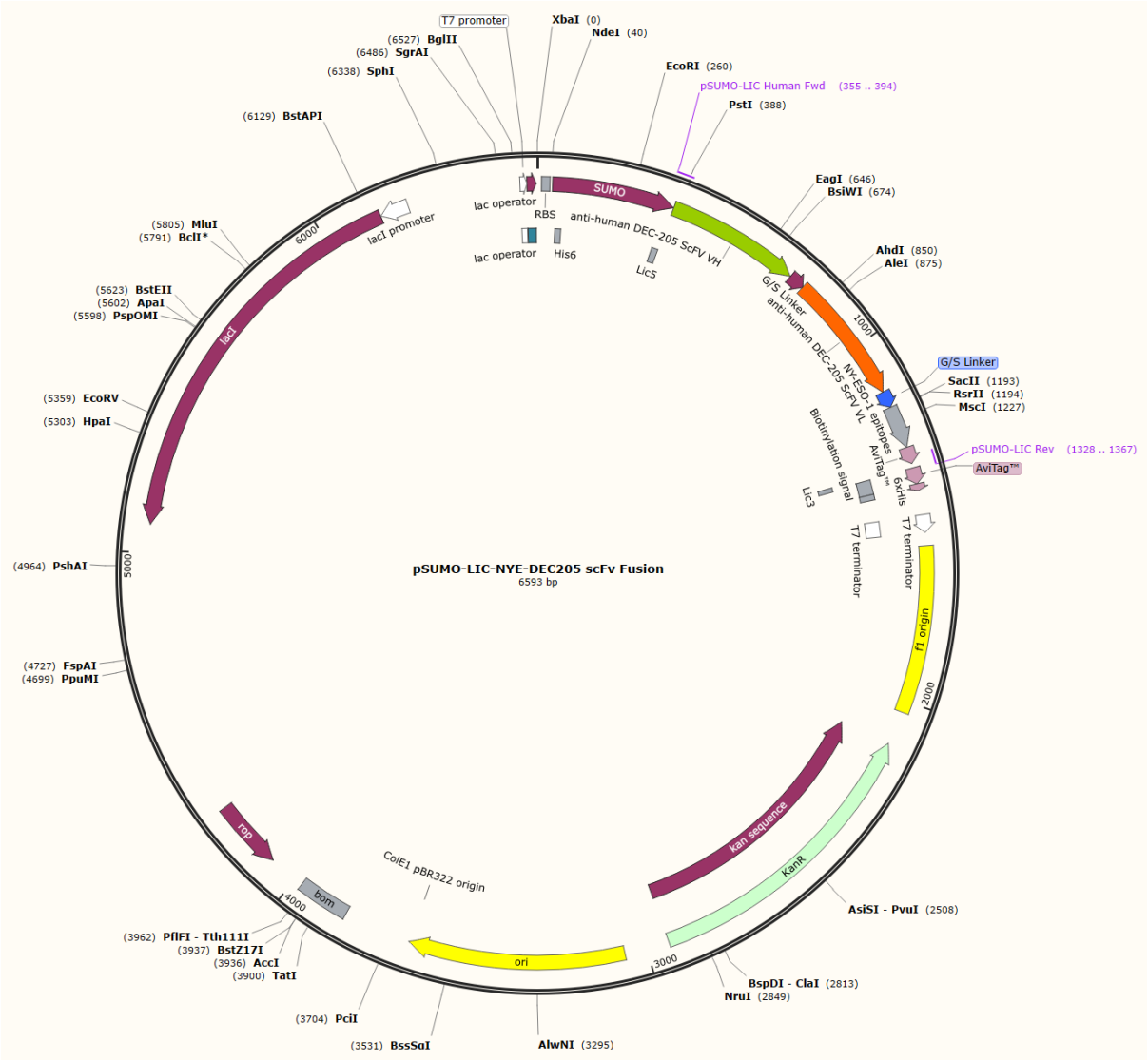
SUMO
DEC-205 scFv VH
G/S Linker
DEC-205 scFv VL
OVA Epitopes
Avitag

ctagaaataattttgtttaactttaagaaggagatatacatatgtgcagcagccatcatcatcatcacggcagcggcagcggct
ctgaccaggaggcaaaaccttcaactgaggacttgggggataagaaggaaggtgaatatattaaactcaaagtcattggacag
gatagcagtgagattcacttcaaagtgaaaatgacaacacatctcaagaaactcaaagaatcatactgtcaaagacagggtgtt
ccaatgaattcactcaggtttctctttgagggtcagagaattgctgataatcatactccaaaagaactgggaatggaggaagaag
atgtgattgaagtttaccaggagcaaacgggaggtgaagttaaactgcagcagagcggcactgaagtggtcaaacctggtgctt
ctgtgaaattatcctgtaaagcgagcggttatatttttacgtcctacgacatagactgggtacgtcagacccccgaacaggggctg
gagtggattggctggatttccctggggaggggtcgactgagtacaatgagaaattcaaggggagagccacgttgtcggttgata
agtcaagttctaccgcctatatggaattgactagactgacctccgaggactcagcagtctatttctgtgctcgcggcgattactaccg
ccggtactttgacttatggggtcaaggaaccacagtaacagtcagttcggaggaggcggaagcggcggaggaggaagcgg
tgggggaggatctgatattcaaatgacccaatcaccctctttcttatccacgagcttaggcaacagcatcacgataacttgtcatgc
ctcgcaaaacattaaaggctggctggcatggtaccaacaaaagtctggtaacgcaccccaacttcttatctataaggccagtagc
ttgcagtccggggtgcccagccgttttagtggttcaggctccgggaccgactacattttcacaataagcaacttacagccagaaga

tatagcgacgtactactgtcaacattaccagtccttcccgtggaccttcggaggcgggactaaattggagatcaaaagagcagc
cggcggaggggttccggtggaggtggtagtggaggaggcgggagt**tccatcattaattttgagaagttgatttcccaagcg**
gtacacgccgcgcacgcagaaataaatgaagcggggagagggctgaacgacatatttgaagcccagaaaatcgaatg
gcacgaataaagcggtggcggtctgaacgacatcttcgaggctcagaaaatcgaatggcacgaacaccaccaccaccacca
ctgagatccggctgctaacaaagcccgaaaggaagctgagttggctgctgccaccgctgagcaataactagcataaccccttg
gggcctctaaacgggtcttgaggggttttttgctgaaaggaggaactatatccggattggcgaatgggacgcgccctgtagcggc
gcattaagcgcggcgggtgtggtggttacgcgcagcgtgaccgctacacttgccagcgccctagcgcccgctcctttcgctttcttc
ccttcctttctcgccacgttcgccggctttccccgtcaagctctaaatcgggggctccctttagggttccgatttagtgctttacggcacc
tcgaccccaaaaaacttgattagggtgatggttcacgtagtgggccatcgccctgatagacggtttttcgccctttgacgttggagtc
cacgttctttaatagtggactcttgttccaaactggaacaacactcaaccctatctcggtctattcttttgatttataagggattttgccga
tttcggcctattggttaaaaaatgagctgatttaacaaaaatttaacgcgaattttaacaaaatattaacgtttacaatttcaggtggc
actttttcgggaaatgtgcgcggaacccctatttgtttatttttctaaatacattcaaatatgtatccgctcatgaattaattcttagaaaa
actcatcgagcatcaaatgaaactgcaatttattcatatcaggattatcaataccatatttttgaaaaagccgtttctgtaatgaagga
gaaaactcaccgaggcagttccataggatggcaagatcctggtatcggtctgcgattccgactcgtccaacatcaatacaaccta
ttaatttcccctcgtcaaaaataaggttatcaagtgagaaatcaccatgagtgacgactgaatccggtgagaatggcaaaagttta
tgcatttctttccagacttgttcaacaggccagccattacgctcgtcatcaaaatcactcgcatcaaccaaaccgttattcattcgtgat
tgcgcctgagcgagacgaaatacgcgatcgctgttaaaaggacaattacaaacaggaatcgaatgcaaccggcgcaggaac
actgccagcgcatcaacaatattttcacctgaatcaggatattcttctaatacctggaatgctgttttcccggggatcgcagtggtga
gtaaccatgcatcatcaggagtacggataaaatgcttgatggtcggaagaggcataaattccgtcagccagtttagtctgaccatc
tcatctgtaacatcattggcaacgctacctttgccatgtttcagaaacaactctggcgcatcgggcttcccatacaatcgatagattgt
cgcacctgattgcccgacattatcgcgagcccatttatacccatataaatcagcatccatgttggaatttaatcgcggcctagagca
agacgtttcccgttgaatatggctcataacacccttgtattactgtttatgtaagcagacagttttattgttcatgaccaaaatccctta
acgtgagttttcgttccactgagcgtcagaccccgtagaaaagatcaaaggatcttcttgagatcctttttttctgcgcgtaatctgctg
cttgcaaacaaaaaaaccaccgctaccagcggtggtttgtttgccggatcaagagctaccaactctttttccgaaggtaactggctt
cagcagagcgcagataccaaatactgtccttctagtgtagccgtagttaggccaccacttcaagaactctgtagcaccgcctaca
tacctcgctctgctaatcctgttaccagtggctgctgccagtggcgataagtcgtgtcttaccgggttggactcaagacgatagttac
cggataaggcgcagcggtcgggctgaacgggggttcgtgcacacagcccagcttggagcgaacgacctacaccgaactga
gatacctacagcgtgagctatgagaaagcgccacgcttcccgaagggagaaaggcggacaggtatccggtaagcggcagg
gtcggaacaggagagcgcacgagggagcttccagggggaaacgcctggtatctttatagtcctgtcgggtttcgccacctctga
cttgagcgtcgatttttgtgatgctcgtcaggggggcggagcctatggaaaaacgccagcaacgcggccttttacggttcctggcc
ttttgctggccttttgctcacatgttctttcctgcgttatcccctgattctgtggataaccgtattaccgcctttgagtgagctgataccgctc
gccgcagccgaacgaccgagcgcagcgagtcagtgagcgaggaagcggaagagcgcctgatgcggtattttctccttacgca
tctgtgcggtatttcacaccgcatatatggtgcactctcagtacaatctgctctgatgccgcatagttaagccagtatacactccgcta
tcgctacgtgactgggtcatggctgcgccccgacacccgccaacacccgctgacgcgccctgacgggcttgtctgctcccggca
tccgcttacagacaagctgtgaccgtctccgggagctgcatgtgtcagaggttttcaccgtcatcaccgaaacgcgcgaggcag
ctgcggtaaagctcatcagcgtggtcgtgaagcgattcacagatgtctgcctgttcatccgcgtccagctcgttgagtttctccagaa
gcgttaatgtctggcttctgataaagcgggccatgttaagggcggttttttcctgtttggtcactgatgcctccgtgtaagggggatttct
gttcatgggggtaatgataccgatgaaacgagagaggatgctcacgatacgggttactgatgatgaacatgcccggttactgga
acgttgtgagggtaaacaactggcggtatggatgcggcgggaccagagaaaaatcactcagggtcaatgccagcgcttcgtta
atacagatgtaggtgttccacagggtagccagcagcatcctgcgatgcagatccggaacataatggtgcagggcgctgacttcc
gcgtttccagactttacgaaacacggaaaccgaagaccattcatgttgttgctcaggtcgcagacgttttgcagcagcagtcgcttc
acgttcgctcgcgtatcggtgattcattctgctaaccagtaaggcaaccccgccagcctagccgggtcctcaacgacaggagca
cgatcatgcgcacccgtggggccgccatgccggcgataatggcctgcttctcgccgaaacgtttggtggcgggaccagtgacg
aaggcttgagcgagggcgtgcaagattccgaataccgcaagcgacaggccgatcatcgtcgcgctccagcgaaagcggtcct
cgccgaaaatgacccagagcgctgccggcacctgtcctacgagttgcatgataaagaagacagtcataagtgcggcgacgat
agtcatgccccgcgcccaccggaaggagctgactgggttgaaggctctcaagggcatcggtcgagatcccggtgcctaatgag
tgagctaacttacattaattgcgttgcgctcactgcccgctttccagtcgggaaacctgtcgtgccagctgcattaatgaatcggcca
acgcgcggggagaggcggtttgcgtattgggcgccagggtggttttttcttttcaccagtgagacgggcaacagctgattgcccttc
accgcctggccctgagagagttgcagcaagcggtccacgctggtttgccccagcaggcgaaaatcctgtttgatggtggttaacg
gcgggatataacatgagctgtcttcggtatcgtcgtatcccactaccgagatatccgcaccaacgcgcagcccggactcggtaat
ggcgcgcattgcgcccagcgccatctgatcgttggcaaccagcatcgcagtgggaacgatgccctcattcagcatttgcatggttt
gttgaaaaccggacatggcactccagtcgccttcccgttccgctatcggctgaatttgattgcgagtgagatatttatgccagccag
ccagacgcagacgcgccgagacagaacttaatgggcccgctaacagcgcgatttgctggtgacccaatgcgaccagatgctc
cacgcccagtcgcgtaccgtcttcatgggagaaaataatactgttgatgggtgtctggtcagagacatcaagaaataacgccgg
aacattagtgcaggcagcttccacagcaatggcatcctggtcatccagcggatagttaatgatcagcccactgacgcgttgcgcg

agaagattgtgcaccgccgctttacaggcttcgacgccgcttcgttctaccatcgacaccaccacgctggcacccagttgatcgg
cgcgagatttaatcgccgcgacaatttgcgacggcgcgtgcagggccagactggaggtggcaacgccaatcagcaacgactg
tttgcccgccagttgttgtgccacgcggttgggaatgtaattcagctccgccatcgccgcttccactttttcccgcgttttcgcagaaac
gtggctggcctggttcaccacgcgggaaacggtctgataagagacaccggcatactctgcgacatcgtataacgttactggtttc
acattcaccaccctgaattgactctcttccgggcgctatcatgccataccgcgaaaggttttgcgccattcgatggtgtccgggatct
cgacgctctcccttatgcgactcctgcattaggaagcagcccagtagtaggttgaggccgttgagcaccgccgccgcaaggaat
ggtgcatgcaaggagatggcgcccaacagtcccccggccacggggcctgccaccatacccacgccgaaacaagcgctcat
gagcccgaagtggcgagcccgatcttccccatcggtgatgtcggcgatataggcgccagcaaccgcacctgtggcgccggtga
tgccggccacgatgcgtccggcgtagaggatcgagatctcgatcccgcgaaattaatacgactcactatagggaattgtgagc
ggataacaattcccct

pSUMO-LIC-NYE-DEC-205 scFv Fusion Construct Sequence Map



pSUMO-LIC-NYE-DEC-205 scFv Fusion DNA Sequence

SUMO
DEC-205 scFv VH
G/S Linker
DEC-205 scFv VL
NY-ESO-1 Epitopes
Avitag

ctagaaataattttgtttaactttaagaaggagatatacatatgtgcagcagccatcatcatcatcacggcagcggcagcggct
ctgaccaggaggcaaaaccttcaactgaggacttgggggataagaaggaaggtgaatatattaaactcaaagtcattggacag
gatagcagtgagattcacttcaaagtgaaaatgacaacacatctcaagaaactcaaagaatcatactgtcaaagacagggtgtt
ccaatgaattcactcaggtttctctttgagggtcagagaattgctgataatcatactccaaaagaactgggaatggaggaagaag
atgtgattgaagtttaccaggagcaaacgggaggtgaagttcagctgcagcagagcggtccagtgctggtcaagccaggtgcg
agcgtgaaaatgtcgtgcaaggcatctggtaatacctttacagattcatttatgcactggatgaagcagtcccatgggaagagcct
ggaatggataggtattattaatccttacaatgggggtacttcatacaatcagaagtttaaggggaaagccacgttgacagtggata
aaagttcgtcaacagcatatatggaactgaactctttaacctccgaagactcggccgtttattactgcgcacgtaatggcgtacgct
attatttcgactattggggtcagggaactactctgacagtatcatcggcatcaggagccggtggtgggggtagcggaggagggg
ggagcggtggaggcggtagcgctgcacaaccggccatggcggattataagcaagctgtagtgacccaggagtccgccctga
ccaccagtccaggcgaaaccgtcacacttacgtgccgctcctcaacgggagccgtgactatcagcaactacgcaaactgggtg
caagaaaaacccgatcacctgttcacagggttgattggaggtactaacaaccgtgccccgggtgttcctgcgcgcttcagtggga
gtctgatcggagataaggcggccttaaccataacaggagcgcagactgaagatgaagccatctacttctgtgccttgtggtacaa
caaccaattcatctttggttcaggaaccaaggtcacagttcttggaggcggtggctcaggggggaggtggttcaggtggcggagg
ctca**gcccgcggaccggagagtcggctgctggaattttatctggccatgccatttgccacaccgatggaagccgagtt**
ggcacggcgcagcttatcccttctgatgtggatcacgcagtgcggtctgaatgatatttttgaagcccagaaaatcgaatgg
cacgaataaagcggtggcggtctgaacgacatcttcgaggctcagaaaatcgaatggcacgaacaccaccaccaccaccac
tgagatccggctgctaacaaagcccgaaaggaagctgagttggctgctgccaccgctgagcaataactagcataaccccttgg
ggcctctaaacgggtcttgaggggttttttgctgaaaggaggaactatatccggattggcgaatgggacgcgccctgtagcggcg
cattaagcgcggcgggtgtggtggttacgcgcagcgtgaccgctacacttgccagcgccctagcgcccgctcctttcgctttcttcc
cttcctttctcgccacgttcgccggctttccccgtcaagctctaaatcgggggctccctttagggttccgatttagtgctttacggcacct
cgaccccaaaaaacttgattagggtgatggttcacgtagtgggccatcgccctgatagacggtttttcgccctttgacgttggagtcc
acgttctttaatagtggactcttgttccaaactggaacaacactcaaccctatctcggtctattcttttgatttataagggattttgccgatt
tcggcctattggttaaaaaatgagctgatttaacaaaaatttaacgcgaattttaacaaaatattaacgtttacaatttcaggtggcac
ttttcggggaaatgtgcgcggaacccctatttgtttatttttctaaatacattcaaatatgtatccgctcatgaattaattcttagaaaaac
tcatcgagcatcaaatgaaactgcaatttattcatatcaggattatcaataccatatttttgaaaaagccgtttctgtaatgaaggaga
aaactcaccgaggcagttccataggatggcaagatcctggtatcggtctgcgattccgactcgtccaacatcaatacaacctatta
atttcccctcgtcaaaaataaggttatcaagtgagaaatcaccatgagtgacgactgaatccggtgagaatggcaaaagtttatg
catttctttccagacttgttcaacaggccagccattacgctcgtcatcaaaatcactcgcatcaaccaaaccgttattcattcgtgattg
cgcctgagcgagacgaaatacgcgatcgctgttaaaaggacaattacaaacaggaatcgaatgcaaccggcgcaggaaca
ctgccagcgcatcaacaatattttcacctgaatcaggatattcttctaatacctggaatgctgttttcccggggatcgcagtggtgagt
aaccatgcatcatcaggagtacggataaaatgcttgatggtcggaagaggcataaattccgtcagccagtttagtctgaccatctc
atctgtaacatcattggcaacgctacctttgccatgtttcagaaacaactctggcgcatcgggcttcccatacaatcgatagattgtc
gcacctgattgcccgacattatcgcgagcccatttatacccatataaatcagcatccatgttggaatttaatcgcggcctagagcaa
gacgtttcccgttgaatatggctcataacacccttgtattactgtttatgtaagcagacagttttattgttcatgaccaaaatcccttaa
cgtgagttttcgttccactgagcgtcagaccccgtagaaaagatcaaaggatcttcttgagatcctttttttctgcgcgtaatctgctgct
tgcaaacaaaaaaaccaccgctaccagcggtggtttgtttgccggatcaagagctaccaactctttttccgaaggtaactggcttc
agcagagcgcagataccaaatactgtccttctagtgtagccgtagttaggccaccacttcaagaactctgtagcaccgcctacat
acctcgctctgctaatcctgttaccagtggctgctgccagtggcgataagtcgtgtcttaccgggttggactcaagacgatagttacc
ggataaggcgcagcggtcgggctgaacgggggttcgtgcacacagcccagcttggagcgaacgacctacaccgaactga
gatacctacagcgtgagctatgagaaagcgccacgcttcccgaagggagaaaggcggacaggtatccggtaagcggcagg
gtcggaacaggagagcgcacgagggagcttccagggggaaacgcctggtatctttatagtcctgtcgggtttcgccacctctga
cttgagcgtcgatttttgtgatgctcgtcaggggggcggagcctatggaaaaacgccagcaacgcggcctttttacggttcctggcc
ttttgctggccttttgctcacatgttctttcctgcgttatcccctgattctgtggataaccgtattaccgcctttgagtgagctgataccgctc
gccgcagccgaacgaccgagcgcagcgagtcagtgagcgaggaagcggaagagcgcctgatgcggtattttctccttacgca
tctgtgcggtatttcacaccgcatatatggtgcactctcagtacaatctgctctgatgccgcatagttaagccagtatacactccgcta
tcgctacgtgactgggtcatggctgcgccccgacacccgccaacacccgctgacgcgccctgacgggcttgtctgctcccggca
tccgcttacagacaagctgtgaccgtctccgggagctgcatgtgtcagaggttttcaccgtcatcaccgaaacgcgcgaggcag
ctgcggtaaagctcatcagcgtggtcgtgaagcgattcacagatgtctgcctgttcatccgcgtccagctcgttgagtttctccagaa
gcgttaatgtctggcttctgataaagcgggccatgttaagggcggttttttcctgtttggtcactgatgcctccgtgtaagggggatttct
gttcatgggggtaatgataccgatgaaacgagagaggatgctcacgatacgggttactgatgatgaacatgcccggttactgga
acgttgtgagggtaaacaactggcggtatggatgcggcgggaccagagaaaaatcactcagggtcaatgccagcgcttcgtta
atacagatgtaggtgttccacagggtagccagcagcatcctgcgatgcagatccggaacataatggtgcagggcgctgacttcc
gcgtttccagactttacgaaacacggaaaccgaagaccattcatgttgttgctcaggtcgcagacgttttgcagcagcagtcgcttc
acgttcgctcgcgtatcggtgattcattctgctaaccagtaaggcaaccccgccagcctagccgggtcctcaacgacaggagca

cgatcatgcgcacccgtggggccgccatgccggcgataatggcctgcttctcgccgaaacgtttggtggcgggaccagtgacg
aaggcttgagcgagggcgtgcaagattccgaataccgcaagcgacaggccgatcatcgtcgcgctccagcgaaagcggtcct
cgccgaaaatgacccagagcgctgccggcacctgtcctacgagttgcatgataaagaagacagtcataagtgcggcgacgat
agtcatgccccgcgcccaccggaaggagctgactgggttgaaggctctcaagggcatcggtcgagatcccggtgcctaatgag
tgagctaacttacattaattgcgttgcgctcactgcccgctttccagtcgggaaacctgtcgtgccagctgcattaatgaatcggcca
acgcgcggggagaggcggtttgcgtattgggcgccagggtggtttttctttcaccagtgagacgggcaacagctgattgcccttc
accgcctggccctgagagagttgcagcaagcggtccacgctggtttgccccagcaggcgaaaatcctgtttgatggtggttaacg
gcgggatataacatgagctgtcttcggtatcgtcgtatcccactaccgagatatccgcaccaacgcgcagcccggactcggtaat
ggcgcgcattgcgcccagcgccatctgatcgttggcaaccagcatcgcagtgggaacgatgccctcattcagcatttgcatggttt
gttgaaaaccggacatggcactccagtcgccttcccgttccgctatcggctgaatttgattgcgagtgagatatttatgccagccag
ccagacgcagacgcgccgagacagaacttaatgggcccgctaacagcgcgatttgctggtgacccaatgcgaccagatgctc
cacgcccagtcgcgtaccgtcttcatgggagaaaataatactgttgatgggtgtctggtcagagacatcaagaaataacgccgg
aacattagtgcaggcagcttccacagcaatggcatcctggtcatccagcggatagttaatgatcagcccactgacgcgttgcgcg
agaagattgtgcaccgccgctttacaggcttcgacgccgcttcgttctaccatcgacaccaccacgctggcacccagttgatcgg
cgcgagatttaatcgccgcgacaatttgcgacggcgcgtgcagggccagactggaggtggcaacgccaatcagcaacgactg
tttgcccgccagttgttgtgccacgcggttgggaatgtaattcagctccgccatcgccgcttccacttttcccgcgttttcgcagaaac
gtggctggcctggttcaccacgcgggaaacggtctgataagagacaccggcatactctgcgacatcgtataacgttactggtttc
acattcaccaccctgaattgactctcttccgggcgctatcatgccataccgcgaaaggttttgcgccattcgatggtgtccgggatct
cgacgctctcccttatgcgactcctgcattaggaagcagcccagtagtaggttgaggccgttgagcaccgccgccgcaaggaat
ggtgcatgcaaggagatggcgcccaacagtcccccggccacggggcctgccaccatacccacgccgaaacaagcgctcat
gagcccgaagtggcgagcccgatcttccccatcggtgatgtcggcgatataggcgccagcaaccgcacctgtggcgccggtga
tgccggccacgatgcgtccggcgtagaggatcgagatctcgatcccgcgaaattaatacgactcactatagggaattgtgagc
ggataacaattcccct